EARTHQUAKE, BLAST AND IMPACT

Measurement and Effects of Vibration

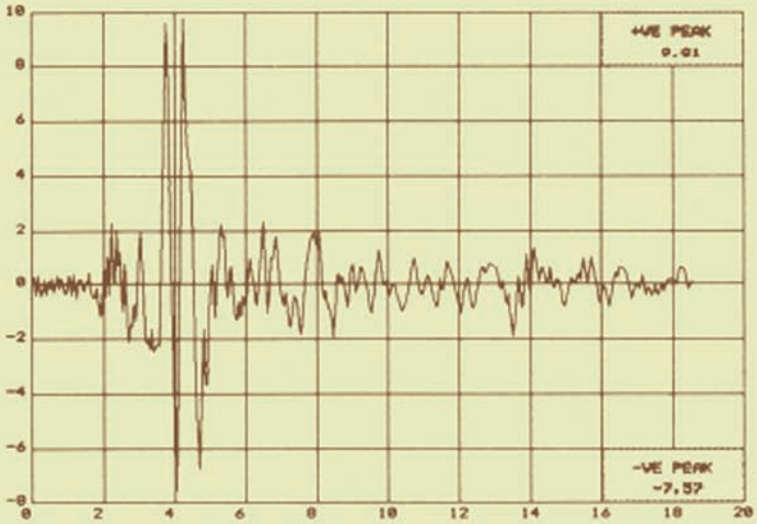

EDITED BY
THE SOCIETY FOR EARTHQUAKE AND CIVIL ENGINEERING DYNAMICS

SECED

@seismicisolation

EARTHQUAKE, BLAST AND IMPACT

Measurement and Effects of Vibration

@seismicisolation

This volume consists of papers presented at the International Conference on Earthquake, Blast and Impact held at the University of Manchester Institute of Science and Technology, UK, 18–20 September 1991, organised by the Society for Earthquake and Civil Engineering Dynamics (SECED) and supported by the Institution of Civil Engineers, the Institution of Mechanical Engineers and the Institution of Structural Engineers.

Organising Committee

J. R. MAGUIRE (*Chairman*)
J. BARR
E. D. BOOTH
C. W. A. BROWITT
A. S. ELNASHAI
R. R. KUNAR
P. A. MERRIMAN
R. S. STEEDMAN

Co-Sponsors

W. S. Atkins
Lloyd's Register
Institute of Explosives Engineers

Student Sponsors

Ove Arup Partnership
British Geological Survey

@seismicisolation

EARTHQUAKE, BLAST AND IMPACT

Measurement and Effects of Vibration

Edited by

SECED

The Society for Earthquake and Civil Engineering Dynamics

ELSEVIER APPLIED SCIENCE

LONDON and NEW YORK

@seismicisolation

Transferred to Digital Printing 2005

ELSEVIER SCIENCE PUBLISHERS LTD
Crown House, Linton Road, Barking, Essex IG11 8JU, England

Sole Distributor in the USA and Canada
ELSEVIER SCIENCE PUBLISHING CO., INC.
655 Avenue of the Americas, New York, NY 10010, USA

WITH 70 TABLES AND 335 ILLUSTRATIONS

© 1991 ELSEVIER SCIENCE PUBLISHERS LTD
© 1991 OVE ARUP PARTNERSHIP—pp. 53–62, 307–318, 482–491
© 1991 CROWN COPYRIGHT—pp. 163–175, 193–200

British Library Cataloguing in Publication Data

Earthquake, blast and impact: measurement and effects of vibration.
I. Society for Earthquake and Civil Engineering Dynamics
624.1762

ISBN 1 85166 705 9

Library of Congress CIP data applied for

No responsibility is assumed by the Publisher for any injury and/or damage to persons or property as a matter of products liability, negligence or otherwise, or from any use or operation of any methods, products, instructions or ideas contained in the material herein.

Special regulations for readers in the USA

This publication has been registered with the Copyright Clearance Center Inc. (CCC), Salem, Massachusetts. Information can be obtained from the CCC about conditions under which photocopies of parts of this publication may be made in the USA. All other copyright questions, including photocopying outside the USA, should be referred to the publisher.

All rights reserved. No part of this publication may be reproduced, stored in a retrieval system, or transmitted in any form or by any means, electronic, mechanical, photocopying, recording, or otherwise, without the prior written permission of the publisher.

@seismicisolation
@seismicisolation

Preface

Following its successful conferences in East Anglia in 1985 and Bristol in 1988, SECED (The Society for Earthquake and Civil Engineering Dynamics) decided to hold the third in this series of international technical conferences at UMIST, Manchester, on 18–20 September 1991.

This book contains the 47 papers which were accepted for formal presentation at the conference. The choice of papers was made on the basis of over 80 abstracts offered, some of which were selected for presentation at a poster session. The papers are organised into nine groups as follows:

Session 1: Ground Motion and Field Studies (Papers 1–6)
Session 2: Analysis and Case Histories (Papers 7–11)
Session 3: Isolation and Damping (Papers 12–15)
Session 4: Blast (Papers 16–20)
Session 5: Members and Joints (Papers 21–25)
Session 6: Instrumentation and Testing (Papers 26–32)
Session 7: Impact (Papers 33–37)
Session 8: Piling and Demolition (Papers 38–43)
Session 9: Code Issues and Feedback (Papers 44–47)

This book contains a wealth of information and we hope that engineers and researchers will find it useful.

J. R. MAGUIRE
Chairman,
SECED Conference Organising Committee

@seismicisolation

Taylor & Francis
Taylor & Francis Group
http://taylorandfrancis.com

@seismicisolation
@seismicisolation

CONTENTS

Preface v

Ground Motion and Field Studies

Far-field ground motions in the Bishop's Castle earthquake of 2 April 1990 1
W. P. Aspinall, G. Woo and D. J. Mallard

Reducing conservatisms from broad band spectra in low to moderate seismic environments 9
J. Donald and R. Kunar

A parameterless scale of seismic intensity for use in seismic risk analysis and vulnerability assessment 19
R. J. S. Spence, A. W. Coburn, S. Sakai and A. Pomonis

A comparison between real, UK suited, response spectra with the present design spectra 31
J. Menu and J. Colloff

On the use of data from microearthquake networks for grading instrumental hypocentre parameters and quality classification of fault plane solutions for seismic hazard assessment 41
W. P. Aspinall, B. O. Skipp and D. J. Mallard

The Luzon, Philippines earthquake of 16 July 1990 53
E. D. Booth, A. M. Chandler, P. K. C. Wong and A. W. Coburn

Analysis and Case Histories

Investigation of the validity of equivalent linearization of non-linear material properties 63
S. K. Sarma and K. Breitwieser

Seismic response of conventional power station structures . . . 79
D. B. Thompson, M. M. Khabbazan, D. C. Mackay and P. S. Fashole-Luke

Parametric studies of the seismic response of concrete gravity dams to UK-type earthquakes 91
W. E. Daniell, C. A. Taylor and J. L. Banks

@seismicisolation

Dynamic testing and analysis of Lloyd's Register House 100
J. R. Maguire

Seismic qualification and construction of safety related pipebridges utilising isolation techniques 110
J. B. Riding, P. Clark and C. Rogers

Isolation and Damping

Some design aspects of dynamic isolation of buildings from seismic ground vibrations 121
R. Shepherd and L. J. Billings

The use of discrete dampers to reduce the torsional response of structures to earthquakes 131
D. Key

Seismic isolation with high damping rubber bearings: theory and practice 141
K. N. G. Fuller, H. R. Ahmadi and V. A. Coveney

Application of fractional calculus in modeling viscous dampers . . 151
N. Makris and M. C. Constantinou

Blast

The effect of detonator variability on explosively induced ground vibration 163
B. M. New

Methods for the assessment of the blast response of engineering structures 176
M. S. Williams and J. P. Newell

Estimation of design forces on structures near quarries from field blast tests 186
V. K. Puri and S. Prakash

On the significance of internal gas explosions in buildings . . . 193
B. R. Ellis

Experimental studies of vibrations caused by blasting for tunnel excavation 201
G. Bongiovanni, V. Gorelli, G. Rienzo and D. Rinaldis

@seismicisolation

Members and Joints

Experimental behaviour of ductile partially-encased composite beam-columns 211
A. Y. Elghazouli, A. S. Elnashai and P. J. Dowling

The behaviour of plastic hinge zones in seismic resistant concrete structures 221
R. Fenwick

Design and performance of model floor-column joints for simulation of inelastic structural response under earthquake loading 231
E. A. Nichol, A. M. Chandler and R. H. Bassett

Seismic resistance of connections in existing flat-plate buildings . . 241
A. J. Durrani

A computational strategy for the cracking process in concrete structures under shock and earthquake loading conditions . . . 249
F. B. A. Beshara and K. S. Virdi

Instrumentation and Testing

'In situ' dynamic tests of a gated gravity dam 264
R. Câmara and A. Portugal

Experimental study of hysteretic energy absorption and load capacity of reinforced concrete columns subjected to different cyclic loading rates 275
G. Verzeletti, S. N. Bousias, E. Gutierrez, G. Magonette and P. Tognoli

Physical modelling of earthquake excitation for geotechnical engineering 285
R. S. Steedman and X. Zeng

University of Nottingham cyclic triaxial test facility 295
M. Raybould

Comparison between analytical and shaking table results for extreme response of a model steel building 307
A. Blakeborough, P. D. Murphy and E. D. Booth

Comparison of calculated seismic response of a 1/4 scale reactor building with measured response 319
J. M. Llambias and R. S. Johnston

@seismicisolation

Effects of test apparatus boundaries on shaking table test results . 333
M. Budhu, G. Neelakantan and A. Al-Karni

Impact

Laboratory and centrifuge modelling of impact loading on buried structures 342
M. C. R. Davies

Ground velocity attenuation associated with the Lockerbie air crash impact 352
D. W. Redmayne and T. Turbitt

Dynamic response of impacted cemented backfill 363
G. N. Nnadi

Methodology for assessment of high mass low velocity impacts on concrete structures 374
B. R. Evason and K. Fullard

Experimental study and theoretical analysis of reinforced concrete structures under accidental impact loading 385
A. V. Zabegayev

Piling and Demolition

Estimation of piling-induced ground vibrations 395
A. Oliver and A. R. Selby

Dynamic debonding of grouted prestressing tendons cut during demolition 411
A. Belhadj, P. Waldron and A. Blakeborough

Ground and structural vibrations induced by explosive demolition of adjacent structures 421
J. M. W. Brownjohn, Z. A. Lubkowski, J. W. Pappin and C. A. Taylor

Dynamic monitoring of large diameter driven piles, New Galata Bridge, Istanbul, Turkey 430
J. S. Young

Effects of constructional vibrations upon an urban environment . 442
I. D. Isaac

@seismicisolation

Non-monotonical decay of ground surface vibrations caused by pile driving 463
P. B. Attewell, A. R. Selby and A. Uromeihy

Code Issues and Feedback

Choice of design seismic hazard parameters for Eurocode 8 in areas of low seismicity 482
E. D. Booth and B. O. Skipp

Evaluation of effects of simplification used in current seismic reliability analysis 492
S. Rahman

Seismic behaviour of structures during the Manjil earthquake, 1990 in Iran 502
H. A. Moghaddam

Seismic design of ductile R/C members 510
K. Pilakoutas and A. S. Elnashai

Index of Contributors 521

@seismicisolation

Taylor & Francis
Taylor & Francis Group
http://taylorandfrancis.com

@seismicisolation
@seismicisolation

FAR-FIELD GROUND MOTIONS IN THE BISHOP'S CASTLE EARTHQUAKE OF 2 APRIL 1990

W.P. ASPINALL[1], G. WOO[2] and D.J. MALLARD[3]

[1]Aspinall & Assocs., Sunbury-on-Thames, Middx.
[2]BEQE Ltd., Cambridge.
[3]Nuclear Electric plc, Barnwood, Glos.

ABSTRACT

The Bishop's Castle earthquake of 1990 April 2 13:46 GMT in the Welsh Borders was widely felt throughout western Britain. An event of this kind occurs infrequently in Britain, every few decades on average, so it was fortunate that it was well recorded on the digital microseismic networks at Hinkley Point and Dungeness. Recordings from these networks, on three-component instruments with bandwidths to 30Hz at distance ranges of 117 to 160 km and 303 to 306 km from the hypocentre, allowed recovery of the first useful far-field horizontal acceleration time histories for British earthquake engineering purposes.

Peak horizontal ground accelerations in the nearer range of distances were in accord with the expected values predicted by current UK uniform risk spectra, notwithstanding some uncertainty in the instrumental magnitude of this earthquake. At the greater distances, peak values were significantly lower than predicted. The recorded response spectra at intermediate and lower frequencies were substantially lower than would be anticipated from the expected uniform risk spectra, reflecting the conservatism of these spectra, and perhaps indicating particular spectral characteristics of this earthquake. Instrumental and macroseismic evidence suggests reduced low and intermediate frequency content of this event compared with the 1984 Lleyn earthquake.

The contribution of these new observations to the quantification of British seismic hazard and its conservatism would be enhanced by a fuller analysis of the instrumental magnitude of the Bishop's Castle earthquake, by a detailed appraisal of the extensive intensity information, and by the deployment of further digital seismographs with good dynamic range and bandwidth.

@seismicisolation

BACKGROUND

The ordinary Monday afternoon tranquillity of seismologists around Britain was rudely interrupted on 2 April 1990 by the Bishop's Castle earthquake, epicentred near the village of Clun in Shropshire, with its sweeping instrumental registrations and ample intensity observations. Ritchie et al. [1] reported a hypocentral location at 52.434°N -3.035°W, depth 14.3 km, and magnitude 5.1M_L; they ascribed a maximum epicentral intensity of 6MSK. Other, preliminary instrumental magnitude measurements for this event were 4.22 ±0.27 M_S and 5.45 M_W, [2]; as far as is known, no authoritative felt-area magnitude assessment has yet been published but a tentative estimate using the approximate radius of the isoseismal III in [1] and the PML (1982) relationship [3] suggests a felt-area magnitude in the range 4.5 to 4.8 M_{SA}. A discussion of the differences between these magnitude estimates is outside the scope of this paper. The earthquake was felt at Intensity III or III+ in the region of north Somerset where Nuclear Electric plc operate their Hinkley Point microseismic network, and was also reputedly felt as far south and east as Canterbury in Kent, not far from the Dungeness network. An approximate estimate of ground acceleration corresponding to intensity may be found from the standard Murphy-O'Brien formula [4]:

$$\text{Log (acc)} = 0.25*(\text{int} + 1)$$

According to this, an Intensity of III roughly corresponds to a peak acceleration of 0.01g.

The Nuclear Electric microearthquake networks [5] each consist of seven telemetered digital outstations, comprising three three-component seismometer sets and four single components using Willmore Mk. III seismometers and Earth Data Ltd. telemetry. The system has an effective dynamic range of 96dB provided by 10-bit digitization with 2-bit gain-ranging. With the exception of some of the vertical components on the Hinkley Point network (which had been modified to assist event detection), data are recorded with a frequency cut-off at 30Hz. The outstations equipped with horizontal seismometers are housed in single-storey brick-built electricity supply industry substations or radio sites; their locations and the epicentre of the Bishop's Castle earthquake are shown on Fig. 1.

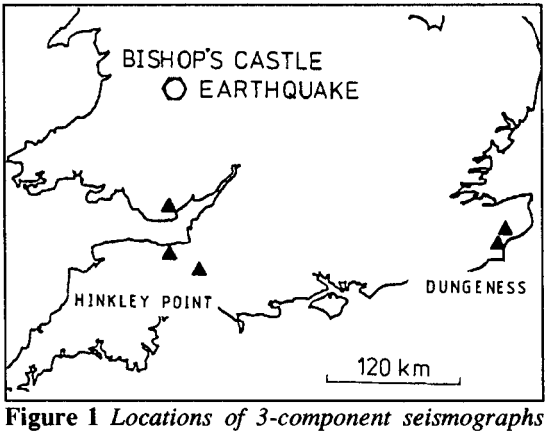

Figure 1 *Locations of 3-component seismographs and the earthquake epicentre.*

@seismicisolation

Since the Lleyn earthquake of 1984 July 19 occurred before the advent of full digital seismometry in Britain, these data essentially contribute the first far-field acceleration time histories for a significant British earthquake. But it must be stressed that the purpose of the networks is to detect and record low-magnitude microearthquakes; the instrumentation has not been configured for precisely recording ground acceleration *per se*.

DATA ANALYSIS

The Willmore Mk. III seismometer is a velocity transducer and the manufacturer's specifications have been assumed for correcting raw data for instrument response; the individual geophones recording the Bishop's Castle earthquake have not been independently calibrated or matched. Data from the two sets of instruments closest to the epicentre, at Leckwith and Holford, suffered slight clipping in limited parts of the record when seismometer outputs exceeded the dynamic range of the acquisition system. This has been corrected by curve-fitting to the missing short segments. The velocity records have been converted to equivalent acceleration time histories using a simple three-point central difference derivative estimator which has only modest pretensions to numerical sophistication. (More complex approaches, such as quadratic least-squares estimators, must be used with caution as some impose low-pass filtering which limits peak response). As a consequence of non-calibration and numerical limitations, the acceleration observations which follow are probably accurate only to about 10 - 20% at best. An example of a processed velocity record and its companion acceleration time history is shown in Fig. 2. Because the vertical instruments of the Hinkley Point network were operated at that time with reduced bandwidths, records of vertical ground motions are not suitable for conversion to acceleration.

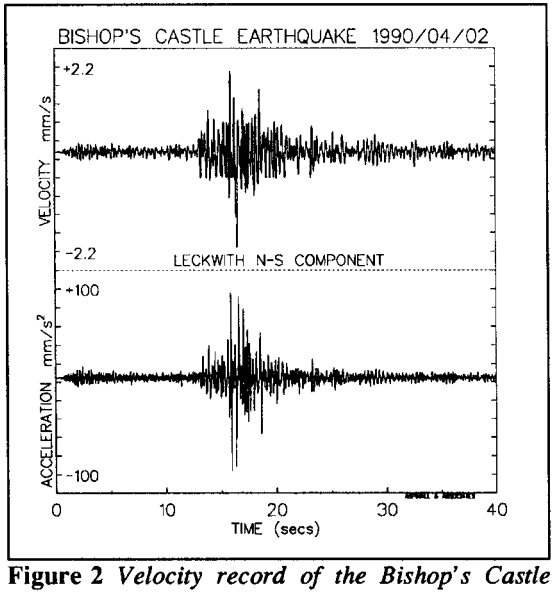

Figure 2 *Velocity record of the Bishop's Castle earthquake, recorded on the N-S component at Leckwith in south Wales, and the derived acceleration time history.*

@seismicisolation

The peak horizontal accelerations recorded at the various seismographs, arising from the Bishop's Castle earthquake, are summarised on Table 1 with their hypocentral distances. According to these estimates, the peak horizontal ground accelerations at Leckwith and Holford were slightly higher than 1%g, consistent with the Intensity III reported from these areas. The horizontal acceleration at Somerton (available from only one instrument) was also close to 1%g. There is negative evidence that these accelerations could not have been much higher: Nuclear Electric had installed two Kinemetrics SMA-1 strong-motion accelerographs, one at Hinkley Point Power Station (a few kms from Holford) and the other at the Somerton substation, and neither had triggered in the earthquake. These devices were set to start at 0.01g but on a vertical trigger; as vertical motions in an earthquake are generally less than horizontal, it is quite plausible that the vertical shaking in this event was below the instruments' trigger thresholds.

TABLE 1. FAR-FIELD PEAK HORIZONTAL GROUND ACCELERATIONS

STATION	COMP.	HYPOCENTRAL DIST. (km)	PGA (g)
LECKWITH	N-S	117	0.012
LECKWITH	E-W	117	0.017
HOLFORD	N-S	140	0.013
HOLFORD	E-W	140	0.008
SOMERTON	E-W	160	0.010
RUFFINS	E-W	303	0.0005
ROMNEY	E-W	306	0.0008
ROMNEY	N-S	306	0.0005

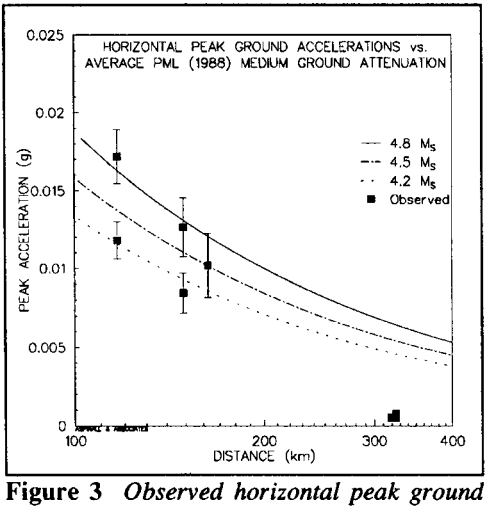

Figure 3 *Observed horizontal peak ground accelerations as a function of hypocentral distance. The curves show expected attenuation from the PML (1988) relationship, for medium ground sites.*

These peak ground acceleration (PGA) values are plotted, with approximate error bars, as a function of hypocentral distance on Fig. 3, together with expected attenuation curves for magnitudes 4.2, 4.5 and 4.8 M_S for medium ground conditions given by the PML (1988) relationship [6]. In the main, the observed PGA's for the Hinkley Point network stations congregate around the lower of the two expected curves while the more distant Dungeness values fall well below the curves. It should be noted that, for this small dataset, ground conditions at the outstation sites are not considered: the Hinkley Point stations would probably be classified as medium

@seismicisolation

whereas those in Kent are probably soft. Local soil properties and topography both will have influenced the observations, in addition to any source directivity effects.

Response spectra for 5% critical damping have been computed for the eight acceleration time histories, and these are plotted on Fig. 4. The gross effect of distance attenuation is shown by the amplitude partitioning of the spectra into two groups corresponding to the Hinkley Point network data and the Dungeness data, whilst the shapes of the latter set show the expected shift to longer periods. The intra-set variability is not very great and such as there is probably contains information about recording site conditions; an analysis of this aspect of the data is outside the scope of this paper.

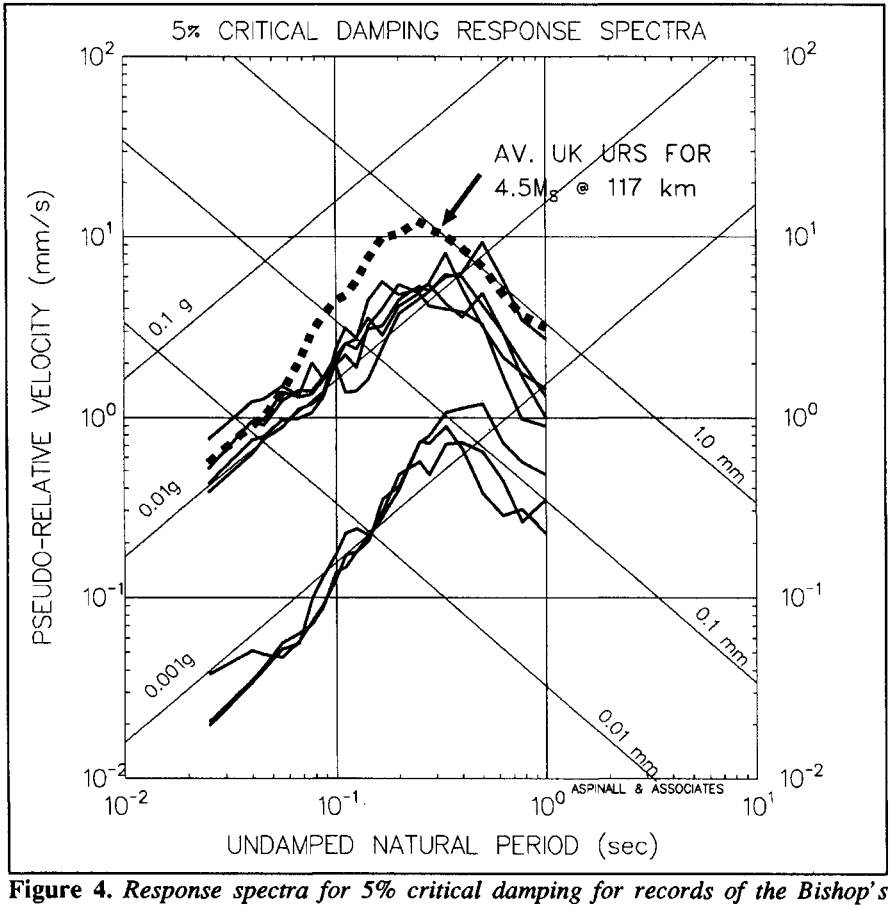

Figure 4. *Response spectra for 5% critical damping for records of the Bishop's Castle earthquake. The comparison curve is the expected UK uniform risk spectrum for medium ground for 4.5 M at 117km range.*

@seismicisolation

For comparison, the current expected UK uniform risk spectrum [6] for a medium ground site at a hypocentral distance of 117 km (i.e. corresponding to the closest seismograph in this dataset) for a magnitude 4.5 M_s earthquake is also plotted. Across a major spread of the spectrum, from 0.06 sec to 0.4 sec period (2.5Hz to 16Hz frequency), the observed responses at the Hinkley Point stations are significantly lower than the expected URS curve. In this period band, a more valid (but extreme) comparison of the observations with the predicted response, which incorporates distance attenuation, is shown on Fig. 5 at one frequency (5Hz). The measured spectral responses are about half that predicted for the Hinkley Point stations, and about a factor of 10 lower at the distant Dungeness locations, even for the lowest magnitude ascribed to this event (4.2 M_s). This tendency to very low observed responses at the greater distances represented by the Dungeness data is present right across the spectrum.

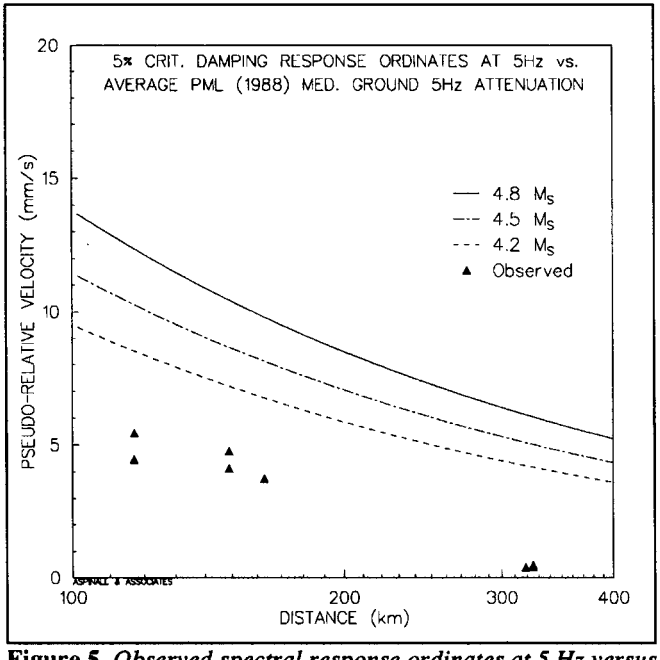

Figure 5. *Observed spectral response ordinates at 5 Hz versus the average PML (1988) medium ground UK uniform risk spectrum attenuation for three representative magnitudes.*

DISCUSSION

The observed peak horizontal accelerations in the distance range 100 to 160 km from the Bishop's castle earthquake fall close to the values predicted by the PML (1988) uniform risk spectra attenuation for an earthquake whose magnitude was somewhere between 4.2 and 4.8 M_s and cannot be regarded as anomalous. At greater distances, attenuation of PGA appears to be stronger than predicted but given the very limited data available and the possibility that this data may be biassed by directivity effects, no firm conclusion on this can be drawn. However, the recorded response spectra at intermediate frequencies are more than one standard deviation below those predicted by this relationship. This marked difference is not

@seismicisolation

so surprising given that the recordings are sufficiently distant as to fall below the threshold for strong ground motion, which is the vibrational regime of engineering interest. The distance regression, upon which the uniform risk spectra attenuation coefficients are based, is conservatively weighted towards the shorter distances contributing more significantly to seismic hazard. For the closer records, it is evident that discrepancy is less great at higher frequencies and at frequencies around 2 Hz; this may be due, at least in part, to the coincidence of direct and reflected crustal seismic waves whose transit times cross in the range 90 to 140 km (depending on crustal structure). This is a condition which is currently giving rise to great interest in seismic hazard assessment in eastern North America [7,8,9], where theoretical predictions of attenuation cannot explain observations of high frequency energy propagation. This effect is already accommodated empirically in the strong motion regression on which the UK uniform risk spectra are founded; the existence of these supportive new British records thus provides an effective rejoinder to those who would claim that the expected uniform risk spectra are not adequately conservative, and would rather prescribe spectra at very high levels of confidence.

The import of these records, as individual observations, would benefit from further analysis of the instrumental surface wave magnitude of this event and, in the context of companion felt-area magnitude relationships, a detailed macroseismic assessment of its intensities. Refinement of British ground motion attenuation relationships, and the reduction of the conservatism which predominantly they engender, would be best advanced by further deployment of digital seismographs; if configured with adequate dynamic range and bandwidth, they could then serve to register faithfully the common microearthquake and the more noble Bishop's Castle class of earthquake.

ACKNOWLEDGMENTS

The Hinkley Point and Dungeness networks are supported by Nuclear Electric plc under the ægis of the Seismic Hazard Working Party. We thank Mr. James Hector (Aspinall & Assocs.) for operating the nets and for his help with data reduction, and Nuclear Electric plc for permission to publish.

This is Seismic Hazard Working Party Contribution No. 50.

REFERENCES

[1] Ritchie M.E.A., R.M.W. Musson and N.H. Woodcock (1990). The Bishop's Castle (UK) earthquake of 2 April 1990. Terra Nova, 2, 390-400.

@seismicisolation

[2] Prof. N.N. Ambraseys - pers. comm.

[3] Principia Mechanica Ltd. (1982). British Earthquakes: an assessment. Report No. 115/82 to CEGB, BNFL and SSEB; London. 255pp.

[4] Murphy J.R. and L.J. O'Brien (1977). An analysis of a worldwide strong motion data sample to develop an improved correlation between peak acceleration, seismic intensity, and other physical parameters. Computer Sciences Corp., Rept. NUREG-0402 to U.S. Nuclear Regulatory Commission. 68pp.

[5] Aspinall W.P., B.O. Skipp and M.E.A. Ritchie (1990). Mictrotremor networks and seismic hazard assessment in the UK. Quart. J. Eng. Geol., **23**, 193-208.

[6] Principia Mechanica Ltd. (1988). Uniform Risk Spectra. Report for NNC Ltd.

[7] Somerville P.G., J.P. McClaren, C.K. Saikia and D.V. Helmberger (1990). The 25 November 1988 Saguenay, Quebec, earthquake: source parameters and the attenuation of strong ground motion. Bull. Seism. Soc. Am., **80**, 1118-1143.

[8] Atkinson G.M. (1990). A comparison of eastern North America ground motion observations with theoretical predictions. Seism. Res. Lett., **61**, 171-180.

[9] Hough S.E., K.H. Jacob and L. Seeber (1990). High-frequency seismic wave propagation in northeastern North America. Seism. Res. Lett., **61**, 193-208.

@seismicisolation
@seismicisolation

REDUCING CONSERVATISMS FROM BROAD BAND SPECTRA IN LOW TO MODERATE SEISMIC ENVIRONMENTS

J Donald Senior Engineer BEQE Ltd
R Kunar Managing Director BEQE Ltd

Abstract

It is commonly recognised that the standard response spectrum adopted by the nuclear industry in the UK is conservative. One of the reasons for this relates to its broad band nature. This paper suggests that for low to moderate seismic environments such as the UK a narrow band spectrum is more appropriate.

It proposes a logical approach to providing a modified spectrum which reduces the energy content whilst still allowing enough conservatism to cover the uncertainties. An example is provided to demonstrate the benefits.

The current UK Design Response Spectrum

The response spectra currently used for the seismic qualification or design of most nuclear installations in the UK is based on studies undertaken on behalf of Nuclear Electric and BNFL in 1981, described in [1]. The design response spectra were developed in a broadly conservative manner for three site conditions viz: soft, medium and hard.

The design response spectra and the values of spectral amplification factors for a given frequency were developed from a selected database of earthquake strong ground motion time histories. These time histories were selected as being representative of earthquakes which might occur in the UK (based on magnitude and duration). The number of earthquakes whose time histories were used to develop the UK design response spectrum was approximately twenty for each type of site condition. Since this study was completed in 1981, a great deal more strong ground motion records have been collected and it is probable that some of the conservatisms associated with the UK design response spectrum could now be reduced.

The standard UK design response spectra were developed from a statistical treatment of the strong motion records in the selected database. Each of the records was first scaled to a nominal peak ground acceleration of 1.0g and then analysed to produce a response spectrum at varying damping levels. All of the resulting response spectra were then combined using statistical methods to generate a single spectrum corresponding to the mean plus one standard deviation. This spectrum when appropriately smoothed provided the standard UK design spectrum. This process was repeated for the data sets corresponding to the soft, medium and hard sites to produce the three different design spectra. An example of the mean plus one standard deviation response spectrum at 5% damping for the medium site is given in Figure 1.

It should be noted that the UK standard spectra were derived by statistically combining the response spectra of all the individual strong motion records. Because of the apparent randomness of strong motion, there is considerable scatter of the frequencies at which the predominant spectral amplifications (or response spectra peaks) occur. As such, it is inevitable that the UK standard spectrum exhibits a broad band of frequency over which the spectral peak is spread. This corresponds to

© SECS - Seismic Engineering Conferences eprints archive

the plateau shown in Figure 1. For this and other reasons, it is recognised that the standard design spectra are conservative. This paper suggests that this conservatism can be reduced by examining the nature of the spectra of earthquakes in low to moderate seismic regions and proposing a logical way forward to reducing the conservatism.

A uniform risk spectrum has been developed for the UK environment and is starting to be used by some members of the UK Nuclear Industry. Use of this spectrum has been relatively limited and has been mainly used for probabilistic safety assessments to date. The use of uniform risk spectra for design has not to the authors knowledge been accepted by the licensing authorities.

The Nature of Earthquake Spectra for Low to Moderate Seismic Environments

Each earthquake has its own unique strong ground motion based on many factors which include effects such as the type of fault on which the earthquake occurred. Therefore the response spectra will have unique spectral shapes and the amplifications associated with each frequency will be different from any other earthquake. In general however, certain observations can be made about the response spectrum from a given earthquake. Large magnitude earthquakes of relatively long durations that are typical of plate boundary areas tend to exhibit significant energy content over a wide range of frequencies. Thus, the spectral peak is spread over a wide range leading to a broad band response spectrum. On the other hand, for regions of low to moderate seismicity such as the UK, there is a tendency for the spectral peak to be narrower. This observation is supported by studies performed in the United States and described in [2]. Also, a cursory examination of the individual spectra of the time histories in the selected database corroborates this hypothesis. For example, Figure 2 shows the response spectra plots for two real acceleration time histories taken from the selected database. This figure shows that both spectra have narrow banded spectral peaks and it can be seen that the majority of the motion is associated with this dominant peak and that the spectral amplification factors decay rapidly from the peak. This observation is of great significance when considering structural responses.

Conservatisms from Broad Band Spectra

The word conservatism is one that is used frequently by the majority of earthquake engineers. Conservatism is most often introduced when there is a high degree of uncertainty associated with any given parameter. However conservatisms can also be developed by the practise of earthquake engineers and analysts to make their part of a scope of work easier to the detriment of those following behind. There is an important place for the use of conservatism in all forms of earthquake engineering, but the degree of conservatism used should always be assessed, and its effect on the validity of the results reviewed. This is particularly true for the assessment of very complex structures which can have several forms of analysis before the development of secondary response spectra.

The input motion and particularly the spectral shape which can occur from any given earthquake exhibits a degree of uncertainty and a conservative value for the spectral amplification factor for each frequency has been selected historically. Each stage of the analysis of a structure involves its own uncertainty and the conservatism introduced to counter each uncertainty is cumulative. Therefore the conservatism introduced from the input motion is scaled through the analysis and significantly effects the results produced.

A broad band spectrum by its very nature includes a significant amount of energy over the whole width of the plateau of the spectrum. Thus it is conceivable for typical nuclear structures that a number of modes will experience the maximum spectral accelerations if the frequencies of these modes fall within the plateau of the broad band spectrum. If however, a narrow band spectrum is adopted then the excitation energy is contained primarily within a single peak (see Figure 2) and as such one or possibly two of the modes will experience the maximum spectral values. Modes corresponding to frequencies outside of the plateau will therefore have less response. On the basis therefore that the spectrum for a UK type of environment is narrower banded than the standard UK spectrum, it is clear that significant conservatisms are introduced into structural responses

© SECS/TNO/CIB/RILEM

when the standard spectrum is used. This can lead the significant overstatement of structural or sub-structural (equipment) responses. It is fruitful therefore to investigate ways in which a narrow banded spectrum can be adopted without losing sight that some conservatism is still necessary to counter uncertainties.

It is not sufficient to propose that a narrow band spectrum should be used. The narrow band spectrum must also be defined with a justifiable basis. The first question to answer is at what frequency should the peak value of the narrow band spectrum be assumed to occur. From the current state-of-the-art in seismology, it is not possible to define this frequency. To counter this uncertainty therefore, this paper proposes that the frequency of the spectral peak should correspond to the fundamental frequency of the structure under consideration. It is recognised that this is a conservative assumption, although it is no more conservative than when the broad band spectrum is used. However, for a narrow band spectrum it is assumed that outside of this frequency the spectral peak reduces rapidly and as such all modes except the fundamental mode will experience lower spectral excitations.

The next answer to be provided concerns the width of the narrow band and to what level does the spectrum drop outside of this narrow band. There are a number of rules that can be suggested for this. This paper proposes a very logical approach still considering the need to deal with uncertainties. It is proposed that the width of the plateau should be over the range of plus or minus 15% of the computed fundamental frequency of the structure. This figure is proposed based on the uncertainty associated with calculating the primary frequency of a structure and could be varied depending upon the accuracy of calculation.

It further proposes that outside of this range the spectral amplitudes reduce in a logical manner to those corresponding to the UK spectrum computed as the mean not the mean plus one standard deviation as is the case in the standard UK spectrum.

The resulting generic hybrid spectrum as demonstrated in Figure 3 will have significantly lower energy content outside of the narrow band than if the mean plus one standard deviation spectrum is used. This would therefore lead to reduced responses particularly for plant or equipment in the structure. The new spectrum reflects the narrow band nature of earthquakes in low to moderate seismic regions and still maintains a reasonable energy content outside of the narrow band.

A Modified UK Spectra

The previous section describes the principles of a modified design response spectrum which considers the nature of real earthquakes for regions of low to moderate seismicity such as the UK.

It provides for the narrow band features of such earthquakes by using a hybrid between the standard UK spectrum which represents a mean plus one standard deviation with a mean UK spectrum.

Figure 4 shows a mean UK spectrum developed by combining the spectra for the time histories in the selected database. A comparison of this mean spectra and the standard UK spectrum (Figure 1) shows significant reductions on the spectral amplification factors, typically of the order of 1.5 over the frequency range of interest.

The mean response spectrum by definition provides spectral amplification factors that have a 50% probability of exceedence. However bearing in mind that the earthquake is likely to show one dominant peak it is expected that the 50% probability of exceedence applies only to this peak and for off peak values, the probability of exceedence will be lower. This mean spectrum underlies the discussion in that it provides a satisfactory degree of conservatism for modes outside of the dominant structural response and would also provide significant reductions in any developed secondary response spectra.

Following the principles stated above, the spectrum proposed for the UK will be a hybrid of the mean plus one standard deviation spectrum and the mean spectrum from the earthquakes used for the selected database as shown in Figure 5.

@seismicisolation

The effects of the modified spectrum on a trial analysis

The beneficial effects of the use of the modified spectrum is best shown by the analysis of a building and of a building subsystem. This was completed for a trial analysis of a steel framed structure with a secondary subsystem located on the roof. A model of the building was developed and two response spectrum analyses performed, one for the current UK design response spectrum input and the second using a modified spectrum input. The loads predicted by the two analysis were then compared. Following this, time histories were developed which were compatible with the input response spectra and the building was analysed using these time histories. The displacement results were then used to develop secondary response spectra at the roof level. These spectra were then input to a simple model of a tank supported on the roof and the results compared. All of the analysis was performed using the general purpose finite element analysis code ANSYS and the generation of the matching response spectra was completed using in-house BEQE software.

The building modelled was considered to be constructed from steel. The floors used in the structure were in-situ concrete floor slabs which spanned between major steel cross beams. The building lateral stiffness is provided by portal action in the transverse direction and by cross bracing in the longitudinal direction. A plot of the developed model is included as Figure 6.

The response spectrum analysis of the building produced the fundamental modes of vibration and the spectrum was modified in accordance with the rules developed previously. Table 1 provides a summary of the building major modes, the mass participating in these modes and the spectral accelerations input based on the current UK motion and the modified spectrum. It can be immediately recognised that for some frequencies, the mean plus one standard deviation values used for the modified spectrum exceed the current design spectrum. This is particularly true for the lower frequency response in the Y-direction.

The nodal accelerations which results from this analysis are shown on Table 2. It can be seen from this table that the typical reduction in the nodal accelerations is of the order of 20%, with a few cases of highly similar accelerations, notably at the top of the structure in the Y-direction, which is the result of the input motion being higher for the first mode in the response spectrum analysis. In general however the results show a significant reduction.

The beam element forces and moments predicted by the two analyses are shown for representative members in Table 3. These results show that the beam forces and moments are also typically reduced in proportion to the reductions seen for the nodal accelerations. As before, the moments due to Y-direction motion have not reduced, and in some cases have actually increased for the modified input motion.

The secondary response spectra were developed from a time history analysis of the model using compatible time histories developed for the differing input motions. The calculated response spectra were for four nodes on the structure, nodes 64, 68, 84 and 88. The spectra from each analysis type in each direction were then enveloped to produce input motion for the subsystem. No broadening of the spectra was completed, and although this is unusual, it was considered to be more realistic for this trial study in that it allows a more direct comparison to be made.

The subsystem considered for this trial analysis was a water tank supported on a low steel frame on the roof the of the steel framed building. The water tank mass used was 10 Te with an effectively full tank, hence removing any sloshing motion. The frame was considered to be a small moment frame constructed from standard small rolled steel sections. Figure 7 indicates the layout of the model used for the tank and the support frame, together with the nodes and element numbers used in the representation.

Table 4 lists the primary modes of vibration of the tank together with the mass participating and the input spectral accelerations from the two sets of developed secondary response spectra. It can be seen that the tank and the frame provide low frequency response of an order similar to that of the primary structure. The input accelerations therefore do not reduce spectacularly from the current design compatible secondary

@seismicisolation

response spectrum and that developed from the modified spectrum. Nevertheless, there are reductions of the order of 10% to 40%.

The accelerations predicted for the nodes of the tank and frame are listed in Table 5 and the elemental forces and moments are compared in Table 6. These tables show similar reductions of the order of 10% to 40%. This reduction would make the design of the tank and its support frame and connections much more simple and would also significantly reduce the loading predicted for the anchorage of the frame to the roof of the steel framed building.

It should be noted that whilst the example used in this paper produces reductions in the loads calculated for the member design of both the main building and the subsystem, these reductions could be smaller or greater dependent upon the system analysed. In general, the reductions would be much larger, and it would require an unusual system for the predicted loads to increase based on the modified input motion, but this is possible, particularly for low frequency structures. High frequency structures and sub-systems whose modal response are well separated from the building below will see very large reductions in loads, usually to the order of half or less.

Conclusions

It has been identified that the current UK design response spectrum is conservative in that the broad band spectrum contains more energy than any probable earthquake in the UK which is a region of low to moderate seismicity. This conservatism is widely accepted within the earthquake engineering industry in the UK, but few have attempted to challenge it. An approach has been presented which provides an idea of the way forward for design response spectra in low to moderate seismic environments, the study is not presented as definitive and would benefit from further work, perhaps using more real time histories from similar environments.

This paper has shown that the principle of using a mean plus one standard deviation for the dominant response of a structure is not unreasonable in that it provides a low probability of exceedence of the loads calculated from this mode. However, the narrow band motion which is most likely from an earthquake in this seismic region shows that a lower spectral amplification is reasonable for off-peak modes of vibration. The statistical approach adopted also allows a calculation of the probability of exceedence of the amplifications used to calculate the higher modal response.

It has also been shown that the adoption of a mean spectrum with modifications for the dominant modes of a structure will produce significant reductions in the loads calculated in a primary structure. Most importantly however, the loads calculated for secondary systems reduce by even greater amounts, particularly for sub-systems with primary modal response away from that of the primary structure below. These reductions would significantly reduce the cost of qualification of secondary systems and would also allow a movement towards a complete system qualification where there is a uniform, consistent and reasonable level of conservatism throughout the whole system.

References

1. Seismic Ground Motions for UK Design for British Nuclear Fuels and Central Electricity Generating Board Principia Mechanica Ltd. April 1981.

2. Selection of lower bound magnitude for seismic hazard assessment. Research Project 2556-25. For Seismicity Owners Group and Electric Power Research Institute.

@seismicisolation

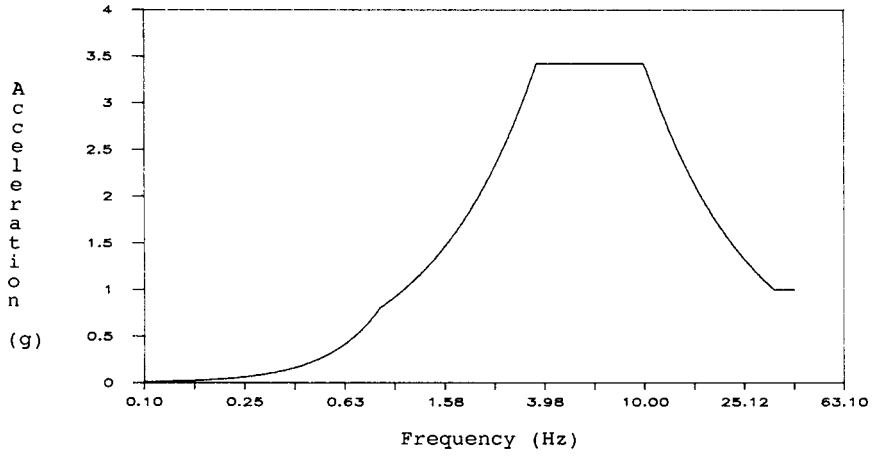

Figure 1 : Medium site UK design spectrum

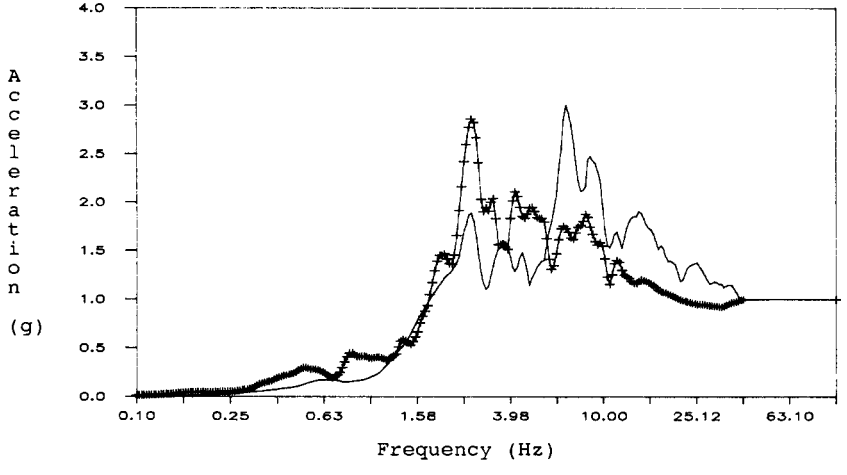

Figure 2 : Two real time history response spectra

@seismicisolation

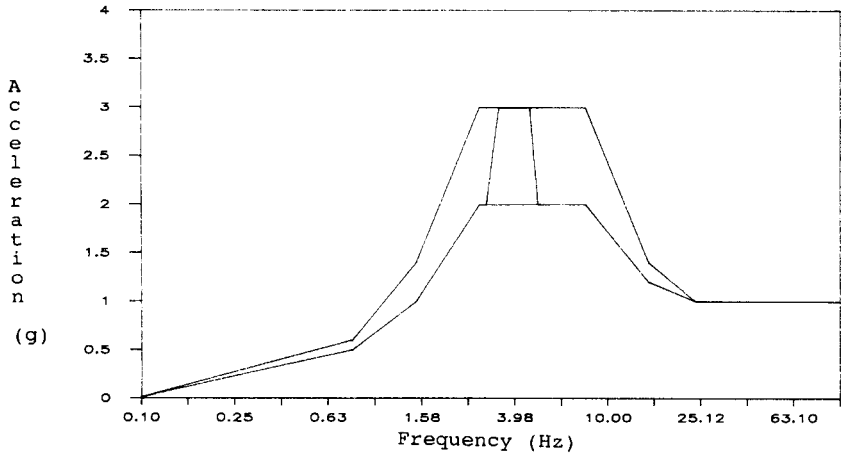

Figure 3 : Generic hybrid spectrum

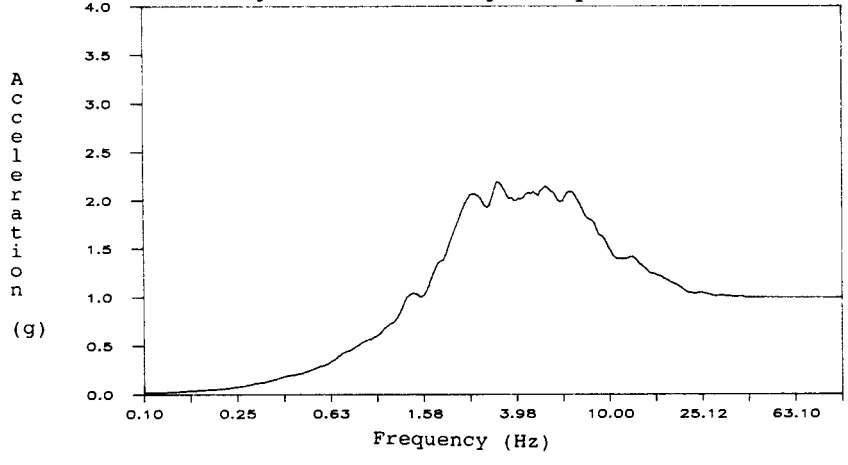

Figure 4 : Mean UK spectrum

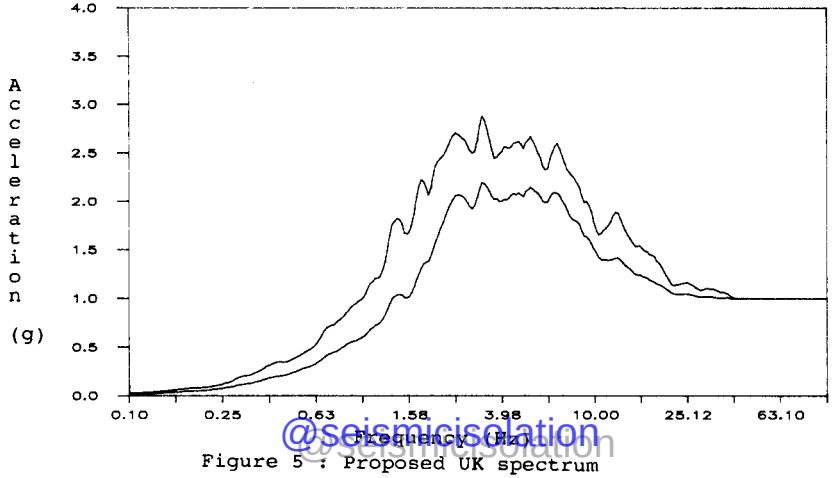

@seismicisolation

Figure 5 : Proposed UK spectrum

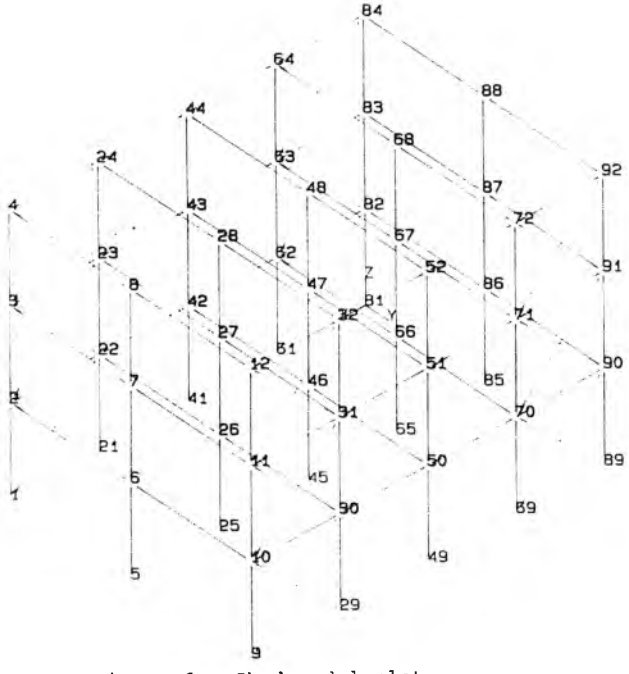

Figure 6 : Shed model plot

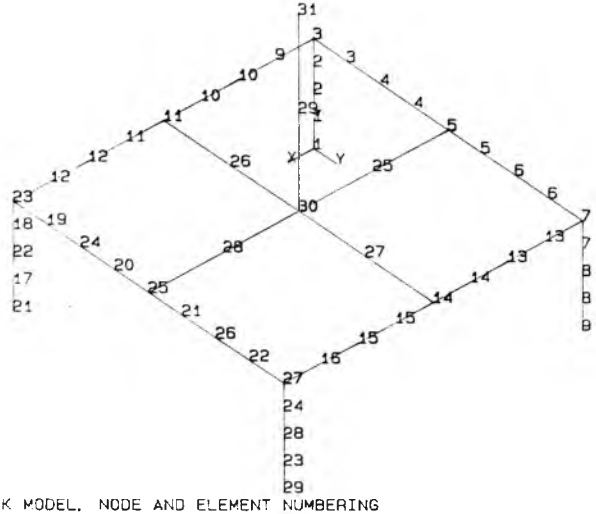

TANK MODEL. NODE AND ELEMENT NUMBERING

Figure 7 : Tank model plot

@seismicisolation

Mode No.	Direction	Frequency (Hz)	Mass (Te)	Acceleration Input (m/s^2) UK	Proposed
2	X	2.5	510.3	5.77	4.91
6	X	8.0	90.9	8.41	4.47
8	X	13.2	9.1	6.31	3.20
1	Y	0.9	594.8	2.00	2.18
4	Y	3.4	14.2	7.73	5.27
9	Z	13.6	463.2	4.09	4.10
12	Z	18.1	35.7	3.06	1.91
16	Z	25.7	48.7	2.12	1.70
21	Z	37.6	37.4	1.64	1.66

Table 1 : Summary of modal analysis results and input motion

Node Number	UK Spectra Acceleration x	y	z	Proposed Spectra Acceleration x	y	z
2	4.61	2.18	0.98	2.85	1.97	0.85
4	7.93	2.65	2.20	6.48	2.66	1.78
6	4.79	2.18	1.35	2.93	1.97	1.18
8	8.01	2.65	3.01	6.52	2.66	1.78
10	4.61	2.18	0.98	2.85	1.97	0.85
12	7.93	2.65	2.20	6.48	2.66	1.78
42	4.72	2.18	1.87	2.90	1.97	1.79
44	7.98	2.65	4.16	6.50	2.66	3.98
46	4.74	2.18	4.24	2.91	1.97	4.19
48	7.99	2.65	9.03	6.51	2.66	9.09
50	4.72	2.18	1.87	2.90	1.97	1.79
52	7.98	2.65	4.16	6.50	2.66	3.98

Table 2 : Comparison of accelerations in m/s^2 between UK and the proposed input spectrum from response spectrum analysis.

Member	UK Spectrum Results Axial (KN)	Moment (KNm) Mx-x	My-y	Proposed Spectrum Axial (KN)	Moment (Knm) Mx-x	My-y
Bracing (Ground El. 130 level)	539.4	0.0	0.0	451.2	0.0	0.0
Bracing (Upper El. 135 level)	281.2	0.0	0.0	229.5	0.0	0.0
Column (Corner ground level) El.1	1347.4	291.9	4.45	1151.6	317.9	3.29
Column (Corner upper level) El. 3	192.8	73.0	2.65	157.3	73.0	1.98
Column (Internal ground level)El.24	356.2	370.2	4.53	356.1	403.6	3.32
Column (Internal upper level) El.26	158.9	105.4	2.70	158.9	107.3	2.00
Beam (Gable first level) El.50	12.3	345.9	0.03	8.0	377.7	0.02
Beam (Gable top level) El.52	22.4	73.0	0.05	18.4	73.1	0.04

Table 3 : Comparison of forces and moments predicted by response spectrum analysis using the UK and proposed input

@seismicisolation

Mode No.	Direction	Frequency (Hz)	Mass (Te)	Acceleration Input (m/s^2) UK	Proposed
1	X	3.9	10.0	13.43	10.11
3	Y	4.6	3.1	4.43	2.94
5	Y	8.2	7.2	3.77	2.50
6	Z	12.5	10.2	40.75	35.99

Table 4 : Summary of modal analysis results and input motion

Node Number	UK Spectra Acceleration x	y	z	Proposed Spectra Acceleration x	y	z
2	9.39	3.70	0.40	7.49	3.08	0.36
3	11.92	3.27	0.88	8.94	2.19	0.78
4	12.03	3.26	23.37	9.02	2.17	20.62
5	12.09	3.27	38.95	9.06	2.17	34.38
10	11.94	3.34	26.56	8.95	2.22	23.45
11	11.96	3.38	39.78	8.97	2.24	35.12
30	12.09	3.38	40.90	9.07	2.24	36.13
31	14.02	2.95	40.96	10.56	1.96	36.17

Table 5 : Comparison of accelerations in m/s^2 between UK and the the proposed input spectrum from response spectrum analysis

Member		UK Spectrum Results Axial (KN)	Moment (KNm) Mx-x	My-y	Proposed Spectrum Axial (KN)	Moment (Knm) Mx-x	My-y
Post Element 1	i	117.0	0.0	0.0	100.2	0.0	0.0
	j	117.0	22.2	17.7	100.2	19.0	13.6
Post Element 2	i	117.0	22.2	17.7	100.2	19.0	13.6
	j	117.0	44.3	34.4	100.2	37.9	27.1
Beam Element 3	i	44.1	44.3	0.3	37.7	37.9	0.2
	j	44.1	11.5	0.1	37.7	9.6	0.1
Beam Element 4	i	44.1	11.5	0.1	37.7	9.6	0.1
	j	44.1	64.9	0.3	37.7	55.8	0.2
Beam Element 9	i	34.6	35.4	0.3	26.5	27.1	0.2
	j	34.6	24.8	0.1	26.5	20.3	0.1
Beam Element 10	i	34.3	24.8	0.1	26.3	20.3	0.1
	j	34.3	47.5	0.1	26.3	41.4	0.1

Table 6 : Comparison of forces and moments predicted by response spectrum analysis using the UK and proposed input

@seismicisolation

A PARAMETERLESS SCALE OF SEISMIC INTENSITY FOR USE IN SEISMIC RISK ANALYSIS AND VULNERABILITY ASSESSMENT

R.J.S. SPENCE, A.W. COBURN, S. SAKAI, A. POMONIS
The Martin Centre for Architectural and Urban Studies,
University of Cambridge, 6 Chaucer Road, Cambridge CB2 2EB, United Kingdom

ABSTRACT

This paper is a summary of analysis [1] carried out on the Martin Centre vulnerability database, which comprises some 70,000 buildings surveyed in 13 different earthquakes and an extensive compilation of published damage data. A continuous scale of seismic intensity is derived from the damage distributions which allows more accurate predictions of damage than the standard aggregation by intensity assignment using MM or MSK intensity scales. Using the Parameterless Scale of Intensity, (ψ PSI) predictions of damage can be made within 25 percentage points with 90% confidence. This compares with 75 percentage points using assigned intensity. PSI is correlated with instrumentally recorded ground motion and shown to correlate well with parameters of acceleration. Predictions of seismic hazard using PHGA or MRSA can be made within $\pm$ 2.5 PSI units with 90% confidence.

INTRODUCTION

Seismic risk assessment is an important activity in any earthquake region because it enables choices to be made in the level of protection employed. The three principal components of a seismic risk analysis are seismic hazard assessment, inventory and categorization of the elements at risk and vulnerability assessment for each element of risk.

Methods of vulnerability assessment are at present at a much less advanced state of development than those of seismic hazard, reducing the accuracy of seismic risk analysis.

The standard methodology for defining vulnerability functions for use in damage estimation is to aggregate damage data relevant to the building types of interest, at given levels of ground motion severity. The average or probabilistic distribution of this data at a given level of ground motion severity can then be used to predict future damage levels to similar building types for a recurrence of that level of ground motion severity. Data on earthquake damage to all the building types that are of interest are relatively sparce and most vulnerability derivations have tended to aggregate damage surveys from a number of earthquakes, and, quite commonly, aggregating damage surveys from a number of different countries [2].

The definition of seismic intensity scales has long assumed that the performance of broad categories of building type is similar irrespective of location and the damage levels to commonly-occurring building types is used to define various levels of intensity. Damage to brick masonry buildings, for example, has formed the definition of intensity levels in successive generations of intensity scales from the Rossi-Forel scale of 1883 to the Mercalli Cancani Seiberg (MCS) Scale of 1912, the Modified Mercalli Scale of 1931, to the Medvedev Sponhuer Karnik (MSK) Scale of 1964 [3].

© Seismicisolation

Earthquake Damage Distributions of

Brick Masonry Buildings

Data Presentation

Loadbearing, fired-clay unit masonry construction, unreinforced, cement or lime mortar, low rise.

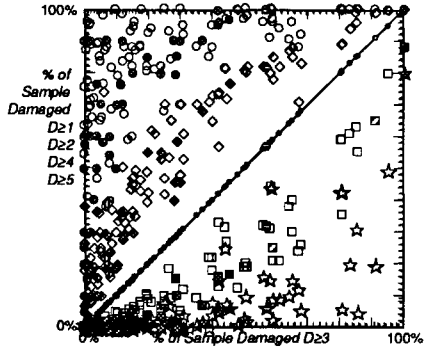

Analysis by Each Damage Degree

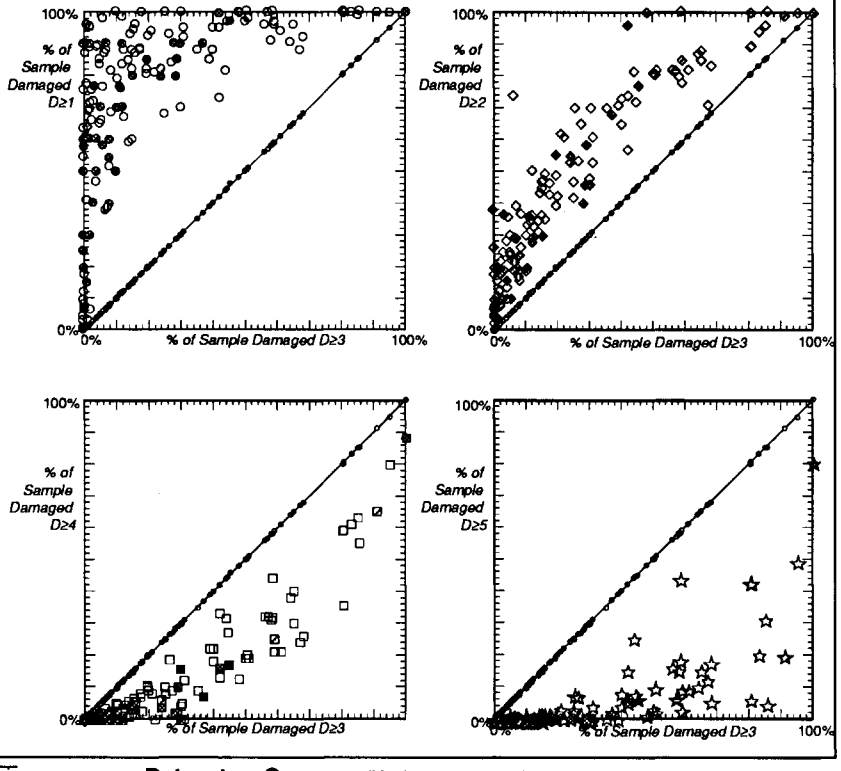

100%
- D≥1 Slight Damage
- D≥2 Moderate Damage
- D≥3 Heavy Damage
- D≥4 Partial Destruction
- D≥5 Collapse

0%

Survey Samples of more than 20 Buildings.

Datasets

- Italy 1980 (Martin Centre Survey)
- Turkey 1983 (Martin Centre Survey)
- Greece 1986 (Martin Centre Survey)
- Romania1990 (Martin Centre Survey)
- Iran 1990 (Martin Centre Survey)
- Australia 1990 (EEFIT Survey)
- China 1976 (Zhang 1982)
- Romania 1977 (INCERC Survey)
- Algeria 1980 (CNT Survey)
- Italy 1980 (CNR Survey)
- USSR 1985 (EERI Survey)

Published Distributions of Damage for Brick Masonry Buildings at Various Intensity Levels:

1. Monge (1969) Chile, 6 equakes
2. Whitman (1975) USA
3. Tzenov (1982) Bulgaria
4. Sandi (1982) Romania
5. Petrovski et al. (1984) Yugoslavia
6. Yang et al. (1984) China

@seismicisolation

Figure 1. Distributions of damage states D1-D5 surveyed in samples of brick masonry buildings in earthquakes around the world

Earthquake Damage Distributions of

Brick Masonry Buildings

Analysis

Loadbearing, fired-clay unit masonry construction, unreinforced, cement or lime mortar, low rise.

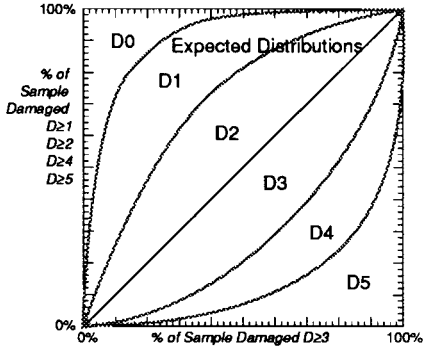

Analysis by Each Damage Degree

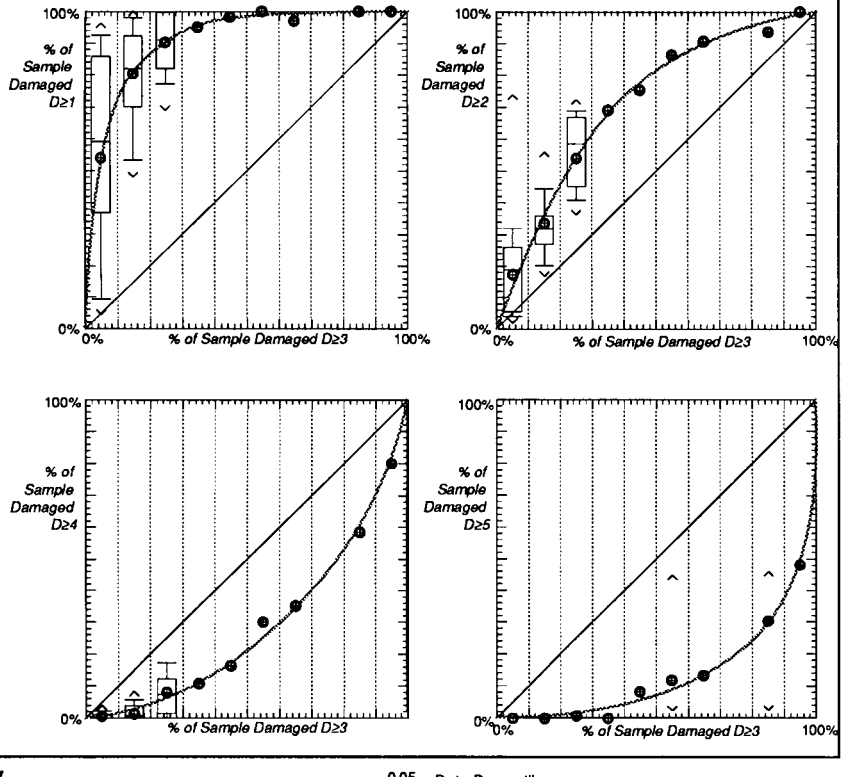

Key

Analysis of data in each 10 point range

Mean

Upper limit of data

Lower limit of data

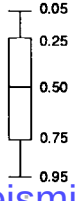

Data Percentiles (Probability of Exceedance)

@seismicisolation

Figure 2. Analysis of damage distributions for brick masonry buildings to derive expected distributions and confidence limits

An initial compilation of earthquake damage surveys in 1986 [4] indicated that significant variations existed between the interpretation and classification of intensity levels from one survey group to another, but that their assessment of damage state distributions in particular building types and the relative damage levels between two building types were consistent across most of the surveys. Collection of a considerably expanded dataset of damage surveys since then has enabled an increased analysis of the vulnerability of a range of building types and, perhaps more importantly, has made it possible to assess the confidence limits for various methods of analysing data and thus the accuracy with which prediction of future damage for levels can be made [1].

DAMAGE DISTRIBUTION DIAGRAMS

Distributions of damage states (presented as cumulative histograms) for 103 surveys of brick masonry buildings in a number of different earthquakes and across a range of different countries are presented in Figure 1, ranked according to the percentage of the sample to have suffered the middle damage state, D3 (Heavy damage) or greater. The term D3, D2 etc will be used here to mean equal to or greater than the particular damage degree (D≥3, D≥2). Most distributions given here consist of over 50 buildings, and surveys of less than 20 buildings are excluded as unreliable. Although there is some variation, it can be seen that there is a degree of consistency in the distributions of damage states found in all the survey samples.

These diagrams display only the distributions of damage surveyed and do not relate the distribution to any assessment of ground motion intensity, and yet it is clear that the increasing percentages of damage states, from left to right, represent increasingly severe levels of intensity.

Expected distributions, and the variation of distributions probabistically can be obtained by averaging and carrying out percentile analysis in segmented bands of the abscissa, as shown in Figure 2. This analysis shows that the average distribution percentages, relative to D3, appear to conform to a series of curves. These curves can be used to predict damage distributions for brick masonry buildings - or at least the ratio of buildings likely to have suffered one damage state relative to another damage state at a given level of damage. For example, when 25% of brick masonry buildings are heavily damaged (D3), it can be expected that 90% will be slightly damaged (D1), 54% moderately damaged, (D2) 8% will suffer partial destruction (D4) and less than 1% will suffer collapse (D5). The confidence limits on this prediction can be obtained from the percentile analysis. When D3 = 25%, the expected average for D2, for example will be 54%, but there is a probability of 0.9 that D2 will be between 41% and 69% - i.e. 90% of the data falls between those two values, (marked by the lower 0.95 percentile and the upper 0.05 percentile).

The confidence limits vary from one damage state to another - for example there is more variation in surveys of slight damage (D1) than in moderate damage (D2) - and also varies with the percentage of that damage state, - for example where the average is close to 0 or 100%, the variation is less. The distribution, being between 0 and 100% is *confined* - variations and confidence limits close to the upper and lower limits are unsymmetrical - where the average is 98%, for example, some points may fall a long way below the average, but those that are above average fall between 98-100%. For this reason error descriptions like standard deviation, which imply symmetrical error distributions are less useful than percentile descriptions.

The measurement of errors and the mathematical solution of the curves that describe the damage distributions are discussed below. Damage distributions have similarly been built up for other building types from the Martin Centre database, including adobe masonry, rubble masonry, stone masonry, reinforced brick masonry, reinforced concrete structures and timber framed buildings [1].

@seismicisolation

DAMAGE DISTRIBUTIONS AND ASSIGNED INTENSITY

Having derived a description of damage distributions for a building type, it is necessary to relate the damage to parameters of ground motion in order to predict the damage that is likely to result from the occurrence of earthquakes of various strengths. Applying the standard methodology of relating the surveyed damage to assigned levels of seismic intensity gives Figures 3 and 4. Many of the survey teams have surveyed damage distributions in an area assigned an MM or MSK intensity level, and their various damage survey results are here aggregated by assigned intensity level.

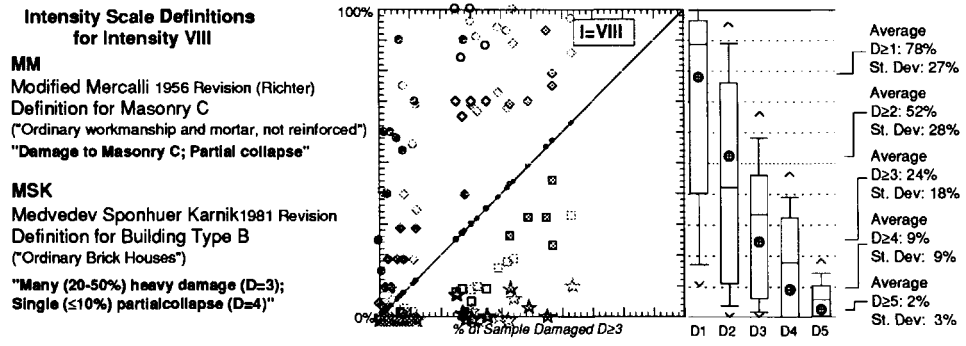

Figure 3. Damage distributions of brick masonry buildings classified by the MM or MSK Intensity level as assigned by survey team (example of Intensity VIII)

Average damage distributions can be derived for each intensity level, as shown on the right in Figure 3 for intensity VIII. At intensity VIII, the expected % of buildings with moderate damage or worse (D2) is 52%, but the confidence limits that have to be placed around that figure if used as a damage forecast are wide: 0.9 probability of the figure falling between 4% and 88%, and 0.5 probability between 12% and 76%. Thus although intensity assignment gives a coarse indication of damage levels, the confidence limits associated with it are poor.

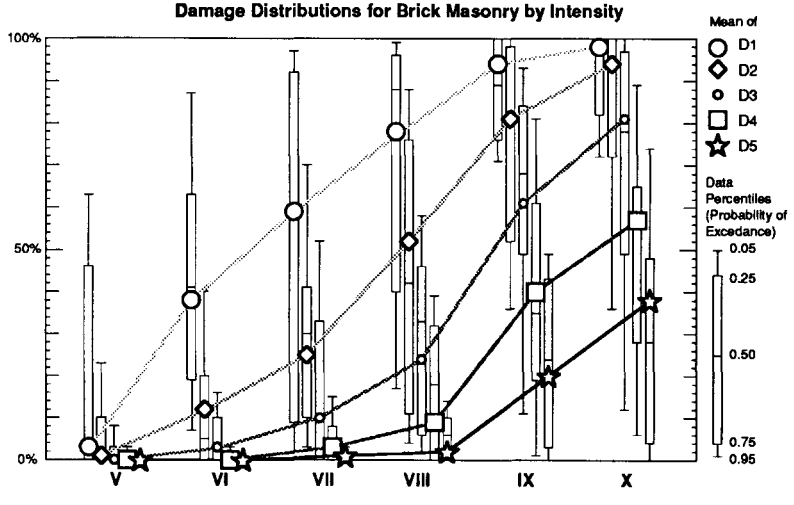

Figure 4. Expected damage distributions and confidence limits for damage predictions by assigned intensity level.

@seismicisolation

It is clear that the assignment of intensities by the various assessors varies considerably. Intensity assignment is usually carried out fairly rapidly after an earthquake and field experience suggests that rapid appraisals of appearance of damage and engineering experience are relied on more than systematic counts of buildings and their damage. In the analysis of damage distributions carried out here, it has been shown that relatively large samples (50+) are needed to derive a representative performance - it is likely that rapid 'eyeball' assessments of damage level are influenced by much smaller numbers of buildings, by their clusterings and visibility of damage.

The aggregating of data on the basis of assigned intensity (Figure 4) produces considerably larger error distributions than are present in the original data (Figure 2), so it can be concluded that intensity assignment is a poor model of vulnerability. A better model of vulnerability would be one in which the intensity of ground motion was defined directly from the damage surveys, and predictions of intensity can be used to derive damage estimates with as much confidence as the data allows.

MODELLING DAMAGE DISTRIBUTIONS

The curves of increasing damage distribution given in Figure 2 represent the increase of each damage degree relative to that of damage degree D3. Here damage degree D3 is being used as non-linear indicator of intensity, and one with a limited range.

The definition of an intensity scale that describes the damage distributions with some accuracy can be derived from the shape of the curves in Figure 2. The solution requires that each of the curves, D1 to D5, including the linear function D3, can be described as a function of intensity as a family of similar mathematical functions. Each curve, for example D2:D3 is the resultant relative displacement of two similar vulnerability functions F(A) and F(A'). (The mathematical derivation of the geometry of the damage distribution curves is given in [1].

The best fit for the curves given in Figure 2, and for all relative damage curves of all building types and damage states, can be shown to be Gaussian - the cumulative function of a normal distribution. This can be rationalised by an assumption of normalised distributions of structural resilience in statistically significant samples of similar building stock. For a large number of similar structures, it can be assumed that the intensity at which each individual structure passes a given damage threshold will be clustered around an average intensity, with some variation: slightly weaker structures will pass the threshold at lower intensity and slightly stronger-than-average structures will pass it at higher intensities. This scatter around the mean performance can be assumed to be normally distributed, along with many other phenomena of natural variation.

A normal distribution is defined by a mean, M, and a standard deviation, σ, as:

$$y = \frac{1}{\sqrt{2\pi}\,\sigma} \exp\left[-\frac{1}{2} \left(\frac{x-M}{\sigma} \right)^2 \right] \qquad [1]$$

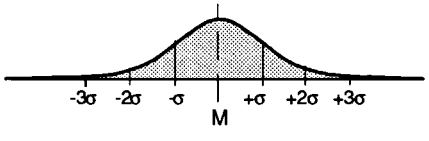

where the total area enclosed under the graph ($-\infty < x < +\infty$) is equal to unity, 1.0.

@seismicisolation

The cumulative distribution function, D = Gauss [M,σ,ψ] is then defined by:

$$D = \int_{M-n\sigma}^{\psi} \frac{1}{\sqrt{2\pi}\,\sigma} \exp\left[-\frac{1}{2}\left(\frac{\psi - M}{\sigma}\right)^2\right] \qquad [2]$$

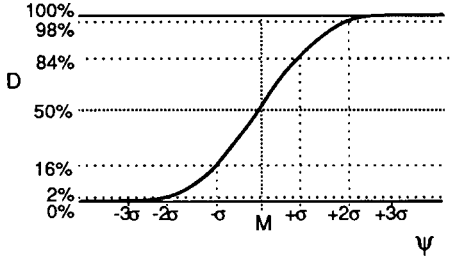

where D is the percentage of the building stock damaged (0-1.0) and ψ is the intensity.

The inverse function, $\psi = \text{Gauss}^{-1}$ [M,σ,D] can also be used to derive an intensity value from a known level of damage.

The relative vulnerability function derived in damage distribution diagrams or relative damage diagrams, such as that shown in Figure 2, can be seen to be the difference between two Gaussian vulnerability functions.

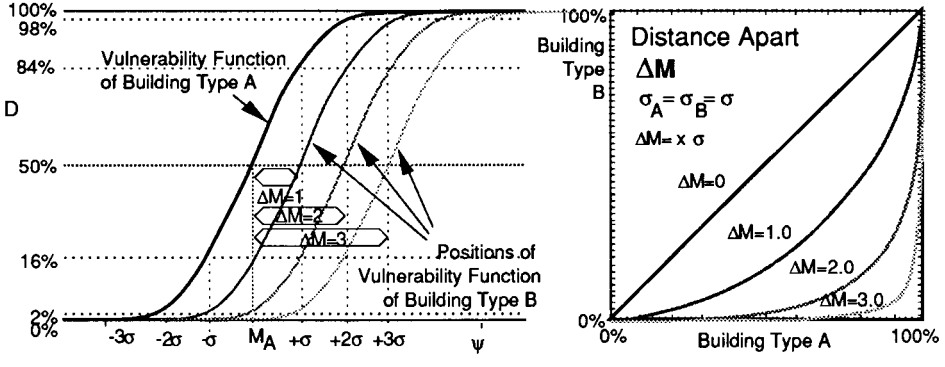

Figure 5. Geometrical Properties of Relative Vulnerability Functions

If the vulnerability function for damage degree D3 has a mean of 0 and a standard deviation of 1, then the best fit for the vulnerability function of damage degree D2, relative to it, has a mean of -0.89 and a standard deviation of 1.11.

The standard deviations of the two curves - the 'slopes' of the lines are very similar, as are the best fit vulnerability functions for the other damage degrees, relative to damage degree D3. The standard deviations of the curves D1 to D5 range from 0.88 to 1.07 and suggest, certainly as a first approximation, that the vulnerability functions of all five damage states may have the same standard deviation. If this is assumed, the accuracy of the fit of the points to the vulnerability functions is affected only marginally. It is logical that if the rationalization of the Gaussian function is that structural resiliance is normally distributed in the building stock sample, then the normal distribution should be consistent for successive damage states.

For brick masonry buildings, the analysis of best-fit vulnerability functions for each damage degree is derived relative to that of D3. If the vulnerability function for damage degree D3 has

@seismicisolation

a mean of O and a standard deviation of 1, then all other damage degrees can be assumed also to have a standard deviation of 1 and their best-fit mean is given in Table 1.

TABLE 1
Vulnerability Functions of Brick Masonry Damage Distributions Relative to D3

	Relative Curves		PSI ψ	
	Mean Relative to D3=0	Standard Deviation Assuming D3 = 1	Mean Relative to D3=10	Standard Deviation Assuming D3=2.5
D1	-2.05	1	4.87	2.5
D2	-0.89	1	7.78	2.5
D3	0	1	10	2.5
D4	0.65	1	11.62	2.5
D5	1.31	1	13.28	2.5

PARAMETERLESS SCALE OF SEISMIC INTENSITY

The definition of the vulnerability functions as a series of Gaussian functions gives an absolute horizontal scale for intensity against which the damage curves can be plotted rather than having to plot them relative to one another as the curves of Figure 2. This absolute scale of intensity is expressed in units of the standard deviation of the D3 curve. Other curves are defined in terms of the number of D3 standard deviations that they are away from the D3 curve.

This scale can be used as an intensity scale which will generate the highest confidence predictions of vulnerability from the damage data available. The intensity scale has no parameters - it is defined directly from the relative shapes of damage distributions - and so will be referred to as the Parameterless Scale of Seismic Intensity - PSI, or represented by ψ, (the Greek character psi.) The examples given above are derived from an assumption that the D3 curve has a mean of 0 and a standard deviation of 1, which means that the D1 and D2 curves have a negative mean. To avoid having negative values of PSI intensity, it will instead be assumed that the D3 curve has its mean at 10 and the standard deviation will be taken as 2.5. Negative intensities are still possible at less than four standard deviations from the mean of brick D3, but these are low intensities and are unlikely to be commonly encountered. A value for the standard deviation of 2.5 means that the range of intensity that causes building damage will be encompassed within approximately 20 units, and accuracies of a single decimal point will generally be sufficient.

The curves for D1 to D5 for brick masonry buildings, defined in terms of the PSI intensity scale are given in the right hand columns of Table 1, and are plotted out in Figure 6, with the damage distributions of Figure 1 replotted for best fit with the curves. The percentile distributions of the data points around the predicted values are given in Figure 7.

The percentiles give the accuracy of prediction for this model of vulnerability. It can be seen that the accuracy of prediction is fairly uniform, although D1 has more variation at higher intensities and D5 is more scattered than other damage degrees. In mid-range estimates of damage - where the prediction is for damage states to be between say 16% and 84% (within one standard deviation of the mean) - most percentiles show the 0.9 probability range covering about 25 percentage points, and the 0.5 probability range covering 10 to 15 percentage points.

This can be compared with the prediction accuracy obtained from using assessed intensity shown in Figure 4. The prediction of a damage level in mid-range (16-84%) derived from assessed intensity in Figure 4 has an average 0.9 confidence of lying within a range of 75 percentage points and an average 0.5 confidence of lying within a 47 percentage point range. The use of PSI intensity to predict a level of damage gives an improvement of prediction accuracy of a factor of 3.

@seismicisolation

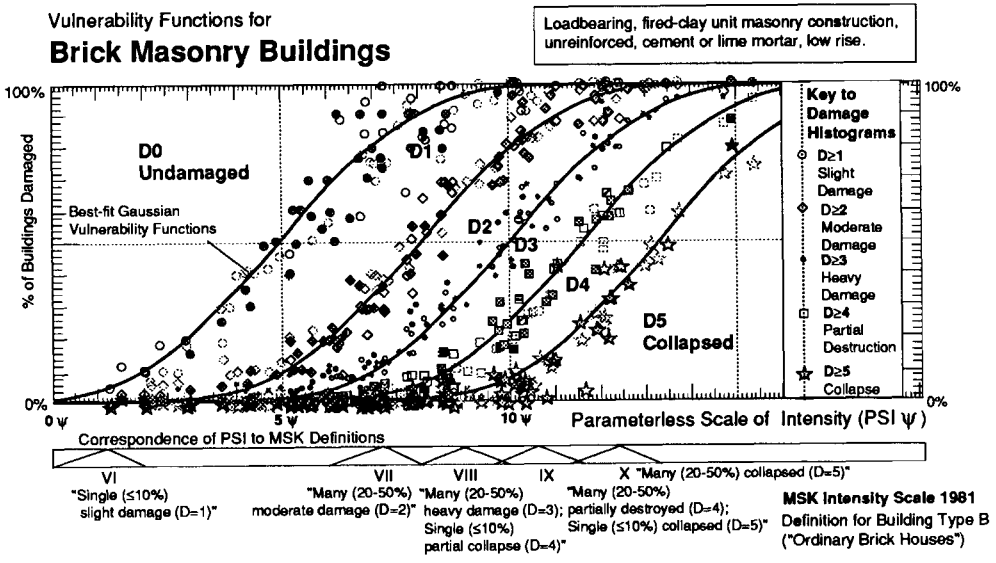

Figure 6. Gaussian vulnerability functions derived from the data are calibrated against a Parameterless Scale of Intensity. Damage distributions have a best-fit PSI value.

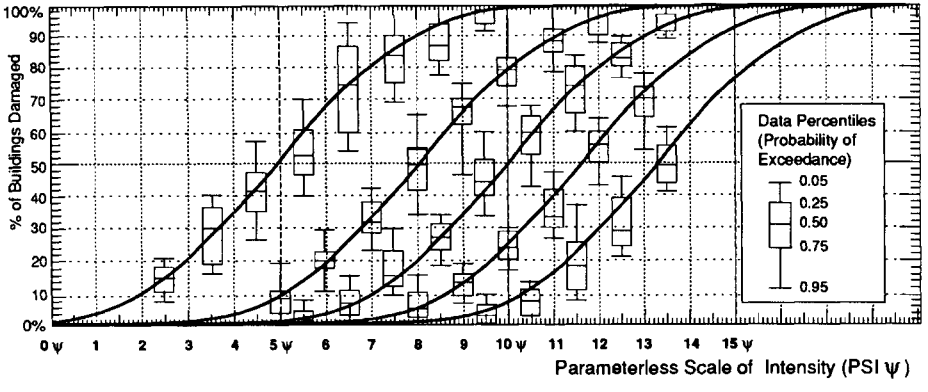

Figure 7. Confidence limits for prediction of brick masonry damage distributions using PSI are obtained from percentile analysis of data scatter.

The accuracy of predicting damage using the PSI intensity scale thus depends on an accurate prediction of the PSI intensity level to be experienced at a location. If the PSI intensity cannot be predicted more accurately than the broad bands of intensity contained within the MM or MSK assigned intensity scales, then the use of PSI will not result in a significant improvement of accuracy over the use of assigned intensity. Work is currently in progress both to define Magnitude:PSI attenuation functions and to correlate PSI with engineering parameters of hazard, presented here.

RELATING PSI INTENSITY TO GROUND MOTION

Several past studies have obtained relationships between ground motion (mostly peak horizontal acceleration) and various intensity scales [5]. Almost all of these studies predict higher accelerations for each intensity level than those values expected in the original definition

©Seismicisolation

of the MSK intensity scale. It is also noteworthy that the relationship between intensity and peak acceleration seems to be largely different in Southern Europe from that in Western USA, where the strong motion data of most of these studies originate.

The low confidence that can be placed in intensity assignment, as demonstrated in Figure 4, suggests that these relationships are highly approximate. The definition of the PSI intensity scale directly from damage allows investigation of the parameters of destructiveness in ground motion. Few attempts have been made to investigate in detail the relationship between recorded ground motion and statistically surveyed damage to buildings that have experienced it. The PSI methodology allows statistical damage distributions of common building types (principally masonry) to be related to a measure of intensity with a relatively high degree of confidence. Where damage distributions are surveyed close to a measured point of ground motion, the relationship between ground motion and damage can be ascertained. Surveys of building damage around locations where strong motion instruments have been triggered has formed part of the Martin Centre damage surveying methodology over the past ten years. Some 14 damage surveys have been carried out in the immediate vicinity of recording instruments (within a radius of maximum 400 metres where soil conditions remain constant). A summary of the data points and their ground motion characteristics are presented in Table 2.

TABLE 2
Building damage surveys around a strong motion instrument to relate PSI to recorded parameters of ground motion

Site	Mag *Ms*	No. Bldgs	Bldg Types	**PSI** ψ	Phga *cm/s2*	Pvga *cm/s2*	Prsa *cm/s2*	T pred *sec*	Mepa *cm/s2*	Mrsa *0.1-0.3s*	Mrsa *0.5-1 s*
1 Bucharest, Romania	7.3	115	B	**7.5**	215	115	625	1.19	129	295	425
2 Brienza, Italy	6.8	44	AB	**4.9**	224	188	890	0.14	178	540	160
3 Bagnoli Irp., Italy	6.8	47	AB	**1.7**	188	105	505	0.12	118	305	290
4 Calitri, Italy	6.8	32	AB	**1.2**	177	165	585	0.33	149	340	375
5 Bisaccia, Italy	6.8	25	AB	**0.0**	96	61	270	0.46	74	145	177
6 Auletta, Italy	6.8	9	AB	**1.4**	63	37	185	0.26	51	135	80
7 Corinthos, Greece	6.6	112	ABC	**7.1**	281	110	865	0.26	225	625	345
8 Kalamata A, Greece	6.0	866	ABC	**10.6**	300	390	1030	0.32	343	840	530
9 Kalamata B, Greece	6.0	514	ABC	**9.0**	270	180	1250	0.34	311	620	515
10 Gukasyan, USSR	6.8	20	B	**7.7**	181	139	555	0.31	162	375	310
11 Buzau, Romania	6.8	105	AB	**4.3**	250						
12 Focsani, Romania	6.8	46	B	**6.0**	260						
13 Valenii, Romania	6.8	31	B	**3.2**	170						
14 Abbar, Iran	7.3	176	AB	**11.6**	600						

Building Types: A: Weak masonry, adobe or rubble stone; B: Brick masonry, unreinforced; C: Reinforced concrete frame; **PHGA** : Peak Horizontal ground acceleration, the strongest peak from the two components; **PVGA** : Peak Vertical ground acceleration; **PRSA** : Peak response spectral acceleration at 5% damping, strongest of the two components; **Tpred** : Predominant period, at which PRSA occurred; **MEPA** : Mean Effective Peak Acceleration, equivalent to the average response spectral acceleration over the 0.1-0.5 seconds period range, divided by a factor of 2.50 which is the average amplification factor between absolute and response accelerations in California. Averaged between the two horizontal components; **MRSA** : Mean Response Spectral acceleration for 5% damping, average response spectral acceleration in period range 0.1-0.3 or 0.5-1.0 seconds, averaged between the two horizontal components.

Although the dataset is limited, the correlation of PSI with several commonly used ground motion parameters is important to indicate which of these parameters gives the best prediction of damage. Acceleration parameters generally appear to be stronger primary parameters than velocity or duration, although each of these secondary characteristics may contribute to the damageability of ground motion. Exploration of these in more detail is given in [1].

©SeismicSoftware

Table 2 shows PSI intensity values with a number of different parameters of ground motion acceleration recorded in the vicinity of the damage surveys. These are plotted in Figure 8. Linear regression analyses carried out for these parameters are summarised in Table 3.

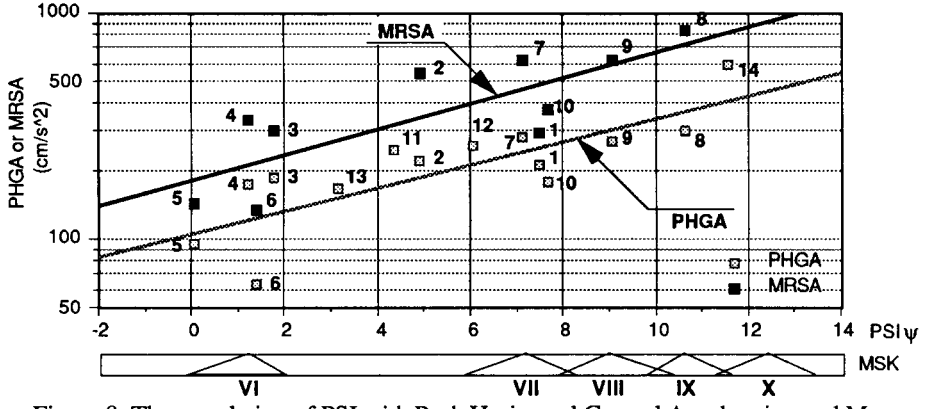

Figure 8. The correlation of PSI with Peak Horizontal Ground Acceleration and Mean Response Spectral Acceleration (period range: 0.1-0.3s).

TABLE 3
Linear regression analysis between PSI and Ground Motion Parameters

Ground Motion Param.	a	t_a	b	t_b	n	r	$s_{y.x}$
Log(PHGA)	2.026	26.259	0.050	3.757	14	0.7495	0.1276
Log(MPHGA)	1.956	22.529	0.051	3.528	10	0.7802	0.1300
Log(PVGA)	1.774	13.541	0.061	2.821	10	0.7062	0.1967
Log(PRSA)	2.440	22.877	0.063	3.578	10	0.7845	0.1600
Log(MEPA)	1.824	19.845	0.068	4.448	10	0.8438	0.1367
Log(MRSA 0.1-0.3s)	2.210	21.497	0.067	3.937	10	0.8122	0.1533
Log(MRSA 0.5-1s)	2.148	17.348	0.057	2.801	10	0.7036	0.1867
Log(MRSA*MRSV 0.1-0.3s)	2.881	12.375	0.133	2.997	9	0.7496	0.3150

a : Intercept; t_a: t-value for the intercept a (95% confidence); **b** : Slope; t_b: t-value for the slope b (95% confidence); **n** : Number of data; **r**: Coefficient of determination (correlation); $s_{y.x}$: Standard Error of estimate of "y" on "x".

Table 3 shows that PSI has a general correlation with all the acceleration parameters. Furthermore the difference in the ability of each one of these paramaters to explain damage occurrence is well illustrated by the differences between the correlation coefficients. Expectedly, in the case of acceleration parameters, the lowest correlation is obtained when only the peak vertical acceleration is considered. The data give a correlation between PSI and PHGA of 0.75. For peak horizontal acceleration it is preferable to use the mean between the two peak values from each component (MPHGA). The correlation between PSI and peak response spectral acceleration (PRSA) is moderately good but can be misleading because these peaks are occurring at different periods. For this reason the predominant periods of each record are also shown (T_{pred}). Using the acceleration response spectrum instead of the absolute acceleration time history means that it is possible to obtain the values of response acceleration over the period ranges relevant to our building stock.

Higher correlations are obtained when the 5% damping spectral acceleration is used instead of the peak accelerations. The effective peak acceleration (EPA) is commonly used in USA as an alternative to peak acceleration and as is shown has the highest correlation with PSI.

@seismicisolation

However the division of the response spectral acceleration with an average amplification factor of 2.50, typical for Western USA, is somewhat arbitrary especially when used with damage that occurred in other tectonic regions.

The majority of the masonry buildings in the 14 sites examined here are residential houses of 1 to 3 storeys high, and it is likely that the best parameter to describe the action of ground motion upon these buildings is the mean response spectral acceleration in the range of 0.1 to 0.3 seconds. This is obtained for each horizontal component and a mean between the two components is calculated (MRSA). In order to illustrate the influence of frequency content of the motion and natural period of the buildings, the last column of Table 2 gives the mean response spectral acceleration in the period range of 0.5 to 1 seconds. The correlation of this long-period component with the damage observed to low-rise masonry buildings is the poorest. The product between acceleration and velocity has one of the highest correlations with observed damage if the mean response spectral values are used (MRSA*MRSV).

CONCLUSIONS

The conclusions that can be drawn from the analysis of relating PSI to ground motion are that acceleration parameters in general are more closely related to damage than other parameters, such as velocity and duration. Among the acceleration parameters, peak horizontal ground acceleration (PHGA) gives an adequate prediction of PSI intensity, but mean response spectral acceleration (MRSA) in the short period range 0.1-0.3 seconds gives a marginally better fit for this data set, probably because these data points represent short-period, mainly masonry buildings. It may be that for longer period buildings, other period ranges would give a better fit. The measures of goodness of fit of the data show that a hazard prediction of a certain value of PHGA or MRSA can be related to PSI intensity in the range 0-12ψ with the following degree of confidence: 0.5 probability that the PSI value falls within ± 1.5 PSI units of the predicted and 0.9 probability of it falling within ± 2.5 PSI units. This accuracy can be verified and may improve in future with further correlation between surveyed damage and recorded ground motion. This accuracy is significantly better than predicting PSI using MM or MSK intensity levels (Figure 5) which would give a 0.5 probability that the PSI value would fall within ± 2.2 of the predicted value and 0.9 probability of it falling within ± 3.7. The use of acceleration parameters to predict PSI is more accurate than assigned intensity by a factor of about one and a half.

REFERENCES

1. A.W. Coburn, S. Sakai, R.J.S. Spence, A. Pomonis, *A Parameterless Scale of Seismic Intensity for Use in Vulnerability Assessment*, Martin Centre Report, March 1991.

2. R.J.S. Spence, `Seismic Risk Modelling: A Review of Methods', *"Verso il New Planning", First International Convention on Methods and Tools for Planning*, University of Naples, Faculty of Architecture, June 1986.

3. Coburn, A.W., *The Use of Intensity in Earthquake Vulnerability Assessment*, Discussion Paper for the European Association of Earthquake Engineering Working Group 3, Vulnerability and Risk Analysis. August 1987.

4. Coburn, A.W., *Relative Vulnerability Assessment,* Proceedings of the Eighth European Conference on Earthquake Engineering, Lisbon, Portugal, September 1986.

5. Pomonis, A., Spence, R.J.S. and Coburn, A.W., *Strong ground motion and damage to masonry buildings*. Final Report for SERC Research Project No., March 1991.

@seismicisolation

A COMPARISON BETWEEN REAL, U.K. SUITED, RESPONSE SPECTRA WITH THE PRESENT DESIGN SPECTRA

J. MENU‡ AND J. COLLOFF†

‡ Seismic Consultant, Seismotec, Milton Keynes, Bucks.

† Seismic Engineering Co-ordinator, BNFL, Risley, Warrington, Cheshire.

ABSTRACT

A selection of real earthquake strong ground motion time histories reflecting plausible seismological and engineering conditions to be expected during an earthquake in the U.K. has been performed. Control parameters included Magnitude, focal depth, macro-seismic Intensity, peak acceleration, effective duration and ground conditions.

A set of ten records (3 components each) whose parameters reasonably fit the target parameters were extracted from world- wide strong motion databases.

A comparison with the design spectra presently used in the U.K. in the nuclear industry shows that a reasonable adequacy is achieved both for hard soil and medium soil conditions. On the contrary, for soft soil sites, the actual spectra appears to be insufficient, reaffirming the need for the determination of site specific design spectra in these conditions.

INTRODUCTION

The accurate definition of a safe, but not overestimated, earthquake loading to structures, is always a formidable task since the detailed characteristics of a future earthquake may vary within wide ranges of multiple parameters. For practical applications seismic ground motions are expressed commonly in the form of response spectra, obtained by treating statistically a sample of response spectra derived from a number of acceleration records. This simple procedure was first used by [1] and [2] to develop horizontal and vertical design response spectra for nuclear facilities.

Similar studies were performed in the U.K., [3], and broad-band elastic spectra were defined based on the analysis of events which occurred outside the U.K. but in similar tectonic and seismological conditions. When adequate data are available, improvements of this early statistical technique, in the form of uniform risk spectra of [4] may also be used to provide a better assessment of the seismic risk at a site.

@seismicisolation

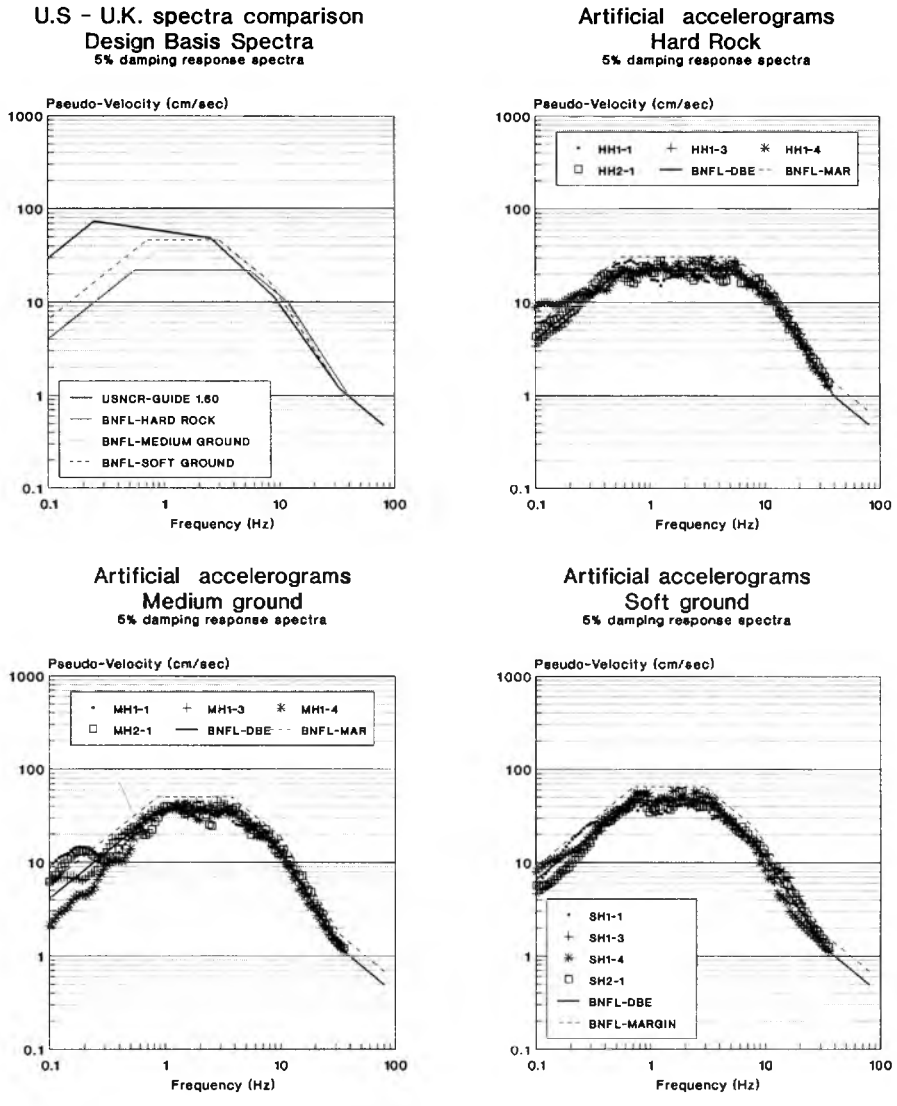

Figure 1. The U.K. DBE response spectra.

a. Comparison of the 3 sub-group spectra with USNRC 1-60.

b. Fitting of artificial time histories on hard rock spectrum.

c. Fitting of artificial time histories on medium ground spectrum.

d. Fitting of artificial time histories on soft ground spectrum.

@seismicisolation

However, other possible approaches to the definition of seismic loading should not be eliminated. They range from the determination of Fourier spectra to the simulation of motion from geophysical models. In this paper, one of these methods, i.e. the selection of real earthquake time histories, from world-wide acceleration records database is presented. A detailed comparison of their elastic response spectra with the present design spectra retained for nuclear constructions in the U.K. is also discussed.

PROBABILISTIC RESPONSE SPECTRA

Earthquake ground motion specification for the design of nuclear facilities in the U.K. has not evolved since the early provisions of 1982 and it is still considered that the design response spectra should be determined by scaling a spectral shape to a PGA of 0.25g (Design Basic Earthquake). The DBE value has been determined assuming that the earthquake occurrence, in the U.K. as a whole, follows an homogeneous Poisson process. It corresponds to a risk or annual probability of exceedence of 10^{-4} irrespective of the soil conditions. The concomitant vertical component is taken as $\frac{2}{3}$ of the horizontal.

The U.K. characteristic earthquake is of small to medium magnitude and shallow depth; distant earthquakes are not likely to influence the spectral shape. The selection process of accelerograms fulfilling these gross tectonic and seismological conditions left a total of 145 records from Central and North America, Italy, Germany and Australia to compose the basic ground motion database. The conventional statistical analysis was then performed to define broad-band elastic response spectra for the design of nuclear facilities. As for the similar spectra determined in the U.S., average smoothed lines corresponding to the mean plus one standard deviation were retained.

Figure 1-a shows the 5% damping smooth spectral shapes scaled to 0.25g for the three local soil conditions commonly envisaged (hard, medium and soft ground). They may be compared with the [5] spectral shape derived from early study by [6].

Variation with the U.K. spectra may be observed both in the high frequency and low frequency ranges. They reflect the expected influence of the selected data sets which comprise different selections of accelerograms and different distributions of event magnitude and site distance.

In the acceleration region, the 5% damping amplification of the U.K. spectra reach 3.04, 3.42 and 3.51 for the hard, medium and soft soil respectively, compared with the average value of 2.87 for the USNRC spectrum. Such strong high frequency amplifications are characteristic of small to medium earthquakes and similar values have already been obtained by [7] on rock as well as on medium thickness alluvium deposits. Recently, [8] made similar observations after analysing a strong motion data set representation of European conditions. In the displacement region, the significant reduction in amplitude simply expresses the shortage of long periods in the U.K. events. It is also worthwhile noting that the low frequency region of the NRC spectra is, to some extent, contaminated with low frequency noise present in many strong motion accelerograms recorded prior to 1975.

@seismicisolation

Artificial acceleration time histories of total duration varying from 10 to 12 sec were

derived from the DBE spectra; the fits of the achieved motions are shown in fig 1-b/c/d. Figure 2 shows one particular movement generated in that manner for the case of medium local ground conditions.

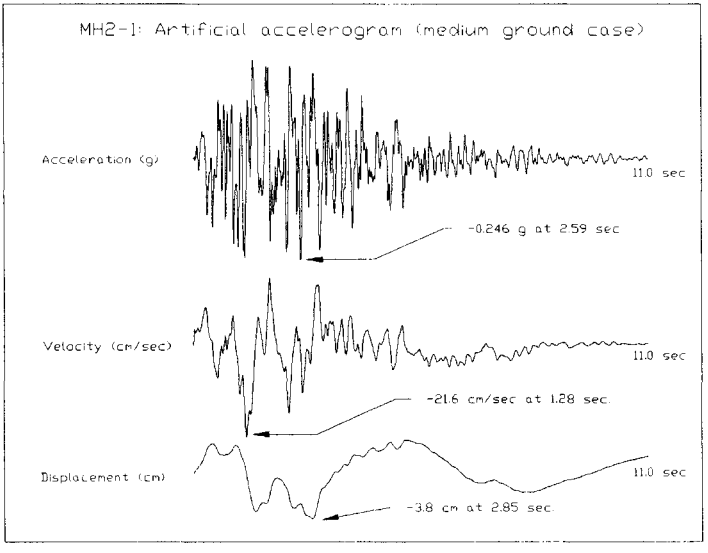

Figure 2. Example of artificial time history for medium ground case.

REAL ACCELEROGRAMS

An alternative and/or a complement to the set of previously generated time histories may be obtained from world-wide earthquake ground acceleration database. This approach, is fundamentally different from the conventional probabilistic analysis and consists of choosing amongst all the acceleration time histories recorded in the world those that would largely resemble future motions in U.K. situations. In order to implement a realistic search, ***fuzzy parameters*** have to be considered. Fuzziness, far from being a disadvantage in the selection process, enables the grouping of several seismological variables in the vicinity of the target parameters which are in any case uncertain.

The following characteristics were chosen to represent the U.K. Design Basis Earthquake (for nuclear design purpose):

Magnitude	$5\frac{1}{2}$
Intensity	VIII
Focal depth	8 to 15 km

Although these parameters are very crude to define a seismic event they provide, if not too strictly applied, a fair definition of a limiting case for the U.K. In addition, they allow

©seismicisolation

the majority of the database records to be discarded. Besides these values other parameters or features have been added which would aim at accelerograms likely to have occurred in the U.K.:

Peak ground acceleration	0.15g - 0.45g.
Total record length	10 to 15 sec.
Strong motion duration	about 3 sec.

Only motions recorded in the free field or in the basement of a building not founded on soft soil were retained. Various local site conditions were allowed.

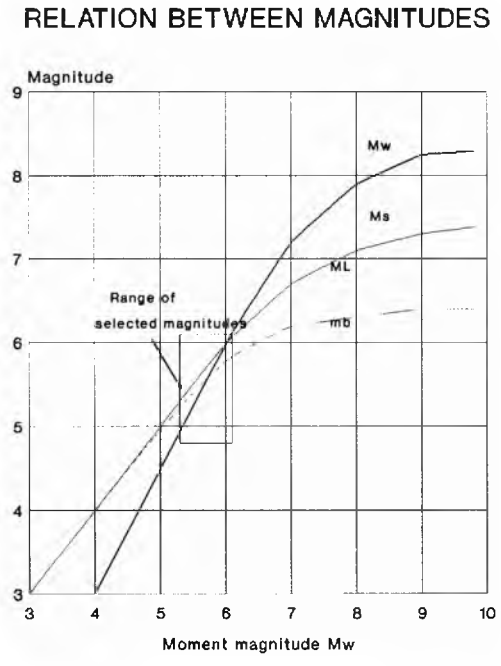

Figure 3. Range of magnitudes of the selected real accelerograms.

Voluntarily, magnitude scale was not defined accurately to avoid eliminating database entries which were not described in that particular scale. Instead, any of M_L, m_b or M_S could be selected as long as they were located in the rectangle shown in figure 3.

M_L	from	5.4	to 6.0
m_b	from	5.3	to 5.7
M_S	from	4.9	to 6.1

@seismicisolation

Similarly, a site macro-seismic Intensity of VII was accepted together with the target value

of VIII. This relative freedom in the selection of Intensity is consistent with the uncertainty of this parameter and helps to realise the poorness of our constraints.

For example, Figure 4 which replots some of the numerous mean regression curves between PGA and Intensity shows that a large variation in PGA may be expected for a given Intensity. For these parameters, the target was located in the upper part of the $VII - VIII$ range where maximum PGA may vary from 0.15g to 0.45g.

Table 1 summarises the main characteristics of 10 of the selected accelerograms. The PGAs correspond to the maximum of the three components of the records. They vary from 0.145g to 0.535g and their associated Intensities are VIII and VII respectively: an indication, if still needed, that peak acceleration is not always the best parameter to define the strength of a ground motion.

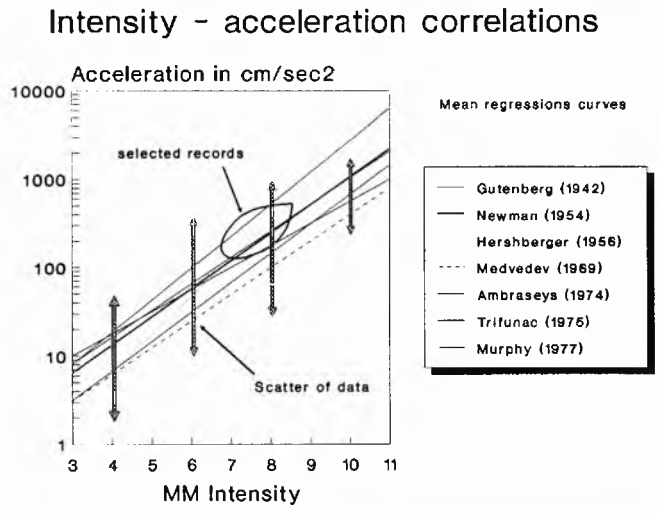

Figure 4: Intensity-PGA selection zone of real time histories.

Figure 5 represents the selected time history SMUK01 recovered during the Friuli (Italy) earthquake of 15 September 1976 (main aftershock). It was corrected and integrated using the Ellicor procedure.

@seismicisolation

TABLE 1
Characteristics of the real accelerograms selected for the U.K.

Code	Recorded in	M_L	M_b	M_S	H km.	I_{max} MM	A_{max} g.	Soil	Dur sec.	Dis km.
SMUK01	Italy	6.0	5.4	6.0	12		0.243	hard	17	16
SMUK02	California	5.7	5.7	5.9	15	VIII	0.145	hard	12	14
SMUK03	Greece	5.6	5.6	5.7	13	VII	0.535	soft	16	18
SMUK04	California	5.5	5.3	6.1	10	VII	0.288	hard	30	7
SMUK05	California	5.5	5.3	6.1	10	VII	0.280	med.	26	12
SMUK06	Canada	5.5	5.4	5.2	10		0.236	med.	20	15
SMUK07	San Salvador	5.4	5.0	5.4	8	VIII	0.430	soft	22	5
SMUK08	San Salvador	5.4	5.0	5.4	8	VIII	0.321	soft	23	7
SMUK09	California	5.3	5.3	4.9	11		0.571	med.	10	2
SMUK10	California	5.4	5.3	5.5	8	VII	0.209	hard	17	15

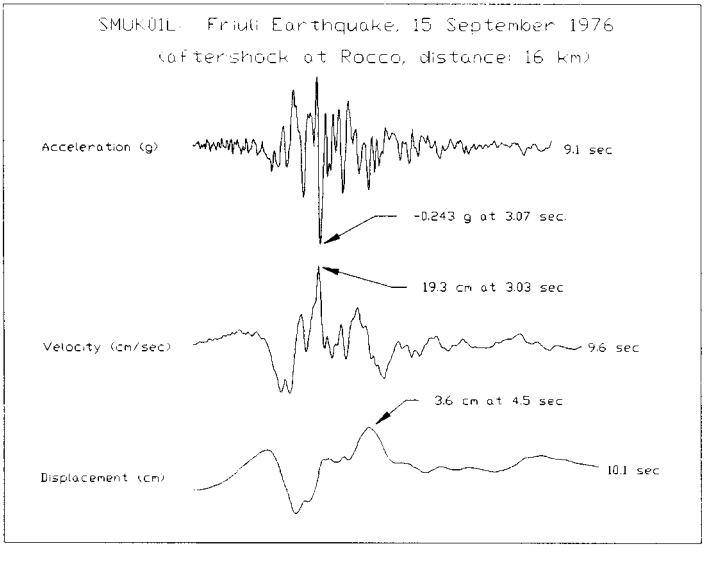

Figure 5. Example of real time history for hard rock conditions.

In Figure 6-a, a plot of some of the typical PGA attenuations with distance is shown together with crosses representing the maximum of the three component peaks reported in Table 1. They are, in average, located around the Joyner and Boore (1981) [10] plus one standard deviation curve. Figures 6- b/c/d show, for each soil condition, the 5% damping

@seismicisolation

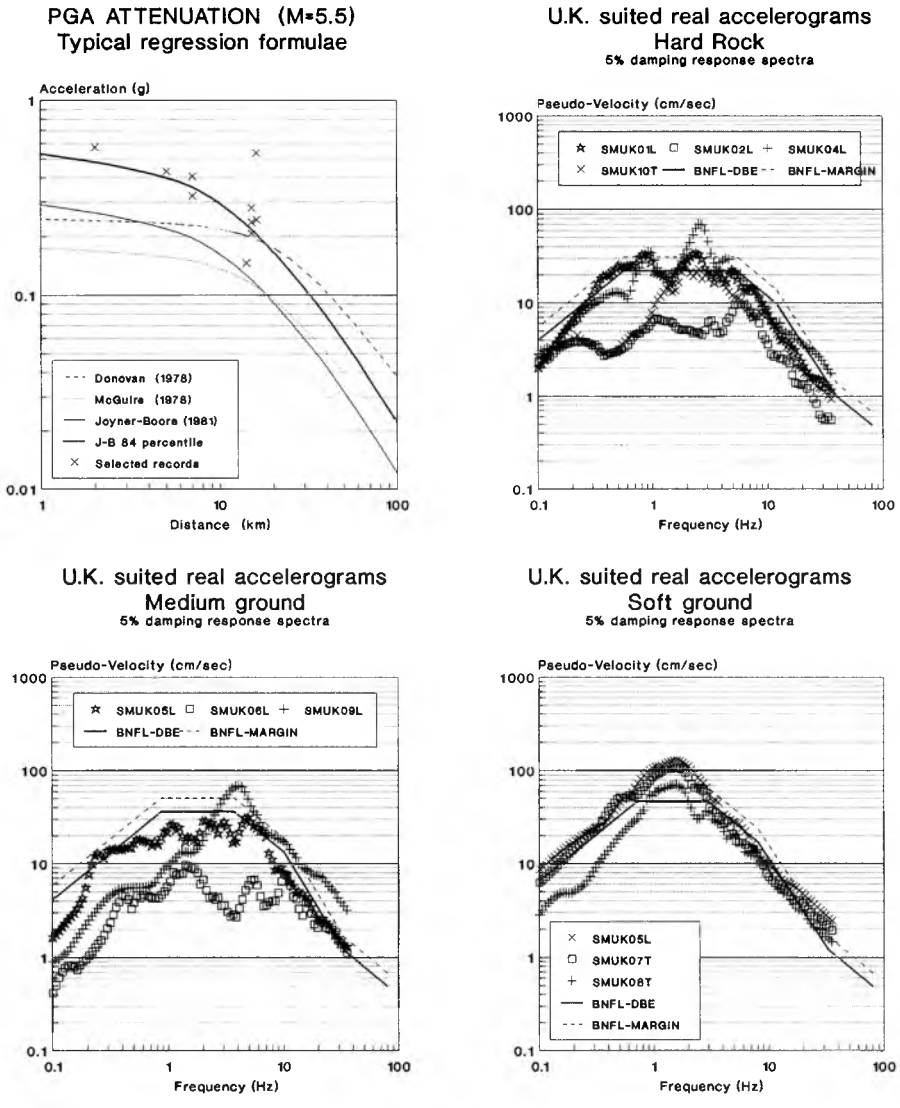

Figure 6. Selected real time histories.

a. Locations of PGAs relatively to typical attenuations laws.

b. 5% damping response spectra of hard rock motions.

c. 5% damping response spectra of medium soil motions.

d. 5% damping response spectra of soft soil medium.

@seismicisolation

elastic response spectra calculated directly from the time histories. For both the hard rock and the medium ground conditions, the DBE response spectra envelope reasonably well, the maximum of the real response spectra. In the acceleration region, localised overshoots are observed and correspond to motions of higher PGA. In the displacement range, the smoothed design line appears to be satisfactory, although many of the records fall below, implying therefore that the present design curves are conservative in the lower frequencies.

For figure 6-d, representing the case of soft ground conditions, an opposite conclusion is reached. Most of the real accelerogram spectra lie above the DBE spectra and particularly in the velocity region predominantly affected by local site amplification. Both acceleration and displacement branches of the present design spectra also appear to be too low. Since the DBE spectra for soft ground conditions is, after all, a mean on many cases, the above observation may reflect a poor sample of soft ground conditions in the U.K. database. This also reaffirms the need for the determination of specific site spectra each time facilities are to be built in these conditions.

CONCLUSIONS

As an alternative and a complement to the definition of design response spectra for nuclear facilities in the U.K., a selection of real accelerograms was carried out in the world-wide strong motion database.

The search retained recorded motions generated by seismic events of magnitudes close to $M = 5\frac{1}{2}$ and of a focal depth between 8 and 15 km. The selected record showed PGA varying from 0.15g to 0.45g for distance between 5 to 18 km from the epicenter.

Examination of the elastic response spectra exhibited good agreement with the DBE spectra presently used for nuclear facilities in the U.K. both for hard rock and medium ground conditions. In the low frequency range many real spectra fall below the design line implying a lower risk in this region compared to the high frequency region. High frequencies of the real accelerograms seem to be sufficiently covered, although there are some local overshoots.

For the soft ground conditions, the present design spectra may be insufficient, in particular in the middle frequency range which can exhibit large amplifications. Failures in Mexico City and San Francisco have been attributed to amplification of soft sites. This effect may not have been adequately represented in the present spectra.

@seismicisolation
@seismicisolation

REFERENCES

1. Blume, J.A., Sharp, R.L. and Dalal, J.S., Recommendations for shape of earthquake response spectra. John A. Blume and Associates, San Francisco, AEC Report WASH-1254, 1972.

2. Mohraz, B., Hall, W.J., and Newmark, N.M., A study of vertical and horizontal earthquake spectra. Nathan M. Newmark Consulting Engineering Services, Urbana, IL. AEC Report WASH-1255, 1972.

3. Principia Mechanica Ltd., Seismic Ground Motions for UK design. Report prepared for CEGB, BNFL and SSEB 1981.

4. Anderson, J.G., and Trifunac, M.D., On uniform risk functionals which describe strong earthquake ground motion.: definition numerical estimation on application to the Fourier Amplitude of Acceleration. Report No. CE77-02, Civil Engineering Department, University of Southern California, Los Angeles. 1977.

5. United States Nuclear Regulatory Commission, Design response spectra for seismic design of nuclear power plants. Guide 1-60, 1973.

6. Newmark, N.M., Blume, J.A., and Kapur, K.K., Seismic design criteria for nuclear power plants. J. Power Div., ASCE, 99. No. PO2, 287-303, 1973.

7. Mohraz, B., A study of earthquake response spectra for different geological conditions. Bull. Seism. Soc. of Am. Vol. 66, No. 3, 915-935, 1976.

8. Hosser, D., Keintzel, E., and Schneider, G., Background Documents for Eurocode 8. Part 1. Vol. 1 Seismic input data Commission of the European Communities. DG III/8075/89N, 1988.

9. Heaton, T.H., Tajima, F., and Mori, A.W., Estimating ground motions using recorded accelerograms. Report to Dames and Moore to Exxon Production Res. Co., Houston. 1982.

10. Joyner, W.B., and Boore, D.M., Peak Horizontal acceleration and velocity from strong-motion records including records from the 1979 Imperial Valley, California earthquake. Bull. Seism. Soc. Am. Vol. 2, No. 6, 2011-2038. 1981.

@seismicisolation

ON THE USE OF DATA FROM MICROEARTHQUAKE NETWORKS FOR GRADING INSTRUMENTAL HYPOCENTRE PARAMETERS AND QUALITY CLASSIFICATION OF FAULT PLANE SOLUTIONS FOR SEISMIC HAZARD ASSESSMENT

W.P. ASPINALL[1], B.O. SKIPP[2] and D.J. MALLARD[3]
[1]Aspinall & Assocs., Sunbury-on-Thames, Middx.
[2]Soil Mechanics Associates, Wokingham, Berks.
[3]Nuclear Electric plc, Barnwood, Glos.

INTRODUCTION

In order to ensure the integrity and robustness of results obtained in a site-specific probabilistic seismic hazard assessment, criteria for the confidence which may be vested in the available instrumental data are needed. Such data may contribute both to seismotectonic understanding and to decisions on the parameters of calculational seismic source models for hazard evaluation, for example, by informing judgements on seismogenic depths or the relative vulnerability of faults to reactivation.

Recent work by the Seismic Hazard Working Party (SHWP), on behalf of Nuclear Electric plc, has drawn attention to the capabilities of local microearthquake networks [1,2,3]. Instruments around Hinkley Point in Somerset, Dungeness in Kent, in North Wales and Heysham in Lancashire have, during their operation yielded 216 hypocentres of events with local magnitudes ranging from -0.6 to 2.7, and focal depths from 0.5 to 24.9 km, together with a total of 76 focal mechanisms (to December 1990).

Before using such information, its quality needs to be assessed. Only earthquakes of the best Grades of epicentral location and depth determination are suitable for testing association with known individual faults. Properly, inferences of a scientific character concerning spatio-temporal distributions of seismicity should only be drawn from a complete, or very nearly complete, dataset. Uncertainty in depth determination is also significant in classifying fault plane solutions which may be used to test individual fault activity status.

The approach to quality classifications proposed here, follows generic principles adopted by the SHWP [3,4,5,19], and is illustrated mainly by data provided by two contiguous networks in north Wales (for Wylfa and Trawsfynydd) operated for Nuclear Electric by the British

©seismicisolation

Geological Survey (BGS). Accuracy and grading of epicentral location are considered first, then accuracy and grading of hypocentral depth followed by the introduction of a method for appraising and grading focal mechanisms which makes use of the locational Grades. The import of Grade and quality classifications on data completeness assessment and seismic hazard modelling is briefly discussed.

ACCURACY AND GRADING OF INSTRUMENTAL EPICENTRES

Without quantification of locational uncertainty, it is not rational even to consider pursuing associations between earthquakes and geology. The methodology for Grading the accuracy of macrocentres assigned to historical earthquakes into four classes has been described by Mallard [4]. With confidence adjudged to be at about the 80% level, Grade 1 locations are known to better than 5 km, Grade 2 to better than 10 km, Grade 3 to better than 20 km, and Grade 4 locations have an uncertainty of more than 20 km. Instrumentally located events may be similarly classified and, ideally, their treatment should be such that the uncertainties on such epicentres (which, for instrumental solutions, can be calculated statistically) can be harmonised with the more subjective locational Grades of the macrocentres. The link between the two is the confidence level associated with the macrocentral location Grades, that is, 80%. Therefore, if the calculated instrumental locational uncertainty is expressed as the standard deviation value ($\pm 1\sigma$) on the epicentre location estimate, the radius of uncertainty, by which the corresponding Grade is determined, needs to be based on 1.28 times the standard deviation.

Such quantification is required of older instrumental solutions as well as results from the new local networks and, in the case of the former, may call for complete reworking of original records or, at least, some form of group or period assessment. For the north Wales study, a detailed review programme of older solutions was commissioned from the Global Seismology Research Unit of the British Geological Survey having three main objectives:

(i) to reveal errors in identification of event type, in phase picking, in data reduction or in cataloguing;

(ii) to provide a new best-estimate hypocentre for each event, enabling comparison to be made between prior and post-revision solutions;

(iii) to provide estimates of the numerical uncertainty in the revised location by use of statistical 'perturbation' analyses which test the stability of the new solution.

Forty-one catalogued events on the primary list of earthquakes, assembled for the hazard study, form the sample which has been reviewed. As a consequence of objective (i) above, six have now been declared to be quarry blasts and five have been ascribed to planned or unplanned explosions. However, these artifical sources can validly contribute to an assessment of locational accuracy, particularly because of their known, shallow origins, even though they may have been removed from the earthquake catalogue. For all 41 events, the changes in principal hypocentral parameters are listed in Table I. The data are grouped according to the level of instrumental coverage in force at the time.

@seismicisolation

Table I. *FINAL HYPOCENTRAL PARAMETERS OF REVIEWED EVENTS, WITH CHANGES FROM CATALOGUE ENTRIES*

ORIGIN TIME: year	mo	dy	hr	mn	secs	δ(OT) secs	EPICENTRE: OS E km	OS N km	δ(x) km	σ(x) km	80% conf.	DEPTH: δ(z) km	σ(z) km	80% conf.	MAGNITUDE ML	δ(M)	LOCATION GRADES Gx	Gz	Event type
1940	12	12	21	20											4.7	0.0	4	4	EQ
1967	4	28	5	32											2.6	-0.4	4	4	EQ
1969	12	26	14	57	57.11	-13.2	237.6	359.3	56.2	±20.10	25.7	34.6		± 9.20	11.8	3.0	0.3	4	3	EQ
1970	7	27	2	45	13.10		201.0	404.6				5.0				2.7	0.0	4	4	EQ
1974	1	23	20	38	0.85	-0.8	300.1	343.3	13.3	± 8.89	11.4	7.5	-7.5	±12.50	16.0	3.5	0.0	3	3	EQ
1974	8	30	11	22	39.11		278.2	357.9	4.5	± 3.90	5.0	7.8		± 4.27	5.5	0.5		1	2	EQ
1974	9	1	5	27	59.83		241.1	349.4		± 7.00	9.0	13.0		± 6.26	8.0	0.6		2	2	EQ
1978	7	12	20	4	4.90	0.3	247.2	390.4	4.0	± 0.96	1.2	13.9	3.9	± 9.90	12.7	2.3	-0.4	1	3	EQ
1979	1	24	2	49	54.09	4.1	275.0	272.8	11.8	± 8.56	11.0	1.3		± 4.95	6.3	1.8	-0.2	3	2	EQ
1980	11	10	16	2	30.27	0.8	261.4	369.7	17.9	± 4.70	6.0	0.0		± 3.04	3.9	1.9	0.0	2	1	QB
1980	12	28	21	47	42.80	-0.1	253.3	400.9	0.9	± 4.74	6.1	5.8		± 5.81	7.4	2.2	-0.2	2	2	EQ
1981	3	30	4	6	51.02	-9.0	204.5	392.0	14.6	± 4.25	5.4	6.6		± 7.49	9.6	1.5	0.1	2	2	EQ
1981	4	28	21	41	56.59	-3.4	342.8	272.7	1.2	± 1.15	1.5	13.0		± 3.34	4.3	1.5	-0.1	1	1	EQ
1981	6	21	2	0	33.82	-0.4	229.5	360.1	3.4	± 1.77	2.3	2.4		± 4.71	6.0	1.9	-0.3	1	2	EQ
1982	8	9	11	25	5.79	-0.6	269.8	347.0	10.0	± 2.00	2.6	8.4	8.2	± 5.54	7.1	2.6	-0.5	1	2	EQ
1982	9	24	16	28	26.12	1.8	155.6	385.7	9.8	± 3.19	4.1	2.3	-1.7	± 3.18	4.1	1.4	0.0	1	1	EX
1983	5	24	21	54	41.85	-0.8	330.0	456.1	5.7	± 3.11	4.0	0.2	-4.8	± 1.22	1.6	2.3	0.0	1	1	EX
1983	8	17	10	54	36.73	-0.8	288.0	324.5	8.9	± 6.05	7.7	9.5	7.0	± 3.70	4.7	1.6	0.1	2	1	EQ
1983	9	15	14	32	43.32	-0.6	264.4	312.1	7.1	± 5.46	7.0	6.7	3.9	± 4.67	6.0	2.4	-0.1	2	2	EQ
1984	3	9	17	29	34.01	-0.2	272.1	346.4	4.3	± 4.09	5.2	0.8	-4.6	± 2.69	3.4	1.7	-0.1	2	1	QB
1984	4	15	21	5	34.92	0.1	315.0	279.9	0.9	± 2.16	2.8	12.7	2.9	± 7.90	10.1	3.3	0.1	1	3	EQ
1984	5	3	17	15	22.33	-0.8	216.0	384.1	14.5	± 1.99	2.5	13.0		± 5.81	7.4	1.3	-0.2	1	2	EQ
1984	5	13	18	45	26.50	0.0	309.6	442.3	4.5	± 2.68	3.4	0.1	-1.1	± 4.21	5.4	1.8	0.0	1	2	EX
1984	5	28	9	5	26.30	-1.0	194.9	321.9	9.5	± 4.70	6.0	1.1	-8.9	± 3.82	4.9	2.0	0.1	2	1	EX
1984	6	22	13	38	22.50	-1.4	270.1	348.0	7.8	±10.01	12.8	0.7	-5.3	± 1.83	2.3	1.8	0.0	3	1	QB
1984	7	9	11	5	7.66	-2.5	262.7	376.7	17.0	±10.11	12.9	0.2	0.2	± 1.93	2.5	1.7	0.0	3	1	QB
1984	7	10	3	58	52.94	-1.0	354.3	359.5	6.1	± 3.84	4.9	6.0	-2.3	± 4.74	6.1	1.6	0.3	1	2	EQ
1984	7	10	14	28	12.47	-3.0	312.2	365.7	16.9	± 5.54	7.1	2.5	2.5	± 1.89	2.4	1.2	0.1	2	1	QB
1984	7	10	17	5	7.78	-4.1	307.9	414.2	26.7	± 1.55	2.0	6.0	1.6	± 5.09	6.5	1.6	0.0	1	2	EX
1984	7	18	11	4	40.19	-1.5	262.9	383.2	13.8	± 7.44	9.5	4.0	4.0	± 4.88	6.2	1.8	0.1	2	2	QB
1984	8	26	20	17	42.42	0.0	314.8	267.0	2.1	± 0.84	1.1	12.1	2.5	± 4.47	5.7	0.7	0.1	1	2	EQ
1984	9	4	3	26	4.03	-0.1	224.4	334.6	0.4	± 1.40	1.8	9.3	1.3	± 0.71	0.9	0.7	0.0	1	1	EQ
1984	9	8	2	35	47.62	-0.1	224.4	349.9	0.3	± 0.83	1.1	14.2	1.4	± 1.25	1.6	0.6	0.0	1	1	EQ
1984	12	4	8	18	2.24	0.1	258.6	438.3	3.2	± 1.80	2.3	6.9	-3.8	± 4.69	6.0	2.0	0.2	1	2	EQ
1984	12	4	9	8	30.64	0.1	263.0	435.9	9.9	± 8.09	10.4	6.6	-2.9	± 5.73	7.3	1.8	0.6	3	2	EQ
1984	12	22	18	5	1.22	1.2	235.2	351.6		± 0.44	0.6	14.1		± 0.43	0.6	0.9	-0.2	1	1	EQ
1985	3	23	19	0	25.56	0.5	262.0	314.6	2.2	± 1.93	2.5	10.5	-2.2	± 2.53	3.2	1.1	-0.1	1	1	EQ
1985	9	5	15	1	4.89	0.3	289.2	384.0	2.0	± 1.81	2.3	6.3	2.2	± 5.30	6.8	2.1	0.0	1	2	EQ
1985	9	19	12	7	55.59	3.0	238.7	343.4	12.5	± 1.76	2.3	21.5	-17.4	± 0.73	0.9	1.0	0.2	1	1	AS
1985	9	27	11	59	51.91	1.0	249.2	308.4	2.5	± 1.36	1.7	15.3	-11.3	± 5.51	7.1	1.6	0.2	1	2	EQ
1986	7	28	23	58	41.52	-0.1	320.9	274.5	0.3	± 0.93	1.2	16.1	1.6	± 3.89	5.0	0.7	-0.1	1	1	EQ
PERIOD SUMMARIES:																		80% conf. statistics	and Grades
1940					(avg.)	-2.4			18.0	±8.2			-1.8	±7.8			-0.1	45.1±14.2	4 4
-1979					(s.d.)	±6.5			±19.5	-			±5.7	-			±0.2		
1980					(avg.)	-1.4			9.6	±4.3			0.1	±4.2			0.0	19.6 ±8.2	3 3
-1984/7/19					(s.d.)	±2.2			±6.5	-			±4.7	-			±0.2		
1984/7/20					(avg.)	0.3			3.0	±2.2			-0.6	±2.8			0.1	8.9 ±5.3	2 3
-1985/6/30					(s.d.)	±0.4			±3.2	-			±2.4	-			±0.2		
1985/7/1					(avg.)	1.4			5.7	±1.6			-8.8	±3.8			0.1	12.2±20.1	3 4
-1985/10/14					(s.d.)	±1.2			±4.8	-			±8.2	-			±0.1		
1985/10/15					(avg.)	-0.1			0.3	±0.9			1.6	±3.9			-0.1	8.9 ±5.3	2 2
-1988/10/31					(s.d.)	-			-	-			-	-			-		

KEY

δ(OT), δ(x), δ(z) and δ(M) are changes in origin time, location, depth and magnitude
σ(x) and σ(z) are the estimated 1 std. dev. location and depth errors on the revised solution
Gx and Gz are the instrumental Grades of location and depth

EQ = earthquake; EX = explosion; AS = aftershock; QB = quarry blast

Prior to 1980, there was an absence of regional seismograph coverage for north Wales until the installation of the station at Bryn Du (SBD). The next impetus to local monitoring was the widely felt Lleyn earthquake of 1984 July 19 which led to the deployment of a temporary BGS network in the area. Apart from a minor hiatus in the late summer of 1985, when the temporary network was being repositioned and extended for the Nuclear Electric study, coverage and accuracy of location of local activity has been maintained at a very high level since July 1984.

@seismicisolation

This is borne out by considering the data of Table I where the columns marked "δ(OT)", "δ(x)", "δ(z)" and "δ(M)" represent respectively the changes in origin time (in seconds), epicentre (in km), depth (in km) and magnitude for each event from its original cataloguing to its final revised solution. Inspection of the mean epicentral changes listed in the period summaries on Table I shows an average revision shift in epicentre of 18.0 km with a spread of ± 19.5 km (at 1σ) in the early period, through 9.6 ± 6.5 km in the early 1980's to 3.0 ± 3.2 km when the local networks were operating. This demonstrates the real improvement in accuracy of epicentral location which results from the use of a local network coupled with dedicated data processing.

The columns marked "σ(x)" and "80% conf" for each epicentre give the values of the one standard deviation uncertainty on the revised location (as determined by the BGS perturbation analysis - see [6]) and the corresponding 80% confidence levels: the latter allow comparison with the historical macrocentre data. These values represent the residual uncertainty on each event after revision. Group averages for each time period of monitoring are given in the "Summaries" section on Table I. The statistics of the residual uncertainties and the revision shifts can be combined to provide an estimate of the average 80% confidence radius on the location of an original, unrevised location as a function of recording period: before 1980, a typical instrumental epicentral location for north Wales would be classed as Grade 4; after 1980 and before the local network was in operation, the average Grade was 3; for events recorded in the presence of the network but processed only routinely for the national catalogue, average locational Grades of 2 are found. This last result contrasts with the typical Grade 1 location furnished by dedicated processing of recordings from the Nuclear Electric networks.

It will be noted from the column "δ(M)" on Table I that, in general, adjustment to the local magnitude estimate for a revised event appears small, as befits a quantity expressed on a logarithmic scale.

The comparison between these particular original and revised solutions thus provides an indication of the extent of gross errors in routinely catalogued instrumental data. It does not, however, throw any light on the extent of which errors may be present in any individual, unrevised event. For such cases, therefore, the behaviour of the tested sample might have to be adopted as indicative of the uncertainties for any untested individual within the rest of the population of events for that period.

The number and quality of recent instrumental earthquake recordings from north Wales might suggest that the entire dataset would be amenable to more detailed location analysis by techniques such as joint hypocentral determination [7], for example. However, the solution for the largest recent instrumental earthquake in this area (1984/07/19) already embodies a detailed local velocity model review and, as the BGS revision exercise has been influenced by the relocation of this event, wholesale relocation of the remaining events has not been pursued.

@seismicisolation

ACCURACY AND GRADING OF INSTRUMENTAL DEPTHS

A quantified estimate of focal depth using intensity data only is rarely justified for British macroseismic events and, in the SHWP praxis, uncertainty Grades are not attributed to such macroseismic depth estimates as are made. However, the uncertainties in instrumental depths need to be assessed if data from these events are used for further analysis or interpretation, such as focal mechanism studies. The conversion from numerical locational uncertainty to an equivalent depth Grade follows the same formula as that for epicenters given above with the extensive review exercise undertaken by BGS for north Wales instrumental locations also providing a basis for assessing the Grades of depths from unrevised events.

An inspection of the figures for depth changes "$\delta(z)$" and their period averages on Table I shows a similar pattern to that for epicentral changes: before 1980, the mean and 1σ figures are -1.8 km and ± 5.7 km; between 1980 and mid-July 1984, +0.1 km and ± 4.7 km, and with the networks operating, -0.6 km and ± 2.4 km. For the short interruption in 1985 mentioned above, the poorer figures of -8.8 ± 8.2 km result mainly from major revisions to the two events of 1985/09/19 and 1985/09/27. These two earthquakes exemplify the potential difference in quality between the results from a dedicated local study and the output from routine processing, particularly in the determination of focal depth.

It is interesting to note that, whereas the standard deviations on the mean values of epicentral shift for each period are systematically greater than the average of the standard deviations derived by the perturbation method for the same data, this is not true for the estimations of depth. This observation is consistent with the fact that depth is the least well-constrained parameter in a hypocentre determination (unless additional data are used, such as depth-sensitive phases); removal of gross errors from original data has a more marked effect on the accuracy of epicentral coordinates than on the accuracies of origin time or depth, which suffer from a trade-off, the one against the other, which cannot be constrained.

With respect to depth Grades, there is further complication involving an apparent dependence of event depth with distance to nearest recording station. For earthquakes in north Wales, this was first noted in Ref.[1]. It would be surprising, if such a condition were not present in the UK catalogued database generally. Thus, when local seismograph coverage is absent in a area of interest, the possibility exists that reported hypocentres may be systematically biased to shallower depths. The degree of this bias, at long epicentral ranges, can easily exceed the uncertainty estimated by the perturbation technique which examines the stability of the individual solution against small changes in the travel-time model but does not constrain the depth/origin time trade-off problem. For the north Wales data, a linear trend was fitted to data which, when removed, gave a new distribution of depths in the range 6.6 to 21.1 km. In the light of this effect, attributed depth Grades are demoted to the next Grade if the nearest seismograph reporting the event is more than 30km from the epicentre. Accordingly, typical depth Grades for unrevised events before the advent of the local network (see Table I) are also reduced by one Grade to reflect this source of uncertainty. As focal depth may have an important influence on the level of ground shaking for critical facilities, these examples of diminished quality in estimates of this parameter argue strongly for a detailed review of old, catalogued data and for the use of local networks in site-specific seismic hazard assessments.

@seismicisolation

FOCAL MECHANISMS

Crustal stress states may, in principle, be established from well-constrained focal mechanisms. In Britain, the growing accumulation of solutions of focal mechanisms over the past decade has been notable: from a few at the end of the 1970's to over 80 by the early 1990's, they now span focal depths from a few kilometers to over 20 km, and local magnitudes from less than 0 to over 5. Deduction of the stress tensor, in already fractured crust, from single or multiple focal mechanisms by inversion is a burgeoning area of research [8,9,10,11] and cannot be dealt with here. Nevertheless, the need to assess quality and completeness in a sample of focal mechanisms before indulging in seismotectonic model-making is as important as in dealing, for example, with locational uncertainty when considering association with faults.

For north Wales, a number of independent but closely similar fault plane solutions have been published for the Lleyn earthquake of 1984/07/19 [12,13,14,15]; with the exception of these, and one dubious event on the edge of the present area of interest, all other fault plane solutions in the region have been derived from earthquakes examined uniformly with the focal hemisphere searching program FOCMEC [16]. Forty-two events up to 31 October 1988 were so treated, eleven analysed in the review exercise and thirty-one recorded by the local networks. For consistency, the Lleyn mainshock has also had a FOCMEC solution generated specifically for the present study (see Fig. 1) using polarity data only; the program produced five compatible possible solutions in two narrow ranges of angular distribution, consistent with the strike-slip movement inferred in all the previous studies.

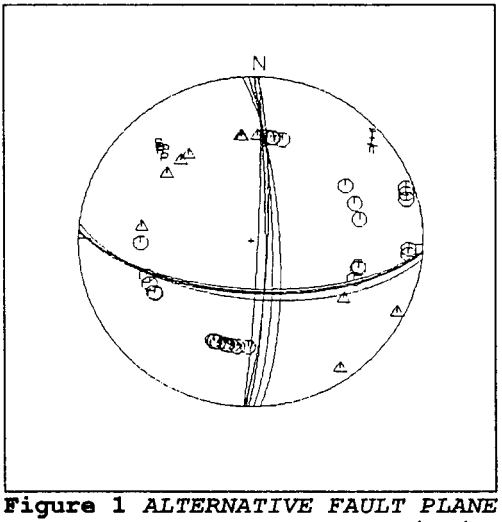

Figure 1 *ALTERNATIVE FAULT PLANE SOLUTIONS FOR THE 1984/07/19 LLEYN EARTHQUAKE FOUND BY PROGRAM FOCMEC (after Turbitt and Ritchie, pers. comm.)*

Before any tectonic implications of the mechanisms can be considered, it is necessary to consider the fitness for use of the individual solutions by assessing their quality. To-date, no straightforward, purely numerical method has been devised which quantifies confidence in fault plane solutions for an idividual earthquake, such as is provided by the statistically-based Grades of uncertainty for location and depth described above, although efforts are being made in this direction (e.g. [10]). The FOCMEC program does give a measure of the goodness-of-fit of the input data to the found solution, in an RMS error sense, but it does not incorporate the effects of uncertainties in the data so that the RMS values for two events, with differing amounts and quality of data, are not strictly comparable. This is an exact parallel with the RMS error calculated by standard earthquake

@seismicisolation

location programs, such as the HYPO series: notwithstanding the superior probity of their solutions, handsomely overdetermined events sometimes produce higher RMS error values than solutions calculated with mimimal data.

A scheme for assessing the quality of focal mechanisms has, therefore, been devised whereby the solutions are ranked according to a number of partially quantitative factors. (While its aims are similar, this scheme should not be confused with the ranking of crustal stress directions proposed for the preparation of a global map of crustal stress, see [17]). In descending order of importance, the factors considered here are as follows:

(i) The most significant criterion concerns the accuracy of depth determination. A well-constrained depth is essential because of the effect of crustal discontinuities on the geometry of raypath take-off angle. A modest change in depth can swing an important raypath from emergence in one quadrant on the focal hemisphere to a different orientation in another, thereby completely altering the sense of the solution. For this reason only Grade 1, or exceptionally, Grade 2 depths should be accepted.

(ii) Next, there should be a sufficient distribution of clear first motion readings. Preferably, all four quadrants of polarity should be populated by some unequivocal first motion data although this requirement may be relaxed where the data include closely-spaced first motions of opposite polarity, serving to constrain either or both focal planes. Indeed, a good fault plane solution may be achieved by as few as four well-disposed, mutually opposed ray trajectories without all quadrants being extensively populated. On the other hand, a hemisphere carrying a good smattering of arrivals in all four quadrants may not provide a well-constrained solution. The merits of a limited distribution of first motion observations can only be readily assessed by inspection.

(iii) Lastly, consideration must be given to the number of polarity errors (and amplitude ratio errors, where these are used) which have had had to be accepted in arriving at the preferred solution. A large proportion of discordant data must undermine confidence in the robustness of the solution.

All three of these factors have been appraised, using the summary information on Table II, for forty-two earthquakes in the north Wales dataset which have FOCMEC solutions. Each solution has then been placed in a classification from A to D:

Events of Quality A have well-defined, unequivocal solutions of high confidence, such that any seismologist would arrive at the same conclusion regardless of method; five earthquakes are placed in this category.

Seven other earthquakes have satisfying solutions which lack only some data completeness or the depth control for an A rating; these are accorded Quality B.

There remain 19 events with solutions which are classified as Quality C, and 11 which are given Quality D.

@seismicisolation

Table II. *QUALITY ASSESSMENT OF FOCAL MECHANISMS FOR EARTHQUAKES IN NORTH WALES (up to 31 Oct 1988)*

DATE:	DELTA: km	GRADES: Gx	GRADES: Gz'	DATA: Npol	DATA: Nrat	SOLUTIONS: Nsol	SOLUTIONS: Nquad	ERRORS: P	ERRORS: Sv/P	SSE: All	SSE: Accepted	MECHANISM QUALITY
1982 8 9	47.1	1	3	9	8	16	2	1	3	10.420	0.021	C
1984 4 15	29.3	1	3	11	3	1	4	0	1	6.943	0.064	B
*1984 7 19	75.8	1	1	42	0	5	4	1	-	-	-	A
1984 8 26	27.9	1	2	4	3	12	4	0	0	0.007	0.007	C
1984 9 4	5.3	1	1	7	5	27	3	0	1	0.541	0.081	B
1984 9 8	12.3	1	1	6	3	2	3	0	1	1.964	0.049	B
1984 12 4	69.5	1	3	6	4	1	4	0	0	0.122	0.122	C
1984 12 22	6.5	1	1	8	5	17	3	0	3	6.930	0.005	C
1985 3 23	2.7	1	1	6	15	1	2	0	2	1.501	0.271	B
1985 9 5	40.5	1	3	6	7	2	3	0	0	0.159	0.159	C
1985 9 27	33.7	1	3	5	11	2	3	0	2	1.257	0.128	B
1985 11 3	15.8	1	1	4	6	4	2	0	0	0.105	0.105	C
1985 12 18	8.4	1	1	5	6	59	3	0	3	1.763	0.011	C
1986 1 21	10.8	1	1	6	10	14	3	0	3	3.782	0.062	B
1986 5 7	5.7	1	1	6	10	3	1	0	2	2.272	0.124	C
1986 5 7	24.3	1	1	1	3	57	1	0	0	0.002	0.002	D
1986 6 22	13.2	1	1	5	12	5	2	0	4	2.322	0.149	C
1986 7 9	3.8	1	1	6	11	4	3	0	3	0.504	0.121	B
1986 7 28	25.3	1	1	2	4	11	1	0	0	0.019	0.019	D
1986 9 19	9.1	1	1	7	12	12	4	1	3	2.544	0.106	C
1986 9 24	13.1	1	1	3	5	33	3	0	1	1.105	0.017	C
1987 1 24	22.7	1	1	2	5	13	2	0	0	0.039	0.039	D
1987 2 23	5.6	1	1	5	7	5	3	0	1	2.002	0.104	C
1987 4 12	21.9	1	2	10	6	1	3	0	4	1.144	0.036	A
1987 4 14	21.3	1	1	3	5	34	2	0	1	0.270	0.014	D
1987 6 10	8.0	1	1	2	4	48	2	0	1	2.289	0.007	D
1987 9 7	6.7	1	1	4	11	26	2	0	2	0.650	0.103	C
1987 10 19	6.7	1	1	5	9	9	2	0	3	3.285	0.048	D
1987 11 29	28.1	1	2	5	6	28	1	0	1	0.750	0.033	D
1988 1 4	3.5	1	1	2	5	11	2	0	0	0.023	0.023	D
1988 1 7	53.5	1	3	4	6	13	1	0	1	0.662	0.025	D
1988 1 12	12.6	1	1	6	9	2	4	0	3	3.448	0.041	A
1988 2 6	5.8	1	1	5	5	8	2	0	3	3.522	0.011	C
1988 2 27	12.4	1	1	3	3	12	1	0	1	1.974	0.002	D
1988 3 8	41.0	1	3	4	5	7	2	0	2	2.113	0.001	C
1988 3 28	39.2	1	3	3	4	5	2	0	0	0.018	0.018	C
1988 4 3	21.6	1	2	9	7	8	4	1	4	4.693	0.018	A
1988 4 10	10.1	1	1	5	4	2	3	0	1	6.352	0.050	A
1988 8 7	39.6	1	3	4	3	16	2	0	0	0.008	0.008	C
1988 8 8	39.0	1	3	3	3	11	2	0	0	0.006	0.006	D
1988 8 8	39.1	1	3	3	3	9	2	0	0	0.009	0.009	C
1988 9 17	6.2	1	1	3	4	1	2	0	0	0.016	0.016	C

KEY:
DELTA: the distance to the nearest station, in km.
DATA: Npol is the no. of polarity readings; Nrat is the number of amplitude ratios for each earthquake.
SOLUTIONS: Nsol is the no. of solutions found for the given search angles, which vary from event to event.
Nquad is the no. of quadrants on the focal sphere which contain at least one polarity reading.
ERRORS: the columns give the no. of polarity and amplitude errors which have to be accepted for the solution.
SSE: the columns give the sum of squared errors of the log ratios for 'All' amplitudes and for 'Accepted' amplitudes, respectively.
NOTE:
* The 1984/7/19 Lleyn earthquake focal mechanism did not use Sv/P amplitude ratios.

The focal mechanism solutions of Qualities A and B are deemed to be of sufficent quality that they can reasonably be used in testing associations with geology. Only marginal confidence is vested in Quality C events as individuals although, with suitable caution, they might be considered for composite mechanisms or as contributing to the regional data on P- and T- axis directions, for example. The Quality D solutions cannot be relied upon.

In addition to summarising the input data, Table II gives the sum-of-squared errors for the logarithms of the Sv/P amplitude ratios for "All" readings and for those which are "Accepted" (at an arbitrary threshold) as belonging to a valid fault plane solution. Rejected ratios (which are included in the category "All") are regarded as gross errors, providing no

@seismicisolation

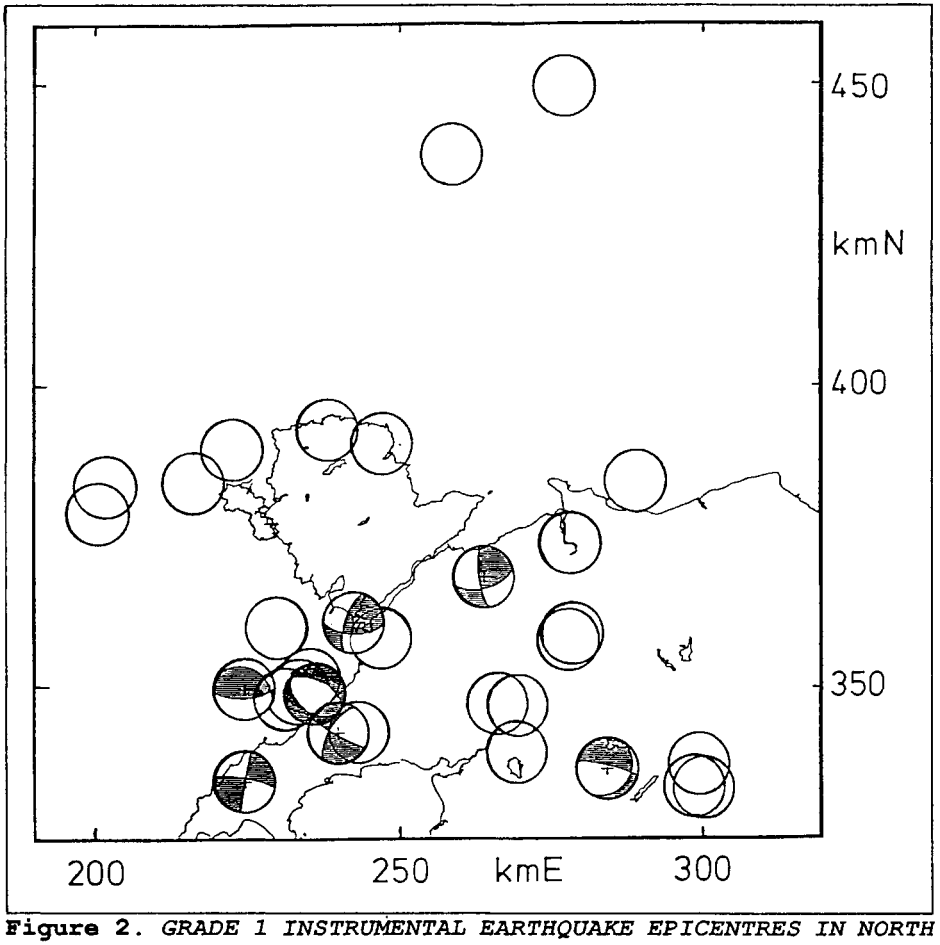

Figure 2. *GRADE 1 INSTRUMENTAL EARTHQUAKE EPICENTRES IN NORTH WALES, WITH QUALITY A OR B LOWER HEMISPHERE FAULT PLANE SOLUTIONS (to Oct. 1989).*

real guidance to the best solution which here is taken to be that which has the least sum-of-squared errors for "Accepted" ratios only. The preferred solutions have been determined bythe SHWP from BGS working papers together with the corresponding orientations of theirplanes and axes, and inferred style of faulting. A subset of these results from the Wylfa study are depicted on Fig. 2; it should be noted that these events have not been tested for completeness and, therefore, should not have spatial significance construed with them. The diagram shows 31 Grade 1 instrumental locations (the circles have radii of 5 km), of which only seven have Quality A or B focal mechanisms. It is noteworthy that the latter are all within the ambit of the local network stations.

@seismicisolation

DISCUSSION

In low seismicity areas where data are sparse, there is a natural tendency to 'make the most of it' and accept every scintilla of information, whatever its worth. However, in this case, the relative abundance of events and fault plane solutions, provided by the north Wales networks, has enabled us to develop an event quality classification. The numbers on Table III summarise the breakdown into Grades of instrumental earthquakes in the north Wales dataset; they include both revised older data and recent results from the local networks. It can be seen that more than 80% of epicentral locations are Grade 1 or 2, and that 60% have similarly reliable depth determinations. In both cases, the majority of good Grades are for the more recent events, recorded on the local networks.

Table III. *NUMBERS OF EVENTS IN EACH GRADE FOR THE NORTH WALES DATASET (to Oct 1989).*

GRADE	EPICENTRE	DEPTH
1	53	29
2	16	17
3	8	28
4	7	6
TOTALS	84	80

Any consideration of the use of seismological data requires, at least, recognition of the importance of completeness of the dataset and it is almost axiomatic that deductions of spatio-temporal patterns need a complete dataset. However, discussion of the methods of testing the completeness of a particular sample, using *a priori* stochastic models or deterministic procedures, is beyond the scope of this paper and has already been presented elsewhere [1,5]. In so far as a site-specific seismic hazard model is concerned, the identification of complete datasets, accompanied by the quality assessments described in this paper, permits rational indentification and parameterisation of seismic sources, including potentially 'active' faults, in a logic-tree hazard program such as PRISK [18] and opens the way towards procedures for statistically weighting the distribution of focal depths assigned to those sources, for example. Already, this approach has confirmed the conservative focal depth assumptions made for the Hinkley Point seismic hazard model which, at the time of its construction (before many local network data were available), had to reflect the contemporary wisdom of very shallow focal depths for British earthquakes. The operation of the Nuclear Electric networks at Hinkley Point and in north Wales have both shown that, locally at least, most well-constrained events nucleate at mid-crustal depths whereas hypocentres which rely only on distant stations may be strongly biased upwards.

Computer programs are now available which permit inversion of fault mechanisms for groups of events to a stress tensor and, in due course, this will be undertaken for the data referred to in this paper. At this stage, however, it is salutory to note the limited proportion of high quality hypocentral locations, especially in depth, and the very modest number of fault plane solutions which achieve a reasonable quality: for north Wales, 12 events only are Quality A or B out of a total of 42, even with the advantage of a thirteen station local

@seismicisolation

network. This underlines the extreme caution which needs to be exercised in associating discrete events with known or postulated geological features, especially if correlation of style of faulting is not considered in the association.

Finally, of more scientific interest, is the perspective that inversion of properly selected high quality fault plane solutions for the stress tensor could help resolve the question as to whether or not throughout Britain, the **major principal stress** is, as is usually assumed, indeed horizontal.

ACKNOWLEDGEMENTS

The north Wales microseismic networks are funded by Nuclear Electric plc and operated by the British Geological Survey under the direction of the SHWP. We gratefully acknowledge the important contributions to this study of Maureen Ritchie, Terry Turbitt, Chris Browitt and their colleagues in the BGS Global Seismology Research Group. We thank Nuclear Electric for permission to publish.

This is Seismic Hazard Working Party Contribution No. 51.

REFERENCES

[1] Aspinall W.P., B.O. Skipp and M.E.A. Ritchie (1990). Microtremor networks and seismic hazard assessment in the UK. Quart. J. Eng. Geol., 23, 193-208.

[2] Skipp B.O., W.P. Aspinall, D.J. Mallard and M.E.A. Ritchie (1990). On the use of microearthquake networks in seismic hazard assessment in Britain. In: Proceedings, 9th European Conference of Earthquake Engineering, Moscow, Sept 1990.

[3] Mallard D.J., I.E. Higginbottom, R. Muir Wood and B.O. Skipp (1991). Recent developments in the methodology of seismic hazard assessment. Paper presented to Institution of Civil Engineers Conference "Civil Engineering in the Nuclear Industry", Windermere, UK, 20-22 March 1991.

[4] Mallard D.J. (1986). The investigation of historical earthquakes and their role in seismic hazard evaluation for the UK. Reproduced in: IAEA-TC-472.2, Vol. 1, 201-219, IAEA, Vienna, 1989.

[5] Skipp B.O. (1985). Completeness and quality of seismological data for hazard analysis. In: Proceedings, 12th Regional Seminar on Earthquake Engineering, EAEE Earthquake Planning and Protection Organisation, Helkidiki, Greece.

[6] Richie M.E.A. (1987). North Wales seismic monitoring for the period 15 October 1985 to 31 October 1986. Brit. Geol. Surv. Glob. Seismol. Report No. 325, Edinburgh, UK.

[7] Douglas A. (1967). Joint epicentre determination. Nature, 215, 47-48.

@seismicisolation

[8] Vasseur G., A. Etchecopar and H. Philip (1983). Stress state inferred from multiple focal mechanisms. Ann. Geophys., **1**, 291-298.

[9] Michael A.J. (1987). Use of focal mechanisms to determine stress: a control study. J. Geophys. Res., **92**, 357-368.

[10] Gephart J.W. (1990). Stress and the direction of slip on fault planes. Tectonics, **4**, 845-858.

[11] Rivera L. and A. Cisternas (1990). Stress tensor and fault plane solutions for a population of earthquakes. Bull. Seism. Soc. Am., **80**, 600-614.

[12] Ansell J., W. Aspinall, G. King and R. Westaway (1986). The 1984 July 19 North Wales earthquake - a lower crustal continental event indicating brittle behaviour at an unusual depth. Geophys. J. R. astr. Soc., **84**, 201-206.

[13] Blenkinsop T.G., R.E. Long, N.J. Kusznir and M.J. Smith (1986). Seismicity and tectonics in Wales. J. Geol. Soc. London, **143**, 327-334.

[14] Trodd H., P. Warburton and C.I. Pooley (1985). The great British earthquake of 1984 seen from afar. Geophys. J. R. astr. Soc., **83**, 809-812.

[15] Turbitt T., E.J. Barker, C.W.A. Browitt, M. Howells, P.C. Marrow, R.M.W. Musson, R.H. Newmark, D.W. Redmayne, A.B. Walker, A.W.B. Jacob, E. Ryan and V. Ward (1985). The North Wales earthquake of 19 July 1984. J. Geol. Soc. London, **142**, 567-571.

[16] Snoke J.A., J.W. Munsey, A.G. Teague and G.A. Bollinger (1984). A program for focal mechanism determination by combined use of polarity and Sv-P amplitude ratio data. Earthquake Notes, **55**, 15.

[17] Mastin L., B. Muller and M.L. Zoback (1989). World stress map. Eos, Trans. AGU, **70**, 1520-1521.

[18] Principia Mechanica Ltd. (1986). PRISK Manual, Report for CEGB, London, UK.

[19] Seismic Hazard Working Party (1988). A Review of Seismic Hazard Assessment Methods and their Adaptation for Britain, Vol. 3M of Report on Seismic Hazard Assessment, CEGB, Barnwood, Gloucester, UK.

@seismicisolation

THE LUZON, PHILIPPINES EARTHQUAKE OF 16 JULY 1990

E.D. BOOTH[1], A.M. CHANDLER[2], P.K.C. WONG[3] & A.W. COBURN[4]

ABSTRACT

On 16th July 1990, a major earthquake struck the centre of Luzon, the largest and most developed of the Philippine Islands. The official statistics indicate that 1,200 people died, a further 1,000 are reported missing, 2,700 people were injured and 120,000 were rendered homeless. The earthquake caused widespread damage to engineered and non-engineered structures and gave rise to both extensive liquefaction and a major surface fault break. This paper briefly summarises the findings of an EEFIT team which visited the Philippines soon after the earthquake. More details are given in the team's full report (1).

INTRODUCTION

The UK based Earthquake Engineering Field Investigation Team EEFIT was formed in 1982. Its principal activity (2) is conducting field investigations of damaging earthquakes, in order to report back to the engineering community the lessons to be learnt. Its members are engineers from both academic and industrial backgrounds. EEFIT investigated nine earthquakes in the period 1983 to 1991 and reports have been published or are in preparation for all these events.

The Philippines earthquake was of particular interest. Not only had engineered buildings been damaged in a country which has adopted the main seismic provisions of the US Building Code of Practice UBC (3) but there were also reports of widespread liquefaction and a major surface fault break. Therefore, two weeks after the earthquake, a three man EEFIT team, comprising the first three authors of this paper, travelled to the Philippines and spent 9 days in the country. During that time they travelled through a representative number of sites in the epicentral area, carrying out visual inspections, photographic surveys and discussions with local engineers and others. In November 1990, the fourth author, A.Coburn, visited the Philippines as part of a United Nations reconstruction team (4).

1] Ove Arup & Partners, London 2] University College, London
3] Ove Arup & Partners, Hong Kong 4] CAR Ltd, Cambridge, UK

@seismicisolation

SEISMOLOGICAL FEATURES

The earthquake was located on the highly active subduction zone between the Eurasian and Philippine plates. It occurred at 16:26 local time on 16.7.90 and ruptured part of the Philippines fault, east of Cabanatuan (Figure 1). It was of magnitude M_s = 7.8 at shallow depth. Surface faulting along at least 100km was recorded on clearly defined geological features. Up to 6m of left lateral movement and 1m of vertical movement was recorded at the surface, the upthrow side being to the east. 15 aftershocks of magnitude 5 to 6 were recorded within the first two days of the earthquake.

DIRECT EFFECTS OF STRONG GROUND MOTION ON STRUCTURES

As described in subsequent sections, the consequences of liquefaction, slope instability and the surface fault break caused at least as much damage as the direct effects of ground vibration. Nevertheless, strong ground motion produced devastation in parts of the epicentral area, particularly the major city of Baguio. However, since there were no strong motion recordings, the amplitude of motions must be inferred approximately from other data.

Throughout Baguio and other towns and cities visited, the majority of engineered structures consisted of reinforced concrete moment-resisting frames, usually with blockwork infill. Newer structures occasionally included shear walls for resisting earthquake loads.

Strong ground motion effects at Baguio

Baguio City, a popular vacation resort with a permanent population of about 200,000, is situated about 270 km north of Manila in the Cordillera Central mountains (Figure 1) and is about 30 km from the main fault break. It is a major mining area, with several gold and copper mines in current operation, and is also a centre for light industry. Baguio is at an altitude of about 1500m and is surrounded by very hilly terrain. As a result of the prominent role which Baguio plays in the tourist economy of the Philippines, together with the fact that most of the better hotels were severely damaged in the earthquake, the Philippines government estimated that there would be a 15 to 20 per cent drop in tourist revenue for the country in 1991.

The earthquake caused severe structural damage to at least 20 modern engineered buildings in Baguio, and resulted in the collapse of a number of medium-rise modern reinforced concrete buildings. The collapsed buildings, which were mainly hotel and educational establishments, were founded on weathered rock, often on steep slopes. The percentage of low-rise buildings affected was much lower. This is illustrated by the results of an indicative but non-comprehensive survey carried out by EEFIT in the central part of Baguio. This indicated that the percentage of buildings of four or more storeys suffering major damage or collapse was 40% percent, compared with under 5% percent in low rise buildings.

Although signs of ground failure were observed around many of the damaged buildings, in EEFIT's opinion these were not the primary cause of structural failure in most instances. It is expected that other more detailed surveys will confirm this and will support the conclusion that had the buildings conformed to the current requirements of UBC, which is effectively the governing code of practice for earthquakes in the Philippines, the scale of

@seismicisolation

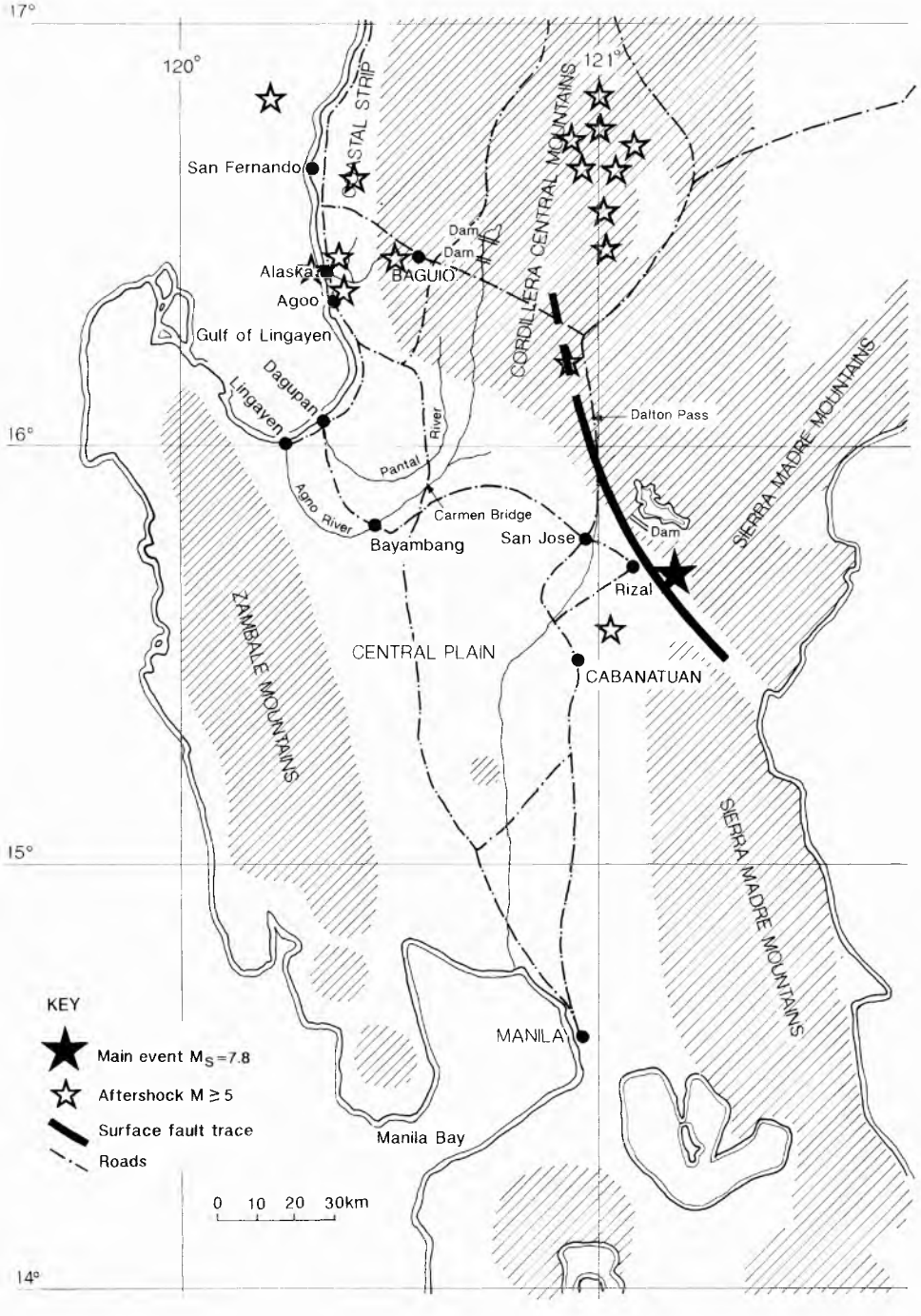

Figure 1. Map of epicentral area

@seismicisolation

the damage would have been very greatly reduced. EEFIT's finding was that the scale of damage in Baguio can be attributed primarily to well understood defects in conceptual and detailed design, and in quality of construction, as further detailed in Conclusion 1 at the end of this paper.

Nevertheless, it is clear that intense ground motions did occur at Baguio and, from the height of buildings affected, it appears that they were predominantly of medium to long period. The fact that steep slopes exist at Baguio rules out the presence of deep soft soil deposits such as caused long period amplification of motions at Mexico City in 1985 (5) and around San Francisco Bay in 1989 (6). Other reasons for the possible amplification must therefore be sought. The lack of strong motion instruments at Baguio makes it difficult to postulate a solution. It may be speculated that topographical effects played a part, whereby the steep hills in the town acted as local resonators amplifying certain frequencies. In Baguio, the Hyatt Terraces Hotel (Figure 2) was near a ridge, but other collapsed buildings were on the sides or near the bottom of slopes. If topographical effects were influential at Baguio, they appear to have been complex. It is important to study them further, since they have implications not just for future construction in Baguio, but also in similar mountainous terrain elsewhere. The first step would be to establish a strong motion instrument network in and around Baguio to record response to the minor earthquakes that may be expected in the near future.

Strong ground motion effects at Agoo

Agoo lies on the main highway running along the west coast of northern Luzon (Figure 1). It is situated about 2 km inland, and has an estimated 20,000 inhabitants. Most of the buildings are one or two storeys high, and there was extensive damage to these low-rise buildings, which had a much greater percentage of serious damage than was the case for similar buildings in Baguio. The buildings affected included simple concrete structures of poor quality, masonry buildings and single storey steel frame classrooms with masonry infill walls. The tallest structure standing was the cathedral, a building at least 50 years old and possibly much older. This had suffered some damage, and another one was reported to have collapsed. In Agoo itself, there was no sign of liquefaction or foundation movement, despite being built on flat (almost certainly alluvial) ground with a high water table, close to areas which had liquefied. Shallow deposits of soil overlying rock, which may well have been present in Agoo, are known to amplify the underlying rock motions by factors up to 5 at short periods (7). It can be postulated that this occurred in Agoo, but that conditions were not such that liquefaction took place.

Strong ground motion effects at Cabanatuan

Cabanatuan is a sizeable town of around 80,000 inhabitants on a very flat area in the Central Plain (Figure 1). The main buildings are single or two storey houses, shops or workshops of reasonable quality, mainly in masonry. There was one catastrophic collapse of a 6-storey reinforced concrete frame building. This was part of the Christian College of the Philippines. It was reported that the upper storeys were added after the original construction. Surrounding concrete frame buildings of similar height which formed part of the College appeared completely undamaged. The library building of the Central Luzon State University was also reported to have suffered partial collapse, but there were few other signs of damage, let alone collapse,

@seismicisolation

elsewhere in the town which appeared to be busy and operating normally.

Structural Damage in Manila

The earthquake was strongly felt in Manila, which lies 100 km from the causative fault, but there was little structural damage and a tentative intensity V was assigned by EEFIT. Calculations by EEFIT (1) suggest that motions during the event were less than 30% of code design values, even allowing for the deep alluvial deposits which are present in parts of Manila. The lack of a strong motion recording referred to previously make this an approximate figure. Nevertheless, there is little doubt that the intensity of the motion was substantially less than that envisaged by the Code.

This earthquake was not therefore the most onerous test of buildings in Manila, which suffered much more devastating events in 1645 and 1863 and will at an unknown but inevitable date in the future be subjected to much more severe shaking than that experienced in 1990. There are well founded concerns that some of the construction in Manila is of the same inappropriate standard as that of the buildings that collapsed in Baguio; any such substandard buildings would be bound to suffer a similar fate unless appropriate strengthening measures are taken.

Structural damage elsewhere in the northern Central Plain

There were few signs of damage due to strong ground motion in the other parts of the Central Plain visited by the EEFIT team, although as reported below, liquefaction and other ground failure effects were more widespread. A tentative MSK intensity of VI was assigned by EEFIT, based on ground vibration damage to low rise buildings.

LIQUEFACTION PHENOMENA

Widespread liquefaction occurred in the north of the Central Plain, which is a very flat area with a number of major rivers which drain the Central Cordillera mountains to the north. The coastal strip to the west of the Central Cordillera also suffered extensive liquefaction accompanied by settlements of up to 1m. The alluvial materials deposited by the rivers in these areas would be expected to create liquefiable soils. Liquefaction was found up to 60km from the source zone which is in agreement with what Ambraseys (8) reports would be expected for this size of event.

Dagupan, a low lying town with a population of 120,000 situated to the north of the Central Plain on the Gulf of Lingayen (Figure 1) was the worst affected city. The central area liquefied extensively, causing roads to break up, buildings to settle and tilt (Figure 3), underground services to be disrupted and a major bridge crossing the Pantal River to fail (Figure 4).

Elsewhere on the Central Plain, the EEFIT team inspected four major bridges which were either impassable or in a dangerous condition as a result of liquefaction induced settlements. Overall the effect of liquefaction and landslides on the road network is likely to prove the most damaging feature of the earthquake.

The EEFIT team visited the site of a small village called Alaska, (Figure 1) on the mouth of a large river flowing west into the sea from the Cordillera

@seismicisolation

Figure 2 Hyatt Terraces Hotel, Baguio

Figure 3 Liquefaction settlement, Dagupan

Figure 4 Magsaysay Bridge, Dagupan

Figure 5 Landslide on Dalton Pass

Figure 6 Bridge at Rizal destroyed by fault movement

@seismicisolation

Central mountains. The village was built on low lying ground and had been destroyed by the earthquake. Moreover, the land had settled by around a metre and sea water had flowed into the surrounding farmlands. There were many liquefaction blowholes to be seen in the area.

SLOPE STABILITY FAILURES

A large number of landslides were triggered by the earthquake in the steep slopes of the Cordillera Central mountains to the north of the Central Plain (Figure 1) and heavy rains in the days following the earthquake caused further slides. It is estimated (4) that in some areas 10% of the topsoil was lost at the time of the earthquake and a further 30% in the following days.

Many buildings were rendered uninhabitable by landslides and rock falls but the extent of the damage may have been lessened by the fact that slope failures are a frequent occurrence in the mountains, even without earthquakes and the most unstable locations have been avoided as a result of previous experience.

The major impact of slope failure is likely to be associated with the disruption caused to the road network. All four access roads to the city of Baguio were blocked after the earthquake; one was reopened to restricted traffic after 3 days but the others took many weeks to clear. The Dalton Pass (Figure 1) carrying the main highway to northern Luzon through the Cordillera Central Mountains, was also blocked by numerous slides (Figure 5).

Three major rockfill dams are in the epicentral area. They were reported to have survived the earthquake with only minor surface cracking and the associated hydroelectric facilities continued to operate.

EFFECTS OF FAULT MOVEMENT

As reported previously, there was a major surface fault. This further disrupted the road through the Dalton Pass. It also passed through the centre of Rizal, a town of about 20,000 inhabitants consisting almost entirely of non-engineered timber and masonry low rise buildings. Buildings straddling the fault generally (though not exclusively) collapsed and there was some damage to buildings immediately to either side. The surprising feature was that even around the fault the intensity was only an estimated MSK VII. Elsewhere in Rizal, the damage was very isolated; life was continuing normally and no-one had been killed by the event, although there were a few minor injuries.

A single span concrete bridge straddling the fault just north of Rizal had been destroyed by the fault movement (Figure 6) but an identical bridge 1km away which was 80m from the fault trace was totally undamaged.

EFFECTS ON SERVICES

Electricity and telephone services survived the earthquake well and were in operation in all the towns visited by EEFIT two weeks after the earthquake. Water supplies were worse affected; Dagupan and Baguio (Figure 1) still had areas which were unsupplied during EEFIT's visit.

@seismicisolation

ECONOMIC LOSSES AND CONSEQUENCES

Property losses to all the hotels, houses, commercial establishments and agricultural installations are estimated to have exceeded 15 billion pesos (US$550 million), but the estimated cost of reconstruction and associated development will be more than three times that at 45 billion pesos (US$1.5 billion).

Physical damage was generally confined to localised pockets, except in highland areas of Benguet and Nueva Vizcaya, where it was extensive. The nation's capital, Manila, although badly shaken, suffered only light damage.

The destruction caused by the earthquake is having serious repercussions on the lives and economic activities of not only the population of the earthquake-affected areas but of Filipinos in general. The disruption of transportation services by the earthquake has had major impact on the Philippine economy. It has choked the flow of goods and supplies for farmers and manufacturers and has cut the agricultural and industrial areas in northern Luzon from their major markets in southern Luzon. As a result, people who barely noticed the seismic event have felt their standard of living decline in its aftermath. The earthquake has increased food prices, unemployment and pressure on the national balance of payments.

The economic losses caused by the earthquake to the production sector far exceeded the cost of repairing the physical damage. The biggest impact of the earthquake came in the form of displaced labour and foregone revenues and opportunities. Labour displacement in industry, trade and tourism has been estimated at 30,000 jobs, a proportion of which may be permanent as a result of reduced economic activities and reduced consumer spending (9).

CONCLUSIONS

The following conclusions were reached by the EEFIT team and are further justified in their report (1).

1. The causes of life threatening failure in the buildings studied by EEFIT appeared in all cases to be due to well understood deficiencies in design and construction. In particular, these were:

   i) Inadequate provision of confining steel and other defects in reinforcement detailing.

   ii) Inappropriate structural forms, particularly soft storeys and plan eccentricities.

   iii) Poor detailing of infill blockwork leading to unintended soft storeys and torsional eccentricities and to dangerous 'short columns' above the tops of partial height blockwalls.

2. The defects noted above are well treated in current codes of practice, including the Philippine code NSCP and the US code UBC:88. No major shortcomings in those codes were revealed by the earthquake for the types of building in the earthquake area. The most urgent need is therefore not to improve the codes themselves, but to improve understanding of them and to ensure that they are enforced.

@seismicisolation

3. These defects are considered to have been the major cause of building damage in Baguio and ground failure appears to have played only a minor role there. Nevertheless, it appears that intense, medium to long period motions were present at Baguio and that short period motions were of relatively lower intensity. The reasons for this are not clear and are certainly different from the site effects associated with deep soft soils, for example in Mexico City and San Francisco Bay. It may be that the steep topography of the area caused these apparent local amplification effects. This area is scarcely discussed by current codes of practice and needs study.

4. One of the major effects of the earthquake was disruption to the road network. This was not directly due to the effects of strong ground shaking causing structural damage, but to the secondary effects of landslide, liquefaction and fault movement.

5. The extent of liquefaction in the earthquake was predictable and is likely to occur again in the Philippines. The liquefaction resulted in bridge and building failures due to gross foundation movements and also disrupted underground services. Measures to assess liquefaction potential and to counter its effects are well covered in the literature, although they are not directly discussed in current Philippine or US codes.

6. The importance of landslides, liquefaction and fault movements in this event emphasises the need for proper geotechnical advice for major projects in earthquake country, which includes the whole of the Philippines.

7. The general lack of damage in Metro Manila in the 1990 earthquake is no guarantee of good performance in future earthquakes, because it is likely that the 1990 intensity of shaking will be considerably exceeded in the lifetime of the current building stock.

ACKNOWLEDGEMENTS

E.Booth and P.Wong were funded by their company, Ove Arup & Partners, A.Chandler was funded by the British Government through the SERC and A.Coburn was funded by the United Nations UNCHS. The support of these organisations is gratefully acknowledged. The views expressed in the paper are the personal views of the authors.

REFERENCES

(1) The Luzon Philippines earthquake of 16 July 1990: A field report by EEFIT. EEFIT, Institution of Structural Engineers, 11 Upper Belgrave Street, London SW1X 3BH.

(2) EEFIT Aims and Methods booklet. Available free from the Institution of Structural Engineers, London.

(3) UBC: Uniform Building Code Chapter 2312: Earthquake Provisions. ICBO, Whittier, California.

@seismicisolation

(4) Armillas I, Petrovski J, Coburn A.W, Corpuz A, Lewis D. Technical Report on Luzon Earthquake of 16 July 1990. United Nations Centre for Human Settlements, Nairobi, December 1990.

(5) EEFIT. The Mexican earthquake of 19 September 1985. SECED, Institution of Civil Engineers, London, 1986.

(6) EEFIT. The Loma Prieta earthquake of 17 October 1989. A field report by EEFIT. Inst. Structural Engineers, London 1991.

(7) Henderson P. et al. Site response effects for structures located on sand sites. Canadian Geotech Jnl, Vol 27 June 1990.

(8) Ambraseys N.N. Engineering Seismology. The first Mallet-Milne lecture. Earth.Engg.Struct.Dyn. Vol 17 No 1, September 1988.

(9) Reconstruction and Development Program following the earthquake of 16.7.90. NEDA, Republic of the Philippines, 1990.

@seismicisolation

INVESTIGATION OF THE VALIDITY OF EQUIVALENT LINEARIZATION of NON-LINEAR MATERIAL PROPERTIES

By

Dr. S.K. Sarma [1]
Miss K. Breitwieser [2]

ABSTRACT

Non-linear material properties are often represented by equivalent linear ones and are used in the analysis of response of structures and soils subjected to earthquake loads. The paper looks at the validity of this approach of analysis in connection with soils by comparing response obtained from non-linear ones with that from equivalent ones. Only a single degree of freedom system is used for this comparison.

Introduction:

The stress-strain behaviour of most material shows non-linear inelastic nature. Some materials may be conveniently treated as linear, elastic with a high degree of accuracy while some others, particularly soils, show non-linear behaviour even for very small strain. On the other hand, for dynamic problems, the non-linear inelastic analysis is time consuming and the so called accuracy achieved by such non-linear analysis may not be accurate in reality due to the very variable nature of material properties. While an elastic material needs only two parameters i.e. the elastic modulus and the damping capacity, a non-linear material may need several parameters to define its properties. It is therefore a matter of convenience to use equivalent linear visco-elastic properties, instead of non-linear inelastic ones for dynamic analysis. It is immediately realised that the response obtained from such an analysis can never be the same as the real response of the system. The aim of this investigation is to study and compare response obtained from an equivalent linear system with that of a non-linear inelastic one. The material to be used is soil.

[1] Civil Engineering Department, Imperial College, London SW7 2BU
[2] Formerly, M.Sc Student, Imperial College, London SW7 2BU

@seismicisolation

In order to define an equivalent visco-elastic linear soil properties, two parameters need to be assessed:

i) an equivalent modulus, usually the shear modulus of the material to resist deformation.

ii) an equivalent viscous damping factor, to account for the dissipation of energy from the vibrating system.

It must be realised at the very outset that these parameters are not the constitutive properties of the material but merely an effect of the visco-elastic interpretation of the real behaviour.

Non-linear material properties of soils:

Soil exhibits nonlinear material properties even at very small strain and yielding at large strain is a well known phenomenon. On reversal of loading, even after yielding, the soil shows strength which is similar to the original material except when it is saturated. Saturated soil may show strength degradation due to cyclic nature of earthquake loading. There are also soils, which shows loss of strength with large strain. Such degrading material is outside the scope of the present discussion. We only consider those materials which show very ductile property without loss of strength. Many researchers have defined the non-linear stress strain properties of soils such as by hyperbolic stress-strain relationship, Duncan and Chang(1970), Hardin and Drnevich(1972), Ramberg and Osgood(1943) or by mechanical models, Iwan (1967) or by curve-fitting the stress-strain relationship. Iwan model appears to be a very convenient approximation and this generally obeys the Masing(1926) rules. Other, more complex soil models are available as well but the number of parameters increases with complexity, making it difficult to find an equivalent physical meaning. The references given above are merely examples and do not constitute a full bibliography.

Modulus and damping in soils:

The mechanism of energy dissipation in a soil mass is influenced by many parameters, see for example, Hardin and Drenvich (1972). It is generally agreed that this mechanism is of hystetretic nature and not viscous. Hysteretic nature implies different loading and

@seismicisolation

unloading stress–strain behaviour. Such behaviour is usually associated with dry friction; it is influenced by the magnitude of the induced strain and not by the strain rate and therefore not by the frequency of loading, Wilson(1985), Hardin and Black (1966). A truly hysteretic material would give the same stress – strain relationship, whether in static or in dynamic tests. However, soil does show some strain rate effect (a viscous component) at very small strains but it is negligible and can generally be ignored. The amount of energy which is lost during vibration due to a full cycle of loading and unloading is represented by the area enclosed by the "hysteresis" loop and is dependent on the strain level.

In a non-linear inelastic material, such as soil, there is no real elastic modulus except perhaps at very low strains. However, during a full cycle of loading and unloading, statically, to a certain strain level (strain controlled tests), a modulus can be defined as the ratio of the stress and the strain at that strain level. This is termed as the secant modulus. The modulus therefore varies with the strain level.

Thus, from a strain controlled loading and unloading tests, it is possible to define a modulus (secant) and compute an area of "hysteresis loop" as a function of the strain level, figure 1. This has been done by many researchers, the most commonly known of these are Seed and Idriss(1970), Hardin and Drenevich(1972), Sun, Golesorkhi and Seed (1988).

Equivalent linear modulus and viscous damping:

The concept of equivalent linearization is developed in order to be able to obtain the response of a non-linear system in an approximate manner. We shall consider a Single Degree of Freedom (SDF) system to check the validity of this approximation. The SDF system consists of either a nonlinear spring or an elastic spring and a viscous dashpot. The system is subjected to a seismic ground acceleration $\ddot{x}(t)$

In the non-linear system, the equation of motion is defined by

$$m\ddot{u} + f(u) = -m\ddot{x} \qquad (1)$$

where f(u) is any function which expresses the non-linear spring behaviour.

@seismicisolation

In the case of the linear spring–dashpot system, the equation of motion is

$$m\ddot{u} + c\dot{u} + ku = -m\ddot{x} \qquad (2)$$

where $c\dot{u}$ = the resistance offered by the damper
and ku = the resistance offered by the spring.

The problem is to define the non-linear inelastic spring force f(u) of the real system by an equivalent hypothetical visco–elastic (spring–dashpot) system, so that approximate analysis can be performed.

Different approaches exist to find a suitable criterion to define the equivalent linear properties in terms of the real soil behaviour .

Jacobsen Approach:

The most popular criterion is based on the equivalence of energy being dissipated during one cycle in the real and in the linearized, hypothetical system. This concept was originally formulated by Jacobsen (1930).

In a hysteretic system the complete load reversal will reveal a loop in a plot of displacement versus resisting force. The same plot for a visco–elastic system would also yield a similar loop when the frequency of the forcing function is in resonance with the frequency of the SDF system.

When a linear visco–elastic system is excited with a harmonic force $[C\sin(\Omega t)]$, then at steady state vibration, the energy loss in a full cycle is given by $[\int c\dot{u}\, du]$ which is represented by the area of the loop. For a quarter of the same cycle, $[\int ku\, du]$ gives the maximum recoverable energy, which is represented by the area of the triangle. The ratio of the two relates to the damping capacity by the following relationship: (see figure 2)

$$\lambda = 1/4\pi\ (\Delta E/E)\ \omega/\Omega \qquad (3)$$

where

ΔE = Area inside the loop
E = Area inside the triangle
ω = The system frequency = $\sqrt{(k/m)}$
Ω = The forcing frequency
λ = Viscous damping coefficient as a fraction of the critical value.

@seismicisolation

Note that in a linear system

a) The maximum force $(c\hat{u} + ku)_{max}$ and the maximum displacement u_{max} do not occur at the same time.

b) In free vibration, the final displacement is always zero.

c) The energy loss depends on the frequency of the loading function.

d) A complete loop similar to the hysteresis one occurs when ω/Ω equals one.

In the non-linear system, we define the equivalent linear stiffness which corresponds to the secant modulus, as that which will produce the same maximum displacement u_{max}. Then corresponding to this stiffness, from the force displacement loop, λ can be calculated from equation (3) assuming that ω/Ω equals one. It is also possible to define equivalence in terms of maximum force i.e. $(c\hat{u}+ku)_{max}$.

Seed and Idriss (1970) has produced curves of equivalent normalised modulus and damping factors as a function of strain, which is shown in figure 3 . The curve is normalised to a s_u/p' ratio where s_u is the undrained strength. This curve refers to clayey soils. These curves are determined on the basis of equal maximum displacement.

Jacobsen, who originally suggested such an approach, describes E as " work area under the skeleton" which is different from the definition of E which is generally accepted now and used in the present discussion.

Hudson Approach:

Basically Hudson (1965) uses exactly the same approach as described above but, for the spring stiffness of the linearized system he takes the initial slope of the hysteresis curve.

By using the initial modulus and at the same time the condition of equal maximum displacement of both systems, the term in his equation, which corresponds to E in the previous approach, represents a bigger strain energy at maximum displacement. Therefore it results in a smaller equivalent damping ratio.

@seismicisolation
@seismicisolation

The equations for λ_{eq} in his paper are only valid for the case of the excitation frequency being equal to ω of the linearized system, which in his approach corresponds to the square root of the initial spring stiffness of the hysteretic system.

Kryloff & Bogoliuboff-type of Approach:

Kryloff and Bogoliuboff approached the problem from a rather different point of view. They replaced the equation for the nonlinear system:

$$m\,\ddot{u} + k\,u + f(u,\dot{u}) = 0$$

by a linear equation:

$$m\,\ddot{u} + \bar{c}\,\dot{u} + \bar{k}\,u = 0$$

with

$\bar{c}$ & $\bar{k}$ ....equivalent coefficients

$\bar{c}$ and $\bar{k}$ are chosen so that the solution of the linear equation is an approximate solution of the nonlinear equation . An equivalent linear damping coefficient as well as an equivalent spring constant is determined for every time step. However, this method is not a convenient one.

Steady State Response:

Considering a harmonic forcing function $C\sin(\Omega t)$, the resulting displacement response of the linearized, **visco-elastic system** will be harmonic with the period $2\pi/\Omega$ in the steady state.

The maximum value of the steady state response u_{max} at resonant frequency is given by

$$u_{max} = C/(2\lambda\Omega^2) \qquad (4)$$

Similarly, at resonance, the maximum inertia acceleration which relates to the maximum force is given by

$$u_{abs} = C\,\sqrt{(1+4\lambda^2)}/2\lambda \qquad (5)$$

@seismicisolation

Thus, for a linearized system, assuming a value for u_{max}, we can select the stiffness and therefore the frequency of the input (resonance) and the corresponding λ. Equation (4) will give the required amplitude of the input motion. Similarly, assuming a value for the maximum $\ddot{u}_{abs}$, we can select a stiffness and damping and obtain the required amplitude of the ground motion. The same input can then be used for the non-linear analysis for comparison.

Response of the non-linear system:

A hysteretic stress- strain curve is shown in figure 4. This curve is derived from the Seed and Idriss(1970) curve, fig 3, for an s_u/p' ratio of 0.2 and Iwan(1967) model is used to describe its piece-wise linear behaviour in loading and unloading. From this model, the damping versus strain model is derived, which is somewhat different from the Seed and Idriss curve. In the linearized analysis, these computed damping values are used.

Comparison of results:

Comparison of results from linear and non-linear analysis with resonant harmonic input (4 cycles) showed that the maximum displacement is similar but the non-linear one carries a plastic non-recoverable element which is expected. The dissipated energy is comparable but it is about 30% bigger in the case of the linear one which is surprising. The maximum inertia load in the case of the equivalent linear system is also about 30% bigger than the non-linear one. It is obvious that with large number of input cycles, the difference in the maximum displacement may also increase considerably.

However, seismic input is hardly likely to be in resonance with the equivalent linear system and it is therefore of interest to compare results when the input is not in resonance. For this, we have selected 4 cycles of harmonic input with maximum acceleration of 1.0g and of period 0.3 sec. Also the longitudinal component of the Koyna earthquake record is chosen for the analysis which has a maximum acceleration of 0.63g and is predominantly of very high frequency.

Figure 5 shows the response of the equivalent linearized system subjected to the harmonic input and figure 6 shows results for the earthquake input.

@seismicisolation
@seismicisolation

Results show that

1) The non-linear system may produce much larger displacement than the linear system. The displacement time histories of the two systems do not match at all which is not surprising. The linear system produces larger inertia force compared to the non-linear one.

2. At the end of the input motion, the non-linear system may show large plastic yielding as a final displacement while the linearized system shows no final displacement.

3. The curve of the work energy $[\int(c\hat{u}+ku)du]$ versus time shows the energy dissipation as a function of time. Surprising result is that the dissipated energy in the equivalent linear system is larger than the nonlinear one.

4. For the harmonic input, which is not in resonance with the linear structure, the maximum response in the linear system may occur during the transient stage.

CONCLUSIONS

The response obtained from equivalent linear system is reasonable provided that the excursion into the plastic domain is not very large. When the equivalence is based on the maximum displacement, the maximum force is higher than the non-linear ones. The displacement in the non-linear response always contain a plastic element which is difficult to quantify.

An equivalent linear analysis should be treated with caution. While it is reasonable to perform such an analysis to gain an insight into the behaviour of material or structure during an earthquake, it is unreasonable to treat it as an exact equivalent. Therefore, to use such an analysis to obtain base-rock acceleration from a soil layer record or similar complicated process is not justified.

LIST OF REFERENCES

Duncan J.M., Chang C.Y. (1970) " Non linear analysis of stress and strain in soils" Jour. Soil Mech & Found. Div. ASCE 96, SM5, 1629-1653.

Hardin B.O., Black W.L. (1966) "Sand Stiffness Under Various Triaxial Stresses", ASCE SM2, vol 3.

Hardin B.O.,Drnevich V.P.(1972a) "Shear Modulus and Damping in Soils: Design Equations and Curves", ASCE, 98, SM7.

@seismicisolation

Hardin B.O., Drnevich V.P.(1972b) "Shear Modulus and Damping in Soils: Measurement and Parameter Effects", ASCE, 98, SM6.

Hudson D.E. (1965) "Equivalent Viscous Friction for Hysteretic Systems with Earthquake-like Excitation", Proceed. of 3rd World Conference of Earthquake Engineering, Vol II, New Zealand.

Iwan W.D. (1967) "On a class of models for the yielding behaviour of continuous and composite systems" Journal of Applied Mechanics, 34, E3, 612-617.

Jacobsen L.S. (1930) "Steady Forced Vibration as Influenced by Damping", ASME Transactions.

Kryloff N., Bogolinboff N. (1943) "Introduction to nonlinear mechanics" Princeton University Press, Princeton.

Masing G. (1926) "Eigenspannungen und verfestigung beism messing" Proc. 2nd Int. Cong. App. Mechanics., Zurich, 332-335

Ramberg W., Osgood W.R. (1943) "Description of stress strain curves by three parameters" Technical note no. 902, National Advisory Comm. for Aeronautics, Washington DC.

Seed H.B., Idriss I.M. (1970) "Shear Moduli and Damping Factors for Dynamic Response Analysis", EERC 70 -10

Wilson J.M.R., "The Dynamic Properties of Soil", M Phil dissertation, Engineering Department, Cambridge University, 1985

@seismicisolation

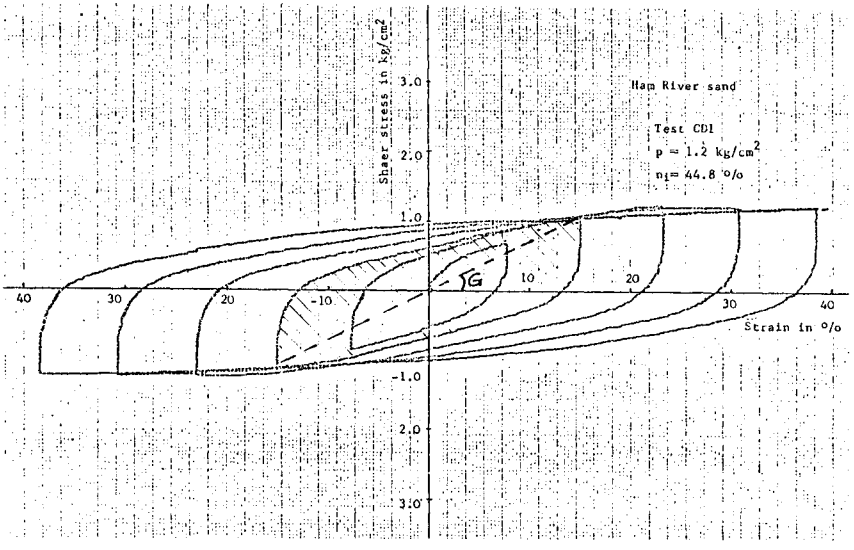

Figure 1 (G = Shear Modulus)

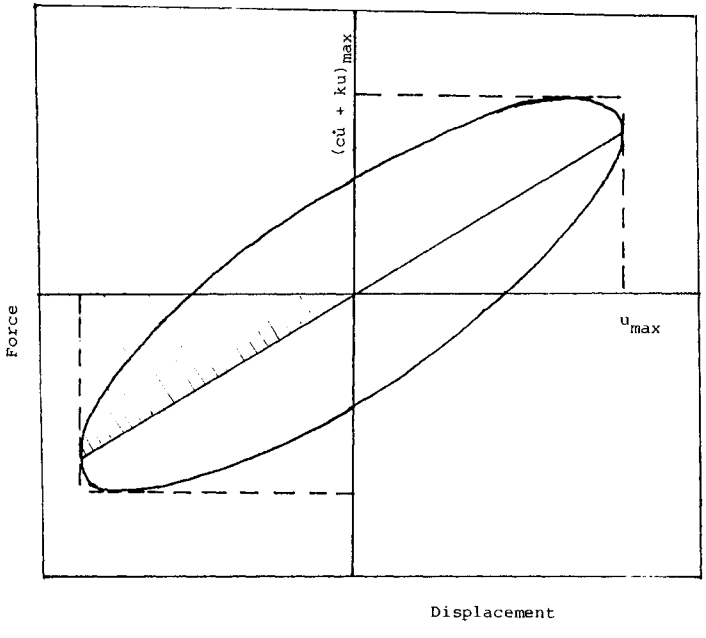

Figure 2 (Linear Analysis)

@seismicisolation

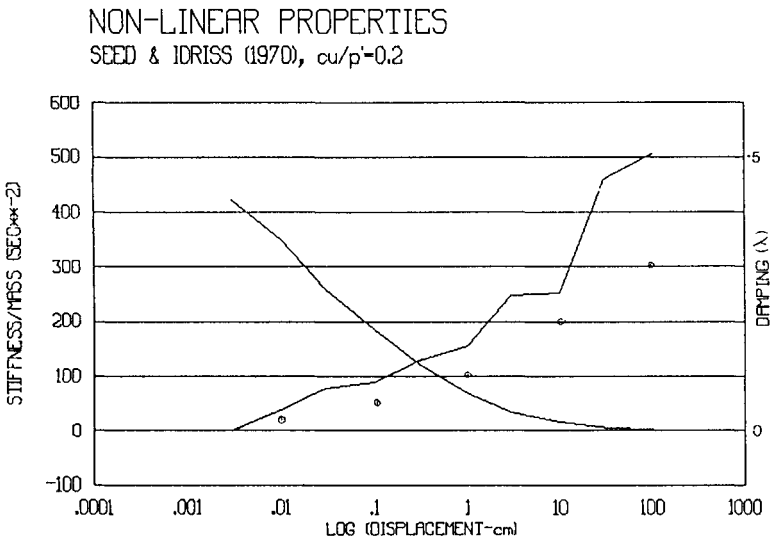

Figure 3 (Ø - Damping Values from Seed & Idriss (1970))
__ Computed damping values

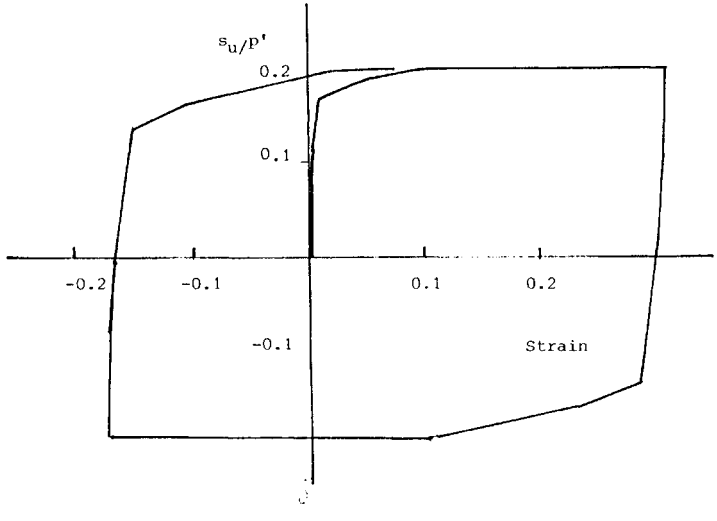

Figure 4 (Model of the Stress Strain Relationship)

@seismicisolation

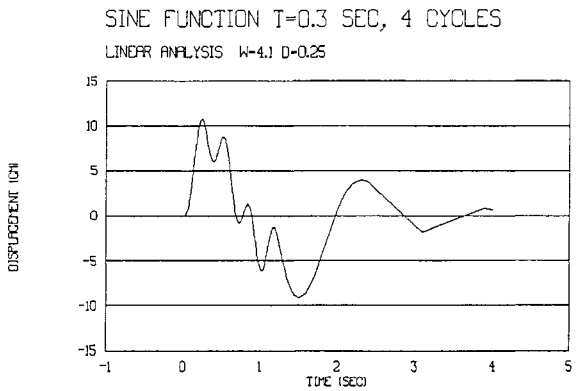

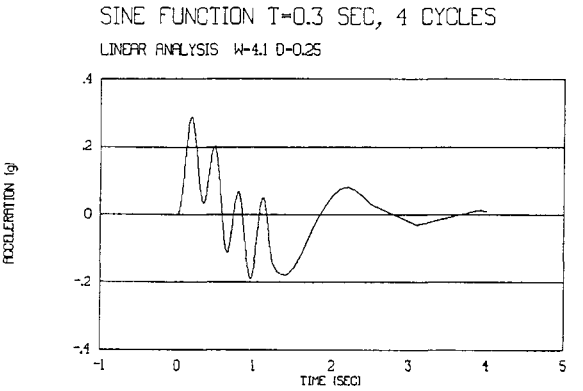

Figure 5a

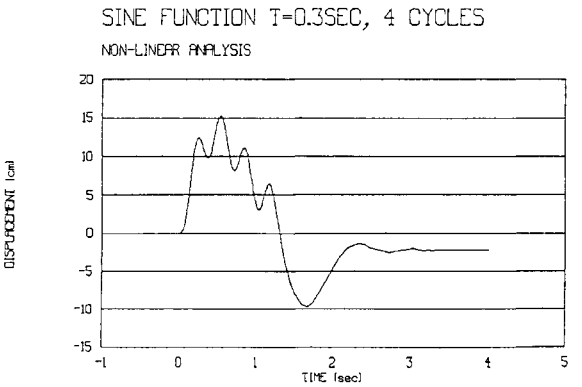

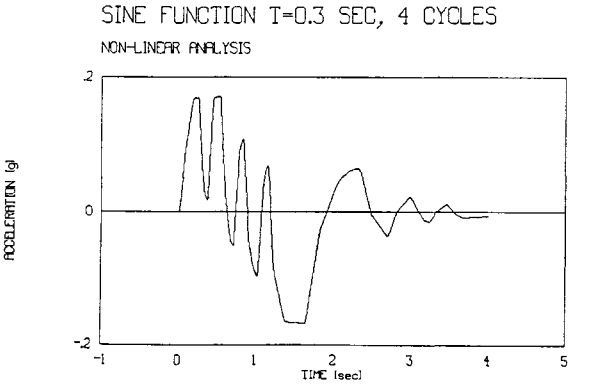

@seismicisolation

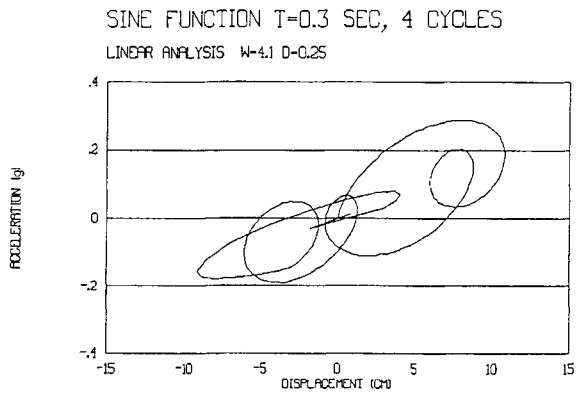

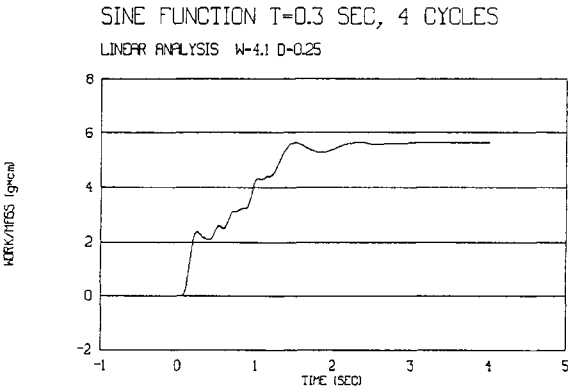

Figure 5b

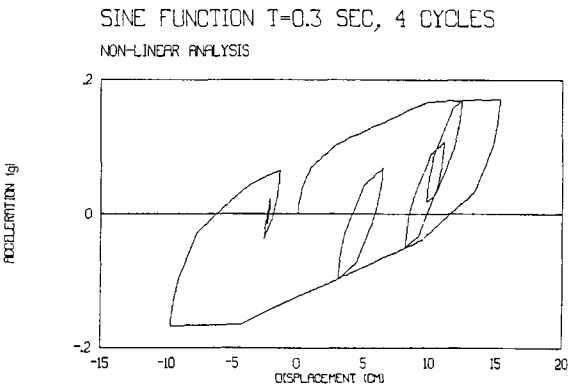

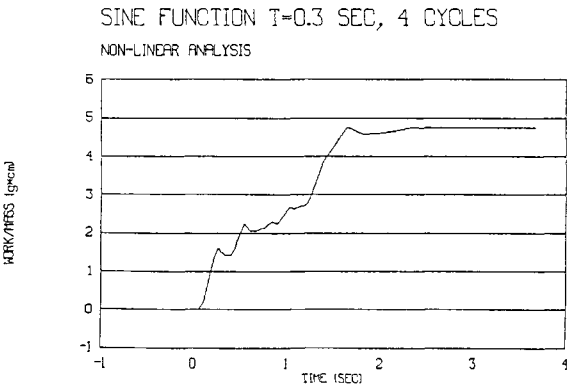

@seismicisolation

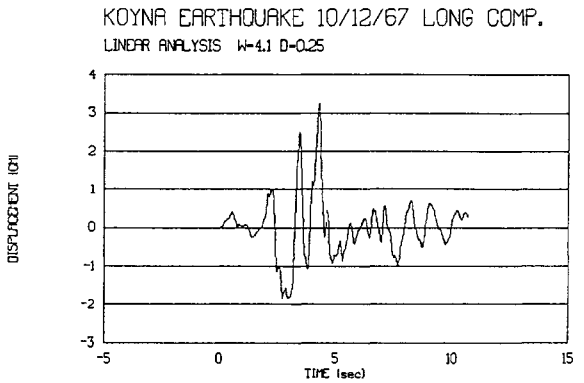

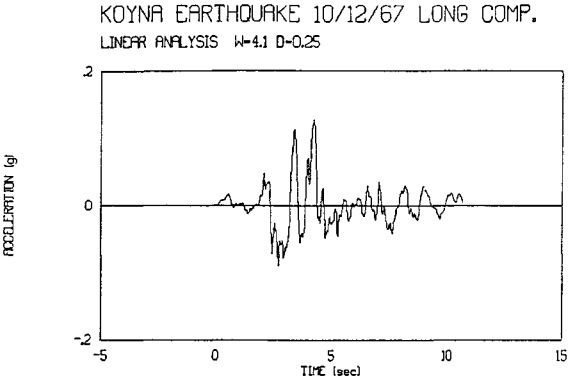

Figure 6a

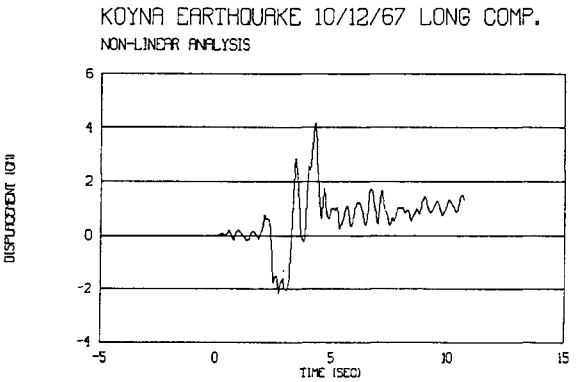

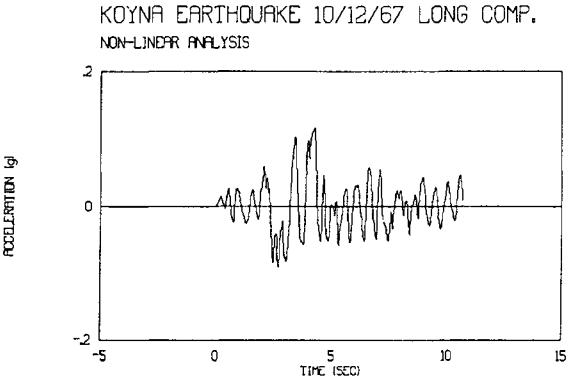

@seismicisolation
@seismicisolation

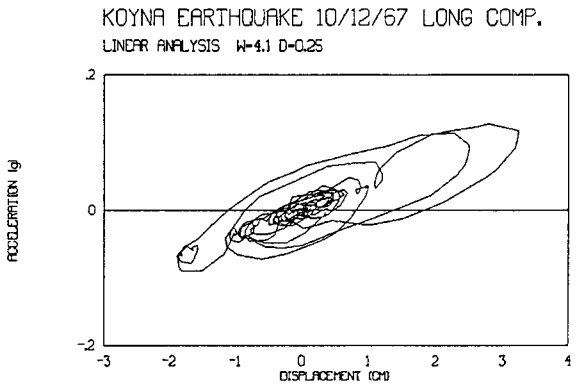

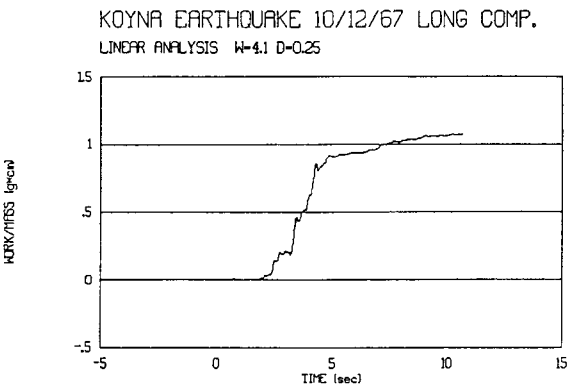

Figure 6b

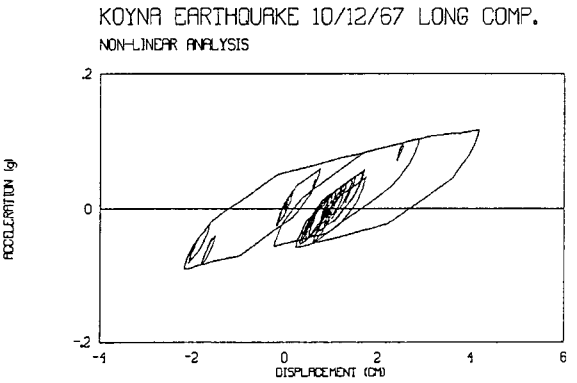

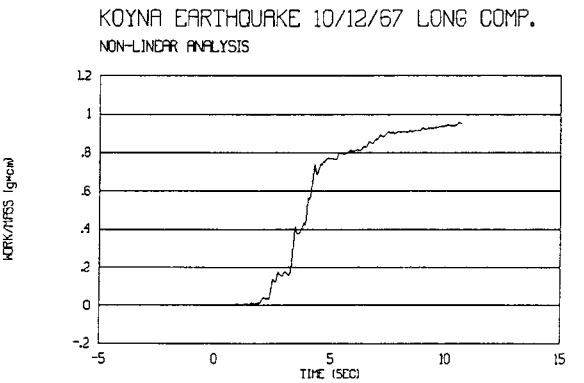

@seismicisolation

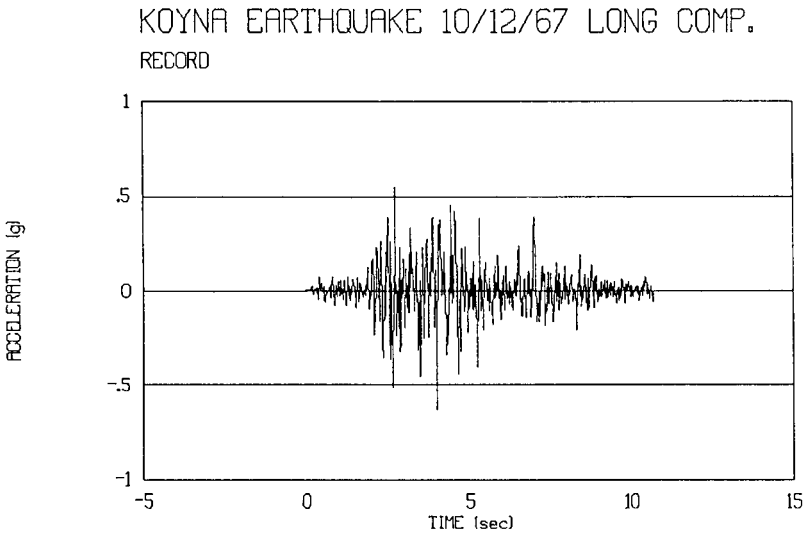

Figure 7

@seismicisolation

SEISMIC RESPONSE OF CONVENTIONAL POWER STATION STRUCTURES

D.B. Thompson, Director - Civil Engineering Division
Dr. M.M. Khabbazan, Principal Engineer
Dr. D.C. Mackay, Head of Special Structures Group
Dr. P.S. Fashole-Luke, Graduate Engineer
L G Mouchel & Partners Limited, UK

ABSTRACT

The dynamic response of a steel building composed of single and multi-storey spans, often used for the Main Building of a conventional power station, was studied using the modal response spectrum analysis approach. The effects of irregularities inherent in these buildings due to mass, stiffness and storey height were investigated using the structural properties of a typical power station Main Building proportioned for gravity loads as well as seismic loads. The seismic response of the building was also calculated approximately using the seismic provisions of the Uniform Building Code and the results compared with the dynamic analysis. The base shear and overturning moment due to the elastic response spectrum approach were found to be within the Code's static approach for most irregularities considered.

INTRODUCTION

The Main Building of a conventional power station usually consists of a single storey Turbine Hall, housing the principal generating plant, and multi-storey annexes on either one or both sides of the Turbine Hall depending on the plant layout. Typical transverse frames of such structures are shown in Figure 1. These buildings usually do not satisfy design code requirements for regularity of structural form and distribution of stiffness due to the combination of single and multi-storey spans and the variation in storey heights between the floors. In addition, the distribution of mass is irregular because of the positioning of plant.

Although Design Codes permit the use of an equivalent static lateral force procedure only when the building meets requirements for regularity, it is common practice to design conventional power station structures using such techniques. The nature and extent of any

@seismicisolation

approximations due to this approach have been investigated in this work.

A simplified structural analysis model of a power station Main Building composed of lumped nodal masses and beam elements has been analysed with seismic loading simulated by response spectra and equivalent lateral static forces, both recommended in the UBC. Dynamic analyses have been carried out for a number of irregular cases, which reflect vertical irregularities due to mass, storey-height and stiffness. The results of the analyses have been compared in order to identify the important characteristics of seismic response of this type of structure and to provide recommendations for the design of power station structures based on the equivalent static lateral force procedure.

Equivalent Static Force Approach

The static approach recommended in seismic codes applies, in general, to multi-storey buildings, which do not have severe irregularities in either plan or height. Power station structures are, however, a combination of multi-storey and single storey bays (Fig 1). In these cases the boiler house has been assumed to be a separate structure. As may be seen from Figure 1b, the two multi-storey annexes are linked together by means of a roof truss. The structure of Figure 1a, where only one multi-storey bay is linked to a column supporting the overhead travelling crane, is a less extreme example. Dynamic response of these structures depends on each individual multi-storey bay and the interaction between them. In the static approach, it is assumed simply that there is no interaction between the multi-storey bays and they will be excited with a frequency which can be obtained from a seismic code. Here, the seismic provisions of the UBC [1] have been used and its important features are highlighted as follows:

1) Fundamental period of vibration, T in seconds, of a steel structure may be approximated from:

$$T = 0.085\ (h)^{3/4} \qquad (1)$$

where h is the height of structure in metres above the base level.

2) Total design lateral force (base shear), V at the base is obtained from:

$$V = kw \qquad (2)$$

where w is the total seismic dead load (total dead load plus applicable portion of live loads), and k is obtained from:

$$k = \frac{ZIC}{R_w} \qquad (3)$$

where:

Z = the maximum effective peak ground acceleration, for this study = 0.3g

@seismicisolation

I	=	importance factor, for this study = 1.0
R_w	=	ductility factor, for this study = 6
C	=	representing spectral shape which is obtained from: $\frac{1.25S}{T^{2/3}}$ but $\not> 2.75$
S	=	site coefficient for soil characteristics, for rock site which is considered in this study = 1
T	=	period calculated from Eq (1)

3) Base shear V should then be distributed over the height of the structure in accordance with the following formula:

$$F_i = (V-F_t)\ \frac{W_i h_i}{\Sigma W_i h_i} \qquad (4)$$

where:

F_i	=	lateral force applied to level i
W_i	=	seismic dead load assigned to level i
h_i	=	height above the base to level i
F_t	=	$0.07TV \leqslant 0.25V$ if $T > 0.7$ second
F_t	=	0.0 if $T \leqslant 0.7$ second

F_t acts at the top level only.

4) Overturning moment at the base level may be obtained from:-

$$M = \Sigma F_i h_i \qquad (5)$$

where F_i and h_i are as defined above.

Dynamic Analysis

Modal response spectrum analysis has been carried out using the ANSYS program [2]. To provide a basis for comparison of dynamic analysis with the static approach, the standard spectra of the UBC corresponding to a rock site, which is also the basis of the equivalent static force procedure contained in the code, was used to represent the ground motion. The

@seismicisolation

spectrum shapes given in the UBC are a smoothed average of normalised 5% damped elastic response spectra. For consistency with the static approach, the spectrum shape for rock soil was scaled by $0.3/R_w$ for frequencies between 0.67 to 33 H_z.

The above ground excitation is used for both horizontal and vertical components of ground motion with identical peak amplitude. According to the code provisions, in calculating the total response of a structure, only those modes in which at least 90 per cent of the participating mass of the structure is included need be considered. A preliminary dynamic analysis of a typical multi-storey structure showed that the first five natural modes including horizontal and vertical modes would be sufficient to meet the code requirement.

The modal maxima have been combined using the Square Root of the Sum of the Squares (SRSS) method. This method provides a good estimate of maximum response for systems with well separated natural frequencies, because there is no significant coupling between their responses. In practice, when a natural frequency of a mode differs by less than 20% from the frequency of the next lower mode coupling between the modes is considered to occur. However, observation of results of the dynamic analyses in this study showed clearly that the natural frequencies due to different modes of vibration were not closely spaced.

Analytical Modelling

A power station Main Building is normally a structure with a uniform rectangular plan without setbacks. It contains parallel main frames in the transverse direction (Fig 1) which resist gravity loads as well as transverse wind or seismic loads, whilst bracing systems may be provided in all longitudinal axes to carry longitudinal loads. Diaphragm action is provided by slabs at floor levels of multi-storey annexes. The distribution of mass at each floor level is assumed to be uniform. In other words, the torsional effect due to asymmetry of mass is neglected.

Consequently, it is reasonable to assume that coupling between transverse and longitudinal modes of vibration will be insignificant. Two-dimensional lumped mass models of the structure in its transverse direction were therefore prepared to study its dynamic response.

Geometrical properties of the main frame are presented in Fig 2a, and the corresponding lumped mass dynamic model is shown in Fig 2b. The properties are typical of conventional power stations and were used to obtain results which would be of practical use.

The lateral stiffness of beam elements in Fig 2b, was determined from a preliminary static analysis of each separate multi-storey annexe of Fig 2a. These stiffnesses were determined so that the maximum horizontal displacement of each annexe with a horizontal point load applied at its top was equal to the displacement of its lumped mass model under the same load.

Only two degrees of freedom consisting of horizontal and vertical translations were allowed at each node of the model. No account was taken of the joint rotation as the inertia

@seismicisolation

effects associated with rotational motion of a joint is generally negligible. As the structure was assumed to be supported by rigid ground, no account of the influence of soil-structure interaction was required.

Effects of Irregularities

Likely irregularities inherent in this type of structure are, first physical discontinuity of the structure in plan at floor levels, and second vertical irregularities such as mass, stiffness and storey-height changes within multi-storey annexes. The effects of the second type of irregularity were investigated with each annexe treated as a separate structure and the results were then compared with those for the building as a whole.

In order to cover a wider range of annexes, three different types of multi-storey structure having 2, 5 and 7 storeys were studied. Each type was developed from a regular case having equal nodal lumped masses and equal storey heights with a constant value of lateral stiffness I, for all beam elements. The irregularities of mass, storey-height and lateral stiffness were then introduced.

Mass irregularity was investigated by assigning a single lumped mass of 2W to a particular floor while a mass of W was assigned to every other floor. The storey height and stiffness of beam elements as well as the sum of the nodal masses were unchanged. Dynamic and static analyses were performed with the heavier mass at each floor level in turn. The choice of a single mass of 2W as compared to equal masses of W, conforms with the limits on mass irregularity given in the UBC. An extreme case was also considered using a single mass of 6W assigned to a chosen storey. The selection of this storey was based on the most critical case of the mass irregularity.

The effect of storey height irregularity was studied in a similar fashion using a single storey height of 2h compared to h for the others. Lateral stiffness irregularity was considered by first assigning 2I to the first floor column and I to the others and then, assigning values 2I to the columns of the first two floors and I to the others, and so on.

Again, the extreme cases relating to 6I and 6h, although impractical were also studied. A comparison of the results for these extreme cases and the extreme case of mass irregularity (6W) showed that the mass irregularity is the case which normally governs. Fig 3 shows some examples of the irregular features described above. The first three fundamental mode shapes of a 5-storey building which are fairly typical for multi-storey buildings are presented in Fig 4.

The numerical results for these cases are presented graphically in Fig 5. The base shear and overturning moment ratios are plotted against frequency ratio, where the frequency ratio is the ratio of frequency due to the dynamic approach, f_d, to that of the static approach, f_s, and base shear and overturning moment ratios are defined in a similar fashion. The overturning moment has been assumed to reflect the effects of the structure's dynamic characteristics on the vertical distribution of lateral force. The fact that these buildings are of a usual configuration and normally do not incorporate severe setbacks justifies this assumption.

@seismicisolation

As may be seen from these Figures, with the exception of the extreme mass irregularity cases, which are denoted by solid squares, almost all other points are spread about the frequency ratio of unity. Also, most of the base shear ratios and overturning moment ratios are below 1 and almost always between 0.6 and 0.8. The base shear ratio and overturning moment ratio in each case are generally within the same order with the latter being almost always smaller than the former.

Combination of Various Annexes

In the above discussion, each multi-storey annexe was treated as a separate building. However in a power station Main Building, the two annexes are linked by means of a roof truss. Therefore, it was necessary to investigate the dynamic response of this structural form for a number of combinations of different multi-storey annexes. The roof truss, depending on its end support conditions may be modelled as a pin- or rigid-ended bar element. Roof trusses of Fig 1 were considered to be pin-ended bar elements.

To separate the influence of roof slope, the study was started with flat roof structures, and then continued with mono-pitched roof buildings with a slope of 7.5 degrees. In these examples, the right hand annexe always remained the same as the regular 5-storey building used in the previous analyses of individual annexes, while the left hand annexe was altered.

These structures have been analysed using both dynamic and static approaches and the results for flat and sloped roof type buildings are presented in Tables 1 and 2, respectively. In the static approach, the frequency of each structure was obtained from Eq (1) using the maximum height of the structure above the base level. The distribution of base shear between the annexes was carried out in proportion to their relative masses. The first six modes of vibration of the most regular case subject to horizontal and vertical excitations are illustrated in Fig 6. Inspection of the mode shapes of other irregular cases showed that they were similar to those of the regular case.

Discussion of Results

Graphic representations of Tables 1 and 2 are shown in Figs 7 and 8, respectively. As with Fig 5, the variation of base shear ratio and overturning moment ratio have been presented against frequency ratio. These ratios are seen to be mostly between 0.8 and 1.0 compared to 0.6 - 0.8 for individual multi-storey buildings. The base shear and overturning moment ratios for structures with sloped roofs are slightly closer to unity as compared with those for flat roofs, as the flat roof structures are more regular.

A comparison of results for multi-storey annexes, treated separately (Fig 5), and those for linked annexes (Figs 7 and 8), shows that greater values of base shear in both cases were calculated by the static approach. This difference was reduced by about 15% for linked annexes and was decreased further as the structure became more irregular.

In graphs of Figs 7 and 8, each multi-storey annexe has a uniform distribution of mass, stiffness and storey height. In practice, however, the distribution of some or all of these properties may be irregular and consequently the results may incorporate larger errors. These effects were studied earlier in terms of individual multi-storey structures and it was

@seismicisolation

TABLE 1
Dynamic responses of Main Building with Flat Roofs

STRUCTURE		$W_1 = W_2$, $I_1 = I_2$ (Series 1)		$W_1 = \frac{1}{2} W_2$, $I_1 = \frac{1}{2} I_2$ (Series 2)		$W_1 = \frac{1}{3} W_2$, $I_1 = \frac{1}{3} I_2$ (Series 3)	
		D	S	D	S	D	S
	f	1.185	1.12	1.18	1.12	1.17	1.12
	V	8.53	13.2	6.45	9.9	6.73	8.8
	M	14.61	22.8	11.44	17.1	10.65	15.2
	f	1.38	1.12	1.3	1.12	1.26	1.12
	V	9.57	11.88	7.33	9.24	6.57	8.36
	M	15.02	18.85	11.45	14.66	10.31	13.27
	f	1.52	1.12	1.37	1.12	1.31	1.12
	V	8.33	10.56	7.07	8.58	6.39	7.92
	M	13.56	15.73	10.8	12.78	9.93	11.8
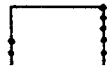	f	1.58	1.12	1.4	1.12	1.33	1.12
	V	8.28	9.24	6.7	7.92	6.17	7.48
	M	11.9	13.45	10.1	11.54	9.45	10.89
	f	1.6	1.12	1.41	1.12	1.34	1.12
	V	7.81	7.92	6.43	7.26	6.12	7.04
	M	11.44	12.01	9.84	11.01	9.31	10.68
	f	1.6	1.12	1.41	1.12	1.34	1.12
	V	6.55	6.6	5.86	6.6	5.59	6.6
	M	10.75	11.4	9.53	11.4	9.03	11.4

TABLE 2
Dynamic responses of Main Buildings with Sloping Roofs

STRUCTURE		$W_1 = W_2$, $I_1 = I_2$ (Series 1)		$W_1 = \frac{1}{2} W_2$, $I_1 = \frac{1}{2} I_2$ (Series 2)		$W_1 = \frac{1}{3} W_2$, $I_1 = \frac{1}{3} I_2$ (Series 3)	
		D	S	D	S	D	S
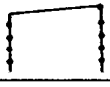	f	1.43	1.12	1.34	1.12	1.29	1.12
	V	10.1	11.88	7.47	9.24	6.27	8.36
	M	15.3	18.85	11.58	14.66	10.22	13.27
	f	1.62	1.12	1.44	1.12	1.36	1.12
	V	9.57	10.56	7.33	8.58	6.53	7.92
	M	13.99	15.73	11.04	12.78	10.02	11.8
	f	1.71	1.12	1.49	1.12	1.4	1.12
	V	8.72	9.24	6.99	7.92	6.53	7.48
	M	12.38	13.45	10.34	11.53	9.58	10.89
	f	1.73	1.12	1.5	1.12	1.4	1.12
	V	7.65	7.92	6.48	7.26	6.1	7.04
	M	11.39	12.01	9.89	11.01	9.33	10.68
	f	1.73	1.12	1.5	1.12	1.4	1.12
	V	7	6.6	6.17	6.6	5.83	6.6
	M	10.96	11.4	9.68	11.4	9.16	11.4

D and S denote dynamic and static analyses, respectively. f, v and m denote frequency, base shear and overturning moment, respectively.

@seismicisolation

seen that for most practical cases they do not significantly influence the response of the regular model. The extent of any approximation, however, depends on the level of irregularities and roof slopes in each individual case.

The structure of Fig 2, described earlier, is a practical example and incorporates irregularities of mass, height and stiffness. The dynamic response of this structure was obtained from the response spectrum analysis and static equivalent force methods, and the results were found to be as follows:

$f_d = 1.10\ H_z$,	$v_d = 646$ kN	$M_d = 9620$ kNm
$f_s = 1.12\ H_z$,	$v_s = 839$ kN	$M_s = 14100$ kNm

The base shear and overturning moment due to the static approach, V_s and M_s, are about 25% greater than those calculated using the dynamic technique. The two frequencies due to both approaches are seen to be almost identical.

Conclusions

An investigation has been made into the dynamic response of Main Buildings of conventional power stations. The frequency, base shear and overturning moment of structures, calculated using both response spectrum and equivalent static analyses, have been compared for a range of realistic examples. These consisted of individual multi-storey annexes, with a range of irregular distributions of mass and stiffness over their height, and twin annexes linked by flat or sloping roofs.

Base shear estimated by the static approach exceeded the values calculated by dynamic analysis by about 25% for individual annexes and by 10% and 5% for twin annexes with flat and sloping roofs, respectively. Inspection of the results of the dynamic analyses revealed that this difference was mainly because the participating mass of the annexes in their fundamental mode of vibration was significantly smaller than the dead load used in the static approach. The results of this study show that this is true, not only for regular annexes, but also for those with irregular features, even outside the limits adopted in the UBC.

Overturning moments calculated by static analysis also exceeded the corresponding dynamic values by ratios almost similar to those of the base shears. This demonstrates that the assumption of linearly varying lateral force along the height of the structure assumed in the static approach holds for all structures studied in this paper.

However, the UBC recommends that the results of the dynamic analysis are scaled to yield the same base shear as the static calculation and that the structure is designed for the most onerous forces, either scaled dynamic or static. As the calculated ratios of statically to dynamically calculated base shear and overturning moment are almost similar for each category of structure considered in this paper, it is expected that the use of either the scaled dynamic or static results would lead to similar designs.

In the absence of site specific design spectra, the static code approach may be employed to

@seismicisolation

characterise the dynamic response of this type of structure. In practice, however, depending on the relative significance of the torsional mode of vibration in each individual case, coupling may exist between torsional and translational modes, which can lead to increased dynamic loads. A full dynamic analysis may be required for these cases.

The distribution of base shear between the twin annexes in the static approach was determined with regard to their relative mass only. A more comprehensive approach would take account of their relative stiffness and the distribution of weight over their height.

REFERENCES

1) International Conference of Building Officials, 'Uniform Building Code', 1988 Edition, Whittier, California, 1988.

2) ANSYS, Engineering Analysis System User's Manual, Revision 3.4, Swanson Analysis Systems, Inc, 1989.

@seismicisolation

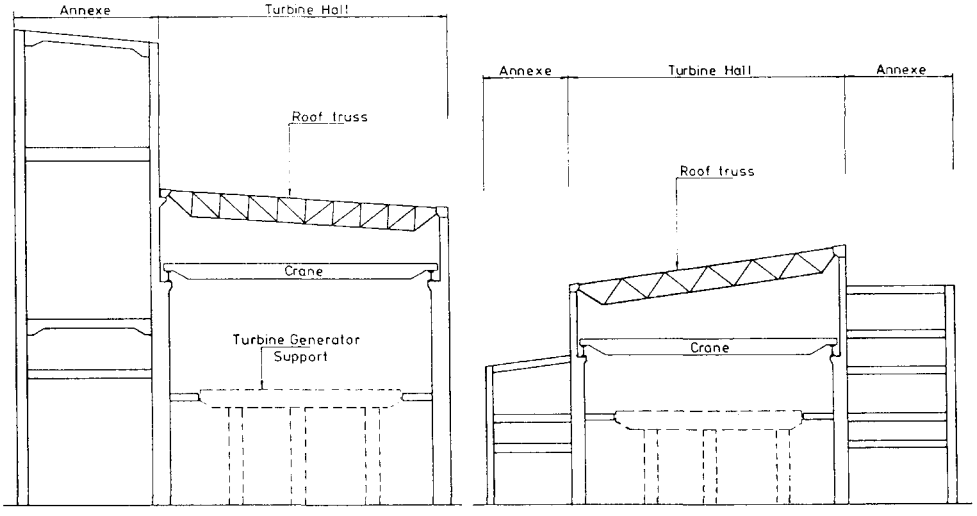

(a) Annexe on one side (b) Annexes on both sides

Figure 1. Typical sections through power station Main Buildings

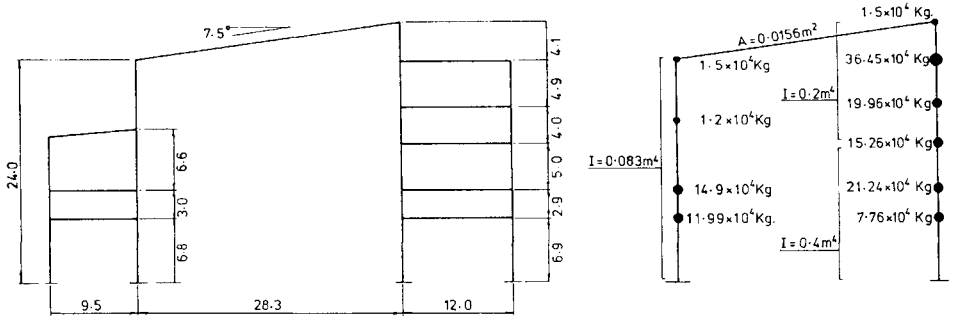

(a) Static (b) Dynamic

Figure 2. Main Building static and dynamic models

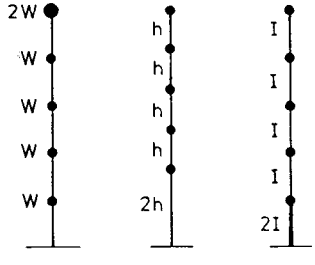

Figure 3. Modelling of irregular features in a 5-storey annexe

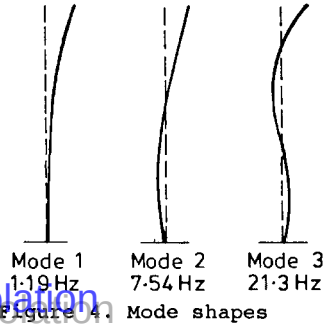

Figure 4. Mode shapes

@seismicisolation

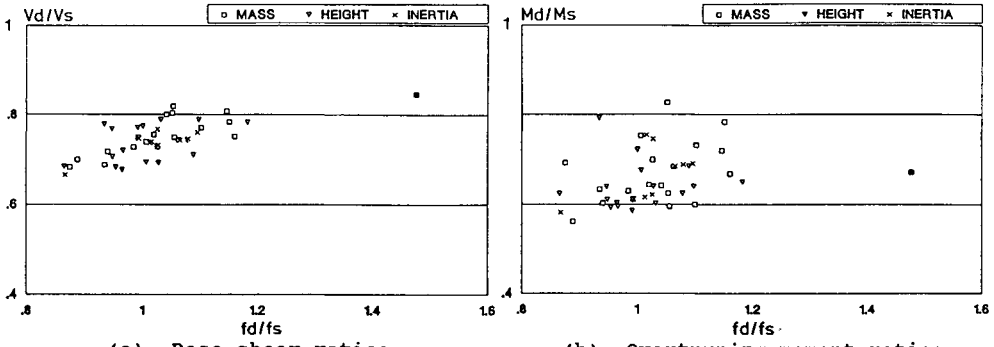

(a) Base shear ratios (b) Overturning moment ratios

Figure 5. Variation of base shear and overturning moment ratios with frequency ratios for individual annexes

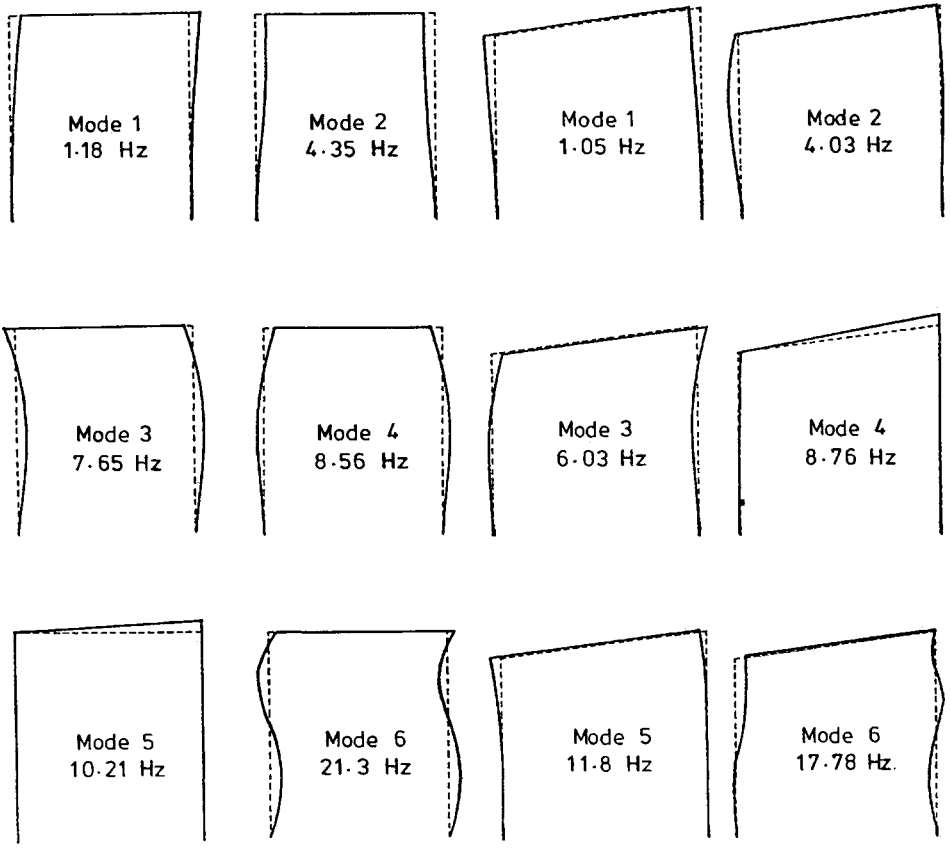

(a) Flat roof (b) Sloping roof

Figure 6. First six modes of regular buildings

@seismicisolation

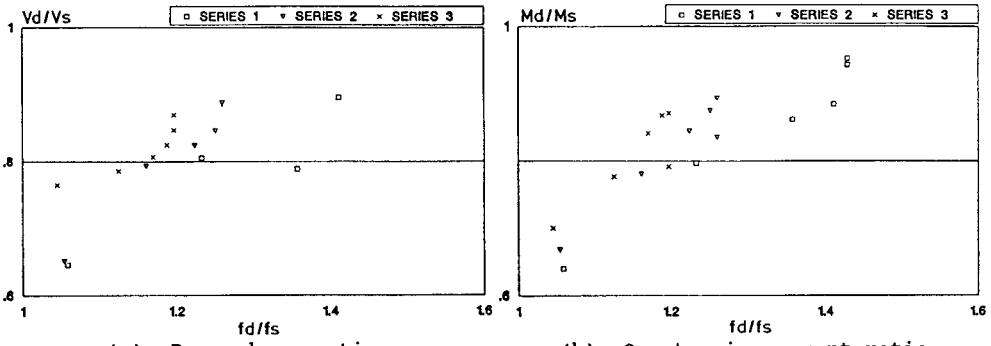

(a) Base shear ratios (b) Overturning moment ratios

Figure 7. Variation of base shear and overturning moment ratios with frequency ratios for Main Buildings with flat roofs

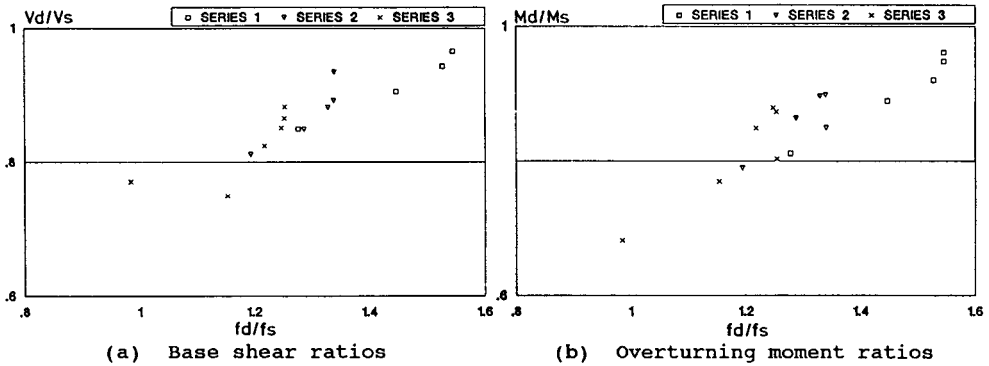

(a) Base shear ratios (b) Overturning moment ratios

Figure 8. Variation of base shear and overturning moment ratios with frequency ratios for Main Buildings with sloping roof

@seismicisolation

PARAMETRIC STUDIES OF THE SEISMIC RESPONSE OF CONCRETE GRAVITY DAMS TO UK-TYPE EARTHQUAKES

W.E. DANIELL
Research Assistant

C.A. TAYLOR
Lecturer
University of Bristol
Earthquake Engineering Research Centre
Bristol BS8 1TR

J.L. HINKS
Principal Engineer
Sir William Halcrow and Partners
Burderop Park
Swindon

ABSTRACT

The initial findings of a parametric study of the response of UK concrete gravity dams to seismic loading are reported. Three dam heights were studied using a number of analytical techniques. It is shown that seismic loading can be important for UK gravity dams and must be properly considered in any stability assessment. Significant variations in the results from different methods of analysis are shown, and the importance of selecting appropriate analytical method is emphasised.

INTRODUCTION

Recent studies of the seismic hazard in the United Kingdom, sponsored by the Department of the Environment, have led engineers to review the seismic behaviour of typical UK dam configurations subject to short duration earthquake motions. This paper reports the initial findings of an on-going parametric study of the seismic behaviour of UK gravity dams being carried out at the Earthquake Engineering Research Centre at Bristol University with the support of Sir William Halcrow and Partners.

The study has selected a typical gravity dam cross-section and three dam heights, 15m, 25m and 50m, as being representative of dam configurations commonly used in the UK. These have been analysed by three methods using as input motions a set of synthesized ground acceleration histories which fit a hard rock acceleration response spectrum proposed for a 1 in 10,000 year UK event.

The objectives of the study are to examine the likelihood of damage to typical gravity dams in the UK and to review the suitability of available analytical methods. This paper

©Seismicisolation

presents a factual report on the progress of the study, but illustrates the importance of careful consideration of seismic effects on UK gravity dams and of the selection of appropriate analytical methods.

FACTORS INFLUENCING EARTHQUAKE RESPONSE OF GRAVITY DAMS

There are many factors which should, ideally, be accounted for in the seismic analysis of gravity dams. It is beyond the scope of this paper to describe these in detail, but the most important will be briefly discussed. A more comprehensive discussion may be found in [1]. Various analytical methods have been developed to handle many of these factors, but they tend to incorporate major simplifications of actual material properties and behaviour. They should therefore be used with care otherwise serious over- or under-estimates of dam response may result.

Dam-reservoir interaction

During an earthquake, a dam interacts dynamically with the impounded water, affecting the dam's natural frequencies and damping characteristics and imposing additional hydrodynamic forces on top of the usual hydrostatic forces. In 1930, Westergaard [2] showed that the water could be represented by an added mass distribution on the dam. Recent analytical developments in reservoir modelling by the Bristol EERC have indicated the very complex structure-reservoir interactions which can occur, with the dam appearing to exhibit the same mode shape response at a range of frequencies. This effect has been noticed in forced excitation tests of prototype dams by the EERC, but further research is needed to confirm this conclusion [3].

Hydrodynamic interaction reduces the fundamental frequency of the dam significantly, by up to 30%, but has a smaller effect on higher resonant frequencies. In general, damping is increased by the presence of the water, but this is most significant for structural resonant frequencies which are close to or greater than the reservoir natural frequency. In such cases, the compressibility of the water gives rise to radiation of energy away from the dam and increased damping.

The reservoir frequency, F_r (in Hertz) is given by the expression

$$F_r = c/4H \qquad (1)$$

in which c is the velocity of sound in water, and H is the depth of the reservoir.

For dams less than about 50m high, the natural frequency of the reservoir usually lies in the range of the higher structural modes and leads to a significant increase in damping of these modes due to the radiation effect. However, earthquake motions, including those predicted for the UK, contain little energy at such frequencies and therefore these modes contribute little to the overall structural response.

For dams greater than 50m high, the reservoir frequency tends to be closer to the fundamental and lower structural frequencies, leading to greater damping and a more significant effect on structural response which is dominated by these lower modes.

Reservoir bottom absorption

Sediment on the bottom of the reservoir tends to absorb pressure waves radiating from the dam, resulting in an effective increase in damping [1]. The effects of this phenomenon can be readily shown analytically, but there is little experimental evidence to show that it is significant at prototype scale or on which to judge the degree to which it should be incorporated in an analysis. Ignoring this effect is conservative.

Dam-foundation interaction

Interaction between the dam and foundation rock tends to reduce the dam's natural frequencies, particularly for the fundamental mode. Damping is increased, particularly for

©Seismicsolution

the higher structural modes, due to material and radiation damping in the rock. Accurate modelling of these effects is difficult due to the complex and often ill-defined nature of the foundation rock. Common practice is to model elastically a substantial portion of the foundation rock, at least to a depth equal to the height of the dam. This accounts for the deformation of the rock, but does not allow for radiation damping. An alternative approach is to model the foundation rock as a visco-elastic half space. This incorporates both rock deformability and radiation damping, but assumes a homogeneous unfaulted rock mass which is unlikely to occur in reality.

METHODS OF ANALYSIS USED IN THE STUDY

Throughout the study, the dams have been analysed as 2-dimensional, plane sections. Technically, this can only be justified where three dimensional effects do not significantly influence the dynamic response of the dam.

A 2-D plane stress analysis may be appropriate for a dam with straight construction joints between monoliths. In such a case, the monoliths could be expected to vibrate independently. However, it is important to consider whether the length of the monolith is such that its bending modes might significantly contribute to its response.

If construction joints are keyed, a 2-D plane strain analysis may be appropriate. This assumes that the dam behaves uniformly across the valley, but long dams will exhibit many modes in plan along the crest as a result of their actual 3-D behaviour. One must therefore be satisfied that the fundamental mode of the 2-D plane strain analysis contributes nearly all of the overall response.

Pseudo-static analysis

The simplest method of seismic analysis is to represent the earthquake forces by equivalent static horizontal and vertical accelerations acting on the dam. These should include the amplification effect of the dam and should not be taken simply as the peak ground accelerations. Hydrodynamic effects may be incorporated using the Westergaard or Zangar added mass approximations. Overall stability of the dam is calculated by traditional equilibrium methods, leading to factors of safety against sliding and overturning. This technique is the least satisfactory since it does not properly model the dynamic behaviour of the dam-reservoir system, nor does it take into account the momentary nature of the peak earthquake accelerations. In view of these limitations, the pseudo-static method was not used in the present study.

Standard finite element method (SFE)

In a standard finite element analysis, the dam-foundation system is modelled as an elastic finite region with a rigid rock boundary. Hydrodynamic effects may be represented using Westergaard's added mass concept or by explicitly modelling the reservoir fluid as a pressure (Eulerian) or displacement (Lagrangian) domain [3]. The latter techniques are computationally intensive and therefore the simpler Westergaard method was adopted for this study. The assumption of a rigid rock boundary precludes radiation damping, but the deformability of the foundation rock is adequately represented.

The input earthquake is represented as a motion of the rigid rock boundary, and is defined either as an acceleration time history, or as a response spectrum. The former method usually yields acceleration, displacement and stress response time histories at various locations in the model. The response spectrum method gives an estimate of the peak response of the dam. It usually advisable to adopt both methods in a detailed analysis.

EAGD84 computer program

EAGD84 is a computer program developed by Chopra and his co-workers [4]. It implements an analytical technique which includes the effects of dam-reservoir-foundation

©SeismicIsolation

interaction and reservoir absorption. The dam is modelled by elastic 2-D finite elements, while the foundation rock is represented by a visco-elastic half space which incorporates radiation damping effects. Reservoir fluid compressibility is included. The ground motion is input as an acceleration time history and the program yields time history outputs. It is suitable for running on a personal computer.

Fenves and Chopra simplified procedure

The techniques incorporated in EAGD84 have been developed into a simplified procedure for the purpose of preliminary design and safety assessment [5]. The fundamental frequency and effective damping of the dam-reservoir-foundation system is estimated from simple formulae. These values are used with the appropriate elastic design response spectra to estimate a peak structural acceleration which is then used in the evaluation of equivalent lateral forces for the fundamental mode. Lateral forces for higher modes may also be included if appropriate. The equivalent forces are then applied in a pseudo-static analysis in which the dam can be modelled as a beam or by 2-D finite elements. This analysis is used to give estimates of peak stresses in the dam.

PARAMETERS USED IN THE STUDY

The typical dam section adopted is shown in Figure 1. Heights of 15, 25 and 50 metres were considered. Two foundation rock elastic moduli, 20GPa and 10GPa, representative of a hard and weak rock respectively, were investigated for each dam height. In the standard finite element analysis, the rock was modelled as a semi-circular plane equal to three time the dam height. In appropriate analyses concrete and rock damping was taken as 5% critical damping, and reservoir bottom absorption was ignored. All models were analysed as plane stress peoblems. The only static loads considered were the dead weight of the dam concrete and the hydrostatic loads.

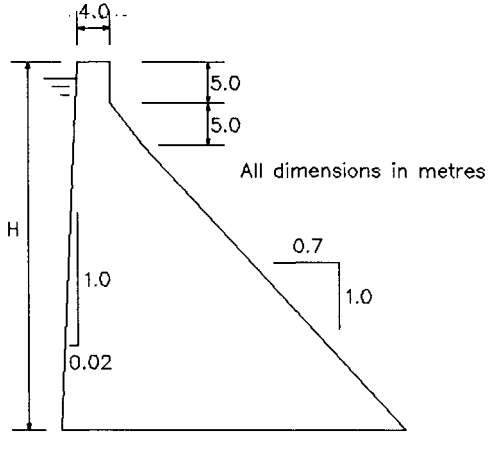

Figure 1. Basic dam configuration

@seismicisolation

Seismic inputs were based on hard rock spectra proposed in [6], and shown in Figure 2, with peak ground accelerations of 0.15g horizontally and 0.1g vertically. Three synthetic spectrum compatible time histories were generated to fit these spectra. Each history lasted 10 seconds and were shaped with a double exponential window giving a strong motion duration of around 5 seconds.

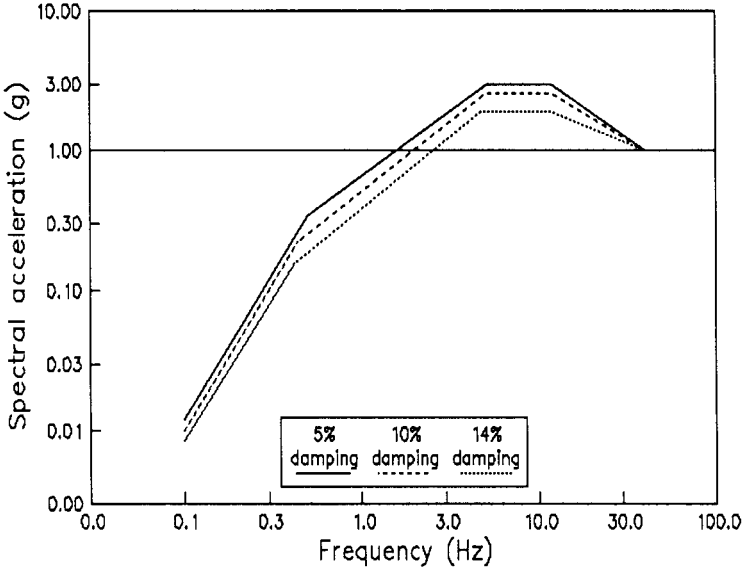

Figure 2. UK hard rock response spectra

RESULTS OF THE ANALYSIS

Fundamental frequencies

Table 1 summarises the frequencies of the fundamental modes of the dams predicted by the three methods for combinations of rigid, 20Gpa and 10GPa foundations conditions and reservoir full and empty for each of the three dam heights.

Those from the Standard Finite Element (SFE) method and the EAGD84 analysis are in good agreement, but the Simplified Procedure (SP) formula gave much higher frequencies. In view of this, the frequencies given by the SFE analysis were used in the subsequent stages of the Simplified Procedure. The frequencies indicate that the Westergaard added mass method may slightly over-estimate the hydrodynamic inertia effects, giving marginally lower frequencies.

Comparing the natural frequencies with the design response spectrum in Figure 1, it will be seen that most occur in the peak spectral acceleration range between 5 and 12 Hertz. Significant seismic response of dams in this range would therefore be expected.

@seismicisolation

TABLE 1
Fundamental frequencies in Hertz

Foundation		Rigid	Rigid	20GPa	10Gpa
Reservoir		Empty	Full	Full	Full
Analytical Method	Dam height (m)	Hz	Hz	Hz	Hz
Standard Finite Element	15	15.2	13.4	11.3	9.9
Simplified Procedure	15	25.0			
EAGD84	15	14.8	14.0	11.8	10.5
Standard Finite Element	25	10.6	8.6	7.3	6.5
Simplified Procedure	25	14.9			
EAGD84	25	10.5	9.4	7.9	7.0
Standard Finite Element	50	6.6	4.6	3.9	3.3
Simplified Procedure	50	7.4			
EAGD84	50	6.60	5.4	4.4	3.8

Peak seismic stresses

Figure 3 shows typical contour plots of peak tensile principal stresses in the 50m high dam on a 10GPa elastic foundation resulting from a horizontal ground motion with 1.0g peak acceleration. Note that these are peak stresses which do not necessarily occur simultaneously. They do not include static stresses and may be scaled linearly for any given acceleration. Similar plots were obtained for the other dam heights and foundation moduli. The SFE stresses shown are from a response spectrum analysis.

@seismicisolation

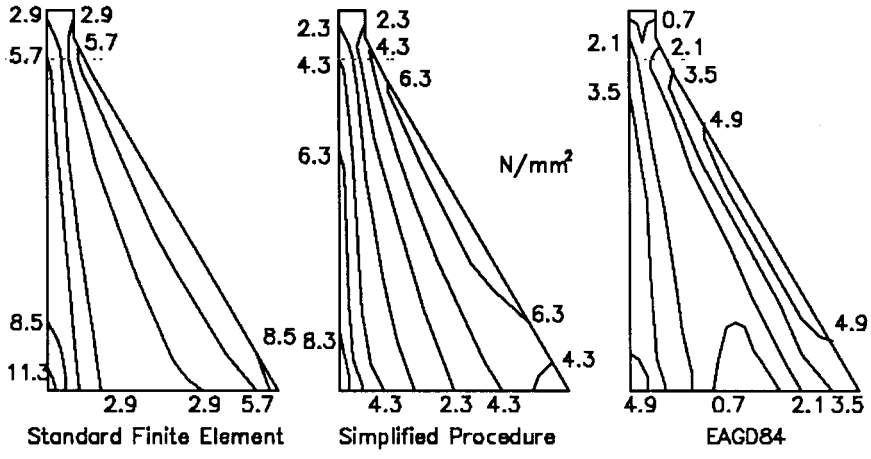

Figure 3 Maximum tensile principal stresses
50m dam, 10GPa rock modulus, 1.0g peak horizontal motion

Inspection of Figure 3 shows that high tensile stresses occur at the upstream heel and on the downstream face, particularly just below the crest at the change in slope. This pattern is typical of gravity dams. It is interesting to note that Koyna dam, in India, suffered serious tensile cracking near the crest at the change in downstream face slope as a result of a reservoir induced earthquake. The SFE and Simplified Procedure predict broadly similar stress levels while those given by EAGD84 are around 50% lower. This is probably due to the much higher effective damping in the EAGD84 analysis (about 14% critical damping compared with 5% in the SFE model) arising from the modelling of radiation damping.

Peak combined static and seismic stresses

Seismic stresses alone are not sufficient to assess the stability of a dam, they must be combined with the pre-earthquake static stresses to give the overall response. Table 2 summarises the peak tensile principal stresses for the various dam configurations resulting from static stresses combined with a horizontal ground motion scaled to 0.15g acceleration and vertical motion of 0.10g. Two sets of stresses are included for EAGD84 to illustrate the effects of different ground acceleration time histories, the two sets being very similar.

It is clear from Table 2 that the Standard Finite Element and Simplified Procedure give very similar results. Peak tensile stresses range from 0.5N/mm^2 in the 15m high dam, to 2.30N/mm^2 in the 50m high dam. These momentary stresses compare with typical permissible tensile stresses of between 0.5 and 1.0 N/mm^2. Maximum compressive principal stresses for combined static and seismic loading were of the order of 5N/mm^2, well within permissible limits.

@seismicisolation

TABLE 2
Maximum tensile stresses for static load combined with 0.15g horizontal and 0.10g vertical ground accelerations

Foundation		20GPa		10GPa	
Dam face		U/S	D/S	U/S	D/S
Analytical Method	Dam Height (m)	N/mm^2	N/mm^2	N/mm^2	N/mm^2
Standard Finite Element	15	0.60	0.60	0.60	0.50
Simplified Procedure	15	0.70	0.60	0.60	0.50
EAGD84	15 15	0.18 0.17	0.27 0.24	0.14 0.16	0.12 0.12
Standard Finite Element	25	0.90	1.00	0.90	1.00
Simplified Procedure	25	1.00	0.90	0.90	0.80
EAGD84	25 25	0.47 0.42	0.59 0.60	0.38 0.32	0.46 0.45
Standard Finite Element	50	2.10	1.60	1.90	1.40
Simplified Procedure	50	2.30	1.40	1.90	1.10
EAGD84	50 50	0.82 0.89	0.82 0.76	0.69 0.72	0.65 0.68

U/S - Upstream D/S - Downstream

Perhaps of most significance from Table 2 are the much lower stresses predicted by EAGD84. As indicated previously, this is almost certainly due to the increased effective damping arising from modelling the foundation as a visco-elastic half-space. There is little experimental evidence to confirm the validity of this assumption. In reality, the actual foundation behaviour, and hence dam response, is likely to be between those represented by the elastic standard finite element analysis and EAGD84.

CONCLUSIONS

The preliminary indications of the on-going parametric study are that seismic loads on UK gravity dams can be significant, particularly for dams greater than 40-50m high, and

©Seismicisolation

must be carefully assessed. The analyses indicate that tensile stresses greater than $1.0N/mm^2$ can occur under the combined action of static and seismic loads, although peak compressive stresses are within normally acceptable limits.

Significant variations in the results from standard finite element analyses and EAGD84 analyses highlight the need to select appropriate analytical methods with care. Further research is needed to quantify foundation radiation damping effects, as well as to assess the dynamic strength and properties of mass concrete.

It is emphasised that the results quoted in this paper should not be used directly in the assessment of the seismic stability of actual dams, but that appropriate specific analyses should be carried out.

REFERENCES

1. Chopra, A.K., Earthquake response analysis of concrete dams. In Advanced Dam Engineering, ed. R.B. Jansen, Van Nostrand, 1988, pp. 416-465.

2. Westergaard, H.M., Water pressures on dams during earthquakes. Trans ASCE, 1933, **98**, 418-472.

3. Greeves, E.J., Analytical modelling of dam-reservoir coupling effects, Ph.D Thesis, University of Bristol, Earthquake Engineering Research Centre, 1991.

4. Fenves, G. and Chopra, A.K., EAGD-84: A computer program for earthquake analysis of concrete gravity dams, Report No. UCB/EERC-84/11, Earthquake Engineering Research Center, University of California, Berkeley, CA, 1986.

5. Fenves, G and Chopra, A.K., Simplified analysis for earthquake resistant design of concrete gravity dams, Report No. UCB/EERC-85/10, Earthquake Engineering Research Center, University of California, Berkeley, CA, 1986.

6. Principia Mechanica, Seismic ground motions for UK design. Report prepared for British Nuclear Fuels Ltd and Central Electricity Generating Board, April 1981.

@seismicisolation

DYNAMIC TESTING AND ANALYSIS OF LLOYD'S REGISTER HOUSE

DR. JOHN MAGUIRE
Lloyd's Register Industrial Division
Civil & Structural Engineering Department
29 Wellesley Road, Croydon, Surrey. CRO 2AJ

ABSTRACT

This paper is a case history, illustrating the use of modern dynamic testing and analysis techniques to assess the structural integrity of buildings. In this example, Lloyd's Register House, Croydon has been studied. This building, constructed in 1984-85, was monitored during ambient (wind) excitation using accelerometers, to determine its natural frequencies, mode shapes and damping values. In parallel, a theoretical dynamic analysis was carried out using the finite element method. Experimental and theoretical results have been compared, and conclusions drawn as to the structural integrity of the building.

INTRODUCTION

There is a growing need to assess the overall structural integrity of buildings post-construction. This need arises from a variety of interested parties such as developers, insurers, designers and builders, all of whom are seeking assurance/confirmation that the building is performing structurally as designed, and that the design has been optimised. The main objective of this case history is to demonstrate such an overall structural "integrity check" using modern dynamic methods, so that interested parties can see the conclusions that may be drawn, and at what cost.

@seismicisolation

STRUCTURAL SUMMARY

The structure is a ten storey, L-shaped, building of height 34.5m, constructed in 1984-85. It was originally known as Green Park House, but is currently known as Lloyd's Register House, and is the home of Lloyd's Register Industrial Division, located in Croydon, Surrey. There is a cellular basement (car parking) beneath the ten storeys and the basement raft is supported by piles end-bearing into the Thanet Sands. The superstructure framing is of reinforced concrete (r.c.), the main load-resisting elements comprising r.c. cores. The idealised superstructure geometry is shown in Figures 1 and 2. Floors are typically 350mm r.c. troughed (250 form plus 100 topping), of dead load 7.5 kN/m^2 (including screed, services, ceilings, and partitions). Design imposed loads are typically $4kN/m^2$ (except for plant room on roof = 7.5 kN/m^2). The curtain walling dead load is $0.5kN/m^2$ on elevation (including glazing, framing, fixings and insulation). The design 28 day characteristic concrete cube strength was $30N/mm^2$, and the reinforcement used had design characteristic strengths of $425N/mm^2$ for main bars (Type 2) and $250N/mm^2$ for the links.

TESTING

The dynamic behaviour of the building, subject to ambient (wind) excitation, was measured during June 1990 to determine its natural frequencies, mode shapes and damping values. This is somewhat analagous to a doctor listening to a patient's heartbeat with a stethoscope - the natural frequency being the "heartbeat" and accelerometers being the "stethoscope". The theory of structural dynamic behaviour is summarised in Reference 1 and is not repeated here for brevity. The testing set up is shown in Figure 3 - major equipment used comprised four servo-accelerometers, a four-channel analogue tape recorder and a two-channel spectrum analyser. A deliberately small arrangement (number of measurement locations) was chosen to determine whether a rapid, low cost test could in fact determine the dominant structural characteristics. With a four-channel recorder this necessitated recording two sets of data (test series A and B as shown in Figure 3) on the ninth floor (top floor). Recorded data was visually monitored using an oscilliscope/chart recorder concurrent with the tape recording. Data processing was carried out "off-line" in Lloyd's Register Laboratories immediately following the tests. Each test series lasted two hours, to minimise random and bias errors and to ensure stationary wind measurements (see Reference 2).

@seismicisolation
@seismicisolation

Main results of the tests are as follows:

TABLE 1
Test Results

Mode	Description	Frequency	Damping (Critical)
1	Translation E-W	1.42 Hz	1.1%
2	Translation N-S	1.73 Hz	0.9%
3	Torsion	4.55 Hz	Not clear

In addition, spectral analysis indicated a possible torsion mode at 1.20 Hz, but there was insufficient time available to research this further.

ANALYSIS

The theoretical dynamic behaviour of the building was studied by constructing a "stick" finite element (f.e.) model. It was assumed that for a short (height less than 50m.), squat (aspect ratio = 1) building founded on piles, that dynamic soil-structure interaction effects would be negligible. The bending stiffness (EI) was based on the gross concrete cross-section of the r.c. cores (hand calculations showed that column stiffnesses were negligible). Young's modulus (E) was initially taken to be 25 kN/mm^2. (See Reference 3 for grade 30 concrete). The torsional stiffness (GJ) was based on CIRIA recommendations (see Reference 4). The torsional stiffness of the cores away from the stiffness/mass centres is particularly significant, and care was needed to input this correctly. The dynamic Poisson's ratio (V) for concrete was assumed to be 0.2, leading to a value of $G = E/2(1 + V) = 10$ kN/mm^2.

The f.e. model adopted is shown in Figure 4. The f.e. code used was NISA II, Version 90, supplied by EMRC Europe Limited. Results of the modal analysis are given in Table 2 below.

TABLE 2
Analysis Results

Mode	Description	Frequency
1	First Bending E-W	1.04 Hz
2	First Bending N-S	1.36 Hz
3	Second Bending + Torsion	4.85 Hz
4	Second Bending + Torsion	6.84 Hz
5	Second Bending + Torsion + Axial	10.71 Hz
6	Third Bending + Torsion + Axial	12.01 Hz

@seismicisolation

COMPARISON OF TEST AND ANALYSIS

The test results yielded fundamental translation (bending) modes at 1.42 Hz (E-W) and 1.73 Hz (N-S). The analysis yielded similar modes at 1.04 Hz (E-W) and 1.36 Hz (N-S), assuming a Young's modulus, E, equal to 25 kN/mm^2 (for grade 30 concrete). If "theory" is revised in line with "reality" this implies an actual E value of:

(1) In E-W direction, E actual = $\left(\frac{1.42}{1.04}\right)^2 \times 25 = 46.6\ kN/mm^2$

(2) In N-S direction, E actual = $\left(\frac{1.73}{1.36}\right)^2 \times 25 = 40.5\ kN/mm^2$

On average, therefore, the actual value of $\underline{E = 43.6\ kN/mm^2}$.
How does this compare with the expected E value for grade 30 concrete at 5 years (the age of the building), rather than at 28 days? BS8110 (Reference 3) relates concrete grade to strength of concrete, at 28 days and 1 year (equation 17 and 18). Neville relates strength at 1 year to strength at 5 years (Reference 5), and BS8110 relates static Young's modulus to dynamic Young's modulus (equation 19). As an example, for grade 30 concrete, the characteristic strength of 30.0 N/mm^2 leads to E static (28 days) = 26 kN/mm^2. This increases at 5 years to 26 x (0.4 + 0.6 x 1.23 x 1.03) = 30.2 kN/mm^2. For E static = 30.2, E dynamic = (E static/1.25) + 15.2 = 39.4 kN/mm^2. Table 3 below gives E values related to concrete grade. Reference 6 suggests that E static is an appropriate value to select for buildings, and this would imply (see Table 3) that although the design specified grade 30 (after 28 days) as a minimum, in practice (after 5 years) in excess of grade 70 has been achieved (E static = 39.4 cf E actual = 43.6). Even if a more conservative E dynamic was used in comparison the desired grade 30 has obviously been achieved - in fact the grade is nearer 55 (E dynamic = 43.9 of E actual = 43.6).

TABLE 3
Concrete Relationships

Grade	f cu (28 days)	E static (28 days) (kN/mm^2)	E static (5 years) (kN/mm^2)	E dynamic (5 years) (kN/mm^2)	E average (5 years) (kN/mm^2)
30	30 N/mm^2	26.0	30.2	39.4	34.8
40	40 N/mm^2	28.0	32.5	41.2	36.9
50	50 N/mm^2	30.0	34.8	43.0	38.9
60	60 N/mm^2	32.0	37.1	44.9	41.0
70	70 N/mm^2	34/0	39.4	46.8	43.1

Notes
1. E static derived from Reference 3, equation 17 and 18.
2. E dynamic derived from Reference 3, equation 19.
3. E average = (E static + E Dynamic)/2

@seismicisolation

It may thus be concluded that the required concrete strength and overall structural stiffness have been achieved. The building structure continues to meet the design requirements and therefore the structural integrity is assured. There is evidence to suggest that the structural design (and construction) is somewhat conservative, and the design (and construction) could therefore be reviewed for further economy.

COSTS

What does a structural integrity check of this nature cost?
A breakdown for this building in terms of man-time, is given below.

TABLE 4
Man-made Breakdown

Activity		Mandays
PHASE I - MOBILISATION		
1.	Initial data collection (drawings, reports, calculations).	1
2.	Study of initial data to extract key parameters.	1
3.	Hand calculations (based on 2.) to determine anticipated dynamic behaviour	1
PHASE II - TESTING (mainly two-man team)		
4.	Select appropriate test equipment (based on 3.), transport to site, set up.	1 + 1
5.	Ambient vibration measurement (including on-site data checking).	2 + 2
6.	Take down equipment, return to laboratory.	1 + 1
7.	Digital signal processing and reporting results.	2
PHASE III - ANALYSIS		
8.	Derive detailed mass and stiffness parameters from item 2.	2
9.	Set up finite element model, test and debug; modal analysis to derive frequencies and mode shapes.	1
10.	Validate results against items 3. and 7.	1
PHASE IV - COMPARISON AND CONCLUSIONS		
11.	Compare test results (7.) and analysis results (10.), and adjust analysis assumptions to match "reality".	1
12.	Compare revised analysis stiffnesses against expected stiffnesses (taking into account age of structure).	1
13.	Report on conclusions as to building structural integrity, including checking.	2
	TOTAL	21 mandays

At a rate of £350/day the mantime cost would be just under £7500. To this should be added the costs of equipment hire and any travel/accommodation expenses during testing. In hindsight, a slightly increased number of mandays should have been allowed for testing (item 5.), to allow clearer definition of mode shapes.

@seismicisolation

CONCLUSIONS

This case history has demonstrated (using modern dynamic methods) that the overall structural integrity of Lloyd's Register House is currently satisfactory and the structure is continuing to behave according to the design. A regular re-assessment ("health check") is recommended at intervals of (say) 5-10 years (see Reference 7). Table 4 indicates that this assurance of structural integrity has been achieved at a modest cost. Studies on other structures would similarly determine their structural fitness for purpose and/or highlight areas where design/construction could be optimised. Further studies could also address adequacy of the weathershield.

ACKNOWLEDGEMENTS

The following assistance is gratefully acknowledged:

1. Prudential Portfolio Managers Ltd (building owner) for their permission to carry out the tests;
2. Bylander Waddell Partnership Ltd (structural engineer) for supplying structural details of the building; (job ref. G3054);
3. Lloyd's Register Technical Investigation Department for carrying out the testing and signal processing;
4. EMRC Europe Limited for carrying out the finite element analysis of the building using the NISA II package.

REFERENCES

1. Maguire, J.R. and Severn, R.T., Assessing the dynamic properties of prototype structures by hammer testing. Proc. I.C.E., Part 2, 1987, Vol. 83, Dec., pp 769-784.
2. Bendat, J.S. and Piersol, A.G., Random Data (Analysis and Measurement Procedures), Wiley-Interscience, 1971.
3. BS8110, The Structural Use of Concrete, Part 2, 1985, Section 7, Table 7.2.
4. CIRIA Report 102, Design of Shear Wall Buildings, 1984, Section 4.1.2.
5. Neville, A.M. Properties of Concrete, Pitman, 2nd edition, 1978.
6. Ellis, B.R. and Littler, J.D., Lessons from dynamic testing of buildings, Paper 8 (and discussion) in Structural Assessment (The use of full and large scale testing), Garas, F.K., Clarke, J.L., and Armer, G.S.T., Butterworths, 1987.
7. The Institution of Structural Engineers, The achievement of structural adequacy in buildings, November 1990, Section 4.2.3 (Durability and maintenance).

@seismicisolation

FIGURE 1

IDEALISED SUPERSTRUCTURE/SIMPLIFIED GEOMETRY

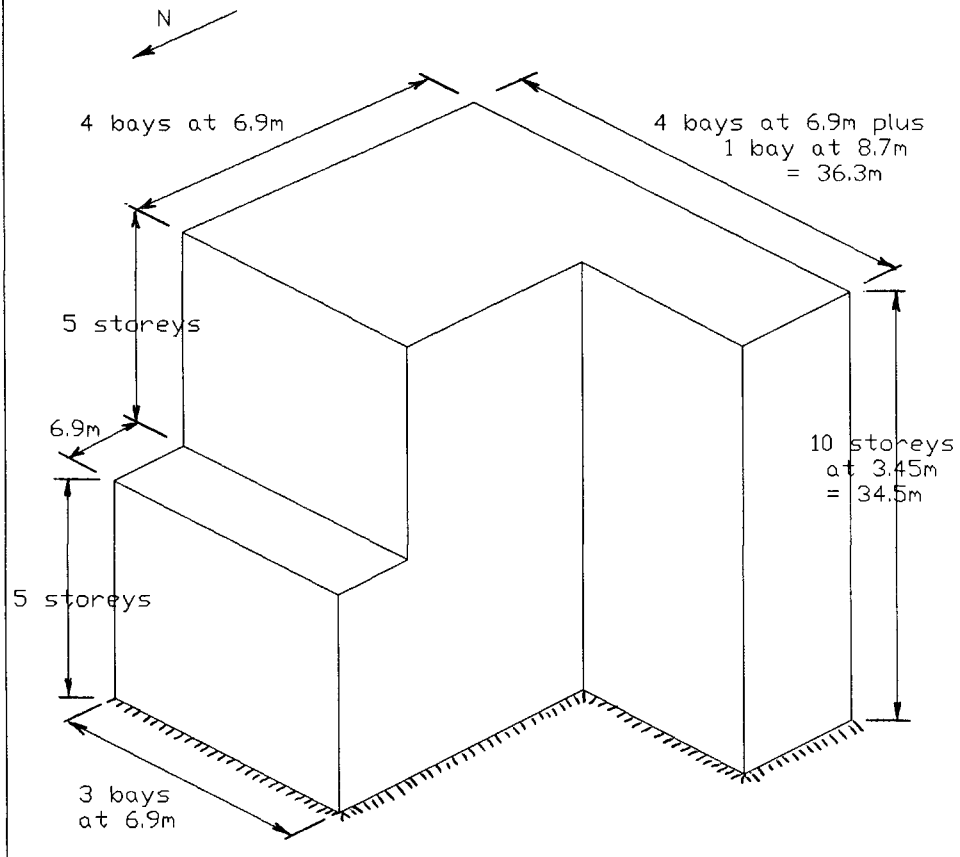

NOTES 1. Full Height atrium (in elbow of "L") not shown.

2. Sloping roof between 5th and 6th storeys not shown.

3. Atrium and sloping roof assumed to be nonstructural.

@seismicisolation

FIGURE 2

TYPICAL FLOOR PLANS (SHOWING CORES)

(A) Upper Five Storeys

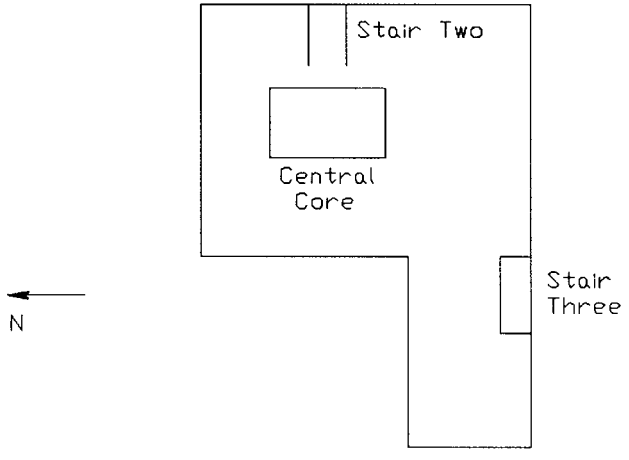

(B) Lower Five Storeys

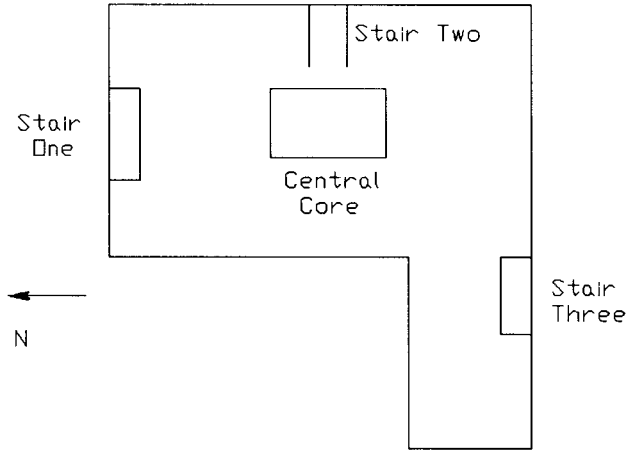

@seismicisolation

FIGURE 3

TEST SETUP ON 9TH FLOOR (PLAN VIEW)

(A) Measurement (Accelerometer) locations

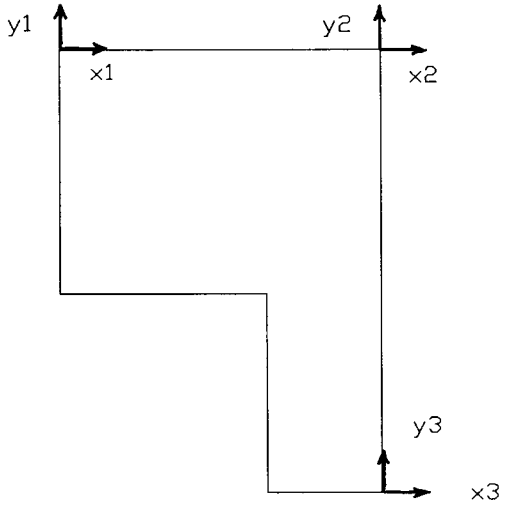

Test series A = measure x1, y1 (ref. point), x2, x3

Test series B = measure x1, y1 (ref. point), y2, y3

(B) Expected Mode Shapes

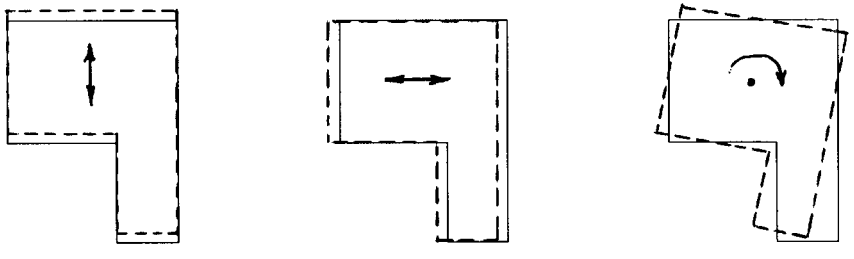

Translation	Translation	Torsion
(y1 y2 y3 large) (and in phase) (x1 x2 x3 small)	(x1 x2 x3 large) (and in phase) (y1 y2 y3 small)	(x1 y1 x2 in phase) (x3 y2 y3 in phase)

@seismicisolation
@seismicisolation

FIGURE 4

DETAILS OF FINITE ELEMENT MODEL

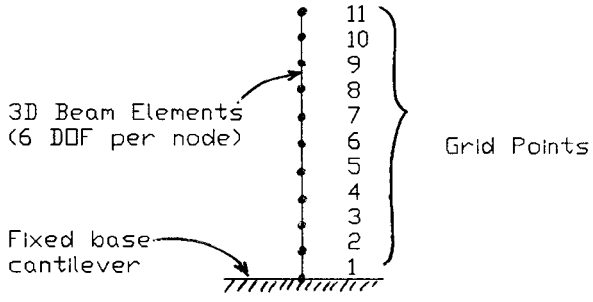

GEOMETRY AND COORDINATES

Grid Point	Elevation z (m.)	Grid point coords x(m.)	Grid point coords y(m.)	Mass point coords x(m.)	Mass point coords y(m.)	Mass values (kg)
1	0.00	+1.59	+2.49	N/A	N/A	N/A
2	3.45	+1.59	+2.49	-0.36	+1.02	0.875×10^6
3	6.90	+1.59	+2.49	-0.36	+1.02	0.875×10^6
4	10.35	+1.59	+2.49	-0.36	+1.02	0.875×10^6
5	13.80	+1.59	+2.49	-0.36	+1.02	0.875×10^6
6	17.25	+1.59	+2.49	-0.36	+1.02	0.875×10^6
7	20.70	+4.31	+1.7	-1.09	-2.09	0.737×10^6
8	24.15	+4.31	+1.7	-1.09	-2.09	0.737×10^6
9	27.60	+4.31	+1.7	-1.09	-2.09	0.737×10^6
10	31.05	+4.31	+1.7	-1.09	-2.09	0.737×10^6
11	34.50	+4.31	+1.7	-1.09	-2.09	1.035×10^6

MEMBERS AND CONNECTIVITY

Member	Connects	$A(m^2)$	$Ixx(m^4)$	$Iyy(m^4)$	$J(m^4)$
1	1-2	15.43	106.5	62.3	582
2	2-3	15.43	106.5	62.3	582
3	3-4	15.43	106.5	62.3	582
4	4-5	15.43	106.5	62.3	582
5	5-6	15.43	106.5	62.3	582
6	6-7	13.30	105.5	47.3	291
7	7-8	13.30	105.5	47.3	291
8	8-9	13.30	105.5	47.3	291
9	9-10	13.30	105.5	47.3	291
10	10-11	13.30	105.5	47.3	291

@seismicisolation

SEISMIC QUALIFICATION & CONSTRUCTION OF SAFETY RELATED PIPEBRIDGES UTILISING ISOLATION TECHNIQUES

J B RIDING - BSc., C.Eng., M.I.Struct. E., MICE
British Nuclear Fuels Plc
Hinton House, Risley, Warrington, Cheshire

P CLARK - BSc., C.Eng., MICE
DGP (Consulting Engineers) Ltd
Brunel House, 54 Princess Street, Manchester

C ROGERS - BSc., C.Eng., M.I.Struct. E., MBCS
DGP (Consulting Engineers) Ltd
Brunel House, 54 Princess Street, Manchester

ABSTRACT

Process Pipebridges utilising bulk radiological shielding perform a key function within the overall reprocessing operations at Sellafield. The pipebridge construction discussed in this paper, consists of a concrete multispan beam and column structure connecting various process buildings within the factory site. The bridge system carries pipe arrays which are contained within a stainless steel liner, over a total distance of 747m. The structure is generally supported on large diameter bored piles, with pad foundations where piles are impracticable. Pre-cast concrete beams of spans between 10m and 27m are supported on columns of typical height 13m. To provide a degree of seismic isolation the majority of beams are seated on elastomeric bearings. Articulation joints are provided at certain locations.

In addition to normal service conditions and 1 in 50 year environmental events, the safety related performance criteria for the structure demands that the design considers 1 in 10,000 year extreme environmental events and operational fault conditions. The bridge structure and its pipework must therefore survive a Design Basis Earthquake defined by a maximum horizontal free field acceleration of 0.25g. The construction of this £50M Project and the testing techniques adopted to satisfy the stringent quality assurance requirements are also addressed.

INTRODUCTION

The design and analysis of Safety Related Pipebridges required to accommodate normal environmental, extreme environmental and operational fault conditions are discussed in this paper.

@seismicisolation

View of Phase 1 of the P.P.B.

The development of the PPB project from functional and safety requirement through to construction and testing is addressed with particular emphasis placed on analysis and design aspects.

FUNCTIONAL AND SAFETY RELATED DESIGN REQUIREMENTS

Functional Requirements

The Process Pipebridge (PPB) is one chain in the infrastructure at Sellafield and links various process buildings (see figures 1, 2 & 3). The fundamental purpose of the PPB is to support and anchor pipework which is required to service the process buildings. All the pipes within the PPB are gravity fed and therefore the height and gradient of the bridge spans were dictated by building entry points and pipework flow requirements. Features on the ground such as roads and railways, buildings and in-ground services limited the scope of route selection, and therefore greatly dictated the basic setting out of the PPB.

@seismicisolation

As active liquors are transferred, the bridge beams are required to provide bulk radiological shielding, in addition to their structural function. The shielding thickness was determined by consideration of source activity and target external dose rates and was achieved by the provision of normal density concrete or where dimensions are restricted, Barytes Concrete.

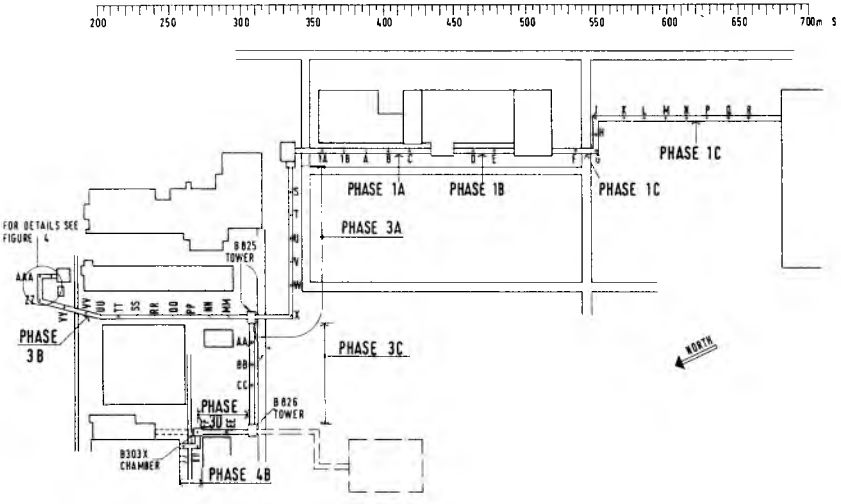

Figure 1 Plan of Process Pipebridge

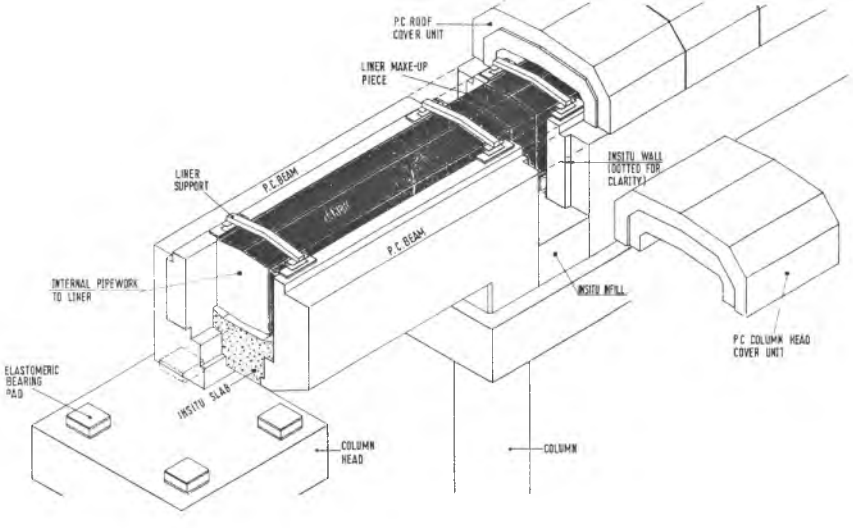

Figure 2 Isometric View of P.P.B.

@seismicisolation

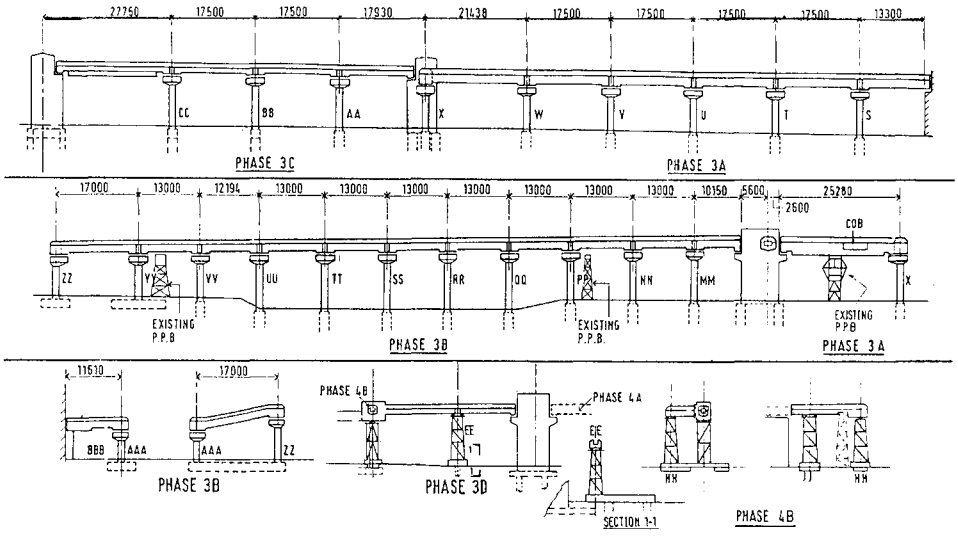

Figure 3 Elevation on Phase 3 of P.P.B.

Safety Related Design Requirements

In addition to Normal Operating Conditions the PPB is required to resist 'Abnormal Operating Conditions' in the form of temperature excursions brought on should a fault in the liquor transfer system occur.

The PPB is designed to sustain, within acceptable criteria, 1:10,000 year environmental events. In particular a Design Basis Earthquake (DBE) having maximum free field acceleration of 0.25g horizontally and 0.167g vertically with assumed design motion as defined in Ref 1. To provide confidence that there exists a margin above the DBE, the structure is assessed for a 0.35g maximum free field acceleration.

In all design cases the displacements of the PPB must not be greater than can be accepted by the pipework.

ANALYSIS

Potential Design Problems

In the consideration of the conceptual design of the process pipebridge structures, it was important to consider various potential design problems before the major analyses were performed.

Existing structures on the route of the bridge had not been specifically designed and analysed for additional loading from the bridge response. It was therefore considered necessary to ensure that the bridges placed the lowest possible additional loads onto these structures.

@seismicisolation

A particular feature of shielded pipebridge structures is that of a relatively high mass, supported at a height above the ground. The mass is supported on single and relatively slender columns resulting in an inverted pendulum type structure.

The entire process pipebridge is designated as a seismic category 3 structure, this allows the structure to exhibit in-elastic displacement within limits defined by the plant designer. The internal mechanical liner however must remain elastic and is defined as a category 2 structure adding further design constraints. The liner, though constructed of thin material (stainless steel of 3mm and 6mm thickness), is a very stiff hexagonal cross section.

It was therefore necessary to carefully consider both seismic and service displacements in the design of the liner. These considerations greatly influenced the structural concept.

Analysis of the Structure

Tests were carried out on analytical models to establish the levels of loading transmitted to the columns and piles. It was very quickly realised that using conventional steel bridge bearings resulted in the superstructure suffering greatly amplified motions. Methods of isolating the superstructure were therefore investigated.

To provide the isolation, rubber bridge bearings were considered, but again the standard types did not provide sufficient isolation due to their stiffness. The design of non standard elastomeric bearings was subsequently undertaken. One of the major advantages of this type of bearing is that its stiffness and damping properties can be modified by careful mix design to provide a bearing of specific properties. The elastomer bearings therefore provided a means of seismic isolation and in addition they provided high levels of critical damping, 10% to 13%, compared to 3% to 5% for well reinforced concrete.

The preliminary analysis indicated unacceptably high shear displacements, of the order of 60mm across the liner, at building entries. It was therefore decided to guide the bridge beams at the building entry. Longitudinal displacement were permitted, this being accommodated by bellows constructed into the liner and the pipes. Initially the bridge beams were analysed as continuous construction spanning horizontally between building entry points. However this continuity resulted in high shear forces within the building supports and to reduce this shear, pin joints were provided over the columns adjacent to building entry points.

The initial testing of the design concepts was performed using modal frequency response techniques. The technique analyses the structure in terms of sets of frequencies, but is limited in that it is not sufficiently sensitive to variations in damping. The structure being designed had elements with high levels of damping and therefore to best represent this feature the transient response technique was adopted. The advantages of transient analysis is that the damping is explicitly included, therefore damping variations through different structural elements can be considered. The output is in the form of a time history. Having identified displacements as a major design

©seismicisolation

criteria, the use of transient techniques provided useful data. Comparisons of the results of the tests performed using modal and time history techniques, demonstrated that the bearing damping was indeed a key factor in the isolation system.

The transient analysis enabled the design team to clearly define the required bearing properties. Permissable displacements and rotations were obtained from the liner designers and a compromise established between structure loading and liner displacements. The chosen properties provided a system with a displacement of approximately 60mm and a natural frequency of 0.8 to 0.9 Hz.

Analysis Model

The analyses were carried out using the industry finite element code ANSYS (2). ANSYS provides several structural analysis modules, including those for modal response and transient solutions. In the case of transient solutions, ANSYS provides a reduced transient module. This reduces the structure by the Guyan Condensation Technique (3), to a selected subset of the structural degrees of freedom. This subset is selected by the analyst to best define the expected structural motions.

The rubber bearings are modelled with spring/damper elements. These elements (ANSYS STIF14) consist of a spring in parallel with a dashpot. Four springs were modelled under each end of each beam that lands on a column head. Three springs are translational in nature, these represent pairs of bearings, acting in shear and axially (see figure 4). The fourth spring is used to represent the rocking resistance of the bearing pair.

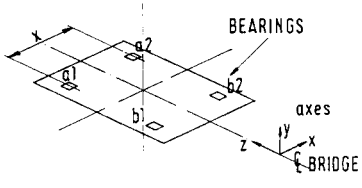

TYPICAL ARRANGEMENT OF COLUMN HEAD BEARINGS

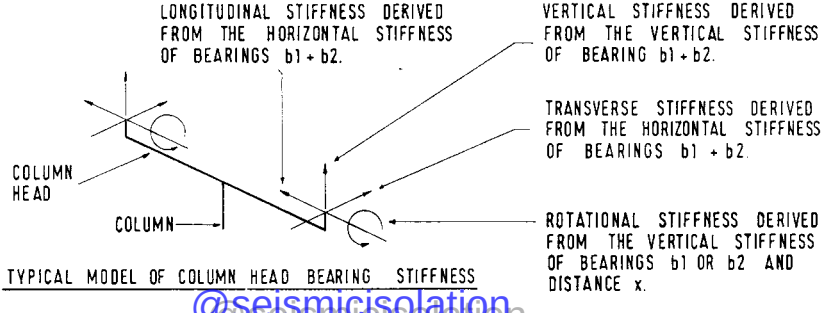

TYPICAL MODEL OF COLUMN HEAD BEARING STIFFNESS

Figure 4 Analysis Modelling of Bearing Arrangement

@seismicisolation

A similar approach was adopted for springs used at the base of the columns to represent the allowable rotational degrees of freedom of the piles. The piles were not modelled explicitly, rather simple pile/soil models were analysed to establish the rotational restraint offered. This resulted in three rotational spring/dampers, which represent the rotation restraint of the piles. The dampers were calculated based upon ground damping properties.

The pin joints were modelled using coupling equations. These are simply instructions to the program that two points in the model should have equivalent displacements. The structural pins provide continuity in the axial direction and in lateral shear, but are free in the other four degrees of freedom.

As the rotational capacity of the bearings had been considered, and beams were modelled at their centre of gravity, torsional responses were included. The modelling was achieved by using stiff offsets rather than adopting the ANSYS STIF44 element. This allowed greater control over the results from the offset, and allowed the modelling of extra mass which is present at the beam ends.

Analysis Input Motion

The input to the model was the BNFL standard digitised ground response (1) for the relevant ground conditions which was input to the base of the columns, as the piles are long and slender and could reasonably be expected to follow the ground motion. For the entry to buildings, time histories from the building analyses were used if available, otherwise stiff elements representing the structure were used, and a driving motion was input at the base level.

The overall response from the modelling allowed forces and moments to be recovered which provided data for the design team. The ability to recover time related results enabled many design problems such as bearing uplift, to be investigated and resolved.

In addition, due to the use of transient techniques, the analysts were able to provide the mechanical design office with design displacements and response spectra for the design of attached items such as the liner.

Achievement of Modelling Assumptions

A close in-house relationship was developed with the analysis team to ensure that analytical assumptions could be achieved in the design. A particular feature of the analysis was the assumption that a pinned joint should be provided within the bridge cross-section at the penultimate bridge support to a building entry. This was achieved by providing an insitu concrete connection allowing rotation but resisting horizontal shears and axial forces, thus reducing distress in the mechanical items.

Although certain bridge beam connections were required to be pinned, the majority of connections over column supports had to provide a fully continuous connection. This in itself would not normally have been a problem however due to requirements for access by the mechanical engineer these connections had to be left temporarily open. ACI code requirements demanded that construction openings had

©Seismicisolation

to be reinstated with mechanical connections of reinforcement rather than utilising lapping bars. This imposed severe design and detailing constraints.

As mentioned earlier limiting displacements to levels acceptable to the mechanical designer was an influential factor in the conceptual design. The north end of Phase 3B of the bridge (see figure 1) in particular had exhibited excessive deflections in the early parametric studies of bridge seismic response. The solution chosen was to anchor the bridge in the analysis at column AAA. This was achieved by providing a pair of steel bearings which anchor the bridge at this location.

These bearings however permit the adjacent bridge spans to articulate about this column thereby eliminating bending moments in the corner units. The articulation provided is illustrated in figure 5.

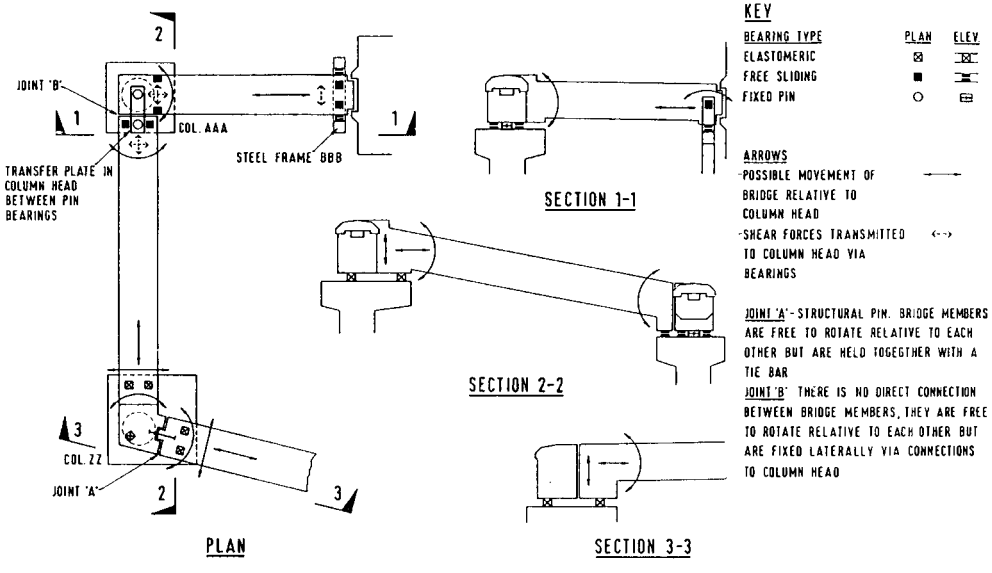

Figure 5 Details of North End of Phase 3B
Illustrating Articulation Features

Uplift on bearings was generally not a problem in the design. However in one or two specific locations the analysis identified that uplift on the bearings could occur. The analytical model assumed that bearings that went into uplift provided the same vertical spring stiffness as bearings that were in compression. Generally when this problem occurred alterations to the geometry of the bridge or location of the bearings resolved the problem. However there were specific locations where uplift on elastomeric bearings could not be avoided. At these positions a restraint was designed which ensured that the bearings remained in compression irrespective of the direction of loading.

@seismicisolation

At interfaces with existing buildings and bridges movement joints are provided to ensure that pounding during a seismic event does not occur.

VALIDATION AND TESTING

Elastomeric Bearings

The use of elastomeric bearings for the dynamic isolation of a structure is not a common solution in the United Kingdom. As a consequence a great deal of attention was paid to the performance of the bearings. Initially tests were carried out on prototype bearings and rubber compound to establish that compression and shear stiffness were within the required tolerances. The bearings were also tested to demonstrate that they would accept without any damage a compressive overload of twice the maximum design load.

Subsequent testing to confirm the dynamic properties of bearings has been jointly undertaken by DGP and BNFL. Shake table testing at Bristol University was undertaken where a test rig was designed and built to achieve full capacity of the test system. The representative earthquake for the Sellafield site was the basis for the comparison between analysis and test. A scaled version of the isolation system demonstrated that the elastomeric bearings were capable of out performing the original manufacturers material data, particularly with regards to damping levels. The most convincing result of the testing performed was the durability of the bearings themselves. Well in excess of a hundred earthquakes were experienced by the bearings, including resonnance tests, with no evidence of distress.

Finally acceptance tests were performed on each and every bearing to confirm that both compression and shear stiffness of the manufactured bearings was within the specified tolerances.

Pile Construction and Testing

As the piles were designed to resist large lateral forces, a means of assessing pile integrity rather than vertical load capacity was desirable. The method chosen was sonic coring, which involved the lowering of probes down pairs of water-filled tubes cast into the pile core. Sonic pulses are transmitted and received through the concrete, with any soil inclusion, gravel or voids reducing the sound velocity considerably when compared with homogeneous concrete.

@seismicisolation

During the piling operation buildings and other structures were monitored to ensure they were not experiencing damaging vibrations. Accelerometers were attached to the structures, at ground level and accelerations and velocities recorded. Upper limits of 0.02g and 0.2m/s for acceleration and velocity respectively were adopted and not exceeded by applying a strict control over the use of the vibrating head or reverting to an oscillating rig.

Erection of Phase 3 A Pre-cast Beams

Couplers

The mechanical connections of reinforcement between beam ends, required by the ACI code, were subject to stringent quality assurance requirements in both their manufacture and assembly. The couplers adopted were tested in accordance with the BNFL specification including performance tests for both initial qualification and production samples.

@seismicisolation

CONCLUSIONS

The relatively high mass of the PPB beams supported at a height above ground level, in combination with the congested site necessitated non-standard design features to engineer a seismically qualified structure. The adoption of structural isolation techniques, elastomeric bearings and articulation joints, reduced seismically induced forces by factors of upto 4. This provided economies of construction and eased the problem of providing foundations in the limited space available.

REFERENCES

1. Principia Mechanica Limited 'BNFL Reprocessing Division, Ground Motion Specification'. BNFL Internal Document, report number TSR ET17.

2. ANSYS General purpose finite element analysis suite. Swanson Analysis Systems Inc., Houston, Pennsylvania, USA.

3. Guyan, R.J., 'Reduction of Stiffness and Mass Matrices', AIAA Journal, Vol 3, No 2, p380, Feb 1965.

ACKNOWLEDGEMENTS

Client : British Nuclear Fuels Plc.; **Conception** : BNFL Engineering (Building & Civil Design Office); **Design** : Design Group Partnership; **Bearing Consultant** : MERL; **Pre-Cast Concrete Manufacturer** : C.V. Buchan Concrete Ltd. The authors would also like to thank their colleagues who participated on this Project, especially Mr R T Day, Dr P A Merriman and Mr A Ireland at BNF Plc and Mr F Testa at D.G.P.

@seismicisolation

SOME DESIGN ASPECTS OF DYNAMIC ISOLATION OF BUILDINGS FROM SEISMIC GROUND VIBRATIONS

Robin Shepherd and Ludi J. Billings
Department of Civil Engineering
University of California
Irvine, California 92717, U.S.A.

ABSTRACT

Within the last decade developments in building base isolation have resulted in this technique being applied in practice to reduce seismic-induced forces, notwithstanding the fact that some aspects of bearing behavior are understood only imperfectly leading to very conservative bearing designs. In this paper the principles of seismic base isolation are reviewed, several approaches to the provision of practical isolation systems are outlined, the design aspects of two specific applications are summarized, and ongoing efforts to examine theoretically the axial load capacity of elastomeric bearings at high shear strains are described. It is anticipated that the availability of improved mathematical models of these bearings will allow designers to achieve more efficient and reliable isolation systems in the future.

INTRODUCTION

The principle of isolating a structural system from ground vibrations has been understood for many years, and many successful implementations exist in which buildings or bridges are mounted on resilient bearings. However, it is only in the last decade that designers have developed sufficient confidence to incorporate dynamic base isolation as the primary means of protecting structures from the devastating effects of earthquake-generated strong ground motion.

The concept of seismic isolation is simple and is not new. A United States patent for an earthquake-proof building was granted in 1906 [1]. Bechtold's concept involved a building supported on a rigid base plate riding freely on a mass of hard spherical bodies. Many similar proposals were made in the following seventy years. All involved the provision of flexible support so that the system is detuned from the excitation. Developments included restricting the motion between the supported structure and the surrounding ground to an acceptable level by the provision of adequate energy dissipation and, in the case of wind or other relatively minor lateral loads, by incorporation of initial stiffness under service load conditions.

@seismicisolation

As with many engineering innovations, successful application of the concept was delayed by difficulty in developing reliable and predictable devices which would not only possess the necessary characteristics at the time of construction, but would preserve these properties throughout the expected life of the structure. Greater understanding of the nature of strong seismic ground movements, and the ability to model structural systems using computers, undoubtedly have benefited the design process, but the most significant recent advances have been prompted by the development of a range of viable isolator devices. These include various combinations of simple rubber blocks, steel torsional and flexural beams, lead extrusion elements and steel plates interlayered with elastomeric materials[2].

One of the most promising of these devices appears to be the laminated steel/elastomer bearing. By sandwiching a series of relatively thin slices of elastomer between horizontal steel shims, a composite block can be formed possessing the desirable properties of large vertical stiffness and large horizontal flexibility.

The design of laminated bearings is still at the stage of progressive refinement. Elementary considerations in typical use necessarily reflect a very conservative approach, as the behavior of these bearings at high strains is imperfectly understood. Current practice in the United States involves verification testing of ten percent of the isolators manufactured for use in a given project. The tested units are then discarded. In Japan, each isolator is tested before installation. The object in both cases is to verify the integrity of the units in the light of the use of a somewhat simplistic design process, and the undoubted difficulty in assuring quality control of the complex production process.

EXAMPLES OF SEISMICALLY ISOLATED BUILDINGS

Seismic base isolation has been applied to several score buildings worldwide, covering both new and existing structures. When applied to structures in this second category the choice is often dictated by the desire to reduce the earthquake damage risk to an historic building without necessitating strengthening procedures which would radically alter the character of the structure.

One such instance is the seismic isolation retrofitting of the Salt Lake City and County Building[3]. This five-storey, massive, unreinforced masonry structure is approximately one hundred years old. It has a central clock tower 76 meters high (Figure 1) and has plan dimensions 40 meters by 80 meters. Some seismic damage has been suffered during the life of the building. However, increasing awareness of the probability of earthquake activity, and of the inadequacy of the structure, prompted a major effort being expended to mitigate the problem in view of the building's historic significance and unusual architecture. Although it was estimated that strengthening by conventional techniques, including the addition of new shear walls, would be cheaper than installing base isolators, the isolation solution was adopted, as it entailed much less architectural disruption than the strengthening option.

The constructed retrofit involved the installation of four hundred and forty three isolators (Figure 3) each 0.43m square in plan and 0.38m high. Those around the perimeter have lead plugs incorporated in the multi-layered steel shim and elastomer configuration. The lead core serves to provide both restraint against low level lateral loads, such as may be generated by wind, and energy absorption, by yielding of the core, during strong motion seismic excitation. The original strip footing walls were first reinforced and then cut to provide space for installation of the isolators (Figure 2). After these were in place and preloaded using epoxy-filled flat jacks inserted below each unit, the footings were cut horizontally so that the building was supported entirely on the isolators.

@seismicisolation

Figure 1 Salt Lake City and County Building

Figure 2 View of two seismic base isolators

The perimeter of the building is separated from the surrounding ground by the construction of a retaining wall providing a 0.30m seismic gap. Analyses predict that the maximum relative deflection that the building will experience in the design earthquake is 0.12m. A backup bumper system is installed in the seismic gap which is covered by sacrificial plates. Provision is also made for the entrance steps to ride over the concrete paths as the building moves on the isolators. It is expected that the maximum lateral acceleration experienced by the isolated structure will be 0.08g, which should ensure that the superstructure stays within the elastic range and that damage will be minimized.

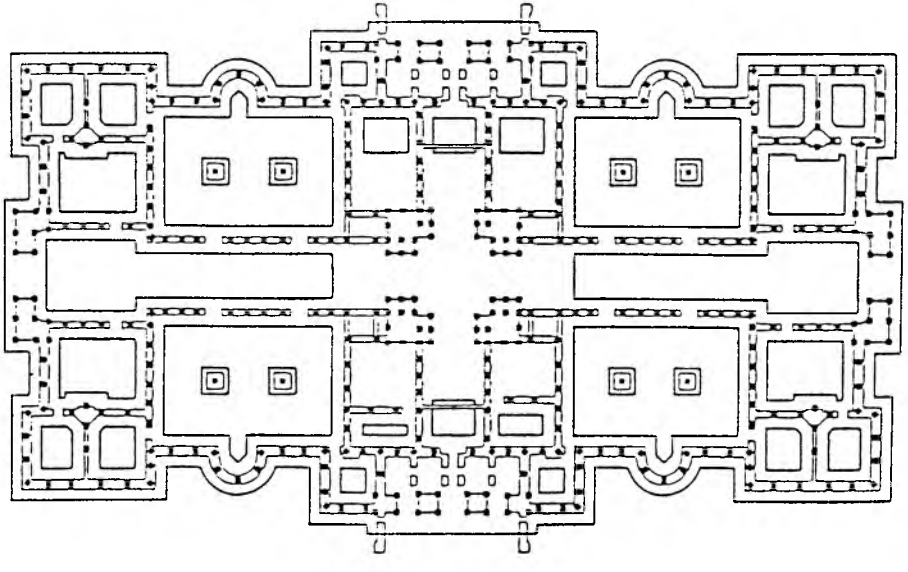

Figure 3 Isolator positions beneath Salt Lake City and County Building

@seismicisolation

Figure 5 (above) Typical Base Isolator under Toranomon building

Figure 4 (left) View of Toranomon building from street

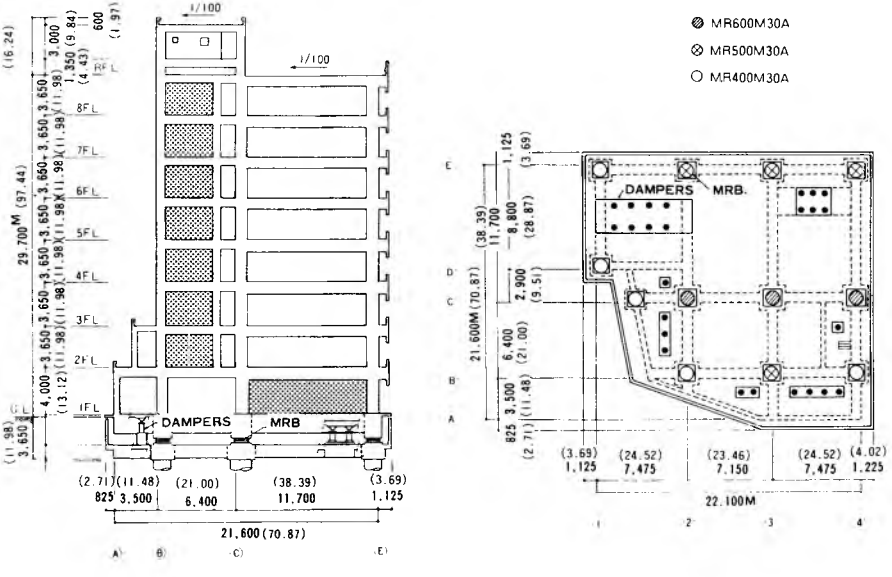

Figure 6 Elevation and plan of Toranomon building

@seismicisolation

Figure 7 Basement of Toranomon building. Oil damper on left. Main bearing on right.

Figure 8 Steel damper units. Twenty-four vertical bars in each one.

Figure 9 Stairs down to basement. Note seismic joint.

Figure 10 Provision for services not to add to building's stiffness.

Although the first base isolated buildings were constructed in New Zealand, more than fifty have been designed in Japan, and many of these have been completed. One example is the eight story, reinforced concrete Toranomon office building (Figure 4) located in Tokyo. This structure, completed by the Shimizu Construction Company in 1989, is supported on twelve low profile Bridgestone bearings (Figure 5). A typical bearing is 0.976 m in diameter and 0.3 m high having twenty-nine steel shims, each 2.2 mm thick and thirty rubber layers, each 6.2 mm thick. Such a unit is rated at 500 tons capacity with a vertical stiffness of 3.5×10^5 t/m and a horizontal stiffness of 2.2×10^2 t/m. The design horizontal displacement is 0.375 m. As is shown in Figure 6, the building is asymmetric in plan thus rendering it susceptible to torsional seismic response. The design called for center of gravity and the torsional center to coincide. Three sizes of isolators were used, namely 400, 500 and 600 t rating. The movement of the building under small excitations, such as wind, is controlled by four oil dampers each installed with its axis horizontal (Figure 7) whereas twenty-four

@seismicisolation

vertical steel rod clusters are installed to provide energy absorption in large movements (Figure 8). The bearings do not have any central cores in this instance but are composed of high damping rubber. Considerable effort has been expended to minimize the unintentional contributions to the horizontal stiffness which is provided frequently by secondary structure and service connections. The stair access to the basement has a discontinuity provided (Figure 9) and loops are provided in both the cables and pipelines carrying services (Figure 10).

OVERALL DESIGN LOAD CONSIDERATIONS

As befits a relatively new concept, no internationally accepted criteria exist for specifying the overall load resistance required of base isolated buildings. Indeed even the nationally applicable criteria are subject to ongoing, effectively continuous revision. A common requirement is that a planned base isolated building shall be treated as a special structure and consequently subjected to extensive time-history computer analyses to determine anticipated responses to selected accelerograms[4]. Whereas in Japan and New Zealand the effects of base isolation are taken into account in determining the required strength of the supported superstructure, with a consequent significant saving relative to a similar non-isolated structure, proposals being advocated recently in California[5] read:

> "Displacement Restraint. The isolation system may be configured to include a displacement restraint that limits lateral displacement due to the Maximum Credible Earthquake to less than 1.5 times the total design displacement, provided that the seismic-isolated structure is designed in accordance with the following criteria when more stringent than the requirements of Section 2333:
>
> (1) Maximum Credible Earthquake response is calculated in accordance with the dynamic analysis requirements of Section 2335, explicitly considering the nonlinear characteristics of the isolation system and the structure above the isolation system.
>
> (2) The ultimate capacity of the isolation system and structural elements below the isolation system shall exceed the strength and displacement demands of the Maximum Credible Earthquake.
>
> (3) The structure above the isolation system is checked for stability and ductility demand of the Maximum Credible Earthquake.
>
> (4) The displacement restraint does not become effective at a displacement less than 0.75 times the total design displacement unless it is demonstrated by analysis that earlier engagement does not result in unsatisfactory performance."

If adopted these requirements will call for California base isolated buildings to be constructed to a stability and ductility level appropriate to the superstructure being supported conventially rather than on base isolators. Application of such a conservative requirement must mitigate against the choice of seismic base isolation except for very special projects where commercial viability is not a major concern.

@seismicisolation

It is likely that the evolution of a more rational set of guidelines will have to await comprehensive examination of the behavior of a representative group of isolated structures which do experience very strong ground motion in future earthquakes. Until this information becomes available it appears very probable that the present degree of uncertainty regarding overall response will persist leading to the almost inevitable trend to excessive conservatism.

In the meantime a better understanding of the internal stress distribution within individual bearings is an area in which progress may be made. Success in this will allow a less conservative approach to be used in the design of individual isolation.

MATHEMATICAL MODELLING

The mathematical model widely used currently to predict the behavior of elastomeric bearings is based on simple small strain elastic theory. Stress is assumed linear with respect to strain and the vertical stiffnesses k_v may be expressed as

$$k_v = \frac{P}{\delta} = \frac{E_c A}{n t} \tag{1}$$

where P is the vertical load, δ the vertical displacement, A the cross sectional area of the bearing, n the number of elastomeric layers, t the thickness of each layer and E_c an equivalent compression modulus of the elastomer.

A similar approach leads to the horizontal stiffnesses k_H being expressed as

$$k_H = \frac{F}{\Delta} = \frac{G A}{n t} \tag{2}$$

where F is the horizontal load, Δ the horizontal displacement, and G the equivalent elastic shear modulus of the elastomer.

Modifications of these expressions for bearings with many layers have been suggested [6], however, use of the simple equations, together with allowable compressive stresses of around 6.9 MPa, a shear modulus of 0.69 MPa, and limiting shear strains of 150% can be used for initial design choices. Clearly the equations do not reflect the observed non-linear behavior of the elastomer, nor do they provide any information on the internal stresses and strains within the bearing. If an improved understanding of the actual behavior of multi-layered isolators is to be developed, a more realistic mathematical model is needed. One possible approach utilizes finite elements to represent the elastomer and the steel shims. A constitutive model of the elastomer is needed for strains greater than unity, whereas most codes utilize small strain theory. Another problem is that it is not easy to determine the material properties experimentally and the analyses are particularly sensitive to the value of shear modulus. The choice of elements to represent the continuum accurately is important. It appears that at least seven elements are required vertically for each elastomer layer if the bulge of the material in compression is to be correctly represented. Many bearings with large numbers of layers, some with thirty two laminates, are now being used. In such cases, the total number of elements may well be of the order of several thousand, and the use of a very large capacity computer is necessary.

@seismicisolation

The availability of PATRAN, a general purpose, 3-D Mechanical Computer Aided Design code has enabled finite element models of elastomeric laminated bearings to be studied. PATRAN uses extensive graphics capabilities, to assist in interpreting input and output data, and can be linked to many major finite element analysis programs as well as its own P/FEA code.

Initial analyses were undertaken on an Apollo Domain 3500 using version 2.3 of PATRAN and the P/FEA finite element program. To avoid excessive computation, a low shape factor bearing for which experimental results were available[7] was chosen for analysis. Details of the bearing are shown in Figure 11. A three dimensional model of the bearing was set up with five hundred and sixty elements. Each steel shim was modeled by one element vertically, and the elastomer layer by four elements vertically. The rubber was assumed to be linear elastic, isotropic and incompressible hence Poisson's ratio was set at one half. The shear modulus was devised from the published experimental results[7] as 0.83 MPa and the elastic modulus was then determined to be 2.5 MPa. When Poisson's ratio was adjusted to 0.49983 good agreement was found between the analytical results and the experimental ones.

Further analyses were undertaken, utilizing a finer mesh, on a DEC 5000/200 system and the latest version of PATRAN namely 2.4. The rubber layers were represented by seven elements, vertically, as shown in Figure 12. As shown in Figures 13 and 14 analytical results matching the experimental ones were obtained using 0.49998 for Poisson's ratio. However it was noted that the internal stress and strain values and distribution were different than those established by the initial analyses. This is consistent with the fact that the P/FEA coding does not allow explicitly for large strain theory. It may be concluded that an analysis of the type undertaken using the P/FEA program is of value to obtain an approximate solution of the conditions inside a bearing but that a more sophisticated technique is called for if reliable accurate analyses are to be carried out.

To this end work has started using a general-purpose finite element program MARC K.4 which is designed specifically for both linear and non-linear analyses of structures including elastoplastic large deformation considerations. Use of MARC K.4 will be facilitated by the availability of MENTAT 5.4 which is a compatible general purpose interactive graphics pre and post processor. The analyses are being undertaken on a CONVEX computer so it is not expected that capacity will prove to be a problem.

Once a viable analysis procedure has been established it is hoped to advance the understanding of the behavior of elastomeric bearings at high strains by investigating some of the following aspects. This distribution of stress and strain at the rubber-steel interface is, as yet, understood imperfectly. The axial stiffness, and particularly the axial stiffness at high shear strains, can not yet be predicted accurately. Similarly, the relationship between the increasing shear strain and the height of the bearing is not readily predicted by current analyses. Methods are not available for determining, at the design stage, the critical displacement at the onset of rollover and the critical buckling load at high shear strains. Also, the effects of the different boundary conditions represented by the top and bottom plates being connected by bolts or dowels to the structure are not thoroughly understood.

@seismicisolation
@seismicisolation

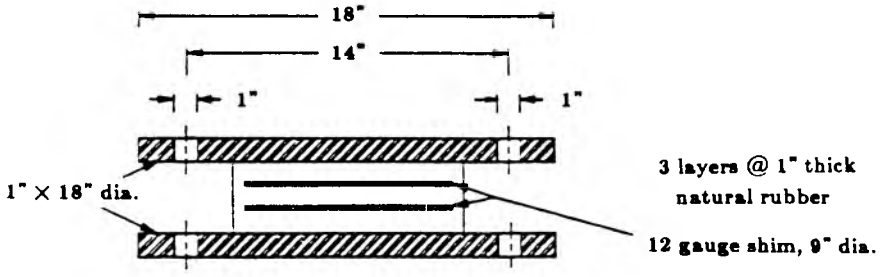

Figure 11 Bearing analysed (after Tajirian 1990)

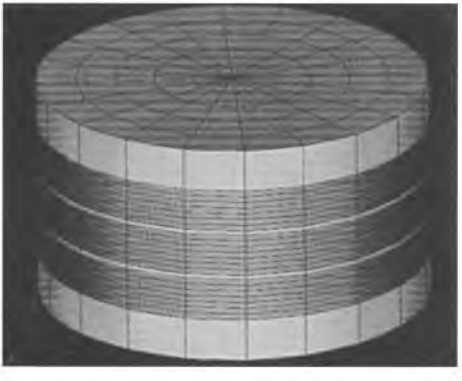

Figure 12 3-D PATRAN model of bearing

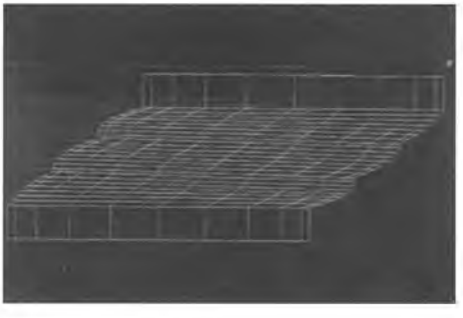

Figure 13 2-D view of model loaded to 133% shear strain

ACKNOWLEDGEMENTS

The information on the Bridgestone Toranomon building was provided by Dr. Tetsuji Itoh of the Ohsaki Research Institute of the Shimizu Corporation who also arranged for the authors to visit the completed structure.

The financial support for the second author's research work at the University of California, Irvine, is provided by the National Earthquake Engineering Research Center, State University of New York at Buffalo. The continuing encouragement of Dr. I.G. Buckle, Deputy Director of the Center is gratefully acknowledged.

@seismicisolation

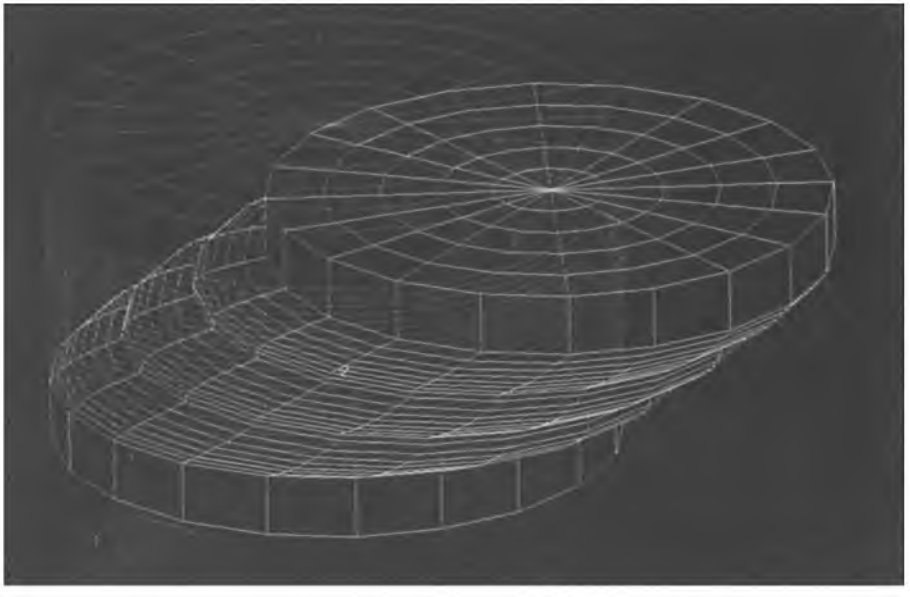

Figure 14 3-D view of model loaded to 133% shear strain

REFERENCES

1. Bechtold, J., Earthquake-Proof Building, United States Patent No. 845, 046, 1907.

2. Buckle, I.G. and Mayes, R.L., Seismic Isolation: History, Application and Performance, Earthquake Spectra, 1990, 6,2, 161-201.

3. Bailey, J.S. and Allen, E.W., Seismic Retrofitting: Salt Lake City and County Building, APT Bulletin, 1988, XX, 2, 32-44.

4. McKay, G.R., Chapman, H.E. and Kirkcaldie D.K., Seismic Isolation: New Zealand Applications, Earthquake Spectra, 1990, 6,2, 203-222.

5. Uniform Building Code, (proposed) 1991 Edition, International Conference of Building Officials, Whittier, California.

6. Kelly, J.M., Aiken, I.D. and Tajirian, F.F., Mechanics of High Shape Factor Elastomeric Seismic Isolation Bearings, Report UCB/EERC 90-01, University of California, Berkeley, 1990.

7. Tajirian, F.F., Aiken, I.D., and Kelly J.M., Seismic Isolation for Advanced Nuclear Power Stations, Earthquake Spectra 1990, 6,2, 371-401.

@seismicisolation

THE USE OF DISCRETE DAMPERS TO REDUCE THE TORSIONAL RESPONSE OF STRUCTURES TO EARTHQUAKES

DAVID KEY
Senior Partner, CEP Research, Consulting Engineers
6 Vyvyan Terrace, Clifton, Bristol BS8 3DF
Visiting Industrial Professor, Department of Civil Engineering, University of Bristol

ABSTRACT

The use of discrete damping systems in reducing lateral response of building structures is well established. This paper examines the combined effect of a simple, single level, discrete damping system on torsional response in combination with lateral reponse. The system is found to be effective in controlling inter-storey shears and displacements.

INTRODUCTION

The use of isolation and discrete damping systems to reduce structural response to earthquakes is being used with increasing frequency. Specific applications are hospitals, offices, retrofitting non seismically qualified structures, laboratories and administrative centres [1,2,3]. Previous studies [4,5] and tests [6] have dealt with lateral response only, although the majority of damper-isolation systems have torsional degrees of freedom.

The object of this study is to establish the effectiveness of discrete dampers in reducing torsional response in combination with a reduction in lateral response. The study comprises the first stage of a more general study of multi-level damping of torsional and lateral response and is limited to the single level, base isolated, case with discrete dampers.

The types of damper developed for use in earthquake resistant structures are described in references [9,10,11] and can be based on yielding steel, shear in lead, friction or lead extrusion.

@seismicisolation

ANALYSIS

The model used for the study is shown in Figure 1 and comprises a stick model with two lateral and one torsional degree of freedom at each floor level. Values of stiffness and mass used are representative of a framed reinforced concrete office building 30 metres square on plan and are shown in Table 1. This stage of the study is limited to the application of dampers at level 1 with the first storey constituting an isolation level corresponding to the introduction of lateral springing within the height of the first storey columns. (Ref. [1] describes an application of this type).

TABLE 1
Structural Model properties

LEVEL	MASS ($kgx10^6$)	ROTATIONAL INERTIA ($kg\text{-}m^2x10^8$)	LATERAL STIFFNESS (MN/m)	TORSIONAL STIFFNESS (MN-m)
1	1.23	1.84	1020	214000
2	1.23	1.84	1020	214000
3	1.23	1.84	320	67200
4	1.23	1.84	320	67200
5	1.23	1.84	320	67200

The damper layout is shown in Figure 2. Each damper comprises a link connecting the rigid ground supported structure to the flexible isolated structure. The hysteretic force displacement properties of the link are shown in Figure 3. The link is treated as hinged at each end so that the structure is free to move on plan. Limitations on damper displacement are taken as 350mm, equal to 70 percent of the link length of 500mm which is used in this study. Dampers are characterised by their peak hysteretic force p_d using the simple bilinear force-displacement relationship shown in Figure 3. This is a simple approximate model for a yielding steel damper and one which is considered to be adequate for the objectives of this study.

Analysis was carried out using SPAN5 which is described in the Appendix. The input accelerograms used are two computer generated events using PSEQGN [7] with a total duration of 20 seconds, 11 seconds of which is strong motion, and a peak acceleration of 0.3g. The spectral properties are representative of firm ground conditions. The accelerograms were applied in the X and Y directions with an eccentricity of 1.5 metres, representing 5% of the plan dimension of the structure. This eccentricity represents a typical seismic code requirement [8] intended to take account of accidental eccentricity of mass and resistance, combined with the effects of torsional ground motion.

@seismicisolation

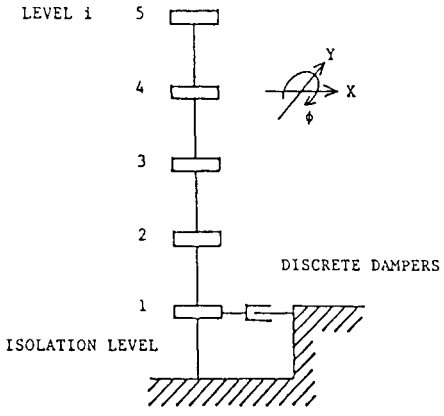

FIGURE 1 STRUCTURAL MODEL

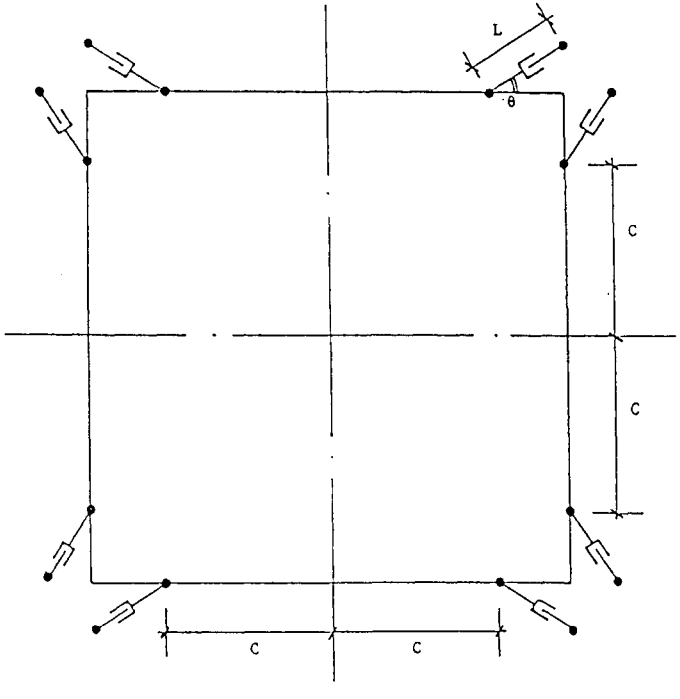

FIGURE 2 PLAN LAYOUT OF DISCRETE DAMPERS
L AND θ EQUAL FOR ALL DAMPERS

@seismicisolation

TABLE 2
Modal Frequencies- Structural Model

MODE	TRANSLATION X,Y (Hz)	ROTATION (Hz)
1	0.974	1.024
2	2.687	2.589
3	3.866	4.101
4	4.771	4.860
5	7.605	8.934

RESULTS

Parameters varied in the study were:-

(a) Inherent structural damping.
(b) Structural stiffness at level 1 (k_1).
(c) Discrete damping parameter (p_d).
(d) Discrete damper configuration.

In the case of (a) the results are relatively insensitive to inherent structural damping so that only the results for a critical damping ratio of 0.02 are presented. The level 1 stiffness k_1 was chosen to represent much lower frequencies than are common in isolation for the reason that this is the region of optimum damper-isolation system performance. The discrete damping parameter p_d was chosen to cover level 1 displacements up to approximately 300mm. In general a practicable acceptable displacement is in the order of 150mm and values were selected to bracket this figure. The damper configuration parameters C, L and θ are defined in Figure 2. C and L were taken as 14 metres and 0.5 metres respectively throughout. Two arrangements were used with θ equal to zero and 45 degrees.

Plots of level 1 response are shown in Figures 4 to 8 using the configuration with θ equal to zero. Displacements are represented in appropriate units, but level 2 shears are shown as proportions of the level 2 shear for the unisolated case with k_1 equal to the value shown in Table 1. Base shear is commonly used as a measure of the earthquake input into a structure so that the ratio to the unisolated case is often taken as a measure of the effectiveness of the isolation-damping system. However it was found that interstorey shears in the isolated structure did not follow the pattern in typical non-isolated structures where the base shear reduces with height. Table 3 shows the ratios of the maximum interstorey shear to the level 2 shear so that the apparent benefit of a reduction in base shear needs to be considered in the light of this redistribution of shear.

@seismicisolation

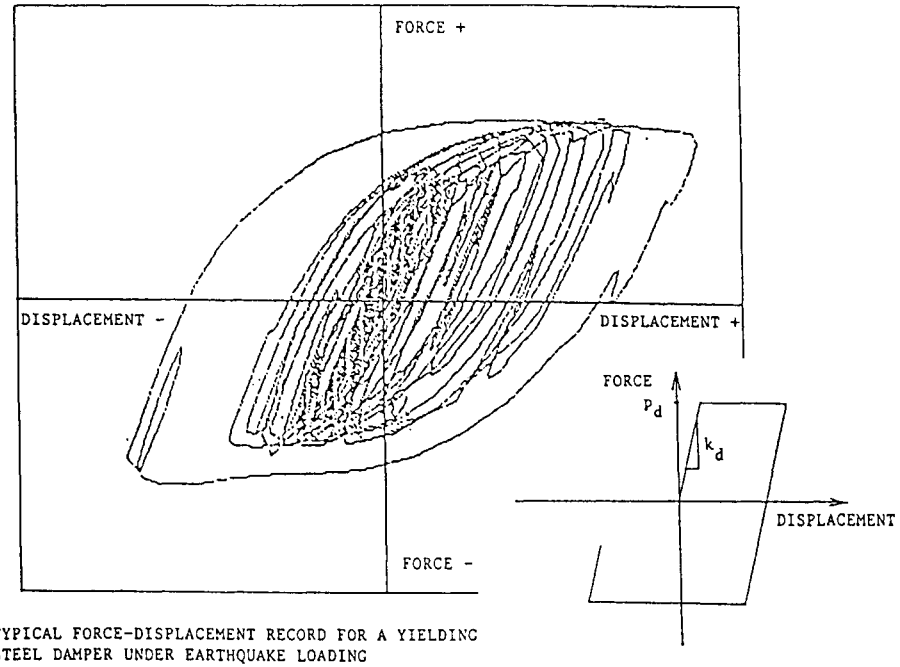

TYPICAL FORCE-DISPLACEMENT RECORD FOR A YIELDING STEEL DAMPER UNDER EARTHQUAKE LOADING

ANALYTICAL MODEL OF DAMPER RESPONSE

FIGURE 3 DAMPER RESPONSE

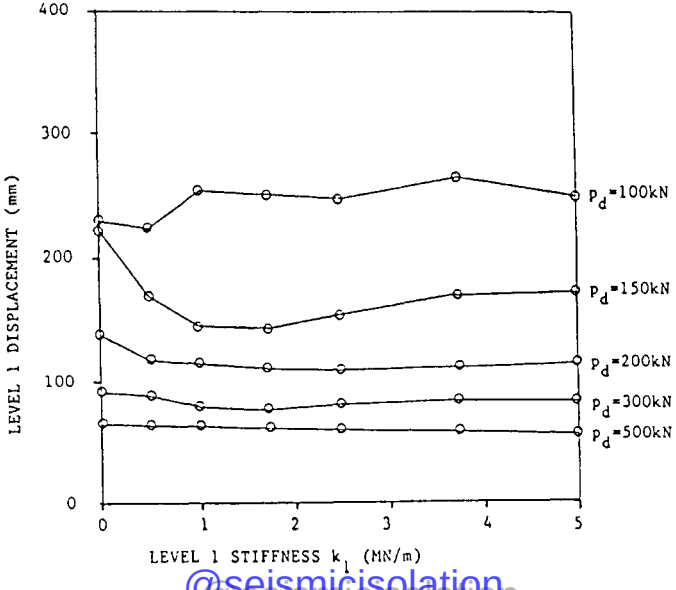

@seismicisolation

FIGURE 4 X AXIS DISPLACEMENT AT LEVEL 1

TABLE 3
Ratios of the Maximum Storey Lateral Shear to Level 2 Shear

p_d(kN)	k_1=50kN	k_1=500kN	k_1=5000kN
0	1.0	1.0	1.0
50	1.24	1.27	1.0
100	1.46	1.62	1.0
150	1.24	1.42	1.16
200	1.32	1.25	1.26
250	1.27	1.28	1.20
300	1.33	1.33	1.29
350	1.29	1.29	1.18
400	1.14	1.14	1.07
450	1.08	1.04	1.03
500	1.04	1.12	1.03

In order to examine the effect of a change in the configuration of the dampers a set of results were obtained for a single value of k_1 equal to 1.75MN, with the angle of the damper link, θ changed to 45°. A comparison of the response values is shown in Table 4.

TABLE 4
Effect of Changed Damper Configuration on Response
Ratio of Response with θ=0 to Response with $\theta=45^o$ for k_1=1.75MN

p_d(kN)	X	Y	φ	V_{x2}	V_{y2}
0	1.0	1.0	1.0	1.0	1.0
50	1.05	0.96	3.93	0.98	1.06
100	0.98	1.05	3.13	1.0	1.07
150	0.78	1.07	2.85	0.88	0.89
200	0.72	0.90	1.13	0.92	0.93
250	0.55	0.71	2.41	0.88	0.99
300	0.57	0.55	3.07	1.0	1.02
350	0.67	0.63	3.33	1.02	0.98
400	1.04	0.66	1.72	0.98	0.89
450	0.90	0.62	2.17	0.91	0.95
500	0.74	0.59	2.96	0.86	0.91
MEAN	0.80	0.77	2.67	0.94	0.97

DISCUSSION

The behaviour of the discrete damper system which has been examined is non-linear and there is strong interaction between the lateral and torsional damper reactions to displacement. For this reason it was not easy to visualise the extent to which the system would be effective in torsion.

The results show response patterns in lateral shear which are similar in form to those found in earlier work [12] for a ten storey structure. The use of discrete dampers enables the

@seismicisolation

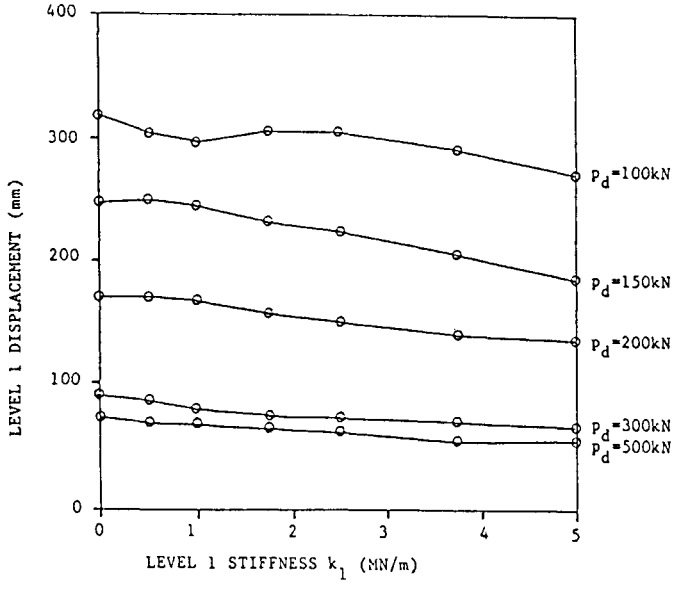

FIGURE 5 Y AXIS DISPLACEMENT AT LEVEL 1

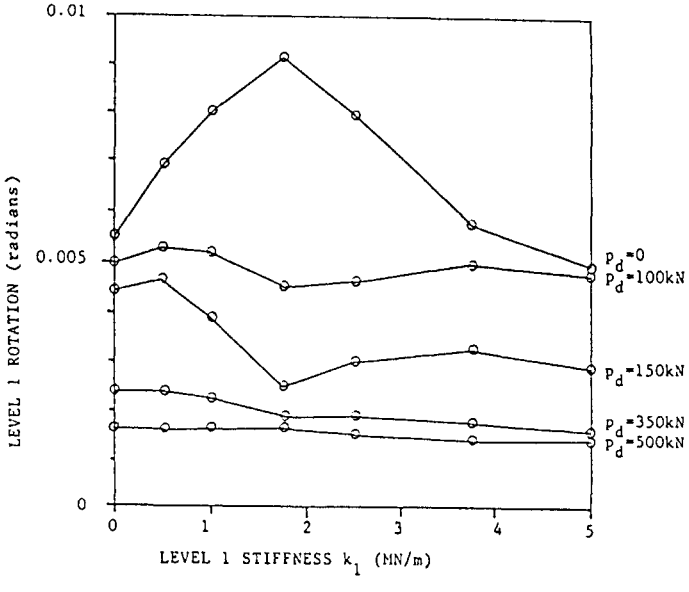

FIGURE 6 ROTATIONAL DISPLACEMENT AT LEVEL 1

@seismicisolation

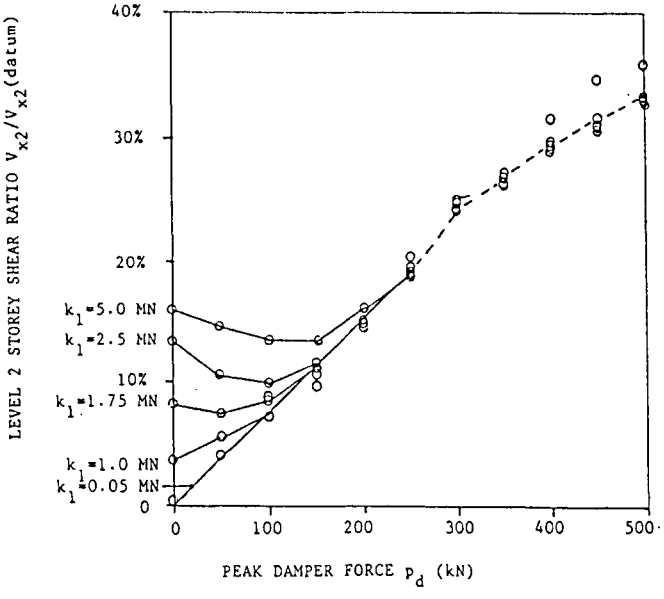

FIGURE 7 LEVEL 2 STOREY SHEAR RATIO
X AXIS

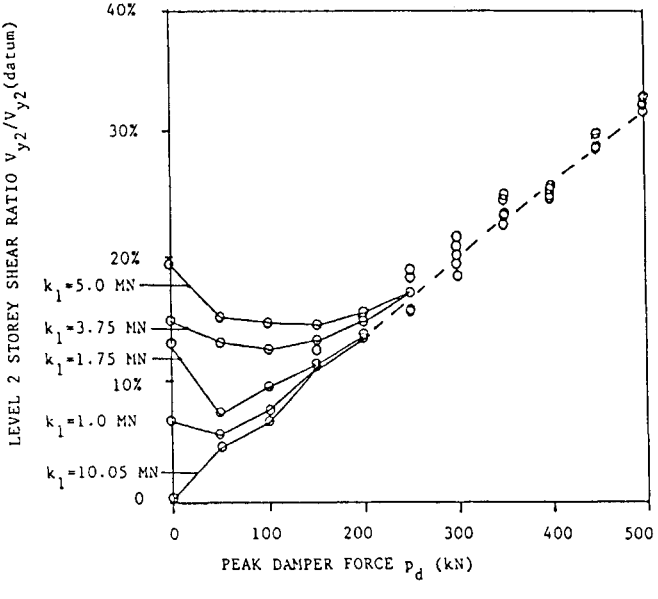

FIGURE 8 LEVEL 2 STOREY SHEAR RATIO
Y AXIS

@seismicisolation

designer to exert control over displacements and the level of inter-storey shears created in the building by ground motion.They also show that the dampers are as effective in reducing torsional response to ground motion as they are in reducing lateral response.

The figures in Table 4 clearly show the effect of changing the damper configuration. By inclining the dampers to the X and Y axes the effective orthogonal damper forces are reduced while the effective lever arm of those forces about the centre of the building is increased. The values in Table 4 are a measure of the effectiveness of the changed configuration in reducing response. In the X and Y directions displacement response is increased although the level 2 shears remain much the same. In the torsional direction however reponse is reduced by a mean factor of 2.67. The significant feature of these figures is that the designer is able to control independently the damping of lateral and torsional response.

Table 3 illustrates the point that the use of base shear alone as a performance indicator for isolation-damping systems needs to take into account the effect on response at higher levels as well, with inter-storey shears running up to 62% higher than at level 2.

Other non-linear structural systems respond to torsional displacement - including friction braced frames [9], eccentric braced frames and knee braced frames [5]. Any such system will also tend to reduce the torsional as well as the lateral response to ground motion.

CONCLUSIONS

Discrete damping systems are effective in reducing horizontal torsional response of building structures and by adjusting the configuration to provide more or less torsional damping independent control can be exerted over the lateral and torsional response of the structure.

ACKNOWLEDGEMENT

This research has been supported by CEP Research, Bristol and the CEP group of consulting engineers in the UK and West Indies.

REFERENCES

1. Civil Engineering, ASCE, November 1989, 64-67
2. Rubber Developments, 43, 1/2, 1990, 18
3. Civil Engineering, ASCE, September 1990, 72-75

@seismicisolation

4. The earthquake response of building structures with energy absorbing dampers, D E Key, PhD Thesis, Department of Civil Engineering, University of Southampton, 1985
5. Knee bracing system for earthquake resisting steel frames, N Bourahla, Department of Civil Engineering, University of Bristol, PhD Thesis, 1990
6. J M Kelly, M S Skinner, K E Buecke, Experimental testing of an energy-absorbing base isolation system, UCB/EERC-80/35, Earthquake Engineering Research Center,University of Berkeley, 1980, 73
7. P Ruiz, J Penzien, Probabilistic study of the behaviour of structures during earthquakes, Report EERC-69-3, March 1969, Earthquake Engineering Research Center, University of California, Berkeley.
8. Recommended Lateral Force Requirements and Commentary, Seismology Committee, Structural Engineers Association of California, 1988
9. A S Pall, Response of friction damped buildings, Eighth World Conference on Earthquake Engineering, San Francisco 1984, V5, 1007-1014
10. R I Skinner, R G Tyler, A J Heine, Steel beam dampers for increasing the earthquake resistance of structures, Seventh World Conference on Earthquake Engineering, Istanbul, 1980, V4, 387,394
11. R I Skinner, R G Tyler, A J Heine, W H Robinson, Hysteretic dampers for the protection of structures from earthquakes, Bulletin of the New Zealand Society for Earthquake Engineering, V13, 1, March 1980, 22-36
12 D E Key, The seismic performance of energy absorbing dampers in building structures, Eighth World Conference on Earthquake Engineering, San Francisco, 1984, V, 1055-1062

APPENDIX A

SPAN5: Program to compute the time domain response of a structure incorporating discrete inelastic dampers

SPAN5 is a purpose written program solving the response of a stick building model to a discretised earthquake ground motion. The model used provides for three degrees of freedom at each floor level as shown in Figure 1. The time history algorithm is identical with that used in the program PANDA which is described in (4) and is based on the Wilson-theta method.

At each time step the resultant force-displacement equations between the dampers and the structure are solved by iteration. Figure 3 shows the force-displacement diagram for a single damper, the resultant forces at each level being obtained by summation in the X, Y and torsional directions for all eight dampers.

@seismicisolation

SEISMIC ISOLATION WITH HIGH DAMPING RUBBER BEARINGS THEORY AND PRACTICE

K.N.G. FULLER, H.R. AHMADI and V.A. COVENEY†
Malaysian Rubber Producers' Research Association
Tun Abdul Razak Laboratory, Brickendonbury,
Hertford SG13 8NL, England

ABSTRACT

The design principles for the use of high damping natural rubber laminated bearings as seismic isolators are outlined. The temperature and frequency dependences of the dynamic properties of the elastomer are discussed. The variation of the modulus with strain amplitude is emphasised. It is shown that despite the non-linearity the level of harmonics generated during the response of the material is low. Furthermore many important aspects of the behaviour of the material can be usefully approximated by linear viscoelastic models.

INTRODUCTION

Medium rise structures and their contents can be particularly vulnerable to earthquake damage because of resonance effects. In seismic isolation the structure is supported on compliant elements to reduce the natural frequency of the system and avoid resonances. Normally, only horizontal isolation is attempted for practical reasons. The concept dates back more than a century but it is only in the last decade that the technique has been gaining widespread acceptance in the United States, Europe, New Zealand [1] and most notably Japan [2].

Numerous designs for seismic isolators have been suggested [3,4] but most implemented schemes use laminated elastomer/steel bearings - with natural rubber being a major constituent of the elastomeric material. The isolators are similar in structure to laminated bridge bearings. However the requirements of low horizontal natural frequency and large displacements lead to earthquake bearings being taller. Specifications tighter in most respects are normally appropriate for seismic isolators than for bridge bearings.

† Now at Bristol Polytechnic

@seismicisolation

A measure of damping is beneficial in most practical base isolation schemes since it reduces peak accelerations, and the maximum displacement of the structure relative to the ground. Much of the benefit of damping is achieved at a level of 10% critical; increasing the damping from 10 to 20% of critical generally results in only a modest further reduction in peak acceleration and relative displacement [5]. Since natural rubber formulations normally give low damping, energy dissipation is sometimes provided by external dampers or, in the case of one class of isolator, by a lead plug within the bearings. Alternatively, high damping levels can be achieved by specialized elastomer formulations, normally based on high loadings of filler and oil in natural rubber. Such high damping natural rubber (HDNR) isolators are simple in design - an important advantage where high reliability with minimal maintenance are required.

DESIGN OF HDNR BEARINGS

Low horizontal stiffness (k_h) is a key requirement of isolators. Typically a horizontal natural frequency of around 0.5Hz is required for effective isolation. To a close approximation k_h of HDNR bearings is given by the simple formula involving the shear modulus of the elastomer (G), the cross-sectional area of the bearing (A) and the total elastomer thickness (T):

$$k_h = GA/T \qquad (1)$$

The stiffness k_h decreases with rise in the vertical load; the extent of this effect depends upon the geometry of the bearing but at a quarter of the buckling load a typical decrease may be about 10% [6]. It should also be borne in mind that G for HDNR materials is a function of shear strain (Fig. 1). Usually a modulus appropriate to the maximum design shear strain is chosen.

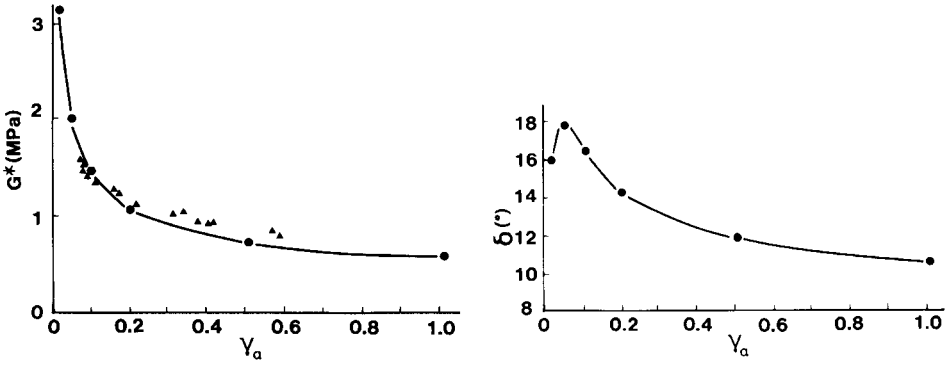

Figure 1. Shear modulus (G^*) and phase angle (δ) against shear strain amplitude (γ_a). ● data from sinusoidal tests (0.5Hz). ▲ modulus obtained from dividing the peak in the force signal to the corresponding peak in a displacement time history similar to that experienced by a bearing during an earthquake (El Centro 1940 earthquake)

@seismicisolation

The concept of shape factor (S) is used in calculating the vertical stiffness (k_v) of the isolator. It is defined as the ratio between the loaded area of the bearing and the force-free area of one elastomer layer. Thus for a circular bearing of diameter D made up of layers of thickness t, S = D/4t. For moderate shape factors (S = 3 to 7):

$$k_v \simeq 6GS^2A/T \qquad (2)$$

where A is the plan area of the bearing. It has been suggested [7] that an appropriate strain level is given by:

$$\bar{\gamma} \simeq \sqrt{6}Sy/T \qquad (3)$$

where y is the vertical deflection. Thus G in equation (2) should be $G(\gamma)$. Some HDNR bearings have very high shape factors; for these the finite bulk compressibility of the elastomer makes a significant contribution to the vertical deflection.

A second key requirement of HDNR isolators is sufficient load bearing capacity. One factor determining this is the maximum shear strain produced in the elastomer by the vertical deflection; the maximum strain (γ_m) occurs in the region at the edge of the reinforcing plate and is approximately given by

$$\gamma_m \simeq 6S\ y/T \qquad (4)$$

HDNR materials are typically capable of withstanding strains of 500% and some recently developed soft compounds fail at strains in excess of 700%. Another factor limiting load bearing capacity is the ability of the steel 'reinforcing' plates to withstand the tensile stresses produced within them. The maximum stress (σ_p) due to a compressive load $\sigma_c A$ on the bearing occurs in the centre of the reinforcing plates and is given by:

$$\sigma_p \simeq \sigma_c(t/t_s)(3+\nu)/2 \qquad (5)$$

where t is thickness of single layer of rubber, t_s the thickness of reinforcing plate and ν the Poisson's ratio of the plate material.

The non-linear behaviour of the HDNR material results in stiffer bearings at low horizontal forces. This fact is exploited to restrain buildings from excessive movement under wind-loading. For example, in one project [8] the displacement of the building due to such loading was reduced to levels comparable to the change in the length of the building due to a 20°C temperature change. An alternative is to use mechanical fuses strong enough to resist the wind force but which would break should an earthquake of significant magnitude occur. Such fuses would be an added complication which is removed by utilizing the elastic non-linearity of the HDNR compounds. The higher stiffness at low forces, however, can reduce the effectiveness of the base-isolation in the case of minor earthquakes.

The British Standard for bridge bearings (BS5400) forbids the placing of laminated rubber bearings into tension. In early base isolation projects this ruling was followed strictly, and isolation bearings located by dowels. The maximum shear displacement (δ_{roll}) which such a bearing (of plan dimension D, height H and supporting a load W) can sustain before

@Seismicisolation

"rolling out" can be found from:

$$X_{roll} \simeq WD/(k_h H + W) \qquad (6)$$

More recently there has been a move away from dowelled and towards bolted connections [9,10]. These enable a bearing of given plan dimension to sustain larger horizontal earthquake displacements since rollout is suppressed. As bolted connections place part of the rubber in tension at large horizontal displacements, cavitation may occur [6]. It is possible, however, that a limited amount of cavitation does not permanently effect the bearings subsequent performance. The bolted option also places higher stresses on the rubber-metal bond. Some bolted bearing designs [10] employ a very high shape factor and a relatively small total elastomer thickness. In order to accommodate the maximum expected earthquake displacements, the rubber must sustain particularly high strains and particularly high stresses are applied to the rubber-metal bond. Good bonds require strict quality control procedures in manufacture and mechanical testing of a large proportion of bearings is advisable especially for bolted bearings. Use of x-rays in non-destructive testing of bonds has been reported [11], and further developments in this area would be beneficial.

Although earthquake base isolation by means of HDNR is a relatively new technology, the use of natural rubber pads in structures extends back over a century. Natural rubber is attacked by oxygen and ozone, but for bulky components (such as earthquake isolation bearings) the effects are only superficial over timescales up to 100 years; large items made from appropriate formulations are relatively immune even to superficial attack. Furthermore the natural material subjected to a constant load is not susceptible to time-dependent crack growth. The bulk properties of suitably formulated natural rubber materials have been found to remain relatively stable over many years [12]. Evidence suggests this is not the case for all engineering elastomers [13].

All elastomers have a finite creep rate when under constant load so that the settlement of elastomeric bearing pads may have to be taken into account. Creep is comprised of a "physical" component due to molecular relaxation processes and a "chemical" component due to the breakage of crosslinks and main chains. The rate of physical creep decreases continuously with time and in fact the amount of creep is linearly proportional to log time. Chemical creep is however proportional to time. For HDNR material the extent of physical creep is likely to dominate for the first few years. The physical creep rate depends quite significantly on details of the natural rubber formulation, mode of deformation and strain. In simple shear at 50% strain typical physical creep rates for a medium (HDNR-1) and a low modulus (HDNR-S) high damping natural rubber material are 7% of the initial displacement per decade of time. Creep rates in HDNR bearings may be significantly less than those indicated if the shape factor is more than about 10 (plan dimension 40 times the elastomer layer thickness), since in this case a significant proportion of the vertical displacement will be due to dilatational rather than deviatoric deformation of the elastomer. If extremely low rates of settlement are required very high shape factor bearings, which are very stiff vertically, can be used.

@seismicisolation
@seismicisolation

DYNAMIC BEHAVIOUR OF HIGH DAMPING ELASTOMERS

The damping of some elastomeric materials (eg. nitrile or epoxidized natural rubber [ENR]) originates largely from molecular interactions associated with the elastomer-glass transition. For this type of material the complex shear modulus and the loss factor depend significantly on temperature and frequency.

Unlike nitrile rubber and ENR, HDNR materials derive their high level of damping mainly from interactions involving solid filler particles added to the elastomer formulation and the sensitivities of shear modulus (G*) and loss angle (δ) to frequency and temperature are low. In Figure 2 a medium modulus HDNR material (HDNR-1) is compared with a harder (HDNR-2) and a softer (HDNR-S) variant; heavily (ENR-HI) and less heavily (ENR-LO) filled ENR; and a material developed in Japan (HD-J). Comparison of the behaviour of δ for the two ENR compounds shows that the more highly filled one gives more damping and a smaller temperature variation. However G* and δ are strongly dependent on strain amplitude (γ_a), for compounds containing significant amounts of filler (Fig 1.)

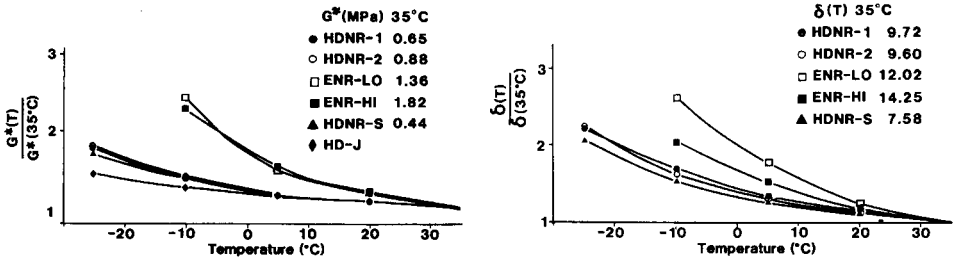

Figure 2. Temperature dependence of the dynamic properties of High Damping elastomers

Models for Dynamic Behaviour of High Damping Natural Rubbers

Because they lead to tractable equations the Kelvin and the standard linear (SL) models are commonly used to represent materials with damping. Both models (and, indeed, all linear models) give sinusoidal force-time signals for sinusoidal displacements; force-displacement plots are elliptical, and no harmonics are generated. Under shear deformation, HDNR materials generally show force-deformation loops which are not elliptical (Fig 3a), except at low strain amplitudes (<1%). The dependence of the dynamic shear modulus $|G^*|$ on the strain amplitude is also manifested by the presence of higher harmonics (mainly odd ones) in the force signal. Numerical simulation of the dynamic behaviour of HDNR materials has been carried out using a Kelvin model (consisting of one spring in parallel with a dashpot) modified to take account of non-linearity. The parameters of the model were set according to the instantaneous applied strain using sinusoidal test data similar to that in Figure 1. The in-phase modulus G' (= $|G^*|$ cosδ) was taken to define the stiffness of the spring. The out of phase modulus G" (= $|G^*|$ sinδ) which is proportional to the

@seismicisolation

viscosity coefficient of the dashpot was kept constant throughout each cycle.

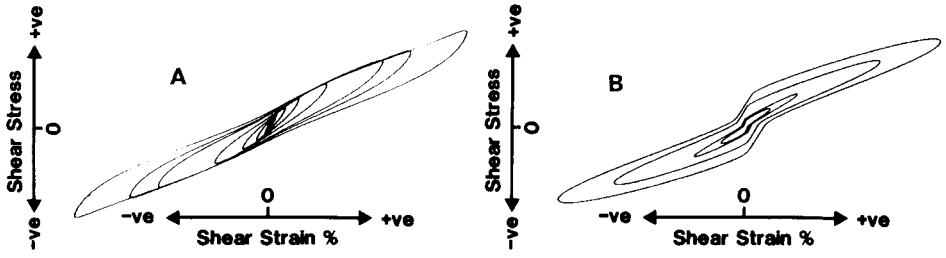

Figure 3. Hysteresis loops (a) observed for High Damping Natural Rubber (HDNR-1) (b) calculated from modified Kelvin Model.

Figure 3b shows the force-deformation loops calculated with the modified Kelvin model for sinusoidal displacements. The form of the loop around low strains is a consequence of the high modulus in this region. The third harmonic in the predicted force signal is the highest as observed experimentally. Table 1 shows the level of the third harmonic observed for HDNR-1 as a function of shear strain amplitude and that predicted by the modified Kelvin model. The latter are much higher than those seen

TABLE 1
Third Harmonic level in force signal (% of fundamental)

	Shear strain amplitude						
	0.02	0.05	0.1	0.2	0.5	0.7	1
(a)	2.4	2.8	2.5	1.9	1.8	2.9	3.9
(b)	0.2	12.2	13.1	12.3	10.9	10.3	9.7

(a) sinusoidal test on HDNR-1 (frequency 1Hz)
(b) Modified Kelvin Model

experimentally. The model predicts a peak in the third harmonic level at a strain close to that at which loss factor is a maximum. Such a coincidence of the peak in the third harmonic and loss factor has been observed [14]. Experiments on HDNR-1, however, have not shown a peak in the third harmonic level. Although the modified Kelvin model predicts some of the features observed, it appears to overestimate the effect of non-linearity on the shape of the hysteresis loop and the level of harmonics.

A test piece of HDNR-1 was subjected to periodic shear using a triangular wave form and the resulting force signal recorded (Fig 4). The force signal has been shifted along the time axis to make the peaks and troughs

@seismicisolation

of the signal coincide. It seems that non-linearity in the force signal is associated with a change of direction in the displacement signal rather than displacements close to zero. This change in stiffness following "retraction" is well known. In contrast with the modified Kelvin model, the force-time signal for the real elastomer does not go through any changes as it passes through the "low strain" region; the non-linearity therefore may be attributed to the "retraction" rather than simply on the variation of the modulus with strain.

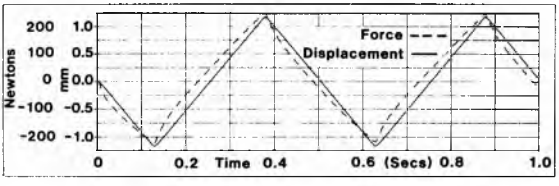

Figure 4. Force and displacement histories for HDNR-1 material subjected to a triangular wave (frequency 2Hz, strain amplitude 0.20)

EARTHQUAKE SIMULATION

Earlier studies [15] suggest that the standard linear solid adequately models the behaviour of HDNR during earthquake-type strain histories. Further experiments have been performed to test the extent to which the behaviour of HDNR during an earthquake can be modelled linearly and the degree to which HDNR materials will introduce higher harmonics into the isolated structure during an earthquake. A testpiece of HDNR-1 was subjected to a 'representative' shear-displacement history and the resulting shear-force history was monitored. The chosen displacement history (EC) was calculated by applying the El Centro 1940 earthquake (SOOE horizontal component) to a single degree of freedom mass on a linear Kelvin model system with a natural frequency of 0.5Hz and damping 0.1 of critical. The displacement history obtained had a very strong component at the isolation frequency and approximated to a modulated 0.5Hz sinusoidal signal (Fig 5).

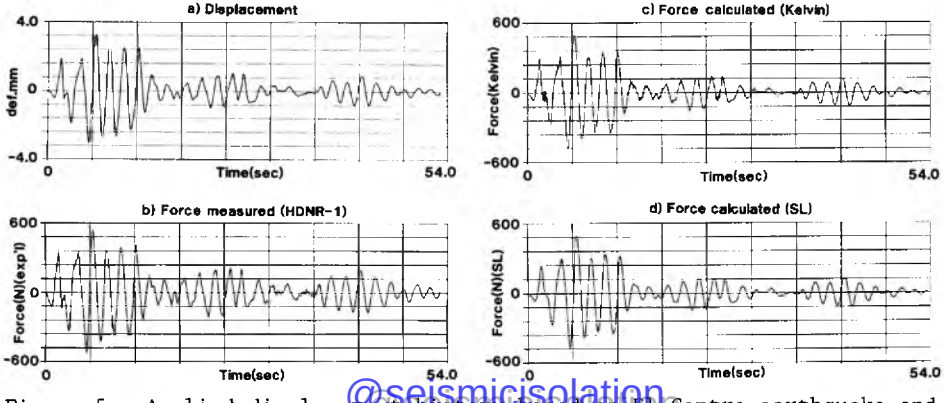

Figure 5. Applied displacement history based on El Centro earthquake and corresponding observed and calculated force histories

@seismicisolation

The experimental force signal shown in Figure 5 was first analysed by dividing force levels at peaks (and troughs) by the corresponding peak displacements. The resulting stiffness values are compared with 6th cycle stiffnesses obtained from standard sinusoidal tests in Figure 1. The two sets of stiffness values are remarkably similar and indicate that large shear strain cycles during an earthquake may exert only a minor effect on subsequent small strain amplitude cycles. In spite of the marked non-linearity the form of the frequency spectrum of the force signal was almost indistinguishable from that of the applied displacement history (Fig 6). The force level at 1Hz was 4% of that at 0.5Hz; this is only slightly greater than the level of applied displacement at 1Hz 3% of that at 0.5Hz).

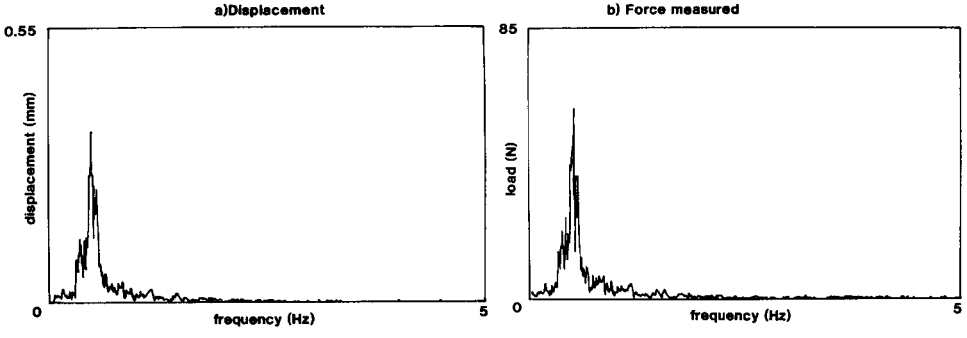

Figure 6. Fourier tranforms of the applied displacement history and observed force history in figure 5

The experiment was repeated with the timescale of the displacement history reduced by factors of 2 and 2.82. The results showed similar nonlinear behaviour regarding amplitude-dependent stiffness in all cases. This suggested that many aspects of the behaviour of HDNR observed in shaking-table tests, in which the timescale is reduced, are valid for full-scale performance.

The force response history of the elastomer to the above calculated displacement history is compared with that predicted by a linear Kelvin and an SL model in Figure 5. The parameters for the two models were chosen in the following way. The loss angles (δ) and the complex shear modulus (G^*) given by the models were matched to those of HDNR-1 when subjected to a steady sinusoidal deformation at 0.5Hz and at a strain amplitude equal to half the peak strain amplitude during the applied strain history. The SL model required an additional parameter which was found by matching the frequency dependence of the loss angle predicted by the model with that observed for the material at 0.5Hz.

Both the Kelvin and SL models represent many of the gross features of the observed material behaviour - the SL offering no significant improvement over the Kelvin model; the linear models do, however, under-estimate the peak force levels during small strain cycles. More accurate predictions of the peak force levels would be given by a Kelvin model modified to have strain-dependent stiffness, but unrealistically high levels at frequencies above 0.5Hz would be predicted in the force signal.

@seismicisolation

CONCLUSIONS

Despite non-linearity of HDNR compounds, many important aspects of the behaviour of earthquake bearings can be successfully predicted by simple linear viscoelastic models. Indeed, attempts to explicitly include non-linearity into the models leads to over estimation of the level of harmonics present.

ACKNOWLEDGEMENTS

We would like to thank A.H. Muhr and A.G. Thomas for their helpful discussions.

REFERENCES

1. Buckle, I.G. and Mayes, R.L., 1. Seismic Isolation: History, Application and Performance - A World View. Earthquake Spectra 1990, 6, pp.161-201.

2. Kelly, J.M., Base Isolation in Japan, UCB/EERC-88/20, University of California, Berkeley.

3. Su, L., Ahmadi, G. and Tadjbakhsh, I.G., A comparative study of performances of various Base Isolation Systems, Part I: Shear beam structures, Earthquake Engineering and Structural Dynamics, 1989, 18, pp.11-32.

4. Su, L., Ahmadi, G. and Tadjbakhsh, I.G., A comparative study of performances of various Base Isolation Systems, Part II: Sensitivity Analysis, Earthquake Engineering and Structural Dynamics, 1990, 19, pp.21-33.

5. Delfosse, G.C., Wood framed individual houses on seismic isolators. In Proceedings of the International Conference on Natural Rubber for Earthquake Protection of Buildings and Vibration Isolation, 1982, Kuala Lumpur, ed. C.J. Derham, Malaysian Rubber Research and Development Board.

6. Thomas, A.G., The design of Laminated Bearings I. Ibid.

7. Muhr, A.H., Tan, G.H. and Thomas, A.G., A method of allowing for non-linearity of filled rubber in force-deformation calculations. J.Nat. Rubb.Res., 1988, 3, pp. 261-276.

8. Derham, C.J., Kelly, J.M. and Thomas, A.G., Non linear Natural Rubber Bearings for Seismic Isolation, Nuclear Engineering and Design, 1985, 84, pp. 417-428.

9. Kojima, H. and Fukahori, Y., Performance and Durability of High Damping Rubber Bearings For Earthquake Protection; Presented at the American Chemical Society Meeting Fall 1989. Reprint No 18.

@seismicisolation

10. Giuliani, G.C., Structural and Practical requirements for the design of Seismically Isolated Buildings. In International Meeting on Base Isolation and Passive Energy Dissipation. Assisi - Italy, June 8-9, 1989.

11. Reinhardt, C.M. and Kovitch, F.J., Elastomer Flexijoints for TLP Tethers/Systems. Proc. 4th International Offshore Mechanics and Artic Engineering Symposium, Dallas, 1985.

12. Stevenson, A., Longevity of Natural Rubber in Structural Bearings, Plastics and Rubber Processing Applications, 1985, 5, pp. 253-258.

13. Babek, M., Franta, I., Hladacek, A. and Petrujova, A., Long-term ageing of rubbers in different environments: water, soil and on the shelf. In 'International Rubber Concerence Brighton' 1972, Paper F5.

14. Harris, J.A., Dynamic Testing Under Non-sinusoidal Conditions and the Consequences of Non-linearity for Service Performance, Rubber Chemistry and Technology, 1987, 60, pp. 870-887.

15. Derham, C.J. and Thomas, A.G., The Design and Use of Rubber bearings for Vibration Isolation and Seismic Protection of Structures. Engineering Structures 1980 2, (July) pp. 171-5.

@seismicisolation

APPLICATION OF FRACTIONAL CALCULUS IN MODELING VISCOUS DAMPERS

NICOS MAKRIS and M. C. CONSTANTINOU
Department of Civil Engineering
State University of New York, Buffalo, N.Y. 14260, U.S.A.

ABSTRACT

A fractional derivative model is proposed for viscous dampers which are used for vibration isolation of equipment and building structures. The development and calibration of the model is based on experimentally observed dynamic characteristics. The model is employed in the dynamic analysis of sliding isolation systems and in isolation systems with coupled horizontal-vertical-rocking motion.

INTRODUCTION

Viscous dampers consist of a moving part immersed in highly viscous fluid as shown in figure 1. These dampers have found application in seismic, shock and vibration isolation of buildings and equipment [1]. To represent the response of viscous dampers a fractional derivative Maxwell model is proposed. Fractional derivatives within the context of viscoelasticity have been used as early as 1936 by Gemant [2], and very recently by Koh and Kelly [3] who proposed a fractional Kelvin model for elastomeric bearings.

The dynamic characteristic of a viscous damper depends primarily on the properties of the viscous fluid. This fluid has both viscosity and elasticity that are frequency dependent. The authors [4,5] conducted dynamic tests on viscous dampers and observed that the frequency dependency of the mechanical properties of the units varied as frequency was raised to fractional rather than integer powers. Consequently a fractional derivative viscoelasticity model was proposed to describe the damper behavior over a wide range of frequencies.

This paper presents the development of the fractional derivative model and its application to the analysis of a) a sliding base-isolated model structure tested on a shake table and b) a seismically isolated structure in California.

FRACTIONAL DERIVATIVE MAXWELL MODEL

Oscillatory shear flow experiments were used to measure the storage and loss shear moduli of the fluid. In the frequency domain, the relation

@seismicisolation

between shear stress, $\bar{\tau}(\omega)$, and shear strain, $\bar{\gamma}(\omega)$ is expressed as

$$\bar{\tau}(\omega)=[G_1(\omega)+iG_2(\omega)]\bar{\gamma}(\omega) \tag{1}$$

where G_1 and G_2 are the storage and loss shear moduli, respectively, i is the imaginary unit and ω is the frequency of oscillation. Fig. 2 shows measured values of moduli G_1 and G_2 as a function of frequency at 5% amplitude of shear strain.

The shear stress-strain relationship in the fractional derivative Maxwell model is

$$\tau+\lambda D^r[\tau]=\mu D^q[\gamma] \tag{2}$$

in which τ and γ are the shear stress and strain, respectively and λ and μ are generalized material constants. $D^r[f(t)]$ is the fractional derivative of order r of the time dependent function f. A definition of the fractional derivative of a function satisfying the condition f(t)=0 for t<0 is via the following series which was given by Grunwald [6]

$$D^r[f(t)] = \frac{d^r f(t)}{dt^r} = \lim_{N\to\infty}\left\{\frac{[\frac{t}{N}]^{-r}}{\Gamma(-r)}\sum_{j=0}^{N-1}\frac{\Gamma(j-r)}{\Gamma(j+1)}\,f(t-j\frac{t}{N})\right\} \tag{3}$$

where Γ is the Gamma function.

The model of equation 2 is a special case of the more general model of Bagley and Torvik, [7]. It may be seen that the model of equation 2 collapses to the conventional Maxwell model when r=q=1, in which case λ and μ become the relaxation time and dynamic viscosity, respectively. Equation 2 may be written in the form of equation 1 by applying Fourier transform. The storage and loss shear moduli are given by

$$G_1 = \frac{\mu\,\omega^q\cos(q\frac{\pi}{2})\,[1+\lambda\omega^r\cos(r\frac{\pi}{2})] + \mu\,\lambda\omega^{q+r}\sin(r\frac{\pi}{2})\sin(q\frac{\pi}{2})}{d} \tag{4}$$

$$G_2 = \frac{\mu\,\omega^q\cos(q\frac{\pi}{2})\,[1+\lambda\omega^r\cos(r\frac{\pi}{2})] - \mu\,\lambda\omega^{q+r}\sin(r\frac{\pi}{2})\cos(q\frac{\pi}{2})}{d} \tag{5}$$

@seismicisolation

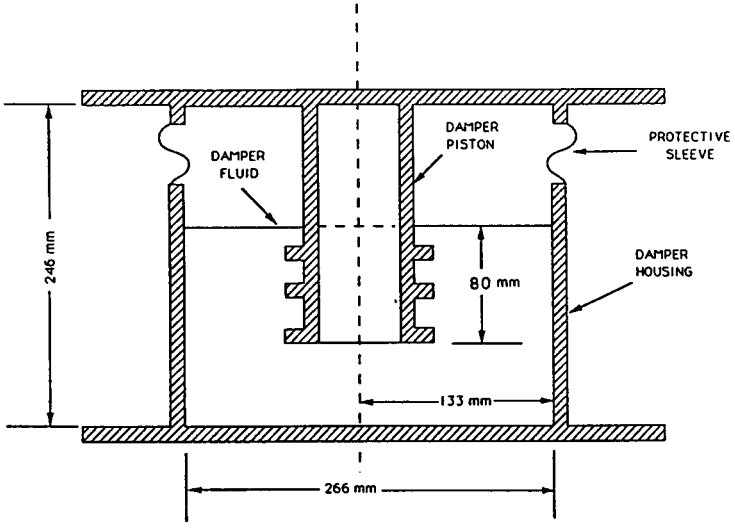

Figure 1. Tested Viscous Damper

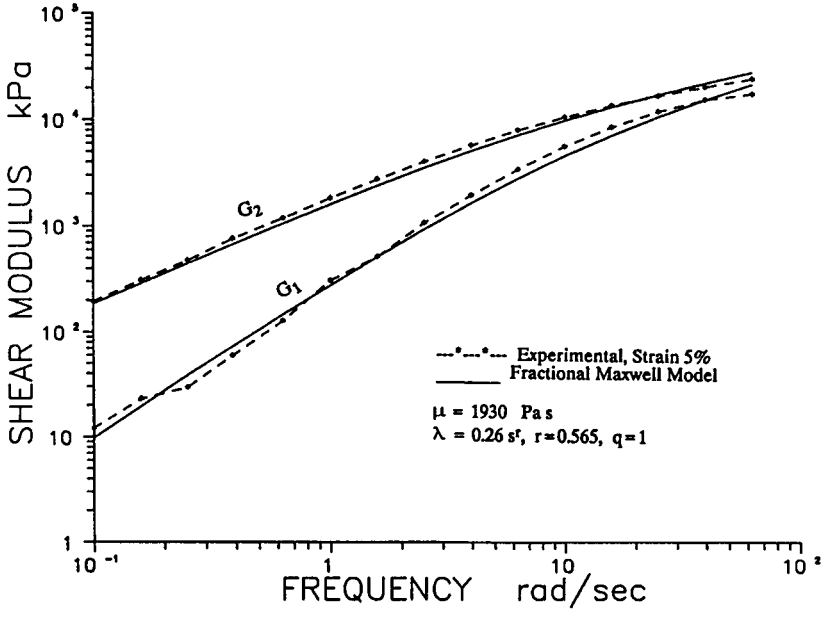

Figure 2. Measured Frequency Dependent Shear Modulus of Damper Fluid and Comparison to Prediction of Fractional Maxwell Model

@seismicisolation

$$d = 1 + \lambda^2\omega^{2r} + 2\lambda\omega^r \cos\left(r\frac{\pi}{2}\right) \tag{6}$$

The four parameters of the model were determined by fitting of the experimental data. The results were $\lambda = 0.26(\text{sec})^{0.565}$, $r = 0.565$ q=1 and $\mu = 1930$ *Pa*-sec. When q equals to unity, μ represents the dynamic viscosity of the fluid.

The force-displacement relation of the damper is expressed in a similar form as the stress-strain relationship of the fluid

$$P + \lambda D^r[P] = C_o D^q[u] \tag{7}$$

in which P is the force at the piston and u is the displacement of the piston. λ and C_o are physical constants.

The relationship between force amplitude, $\overline{P}(\omega)$, and displacement amplitude, $\overline{u}(\omega)$ is obtained by employing Fourier transform to equation 7

$$\overline{P}(\omega) = [K_1(\omega) + iK_2(\omega)]\ \overline{u}(\omega) \tag{8}$$

where K_1 and K_2 are the storage and loss stiffnesses. The mathematical expressions for stiffnesses K_1 and K_2 are identical to those for moduli G_1 and G_2 except that μ is replaced by C_o.

For convenience, the damping coefficient is introduced

$$C(\omega) = \frac{K_2(\omega)}{\omega} \tag{9}$$

so that the force developed at the piston of the damper in steady state harmonic motion is

$$P(t) = K_1(\omega)\ u(t) + C(\omega)\dot{u}(t) \tag{10}$$

where $\dot{u}(t)$ is the piston velocity.

Tests were conducted by imposing harmonic motion of the piston of the damper and measuring the force needed to maintain the motion. The recorded force-displacement loops under steady-state conditions were used to extract the frequency dependent mechanical properties of the damper in vertical and lateral motion for frequencies in the range of 0 to 50 Hz. The parameters of the model were determined in a least square fit of the experimental curves of storage stiffness and damping coefficient. The parameters of the model for the tested damper in vertical motion were q=1, C_o = 15,000 Ns/m, r = 0.6 and λ=0.3(sec)$^{0.6}$. For lateral motion the parameters were q = 1, C_o = 6000 Ns/m, λ = 0.15(sec)$^{0.7}$ r = 0.7.

Figure 3 demonstrates the very good agreement between the model predictions and the measured properties of storage stiffness and damping coefficient of the tested damper in vertical motion.

@seismicisolation

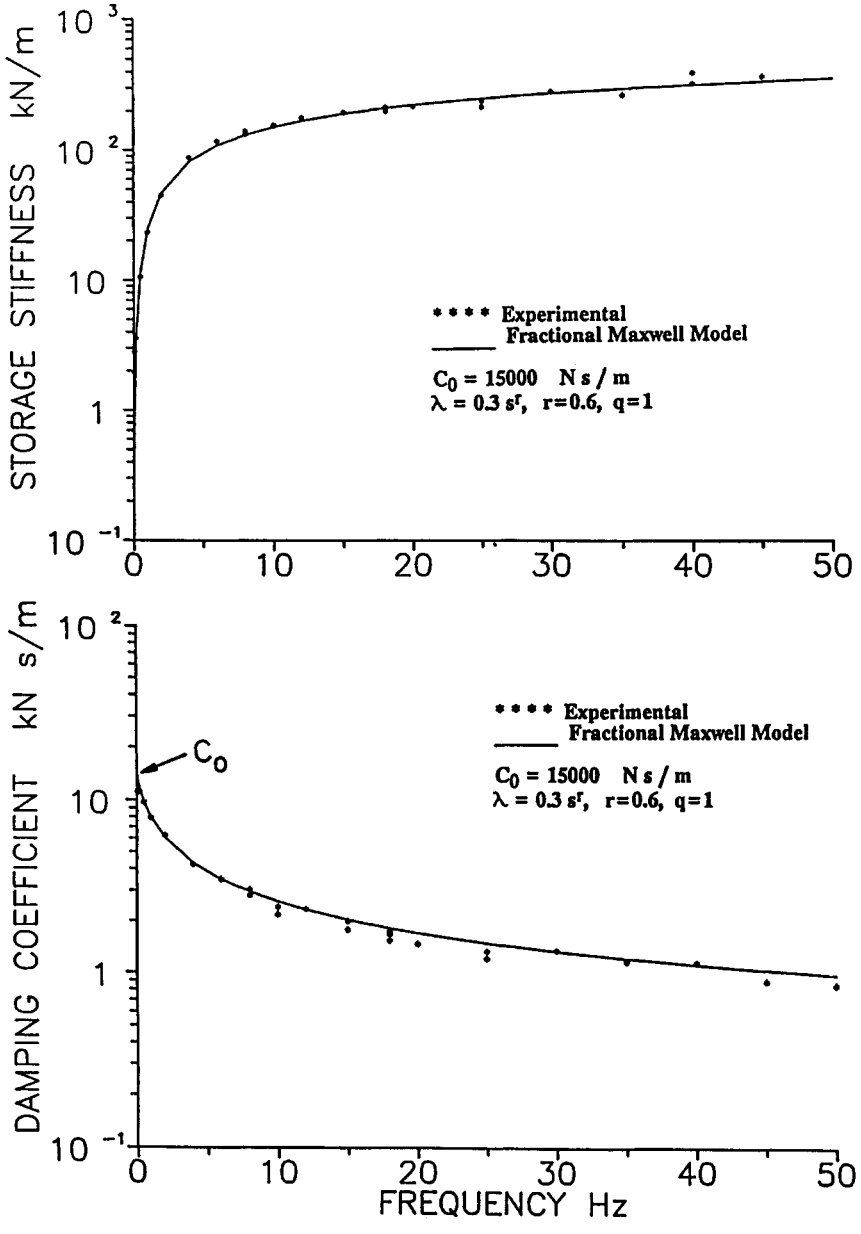

Figure 3, Fitting of Storage Stiffness and Damping Coefficient of Tested Damper in Vertical Motion by Fractional Maxwell Model

@seismicisolation

APPLICATION OF VISCOUS DAMPERS IN A SLIDING ISOLATION SYSTEM

Sliding isolation systems have been used for the seismic protection of structures. They are more stable and have lower bearing displacements than elastomeric isolation systems, at the expense however of higher structural accelerations. One such sliding system has been recently tested on a shake table using a six-story, quarter scale, 230kN model structure (Constantinou et al, [8]). The isolation system consisted of Teflon sliding bearings and restoring force devices in the form of helical steel springs. Initially the system was tested without the addition of viscous dampers. In a series of tests, the model structure was excited by the 1985 Mexico City earthquake with peak ground acceleration of 0.18g. The record was scaled to a peak table acceleration of 0.21g.

The same test was repeated with four viscous dampers added to the isolation system. These dampers were identical to the one tested. Fig. 4 compares the recorded and analytical predicted time histories of the base of the model without and with the viscous dampers.

Evidently, the dampers were effective in reducing the bearing displacement by about 20% (from a peak of 53.8mm to 43.5mm). This reduction in bearing displacement was associated with a slight increase in the interstory drift of the structure above the isolation system.

For the analytical prediction of the response of the system with viscous dampers, the mathematical model of friction presented by Constantinou et al, [6] has been used. In the equations of motion, the force from the four viscous dampers has been accounted for by the model of equation 7 with the experimentally determined parameters for motion in the horizontal direction: $q=1$, $r=0.7$, $\lambda = 0.15(\text{sec})^{0.7}$, $C_o=24{,}000$ Ns/m. The analysis was performed in the time domain so that the nonlinearity of the isolation system (friction) could be included. The evaluation of the damper force, equation. 7, was based on a modification of the G1-algorithm (Oldham and Spanier, [4]). In this algorithm, the fractional derivative is generated from the definition of equation 3 by omitting the $N\to\infty$ operation. More details may be found in the report of Makris and Constantinou [5]. The analysis results are compared in Figure 4 to the experimental results and the agreement is good.

COUPLED LATERAL-VERTICAL-ROCKING RESPONSE OF A RIGID BODY SUPPORTED BY SPRINGS AND VISCODAMPERS

Two residential buildings have been very recently constructed in Los Angeles, California on a seismic isolation system consisting of helical steel springs and viscous dampers. The superstructure is a braced steel frame with fundamental frequency of 7.75Hz. This frequency is considerably larger than the isolated structure frequency (1.4Hz) so that the superstructure is idealized as a rigid body.

The above consideration motivated the formulation and solution of the equations of motion of a rigid-body supported by springs and viscous dampers and undergoing coupled lateral-vertical-rocking motion. All springs and viscodampers are placed at the isolation level so that all elements of the isolation system are at a constant height h below the center of mass of the superstructure (Figure 5). Each spring has vertical stiffness K_{zi} and horizontal stiffness, K_{xi}. Each viscous damper is described by the constitutive law of Eq. 7 with parameters C_{ozj}, r_z, λ_z for vertical motion, parameters C_{oxj}, r_x, λ_x for horizontal motion and $q=1$.

@seismicisolation

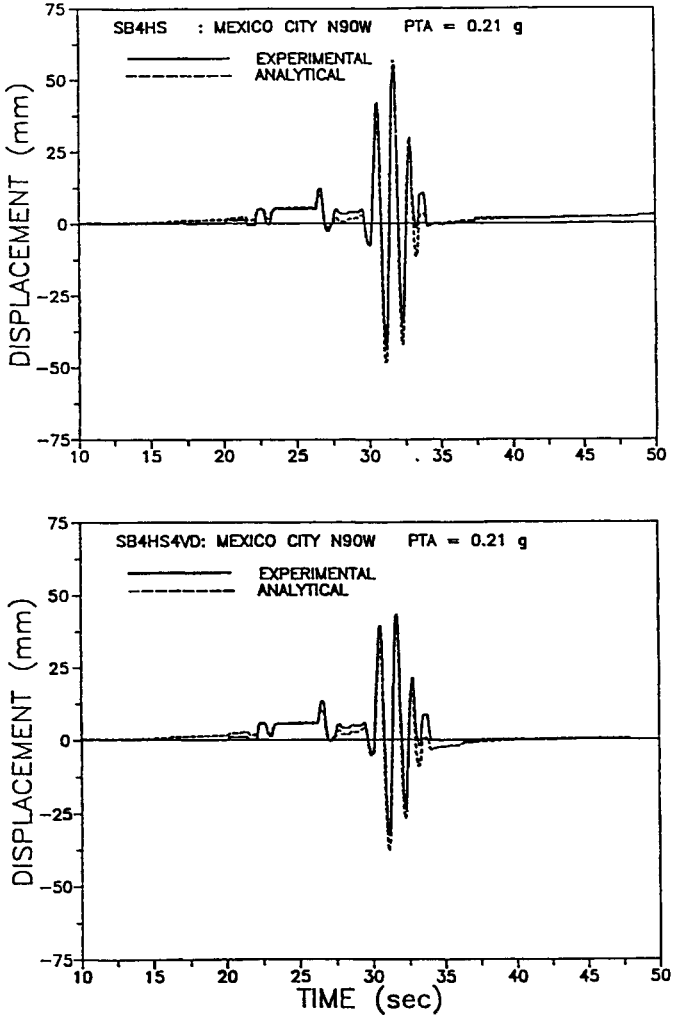

Figure 4. Comparison of Recorded and Analytically Predicted Histories of Displacement of Sliding Isolation System without (Top) and with (Bottom) Viscous Dampers for Mexico City Input

@seismicisolation

Considering motion in a vertical plane and allowing for some horizontal eccentricity between the center of mass of the superstructure and the center of rigidity of the supporting springs as shown in Figure 5, the equations of motion are

$$m\,\ddot{u} + K_x\,u - K_x h\Theta + P_x = -m\ddot{u}_{gx} \tag{11}$$

$$m\,\ddot{v} + K_z\,v - K_z e\Theta + P_z = -m\ddot{u}_{gz} \tag{12}$$

$$I\ddot{\Theta} + K_x\,h^2\Theta + \sum_i K_{zi}\,x_i^2\Theta - K_z hu - K_z\,e\,v - M_x - M_z = 0 \tag{13}$$

where

$$K_x = \sum_i K_x{}^i,\ K_z = \sum_i K_{zi} \tag{14}$$

$$e = \frac{\sum_i K_{zi}x_i^l}{K_z} \tag{15}$$

and $\ddot{u}_{gx}, \ddot{u}_{gz}$ are the horizontal and vertical components of ground motion. Furthermore, P_x, P_z, M_x *and* M_z are forces and moments created by the viscous dampers at the center of mass

$$P_x + \lambda_x D^{r_x}\,[P_x] = C_{ox}(\dot{u} - h\dot{\Theta}) \tag{16}$$

$$P_z + \lambda_z D^{r_z}\,[P_x] = C_{oz}(\dot{v} - e\dot{\Theta}) \tag{17}$$

$$M_x + \lambda_x D^{r_x}\,[M_x] = C_{ox}(h\dot{u} - h^2\dot{\Theta}) \tag{18}$$

$$M_z + \lambda_z\,D^{r_z}\,[M_z] = C_{oz}e\dot{v} - \sum_j C_{ozj}\,x_j^2\dot{\Theta} \tag{19}$$

@seismicisolation

$$C_{ox} = \sum_j C_{oxj}, C_{oz} = \sum_j C_{ozj} \tag{20}$$

$$e = \frac{\sum_j C_{ozj} x_j'}{C_{oz}} \tag{21}$$

Equations 11 to 13 and 16 to 19 form a system of fractional, also known as extraordinary, differential equations. Numerical solutions may be derived by application of Fourier transform to arrive at

$$[H(\omega)]\{\overline{u}(\omega)\} = \{\overline{F}(\omega)\} \tag{22}$$

where $\{(\overline{u})\}$ and $\{(\overline{F})\}$ are the transforms of the response vector and seismic loading vector, respectively. The solution is then derived by the DFT approach [5]. The exact frequencies and damping ratios of the coupled system are derived by solving the eigenvalue problem of matrix $[H(\omega)]$. This requires the application of an iterative procedure as matrix $[H(\omega)]$ depends on the unknown frequencies.

The lack of physical intuition on the response of systems modeled with this approach and the necessity to use an explicit time history of ground acceleration, rather than the usual design specification in the form of response spectrum, represent difficulties in applying the described procedure. In this respect a simplified analysis method is developed in which the force in each viscous damper is described by eq. 10 with the storage stiffness, K_1, and damping coefficient, C, evaluated at the free vibration frequencies of the coupled system.

In this way the equations of motion may be written in the standard mass-damping-stiffness matrix form but with stiffness and damping matrices being dependent on the unknown frequencies of the system.

The approximate frequencies of free vibration and corresponding mode shapes are determined from the undamped equations of motion of the simplified system by employing an iterative procedure because of the dependency of frequency. The associated damping ratios are determined by energy considerations:

$$\xi_n = \frac{W}{4\pi E} \tag{23}$$

where ξ_n is the damping ratio in the nth mode, E is the maximum strain energy of the system and W is the work done by the damping forces in a cycle of period Tn

$$W = \sum_j \left(\int_o^{T_n} P_{xj} \dot{u}_j \, dt + \int_o^{T_n} P_{zj} \dot{v}_j dt \right) \tag{24}$$

@seismicisolation

In eq. 24 $\dot{u}_j$ *and* $\dot{v}_j$ are the horizontal and vertical velocities of damper j (see Fig. 5).

The exact and simplified methods of analysis were applied in the analysis of one of the base isolated buildings in California. The isolation system of the building consists of eleven spring units and six combined spring-viscous damper units. The combined properties of the isolation system are (eqs. 14 and 20): K_x = 7kN/mm, K_z= 17.5 k/N/mm, C_{ox} = 90 kNs/m and C_{oz} = 340 kNs/m. The structure weighs 613 kN with its center of mass at height h = 3.75m (Fig. 5) above the isolation system and radius of gyration about a principal axis passing through the center of mass equal to 3.05m. The earthquake excitation is described by the ATC 0.4g S1 spectrum.

Table 1 compares frequencies, damping ratios and peak response values of the isolated structure as calculated by the two methods. In the exact method, three artificial records compatible with the design spectrum were generated and used in the dynamic analysis. The values in Table 1 are the maxima out of the results of the three records. In the simplified method, the analysis was performed for each mode of vibration and the results were combined by the SRSS rule. It may be seen that the simplified method predicts results in good accord with the exact results. It should be noted that the ground acceleration is not amplified in the structure above the isolation system, whereas analyses of the structure with conventional foundation resulted in more than two-fold increase of the ground acceleration over the height of the structure. This indicates the beneficial effect of isolation.

TABLE 1

Comparison of Exact and Approximate Results of Dynamic Analysis

	Exact	Approximate
f_1 (Hz)	1.35	1.34
f_2 (Hz)	3.47	3.31
f_3 (Hz)	6.54	5.74
ξ_1	0.291	0.263
ξ_2	0.270	0.244
ξ_3	0.445	0.215
Corner Point Horizontal Displ. (mm)	30.00	29.00
C.M. Horizontal Accel. (g)	0.31	0.31
Top Point Horizontal Accel. (g)	0.41	0.42

@seismicisolation

CONCLUSIONS

Viscous dampers exhibit a dynamic force-displacement behavior which may be accurately modeled over a wide range of frequencies by a fractional derivative Maxwell model. The calibration of the model requires the experimental determination of a single physical parameter.

Viscous dampers have been used for energy dissipation in two different types of isolation systems. The developed model for viscous dampers has been implemented in the analysis of a sliding (nonlinear) isolation system and an isolation system with coupled horizontal-vertical-rocking motion. In the first system the analytical results are in good agreement with the recorded data. In the second system which is linear but involves fractional order differential equation of motion, a simplified analysis method has been presented. The simplified method is suitable for use with response spectra which is the usual design specification. The method predicts results which are in good agreement with the analysis results of the exact method.

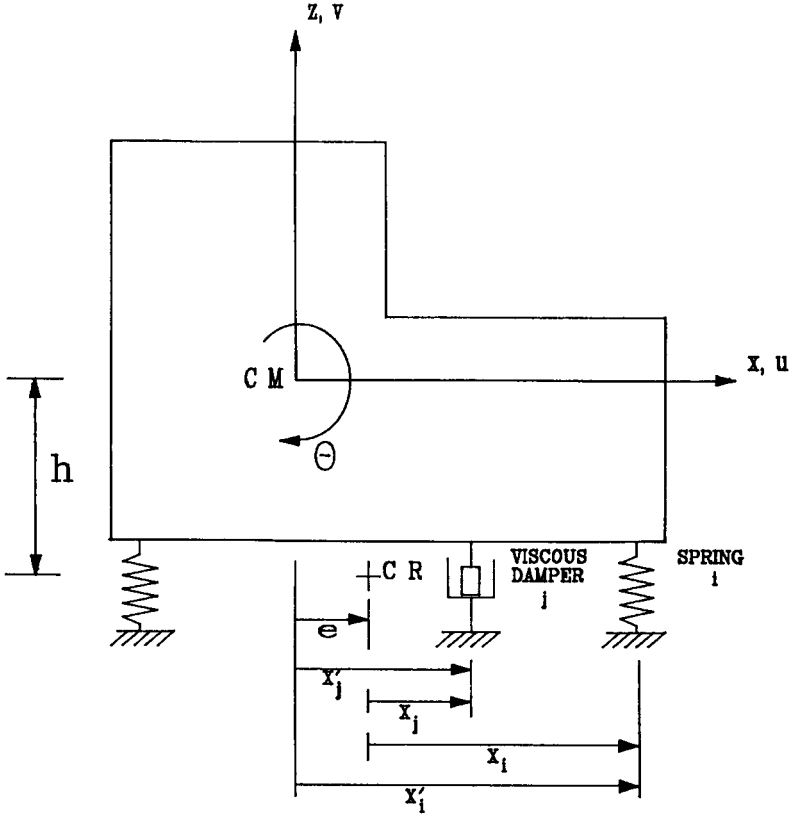

Figure 5 Rigid Body Model of Isolated Structure

@seismicisolation

REFERENCES

1. Huffmann, G. "Full base isolation for earthquake protection by helical springs and viscodampers." Nuclear Engineering and Design, 1985, 84, 331-338.

2. Gemant, A. "A method of analysing experimental results obtained from elasto-viscous bodies." Physics, 1936, 7, 311-317.

3. Koh, C.G. and Kelly, J.M. "Application of fractional derivatives to seismic analysis of base-isolated models." Earthquake Engineering and Structural Dynamics, 1990, 19, 229-241.

4. Makris, N. and Constantinou, M.C. "Fractional derivative Maxwell model for viscous dampers." J. of Struc. Eng., ASCE, 1991, to appear.

5. Makris, N. and Constantinou, M.C. "Viscous Dampers: testing, modeling and application in vibration and seismic isolation." Report No. NCEER 90-0028, National Center for Earthquake Engineering Research, State University of New York, Buffalo, New York, 1990.

6. Oldham, K.B. and Spanier, J. The Fractional Calculus. Mathematics in Science and Engineer, Vol. III. Academic Press, 1974.

7. Bagley, R.L. and Torvic, P.J. "Fractional Calculus - A different approach to the analysis of viscoelastically damped structures." AIAA Journal, 1983, 21(5), 741-748.

8. Constantinou, M.C., Mokha, A. and Reinhorn, A.M. "Study of a sliding bearing and helical steel spring isolation system." J. Structural Eng, ASCE, Vol. 117(No. 4), to appear in April 1991.

@seismicisolation

THE EFFECT OF DETONATOR VARIABILITY ON EXPLOSIVELY INDUCED GROUND VIBRATION

DR BARRY M NEW
Ground Engineering Division
Transport and Road Research Laboratory
Crowthorne, Berkshire

ABSTRACT

The research reported in this paper forms part of a programme concerned with the explosive excavation of rock for highway tunnels and cuttings. In particular the important effect of long delay detonator variability is considered in relation to the prediction of ground vibration.

The paper gives details of construction blasting vibration measurements and describes a numerical technique developed to model the effects of detonator variability. The model allows vibration levels to be predicted with allowance made for detonator inaccuracies which are specified in terms of the standard deviation of the pyrotechnic delay period.

Other factors, such as the frequency distribution of vibration from construction blasts, are also discussed where relevant to the prediction of intrusion or structural damage.

INTRODUCTION

The use of explosives during civil engineering construction can cause ground vibrations which result in damage to nearby property or the adjacent works and substantial nuisance to the local population. These factors may lead to restraints on the working method which lead to additional costs or even, in extreme circumstances, to curtailment of the works. The more accurate prediction of vibration has therefore become an increasingly important part of the site investigation programme for construction works involving blasting.

The comparison of vibration predictions (based on site investigation blasting trials) and the vibration measured during the construction of a major road tunnel has indicated that normal scaled-distance site law analyses of the trial data can overestimate the actual vibration caused by the works. This effect was particularly notable during the firing of the longer duration delays (½ second delay series) firing the heaviest charges in the tunnelling round. This paper investigates the cause of the discrepancy and describes techniques which will allow more accurate predictions to be made in future.

@seismicisolation

The blasting trials and construction blasting measurements [1] were carried out prior to, and during, the construction of the Penmaenbach road tunnel [2]. This tunnel is one of a series of major works for the improvement of the A55 North Wales Coast Road. The contract has been carried out for Welsh Office by Balfour Beatty Construction Ltd and Travers Morgan (assisted by Howard Humphries) were the Engineers for the scheme.

As part of the site investigation the Welsh Office invited the Transport and Road Research Laboratory (TRRL) to advise upon and carry out measurements to establish parameters concerned with the environmental viability of the proposed works. A major consideration was that the new tunnel was to be blasted close to the existing unlined rail tunnel which forms part of the main London-Holyhead route. It was therefore necessary to carry out blasting trials to provide a rational basis for vibration control during tunnel construction and to check that maintaining the integrity of the existing rail tunnel would not unreasonably constrain the Contractors for the tunnel works.

It has been possible to assemble an extensive database commencing with the trial blasting carried out during the site investigation in 1979 and to follow this up with comprehensive monitoring of production explosions during construction of the tunnel in 1986-87. The trial measurements provided pre-contract design information and site control guidance as well as data for research purposes.

Analysis of the vibration time histories showed the important effect of temporal variations in the pyrotechnic delay elements of the detonators. These variations resulted in the non-simultaneous detonation of the individual charges on nominally identical delays and caused significant deviations from the vibration level predicted during the trial blasting.

Frequency domain analyses were carried out and the spectral distribution of energy close to the excavations was investigated. This is important as the effects of vibrations, on structures and people, are heavily dependent on the frequency of the disturbing motions.

BLASTING METHOD AND VIBRATIONS

In order to explain the pattern of vibration produced by tunnelling works, it is necessary to briefly describe the sequence of a typical 'pull' which advances the heading into the rock. Figure 1 shows a sketch of a drilling pattern for the excavation of a tunnel with a face area of about 100 m^2. This type of round is known as the 'burn cut' and has become increasingly common since the introduction of multi-boom drilling jumbos, which are at their most efficient when drilling large arrays of parallel holes. The explosives are initiated from the centre outward as follows:-

A series of short delay (millisecond series) detonators sequentially fire the holes numbered 1 through 9 (inside circles) using the larger uncharged holes, marked R, to provide some relief for bulking of the central pulverised core. The later delays numbered 3 through 12 then fire in generally semicircular groups progressively away from the centre exploiting the partial void formed by the explosion of the earlier charges. After the bulk of the rock has been fragmented, mainly at ½ sec delay intervals, the perimeter holes, which are usually more closely spaced and lightly charged, are fired to produce a smooth finish with minimum overbreak and damage to the remaining rock. Finally, the 'lifting' charges are fired; these excavate the bottom of the heading and lift the rock fragmented by the main part of the round back from the face. This loosens and spreads the rock pile making mucking out easier.

@seismicisolation

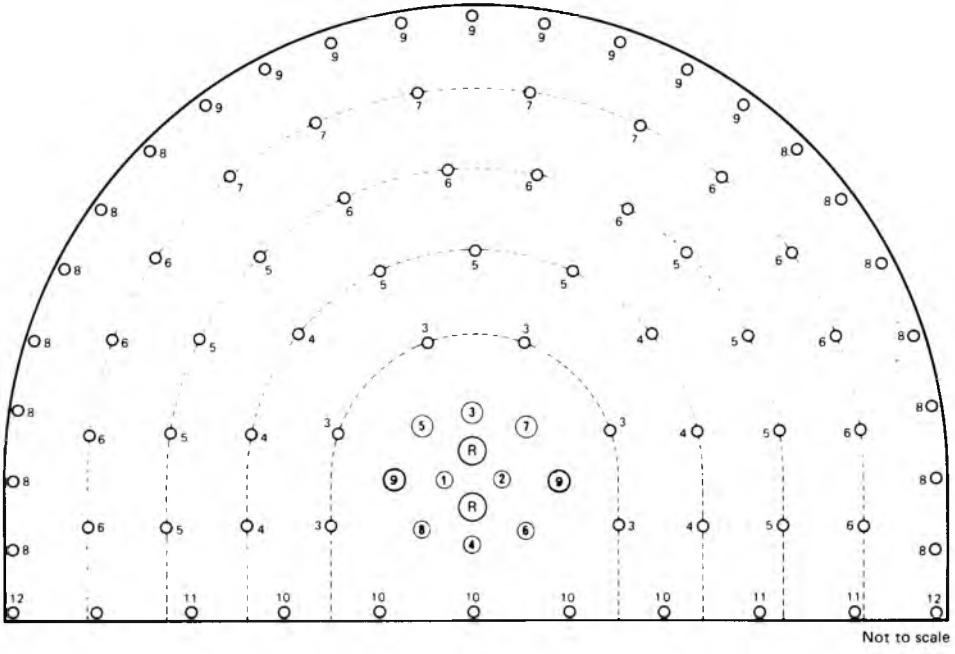

Fig. 1 Typical drilling pattern for 'Burn cut' tunnel round

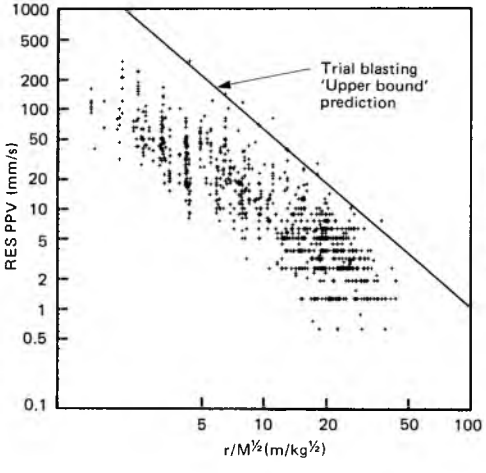

Fig. 2 Data from tunnel blasting (square root scaling method)

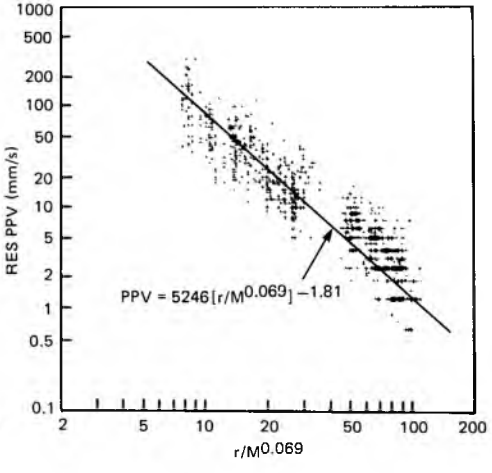

Fig. 3 PPV v Site specific scaling (from multiple regression analysis)

@seismicisolation

Efficient blast design which ensures both good fragmentation and economical use of explosives will exploit the full range of delays available, and tunnelling engineers have come to rely on the use of long delay detonators. The number of holes fired with detonators of a single nominal delay period will vary according to the blast design. The early delays fire only a single hole, whereas the later bulk removal delays may fire over twenty separately initiated and charged holes of the same nominal delay period.

Extensive vibration measurements were taken between mid 1986 and late 1987 during the construction of the Penmaenbach tunnel. Geophone and accelerometer transducer arrays were located in the adjacent railway tunnel, within the new tunnel and on surface rock exposures. Blast to transducer range varied between 4 m and 250 m and charge weights per delay between 2.35 kg and 54 kg.

The variation of peak particle velocity was initially plotted against scaled distance [Figure 2], as had been found most satisfactory for the presentation of the trial blasting data [1]. It quickly became apparent that the actual PPV's were generally lower and much more widely scattered than the trial blasting had predicted. It is of interest to note however that the 'upper bound' equation did provide an excellent prediction of the maximum PPV's actually observed. The variation of PPV with range, r, and charge weight, M, were then examined individually. Whilst the PPV's were very clearly dependent on range no such well defined relationship was apparent for charge weight. A multiple regression analysis confirmed these observations and the following relationship was calculated:

$$PPV = 5246 \quad r^{-1.81}.M^{0.125} = 5246 \ (r/M^{0.069})^{-1.81} \quad \ldots\ldots\ldots\ldots\ldots\ldots\ldots (1)$$

This relationship has been converted to site specific scaling [3] and presented in Figure 3. Whilst the PPV of the vibrations depended on range, as predicted, it appeared only weakly dependant on charge weight per delay, as shown by the exponent value for M of only 0.125.

Records of all the blasts were held on floppy disks and on-site processing provided a printout of the three component particle velocities and the resultant particle velocity for each transducer array location. These time history printouts comprised about one second of very complex motions, as the short duration delays fired in and around the centre of the face, followed by groups of wave packets from each successive delay until the vibration from the last delay (6 secs) had died away: The wave packet having a duration of about 6.5 seconds. Inspection of the records revealed that each group of vibrations, attributable to a nominal delay, comprised a number of separate individual detonations.

Figure 4 shows a short extract, about 1 per cent, from a typical time history obtained at a distance of 20 m from the face. The wave packets shown are induced by the first two holes to fire on nominally four second delay detonators; later in the printout the wave packets from the remaining holes on the same delay are to be found. For these two particular events the instant of detonation is easily identified. Occasionally however two or more detonations occurred within a few milliseconds and the precise detonation time was more difficult to determine.

A large number of time histories from many blasts were analysed and many individual delay times recorded. The variation of each nominal delay detonator was then calculated in terms of its standard deviation. The manufacturer of the detonators was contacted and they provided information on expected variation. In general, the detonators were within the tolerances given by Nitro Nobel [4] (a standard deviation of .05 sec for delays in the range 1.2-2 secs and 0.15 sec for the range 2.5-6 secs).

@seismicisolation

Well over a thousand individual hole firing times were identified from 25 separate tunnel rounds and the Table gives the standard deviation for each group of long delay detonators. At delays of 1 second or less, it was not possible to reliably identify the individual detonator initiations due to the superposition of waveforms.

Although the standard deviations relate specifically to Nonel detonators, similar variations are to be found in the half second delay series of electric detonators made by ICI Nobel and Nitro Bickford, both of which are widely used in the UK and elsewhere (Personal communications with ICI Nobel Ltd and Explosives and Chemical Products Ltd). It should be noted that mean delay period and standard deviation will vary from batch to batch and with storage conditions and duration.

TABLE 1
Nonel detonator delays

Nominal delay period (secs)	Measured mean delay period (secs)	Standard Deviation (secs)
1.2	1.24	0.034
1.4	1.45	0.041
1.6	1.62	0.038
1.8	1.89	0.036
2.0	2.12	0.056
2.5	2.59	0.063
3.0	3.26	0.084
3.5	3.72	0.119
4.0	4.20	0.108
4.5	4.69	0.089
5.0	5.14	0.071
5.5	5.74	0.110
6.0	6.39	0.161

It is of interest to note that, had the detonators all fired precisely at their nominal delay period, then vibration levels in the adjacent railway tunnel would probably have exceeded the prescribed limits. The variations of the delay period effectively spread the release of explosive energy thereby substantially reducing the amplitude of the vibrations to well within the contract limits. The introduction of new electronic delay detonators which are claimed to be extremely precise could, apparently, increase vibration levels, particularly on long delays. However, the effect should be mitigated by the use of many delay periods rather than the ½ second series currently available from detonators using pyrotechnic delay elements. Indeed, the use of detonators which may fire a prolonged series of relatively closely spaced delays would permit the individual charge weight to be kept low. Besides reducing peak particle velocities this would also shift the frequency of the motions to higher frequencies where most structures are considerably less sensitive.

©seismicisolation

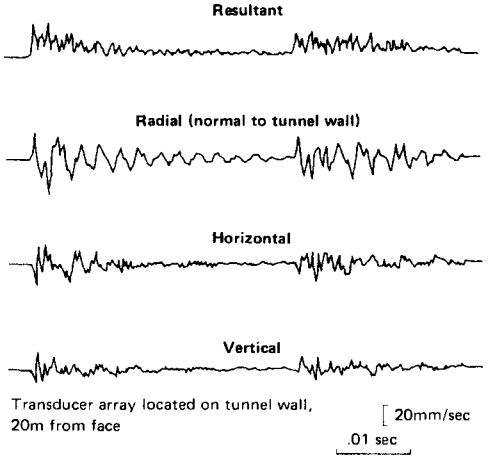

Fig. 4 Extract from particle velocity time history showing two detonations

```
MAXIMUM PEAK PARTICLE VELOCITY CALCULATION

Base signal from file PB69Y3_78

Number of detonations  30

Mean detonation time  1  Secs

Standard deviation of detonation times  .1  Secs

Duration of single detonation wave packet  .060675792  Secs

Max amplitude of base signal  24.5834079295  mm/sec
Number of repetitions of simulation  50


MAX PPV=   40.56   MEAN PPV=   33.30   STANDARD DEVIATION=  2.80


          PEAK PARTICLE VELOCITIES FOR EACH REPETITION

40.56    32.25    30.15    30.94    36.98    37.80    30.17    32.03
38.07    32.43    36.38    35.10    32.21    29.92    29.54    28.68
35.23    34.29    33.04    33.45    34.05    30.49    31.12    29.42
33.37    31.59    33.67    30.91    37.71    30.95    34.09    33.46
31.34    32.09    37.69    30.60    32.30    34.59    32.46    34.15
29.66    31.82    37.32    36.63    37.85    30.02    34.66    33.82
32.27    35.52
```

Fig. 5 Typical printout from SIMWAVE programme

@seismicisolation

THE NUMERICAL MODEL

The vibration levels observed during the construction works were generally lower than those predicted, because the predictive method assumed that all the charged holes on a nominally identical delay were fired instantaneously: the particle velocity time histories showed that this was not the case.

A numerical model was developed to estimate how the PPV might be expected to increase with the increase in charge weight per delay. It must be noted that, for a tunnel round of the type used at Penmaenbach, the charge weight per delay is increased by firing a larger number of similarly charged holes, not by increasing the charge weight in each hole. In these circumstances, the PPV would be expected to increase as the square root of the charge weight if the firings were at precisely the same instant. (Note that for a single spherical charge the PPV would be expected to increase as the cube root of the charge weight).

A computer programme (**SIMWAVE**) was written to assemble the particle velocity time history of a wave packet comprising a number (N) of superimposed single hole detonations fired with timing errors normally distributed about a nominal delay period.

SIMWAVE requests the following inputs:-

1. The number (N) of holes fired on the delay

2. The standard deviation of the detonator delay period and the nominal delay period

3. A data file containing the particle velocity time history from the firing of a single hole. This can be a waveform recorded in the field, or a simulated waveform with specified frequency and damping characteristics.

4. The required number of repetitions of the calculations. (Because of the probabilistic nature of the computation it is necessary to obtain a measure of the variability of the predicted PPV's for a number of wave packet simulations).

SIMWAVE then performs the following operations:-

1. Randomly selects N initiation times with the specified mean and standard deviation.

2. Loads the appropriate source waveform from a data file or generates an artificial waveform as required.

3. Stacks the N individual waveforms to yield the complete wave packet time history

4. Stores the maximum PPV occurring in the wave packet

5. Repeats processes 1 - 4 for the specified number of wave packets to be generated

6. Calculates the mean, maximum and standard deviation of the maximum PPV values for each wave packet

@seismicisolation

7. Prints the output in the form shown in Figure 5

The programme was tested using a number of different single hole source waveforms recorded at the site. The output was found to be relatively insensitive to changes in waveform and yielded similar results for waveforms with similar PPV's, duration and frequency content.

SIMWAVE was run for a range of values (N=1 to 30) for the number of individual holes fired on a single delay and the results are plotted in Figure 6. At Penmaenbach the maximum charge weight per delay was about 54 kg comprising 23 holes each charged with 2.35 kg of 80% strength special gelatine (SG80). Usually this maximum charge was fired on the 4 or 4.5 second delay.

The standard deviation of the detonators was taken as 0.1 seconds which is typical of the longer delay detonators (see Table 1).

Figure 7 shows a simulated wave packet comprising the superposition of 20 similar source waveforms recorded in the field. Note that, although most of the wave packet shows some superposition of waveforms, the chances of the peak motions occurring simultaneously are small. Also, short sections of the wave packet show zero particle velocity. This wave packet is similar to those caused by the actual blasting works.

Figure 6 indicates how the PPV caused by a given delay depends on the weight of charge fired (M) which is proportional to the number of holes fired (N).

A best fit straight line has been fitted to that region of the curve which most closely applies to the field blast design. That is, the range of numbers of holes fired on a single delay was 5 to 30. The regression line indicates that, in this region, the PPV increases as $N^{0.14}$. This compares very favourably with equation (1) which shows that, during the construction blasting, the PPV increased as $M^{0.125}$. Figure 6 also shows how the PPV might be expected to increase with charge weight when all charges are fired precisely at the same moment.

THE FREQUENCIES OF THE BLASTING VIBRATIONS

The way in which an explosive charge transfers its energy to a rock mass and the factors which affect the propagation of the stress wave packet are extremely complex, particularly when the field conditions imposed by excavation works are considered. The near surface weathered rocks encountered during most civil engineering works present a particularly intractable set of problems and multihole arrays of non-simultaneous detonations further complicate the issue. Most explosive excavations involve the firing of a number of holes and the effective source comprises the superimposed wave motions from each hole. Even for single cavities calculations of wave packet form, based on drill-hole or cavity dimensions, have been found inaccurate in practice, although some progress has recently been reported [5]. Other factors which control the source include the strength and velocity of detonation of the explosive, the stemming of the drill-holes and the degree of containment imposed by the rock mass.

Not only is the radiation pattern from such complex sources difficult to define, but it constantly changes with propagation through the rock mass due to the following factors:-

(i) geometrical spreading

(ii) the progressive separation of compressional, shear and surface wave types due to their differing propagation velocities.

@seismicisolation

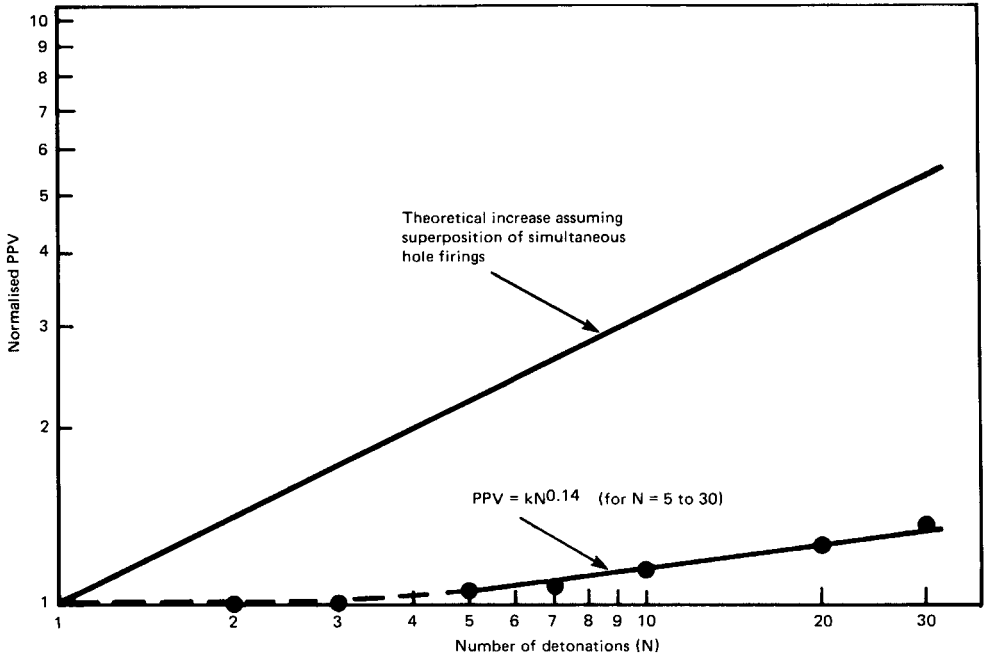

Fig. 6 Increase in PPV (normalised) with increase in number of holes fired

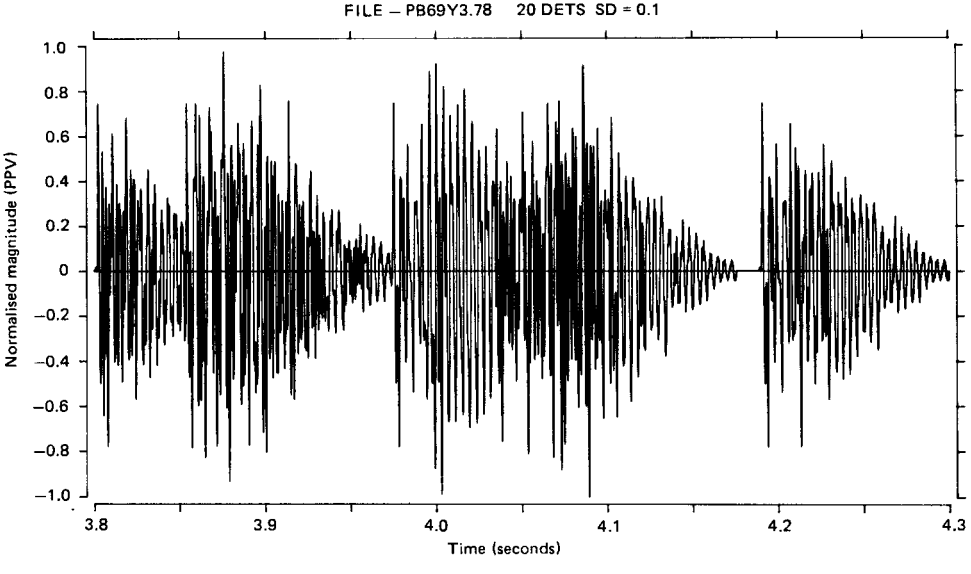

Fig. 7 Simulated wave packet comprising 20 holes fired on a 4 second (nominal) delay

@seismicisolation

(iii) the presence of discontinuities in seismic impedance will cause reflection, refraction, diffraction, scattering and mode conversion processes.

(iv) internal friction will cause frequency dependent attenuation.

The combined effect of these factors causes the amplitude of the motions to be attenuated, particularly at high frequencies, and the wave packet duration to increase with propagation.

At Penmaenbach the detailed form of the spectral distribution was generally varied and complex, however for a given range the bandwidth of the vibration was reasonably consistent. Figure 8 shows the envelopes of energy distribution obtained by averaging groups of individual spectra in three range groupings. These distributions are consistent with those obtained during trial blasting although slightly richer in higher frequencies. This may be due to the rock in the tunnel being much fresher and under considerable in-situ stress compared with the surface rock drilled for the trial blast shots. The similarity is to be expected since the vibrations induced during the construction works were basically caused by holes charged with 2 kg to 3 kg of explosives, just as happened during the trials.

During construction the opportunity was taken to measure the vibrations within 10 to 20 m of the tunnel face. This presented some operational difficulties due to the highly damaging effects of flyrock to the transducers and cabling when close to the face. The spectra obtained were even richer in high frequency motions with significant energy present at frequencies as high as 1 kHz.

Comparison of spectra obtained from locations within the tunnel under construction, the adjacent rail tunnel and the surface exposures above the tunnel showed no significant differences in distribution. However, the time histories obtained within the tunnels did indicate the presence of phenomena related to the presence of the tunnel itself which were not apparent from surface observations. These motions followed the large compressional and shear wave motions and were generally of much lower amplitude. In some cases they considerably prolonged the duration of the wave packet. This effect is shown in Figure 4, where lower frequency motions in the coda of the wave packet indicate a reverberation of the tunnel wall in a radial direction. The motions in the plane of the tunnel wall do not show this characteristic.

It should be noted that the high frequencies measured at this site are not widely reported in case histories from other construction sites. This may stem from the fact that equipment used on construction sites has historically been designed to monitor vibrations caused by mining operations which fire large charge weights and are observed at relatively long ranges. Civil engineering works tend to use smaller charges and are often observed at quite close range. This may have created a situation where damage has been attributed to inaccurately low measures of particle velocity, because the equipment could not respond to the much higher particle velocities actually present at higher frequencies. Systems similar to that specified for Penmaenbach [6], or other recently introduced proprietary equipment, must be used for vibration control on construction sites.

Before tunnel excavations could begin, portal preparation works required the firing of a large pre-splitting charge to yield a near vertical rock face, which was damaged as little as possible by the blasting [7]. This would assist with safety aspects by minimising falling rock both during and subsequent to the works and reduce maintenance costs during

@seismicisolation

tunnel operation. The creation of a pre-split plane some 20 metres wide by up to 14.4 m metres deep required the instantaneous firing of approximately 90 kg of explosives. The main array of pre-splitting drill-holes were 90 mm in diameter at 0.9 m centres and were charged with 250 gms/m of 80 per cent strength blasting gelatine fired by blasting cord at 40 g/m. The individual holes were coupled by a continuous surface run of detonating cord which ensured the near simultaneous firing required to create a successful pre-split plane. The overall charge weight for the pre-split plane was approximately 0.32 kg/m^2 of rock face. Transducer arrays were fixed on rock exposures, and to a deflector wall which had been recently cast just above the portal. At its closest point the wall was less than 10m from the pre-split face and high particle velocities were expected.

Peak particle velocities of up to 375 mm/s were sustained by the deflector wall with no visible signs of vibration induced damage. Subsequent ultrasonic pulse velocity measurements on the wall indicated that the concrete strength had not been adversely affected by the blasting. The spectral distribution of vibration energy is given in Figure 9 for the motions of the deflector wall and of a surface rock exposure about 60 m from the blast. Note that, for this large and spatially diffuse charge configuration, the spectra are dominated by low order harmonics and almost all the energy occurs at frequencies of less than 60 Hz.

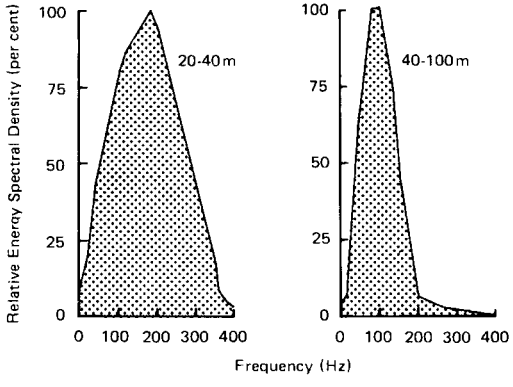

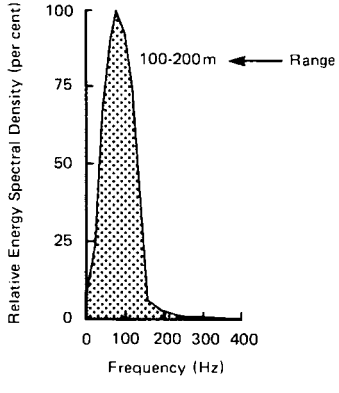

@seismicisolation

Fig. 8 Averaged energy spectral distributions for production blasts in various range bands

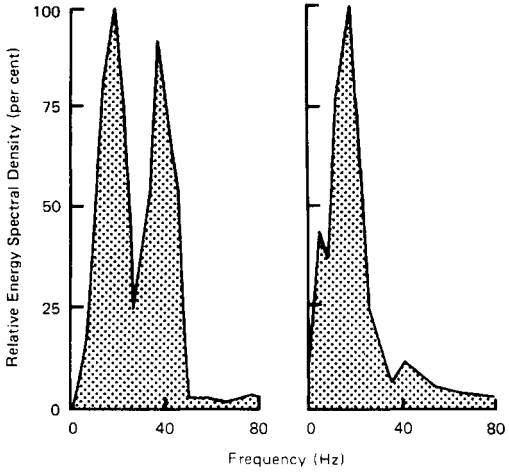

(a) On concrete wall close to face

(b) Surface rock 60 m from face

Fig. 9 Energy spectra from presplit explosion

CONCLUSIONS

Trial blasting provides a sound basis on which the environmental viability of proposed construction works may be assessed. However, it is unlikely that details of the production blasting technique will be available during the site investigation, and the firing of full scale rounds is usually unacceptable prior to the commencement of the contract.

Results from the tunnelling works at Penmaenbach have highlighted the usefulness of good vibration prediction and control and have provided considerable insight into problems which may, nevertheless, still occur. In particular, the site law predictions from the trial blasting generally overestimated the vibration levels likely to occur, particularly at the higher charge weights where many holes were fired on a single delay. The effect of detonator delay variations could not have been realistically taken into account, although the 'upper bound' prediction established during the trials did provide an accurate working guide during design.

A numerical model has been developed and this provides predictions which are closely correlated with the field measurements at Penmaenbach. The model will be used to assist with the prediction of ground vibration at other sites, and this work, together with further production blasting measurements,will serve to test its validity under a variety of conditions.

The frequency domain analysis of the data confirms that high frequency vibrations (>200Hz) may occur during construction works, particularly within 40 m of the blasting. The presence of high frequencies will be particularly pronounced when firing small shots in strong, intact rocks. The results from Penmaenbach should be taken as providing an upper bound with respect to bandwidth, as most sites will be on weaker materials often with soil cover.

The high frequencies measured at this site are not widely reported in case histories from other sites. Where measurements of vibration at construction sites are required it is vital that the equipment chosen has a sufficiently broad frequency response so that peak particle velocities may be correctly recorded.

@seismicisolation

ACKNOWLEDGEMENTS

The work described in this paper forms part of the programme of the Transport and Road Research Laboratory and the paper is published by permission of the Director. The author gratefully acknowledges the assistance given by Welsh Office, Travers Morgan and Balfour Beatty Construction Ltd, without whose willing cooperation this work could not have been carried out.

REFERENCES

1. New, B.M., Trial and construction induced blasting vibration at the Penmaenbach road tunnel. Department of Transport. TRRL Research Report 181, Transport and Road Research Laboratory, Crowthorne, 1989.

2. Watts, R., The A55 North Wales Trunk Road Penmaenbach Tunnel: use of Nonel blasting techniques. Proc.Tunnelling 88, 1988, pp 389-399, IMM, London.

3. New, B.M., Ground vibration caused by civil engineering works. Department of Transport. TRRL Research Report 53. Transport and Road Research Laboratory, Crowthorne. 1986.

4. Larsson, B. The role of correct interval timing in rock blasting. Paper given at the Swedish Rock Blasting Council, March, 1985.

5. Hinzen, K.G., Modelling of Blast Vibrations. Int. J Rock Mech. Min. Sci. Vol.25, No.6, pp 439-445, 1988.

6. New, B.M., and Hood, R.A., The measurement and control of blasting vibration during civil engineering works. Proc. Conf. on Geotechnical Instrumentation in Civil Engineering Projects, Nottingham. I.C.E. London 1989.

7. Matheson, G.D., Presplit blasting for highway rock excavation. Department of Transport. TRRL Laboratory Report LR 1094. Transport and Road Research Laboratory, Crowthorne. 1983.

Crown Copyright. The views expressed in this paper are not necessarily those of the Department of Transport or Welsh Office. Extracts from the text may be reproduced, except for commercial purposes, provided the source is acknowledged.

@seismicisolation
@seismicisolation

METHODS FOR THE ASSESSMENT OF THE BLAST RESPONSE OF ENGINEERING STRUCTURES

MARTIN S. WILLIAMS
Department of Engineering Science,
University of Oxford,
Parks Road, Oxford OX1 3PJ, UK

JOHN P. NEWELL
Manager, Engineering Mechanics,
W.S. Atkins Engineering Sciences Ltd,
160, Aztec West, Park Avenue, Almondsbury,
Bristol BS12 4TU, UK

ABSTRACT

Techniques for the blast analysis of steel and concrete structures are reviewed. Pseudo-static, impulsive and dynamic analyses, using both hand calculation and computational methods, are described. The effects of confinement and partial venting are considered, and guidance is given on the choice of appropriate material parameters under high strain-rate loading. The lack of established procedures and the need for research are highlighted.

INTRODUCTION

Structural design against blast loading has traditionally been a subject of interest mainly to the military sector. However, disasters such as Ronan Point and Piper Alpha have highlighted a growing need for blast-resistant design in a range of non-military structures.

The majority of techniques available for analysing blast events have been developed for use in a military context. Many date from the Second World War, or from the post-war period in which the major advances in nuclear weaponry took place; much important information is classified. Research and development in the civil sector has tended to be limited and problem-specific, so that no clearly established design techniques have emerged. This is in contrast with other extreme load types such as earthquake and impact, where substantial research has led to the

©Seismicisolation

accumulation of a wealth of knowledge and techniques. This paper aims to outline the analysis approaches which are available and to highlight the major deficiencies in the field.

LOADING DEFINITION

Air blast occurs due to explosions at or above ground level. The nature of a blast loading is dependent on the type of explosive used, the amount of reflection occurring and the level of confinement.

High Explosive Air Blast

When a high explosive is detonated in air at ambient pressure p_o, an increase in pressure known as a blast wave is generated. The wave moves outwards from the centre of the explosion forming a spherical wave front, whose peak overpressure, p_s, varies inversely with the cube of the distance from the explosion (the range). Additionally, the surrounding air is set in motion, creating a blast wind. This causes an additional, dynamic pressure p_d on any structure it encounters, given by

$$p_d = \frac{5p_s^2}{2(p_s+7p_0)} \tag{1}$$

Figure 1 shows typical overpressure and dynamic pressure time histories at a fixed distance from an explosion. For time-history analyses, these may be idealised as simple triangular pressure pulses having the same peak value and enclosed area (impulse).

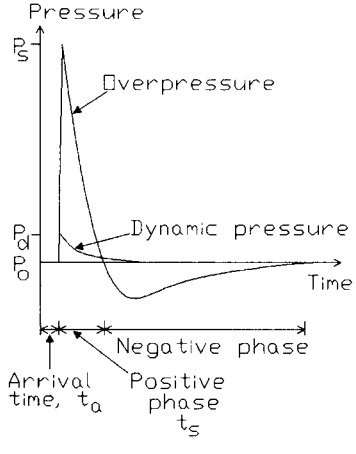

Figure 1. Typical blast pressure time history

Experimental data relating blast parameters to range and charge size for TNT are available in numerous sources, such as [1]. It is usual to convert quantities of explosives to TNT equivalents in order to determine their blast characteristics.

@seismicisolation

Wave reflections: When a blast wave impinges on a surface, reflection occurs. The reflected wave has a higher pressure than the incident wave due to the fact that it is passing through air which has already been heated and pressurised. For normal incidence, the peak reflected overpressure, p_r, is approximately

$$p_r = 2p_s + 2.4p_d \tag{2}$$

Substituting for p_d from (1) gives

$$p_r = \frac{2p_s(4p_s+7p_0)}{(p_s+7p_0)} \tag{3}$$

Thus the reflection causes an amplification factor of between 2 and 8, depending on the magnitude of the incident overpressure.

Surface explosions: Blast parameters for a surface burst can be obtained by applying an amplification factor of 1.8 to data for an air burst. This factor is derived by assuming that the immediate reflection of the blast wave at the ground surface gives an amplification of 2.0, and that 10% of the explosive energy goes into cratering.

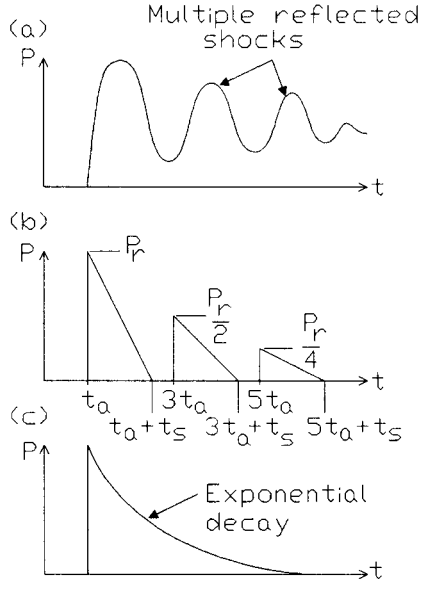

Figure 2. Loading due to confined explosions

Confined explosions: When an HE device is detonated within a building, the characteristics of the resulting blast wave will differ substantially from those due to a free-air explosion [1,2]. Figure 2(a) shows a typical

@seismicisolation

blast loading due to a confined explosion, consisting of multiple reflected shocks combined with a pseudo-static gas pressure caused by the increase in volume of the detonation products.

Loading due to confined explosions may be reduced by venting, i.e. the rapid collapse under blast loading of windows, doors or non-structural partitions, preventing the build-up of gas pressures. The speed of these collapses is not normally sufficient to prevent blast wave reflections.

For the purposes of design, it is common to assume that the blast pressure history can be idealised as shown in Figure 2(b), where the parameters for the first pulse are calculated by treating the detonation as a surface explosion. In cases where the structure responds impulsively, these may be combined to give a single impulse. The gas pressure history is assumed to rise instantly to a peak and then decay exponentially, Figure 2(c), the rate of decay varying with the amount of venting present.

Nuclear Air Blast

Blast parameters for nuclear weapons exploded in air can be calculated in much the same way as for high explosives. However, the stated TNT equivalence for a weapon should first be factored by 0.5, since approximately 50% of the energy in a nuclear explosion goes into generation of heat, light and electromagnetic waves.

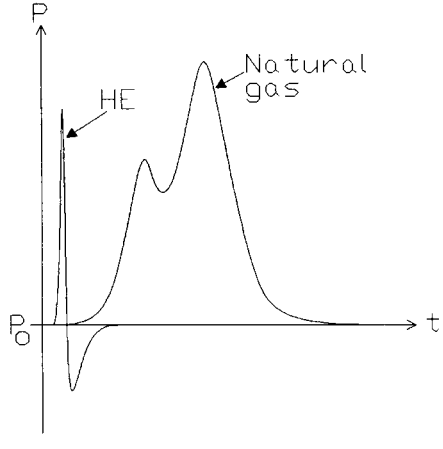

Figure 3. Comparison of blast pressures due to HE and natural gas explosions of the same specific energy

Gas Cloud Explosions

Confined natural gas explosions have received increasing attention since the Ronan Point disaster of 1968. Natural gas explosions differ significantly from HE detonations in that the build-up of pressure is much slower, as shown in Figure 3. Unlike HE blast, it is possible that venting may occur prior to the peak pressure being reached, resulting in the double peak of Figure 3. The maximum pressure achieved by ignition of a room containing a mixture of domestic gas and air appears to be related chiefly to the proportion of the wall area which provides venting [3].

@seismicisolation

REGIMES OF STRUCTURAL RESPONSE

The nature of the structural response to a blast loading is related to the frequency characteristics both of the building and of the loading. Obviously, if the duration, t_s, of the blast wave is close to the natural period of the building, T, then some dynamic amplification of the structural response is likely. However, this will not be as severe as under many other forms of dynamic loading, since the blast wave consists of a single pulse rather than an oscillating load function.

If the positive phase duration is much shorter than the natural period of the structure the effect is an impulsive one, as the structure does not move appreciably until the loading is completed. The blast wave can be assumed simply to have imparted an instantaneous velocity to the structure.

If the positive phase is much longer than the natural period of the structure, dynamic behaviour is unlikely, and the blast wave can be treated as a static pressure loading.

Determination of Structural Dynamic Characteristics

An obvious prerequisite to the analysis of blast resistance is the determination of the dynamic characteristics of the loaded structure. This enables the analyst to make a sensible prediction of the nature of the response, and so to choose an appropriate analysis technique.

For simple structures, natural frequencies can be determined manually by approximating the structure to a one or two-degree-of-freedom system. For more complex structures it will be necessary to use a computational approach. A natural frequency analysis capability exists in most modern finite element codes. The results of an elastic natural frequency analysis should be used only as a rough guide, since the blast loading is likely to cause substantial plasticity, thus modifying the dynamic characteristics.

MATERIAL REPRESENTATION

Structures subjected to blast loading are required to absorb large amounts of energy by plastic deformation. The critical material parameters are therefore the yield strength and the permissible ductility. As a general rule, materials loaded at high rates of strain tend to exhibit higher yield strengths and greater ductilities than under static loading. Variations in other parameters such as Young's modulus are minimal [4].

Steel

The dynamic yield strength of steel increases approximately logarithmically with strain rate [4]. If it is assumed that the structure responds to the blast loading primarily at its first natural frequency, then the appropriate value of yield strength can be deduced from Figure 4.

Steel can sustain temporary displacements as high as 6.0 times the deformation at yield without collapse, although subsequent demolition will almost certainly be necessary after such a severe overload. Structures subjected to motions corresponding to a ductility of up to 3.0 are likely to be reusable after the loading.

@seismicisolation

Reinforced Concrete
Millstein and Sabnis [5] have shown that enhancements in concrete strength of up to 1.6 can be achieved at very high loading rates. Under blast loading it is usual to assume rather more modest increases. The American Concrete Institute [6] suggests strength enhancement factors of 1.25 for concrete, 1.2 for mild steel reinforcement and 1.1 for high yield reinforcement. Most concrete structures are under-reinforced, so that the onset of plasticity is controlled by yielding of the reinforcement.

An appropriate limiting ductility ratio for concrete is 3.0. Alternatively, movement limits can be specified as maximum rotations at plastic hinges or yield lines. Suggested rotation limits vary between 2.0 and 5.0 degrees [6,7].

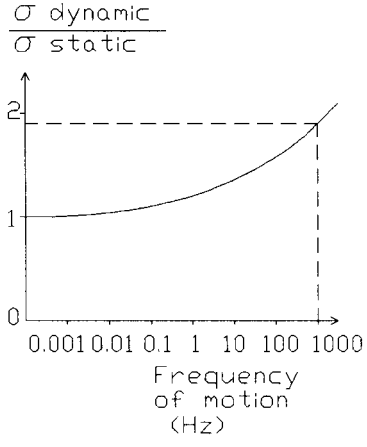

Figure 4. Dynamic Yield Strength of Steel

SIMPLIFIED ANALYSIS METHODS

Equivalent SDOF System
In dynamic analysis it is often convenient to consider an equivalent SDOF system whose displacement corresponds to that of some significant point on the element under consideration, e.g. the midspan displacement of a beam (see Figure 5). Equivalent loads (P_e) and masses (M_e) for the SDOF system can be found from work and energy considerations [8].

A resistance function (load vs. displacement) for the element can be found from plastic collapse considerations. This is then simplified to a bilinear function having the same peak resistance and total energy absorption, (Figure 5).

For short duration loadings such as blast it is common to neglect damping effects. This is because the damping is hard to assess, due to the non-linearity of the system, and because damping forces do not achieve significant magnitude until substantial motion has occurred.

@seismicisolation

Pseudo-Static Analysis
When the blast loading is of considerably longer duration than the natural period of the structure ($t_s \geq 6T$), then the peak reflected pressure is applied as a static load. The structural response is then analysed using an appropriate form of limit analysis, such as plastic collapse or yield line analysis. This approach is only likely to be appropriate for the analysis of long-range blast effects, and is most commonly used for nuclear blast loading.

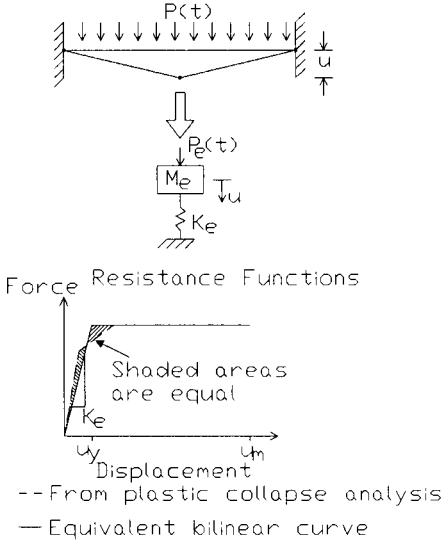

Figure 5. Equivalent single-degree-of-freedom system

Analysis of Impulsive Response
Confined or short-range HE blast waves are usually of very short duration ($t_s \leq 0.1T$), resulting in an impulsive loading of the structure. Analysis of such loadings is a simple matter if it is based on the use of an equivalent SDOF system.

The reflected impulse, i_r, of the blast wave is given by the area under the pressure-time curve, which can be found from published data [1]. This imparts a momentum to the structure, and hence a velocity, given by

$$v = \frac{i_r}{M_e} \tag{4}$$

The strain energy, U, is simply the area under the resistance curve (Figure 5). So the peak displacement, u_m, can be found from energy conservation:

$$u = k_e u_y (u_m - \frac{u_y}{2}) = M_e \frac{v^2}{2} \tag{5}$$

@seismicisolation

The displacement can then be substituted back into the original structure in order to calculate stresses.

Resonant Response

If the loading duration is approximately equal to the structural period, dynamic amplification due to resonance will occur. This case can be dealt with in a number of ways.

Solution of equation of motion: In terms of an equivalent SDOF system, the equation of motion may be written as:

$$M_e\ddot{u}+k_e u = P_e(t) \tag{6}$$

This can be solved in a stepwise manner, since the loading history and initial conditions are known. If a short enough timestep is used, then an assumption of constant acceleration during a timestep will provide sufficient accuracy.

Energy method: Alternatively, if only the maximum displacement is required, an energy approach may prove simpler. This involves equating the work done by the applied load to the strain energy in the structure at its peak displacement. For a SDOF system this is simply:

$$P_e u_m = k_e u_y (u_m - \frac{u_y}{2}) \tag{7}$$

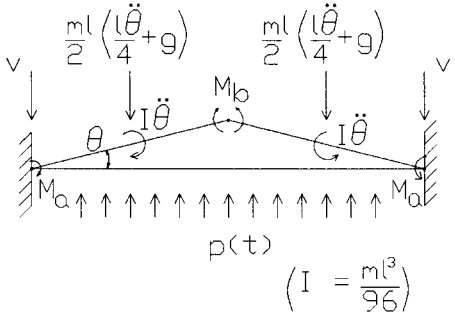

Figure 6. Dynamic plastic collapse of reinforced concrete beam

Dynamic load factor (DLF): In cases where little or no plasticity is expected, a DLF can be deduced from a simple elastic analysis. Plots of DLF vs. natural frequency for various loading pulses are available in numerous references, e.g. [8]. The peak applied load factored by the DLF must not exceed the maximum resistance available.

Dynamic plasticity method: The equation of motion for a structure undergoing plastic collapse can be solved without using an equivalent SDOF system. This approach was first suggested for reinforced concrete beams [9], but can easily be extended to slabs and walls using the yield line method, and to plastic collapse of steel structures.

@seismicisolation
@Seismic Structures

Figure 6 shows the forces on a beam undergoing plastic collapse. The material is assumed to be rigid-plastic, and has mass m per unit length. Consideration of the work done per unit time gives

$$\frac{pl^2}{8} = M_a + M_b + \frac{mgl^2}{8} + \frac{ml^3\ddot{\theta}}{24} \tag{8}$$

Now the static pressure to cause collapse is given by

$$\frac{p_y l^2}{8} = M_a + M_b + \frac{mgl^2}{8} \tag{9}$$

Subtracting (9) from (8) gives:

$$\frac{(p-p_y)\,l^2}{8} = \frac{ml^3\ddot{\theta}}{24} \tag{10}$$

Equation (10) can be solved for successive values of the applied blast pressure p and rotation θ using numerical integration. For vertical members the procedure is slightly more complex, since in-plane forces must be included, and the resulting equations solved numerically using, for example, the finite difference method.

COMPUTATIONAL ANALYSIS METHODS

Improvements in computing power have made it possible to perform highly sophisticated analyses of structures under extreme dynamic loads. Methods available include non-linear FE programs (e.g. ABAQUS), and "hydrocodes" such as DYNA-3D.

Finite Element Methods

While non-linear finite element programs can be applied to blast loading events, many of the limitations of simpler methods remain. Analyses are performed in the time domain, using a stepwise integration scheme and the loading is usually defined in a similar way to hand calculation methods.

Material characteristics may be derived by consideration of plastic hinge formation. However, it is common to attempt a more sophisticated material representation. For example, many attempts to model reinforced concrete include allowances for strain-softening in compression, for incremental plasticity under multiaxial stresses, and for visco-plastic modelling of strain-rate dependency [10]. It is doubtful whether such sophistication is justified, given the level of uncertainty over loading and material characteristics in most analyses.

Hydrocodes

A range of programs for the analysis of very high rate loading events are known as hydrocodes, due to the capability for modelling hydrodynamic behaviour of the loaded material. These can be applied to blast loading, though in many cases the loading rate is not sufficiently high to justify their use. One advantage of such programs (e.g. AUTODYN) is their ability to model the sequential stages of an explosive event (detonation dynamics, blast wave propagation, structural response).

@seismicisolation

CONCLUDING REMARKS

The techniques available for the analysis of structures subjected to blast loading tend to lie at one of two extremes, i.e. hand calculation methods and highly complex, expensive computer analyses. There is a clear need for the development of straightforward analysis methods capable of yielding sufficient detail to the design engineer, but not requiring a wealth of specialist knowledge. Until such methods are available, understanding of blast loading is likely to be confined to a few specialists, mostly in the military field.

REFERENCES

1. Baker, W.E., Explosions in Air, University of Texas Press, Austin, USA, 1973.

2. US Departments of the Army, Navy and Air Force, Structures to Resist the Effects of Accidental Explosions, Technical manual TM5-1300, 1969.

3. Harris, R.J., The Investigation and Control of Gas Explosions in Buildings and Heating Plant, E. and F.N. Spon, London, 1983.

4. Macauley, M.A., Introduction to Impact Engineering, Chapman and Hall, London, 1987, pp. 4-26.

5. Millstein, L. and Sabnis, G.M., Concrete strength under impact loading. Proc. Int. Symp. on Concrete Structures Under Impact and Impulsive Loading, Berlin, 1982, 101-11.

6. ACI Committee 349, Code requirements for nuclear safety related concrete structures. ACI Journal, 1977, 53-8.

7. Kennedy, R.P., A review of procedures for the analysis and design of concrete structures to resist missile impact effects. Nucl. Eng. and Design, 1976, 37, 183-203.

8. Biggs, J.M., Introduction to Structural Dynamics, McGraw- Hill, New York, 1964, pp. 34-76 and 199-244.

9. Alexander, S.J. and Hambly, E.C., The design of structures to withstand gaseous explosions. Concrete, 1970, 62-5 and 107-16.

10. Mikkola, M.J., and Sinisalo, H.S., Nonlinear dynamic analysis of reinforced concrete structures. Proc. Int. Symp. on Concrete Structures Under Impact and Impulsive Loading, Berlin, 1982, 534-47.

@seismicisolation

ESTIMATION OF DESIGN FORCES ON STRUCTURES NEAR QUARRIES FROM FIELD BLAST TESTS

Vijay K. Purl
Assistant Professor, Department of Civil Engineering and Mechanics
Southern Illinois University
Carbondale, Illinois, USA 62901
and
Shamsher Prakash
Professor, Civil Engineering Department
University of Missouri at Rolla
Rolla, Missouri, USA 65401

ABSTRACT

Blasting of large charges for quarry operations results in strong ground motion which may cause damage to structures in its vicinity. Precautions are therefore needed in the design and construction of such structures. Peak ground velocity provides and excellent criteria for assessing the damage due to the blast effects. However, for estimation of dynamic forces for the design of such structures, data on ground acceleration occasioned by the blast is required. This paper describes a study in which the dynamic forces for the design of structures near a proposed lime stone quarry were determined based on acceleration-time history data recorded during field blast tests. Acceleration response spectra was obtained from the recorded accelerograms. Also an equation was developed for this particular site for estimation of the peak horizontal ground accelerations in terms of the amount of charge per delay and the distance, which was subsequently used for modifying the ordinates of response spectra to account for the effect of distance of the structure from the blast and variation in the amount of maximum charge per delay.

INTRODUCTION

Strong ground motion produced by blasting of large amounts of charges for mining operations often results in damage to adjacent structures. Depending on the nature of the rock masses in the area, and the blast parameters, structures several kilometers away may sometimes be affected. Adequate precautions are therefore necessary in the design and construction of structures in the vicinity of mining areas. Efforts are made to minimize damage due to blasting by suitably designing the blast, limiting the amount of explosive per delay, and by adequately strengthening the structures to resist the resulting ground motion. The intensity of ground motion due to large amounts of charges used in modern large scale mining operations may exceed the safety limits, thus, necessitating design of structures to resist the resulting strong ground motion. This requires the determination of dynamic forces which will act on the structures as a result of the blasting operations. Since these forces depend not only on the amount of the charge and the distance of the structure from the blast face, but also on soil and rock conditions in the area, and the characteristics of the structure and its foundation, their accurate estimation often poses problems.

@seismicisolation

Safety Criteria

The structural damage and the peak particle velocity have been observed to show a good correlation over a wide range of frequencies [1,2,3,4,5]. Damage is likely to occur when the peak particle velocity exceeds about 125 mm/sec, which corresponds with earthquake intensity between VII and VIII on Modified Mercalli intensity scale [6]. Codes of practice in many countries specify the safety criteria for determination of safe distance of the structure from the blast point in terms of the peak particle velocity. The values of peak particle velocity may be obtained from empirical equations of the type given below [9].

$$V=K\left(\frac{R}{\sqrt{W}}\right)^{\beta} \quad \ldots\ldots\ldots\ldots (1)$$

where V = peak particle velocity
W = weight of explosive per delay
R = radial distance from the blast point
and, K and β are constants which depend on the nature of the rock and the type of the explosive.

Ground Motion For The Design of Structures

The data on strong ground motion is required for the design of structures. Several investigators [7] have obtained theoretical solutions for the maximum ground acceleration which may result from a fully contained explosion in a perfectly elastic medium. It is difficult to account for the effect of significant parameters such as soil and rock properties, and their local variation in the blasting arena and its vicinity, on the blast generated ground motion. Therefore, determination of ground acceleration for the design of structures may preferably be made based on acceleration--time data recorded during blasting operations [8]. It may be mentioned here that the blast resistant design differs from the aseismic design in the fact that the blasting for mining operations is a repetitive phenomenon, whereas a seismic event is rather infrequent. The structures should therefore be designed to behave elastically for blast loading, whereas some minor damage may be acceptable for seismic loading of moderate size.

This paper presents a case study of field blast tests conducted for the determination of dynamic forces in terms of spectral accelerations for the design of structures to be located at various distances from the blast point in the vicinity of a proposed lime stone quarry. The horizontal ground acceleration for design of the structure could then be determined taking into consideration its characteristics defined by its undamped natural period, and the damping. To account for the effect of distance, or the variations in the maximum amount of charge per delay on the design accelerations, modification factors were also suggested. The details of the field blast tests and the results of this study are discussed herein.

FIELD BLAST TESTS

Five blast tests using various amounts of charges were carried out at different locations in the proposed lime stone quarry area. The details of the charges used and the distances of observation points from the blast holes are summarized in Table 1. The layout of blast holes and observation points was decided in such a way so as to obtain fairly representative average values of data for the site. For each blast, the horizontal component of ground acceleration was measured at predetermined locations using acceleration transducers. The output of the acceleration transducers was amplified through Universal Amplifiers and recorded using ink writing oscillographs. A typical acceleration-time history plot for one of the blast tests is shown in Fig. 1. The data on observed peak horizontal ground accelerations and primary or P-wave velocities is also shown in Table 1.

@seismicisolation

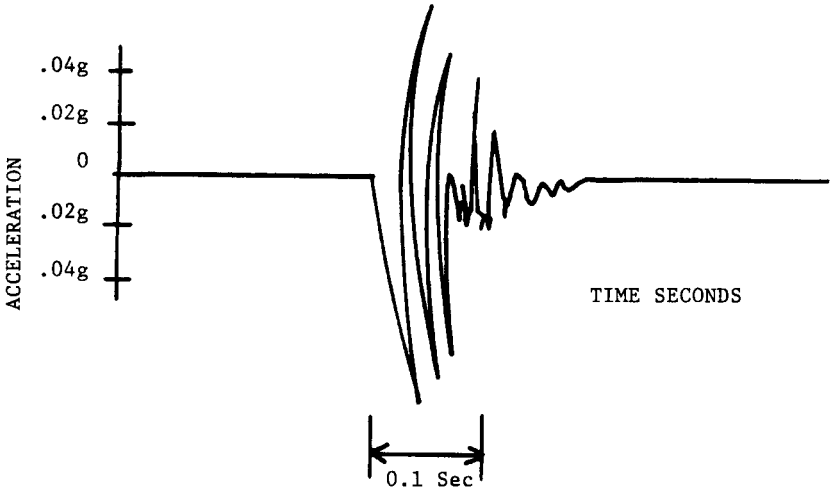

Figure 1. Typical acceleration versus time plot for a charge of 78.75 kg at a distance of 125m from the blast.

ANALYSIS AND INTERPRETATION OF TEST DATA

Peak Horizontal Ground Accelerations

The observed data on peak horizontal ground acceleration 'a', the primary wave velocity 'Vc', the weight of the charge 'W' per delay and the distance 'R' from the center of the blast was analyzed by using dimensional analysis. A plot was made between the dimensionless parameters $aW^{1/3}/Vc^2$ and $(R/W^{1/3})$ which is shown in Fig. 2. The equation of the upper bound (which is straight line on the log-log plot) is found to be:

$$\frac{aW^{1/3}}{Vc^2} = 0.655 \left(\frac{R^{-2.35}}{W^{1/3}}\right)$$

or

$$a = 0.655(R^{-2.35})\ (W^{0.45})\ (Vc^2) \qquad (2)$$

In order to account for the nature of the explosive on the values of ground acceleration, weight 'W' in Eq. 2, may be expressed in terms of the volume given by Q (RBS)/γ_e, where 'Q' is the bulk weight of the explosive, 'RBS' is the relative bulk strength expressed as a ratio, and γ_e is the weight density of the explosive. Equation 2 may then be rewritten as:

$$a = KQ^{0.45}.R^{-2.35} \qquad (3)$$

where

$$K = 0.655\ Vc^2 \left(\frac{RBS^{0.45}}{\gamma_e}\right) \qquad (4)$$

@seismicisolation

Table 1
Details of Field Blast Tests and Data Observed

Site	Charge Description			Max charge in a delay, kg.	Depth of blast holes, m	Distance from blast hole, m	P-wave velocity, m/sec.	Peak horizontal ground acc^n, cm/sec^2
	Type	Total charge	No. of delays					
A	Special gelatine 80%	23.0	-	23.0	4.8	50.0 90.3	3680	47.0 23.1
B	Special gelatine 80%	7.5	-	7.5	4.2	50.0 114.8	3890	55.2 44.4
C	Special gelatine 80%	12.5	-	12.5	4.2	50.0 114.8	3980	58.1 25.6
D	Special gelatine 80%	78.75	-	78.75	6.0	50.0 125.0	3680	348.7 37.6
E	Open cast gelignite	584.0	2	292.00	8.4	106.0 175.0	3500	530.2 126.8

Constant K in Eq. 3 depends on the characteristics of the medium defined by the primary wave velocity, and the charge characteristics defined by its relative bulk strength and density. Equation (3) was used to determine the peak horizontal ground acceleration at different distances from the blast locations for a given charge.

Design Acceleration Spectra

From the recorded accelerograms of different blast tests, spectral accelerations for structures of different periods and damping were computed. Using these values, the design spectra for a blast having a maximum charge of 300 kg of open cast gelganite in any delay, and for a distance of 100 m from the blast was obtained for damping values of 2,5 & 10%, as shown in Fig. 3.

Modification Factors For Ground Acceleration

The values of peak horizontal ground acceleration for the design of structures may be obtained from Fig. 3. This needs information on undamped natural period 'T' and damping in the structure. The undamped natural period can be computed using the principle of vibrations, and the value of damping should be assumed depending upon the type of material used for the structure. It my be noted that the acceleration response spectrum given in Fig. 3 is for a maximum charge per delay of 300 kg of 80% special gelatine, and for a distance of 100 m from the blast point. Since the full scale mining operations had not yet started, the information on a maximum charge per delay to be used in the future was not known. Also, structures will naturally be located at various distances from the blast point. The ordinates of horizontal ground acceleration obtained from Fig. 3 should therefore be modified to account for the effect of the amount of charge per delay actually used, and the distance of the structure from the blast point. Further modification may be made, if an explosive other than special gelatine 80% is used. The design acceleration for a structure may then be obtained by modifying the ordinates of the acceleration response spectrum in Fig. 3 as follows:

$$a_{des} = S_a \cdot \frac{a_2}{a_1} \qquad (5)$$

where, a_{des} = Design acceleration, cm/Sec^2

S_a = Spectral acceleration obtained from Fig. 3. corresponding to the undamped natural period of the structure under consideration, cm/Sec^2

@seismicisolation

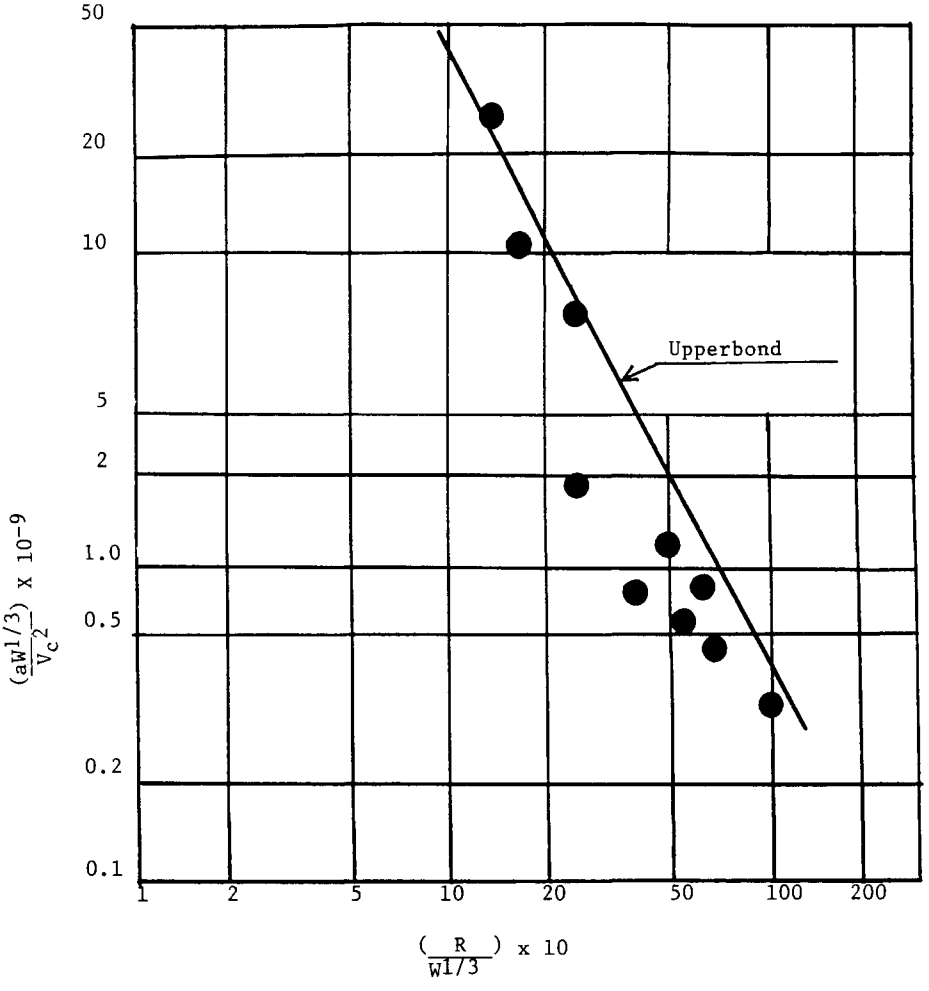

Figure 2. Plot of $\left(\frac{aW^{1/3}}{VC^2}\right) \times 10^{-9}$ versus $\left(\frac{R}{W^{1/3}}\right) \times 10$

a_1 = Peak horizontal ground acceleration at a distance of 100 m for a charge of 300 kg of special gelatine.

and, a_2 = Peak horizontal acceleration at the proposed location of the structure due to the actual blast, cm/sec^2.

The values of a_2 may be computed using Eq. 3.

@seismicisolation

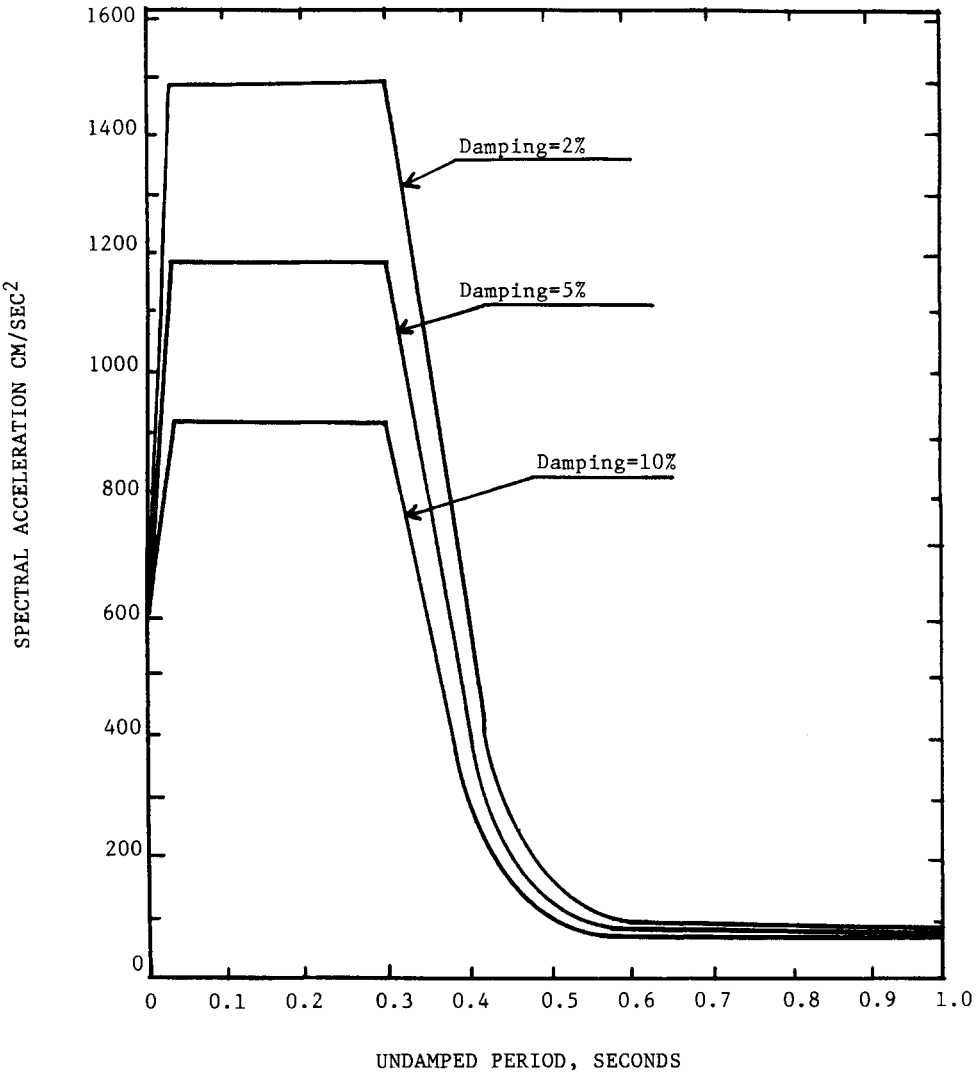

Figure 3. Design Spectra for a charge of 300 kg per delay at a distance of 100m from the blast point.

CONCLUSIONS

This case study demonstrates the process of obtaining horizontal ground acceleration for the design of structures located in the vicinity of a proposed lime stone quarry. The field blast tests should be conducted simulating the charge and blasting pattern used during the actual mining operations, which was not possible in this case. An empirical procedure based upon the peak ground accelerations

@seismicisolation

was therefore proposed to modify the ordinates of the acceleration response spectrum which was developed from recorded acceleration-time history data.

REFERENCES

1. Crandell, F.J., Ground vibrations due to blasting and its effects upon structures," J. Boston Soc. Civil Engineers, 1949, 36, 222-45.

2. Edwards, A.T. and Northwood, A.T., "Experimental studies of the effects of blasting on structures," The Engineer, 1960, 210, 538-46.

3. Duvall, W.I., and Fogelson, D.E., "Review of criteria for estimating damage to residences from blasting vibrations," US Bureau of Mines Report of investigations, 1963, 5968, 1-19.

4. Duvall, W.I., Johnson, C.F., Meyer, A.V.C., and Devine, G.F., "Vibrations from instantaneous and Millisecond-delayed quarry blasts," US Bureau of Mines Report Of Investigations, 1963, 6151, 1-34.

5. Langefors, U. and Kihlstrom, B., The Modern Technique of Rock Blasting, John Wiley and Sons, New York, 1973, pp. 1-405.

6. Hudson, D.E., "Man made ground motion," Shock and Vibration Handbook, McGraw Hill, New York, 1961.

7. Hoek, E., and Bray, J., Rock Slope Engineering, Institute of Mining and Metallurgy, London, 1981, pp. 271-308.

8. Srivastva, L.S., Puri, V.K., Chandra, B., Basu, S., and Arya, A.S., "Response spectra for design of structures subjected to underground blasts," V Symposium On Earthquake Engineering, University of Roorkee, India, 1974, pp. 27-30.

@seismicisolation

ON THE SIGNIFICANCE OF INTERNAL GAS EXPLOSIONS IN BUILDINGS

B R ELLIS
Building Research Establishment, Watford, WD2 7JR, UK.

ABSTRACT

The purpose of this paper is to draw together some of the findings of a number of research projects concerned with gas explosions in buildings. The factors which affect the development of gas explosions are discussed and pressure-time histories are presented to illustrate two different types of explosion. Then the results of a survey are used to show the hazard and risk associated with gas explosions in buildings. Measured results from tests in an experimental rig and tests in two types of buildings are given. Finally, an attempt is made to draw together some of the information and examine the risk inherent in various levels of design loading for tall buildings.

INTRODUCTION

In 1968 a gas explosion occurred in a flat in the south-east corner of the 18th floor of a 22 storey block of flats in Newham, London. The explosion blew out the non-load bearing walls of the kitchen and the living room and the external load bearing wall of the living room. This initiated the progressive collapse of one corner of the whole block. The cause of the explosion was the leakage of town gas from a defective connection on a cooker which was probably ignited by a struck match (1). The explosion was not confined to the kitchen, but propagated into the hall and living room.

This event had significant repercussions within the engineering community and resulted in changes in the Building Regulations to deal specifically with localised damage due to an accident such as a gas explosion. The Building Regulations 1976 required that the building should be so constructed that structural failure consequent on removal of any one member in a storey should be localised and limited in its extent to a certain area of that storey. If this was not possible, that member should be capable of sustaining without structural failure, an additional load corresponding to a pressure of 34 kPa.

These changes were based on the limited information available at the time, and it was realised that further data were required to provide a better understanding of the problem; consequently research was initiated at various institutions. This research has been concerned with measuring pressures in explosions from various gas/air mixtures, noting how frequently gas explosions occur throughout the UK and the severity of the resultant damage, and also examining how structures respond to explosions.

The purpose of this paper is to bring together some of the findings of the research work and to show what level of risk is associated with gas explosions in buildings.

@seismicisolation

FACTORS AFFECTING THE DEVELOPMENT OF A GAS EXPLOSION

A gas explosion may occur if an ignition source is introduced to a mixture of gas and air when the gas concentration is within a certain range. The combustion of the gas-air mixture produces a rise in pressure, which for a stoichiometric* gas-air mixture in a room could reach a maximum pressure of 700-1000 kPa. In most instances the rising pressure will break the weakest element within the room, maybe a window or lightweight partition, thus venting the explosion and limiting the peak pressure to a fraction of the maximum potential pressure. There are many factors which can effect the development of an explosion and the pressures generated, including the amount and type of gas, the turbulence created during the explosion and the size and strength of the vents. To illustrate these points it useful to examine the pressure time histories recorded during two explosions.

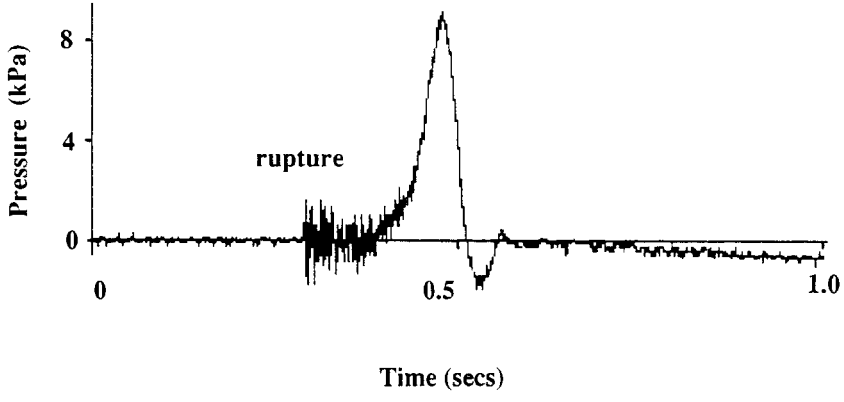

FIGURE 1 Pressure-time history produced using a butane canister

Figure 1 shows the pressure time history recorded for a 'simple' explosion which occurred in the ground floor bedroom of a maisonette. It was created by rupturing an aerosol canister containing butane and igniting the contents. The aerosol canister contained less gas than required to produce a stoichiometric mixture within the room, but even so the maximum theoretical pressure from that source in the room was 41 kPa. The explosion broke the windows and lightweight walls thus venting the explosion and limiting the maximum pressure to 9.0 kPa. This type of simple explosion, which may arise from the leakage of any type of gas, was restricted to one room and is perhaps the most common type of explosion encountered in buildings.

Figure 2 shows a pressure time history of an explosion in the BRE explosion test rig. The explosion was produced by igniting Liquefied Petroleum Gas (LPG) which had been allowed to leak into the test chamber. In this example there is a much greater volume of gas than in the previous example and the resulting pressure time history is more complex. The explosion can be broken into distinct phases and each pressure peak related to a particular mechanism or process occurring during the explosion (2). The first peak Pv is caused by the breaking of vent. The second peak Pe arises from unburnt material expelled ahead of the advancing flame front being ignited as it passes through the vent. The third peak Pa sometimes termed the acoustic peak, arises from the coupling of the combustion process with the acoustic properties of the test chamber. In actual buildings this sort of coupling is unlikely to occur.

*Stoichiometric - mixture when there is just enough oxygen in the air to burn all the gas.

@seismicisolation

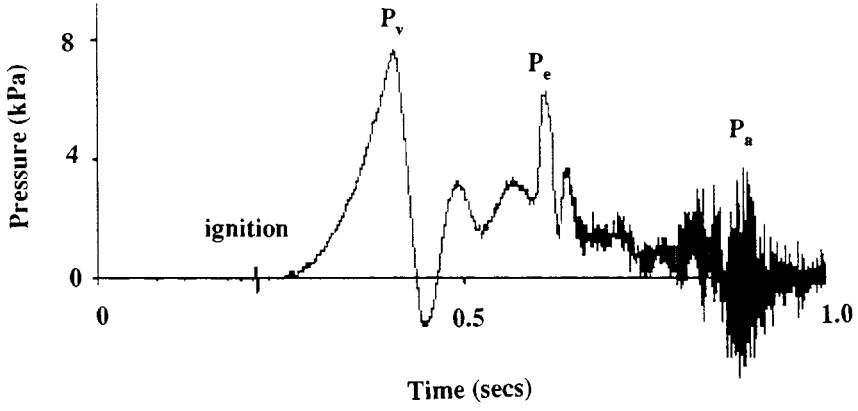

FIGURE 2 Pressure-time history produced by igniting LPG

If a sufficiently large volume of gas leaks into a building, significant concentrations of gas could build up in a number of rooms or corridors. Normal ventilation within the building will help to disperse such accumulations of gas. However, if this situation arises a much more complex and potentially more damaging explosion can result. An initial explosion in one room could propagate into other rooms, but in so doing cause a more turbulent situation and result in a much more violent explosion. This type of explosion which propagates from one room to another has been termed a cascade explosion.

Gas explosions are relatively slow events, at least as far as a building is concerned. For example the first pressure pulse in figure 1 had a duration of 75 ms. This pulse can be approximated as half a sine wave with frequency 6.7 Hz. The fundamental frequency of most structural elements is considerably higher than 6.7 Hz, so the structural element responds to the explosion load as though it were a slowly changing load. For example the ranges of fundamental frequencies noted at Ronan Point (the Newham building which suffered the progressive collapse) are 35 - 130 Hz for the walls and 21-44 Hz for the floors. According to ref 3, the fundamental frequencies of brick walls range from 25-40 Hz. In general, structural elements have fundamental frequencies that are much higher (or alternatively fundamental periods that are much longer) than the corresponding characteristic of a typical gas explosion. Elements with frequencies considerably greater than the 'frequency' of the explosion see the loading as effectively static and the displacement time history of these elements during an explosion will have a similar shape to the pressure time history (4) unless of course the element fails. Some structures like long-span lightweight floors have much lower fundamental frequencies and if these correspond to the 'frequency' of an explosion then some dynamic amplification is possible, up to a maximum value of 2.

If the pressure during a gas explosion is monitored in a number of places within a room, the pressure time histories at the various positions are usually similar, at least for the 'simple' explosions. Hence, the pressure distribution throughout the room is uniform and the loading on the walls, floors and ceiling will be uniformly distributed. For more turbulent explosions variations in pressure distribution can occur. However, the maximum load a structural element has to withstand is the peak pressure multiplied by the area of the element exposed to the explosion multiplied by the dynamic magnification factor. In most cases this dynamic magnification factor is unity.

@seismicisolation

NEWSPAPER SURVEY

To provide statistics on the frequency and severity of gas explosions in housing, DoE have undertaken a survey. The survey of structural damage caused by gas explosions (and other accidental loadings), conducted by CIRIA under contract to the DoE and subsequently under contract and in association with BRE, covers the period 1971-1981. The survey covers cases of accidental damage to non-industrial buildings in Great Britain, details of which were obtained from press reports through a press cutting agency. For some cases there was also direct inspection of damage.

In a report of the survey for the period 1971-1977 (5) incidents are classified by the type of incident and the type of building(s) affected. A basic classification of the severity of a damage incident is given in terms of the type and extent of damage. Three classes are given for explosions as follows:

(i) moderate explosion - destroys relatively weak structures up to and including the typical small bungalow, or for more substantial and larger structures destroys light cladding and windows, damages stud partitioning and similar elements and blows doors off hinges.

(ii) severe explosion - destroys or seriously damages heavier claddings, infills and partitions (eg of brickwork and blockwork) and destroys or damages load bearing elements such as the gable wall and 1st floor of the typical post 1919 2 storey house.

(iii) very severe explosion - destroys or seriously damages stronger load bearing elements (eg of R.C.) or causes very substantial damage over several stories of less substantial construction.

According to these definitions severe and very severe explosion could only occur in buildings of sufficient size and strength.

The number of explosions of different severity for town gas, natural gas and LPG are given in report (5), but there are few other details about the type of explosion. Estimates of peak pressures are made for 'significant' gas explosions where it was possible to inspect damage. However, in general there are few peak pressure values assigned to explosions.

The statistics in the reports (5 & 6) covering the period 1971-1981 give an overall picture of gas explosions which occurred during the period. They also give some indication of the types of structure most commonly affected and the relative hazards of explosions from different types of gas. For the period 1971-1981, 3944 gas explosions were noted.

type of gas	reported explosions	significant explosions
piped gas	2346	345
liquefied gas (aerosols,cylinders)	1598	62

If the significant explosions are classified according to their severity the following table results (6)

type of gas	Moderate	Severe	Very Severe
piped gas	215	113	17
liquefied gas (aerosols,cylinders)	53	9	0

The above statistics imply that explosions due to liquefied gas are less damaging than those due to piped gas. This is as might be expected, as there is less possibility of high concentrations of gas accumulating from sources of fixed gas volume.

@seismicisolation

A discussion of the risk of a gas explosion, in terms of total gas consumption and the number of consumers, is given in (5). When the annual totals of all significant explosions are expressed in terms of gas consumption for 1971-77 it emerges that there is a much greater risk to the users of bottled gas to piped gas, in proportion to energy consumed.

For the period 1971-81 364 significant explosions occurred in domestic buildings of which 10 occurred in buildings of 5 or more storeys., ie 2.75% of the significant explosions occurred in "tall" buildings, which constitute 3% of the total housing stock.

A further survey between 1985 and 1990 has been completed but the results are not yet published. The data from this survey suggest a slight reduction in the annual incidence of explosions from piped gas (in comparison to the 1971-81 data), but a slight increase for gas cylinders.

Other aspects of the survey which are of interest are the risk of fatal injuries and the annual cost of damage from gas explosions. These details are quoted for the years 1971-77. In this time there were 63 deaths due to gas explosions, excluding fatalities due to suffocation or burns during an associated fire. The annual cost at 1977 prices (excluding costs of personal injuries and death) was £1.35M. If the costs are increased by a factor of 4 to inflate them to 1991 prices the figure is £5.4M.

To put the costs in perspective an example of another form of hazardous loading is useful. In the Gales in January and February 1990 (7) it was estimated that 1.16 million domestic houses were damaged and the cost of their repair alone would be approximately £188M. To illustrate the relative risk from gas explosions information given in ref(3) is useful. For the years 1975-78, relative to deaths from natural gas explosions, death from road travel were 500 times more likely, electrocution 5 times more likely and death due to lightning 0.5 times has likely. Thus it can be seen that the costs of gas explosions are relatively insignificant and the risk of fatalities are low.

PHYSICAL TESTS

Although the press survey provides a general overview of the risks of gas explosions in housing, some measurements of pressures during explosions and observations of the resultant damage are necessary to gain a better understanding of the potential hazard. In this section measurements from actual tests are summarised, starting with tests in a steel explosions rig and then followed by two sets of tests in real buildings.

Experimental measurements in a test rig

For a number of years tests have been conducted by staff of the Fire Research Station at their BRE explosion test facility at Cardington to measure the pressure time histories produced by a wide range of gas explosions. The steel explosion cell is a multi-compartment facility consisting of two 22 cubic metre rooms surrounded on three sides by a 1.2m corridor. The modular construction allows building elements such as doors, windows and cells to be incorporated in the cell in a number of configurations and the gas control and monitoring systems cater for a wide variety of flammable gas/air mixtures. This allows explosions designed to simulate a wide variety of conditions to be undertaken.

One series of tests examined explosions from small LPG containers. This type of event is known to have caused damage in buildings, and information on the incidence of this type of explosion and the reported damage from a number of events, plus the range of pressures measured in the test rig are given in ref(8). It should be noted that the damage categories in this report do not correspond to those in the DoE newspaper survey. Peak pressures measured in the rig ranged from 3.5 to 43 kPa, although pressures above 20kPa were only noted with the larger containers when the rig had its smaller vent area fitted (12.5% of one wall). The vents were covered by fibre board which fails at approximately the same pressure as 4mm thick glass.

Another series of tests examined the ignition of LPG from leaking refillable gas cylinders and peak pressures ranged from 3.5 to 20.7 kPa for experiments carried out in single rooms and from 6.9 to 34 kPa for experiments using two rooms separated by a standard domestic door.

@seismicisolation

Further experiments were undertaken to examine cascade type explosions, using various

gases in the rooms and corridors of the rig. These produced the largest pressures measured in the rig (up to 90kPa).

With these tests in a steel rig it should be remembered that on some occasions the worst possible conditions are being artificially created to examine the potential hazard. The rig is sealed so that natural ventilation cannot disperse any gas concentrations as would occur in actual buildings and the venting is restricted to part of one wall.

Chapeltown

To verify some of the conclusions reached in the laboratory tests at Cardington it was thought that some tests in real houses were necessary. Accordingly, possible test sites were investigated until an opportunity arose to test a block of LPS maisonettes at Chapeltown, near Sheffield.

The tests were conducted in a three storey block which contained five flats. The block was constructed by Reema Construction Ltd in 1965 using large prefabricated reinforced concrete panels. Twelve tests were conducted in a number of rooms (9). The explosions were created by rupturing an aerosol canister containing butane and igniting the discharged contents.

A variety of tests were conducted in the largest room which had a volume of approximately 48.3 m^3. Four tests using a 200 ml butane aerosol produced peak pressures ranging from 2.6 to 3.7 kPa and resulted in a range of non-structural damage. Two later tests using 750 ml aerosols, but with the vent areas reinforced, produced peak pressures of 4.8 and 9.0 kPa. Further tests in various rooms using 200 ml aerosols produced peak pressures ranging from 6.1 to 9.0 kPa, and tests using 750 ml aerosols in two second storey bedrooms whose windows were boarded with plywood both produced 9.0 kPa explosions. Although the non-structural damage was significant and aligns with the 'moderate explosion' category used in the newspaper survey, structural damage was not seen, indeed the maximum recorded elastic movement of a R.C. wall was 0.63mm.

With these tests it appeared that the venting and the failure of the non-structural walls was determining the maximum pressures reached. The higher pressures with the larger cans were as much a result of the plywood boarded windows as the larger potential energy.

Potters Marston

Following the progressive collapse at Ronan Point there was some concern over the ability of brickwork to resist the loads produced in gas explosions and to investigate this subject a series of tests was organised by the British Ceramic Research Association (BCRA) at Potters Marston (10 & 11). The investigation involved constructing a special building in load bearing brickwork to simulate the top three storeys of a tall cross wall block. Different types of explosions were set off to investigate the structural stability of brickwork. To complement the results from these tests, further tests were conducted on some granite bunkers on the same site and these have provided some information on the resistance of brickwork and various types of cladding.

The tests in the three storey block can be placed in two categories. The first tests were produced in a single room by igniting the contents of a balloon filled with a gas/air mixture and the second tests were produced by allowing gas to filter into two rooms then igniting the mixture when a selected concentration was reached.

The first experiments with the balloons produced a range of peak pressures from 2.8 kPa to 13.1 kPa although the amount of gas present was potentially able to produce much greater pressures. The peak pressure being limited by the venting which was caused by breaking windows and doors and no damage to the brick work resulted.

The second tests attempted to simulate a typical domestic incident by allowing piped gas to escape into a room and percolate into a second room. For a number of the tests it was necessary to fill cracks etc to prevent gas leakage out of the room to achieve the desired test concentrations. The range of peak pressures reached in the room where the explosion was ignited was from 4.8 to 9.0 kPa, however on two occasions higher peak pressures were reached in the adjoining room with the maximum being 22.8kPa. This largest explosion did considerable damage to the brickwork, although no individual panel blew out completely, and it was judged that the building appeared safe.

@seismicisolation

DISCUSSION

When the changes to the Building Regulations were made to avoid progressive collapse in tall buildings, there was not a great deal of data on which to evaluate the likely hazards from explosions. Even with the information presented in the previous sections it is not a simple task to assess what guidance should be given for compliance with the Building Regulations, because those responsible for the regulations have to decide whether the risks are acceptable (eg the risk of an explosion causing local damage may be acceptable but the risk of consequent progressive collapse disproportionate to the cause may be unacceptable) and a balance has to be achieved between risk and cost.

Proposed revisions to guidance in the Approved Document A (Structure) and the Regulations reflect this approach. The guidance is aimed at reducing the sensitivity of a building to disproportionate collapse by recommending measures (albeit accepting that the building may substantially deform), such as providing effective horizontal and vertical ties in accordance with the structural codes of practice, based on design strengths related to 34 kPa. In case such provisions cannot be made, it is recommended that the structure should be able to bridge over a loss of an untied member and that the area of collapse will be limited and localised. Finally, if it is not possible to bridge over the missing member (which should be the case for a small minority of buildings), such a member should be designed as a protected (or key) member capable of sustaining additional loads related to a pressure of 34 kPa.

It may be felt, however, that in some cases such as the design connections for steel structures, the implied load corresponding to 34 kPa pressure is too onerous. This may lead to considerations for using a reduced value, say 17 kPa, where this can be justified.

The first point about explosions to emphasise is that gas explosions in non-industrial buildings are relatively rare, with the newspaper survey (6) showing an average of only 394 explosions per year throughout Great Britain between 1971 and 1981. Of these explosions only 10% were classified as significant, (from a damage viewpoint) and only 0.43% were very severe. When compared with other hazards the number of deaths from explosions are small and the costs of damage are low.

When piped gas is not supplied there is always the possibility that LPG will be used in preference to electricity. Thus there is a possibility that gas explosions could occur in a building catering for a 17kPa pressure. From the survey, LPG does not seem to be associated with the more severe explosions and this may be because the LPG explosions are generally the 'simple' type of explosions occurring in single rooms and not the cascade type explosions which can generate much higher pressures. This is not to say that LPG could not be the source of a cascade type explosion, just that the chances of getting a sufficient amount of gas, from a limited source, building up in a number of rooms in which normal ventilation would help to disperse the gas, are greatly reduced. A 'simple' explosion in a normally vented room in a building has been shown to generate pressures up to 13 kPa and further tests in real buildings will probably extend this range. This limiting pressure is linked to the structural characteristics of the building rather than the potential energy available from the gas. Larger pressures than this have been noted for LPG in the artificial conditions of the test rig, but do not appear to have been encountered in real buildings. Hence, 17 kPa seems to be a reasonable upper bound based on the limited information available.

When explosions from piped gas and LPG are compared it emerges that there is less risk to users of piped gas in proportion to the energy consumed. For relatively weak structures, explosions from either piped gas or LPG could cause major damage. However, very severe explosions are all linked to piped gas and probably to cascade type explosions. This is probably the type of explosion which occurred at Ronan Point, but the risk of this type of explosion is very small. In the test rig higher pressures than 34 kPa have been monitored during cascade type explosions, but there is no available data from this type of explosion in real buildings, and as can be seen from the comparative tests with other types of explosion, pressures generated in real structures can be much lower than those generated in the test rig.

In the authors opinion further information from tests in real buildings is desirable, especially if the cascade explosions could be generated. The continuation of the newspaper survey is important for monitoring any changes which may result with changes in building practice, like the effects of strengthening doors and windows for security purposes, simply

@seismicisolation

because the structural strengths are an important factor in limiting the pressure generated in a 'simple' explosion. Also the examination of any severe explosions involving LPG would be useful.

Areas without normal venting must remain a separate issue. The pressures generated in confined unvented explosions are great, and it is unlikely that a conventional design could contain these pressures. Therefore, special attention should be given to providing good ventilation in these areas and removing the chance of gas ingress particularly below ground level.

ACKNOWLEDGEMENTS

Although a lot of the results mentioned in this paper have been obtained from work undertaken by BRE, either through the Building Research Station or the Fire Research Station, the author of this paper has only been involved a few recent investigations. For detailed information on this work the original references should be obtained. The tests with which the author has been involved have been undertaken with David Crowhurst at FRS who has been responsible for creating and recording the explosions. The author would like to acknowledge the contribution made by his colleagues Graham Armer and David Crowhurst through many discussions on explosions and other forms of accidental loading. This work is included in the research programme of the Building Research Establishment and is published by permission of the Chief Executive.

REFERENCES

1. Report into the Inquiry into the collapse of flats at Ronan Point, Canning Town, London. HMSO 1968.

2. Cooper, M.G., Fairweather, M. and Tile J., On the mechanisms of pressure generation in vented explosions. Combustion and Flame, Vol 65, pp. 1-14, 1986.

3. Harris, R.J., Gas explosions in buildings and heating plant. British gas/ E & F N Spon Ltd, London, 1983.

4. Ellis, B.R. and Crowhurst D., On the elastic response of panels to gas explosions. Conf. on Structures under Shock and Impact, Cambridge, Massachusetts, July 1989.

5. Mainstone, R.J., Nicholson, H.G. and Alexander, S.J., Structural damage in buildings caused by gaseous explosions and other accidental loadings, 1971-1977. BRE Report, London, HMSO, 1978.

6. Moore, J.F.A., The incidence of accidental loadings in buildings, 1971-1981. BRE Current Paper 2/83.

7. Buller, P.S.J., The gales of January and February 1990; Damage to buildings and structures. *to be published through BRE.*

8. Ames, S. and Crowhurst, D., Domestic explosions from small LPG containers. J. of Hazardous Materials, 19,1988.

9. Ellis, B.R. and Crowhurst, D., The response of several LPS maisonettes to small gas explosions. Joint I.S.E./B.R.E. seminar on Structural design for hazardous loads: The role of physical tests, Brighton 1991.

10. Astbury, N.F., West, H.W.H., Hodgkinson, H.R., Cubbage, P.A. and Clare, R., Gas explosions in load bearing brick structures, BCRA special publication 68, 1970.

11. Astbury, N.F. Gas explosions in load bearing brick buildings. Construction research and development journal, vol 2, no 4, 1971.

@seismicisolation

EXPERIMENTAL STUDIES OF VIBRATIONS CAUSED BY BLASTING FOR TUNNEL EXCAVATION.

G. Bongiovanni, V. Gorelli, G. Rienzo, D. Rinaldis
ENEA Area Energia Ambiente e Salute, C.R.E. Casaccia, P.O. Box 2400, 00100 ROMA A.D.

ABSTRACT

In Valle d'Aosta, north-west of Italy, a freeway from Aosta to the Monte Bianco tunnel is under construction. Due to the geomorphology they are excavating many tunnels using also blasts.

ENEA has been asked to evaluate the risk for some dwellings, mainly masonry type, associated with the use of blasting for the construction of the Chabodey tunnel.

Customarily the safety of the structures is supposed if a threshold is imposed to some parameter controlling the motion of the soil (e.g.,the maximum velocity of vibration) in their vicinity. Most of the empirical relationships relate the maximum expected velocity to the weight of explosive and to the distance from the focus. Hardly the frequency content of the vibrogram and source effects are taken into account.

As a first step of our work a set of tests have been performed along the alignement of the tunnel, using specifically designed blasts and the normal excavation blasts, to determine a statistical set of values suited to fit a relationship of the form:

$$V = K * Q^{m} * R^{-n} \qquad (1)$$

V= maximum vector velocity (mm/s)
Q= weight of explosive (Kg)
R= focal distance (m)
K= constant accounting for the physical effect of the soil
n,m= empirical parameters.

@seismicisolation

Triaxial seismometers have been used to measure V. More than 100 values have been measured. Both linear regressions (using the Log form of (1)) and non-linear regressions have been performed on the whole set of data and on selected sub-set. From these analyses it appears that the relationship shows poor fit to the data near the source (< 50 m), that is a source term accounting for the geometry (at least) should be added. Moreover a frequency analysis of the recorded signals shows a large spread in the energy distribution, that is the physical and geometrical effects tend to be dominant in the propagation of the waves originated by the blastings. The role played by the physical and geometrical inhomogeneity are going to be investigated in a successive study, before the risk for the dwellings can be faced.

INTRODUCTION

The tunnel under construction is one of several along the Aosta-Monte Bianco freeway. In fig. 1 is a plan view of the tunnel and in table 1 are summarized some characteristics of the soil to be excavated. It is apparent that the soil is quite poor and the use of explosive is not so simple [1-4]. Nevertheless the authorities have permitted the utilization of explosives with some limitation and with the duty to control the peak velocity induced near the dwellings (Chabodey, La Pietra, Plassier) by adjusting the K value of the Langefors relationship.

R.A.V., the licensing company for the whole freeway, asked Geoconsult, a consulting company, to assess the safety for the dwellings close to the tunnel. Geoconsult referred to ENEA to make detailed studies and experimentation on the subject.

The authors of this paper decided, as a first step, to verify the reliability of the Langefors relationship for the type of soil of the site.

In the paper is shortly described the in situ measurements, the results of numerical fit to the relationship and some consideration on the frequency content of the recorded time histories.

@seismicisolation

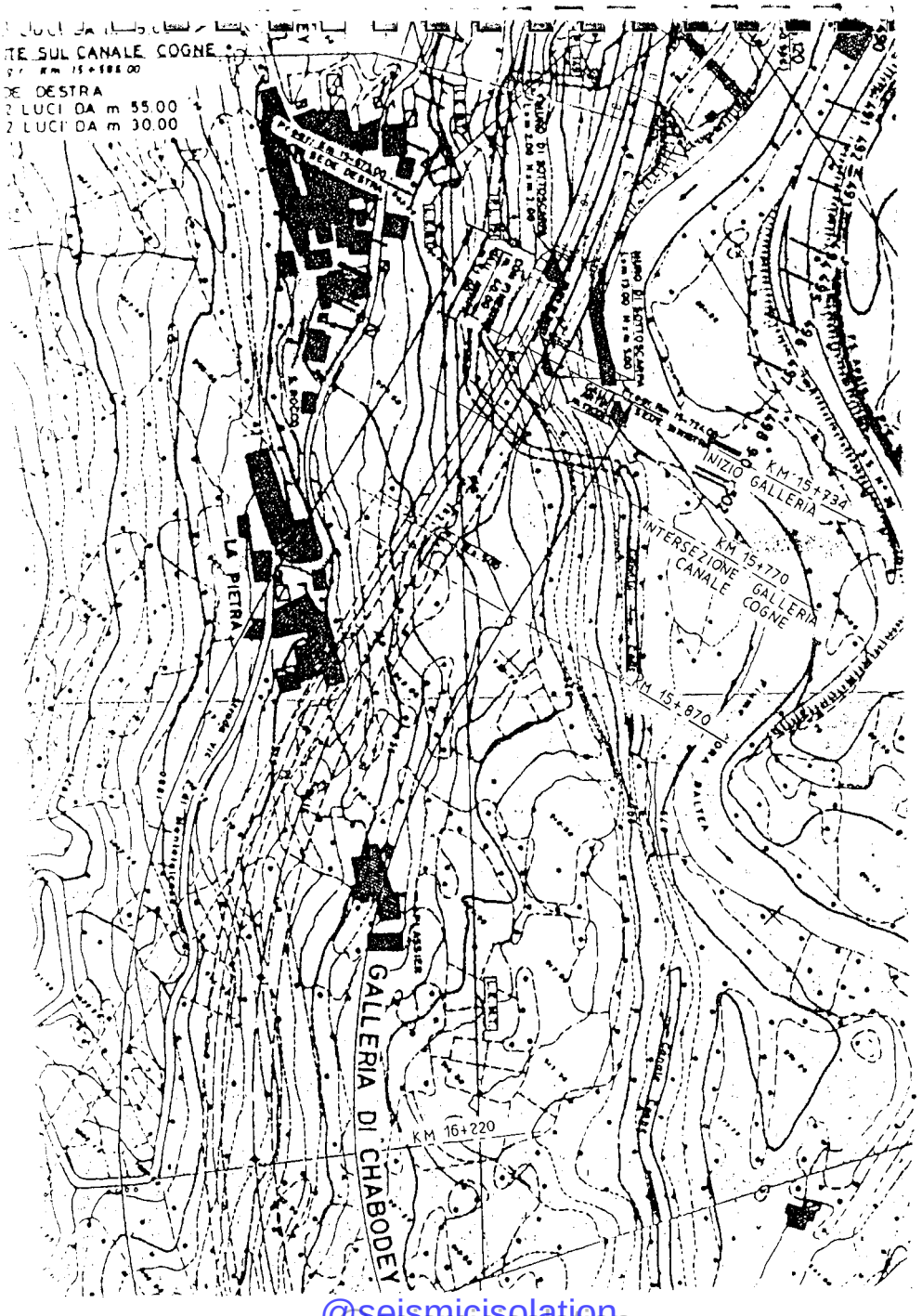

@seismicisolation

Fig. 1 Plan view of the tunnel

TABLE 1
Soil characteristics

m 0 500 1000

Mean Thickness	25	70	70	30
Lithology	Debris	Mica-schists	Schists	Landslide
γ (t/m**3)	2.1	2.5	2.5-2.7	2.2
σ_c (Kg/cm**2)		600	1200-1500	
E (Kg/cm**2)	500	15000	100000-150000	500

EXPERIMENTAL ASPECTS

Nine seismometers Kinemetrics SS-1 in triaxial configuration connected with three Kinemetrics PDR-1 recorders have been used. In addition two accelerographs Kinemetrics DSA-1 and one accelerograph Contraves Codisma with a piezoelectric triaxial sensor have been used [5]. A large set of time-histories have been recorded from the normal excavation blasts. A set of four downhole blast, specifically designed, at depth from 20 to 30m have been performed using single or one second delayed explosions and to test the reciprocal reliability of accelerometers and seismometers with respect to the frequency content. In fig. 2 and 3 are shown two samples of time histories.

The .250 s delay has been used in the normal excavation blasts, but in some cases it has not be possible to separate two successive explosions. While this fact made the available data less, at the same time denotes that the response of the soil is cumbersome.

@seismicisolation

Fig. 2

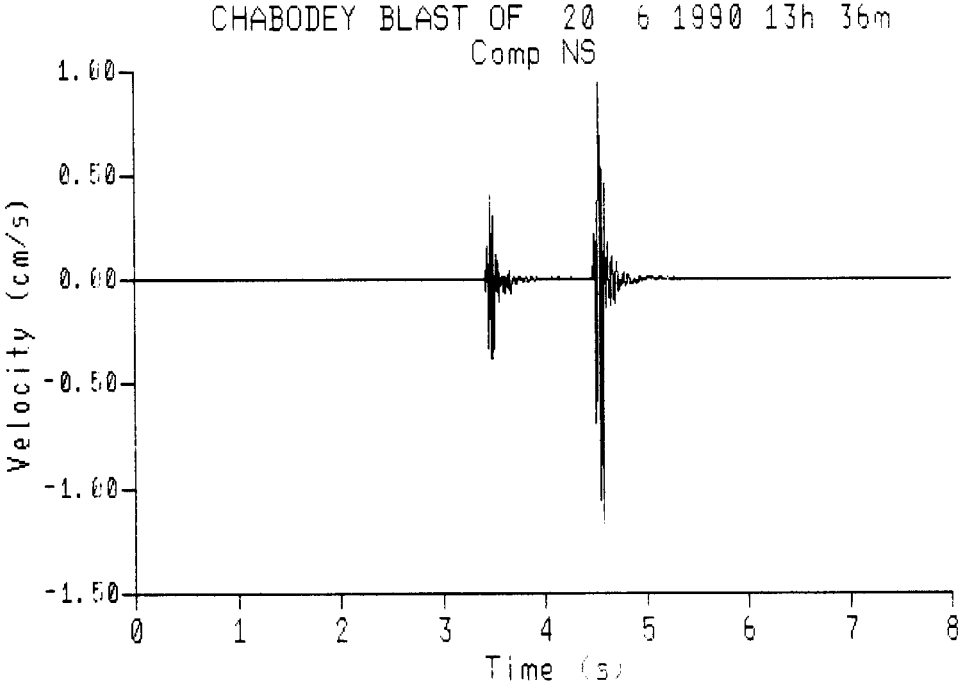

Fig. 3

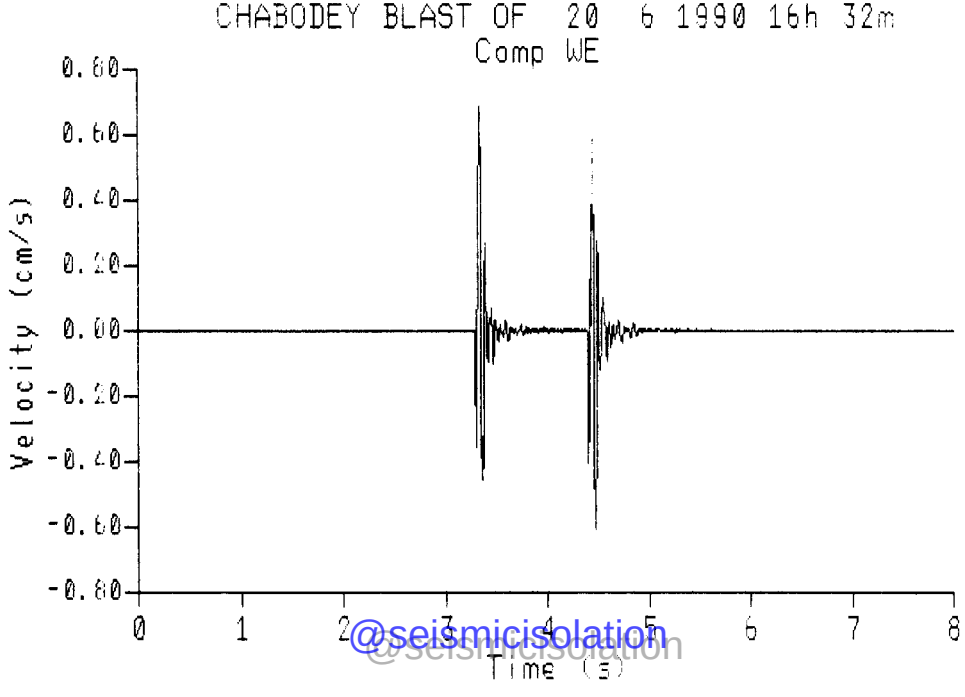

@seismicisolation
@seismicisolation

FITTING THE LANGEFORS RELATIONSHIP

The Langefors relationship, customarily used to control the effect of blasts, has the form [6]:

$$V = K * Q^m * R^{-n} \qquad (1)$$

V= maximum vector velocity (mm/s)
Q= weight of explosive (Kg)
R= focal distance (m)
K,m,n = empirical parameters

A set of 160 values of V, Q, R, obtained from the experimental data, have been used to fit the relationship. Their ranges are:
V= 0.01 to 32. mm/s
Q= .250 to 25. Kg
R= 10 to 520 m
Data have been fitted to the log form of (1)

$$\mathbf{Log(V)= Log(K) + m*Log(Q)-n*Log(R)} \qquad (2)$$

The values obtained are:
Log(K)= 3.9
m= .11
n= -2
R-square=.77
but the T statistic for m cannot be accepted.

Considering that the source effect can be relevant and that data at higher distances could not be reliable the following sub-sets have been examined:
a) R< 100 m (39 values);
b) R> 100 m (121 values);
c) R≤ 111 m (102 values);
d) R>111 m (58 values).

For all of them the fit cannot be accepted. The use of a nonlinear least square fit (Marquardt) for the Langefors relationship gives the following results:
The whole data: K= 785.; m= 0.21 ; n= -1.4

Correlation matrix

	K	m	n
K	1.00	-0.36	-0.69
m	-0.36	1.00	-0.38
n	-0.69	-0.38	1.00

@seismicisolation

Data set a) : K= 300.; m= 0.59 ; n= -1.2

Correlation matrix

	K	m	n
K	1.00	-0.36	-0.65
m	-0.36	1.00	-0.44
n	-0.65	-0.44	1.00

Data set b) : K= 55.; m= 0.24 ; n= -1.06

Correlation matrix

	K	m	n
K	1.00	-0.12	-0.98
m	-0.12	1.00	-0.09
n	-0.98	-0.09	1.00

Data set c) : K= 712.; m= 0.25 ; n= -1.38

Correlation matrix

	K	m	n
K	1.00	-0.36	-0.70
m	-0.36	1.00	-0.36
n	-0.70	-0.36	1.00

Data set d) : K= 196.; m= 0.15 ; n= -1.26

Correlation matrix

	K	m	n
K	1.00	-0.12	-0.98
m	-0.12	1.00	-0.07
n	-0.98	-0.07	1.00

It is apparent that the whole data, as well as the set a) and c), show poor correlation for all of the parameters. The set b) and d) show that the pairs K-m, m-n are independent while K-n are strongly correlated. In any case we must reject the reliability of the Langefors relationship for this kind of soil. For sake of completeness in fig. 4 is shown the distribution of the experimental values around some parametrized curves obtained for the results of case b).

@seismicisolation

Fig. 4
EXPECTED CURVES AND EXPERIMENTAL VALUES

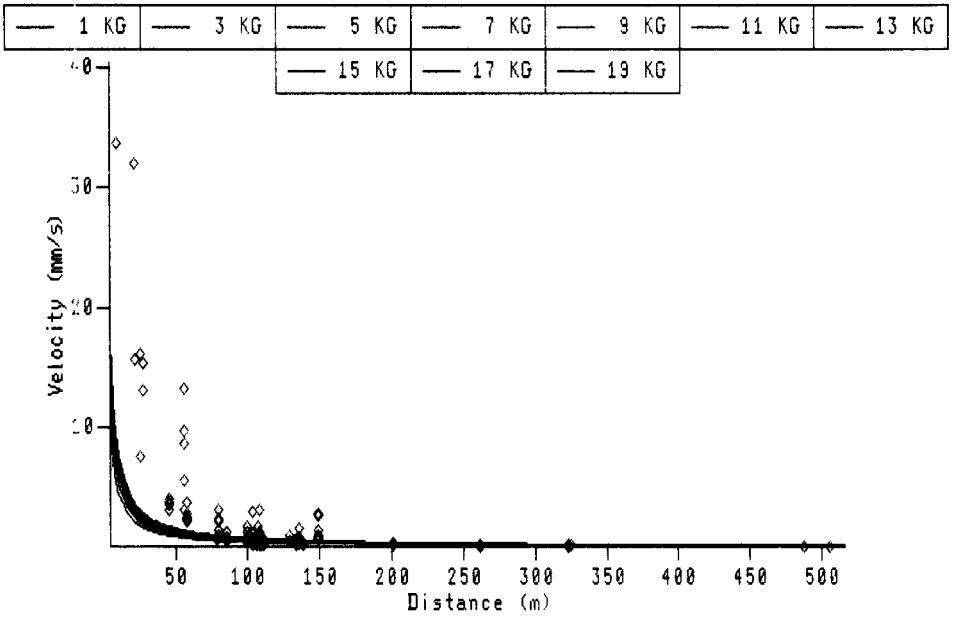

RELATIONSHIP : V= 55.* Q**(0.24)*R**(-1.06)

SOME CONSIDERATION ABOUT THE FREQUENCY CONTENT

In fig. 5 and 6 are shown the Fourier Amplitude Spectra of the time-histories of fig. 2 and 3. It is unusual that ti-hi from explosions give such low frequency content [7]. The main reasons is to be found in the nature of the soil that introduces the low frequencies. Moreover the acceleration time history obtained by derivation of that of fig. 2, shown in fig. 7, has a significant peak. It is reasonable that velocity ti-hi with peak value of 8-10 mm/s can correspond to accelerations typical of strong earthquakes.

CONCLUSIONS

The Langefors relationship is to be considered not reliable to control the motion induced by blasts if the soil has characteristics similar to those of this case. It is in any case advisable to make some experiments to determine the amount of source effect and the possibility of local response of the soil.

@seismicisolation

Fig. 5

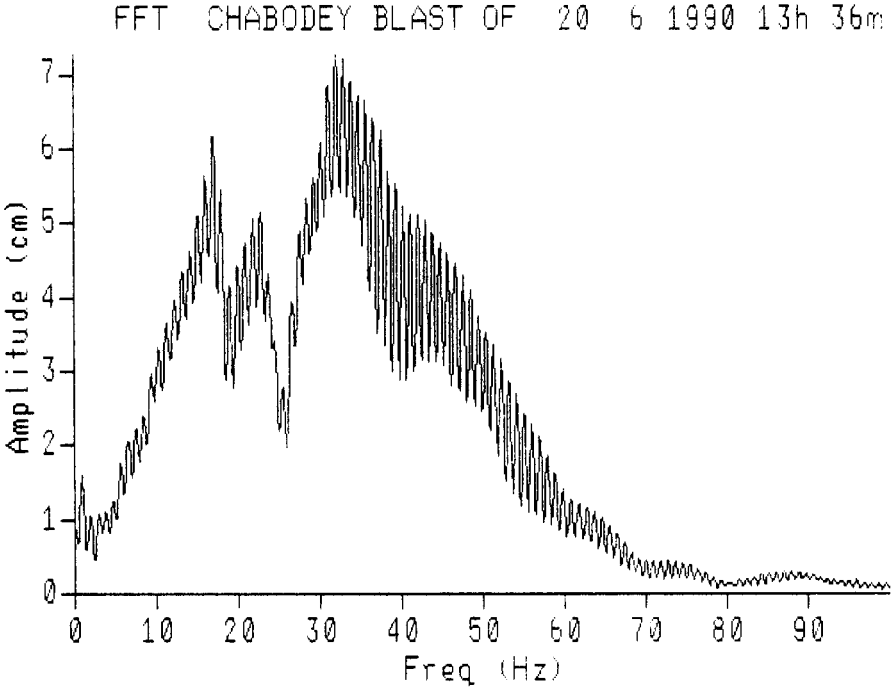

Fig. 6

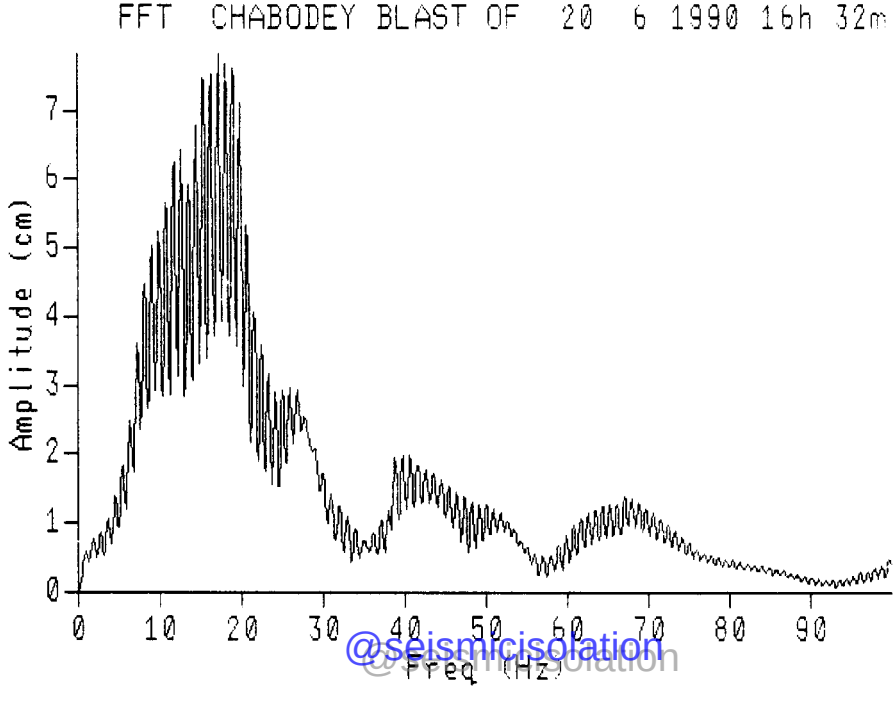

@seismicisolation

Fig. 7

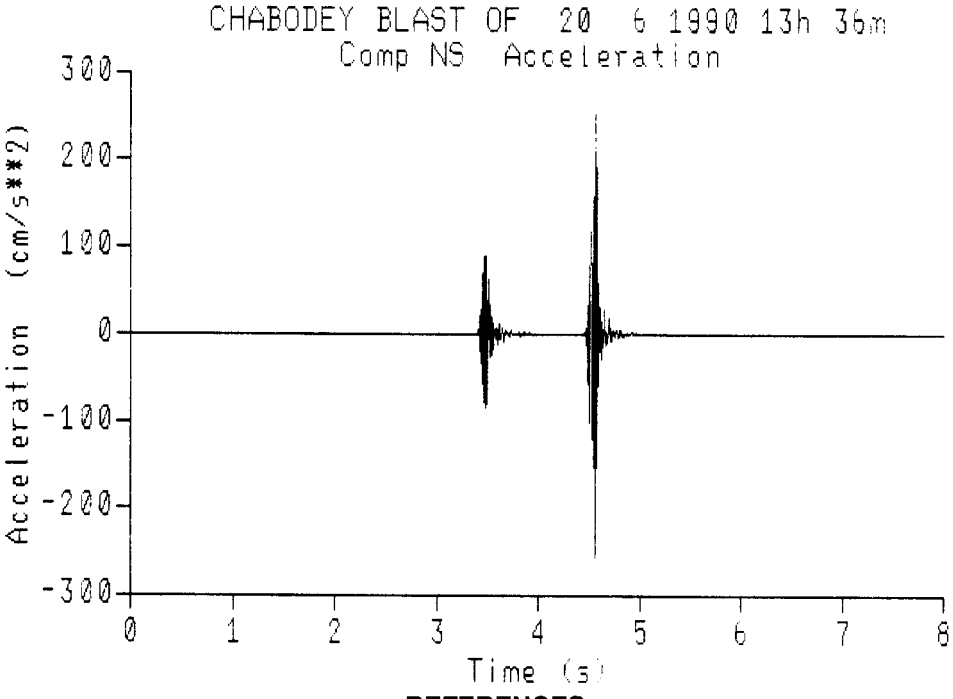

REFERENCES

1. Brosch, F. J., Geology and classification of rock masses, B. of Int. Ass. of Eng. Geol., 1986, **33**, 31-7.
2. Bonvino, U., La velocità delle onde sismiche e le opere di sostegno dei terrapieni. Le Strade, 1988, **1250**, pp. 663-70.
3. Fatteschi, G., Classificazione della massa rocciosa in galleria. Problematiche sulla individuazione delle classi di scavo. Le Strade, 1988, **1250**, pp. 671-80.
4. Hwong, T., Classification of the rock mass structures and determination of rock mass quality. B. of Int. Ass. of Eng. Geol., 1978, **18**, 139-42.
5. Bidussi, G., Coren, F. and Mosca F., Problemi di analisi vibrometrica connessi con l'uso di esplosivo. esperienze e strumentazioni. Cave e Cantieri,
6. Passaro, A. and De Lieto, L., Criteri di controllo delle vibrazioni provocate dall'uso di esplosivi. Le Strade, 1989, **1257**, pp. 487-96.
7. Berta, G., L'esplosivo strumento di lavoro. Italesplosivi, 1985, Chap. 2: Sollecitazioni indotte dalle esplosioni verso l'ambient esterno alla volata, pp. 105-39.

@seismicisolation

EXPERIMENTAL BEHAVIOUR OF DUCTILE PARTIALLY-ENCASED COMPOSITE BEAM-COLUMNS

A. Y. Elghazouli, A. S. Elnashai and P. J. Dowling
Department of Civil Engineering,
Imperial College, London SW7, UK

ABSTRACT

This paper presents a brief account of the results from a series of tests on a new configuration of partially-encased composite steel/concrete beam-columns. The models were designed to provide improved performance for earthquake resistance, incorporating two novel features. The first is variable pitch confining stirrups, with reduced spacing in the potential plastic hinge zone. The second is the provision of additional transverse bars to delay local buckling at large strain levels, and to increase the interaction between the two materials. A number of tests were conducted under constant axial loads and variable amplitude lateral cyclic loading. This was followed by verification tests under realistic earthquake loading, using the pseudo-dynamic testing technique. In addition, the experimental programme included several tests on specimens typical of European practice to quantify the difference in behaviour. In comparison with the conventional models, the new form exhibits significant improvement in ductility and energy absorption capacity.

INTRODUCTION

Composite columns offer an attractive solution to problems such as local and overall buckling for steel columns, and deterioration and shear failures for concrete columns. Besides, the favourable behaviour of composite members under earthquake loading has been recognised by researchers in Japan [1] for many years. Whereas previous European research concentrated on static loading applications [2], attention has recently been directed towards earthquake-resistant behaviour, particularly after the introduction of Eurocode 8 [3].

A detailed assessment of existing code regulations for the design of composite columns was undertaken by the writers [4]. It revealed significant discrepancies even with codes using the same experimental data and design philosophy. Consequently, a research project was initiated with two main objectives. Firstly, to study the behaviour of composite members, typically used in Europe for static design, under cyclic and earthquake loading, in order to derive improved and simplified design regulations. The second aim was to develop new configurations with improved seismic performance.

@seismicisolation

Partially-encased sections, commonly used in Europe, exhibit several advantages, such as simple beam-column connections, reduced or eliminated shuttering and the favouarble fire resistance capability [5]. Tests were carried-out on the conventional form of this type of member, but with a reduced stirrup spacing in the plastic hinge zone. In addition, the experimental programme included tests on a new configuration, recently developed at Imperial College, in which additional transverse bars were provided to delay or inhibit local buckling at large deformations.

The investigation comprised testing under constant axial loads and transverse displacement cycles of increasing amplitudes. Also, several specimens were tested using the realistic pseudo-dynamic testing method. This advanced experimental technique, introduced by Takanashi and his co-workers [6], followed by other researchers in Japan [7] and the USA [8], has been recently employed at Imperial College [9]. A brief description of the tests is given hereafter, and preliminary results and design implications are presented.

TEST LAYOUT

The first group of cyclic and pseudo-dynamic tests were conducted using the self-reacting testing frame shown in Figure 1. A computer was responsible for the control and data acquisition operations. The accuracy of this on-line computer-controlled testing assembly was verified by testing steel cantilevers in the linear and the nonlinear domains [9]. The composite models were tested as cantilever members. In both the cyclic and pseudo-dynamic tests, displacements were applied at the top of the specimens using a double-acting hydraulic actuator.

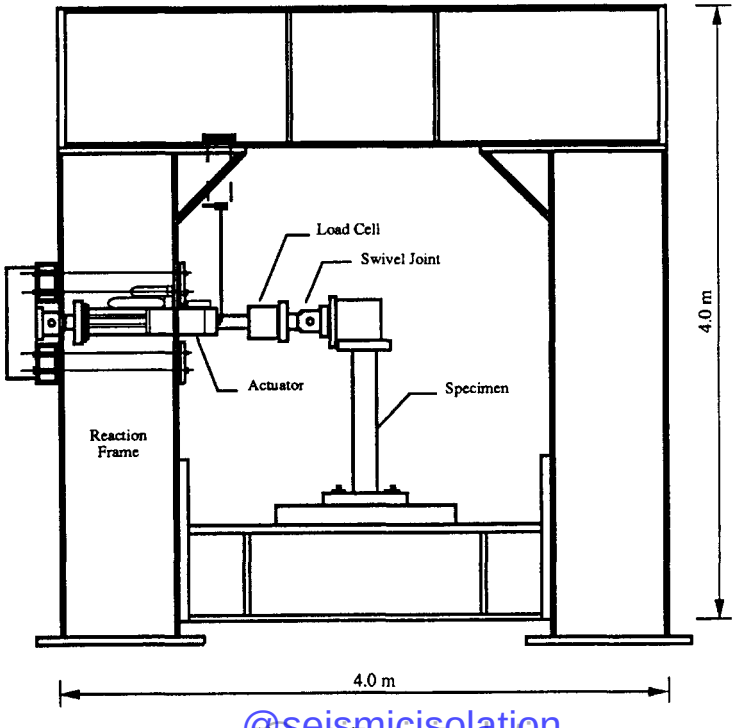

Figure 1. Testing Frame

@seismicisolation

The second group of tests were carried-out as part of a joint activity between Imperial College and the Institute of Industrial Science (IIS), University of Tokyo. The models were designed at Imperial College, and manufactured and tested at IIS [10]. In this case, the models were tested using the set-up shown in Figure 2. Displacements were applied at the intermediate point joining a stiff steel beam on one side and the specimen on the other side, thus simulating a cantilever under varying horizontal displacements. A constant vertical load was also applied throughout the tests. Figure 3 shows the relationship between the different control parameters. A simplified geometry transformation, shown in Figure 3(b), was used. An analytical study of the error involved in this approximation was undertaken and showed that the errors introduced are negligible, within the order of 0.3%. This was later confirmed by the experimental results.

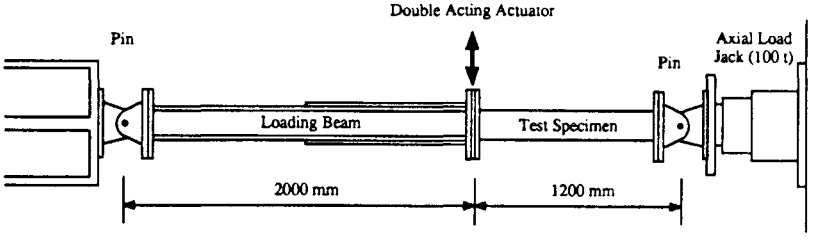

Figure 2. Test Layout

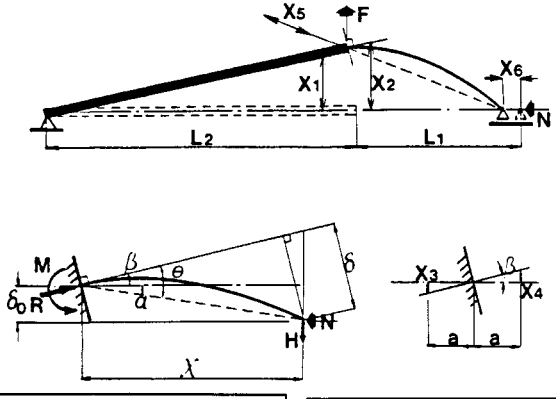

$M = H\chi + N\delta_0$ $\quad \delta = (\chi \tan\beta + \delta_0)\cos\beta$

$\theta = \alpha + \beta$ $\quad \chi = \sqrt{(L_1 - X_5)^2 + \delta_0^2}$

$H = [L_2/(L_1+L_2)]F$ $\quad \delta_0 = (X_1 + X_2)/2$

$\alpha = \tan^{-1}\left(\frac{\delta_0}{\chi}\right)$ $\quad \beta = \sin^{-1}\left(\frac{X_4 - X_3}{2a}\right)$

(a) Detailed Geometry Transformation

$M = H L_1 + N\delta_0$ $\quad \delta = (L_1 \tan\theta + \delta_0)\cos\theta$

$H = [L_2/(L_1+L_2)]F$ $\quad \delta_0 = (X_1 + X_2)/2$

$\theta = \tan^{-1}\left(\frac{X_4 - X_3}{2a}\right)$

(b) Simplified Geometry Transformation

Figure 3. Geometric Relationships for Testing Assembly

@seismicisolation

SPECIMEN DETAILS

Two cross-section details were used, one typical of European practice (EM), with two longitudinal bars on either side of the web, as shown in Figure 4(a). The second type (IC), shown in Figure 4(b), included a modification designed to improve the performance at large strain levels by delaying the outward buckling of the flange. The additional bars were welded to the inside of both flanges, and hence act as connectors for improved interaction. In both cases, reduced stirrup spacing was used in the potential plastic hinge zone to provide sufficient concrete confinement. Table 1 gives the the dimensions of the models, where L is the height of the cantilever measured from the point of lateral load application to the base of the column. In the longitudinal direction, the stirrups were arranged such that the spacing in the plastic hinge zone is half that elsewhere, as shown in Figure 4.

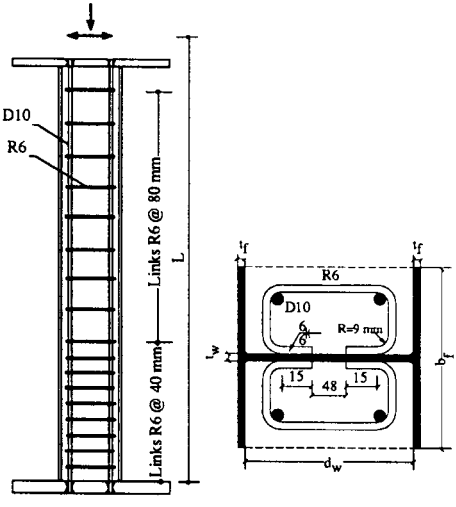

Figure 4 (a). Conventional Model

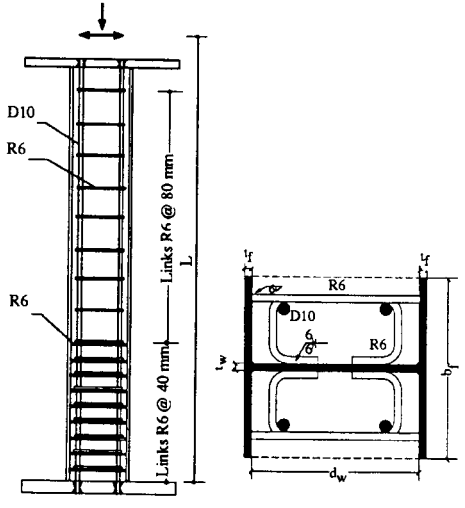

Figure 4(b). Modified Model

TABLE 1
Specimen Dimensions

Model Reference	*L (mm)*	b_f x t_f *(mm)*	d_w x t_w *(mm)*
EM01	1200	150 x 6	138 x 6
EM02	1200	150 x 6	138 x 6
EM03	1200	150 x 6	138 x 6
EM04	1030	152.4 x 6.8	141.4 x 6.1
EM05	1030	152.4 x 6.8	141.4 x 6.1
IC01	1200	150 x 6	138 x 6
IC02	1200	150 x 6	138 x 6
IC03	1200	150 x 6	138 x 6
IC04	1030	152.4 x 6.8	141.4 x 6.1
IC05	1030	152.4 x 6.8	141.4 x 6.1

@seismicisolation

The average material properties of steel and concrete obtained from test samples are presented in Table 2, and are given in N/mm^2. The two sides of the specimens were cast three days apart. The difference in compressive strength should reduce after 28 days, if the two mixes were identical. Nevertheless, this difference has no bearing on the results as the models had the same strength distribution under strong axis bending.

TABLE 2
Material Properties

Model Ref.	*Steel Section*		*Vertical Rft.*		*Horizontal Rft.*		*Cube Strength*	
	σ_y	σ_u	σ_y	σ_u	σ_y	σ_u	*Side 1*	*Side 2*
EM01	274	418	359	501	520	562	40.5	33.4
EM02	274	418	359	501	520	562	40.5	33.4
EM03	274	418	359	501	520	562	40.5	33.4
EM04	297	468	487	637	346	454	38.9	30.1
EM05	283	459	487	637	346	454	36.6	35.5
IC01	274	418	359	501	520	562	40.5	33.4
IC02	274	418	359	501	520	562	40.5	33.4
IC03	274	418	359	501	520	562	40.5	33.4
IC04	297	468	487	637	346	454	38.9	30.1
IC05	283	459	487	637	346	454	36.6	35.5

TESTING PROCEDURE

Table 3 presents the testing procedure for the models, referred to as either European modified (EM) or as Imperial College section (IC). The axial load is given as a percentage of the squash load of of the composite section.

TABLE 3
Testing Sequence

Model Reference	*Testing Method*	*Axial Load*
EM01	Cyclic	15%
EM02	Cyclic	30%
EM03	Pseudo-dynamic	30%
EM04	Cyclic	0%
EM05	Pseudo-dynamic	0%
IC01	Cyclic	15%
IC02	Cyclic	30%
IC03	Pseudo-dynamic	30%
IC04	Cyclic	0%
IC05	Pseudo-dynamic	0%

The cyclic tests were carried-out according to the guidelines given in the ECCS short testing procedure [11]. The models were subjected to multiples of the first yield displacement, with a predefined number of cycles per amplitude. Within the elastic range, one full cycle per displacement amplitude was used. In the inelastic range, up to three cycles per amplitude were applied, depending on the observed changes between the cycles.

@seismicisolation

Models EM03, IC03, EM05 and IC05 were tested using the pseudo-dynamic testing method. EM03 and IC03 were subjected to an 8 seconds acceleration time history from El Centro NS record [12]. To demonstrate the improved behaviour of the modified models, and based on the cyclic test results, a response displacement of about 60 mm in the early peak was sought. Consequently, after a series of analyses using the advanced nonlinear dynamic analysis program 'ADAPTIC' [13], an inertial mass of 20,000 Kg was assumed and the acceleration record was scaled up by 40%. Based on estimated stiffness of 4.7×10^6 N/m, the equivalent cantilever had a period of 0.41 seconds. Hence, a time step of 0.02 was sufficient for the stability of the central difference algorithm employed in the on-line method. Nevertheless, a time step of 0.01 seconds was chosen in order to achieve high accuracy from the control of the test specimen.

Following the same basis as before, specimens EM05 and IC05 were subjected to an 8 seconds acceleration time history of Montenegro earthquake [12]. A mass of 30,000 Kg was assumed in the procedure, and a time step of 0.02 seconds was used. The earthquake record was first scaled down by 10% . This was followed by another 8 seconds of the unscaled acceleration time history, to examine the ultimate behaviour of model IC05.

EXPERIMENTAL RESULTS

Cyclic Tests

Model EM01, tested under 15% axial load achieved a peak load of 59.5 KN at about 33 mm displacement, where the flanges started to buckle. At the onset of local buckling, concrete confinement was suddenly released, hence the concrete crushed very soon after. At a displacement of 44 mm, large buckles appeared in the flanges, with about 15% drop in load. The response of IC01 up to a displacement of 33 mm was almost the same as for EM01, with the curve deviating from the initial linear response at about 11 mm. The strength at 33 mm was only 0.7% higher than EM01. The peak load, however, was reached at a displacement of 44 mm, and was 60.5 KN. At a displacement of 77 mm local buckling was initiated in the flange between the welded bars. The behaviour remained stable up to a displacement of 99 mm, where the weld between the flanges and the straight bars failed. This coincided with a load drop of 20%.

The results from EM02 and IC02 followed similar patterns, but with a more pronounced second order effect. Figure 5 shows the load-displacement relationship for EM02. The measured capacity was 56.5 KN, corresponding to a displacement of 15 mm. Local buckling occurred at a displacement of 30 mm. Thereafter, the strength progressively dropped as local buckling increased causing concrete crushing, aided by the high level of applied axial load. At 44 mm the load was 69% of the ultimate load. Results for model IC02 are shown in Figure 6. The peak load, only 0.4% higher than EM02, is reached at 22 mm. Local buckling of very small amplitude was initiated at 44 mm. At 66 mm, the straight bars snapped, and a large local buckle developed. The corresponding strength was 78% of the ultimate.

Models EM04 and IC04, again followed the same behaviour as before. For EM04, local buckling was initiated at a displacement of 48 mm, at a load of 89 KN. However, the drop in load in subsequent cycles up to a displacement of 80 mm was less than 6%. Concrete started disintegrating after the flange buckled, but at a much slower rate than previous models. Model IC04 showed the same behaviour as EM04 up to a displacement of 48 mm, where the load was only 0.5% higher. However, no sign of local buckling was observed up to a displacement of 90 mm, where the load increased to 93 KN because of strain hardening. At this stage, the test had to be terminated since the limits set for the experiment were exceeded.

@seismicisolation

Pseudo-dynamic Tests

For model EM03, the displacement corresponding to the first significant peak was 19 mm, while the force was 57 KN. The major peak, 2 seconds from the start of the record, produced a displacement of 72 mm, and large amplitude local buckling in the compression flange. Due to loss of stiffness and second order effects, the specimen did not recover, and the displacements increased substantially in the subsequent peak, as shown in Figure 7. The test was then aborted as the displacements exceeded the actuator stroke. Model IC03 was subjected to the same acceleration history. The displacement corresponding to the first peak was again 19 mm. On the reverse peak, the displacement was 62 mm. This did not cause buckling, and the specimen continued to carry its full capacity. The test ran for the full 8 seconds, as shown in Figure 8. At the tail of the record a displacement close to 150 mm was measured, with no clear sign of local buckling.

The response of models EM05 and IC05 are shown in Figures 9 and 10. At the peak, 2.4 seconds from the start of the record, the displacement of EM05 was 78 mm, and local buckling appeared on the compression flange. However, the model displayed stable behaviour up to 13.5 seconds, where the deterioration in stiffness caused the displacements to increase beyond 120 mm. For model IC05, the displacement at 2.4 seconds was 61 mm with no sign of local buckling. The specimen showed response similar to EM05, but with comparatively lower displacement amplitudes. At 10.6 seconds from the start of the test, a small local buckle started in the compression flange between the welded bars, corresponding to a displacement of about 90 mm. However, the specimen did not suffer significant deterioration up to the end of the excitation history.

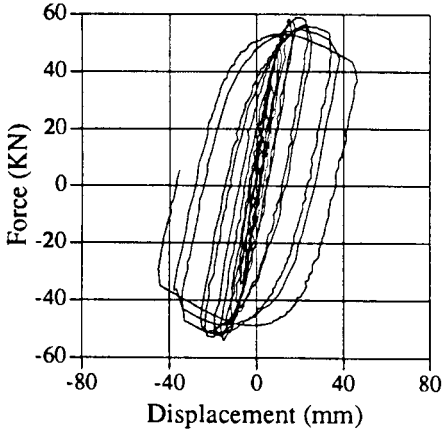

Figure 5. Load-Displacement for EM02

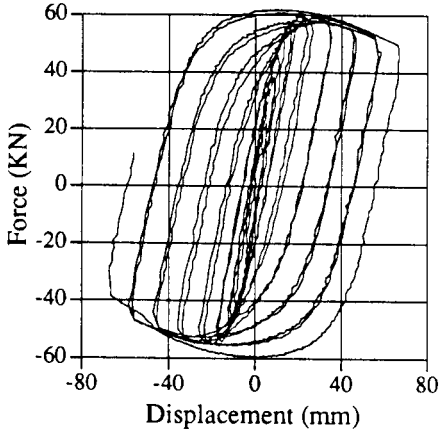

Figure 6. Load-Displacement for IC02

@seismicisolation

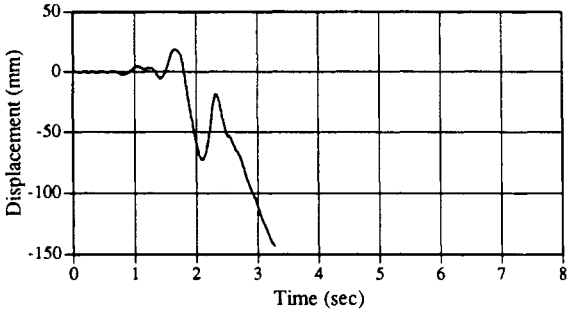

Figure 7. Displacement Response for EM03

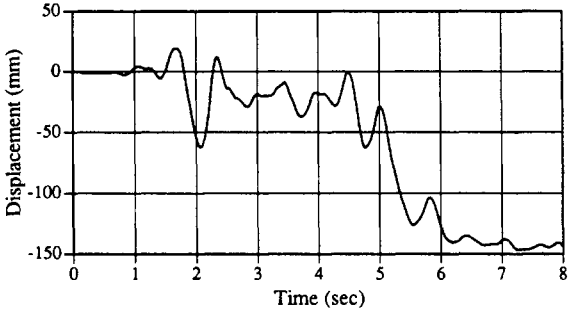

Figure 8. Displacement Response for IC03

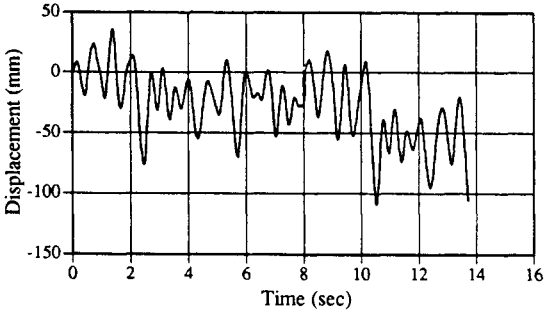

Figure 9. Displacement Response for EM05

@seismicisolation

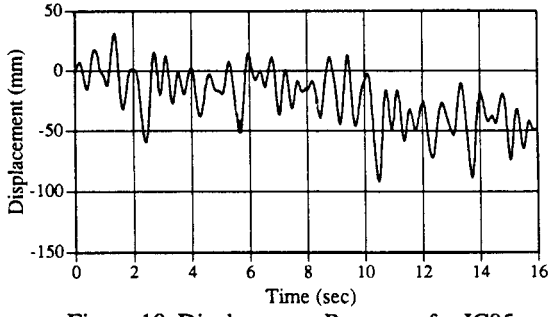

Figure 10. Displacement Response for IC05

CONCLUSIONS

The results clearly indicate the significant improvement in behaviour due to the presence of the additional bars. As shown in Table 4, the rotational ductility of the member was increased by a minimum of 50%, based on an approximate assessment of the results. The pseudo-dynamic tests vindicate the conclusions drawn from the cyclic tests, and demonstrate the substantial increase in ductility and energy absorption capacity of the modified section. Moreover, the development of concrete cracking along the member showed higher spread in the case of the modified section, hence absorbing more energy through crack initiation and propagation.

TABLE 4
Attained Ductilities

Model Reference	*Rotational Ductility*
EM01	4.9
IC01	8.8
EM02	2.7
IC02	4.3
EM03	2.6
IC03	3.9
EM04	7.2
IC04	9.8
EM05	8.1
IC05	10.4

Due to the presence of the additional bars, local buckling was either eliminated or considerably constrained. This can lead to a relaxation of flange slenderness ratios, thus resulting in more economical design and efficient use of sections. It was clear from the test results that the point of initiation of local buckling in pseudo-dynamic tests is different, compared to the cyclic tests. This emphasises the importance of pseudo-dynamic testing to investigate structural behaviour under earthquake loading, since cyclic loading tests may result in over-conservative estimates of deformational capacities.

Further processing of experimental data is underway to accurately quantify the behaviour of such members [14]. Parametric studies are also underway using a nonlinear dynamic analysis program [13] including cyclic constitutive models for concrete and steel and accounting for local buckling of steel sections. The results will be used to derive design recommendations for composite beam-columns under cyclic and dynamic loading [14].

@seismicisolation

ACKNOWLEDGEMENTS

The writers are indebted to the Science and Engineering research council for the financial support provided for this research programme. The support of the Institute of Industrial Science in conducting part of the testing under the supervision of Professor Koichi Takanashi, is very gratefully acknowledged.

REFERENCES

1. Wakabayashi, M, Shibata, M, Matsui, C and Minami, K, "A Study on the Behaviour of Steel-Reinforced Concrete Columns and Frames", IABSE Symposium, Quebec, Canada, 1974.

2. Virdi, K S and Dowling P J, "A Unified Design Method for Composite Columns", IABSE Memoirs, Vol.36-II, 1976.

3. Eurocode No 8, "Structures in Seismic Regions", Commission of the European Communities, Report EUR 12266, May 1988 Edition.

4. Elnashai, A S, Elghazouli, A Y and Dowling P J, "International Assessment of Design Guidance for Composite Columns", Journal of Constructional Steel Research, Vol.15, 1990, pp.191-213.

5. Schleich, J B, "Fire Engineering Design of Steel Structures", Steel Construction Today, Vol. 2, 1988, pp. 39-52.

6. Takanashi, K, Udagawa, K and Tanaka, H, "Pseudo-dynamic Tests on a two Storey Steel Frame by Computer Load Test Apparatus Hybrid System", Proceedings of the Seventh World Conference on Earthquake Engineering, Istanbul, Turkey, 1980, Vol.7, pp.225-232.

7. Takanashi, K and Nakashima, M, "Japanese Activities on On-line Testing", Journal of Engineering Mechanics, ASCE, Vol.113, No.7, 1987, pp.1014-1032.

8. Mahin, S A and Shing, P B, "Pseudo-dynamic Method for Seismic Testing", Journal of Structural Engineering, ASCE, 1984, Vol.111, No. 7, pp.1482-1503.

9. Elnashai, A S, Elghazouli, A Y and Dowling P J, "Verification of Pseudo-dynamic Testing of Steel Members", Journal of Constructional Steel Research, Vol.16, 1990, pp.153-161.

10. Elnashai, A S, Takanashi, K, Elghazouli, A Y and Dowling P J, "Experimental Behaviour of Partially Encased Composite Beam-Columns under Cyclic and Dynamic Loads", Accepted for publication, ICE Proceedings, 1991.

11. European Convention for Constructional Steelwork, "Recommended Testing Procedure for Assessing the Behaviour of Structural Steel Elements under Cyclic Loading", Technical Working Group 1.3- Seismic Design, First Edition 1986.

12. Ambraseys, N N, Basili, M, Martinetti, S and Mohammadioun, B, "CEC Strong-motion Databank and Dissemination Centre", European Earthquake Engineering, Vol.II, 3, 51-52.

13. Elnashai, A S, Izzuddin, B A and Dowling, P J, " Efficient Large Displacement Elastoplastic Dynamic Analysis of Structures", Journal of European Earthquake Engineering, 3, 1989, pp.32-41.

14. Elghazouli, A Y, "Earthquake Resistance of Composite Beam-Columns", PhD Thesis, Imperial College, University of London, to be submitted, July 1991.

@seismicisolation

THE BEHAVIOUR OF PLASTIC HINGE ZONES IN SEISMIC RESISTANT CONCRETE STRUCTURES

RICHARD FENWICK
Associate Professor, Civil Engineering Department
University of Auckland, New Zealand

ABSTRACT

In a severe earthquake two different types of plastic hinge zone may form in the beams of frame structures. These are referred to as reversing and uni-directional plastic hinges and they exhibit very different load deflection characteristics. Beams which form reversing plastic hinge zones are generally more ductile but they undergo greater stiffness degradation under cyclic loading than those that develop uni-directional hinges. With both types of plastic hinge the tensile yielding of the flexural reinforcement causes the beams to elongate to a much greater extent than would be intuitively expected. This largely neglected aspect of behaviour can have a major influence on the seismic performance of a structure and it should be taken into account in the design of the supports for precast floors, cladding and in the detailing of columns.

INTRODUCTION

Current practice in the design of seismic resistant multi-storey frame structures requires them to be proportioned so that in the event of a major earthquake they behave in a ductile manner. To achieve this objective they are generally designed to develop a beam sway in preference to a column sway mechanism so that most of the potential primary plastic hinge zones are located in the beams. Consequently the dynamic performance in a severe earthquake, once yielding has occurred, is dominated by the load deformation characteristics of the plastic hinge zones in the beams.

FORMS OF PLASTIC HINGE

Two different forms of plastic hinge may develop in the beams of a frame when it is subjected to inelastic cyclic displacement, such as may be expected to occur in a major earthquake. Where the gravity load supported by the beam along its length is light reversing plastic hinges may be expected, while uni-directional hinges occur with higher load levels.

@seismicisolation

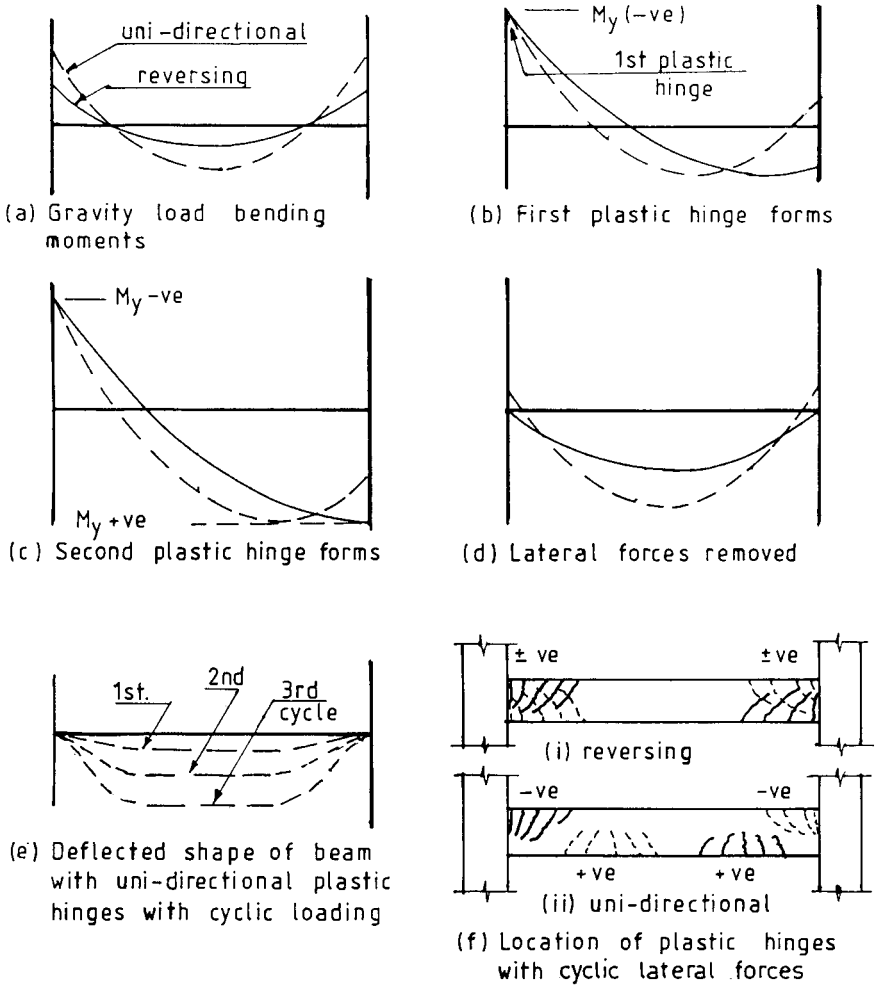

Figure 1. Formation of reversing and uni-directional hinges.

The way in which these two different forms of plastic hinge develop is illustrated in Figure 1. In (a) the gravity load bending moments are shown for the two cases, while in (b) the seismic actions are increased until a negative bending moment hinge forms against the left hand column face. Further increase in the seismic actions results in the formation of a positive moment hinge, as shown in (c). For the reversing plastic hinge it is located against the right hand column face, while for the uni-directional plastic hinge it is situated in the span on the right hand side of the column centre-line. In this state further lateral displacement may occur with rotation occurring at both plastic hinges. If the direction of sway changes, with the reversing hinge the sign of the rotation sustained by each zone is reversed as indicated in (f (i)). However, for the uni-directional case two new hinges are formed, as illustrated in (f (ii)). The negative moment hinge forms

@seismicisolation

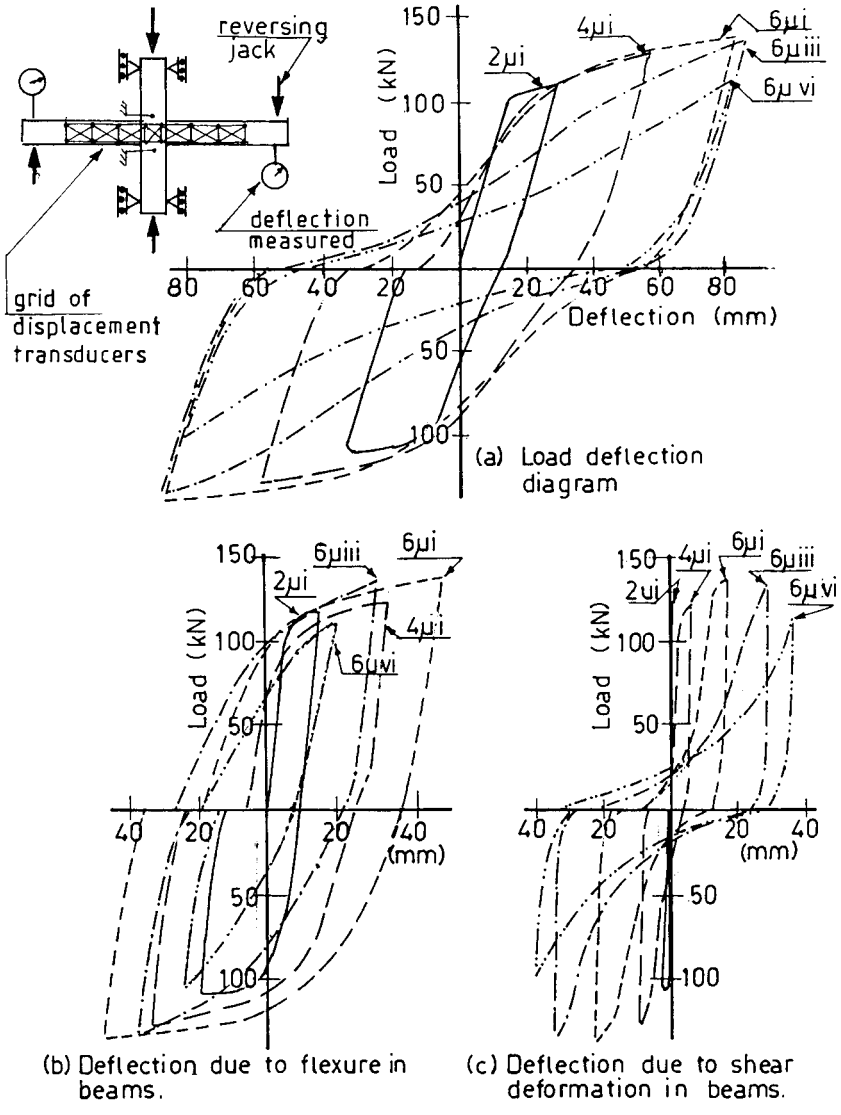

Figure 2. Behaviour of beam-column unit which forms reversing hinges.

against the face of the column on the right hand side and a positive moment hinge forms on the left hand side of the beam centre-line. The inelastic negative moment rotations accumulate at the column faces and the positive moment rotations in the span. Thus with each inelastic cycle of lateral displacement the defection of the beam increases as indicated in Figure 1 (e).

The major difference between the two plastic hinge zones is that in the reversing plastic

@seismicisolation

hinge a change in the direction of the applied lateral inelastic displacement causes a reduction in the magnitude of the rotations that are sustained. However, with the uni-directional plastic hinges each inelastic lateral displacement causes an increase in the hinge rotations. Thus during an earthquake the rotations progressively increase.

BEHAVIOUR OF REVERSING PLASTIC HINGES

This form of plastic hinge has been subjected to extensive research. Many structural tests, which have been carried out to investigate the seismic performance of beams and beam-column sub-assemblies, have resulted in the formation of reversing plastic hinge zones. Some of the results of one such test[1] are reproduced in Figure 2. In this beam-column sub-assembly the column and joint zone was designed to remain elastic. Plastic hinging was confined to the beams in the zones adjacent to the column faces. Loads were applied to the beams, as illustrated in Figure 2, to give two complete cycles in which the load was increased to ± ¾ of the value corresponding to the theoretical flexural strength of the beams. This was followed by displacement controlled cycles. Two complete cycles were applied in which the displacement varied between ± 29 mm. This was followed by two further cycles between ± 58 mm and six additional cycles to approximately 87 mm with failure occurring in the 7th such cycle. These displacement levels corresponded to displacement ductilities of 2, 4 and 6 respectively (2μ etc).

Figure 2 shows the load deflection curves for some of the load cycles. It can be seen that extensive stiffness degradation occurs, with the average stiffness in the 6th ductility 6 cycle being close to 1/11th of the initial value. However, even at this stage of the test there was no evidence of any strength degradation. This did not occur until the 7th ductility 6 cycle.

The measurements from the displacement transducers shown in Figure 2 were used to find the components of displacement. The transducers were mounted on studs welded to the longitudinal reinforcement in the beams. A gap was formed around each stud so that it could not bear against the concrete. The shear deformation was found from the

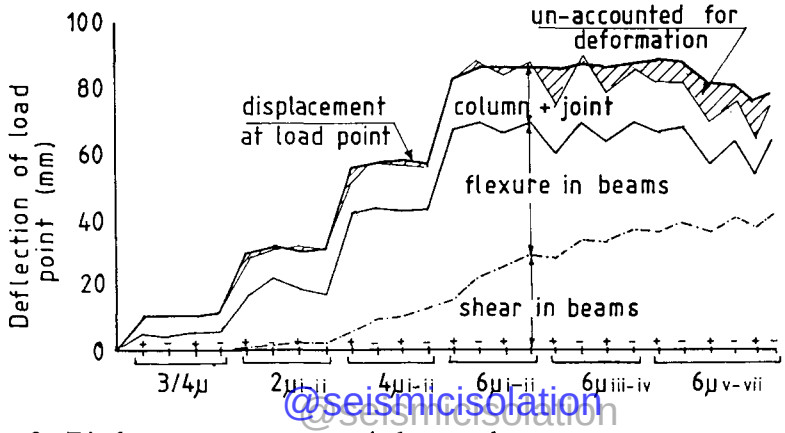

@seismicisolation

Figure 3. Displacement components in beam-column test.

diagonal transducers. The closure errors were principally caused by the buckling of bars causing incorrect transducer readings. In Figure 3 both positive and negative deflections are plotted as positive values.

The results show that the column and the beam column joint zone remained effectively elastic during the test. The small increase in these components of deformation is associated with the increase in load sustained due to strain hardening in the plastic hinge zones and flexural cracking in the column with repeated load cycles. As the test progressed it can be seen that the proportion of deformation associated with flexural rotation in the beams reduced as the shear deformation increased.

The load versus deflection curves associated with the flexural and the shear deformations in the beams are shown in Figure 2 (b) and (c). From these it is clear that the stiffness degradation of the test unit is primarily associated with the shear deformation. The low shear stiffness, which occurs when the direction of the shear force is reversed, is associated with the closing of one set of diagonal cracks and the opening of the other set[2,3].

BEHAVIOUR OF UNI-DIRECTIONAL HINGES

In the context of the seismic performance of concrete structures this form of plastic hinge zone has received very little attention. However, at the University of Auckland, some tests have been made, one of which is briefly outlined below.

A reinforced concrete portal frame with a clear span of close to 5 m, was subjected to inelastic lateral displacements to represent seismic actions, while simultaneously being pulled to the floor by constant forces in two jacks. With this arrangement, which is shown in Figure 4, no P-delta effects are induced. A similar load sequence was used in this test as in the beam-column sub-assembly. There were two elastic lateral load cycles followed by two complete cycles to $\pm$ 19 mm, $\pm$ 38 mm and $\pm$ 57 mm. These corresponded to displacement ductilities of 2, 4 and 6. Failure occurred during the second ductility 6 cycle. Further details may be found in reference 4.

During the test the plastic hinges were predominately of the uni-directional type. There was a little reversing action occurring in the higher ductility cycles. From the lateral load deflection diagram, which is shown in Figure 4, it can be seen that little stiffness degradation occurred until the failure conditions were approached in the last load cycle. With the uni-directional hinges the direction of the shear forces in the plastic zones does not change and consequently the low shear stiffness associated with the shear force reversal does not occur.

As expected each inelastic lateral displacement of the portal frame caused the plastic hinge rotations to accumulate in their respective positive and negative hinge locations with the deflection of the beam progressively increasing during the test, see Figure 5. Failure occurred when one of the negative moment plastic hinges was sustaining a rotation of close to 5°.

@seismicisolation

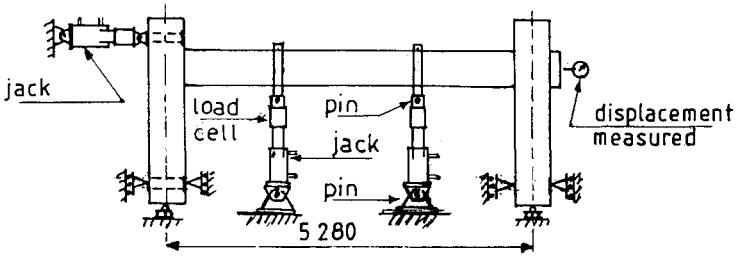

(a) Test arrangement

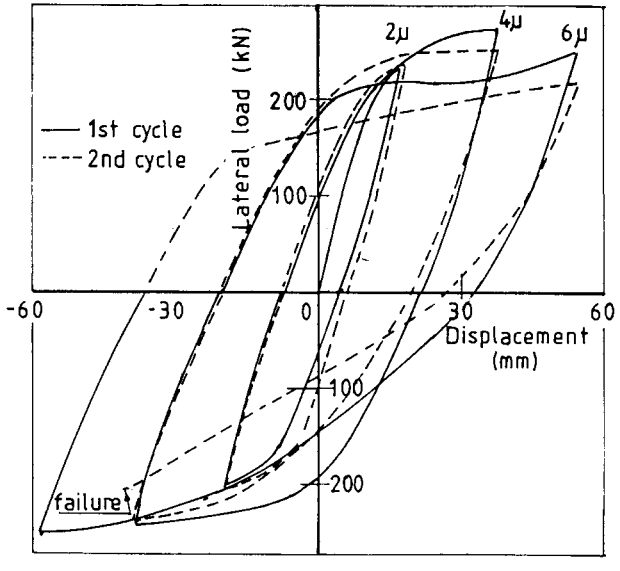

(b) Lateral load versus deflection

Figure 4. Lateral load versus deflection diagram for portal frame.

ELONGATION OF PLASTIC HINGE ZONES

Flexural cracking in a reinforced concrete beam gives rise to elongation as the tensile strains in the reinforcement are greater than the compression strains in the concrete. With the onset of yielding this becomes more significant.

Measurements made in the plastic hinge zones of beams containing uni-directional hinges have shown that the stresses sustained by the compression reinforcement are small. For practical purposes they may be neglected[4]. On this basis the elongation in a beam containing a set of uni-directional hinges is given by the expression -

$$\text{elongation} = \Sigma\theta\,(d - d') / 2 \qquad (1)$$

@seismicisolation

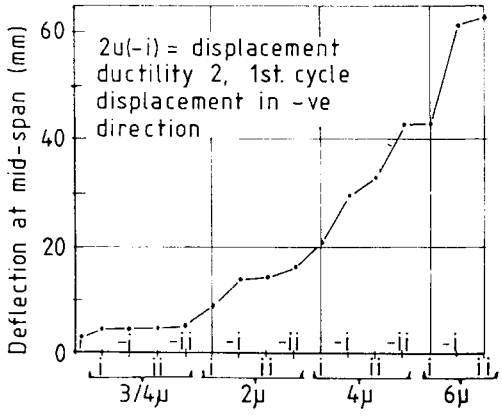

Figure 5. Mid-span deflection of beam in portal frame test

where $\Sigma\theta$ is the sum of the plastic hinge rotations in the member and d - d' is the distance between the centroids of the top and bottom reinforcement. As shown in Figure 6 the agreement between the measured elongations in the portal test and the values predicted by equation 1 is close.

With reversing hinges equation 1 underestimates the elongation. Displacement measurements made in a reversing plastic hinge zone on a beam that contained equal areas of top and bottom reinforcement are shown in Figure 7. With the application of the first inelastic rotation to the hinge small compressive strains were sustained in the reinforcement in the compression zone. However, with the reversal of the direction of rotation it can be seen that the reinforcement, that had been previously yielded in tension did not fully yield back in compression and the cracks did not close. With subsequent cycles of inelastic rotation the elongation of the compression zone reinforcement can be seen to progressively increase. From Figure 7 it is apparent that

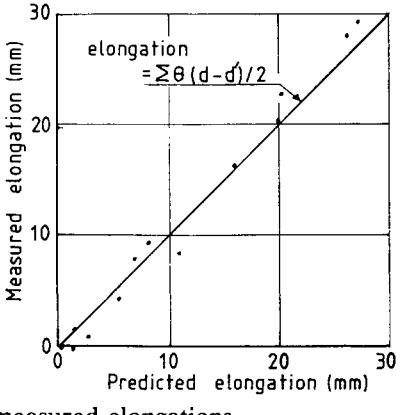

Figure 6. Predicted and measured elongations.

@seismicisolation

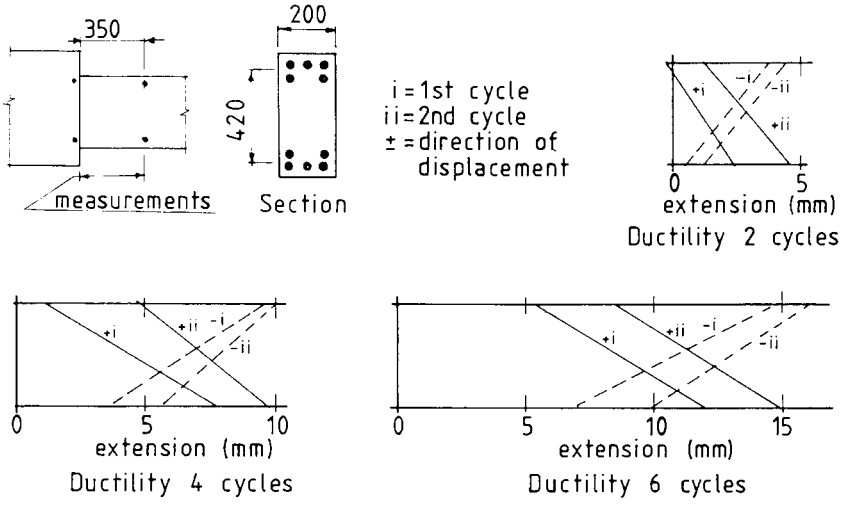

Figure 7. Displacements measured in a reversing plastic hinge.

in the ductility 6 cycles typically ⅓ of the elongation comes from the rotation, as given by equation 1, with the remainder coming from the elongation of the compression zone reinforcement.

There are two reasons why the longitudinal reinforcement in the compression zone of a reversing plastic hinge does not yield back in compression. The first of these arises from the wedging action of aggregate particles which become dislocated from the crack surfaces, and the second arises from the mechanism of shear resistance in the plastic hinge zone. With the formation of intersecting diagonal cracks the only available mechanism of shear resistance is provided by the truss like action illustrated in Figure 8. The equilibrium requirements indicate that the tension force, T, is always significantly greater than the flexural compression force, C. A consequence of this is that inelastic rotation tends to occur by the tensile yielding of the reinforcement rather than yielding of the steel in the compression zone. Tests have shown that quite high axial forces have to be applied to the beam to cause the compression zone reinforcement to yield back to close the cracks.

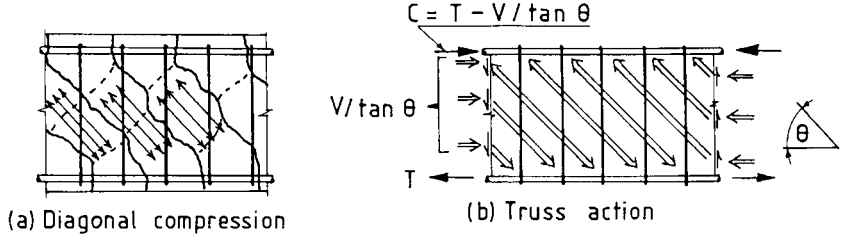

Figure 8. Mechanism of shear resistance in plastic hinge zone

@seismicisolation

Tests on beams with composite slabs and on beams with unequal areas of top and bottom reinforcement have shown that similar magnitudes of elongation occur as in the case of beams with equal top and bottom areas of reinforcement[6]. Slabs generally do not restrain elongation as once some of the longitudinal steel yields it helps to prop open the cracks.

STRUCTURAL SIGNIFICANCE OF ELONGATION

A full scale test of a seven storey frame-wall-building which was subjected to lateral forces to represent seismic actions, demonstrated the importance of elongation[7]. In this case a central structural wall formed a plastic hinge at its base and this caused it to elongate. The growth in length of this member caused a number of the columns to be subjected to axial tension. This resulted in an increase, of the order of 100 percent, in the lateral load carrying capacity of the structure. However, it also reduced the ductility as the shear reinforcement was not provided for this enhanced capacity.

Consider the perimeter frame shown in Figure 9(a). If for example it is assumed that the maximum interstory deflection in a severe earthquake is 0.015 times the interstorey height then the rotation applied to both the plastic hinge zones in each beam is approximately 0.0188 rad. According to equation 1 this would cause an elongation over the whole length of the structure of 68 mm. Assuming that a number of cycles of this order of sway were sustained the expected elongation would be 2 to 3 times this value, that is 130 to 200 mm. Comparable elongations may be predicted if this form of structure is replaced by one which forms uni-directional hinges. Assume that the 6 bay frame is replaced by a 3 bay one with 10 m spans. For this structure $d - d'$ is taken as 800 mm, the column dimension as 900 mm and the positive moment hinge is assumed to form 2 000 mm from the column faces, see Figure 9(b). If it is assumed that in a severe earthquake the interstorey deflection undergoes the equivalent of two complete cycles between + and - 0.015 times the interstorey height, then the elongation of the beam can be calculated to be of the order of 260 mm.

Extensions of this order of magnitude must have a major influence on the performance of the outside columns. The restraint they provide increases the shear they sustain but it is insufficient to prevent elongation. Consequently, a major increase must occur in the rotations imposed on the plastic hinges in the columns at the foundation level.

Elongation of the order described in this section clearly has implications for the design of the supports for cladding and precast components, which should be detailed to accommodate the necessary movement without danger of collapse. There are also implications for the size of seismic gaps that are required and the performance of diaphragms, which may have wide cracks induced in them due to the beam elongation.

CONCLUSIONS

Two different forms of plastic hinge zone, namely reversing and uni-directional, may form in the beams of moment resistant frames subjected to a severe earthquake. The reversing hinge is the more ductile of the two but it suffers greater stiffness degradation.

@seismicisolation

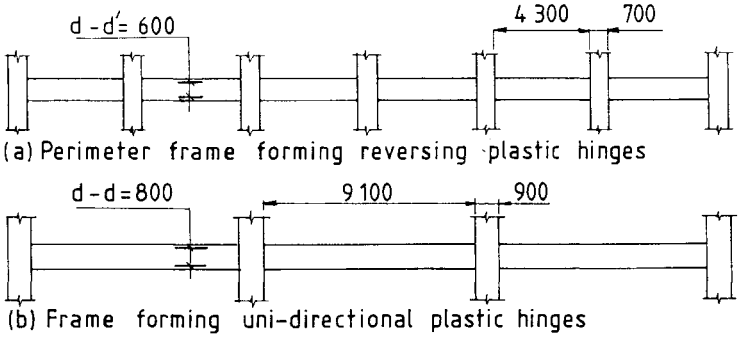

Figure 9. Frames used for estimating likely elongation.

Both forms of hinge zone cause the beams to elongate. This can have a major influence on the seismic performance of a structure. Particular attention needs to be directed to the performance of the outside columns, which are subjected to increased shear and plastic hinge rotations, and to the detailing of the support of cladding and floor units to prevent possible collapse due to elongation

REFERENCES

1. Fenwick, R.C. "Seismic resistant joints for reinforced concrete structures", Bulletin of NZ National Society for Earthquake Engineering, Vol. 14, No. 3, Sept. 1981, pp 145-159.

2. Fenwick, R.C. "Strength degradation of concrete beams under cyclic loading" Bulletin of NZ National Society for Earthquake Engineering, Vol. 16, No. 1, Nov. 1987, pp 25-38.

3. Fenwick, R.C. and Thom, C.W. "Shear deformation in reinforced concrete beams subjected to inelastic cyclic loading". University of Auckland, School of Engineering Report, No. 279, June 1982, pp 50.

4. Megget, L.M. and Fenwick, R.C., "Seismic behaviour of a reinforced concrete portal frame sustaining gravity loads". Bulletin NZ National Society for Earthquake Engineering, Vol. 22, No. 1, Mar. 1989. pp 39-49.

5. Fenwick, R.C., "Member elongation - a neglected factor in seismic design", NZ Concrete Society, Technical Report TR10, 1990.

6. Fenwick, R.C., Tankat, A.T. and Thom, C.W., "The deformation of reinforced concrete beams subjected to inelastic cyclic loading - experimental results", University of Auckland, School of Engineering Report, No 268, Oct. 1981, pp 72.

7. Wight, J.K. (editor), "Earthquake effects on reinforced concrete structures", American Concrete Institute, Special Publication SP84, 1985, pp 428.

© Copyright NZSEE

DESIGN AND PERFORMANCE OF MODEL FLOOR-COLUMN JOINTS FOR SIMULATION OF INELASTIC STRUCTURAL RESPONSE UNDER EARTHQUAKE LOADING

E.A. NICHOL, A.M. CHANDLER and R.H. BASSETT
Department of Civil and Municipal Engineering
University College London
Gower Street, London, WC1E 6BT, UK

ABSTRACT

Hinged joints have been developed for use in experimental inelastic dynamic response studies of modelled buildings. These hinges simulate the formation of plastic hinges either in the columns or in the beams of a building under dynamic loading. Experimental results are presented for an initial series of tests studying the inelastic behaviour of a series of single-storey building models with varying mass asymmetry and different plastic hinge configurations.

INTRODUCTION

This research programme forms the second part of a study on the torsional behaviour of asymmetric buildings. The initial part of this study dealt with the elastic torsional behaviour of multi-storey mass asymmetric buildings, from which the experimental and analytical results have been presented in previous publications [1,2,3]. The current research programme modifies the original elastic experimental model in order to accommodate inelastic structural behaviour through the use of hinges, which simulate plastic yield in the beam-column connections. From this, the effects of inelastic torsional coupling on single and multi-storey buildings can be verified experimentally, and compared to the numerous analytical studies available.

This paper describes the incorporation of hinge units in a series of single-storey building models. Details on the performance of these hinges at various yield levels and

©Seismic Isolation

yielding distributions in buildings subjected to impulse loading and a Eurocode 8 spectrum compatible earthquake ground motion are presented herein.

EXPERIMENTAL MODEL

Description of Experimental Model

The building model used in this series of experiments consists of a single-storey frame with 5 work-hardened brass columns, shown in Figure 1 mounted on the SERC 6-axis earthquake simulator at Bristol University. The floor, measuring approximately 1 metre square, incorporates a series of lead plates which can be placed in different positions within the floor frame to alter the mass eccentricity in the building. Three different mass configurations have been used in this study. These consist of one symmetric mass arrangement (S1, e_r'=0.0) and two coupled asymmetric mass distributions (A2, e_r'=0.07 and A6, e_r'=0.20) [1]. The parameter e_r' is the stiffness eccentricity ratio, defined as the distance between the centre of stiffness or resistance (which in all models coincides with the geometric centre of the floor frame) and the centre of mass, normalized by the floor dimension perpendicular to the applied loading. The mass eccentricity ratio for mass distributions A2 and A6, represent buildings with low and high asymmetry, respectively. The two asymmetric mass distributions are coupled, meaning that in the elastic

Figure 1. Single-storey experimental model, shown with mass configuration A6. The depicted hinge configuration entails floor hinges and rigid column-base connections.

TABLE 1
Hinge pad specifications.

Hinge pad material	M_p friction coefficient, μ_m † (N-m/N)	Minimum M_p (N-m)	Maximum M_p (N-m)
PTFE	0.011	1.1	14.1
Lignum Vitae	0.012	8.4	15.0
Stainless Steel	0.023	13.7	30.0

† $M_p = \mu_m F_c$, where M_p is the initial plastic moment and F_c is the clamping force on the hinge friction pad.

@seismicisolation

range, translational ground excitations result in both translational and torsional structural behaviour. In the inelastic range, other parameters such as the strength eccentricity (distance between the centre of strength and centre of mass) and strength distribution can significantly affect the behaviour.

Displacements are measured by non-contacting transducers mounted on rigid frames adjacent to the model (Figure 1). The column diameters in the model can also be varied to produce different ratios of torsional and translational stiffness [1]. This study concentrates on a column configuration which has a ratio of torsional to translational frequency (Ω) near unity (see TABLE 3), a value which will generally lead to the greatest elastic torsional coupling effects [5].

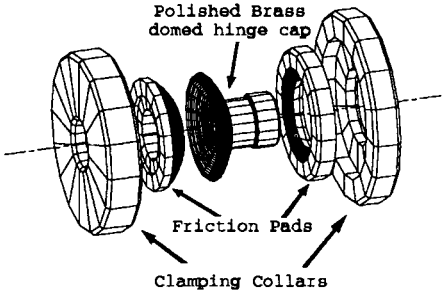

Figure 2. Exploded view of a typical hinge unit.

Description of Hinge Joints

The hinge joint units consist of a set of brass clamping collars with detachable friction pads on a polished brass domed hinge cap (see Figure 2). The yielding moment in the hinge unit can be varied through an adjustment of the clamping force and through the use of different friction pad materials. The clamping force on the friction pads can be accurately adjusted between 0.1 kN and 1.3 kN. Accounting for the different friction pad materials, this variation allows hinge yield moments to be developed anywhere in the range of 1.1 N-m to 30.0 N-m (see TABLE 1). TABLE 2 lists the 6 hinge configurations used in this study, together with the corresponding strength eccentricity ratios. The parameters F_y and M_y are the total translational and rotational strength about the centre of strength of the single storey model, respectively.

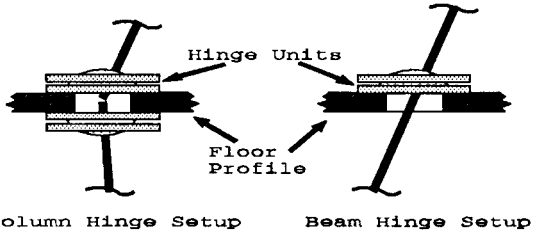

Figure 3. Hinge placement set-ups for the simulation of plastic yield in the columns or in the beams at floor level.

In studies of multi-storey buildings, the hinge units can be attached to the model at the column-floor connections in either of two set-ups (Figure 3). The column yield setup consists of a hinge unit placed on both the top and bottom of each floor, and segmented columns attached to each hinge. This allows for a discontinuity in the column curvature at each floor, thus simulating the formation of a plastic hinge located in the column at floor level. The beam yield setup places a single hinge at either the top or bottom of each floor, and employs a continuous column through the hinge unit. The resisting moment of the floor (beams) on

@seismicisolation

the column is then limited to M_p (TABLE 1).

TABLE 2
Hinge configurations

Hinge Configuration	F_y (N)	M_y (N-m)	F_y / M_y (m^{-1})	Strength eccentricity ratio, e_s' †
1	7.4	3.9	1.90	0.00
2	5.9	2.9	2.03	0.00
3	12.8	2.9	4.41	0.00
4	13.6	3.4	4.00	-0.04
5	27.5	12.5	2.20	-0.36
6	30.4	16.9	1.80	+0.17

† Negative values indicate that the location of the centre of strength is in the direction opposite to the centre of mass, with respect to the geometric floor centre.

For the single-storey model examined in this study, emphasis has been placed on two hinge set-ups. For the impulse tests, hinges are placed at the top of each column, while the base of each column remains fixed. The earthquake tests have hinges at both the top and bottom of each column, thus allowing for the possible formation of a mechanism. A photograph of the latter case is shown in Figure 5.

Figure 5. Single-storey dual hinge set-up.

Static Testing

Static tests have been performed to determine the initial yielding moment in the hinge units, and their yield capacity during repeat testing. For the initial yield tests, the clamping force in the

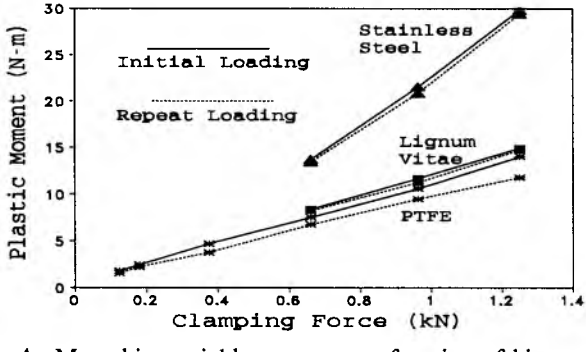

Figure 4. Mean hinge yield moment as a function of hinge clamping force for both initial and repeat loading.

hinge units is completely released, thus ensuring no residual shear stresses on the friction surface. The units are then re-clamped, and loaded until the onset of yielding. For the repeat yield tests, the

@seismicisolution

tests. Figure 4 shows the relationship between the clamping force and the yield moment for both initial and repeat yielding of the hinge units for the different types of friction pad materials. The standard deviation about the mean plastic moment for PTFE (about 1%) is lower than that obtained during the static tests for either lignum vitae or stainless steel. Hence, the stainless steel and lignum vitae friction pads were not tested in the low plastic moment range, where the PTFE friction pads performed more consistently.

DYNAMIC TESTING

Frequencies

The frequencies of the building models have been determined experimentally, and are listed in TABLE 3. The elastic stiffness of the dual hinge set-up is greater then that for the single hinge set-up due to the reduction in column length caused by the additional hinge unit (Figure 5), thus the discrepancies in the structural frequencies for the dual and single hinge models. By definition, Ω is computed from mass configuration S1. As the mass eccentricity is increased, the fundamental translational and rotational frequencies spread apart. This in turn reduces the effects of elastic torsional coupling. However, the increase in the mass eccentricity increases the rotational displacement component in the model. The frequencies listed in TABLE 3 are representative values for prototype 1-2 storey buildings.

TABLE 3

Elastic frequencies of vibration for the 3 mass set-ups. Single hinge indicates hinge unit at the top of each column. Dual hinge denotes hinge units at both top and bottom of every column.

Mass Configuration	Single Hinge $\Omega = 1.09$		Dual Hinge $\Omega = 1.18$	
	Translation	Rotation	Translation	Rotation
S1	5.80 Hz	6.30 Hz	6.80 Hz	8.03 Hz
A2	5.18	6.45	6.65	8.23
A6	4.75	6.53	6.08	8.35

Damping

The damping ratios for the building models have been calculated by both the width of the Fourier transform resonance peak obtained from the displacement response, and through free vibration displacement decay measurements. The translational mode produced better agreement between the two methods. This is partially a result of this being the fundamental mode ($\Omega > 1$). The elastic damping ratios listed in TABLE 4 are fairly low compared with

@seismicisolation

actual buildings, especially for the dual hinge set-up. When fully clamped, the hinge units provide a higher degree of fixity than the column-base connections, as is evident from the lower damping values. The influence of the low elastic damping ratios on the inelastic response become negligible due to the hysteretic damping inherent in the hinge joints.

TABLE 4
Elastic damping ratios for the 3 mass configurations.

Mass Configuration	Single Hinge		Dual Hinge	
	Translation	Rotation	Translation	Rotation
S1	0.97%	0.47%	0.55%	0.23%
A2	0.99	0.58	0.56	0.26
A6	0.82	0.69	0.33	0.34

Impulse Response

In order to examine the influence of the different building parameters (mass eccentricity, strength eccentricity and distribution) on the inelastic response, a series of uniaxial impulse tests were performed. Each model was loaded with two different frequencies of a modified sinusoidal acceleration impulse (Figure 6), each frequency being close to that of either its fundamental translational or rotational mode. Additionally, each impulse test was repeated through a range of peak input accelerations.

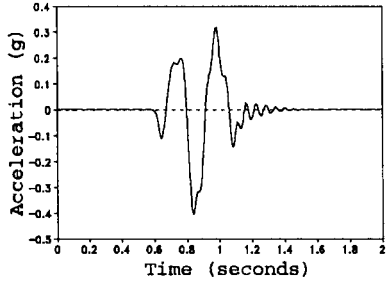

Figure 6. Acceleration time-history of typical impulse response.

Earthquake Response

In addition to the impulse tests, a simulated acceleration time-history, as specified for hard soils or rock by Eurocode 8, was used to measure the structural response. The correction factor for low damping was modified in accordance with the recommendations of reference [6]. The earthquake record has a significant duration of just over 10 seconds, with high energy content in the velocity controlled region of the response spectrum (Figure 7). This is also the range which has the most influence on the building models during inelastic behaviour, due to the reduction in frequency.

ANALYSIS OF RESULTS

Figures 8 through 11 show the peak displacement response of the two sides of the model designated A and B (Figure 1, where side B is closest to the centre of mass) arising from the translational impulse applied at both the translational and rotational modal

@seismicisolation

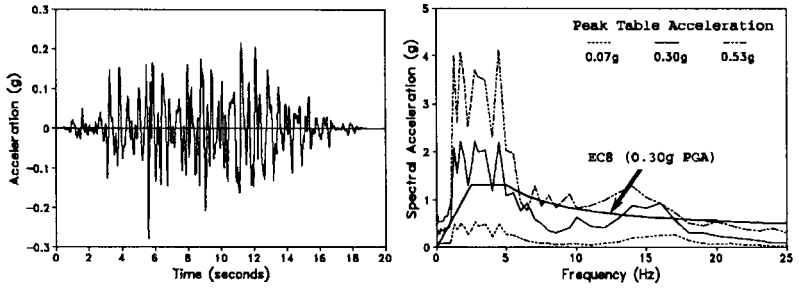

Figure 7. Eurocode 8 spectrum compatible ground acceleration (0.3g PGA, soil type A) shown with the 0.5% damped spectral acceleration response at various levels of peak ground acceleration.

frequencies. The peak displacements for each hinge configuration coincide for a particular side at peak ground accelerations below 0.1g, since the structure is still behaving elastically.

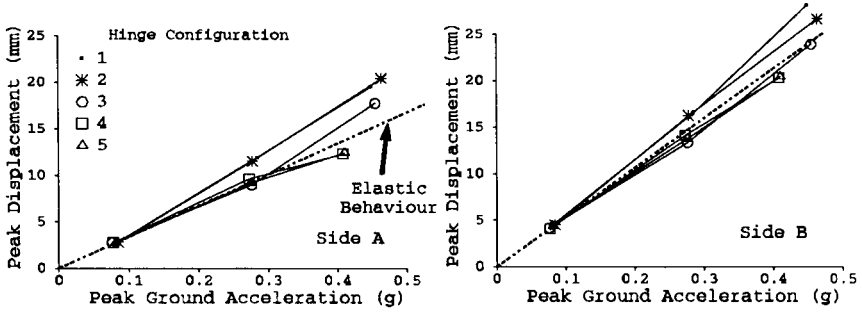

Figure 8. Peak impulse response of model A2 (low mass eccentricity) at fundamental translational frequency.

Figures 8 and 9 show the peak response from the translational frequency impulses for models with low and high mass eccentricities, respectively. The peak response is always greater for side B, with the differences increasing with the mass eccentricity. For both models A2 and A6, hinge configurations A and B result in the highest displacements due to their low translational yield strength, F_y. Larger values of the moment strength, M_y (TABLE 2), tend to reduce the inelastic torsional behaviour of the model.

Figures 10 and 11 show the peak displacement response from the translational impulse applied at the primary rotational frequencies. The peak displacements do not vary greatly

@seismicisolation

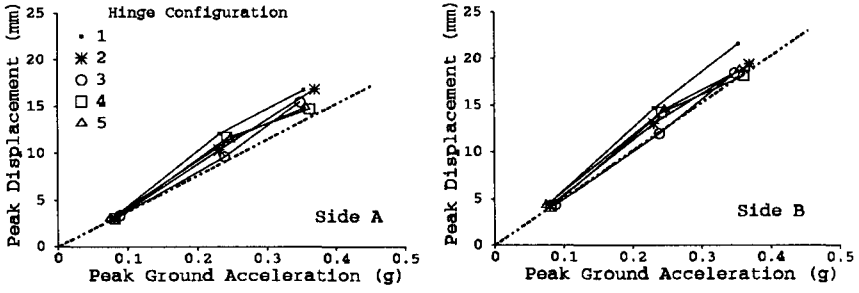

Figure 9. Peak impulse response of model A6 (high mass eccentricity) at fundamental translational frequency.

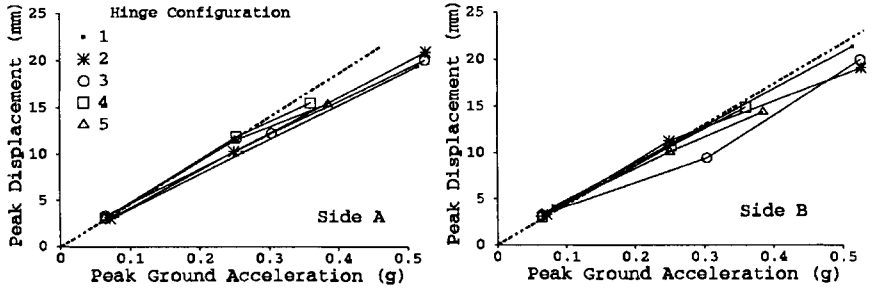

Figure 10. Peak displacements for high mass eccentricity model (A6). Translational impulse at primary rotational frequency.

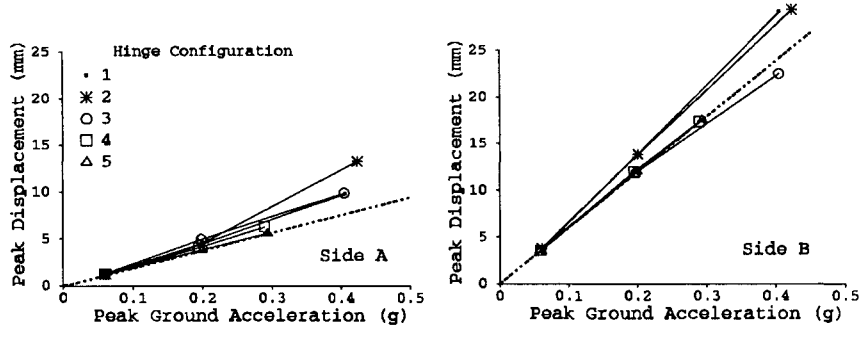

Figure 11. Peak displacement response of high mass eccentricity model (A6) at fundamental translational impulse frequency.

@seismicisolation

between the two sides, in contrast with the translational impulse frequency responses. However, side B is still the more vulnerable in terms of displacement, especially for the low mass eccentricity. This is the result of the modal frequency shifts due to the change in mass eccentricity. Hence, the rotational impulse frequency is much higher than from the fundamental translational frequency. This affects both the resonance response, and the influence from torsional coupling.

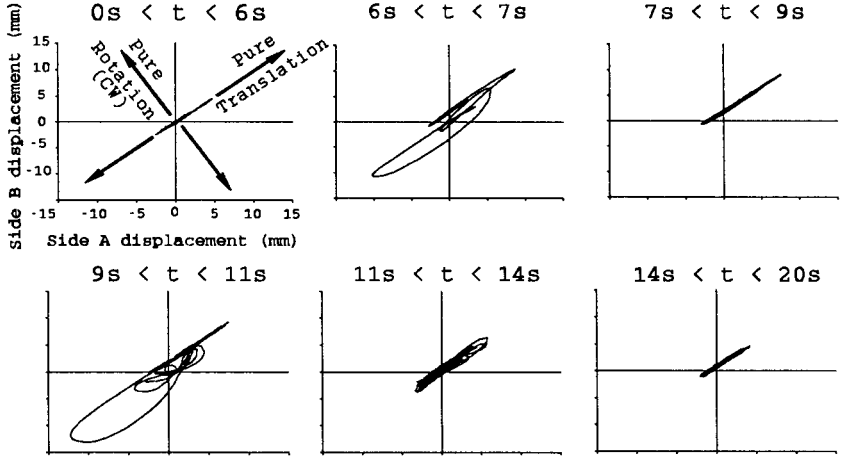

Figure 12. Plot of displacements for side B against side A for the mass symmetric (S1), strength asymmetric model (hinge configuration F, e_s'=+0.17, 0.5g PGA).

The earthquake input was used to determine the performance of the hinge joints under extended dynamic loading. The dual hinge set-up was used in this case (Figure 5). For brevity, only one experimental test is presented. Figure 12 shows the response of side A plotted against side B in a series of time-windows for the model with hinge configuration 6, and 0.5g peak ground acceleration. Because of the particular input motion, the inelastic response is concentrated in two time-windows (6s to 7s and 9s to 11s). It is shown that for the first 6 seconds, the structure behaves elastically, only in translation. Just after 6 seconds into the loading history the hinges yield, producing the first peak displacement pulse (10mm), for both sides. However, some torsional behaviour is introduced into the response from the strength eccentricity, i.e. the yield capacity on side A being less than that on side B ($e_s' > 0.0$). The response again becomes elastic at 7 seconds with inelastic offsets of 2mm and 4mm for sides A and B, respectively. From 10 seconds into the earthquake record, the response again becomes inelastic leading to a final structural deformation of 1mm in translation.

FUTURE RESEARCH PROGRAMME

Currently, inelastic tests are being carried out on multi-storey, variable mass asymmetric building models. These multi-storey structures will also be modified at a later date to incorporate shear walls. The effect of the cyclic stiffness degradation that these shear walls

@seismicisolation

have on the inelastic torsional behaviour, as well as the energy dissipation capacity of both the hinge units and shear walls, are to be studied.

CONCLUSIONS

The overall performance of the hinge joints in simulating plastic yield in the beam-column connections for the single storey experimental model are reasonable and repeatable. The results indicate that the translational yield strength and strength eccentricity are the most influential parameters in the inelastic response of the single-storey model.

ACKNOWLEDGEMENT

This research programme is funded by the UK Science Engineering Research Council (Grant GR/F/60632), whose support is gratefully acknowledged. The findings and recommendations in this paper are those of the authors and not necessarily those of the sponsor.

REFERENCES

1. Maheri, M.R., Chandler, A.M. and Bassett, R.H., Coupled lateral-torsional behaviour of frame structures under earthquake loading, Earthquake Engineering and Structural Dynamics, 1991, **20**, pp. 61-85.

2. Bassett, R.H., Maheri, M.R. and Chandler, A.M., Torsional earthquake response of frame buildings to Eurocode 8 spectrum-compatible design motion, Proc. 9th Eur. Conf. Earthquake Eng., Moscow, 1990, **5**, pp. 97-106.

3. Chandler, A.M. and Nichol, E.A., Experimental evaluation of procedures for earthquake analysis of torsionally asymmetric buildings, European Earthquake Engineering, (in press).

4. Commission of the Europeam Communities, Eurocode 8: Structures in seismic regions, Part 1, Brussels, 1988, Report # EUR 12266 EN.

5. Kan, C.L. and Chopra, A.K., Elastic Earthquake Analysis of a class of Torsionally Coupled Buildings, Journal of Structural Division, ASCE, 1977, **103**, pp. 395-412.

6. Chandler, A.M., Evaluation of Site-Dependent Spectra for Earthquake-Resistant Design of Structures in Europe and North America, Proc. Instn. Civ. Engrs., London, Part 1, (in press)

@seismicisolation

SEISMIC RESISTANCE OF CONNECTIONS IN EXISTING FLAT-PLATE BUILDINGS

AHMAD J. DURRANI
Associate Professor, Civil Engineering Department
Rice University,
6100 S. Main, Houston, Texas 77005, USA

ABSTRACT

The effect of non-ductile reinforcing detail on the seismic resistance of slab-column frames was investigated by testing four half-scale flat-plate subassemblies. The test subassemblies were designed and detailed using the code procedures of late forties for gravity load design of flat-slab buildings. Each subassembly consisted of two exterior and one interior connection and was subjected to several cycles of load reversals of increasing amplitude. The variables included slab reinforcing detail, intensity of the gravity load, and the presence of a spandrel beam. The effect of non-ductile connection detail on the overall lateral-load response of slab-column frame subassemblies with some detail of individual connection performance is presented. Rapid degradation of stiffness, significant reduction in deformation capacity with increased gravity load, and limited moment transfer capacity of connections under reversed loading emerged as principal response parameters of non-ductile slab-column connections.

INTRODUCTION

Flat-plate systems are inherently flexible and susceptible to considerable structural and non-structural damage during moderate to strong ground motions. Relatively poor performance of flat-slab buildings during the Mexico City earthquake [1] and similar observations elsewhere have renewed the concern for the adequacy of existing design procedures. Post-earthquake investigations of slab-column framing systems [2] and recent research efforts have led to signif-

@seismicisolation

icant improvements in the design and detailing of slab-column connections for seismic resistance. These advancements in building codes will only enhance the safety of new buildings. Flat-slab buildings of relatively older vintage pose a serious challenge to earthquake hazard mitigation effort. Case in point is the eastern region of the United States where a large stock of flat-plate and flat-slab buildings of five to fifteen stories height has accumulated during the last sixty years. The reinforcing detail of these buildings is based on gravity load design with some consideration for wind loads in relatively newer construction. Typical characteristics include lightly reinforced floor slabs, discontinuous slab bottom reinforcement through the column and poor anchorage detail. In the event of a moderate earthquake, the safety of most of these buildings could be in jeopardy. This paper briefly presents results of an experimental investigation on evaluating the seismic resistance of slab-column connections in existing flat-plate buildings.

MATERIALS AND METHODS

The design of the slab-column test subassemblies was based on a five story flat-plate building with three bays in the short direction and four bays in the long direction as shown in Fig. 1. In designing the prototype, every attempt was made to simulate material properties and design procedures specified in the ACI 318-47 Building Code [3]. The building was assumed to be an office building with a live load of 50 lbs/ft^2 and a total gravity load of 145 lbs/ft^2.

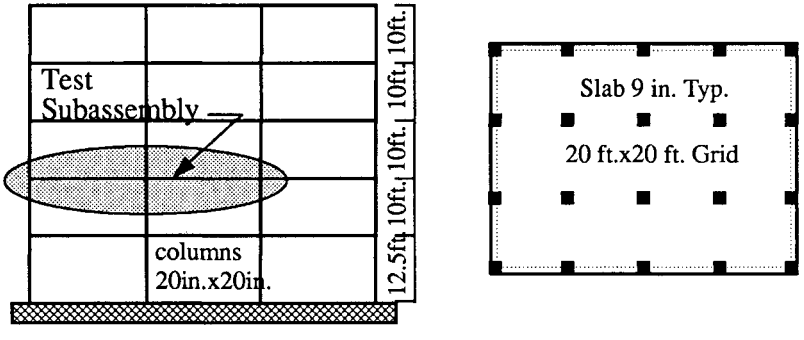

Figure 1. Elevation and Plan of Prototype Flat-Plate Building

Unlike the commonly used testing configuration of individual connections, it was decided to use two-bay slab-column subassemblies to allow redistribution of moments among connections. The test subassembly was extracted from the prototype as indicated in Fig.1. Since the study focucused on slab response in the connection region, the columns were deliberately overdesigned to remain elastic during the load reversals. The overall dimensions of the specimen were approximately one-half of the prototype and the gravity load was adjusted to result

@seismicisolation

in the same level of shear stress at the connections ($1.2\sqrt{f_c'}$ to $1.5\sqrt{f_c'}$ in psi units) as calculated in the prototype design. The level of axial stress in the columns due to the applied gravity load varied from 120 psi to 200 psi. The reinforcement ratio for slab top reinforcement at the column line was approximately 0.6% and that for the bottom reinforcement varied between 0.22 to 0.37% depending upon the reinforcing configuration used. Two types of commonly used slab reinforcing details, straight and bent-up, were investigated. These details have slightly different requirement for extending the slab bottom reinforcement into the column as shown in Fig. 2.

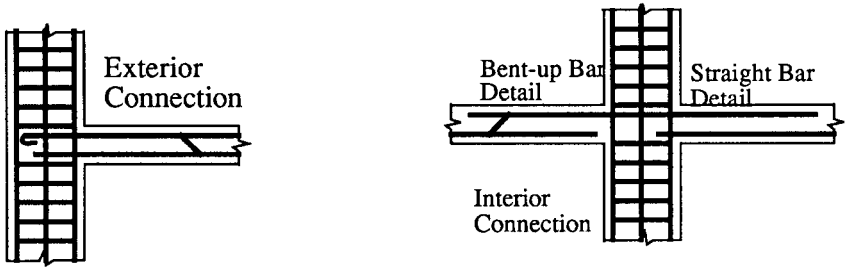

Figure 2. Reinforcing Detail in Connections

The design concrete strength for all specimens was 3000 psi with Grade 40 steel in the slab and Grade 60 steel in the columns. These specimens were constructed in the laboratory with ready-mixed concrete. Prior to casting, the reinforcement in the connection region was appropriately instrumented with strain gages to monitor participation of the slab under load reversals. Other miscellaneous instrumentation included a variety of load cells and displacement transducers. The subassemblies were tested in a stiff steel reaction frame. The bottom columns had a hinge connection to the frame while the top columns were connected to a loading beam capable of applying lateral cyclic load to the subassembly. Load application and data acquisition was carried out through an automated servo-controlled closed-loop hydraulic system. All specimens were subjected to a predefined set of lateral displacement cycles which increased in amplitude gradually to a maximum drift of 6 percent. The gravity load, which simulated the design dead and live loads, was applied to the slab before commencing the test. Further detail of the test set-up and testing detail can be found elsewhere [4]. Table 1 summarizes the configuration, material properties and the level of gravity load applied to each specimen. The response of the specimens was continuously monitored through visual observations of crack development, slab deflection measurements, and lateral load vs. displacement plots. Strain measurements and other transducer outputs were recorded at suitable intervals during each test.

@seismicisolation

TABLE 1

Specimen Configuration and Material Properties

Specimen	Reinf. Detail	Gravity Loading	Concrete Strength	Steel Strength
DNY_1	Bent-up	DL+0.3LL	5115 psi	54 ksi
DNY_2	Bent-up	DL+LL	3731 psi	54 ksi
DNY_3	Straight	DL+0.3LL	3566 psi	54 ksi
DNY_4	Edge Beam	DL+0.3LL	2772 psi	54 ksi

DISCUSSION OF RESULTS

All specimens, except DNY_2, were uncracked under service load prior to the start of the test. Specimen DNY_2, which was subjected to full design load, had minor initial cracks adjacent to columns prior to lateral load application. None of the specimens failed in punching under service loads. Yielding of the slab top reinforcement, at both interior and exterior connections, occurred mostly between 0.75 to 1.0 percent. The lateral load peaked between 2 to 3% drift. Under reversed loading, the moment transfer was limited to cracking strength of the slab. The slab bottom reinforcement, when extending into column, yielded soon after the cracking capacity of the slab was reached. The cracking of exterior connections under negative bending developed in the form of a combined flexural-torsional mechanism at the slab edge which prevented growth of yield lines across the full slab width. Most of the cracking in the connection regions stabilized between 2.5 to 3.0% drit. The presence of the full gravity load in DNY_2 forced a punching failure at interior connection at about 2% drift. Specimen DNY_4, which had a spandrel beam at the exterior connection, developed full yield lines at both interior and exterior connections. Higher initial stiffness of the exterior connection in DNY_4 caused early yielding of the slab reinforcement at about 0.5 percent drift with peak load occurring at 2.0% drift. With the exception of DNY_2, the remaining specimens were able to sustain lateral drifts as high as 4.5 percent. Some degradation of strength was noticed at drift levels above 3.0 percent. The measured peak loads and drift capacities along with the failure mode of the specimens is given in Table 2.

The load-deformation response of all specimens, with the exception of DNY_2 which failed early, was approximately bilinear with some tendency of strength loss at higher drift levels. A typical load-drift response is shown in Fig. 3. The symmetry of the response is attrib-

@seismicisolation

uted to load redistribution and sharing of load among different connections. The individual connections transferred the unbalanced moment only on the column face with slab top reinforcement in tension. The hysteresis loops were severely pinched indicating a rapid loss of stiffness and a low energy dissipation capacity. Most of the energy in specimens was dissipated by yielding of the slab reinforcement and growth of the flexural cracks.

TABLE 2

Ultimate Response and Failure Mode of Specimens

Specimen	Peak Load (kips)	Peak Drift (%)	Ultimate Load (kips)	Ultimate Drift (%)	Failure Mode
DNY_1	10.9	3.0	8.7	4.5	Flexure
DNY_2	9.6	2.0	7.7	2.0	Punching
DNY_3	10.2	2.0	8.2	4.5	Flexure
DNY_4	10.9	2.6	8.7	4.7	Flexure

The failure mode of specimen DNY_2 was clearly of punching type unlike the other specimens which showed a yielding mechanism. The specimen DNY_4 appeared to experience a partial punching towards the end of the test but this could have resulted from unrealistically large drift level. The peak load in both positive and negative loading directions was within ten percent of the average peak load The average peak load in the negative loading direction was approximately five percent less than the average peak load in the positive direction. Damage during the first half the loading cycle appears to have affected the strength during the second half of the loading cycle.

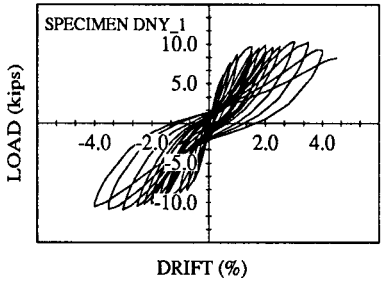

Figure 3. Typical Load-Deformation Plot

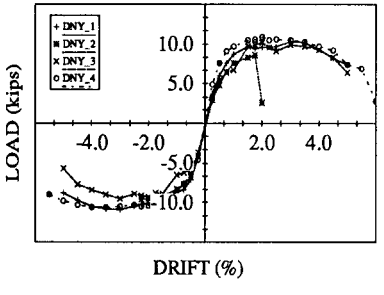

Figure 4. Envelope of Hysteresis Loops

Figure 4 shows the envelope of the load-drift response of all specimens. The difference in the reinforcing detail in the slab, whether bent-up or straight, does not appear to have any

@seismicisolation

significant effect on the overall response. Because of the differences between the two anchorage details of the slab bottom reinforcement, the moment-transfer response of the individual connections was slightly different at low drift levels. The presence of spandrel beam in DNY_4 increased the initial stiffness as well as the general strength and deformation capacity. The effect of increased gravity load, however, was dramatic in reducing the lateral drift capacity. The asymetry of the response in DNY_3 resulted from an initial large displacement imposed on the test subassembly due to a malfunction in the feedback circuitry.

Lateral stiffness of the slab-column framing system has always been of concern to the designers. In seismic regions, flat-plates are seldom built without shear walls. In older buildings, particularly those not specifically designed for lateral load resistance, stiff elements such as stairwells or elevator shafts may provide some resistance to lateral loads. But the non-ductile detail or inappropriate location of such elements may render them ineffective. As such, some understanding of the deterioration of the lateral stiffness of the flat-plate systems is important. Figure 5 shows the secant stiffness of specimen DNY_1 during each half cycle of the loading routine. The initial stiffness of the specimens was affected by factors such as the presence of the spandrel beam, the level of the gravity load, and to some extent by the connection reinfrocing detail. But after 1.5 to 2.0% drift, the stiffness of all specimens became very similar. Approximately 50% of the initial stiffness of the subassemblies was lost during the first 1% drift. Additional 20% of the stiffness was lost when drift reached 2 percent. Only 10% of the initial stiffness remained by the time the specimens reached 5% drift. Such rapid loss of stiffness must be accounted for in analyzing the flat-plate buildings for seismic forces.

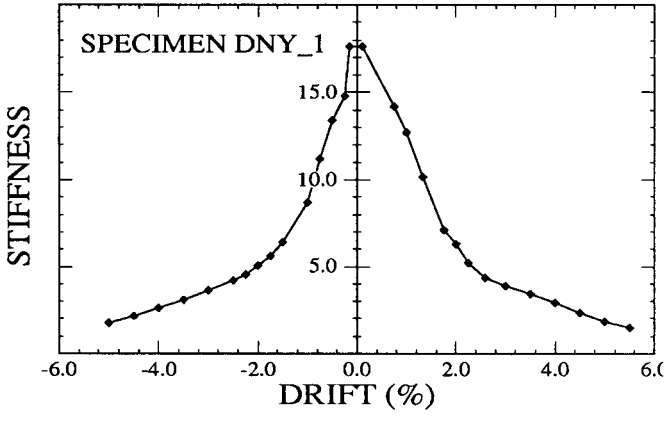

Figure 5. Stiffness Degradation

As mentioned earlier, moment redistribution played an important role in the overall response of the subassemblies. The moment-transfer capacity in non-ductile connections is limited to flexural strength of the slab effective width on one side of the column and to the slab

@seismicisolation

cracking strength on the other side. As soon as the slab cracks under positive bending, it is no longer able to transfer the moment on that side of the column and a part of the unbalanced moment at the connection is transferred to the other end of the slab. The moment transfer between the slab and the column under lateral loading is, therefore, mostly limited to the side of columns facing the loading direction. The location of the cracking moment in the slab relative to the column face depends on the magnitude of the gravity load. When lateral load dominates the response, as in DNY_1, the location of the flexural crack in the slab due to positive moment is closer to the face of the column compared to when the gravity load dominates the response as in DNY_2. The location of the cracking moment was found to have some effect on the anchorage of the slab bottom reinforcement in the connection region.

The combined effect of gravity and lateral load on the distribution of moment can also be observed from the deflected shape of the slab. Figure 6 shows the deflected shape of the slab for specimens DNY_1 and DNY_2 at 2% drift. Under normal service loads the slab appears to maintain the antisymmetric deformed shape with relatively small deflections. Under increased gravity load, the inflection point disappeared from the right span and moved closer to the interior connection in the left span.

The moment transfer capability of the exterior connections degraded much earlier than the interior connections. The low torsional resistance of the slab edge at the exterior connection quickly transformed it into a hinge which protected the connection from punching failure and redistributed. Moment transfer at interior connections occurred primarily on the column side with slab top reinforcement in tension.

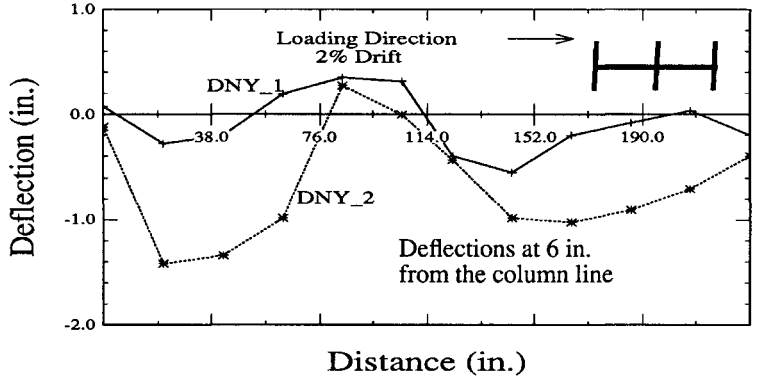

Figure 6. Deflected Shape of the Slab under Increased Gravity Load

@seismicisolation

CONCLUSIONS

Based on the observations made during this investigation, the following conclusions may be drawn regarding the overall response of the non-ductile flat-plate subassemblies:

1. The intensity of the gravity load at the time of lateral loading had the most effect on the response of the subassemblies. It affected the failure mechanism, drift capacity, and initial stiffness of the subassemblies.
2. The configuration of the slab reinforcement, bent-up or straight, did not have any significant effect on the strength or stiffness of the subassemblies. Extension of the slab bottom bars into the column in straight-bar detail improved the moment-transfer in positive bending at low drift levels.
3. Spandrel beam at the exterior connections increased the initial stiffness and improved the distribution of shear and moment transfer among connections.
4. Non-ductile slab-columns resisted lateral loads mostly through slab yielding mechanism unless punching occurred due to high gravity loads. Punching was more likely to occur at the interior connection compared to the exterior connection.
5. The lateral load response of the non-ductile frames is very nearly bilinear with some strength degradation at higher drifts. Stiffness degradation occurred rapidly with roughly 70% of the initial stiffness being lost within first 2% drift.

REFERENCES

1. "Impressions of the Guerrero-Michoacan Mexico Earthquake, September 19, 1985," A Preliminary Reconnaissance Report, EERI, October 1985.
2. I.N. Robertson and A. J. Durrani, "Seismic Response of Connections in Indeterminate Flat-Slab Subassemblies," Structural Research at Rice Report No. 41, Department of Civil Engineering, Rice University, Houston, Texas, July 1990, p. 266
3. "Building Regulations for Reinforced Concrete ACI 318-47," American Concrete Institute, Detroit, Michigan, 1947.
4. Yong Du and A. J. Durrani, "Seismic Resistance of Slab Column Connections in Non-Ductile Flat-Plate Buildings," NCEER Report, March, 1991,(in print)

ACKNOWLEDGEMENT

This research was funded by the National Center for Earthquake Engineering Research at SUNY, Buffalo, under Grant No. NCEER 88-1002D which is gratefully acknowledged. Contribution and assistance of Yong Du in preparing the manuscript is very much appreciated.

@seismicisolation

A COMPUTATIONAL STRATEGY FOR THE CRACKING PROCESS IN CONCRETE STRUCTURES UNDER SHOCK AND EARTHQUAKE LOADING CONDITIONS

F B A Beshara
and
K S Virdi
Structures Research Centre
Department of Civil Engineering
City University
Northampton Square, London EC1V OHB

ABSTRACT

A computational strategy to the cracking process is presented for the finite element analysis of planar and axisymmetric reinforced concrete structures under transient and impulsive loading conditions. A smeared crack formulation is proposed which is based on the fixed crack approach. The crack initiation is controlled by a new rate dependent strain criterion. The postcracking regime is governed by non-linear reversible formulations to model concrete tension softening as a function of concrete fracture energy, tensile strength, cracking strain and crack characteristic length. Crack shear is allowed to take place using a non-linear model dependent on the strain across the crack. Practical recommendations are made to some of the problems associated with the smearing approach. A new crack monitoring algorithm, as part of a comprehensive computer program FEABRS, is developed which follows the cracking behaviour with the time stepping scheme. The solution of some dynamic problems, with beam and circular slab elements, are presented and a comparison is made with results from other sources.

INTRODUCTION

The low probability of incidence of transient and impulsive loads requires the design of structural elements such that some level of irreversible structural deformation and material damage is acceptable, provided that the overall structural integrity is maintained. For the non-linear finite element analysis of dynamically loaded concrete structures, constitutive relationships are required which take into account the inelastic response in compression, the degradation of stiffness due to cracking, the yielding of reinforcing steel, and the effects of high strain rate on the behaviour of concrete and steel. Such history and rate dependent relationships have been developed in [1] and have been presented with examples in [2, 3]. As the tensile cracking process plays a dominant role in the non-linear behaviour of concrete, the main attention in the present paper is paid to

@Seismicisolation

the description of a proposed computational strategy for the crack initiation and propagation process in reinforced concrete structures subjected to severe dynamic loads such as blast, impact and earthquakes.

CONCRETE TENSILE BEHAVIOUR AND NUMERICAL REPRESENTATION OF CRACKS

Concrete tensile strain-softening behaviour

The main characteristic of plain concrete behaviour is its low tensile strength. As a result, tensile cracking is considered as the major factor contributing to the non-linear behaviour of reinforced concrete structures. Several experiments [4, 5] have revealed that this response is primarily controlled by the formation of micro-cracks. Initially a limited number of such cracks develop anywhere in the specimen, but if the tensile stress or strain reaches a certain limit, all deformation due to micro-cracks will localize within a fracture zone. The stress gradually decreases while the strain increases. This phenomenon is known as a tensile strain-softening. The stress strain curve in tension is linear almost up to the peak stress followed by considerable softening. When the end of the descending strain softening branch is approached, the micro-cracks coalesce into one continuous macro-crack. From the study of different testing results carried out at higher strain rates than the conventional static tests, it was concluded [1] that increasing the stress or strain rate in tension or compression results in higher concrete strength. However, the tensile response of concrete is more strain rate sensitive than its compressive strength. The inequality of rate effects in tension and compression induces anisotropic effect. It has also been observed [4, 5] that with the increase of strain rate, the stress strain curves in tension are almost linear and show only curvature in the final phase of pre-cracking range before the activation of tension softening regime.

To account for this observed behaviour, concrete is modelled in tension here as a rate sensitive linear elastic strain softening material. That is, concrete behaves elastically until cracks initiate according to rate dependent cracking criterion and then the crack propagation process is governed by a fracture energy based softening rule in which tensile strength normal to the crack is gradually released in uniformity with the crack width.

Finite element representation of cracks

In the finite element context, two main approaches have been used for crack representation [6]: the discrete crack model and the smeared crack model. The choice between one or the other depends on the purpose of the finite element analysis, with regard to local or overall behaviour of a structure. The discrete concept fits our material conception of fracture since cracking is identified as a geometrical discontinuity. Conversely, it has been stated that a smeared representation might be realistic considering the bands of micro-cracks that blunt fracture in matrix-aggregate composites like concrete. The width of such bands, which occur at the tip of visible crack, has even been claimed to be a material property [7]. At present, however, it is difficult to judge these arguments since experimental detection of crack tip related micro-mechanical process in matrix-aggregate composites is scarce and the question remains whether these processes occur in a discrete manner or not.

@seismicisolation

Following the most common approach, a smeared crack model has been adopted here where cracked concrete is assumed to remain a continuum and

the material properties are modified to account for the damage due to cracking. This approach has been chosen for the following reasons:

1. For severe dynamic loading conditions where the cracking patterns are difficult to predict, and also for situations where the scale of the representative continuum is large compared to the crack spacing, the smeared crack concept provides a realistic approach for distributed fracture representation compared with the discrete model which seems adequate for simple problems involving a few dominant cracks.
2. The proposed constitutive model is suitable for the description of concrete behaviour at the engineering level but not at the microscopic level which will necessitate the discrete approach.
3. The simplicity and the computational advantages of the smeared crack approach such as automatic generation of cracks without pre-defining or re-defining the finite element mesh, and also complete generality in allowing crack initiation in any direction.

CRACK INITIATION PROCESS

Strain rate sensitive cracking criterion

Simple criteria are commonly employed by most analysts to predict tensile fracture. The maximum tensile stress or strain theories [6] are frequently adopted for this purpose. Under severe dynamic conditions, the main limitation of the existing crack initiation criteria is that the strain rate effects are not included in spite of reported experimental results. For the present analysis, the tensile crack initiation is based on a rate sensitive criterion to distinguish the elastic behaviour from tensile fracture. The influence of deformation velocity on the material behaviour is taken into consideration by raising the cracking strain in relation to static condition using a rate sensitivity function as follows

$$\varepsilon_{td} = \phi_t \left(\dot{\varepsilon}_{eff}\right) \varepsilon_{ts} \tag{1}$$

in which ε_{td} is the dynamic cracking strain, ε_{ts} is the static cracking strain and $\phi_t(\dot{\varepsilon}_{eff})$ is the strain rate sensitivity function of concrete cracking and which is assumed to depend upon the effective strain rate. The least squares curve fitting was used to obtain a mathematical relation which fits the experimental results, found in the literature, for concrete tensile strength. Due to lack of sufficient experimental results, the effect of strain rate on the tensile strength and the cracking strain is assumed to be the same [4, 5]. The strain rate sensitivity function ϕ_t is found [1] to be

$$\phi_t\left(\dot{\varepsilon}_{eff}\right) = 2.23 + 0.404 \log \dot{\varepsilon}_{eff} + 0.0351 \left(\log \dot{\varepsilon}_{eff}\right)^2 \tag{2}$$

The advantage of this proposed crack initiation criterion over the other existing criteria is that concrete brittleness observed in dynamic tests, strain rate dependency and the inclusion of strain rate induced anisotropy, can all be considered.

@seismicisolation

Introduction of cracking process for plane and axisymmetric problems

For a previously uncracked point in a plane structure, cracks are assumed

to form in planes perpendicular to the direction of maximum tensile strain as soon as this strain reaches the specified concrete dynamic cracking strain, ε_{td}. Thus for cracking

$$\varepsilon_1 \geq \varepsilon_{td} \quad \text{and/or} \quad \varepsilon_2 \geq \varepsilon_{td} \tag{3}$$

where subscripts 1 and 2 relate to the principal directions in the plane of a structure. Thereafter, the behaviour of concrete is no longer isotropic. It becomes orthotropic and the local material axes coincide with the principal strain directions. Following the fixed crack approach [1], the crack directions are assumed to be fixed in the directions of the primary cracks, irrespective of the possible rotation of stresses and strains. Under further loading, a secondary crack may occur at a sampling point that was originally cracked in one direction if the strain parallel to the existing crack, ε_t^*, satisfies the cracking condition

$$\varepsilon_t^* \geq \varepsilon_{td} \tag{4}$$

Thus for plane problems, two sets of cracks are allowed at each sampling point in mutually orthogonal directions.

In axisymmetry, the hoop stresses and strains are always principal quantities, and therefore cracks lie in radial planes if the hoop strain satisfies the cracking condition

$$\varepsilon_\theta \geq \varepsilon_{td} \tag{5}$$

The other type of cracks, called the circumferential cracks, can occur in the radial-axial (r-z) plane which are similar to those in planar conditions. Thus, taking into account that this third direction, θ, is always a principal direction and is out of plane, the cracking prediction follows the same procedure of plane problems for circumferential cracks.

CRACK PROPAGATION PROCESS

Tension softening rule

In order to account for the post-cracking residual tensile strength of concrete in the present computational model, it is assumed that the loss of tensile strength occurs gradually after cracking. An important consideration in the selection of crack propagation criterion for the smeared cracking concept is the objectivity with respect to mesh elements size. The element size effect is treated here by an approach proposed by Nilsson et al [8], in which the abrupt stress reduction is replaced with a gradual stress reduction to follow a fracture energy based non-linear softening curve as shown in Figure 1. The fracture energy release rate, G_f, defined as a material property is used with local strain softening rule and a characteristic length, L_c, for the subjective treatment of the post-cracking behaviour. As a result the fracture energy concept leads to a non-local format of the equivalent softening relation.

The stress, σ, across an opening crack is assumed to be a function of crack width, w, [8] such that

@seismicisolation

$$G_f = \int_0^{\infty} \sigma\ (w)\ dw \tag{6}$$

It was assumed that inside a control volume, v, containing a crack with a surface area A, all inelastic deformations take place in the crack, so the rest of the control volume remains elastic. The rate of energy dissipation in the crack is

$$\dot{U}_A = \int_A \sigma\ \dot{w}\ d\ A \tag{7}$$

In order to replace the discontinuous crack with an equivalent smeared crack, it is assumed that the control volume is subjected to the same state of stress as the crack, but strained by equivalent strain, ε_c. The rate of energy dissipation in this continuous volume is

$$\dot{U}_v = \int_v \sigma\ \dot{\varepsilon}_c\ dv \tag{8}$$

The relationship between the crack width and the fictitious crack strain is obtained by equating (7) to (8), which leads to

$$\frac{dw}{d\varepsilon_c} = \frac{V}{A} \tag{9}$$

Taking the characteristic length of crack as the ratio between the control volume and the crack surface, equation (9) can be re-written as

$$\frac{dw}{d\varepsilon_c} = L_c \tag{10}$$

Using equation (10), the fracture energy in equation (6) is defined as

$$G_f = L_c \int_0^{\varepsilon} \sigma\ d\ \varepsilon_c \tag{11}$$

Based on various experimental evidence, an exponential function is used to simulate strain softening branch [9, 10] as

$$\sigma = \sigma_{ts}\ e^{-\frac{\varepsilon - \varepsilon_{ts}}{\delta}} \tag{12}$$

where σ_{ts} is the static tensile strength of concrete, ε_{ts} is the cracking strain, δ is the tension softening parameter and ε is the normal tensile strain in the cracked zone. From Figure 1, the stress in the linear elastic part can be defined as

$$\sigma = \varepsilon\ \ \sigma_{ts} / \varepsilon_{ts} \tag{13}$$

Substituting (12) and (13) into (11) and upon mathematical manipulation, the tension softening parameter is found [10] as

@seismicisolation

$$\delta = \left(G_f - \frac{1}{2}\sigma_{ts}\,\varepsilon_{ts}\,L_c\right) / \sigma_{ts}\,L_c \tag{14}$$

In the context of finite element computations, the control volume for a crack is the volume associated with a sampling point in a given element. The characteristic crack length is computed here for each sampling point [10] as

$$L_c = (dv)^{1/3} \tag{15}$$

where dv denotes the volume of concrete represented by the sampling point inside each element.

Shear transfer across the cracks

At the onset of cracking, the ability of concrete to transfer shear stresses across the crack is greatly reduced. However, phenomenon such as aggregate interlock and dowel action due to reinforcing bars must be taken into consideration. Both mechanisms are controlled by the width of the crack, the shear transfer capacity being reduced as the width increases. To account for the shear capacity of cracked concrete in the smeared crack approach, a simplified procedure is generally employed by assigning to the uncracked shear modulus, G, a reduced value, G_c, defined as

$$G_c = \beta_s\,G \tag{16}$$

where β_s is a reduction factor in the range of zero to one. In the present work, the reduction factor is related by a monotonically decreasing function, to the tensile strain normal to the crack plane, a smeared measure of the crack width by the expression

$$\beta_s = 1 - \left(\frac{\varepsilon^*_n}{\varepsilon_m}\right)^{\mu}, \quad \beta_s = 0 \text{ if } \varepsilon^*_n \geq \varepsilon_m \tag{17}$$

where ε_m is the maximum limiting tensile strain and μ is a parameter in the range 0.3 to 1.0 [11]. The value of the maximum limiting strain is often considered in a range of 0.004 - 0.005.

SOME OTHER FEATURES OF COMPUTATIONAL CRACKING STRATEGY

Closing and opening of existing cracks

The redistribution of stresses due to cracking in other sampling points, or further loading or unloading may force some of the previously open cracks to close partially or fully. The current strain normal to the crack direction is used [1] to assess the state of the cracks in already cracked concrete. Thus, a crack is assumed to be fully closed if the strain becomes negative, as

$$\varepsilon^*_n \leq 0 \quad \text{and/or} \quad \varepsilon^*_t \leq 0 \tag{18}$$

and/or additionally for axisymmetric problems

$$\varepsilon_\theta \leq 0 \tag{19}$$

@seismicisolation

The compressive stresses can then again be transmitted across the

cracks. If the strain normal to the crack direction decreases, but is still positive, partial closing of the crack is assumed. This situation may occur when the current strain, ε_n^*, is smaller than the reference strain, ε_{ref}, recorded as the maximum tensile strain reached across the crack under consideration at the previous time steps. In this case, the stress normal to the crack is computed from

$$\sigma_n = \frac{\sigma_{ref}}{\varepsilon_{ref}} \varepsilon \tag{20}$$

in which σ_{ref} is the interpolated stress corresponding to the strain ε_{ref}. This secant unloading path is shown in Figure 1. Re-opening of fully closed crack is also monitored by the tensile strain normal to the crack direction, i.e.

$$\varepsilon_n^* > 0 \quad \text{and/or} \quad \varepsilon_t^* > 0 \tag{21}$$

and/or for axisymmetric problems

$$\varepsilon_\theta > 0 \tag{22}$$

In this case, the crack follows the same secant path until ε_{ref} is exceeded and then the stress is interpolated from the strain softening governing equation (12). It should be mentioned that from the moment of first cracking, for each integration point, a record of the crack angle, the crack state, and the cracking reference values (ε_{ref}, σ_{ref}) are kept and constantly updated at each time step.

Control of stress locking phenomenon

Occasionally in the vicinity of fracture localization zones the principal stress plots exhibit stress locking phenomenon when the stress should actually drop to zero. This leads to overstiff response. The stress-locking is a fundamental consequence of finite element displacement continuity in smeared softening approaches. If a certain element contains an inclined crack at sampling point, GP1, the strain imposed by this crack implies adjacent integration points, e.g. GP2, to be strained as well. Hence, while the stress at GP1 correctly softens, the stress at GP2, which is still in the elastic regime, increases. Then, there are two possibilities [12]: the strain at GP2 will either exceed the limiting cracking strain and start softening, or it will not. The former alternative discourages localizations (spurious cracking), but the latter suffers from spurious stiffening. Stress locking does not disappear on mesh refinement, since refinement does not remove the fundamental assumption of displacement compatibility. As a result, the solution of the problem must be primarily sought in improvements of the finite element approximations. It has been suggested [12] that a possibility is to interactively align the elements with the lines of the fracture, or to use some isotropic softening law, whereby not only the stiffness normal to the crack but also the stiffness parallel to the crack deteriorates. However, with the former method the featuring advantage of smeared cracking as to maintaining the original topology is lost. The latter solution is not realistic since in reality the stiffness of concrete parallel to the cracks does not disappear. In the present work, the use of Guassian quadrature technique with the reduced 2x2 order for the numerical integration of the stress fields proved [1] to be a practical and successful means of handling elastic and inelastic domains within the same 8-node isoparametric elements

©seismicisolation

adopted here for geometry discretization. It gives a partial release of the continuity requirements imposed by shape functions of elements.

COMPUTER IMPLEMENTATIONS AND NUMERICAL APPLICATIONS

Crack monitoring algorithm

A new crack monitoring algorithm is developed in [1] which follows the subsequent cracking of elements. The outlines of the algorithm are given in Table 1. This algorithm is part of a versatile and comprehensive computer program, FEABRS, which has been developed [1] for the finite element linear and non-linear dynamic analysis of plane and axisymmetric reinforced concrete structures under blast and acceleration history excitations. Explicit central difference scheme has been employed for the time discretization of the governing dynamic equilibrium equations. The crack monitoring algorithm is activated after strain evaluation in each time step and for each cracked integration point.

Beam under impulsive concentrated load

A simply supported reinforced concrete beam is subjected to two symmetrically applied concentrated loads which are applied as step loads with a zero rise time. The problem has been solved in [10, 13]. The beam is reinforced in the lower position by 1290 mm^2 steel area. The material properties of concrete and steel are listed in [1]. Using symmetry conditions, only one half of the beam is modelled using the 8-noded isoparametric elements with axial bars to simulate the reinforcing steel. No viscous damping has been considered. The time step size was chosen as 0.000002 sec.

The performance of the rate independent modelling is compared with the rate dependent response of the beam in Figure 2 which shows the variation of the mid-span deflection with time for the non-linear analyses together with the elastic response. Generally, the results of the linear and non-linear rate dependent analyses found to be in good agreement with those reported elsewhere [10, 13]. The following points can be drawn from the Figure:

1. Compared with the linear analysis, the much longer response (almost 50% higher) of non-linear cases is a result of the softening behaviour of the structure with the progression of cracks in the structure.

2. For the non-linear analyses, both the peak displacement and the time corresponding to the peak deflection vary with the rate sensitivity consideration. Ignoring the strain rate effect results in an over-estimate by almost 12% of the maximum deflection obtained for the rate dependent case, and by approximately 64% compared with the elastic case. An elongation of the natural period can also be noticed. Based on the formulation of the proposed concrete constitutive modelling to simulate the experimentally observed phenomena under dynamic loading, two differences exist between the rate dependent and rate independent models that may account for differences observed in the deflection history. First, the inclusion of strain rate effect results in stress-strain diagrams which indicate higher strength and greater energy absorption before concrete fractures. Second, the adopted rate dependent crack initiation criterion introduces additional crack hardening mechanisms associated with the higher limiting cracking strain.

© Seismicisolation

To study the sensitivity of the beam response to variations in the concrete fracture energy, the non-linear analysis is performed with G_f varied between 105.1 and 150.6 Nm/m^2. It can be observed from Figure 3 that the consequence of reducing this material property is an amplification of the effect of concrete cracking which results in an increase in deflection and an elongation of the period. However, the increase in the deflection is not proportional to the change in the fracture energy. As the fracture energy is increased by 50%, the maximum deflection decreases by only 10%.

The beam topology is traced in Figure 4 which shows the deformed shape of beam and how the cracks spread in concrete at different time stations. The deformed beam elevation is represented by considering the horizontal and vertical displacements magnified 20 times. Following the cracking history, the beam behaviour is linear elastic in the initial stages. At time, t = 0.00298 sec, cracking commences near the bottom surface of the beam. With increasing deflection, the cracks develop on the underside of the central part of the beam. The cracking patterns indicate that flexural deformations produce the cracks which are all perpendicular to the tension initiation. As the cracks propagate further into the beam, the compressive strain combines with the shear strain and alters the inclination of the principal tensile strain so that the crack inclines towards the horizontal. The significant increase in displacements with time also reveals the fact that the main factor contributing to the non-linear behaviour is the cracking of concrete.

Circular slab under uniformly distributed dynamic force

The slab is subjected to a uniformly distributed load of intensity 137.3 kN/m^2. This problem has been previously analyzed by several investigators [10, 14]. The plate has a radius of 10 m and a thickness of 1 m. The load is applied with a rise time equal to half of the elastic fundamental period (T = 0.06 sec). The percentage of reinforcement placed near the upper and lower surfaces in the radial and tangential directions is 1%. The material properties employed here are given in [1]. Following the axisymmetric conditions, only a quadrant of the plate is modelled in the r-z plane using 24 isoparametric elements. The reinforcement was simulated as axisymmetric membrane with Poisson's ratio ν = 0.0, which in the adopted model implies four steel layers, each of 1.0 cm equivalent thickness. The analysis was performed with a time step of 0.000005 sec and with no damping.

The numerical results of the time history of mid-span deflection in Figure 5 are presented for linear analysis as well as non-linear response for two different levels of concrete cracking strains. The linear elastic curve and the curve obtained for cracking strain 0.00018 are in good agreement with the results reported in [10,14]. The general trends observed in the previous example are confirmed. Non-linear effects amplify displacements and elongate the period of vibration. The significant variation in responses for different cracking limits indicates the capability of the proposed computational strategy of the cracking process in predicting the behaviour of concrete structures where tensile cracking is the most sensitive and dissipative mechanism.

At different time intervals, the deformed profiles of one half of the structure and the spread of the crack zones through the thickness in the radial and hoop directions are shown in Figure 6 where the deformations are enlarged 20 times. In the initial stages (time = 0.024 sec), the slab behaviour is linear elastic. At time, t = 0.032 sec, the non-linear

@seismicisolation

analysis leads to cracking in the tangential direction in the vicinity of the built-in section at the top of the slab. The first circumferential cracks are predicted at the bottom of the centre of the slab at time, t = 0.0366 sec. With increasing time, the radial cracks spread to the top of the slab at mid-span and to the bottom of the slab at the fixed edge. On the other hand, the hoop cracks extend from the lower face towards the centre at the top of the slab. It can also be seen from the Figure that the increase in deformations is mainly determined by the increasing displacements in the cracked zones.

CONCLUSION

The main conclusions that can be drawn from the present study are:

1. The proposed computational strategy for modelling the cracking process in smeared fashion is a suitable and powerful tool for the non-linear dynamic analysis of planar and axisymmetric reinforced concrete structures under impulsive and transient loading conditions. Such methodology has been shown to be suited for representing overall behaviour as well as for simulating different crack patterns.

2. For all types of concrete structures, tensile cracking process plays a dominant role in the non-linear response. The numerical results indicate that the structural response is sensitive to the crack initiation parameters (cracking strain and strain rate dependency). Decreasing the limiting cracking strain or ignoring strain rate effect results in higher deflections and longer periods. The proposed rate dependent crack initiation criterion numerically introduces a crack arresting mechanism associated with the higher limiting cracking strain.

3. The computed structural response clearly depends on the post-peak tensile behaviour of concrete through concrete fracture energy G_f. The difference in deflection response for lower values of G_f seems to be a direct consequence of the decrease of the effective load-carrying area of concrete in tension. As the slope of the descending branch of the tensile stress-strain curves decreases for higher values of G_f, the cracks propagate more slowly and the load capacity of the structural member increases. The insensitivity of the response to small changes in fracture energy may be due to the fact that increasing the fracture energy primarily stiffens and does not strengthen the structural element.

4. The plane 8-noded isoparametric elements employed for geometry discretization proved to be a successful and computationally economical means of handling elastic and inelastic spatial domains. Moreover, the use of Guassian quadrature technique with the reduced 2×2 order for the numerical integration of the element stress fields, gives reasonable cracking patterns as well as a control of the stress locking phenomenon as a result of the partial release of the continuity requirements imposed by the shape functions.

5. The crack monitoring algorithm developed as a part of the computer program FEABRS offers good possibilities for non-linear dynamic analysis of concrete structures where strain rate dependency effects, tensile strain-softening, crack shear and partial or full closing and opening of cracks are taken into account. The progressive cracking in

@seismicisolation

concrete can be traced where single mode or mixed mode fracture analysis can be performed.

REFERENCES

1. *Beshara, F.B.A.,* "Non-linear finite element analysis of reinforced concrete structures subjected to blast loading", PhD Thesis, City University, London, 1991.

2. *Beshara, F.B.A., and Virdi, K.S.,* "Non-linear finite element dynamic analysis of two-dimensional concrete structures", in the Proceedings of 4th Int. Conf. on Civil and Struct. Eng. Computing, Volume 1, pp. 329-343, 1989.

3. *Beshara, F.B.A., and Virdi, K.S.,* "Non-linear finite element analysis of reinforced concrete structures subjected to blast and impulsive loading", in the Proceedings of second World Congress on Computational Mechanics, Stuttgart, FRG, pp. 57-61, 1990.

4. *Zielinski, A.J., and Reinhardt, H.W.,* "Impact stress-strain behaviour of concrete in tension", Proceedings of RILEM-CEB-IABSE-AISS Symposium on concrete structures under impact and impulsive loading", Berlin (West), pp. 112-124, 1982.

5. *Reinhardt, H.W.,* "Concrete under impact loading - Tensile strength and bond", Heron, Vol. 27, No. 3, 1982.

6. *Chen, W.F.,* "Plasticity in reinforced concrete", McGraw-Hill, N.Y., 1982.

7. *Bazant, Z.P., and Oh, B.H.,* "Crack band theory for fracture in concrete", RILEM, Materiaux et Constructions, Vol. 16, pp. 155-177, 1983.

8. *Nilsson, L., and Oldenburg, M.,* "Non-linear wave propagation in plastic fracturing materials - A constitutive modelling and finite element analysis", •IUTAM Symp. on non-linear deformation waves, Tallin, 1982.

9. *Glemberg, R.,* "Dynamic analysis of concrete structures - Constitutive modelling, dynamic substructuring, Computer implementation", Chalmers Univ. of Technology, Publication 84:1, 1984.

10. *Cervena, M., Hinton, E., and Bicanic, N.,* "Non-linear transient dynamic analysis of three-dimensional reinforced concrete structures using a three-dimensional approach", in numerical methods for transient and coupled problems, ed. by R.W. Lewis et al, 1987.

11. *Cervenka, V.,* "Constitutive model for cracked reinforced concrete", ACI Journal, Vol. 82, pp. 877-882, 1985.

12. *Rots, J.G., and Blaauwendraad, J.,* "Crack models for concrete - discrete or smeared?, Fixed, multi-directional or rotating?", Heron, Vol. 34, No. 1, 1989.

13. *Bathe, K.J., and Ramaswamy, S.,* "On three-dimensional non-linear analysis of concrete structures", Nucl. Engng. Design, Vol. 52, pp. 385-409, 1979.

14. *Rebora, B., and Zimmermann, T.,* "Dynamic rupture analysis of reinforced concrete shells", Nucl. Engng. Design, Vol. 37, pp. 269-297, 1976.

@seismicisolation

TABLE 1 The crack monitoring algorithm in FEABRS

A - Check whether the sampling point (GP) is previously cracked

B - if not previously cracked (crack has just initiated):

1. - Compute and store crack angle
2. - Set appropriate flags for material state (MSTAT)
3. - Stress evaluation for cracked state, go to D

C - if previously cracked:

1. - Compute strains in local coordinate system.
2. - Check whether each of the old cracks is opened by checking the dilation across each existing crack.
3. - For plane problems, if GP (Guass Point) is previously cracked in one direction, check whether a new crack has just opened orthogonal to the direction of first one by checking the strain parallel to the first crack.
4. - For axisymmetric problems, if GP is previously cracked in one direction or two directions check whether new cracks (two for the first case and one for the second) just initiated from the following three possibilities of cracks:

i. radial crack by checking the strain in the hoop direction.

ii. main circumferential crack by checking the strain in the radial direction.

iii. secondary circumferential crack orthogonal to the main one by checking the strain parallel to the main circumferential crack.

5. - Store angle of each new crack
6. - Update appropriate flags for MSTAT
7. - Stress evaluation of cracked state

D - stress evaluation procedure for cracked state:

1. - Evaluate stresses in crack directions using suitable constitutive relationship for cracked concrete, [1].
2. - Update the normal stresses across the cracks using tension softening rule.
3. - Update shear stresses across the cracks using shear transfer model.
4. - Update the crack reference values.
5. - Transform stresses back to global directions.

@seismicisolation

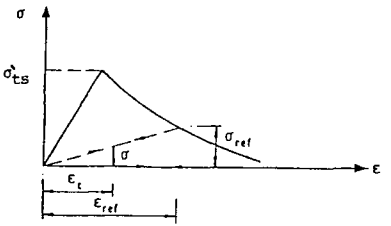

Figure 1 Strain softening curve with secant unloading and reloading

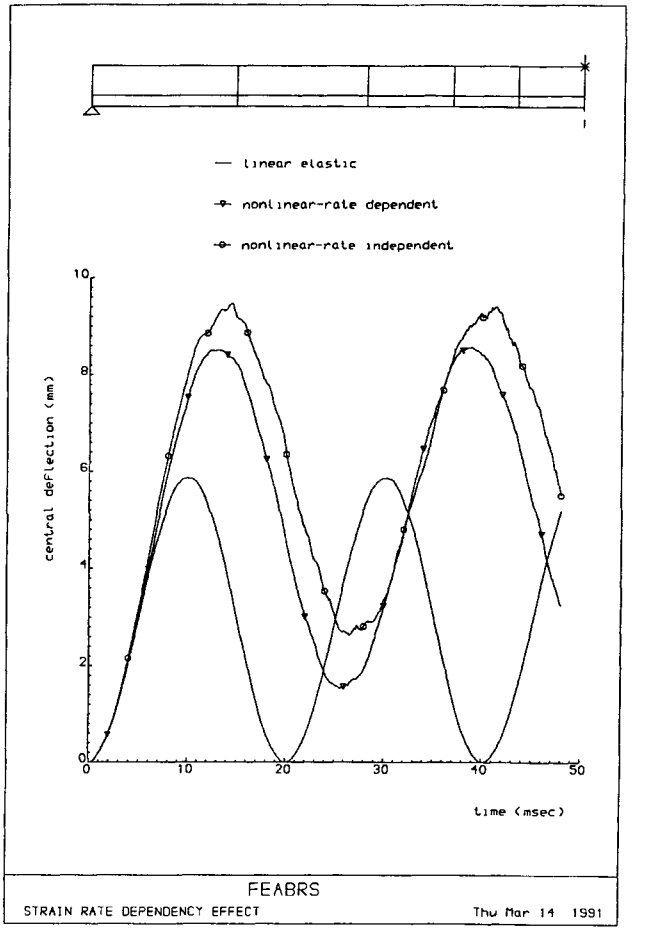

Figure 2 The effect of strain rate on the nonlinear response of Bathe's beam

@seismicisolation

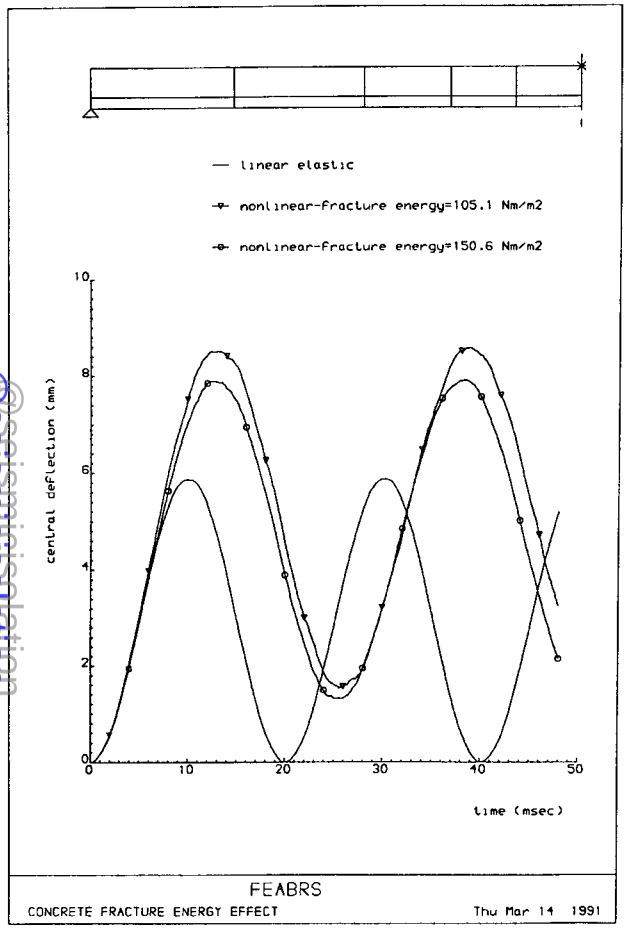

Figure 3 Influence of concrete fracture energy on nonlinear response of Bathe's beam

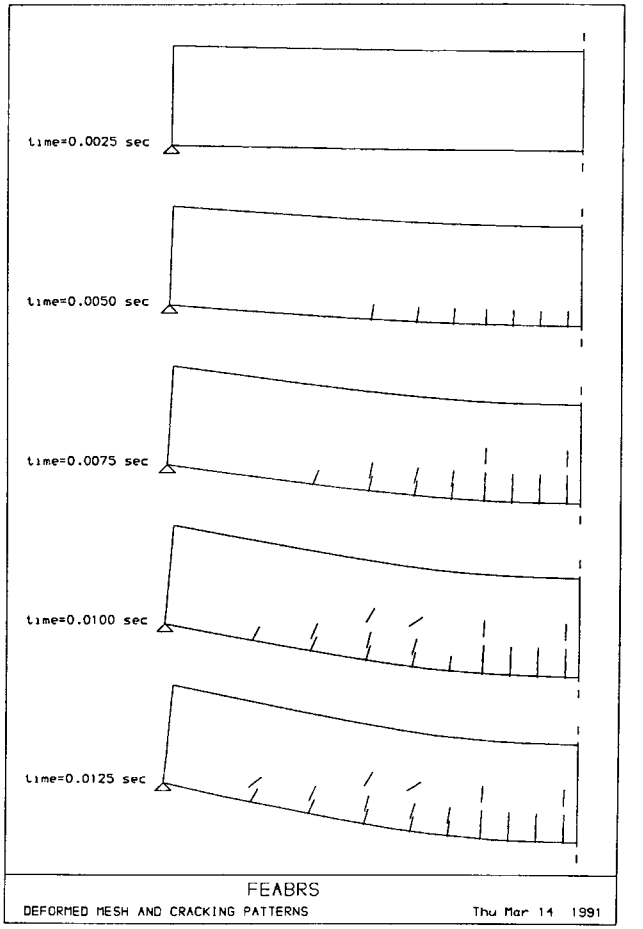

Figure 4 Deformation and cracking history of Bathe's beam

@seismicisolation

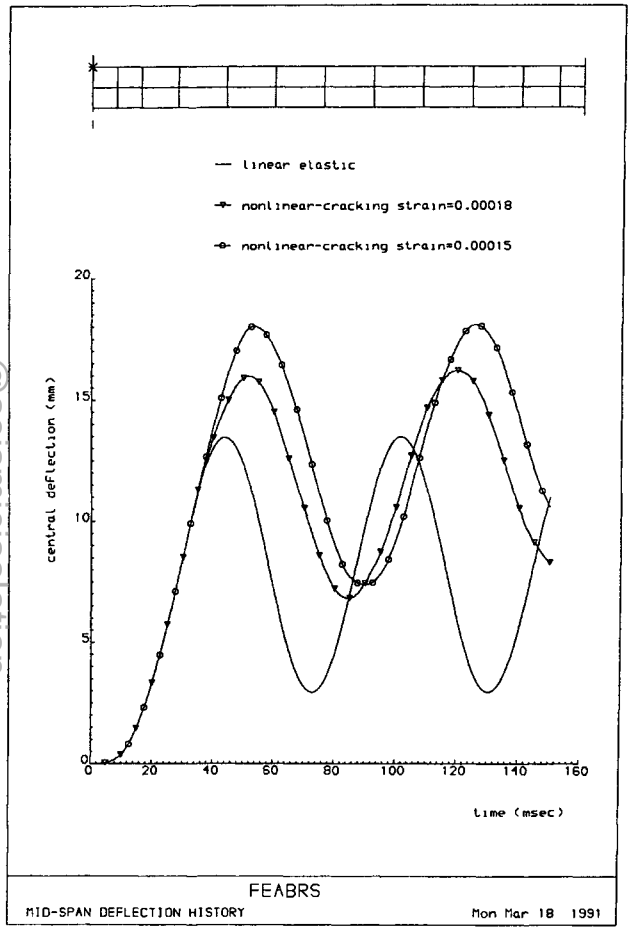

Figure 5 Nonlinear response of circular plate

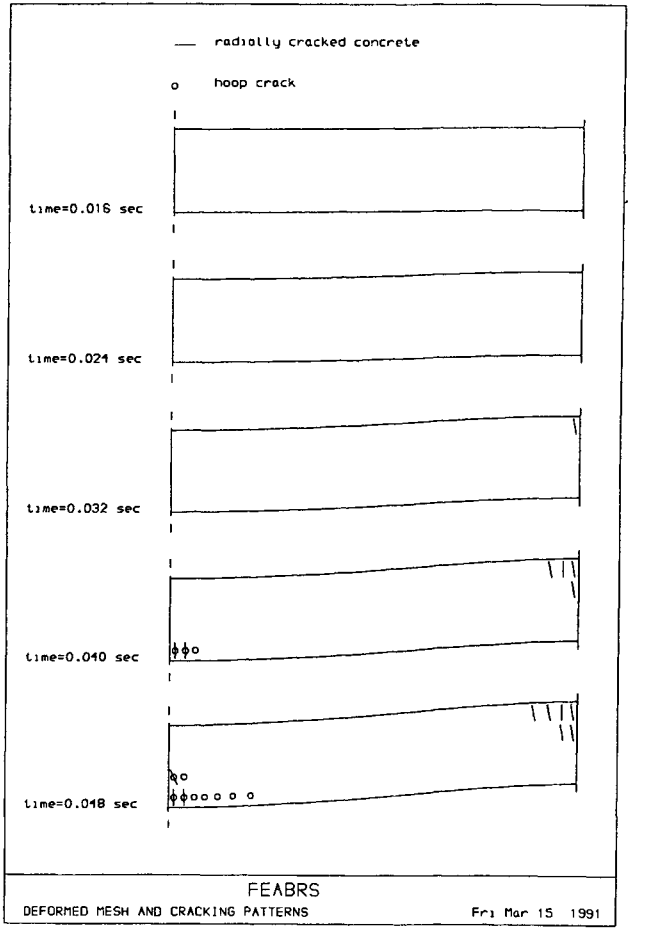

Figure 6 Deformation and cracking history for circular slab

@seismicisolation
@seismicisolation

"IN SITU" DYNAMIC TESTS OF A GATED GRAVITY DAM

ROMANO CÂMARA & ALEXANDRE PORTUGAL
Dams Department
Laboratório Nacional de Engenharia Civil
Av. do Brasil, 101 - 1799 LISBOA CODEX - PORTUGAL

ABSTRACT

This paper presents forced vibration test results of a gated gravity dam, Crestuma dam, located in Douro river near Oporto.

Vibrations generated by ambient noise and hydraulic flow were initially measured aiming at a first identification of fundamental frequencies. The forced vibration of the structure was produced by an eccentric mass exciter and velocities were measured at several points of the dam. Transfer functions were obtained allowing identification of the fundamental frequencies and damping ratios. Results obtained with these tests are compared with those obtained by a finite element model.

INTRODUCTION

The high potential risk of large dams makes their safety assessment an issue of the utmost importance. Laboratório Nacional de Engenharia Civil (LNEC) has had this task in Portugal for several years and so it has been responsible together with Electricidade de Portugal (EDP) and other organizations for the seismic monitoring of concrete dams and their reservoirs. In fact dynamic behaviour observation of concrete dams is a very important feature in safety assessment of these structures owing to the seismic risk in Portuguese territory. The main activities developed in this field by LNEC over the past thirty years include [1,2,3,4,5]: instrumentation of reservoirs aiming at induced seismicity control, "in situ" tests such as ambient noise measurements and forced vibration tests, seismic instrumentation of dams and inspections following earthquakes.

Studies on the seismic behaviour of concrete dams have been developed at LNEC, together with seismic monitoring, namely studies on: idealization of seismic loads, modelling of dynamic behaviour of materials and structures using experimental and numerical approaches.

The scope of this paper is the presentation of some recent research work performed on a large gated gravity dam, Crestuma

@seismicisolation

dam, located in Douro river near Oporto. "In situ" vibration tests were made, as a part of the structure safety assessment, aiming at three different goals: i) to study the structural dynamic behaviour under small amplitude vibrations; ii) to develop and fit the dam-foundation-reservoir mathematical model and; iii) to predict the structural response to seismic loads.

"IN SITU" TESTS

2.1. Crestuma dam

Crestuma is a multi-purpose plant in Douro river near Oporto mainly intended for hydroelectric power, water suply to Oporto and improvement of navigability conditions [6,7].

The main parts of the plant are: a gated movable dam, a navigation lock located near the river left bank, a 120 MW power station and a fish lock.

Figure 1. Crestuma dam.

The movable gated dam (fig. 1) consists on 8 double-fixed roller-gates (hook type), 28 m clear span, 13.7 m in height, supported by 6 m thick, 49 m large concrete piers, founded by the concrete-wall technique on the schist bedrock, 40 m below the alluvium river bed. The stilling basins are in plain concrete poured directly on the alluvium and are structuraly independent from the piers. The piers also support a road bridge connecting the river banks and two beams on which the rails for the gantry crane lie.

2.2. Ambient noise measurements

@seismicisolation

Ambient noise vibrations (wind, hydraulic flow and turbine operation) were initially measured aiming at a previous identification of fundamental frequencies.

Velocities were measured at several points of the dam (fig.

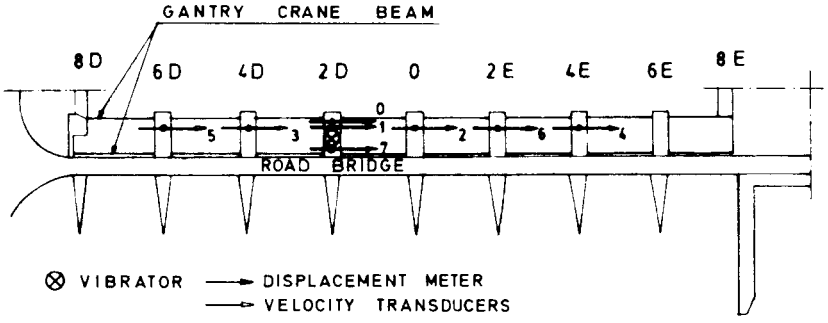

Figure 2. Crestuma dam. Measurement and exciting points.

2). Velocity Kinemetrics SS-1 transducers were used with Kinemetrics SC-1 signal conditioners, connected to an A/D converter included in a Hewlett-Packard series 300 microcomputer. The signal conditioners include analog filters to avoid aliasing in digital series and amplifiers to fit the voltage to the A/D converter. Although not used in this work these signal conditioners also include integrating and differentiating circuits.

Several 2048 point samples were recorded with 100 Hz sampling frequency, i.e., about 20 s in duration. The analog filters were set to low-pass at 30 Hz to eliminate the signal electrical background and to avoid aliasing.

2.3. Forced vibration tests

Forced vibration tests were made aiming at the determination of force to displacement transfer functions (TF) from which modal parameters may be computed.

These tests consisted in loading the structure with harmonic horizontal forces at several frequencies. These forces were generated by an eccentric mass vibrator designed and constructed at LNEC [8]. The single arm vibrator produces a maximum force of about 50 kN in a frequency range between 1 and 7 Hz. The vibrator is attached to the structure by eight steel 30 mm bolts.

The two components of the force generated by this exciter are:

$$F_x(t) = F_0 e^{j\overline{\omega}t} \quad ; \quad F_y(t) = F_0 e^{j(\overline{\omega}t - \frac{\pi}{2})} \tag{1}$$

where

$$F_0 = m\overline{\omega}^2 r \tag{2}$$

where m is the eccentric mass and r is the distance to the rotation center. The angular frequency $\overline{\omega}$ depends on the rotation speed of the vibrator electric engine.

The main pitfalls of this equipment are the impossibility of loading with single direction forces, the narrow frequency vibration band and lacking of measurement of the generated forces.

@seismicisolation

The vibrator was located on pier 2D and velocities were measured at several points (fig. 2). About 80 different samples were taken, corresponding to different exciting frequencies. For each sample 120 Hz sampling frequency and 512 points were used, meaning about 4 s time series.

2.4. Data treatment

A computer code was developed at LNEC for the treatment of ambient noise test results. This code mainly consists in a numerical zoom and an averaging technique. The time series are divided in smaller overlapping samples, which are treated by numerical zoom, and which Fourier spectra are averaged. This technique aims at smoothing the spectral estimates obtained. This is a very plain method whose only purpose is the identification of fundamental frequencies by simple inspection of the Fourier spectra.

The time series obtained in the forced vibration tests were treated by means of a computer code. It starts by applying a cosine-taper window to reduce leakage effects. The Fourier Transform of the time series is then computed. Once in the frequency domain, integration to obtain displacements, deconvolution of transducer TF and band-pass filtering centered in the exciting frequency are performed. At this point the Inverse Fourier Transform is computed yielding a new time series, now almost purely sinusoidal, which amplitude is determined and divided by the exciting force computed by expressions (1) and (2) yielding the value of the force-displacement TF for the exciting frequency.

MODAL PARAMETER IDENTIFICATION

The scheme proposed for modal parameter identification includes three steps. In the first one a single degree of freedom (SDF) algorithm was used for parameter estimation. These first estimates were then used as initial guesses for the N degree of freedom (NDF) identification algorithm. This second algorithm was used twice: the first time it was used to obtain modal estimates for each TF; the new parameters were then used as initial guesses for the last step. In this step modal parameters were found for several TF simultaneously, aiming at obtaining modal parameters for the whole structure rather than for a set of different points studied separately.

3.1. Single degree of freedom algorithm

The SDF algorithm used in this work was proposed by Mau and Wang, 1989 [9]. It replaces the classical Half-Power Bandwidth (HPB) method earlier used at LNEC [10]. The need to replace the HPB comes from its major drawbacks:

i) the frequency-response curve must be suficiently well defined to show a clear bandwidth at the half-power level below the peak, what is not always the case when there is modal interference and;

ii) the whole method depends on a single point of the curve, its maximum (the point where experimental errors are larger).

@seismicisolation

A computer code was developed to identify modal parameters

by this method, using typically 10 to 15 points to each mode.

The drawbacks of the SDF approach are:

i) only modes of vibration for which the TF peaks are well defined can be identified by this method; and

ii) for the same mode of vibration, frequency and damping change from point to point.

3.2. N degree of freedom algorithm

In order to eliminate the drawbacks of the SDF approach a NDF algorithm was developed.

The first step consisted in finding the minimum of the function Δ

$$\Delta = \sum_{k=1}^{N} \left(|H(\overline{\omega}_k)| - \overline{A}_k \right)^2 \qquad (3)$$

where $H(\overline{\omega}_k)$ is the TF value obtained with the fitted parameters, $\overline{\omega}$ is the angular frequency of the exciting force, $\overline{A}_k$ is the experimental value of the TF modulus and N is the number of exciting frequencies, i.e., test points on the TF determined from forced vibration tests. $H(\overline{\omega}_k)$ is:

$$H(\overline{\omega}_k) = \sum_{i=1}^{NM} \frac{P_i}{(\omega_i^2 - \overline{\omega}_k^2) + (j2\xi_i\omega_i\overline{\omega}_k)} \quad ; \quad k=1,\ldots,N \qquad (4)$$

where NM is the number of modes to be identified, ω_i is the modal angular frequency for mode i, ξ_i the modal damping ratio and P_i the modal participation factor.

In equation (4) the modulus of the adjusted TF is used because the experimental technique does not allow the determination of the load-response phase lag.

The minimization of function Δ is done by a general gradient method where the SDF results enter as initial guesses. Function Δ derivatives to the modal parameters ω_i, ξ_i, P_i (i=1,...,NM) are computed from:

$$\frac{\partial \Delta}{\partial \omega_i} = \sum_{k=1}^{N} 2 \frac{\partial |H(\overline{\omega}_k)|}{\partial \omega_i} \left(|H(\overline{\omega}_k)| - \overline{A}_k \right) \qquad (5)$$

where

$$\frac{\partial |H(\overline{\omega}_k)|}{\partial \omega_i} = \frac{1}{2|H(\overline{\omega}_k)|} \frac{\partial |H(\overline{\omega}_k)|^2}{\partial \omega_i} \qquad (6)$$

where $\frac{\partial |H(\overline{\omega}_k)|^2}{\partial \omega_i}$ can be easily computed. Identical formulae were used for the other derivatives.

Results obtained with this method for the first four modes of vibration (12 parameters), are presented in figure 3. Modal parameters are summarized in table I.

A generalization of the NDF algorithm presented above consisted of finding the minimum of a new Δ function:

@seismicisolation

$$\Delta = \sum_{n=1}^{NTF} \sum_{k=1}^{N} \left(|H_n(\overline{\omega}_k)| - \overline{A}_{kn} \right)^2 \qquad (7)$$

Table I - Modal parameters from NDF algorithm

POINT	MODE 1			MODE 2			MODE 3			MODE 4		
	f (Hz)	ξ (%)	p (*)	f (Hz)	ξ (%)	p (*)	f (Hz)	ξ (%)	p (*)	f (Hz)	ξ (%)	p (*)
1	2.79	3.2	1.69	3.32	4.4	1.85	4.41	1.8	0.65	5.50	17.6	20.32
2	2.78	3.7	2.28	3.31	8.1	-.22	4.66	26.6	17.01	5.46	18.1	-16.32
6	2.78	3.9	2.51	3.30	4.9	-1.72	4.45	5.6	-2.32	5.28	27.5	3.76
7	2.76	3.8	2.88	3.29	4.8	3.07	4.39	3.58	2.65	5.35	8.2	6.86

(*) - $\mu m(kN)^{-1} rad^2 s^{-2} x10^2$

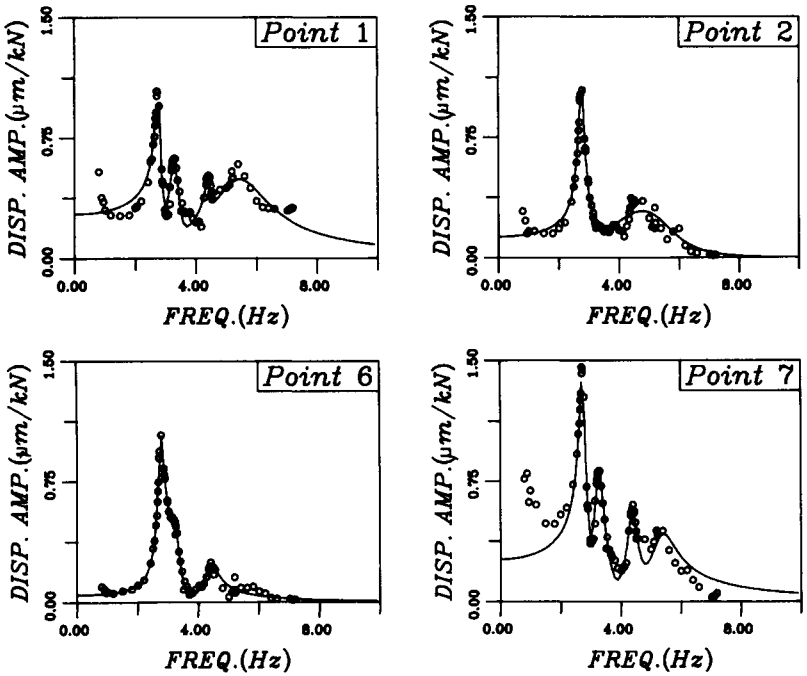

Figure 3. NDF algorithm. Fitted TF.

what is no more than considering the simultaneous parameter fitting over NTF experimental transfer functions, one for each point tested.

The fitted transfer function $H_n(\overline{\omega}_k)$ is now:

$$H_n(\overline{\omega}_k) = \sum_{i=1}^{NM} \frac{P_{in}}{(\omega_i^2 - \overline{\omega}_k^2) + (j2\xi_i\omega_i\overline{\omega}_k)} \quad ; \quad k=1,\ldots,N; \; n=1,\ldots,NTF \tag{8}$$

@seismicisolation

The new set of parameters is:

$$\omega_i \ , \ \xi_i \ , \ P_{in} \qquad i=1,...,NM \ ; \ n=1,...,NTF \tag{9}$$

what means that the number of parameters to be fitted is:

$$NPAR = 2 \times NM + NTF \times NM \tag{10}$$

instead of

$$NPAR = 3 \times NM \tag{11}$$

as in the latter algorithm.

The obvious advantage of this approach is that one may now treat the structure as a whole, i.e., the frequencies and damping

Table II - Modal parameters from NDF generalized method

MODE	f_i (Hz)	ξ_i (%)	POINT [$\mu m(kN)^{-1} rad^2 s^{-2} x10^2$]			
			p_{i1}	p_{i2}	p_{i6}	p_{i7}
1	2.78	3.6	1.79	2.42	2.41	2.75
2	3.31	5.0	2.09	0.42	-1.73	3.15
3	4.41	3.9	1.21	2.16	-1.49	2.37
4	5.36	14.2	16.24	-5.97	2.09	10.59

ratios obtained are much more meaningful.

Table II and figure 4 present results obtained with this method for the first 4 vibration modes and for 7 points in a total of 36 parameters.

FINITE ELEMENT ANALYSIS

4.1. Model characteristics

The mathematical model of the dam-foundation-reservoir system was fitted to the test results. These showed that the structure behaves as a whole and therefore a 3D beam equilibrium model was considered. The 9 piers of the structure were linked by the beams supporting the gantry crane.

Field tests had shown important relative movements between the piers and the bridge. So, no stiffness effects were assumed and the road bridge was only considered as an associated mass.

In order to fit the mathematical model vibration frequencies to the frequencies given by the forced vibration tests it was necessary to assume that the piers are simply supported at stilling basin level [11].

The influence of alluvia was considered negligible and the reservoir was assumed empty.

@seismicisolation

To fit the first vibration frequency the Young modulus was taken as 40 GPa for the upper zones of the piers, while for the zones embedded in alluvia it was taken as 20GPa to take into account the difficult construction conditions. The modal damping

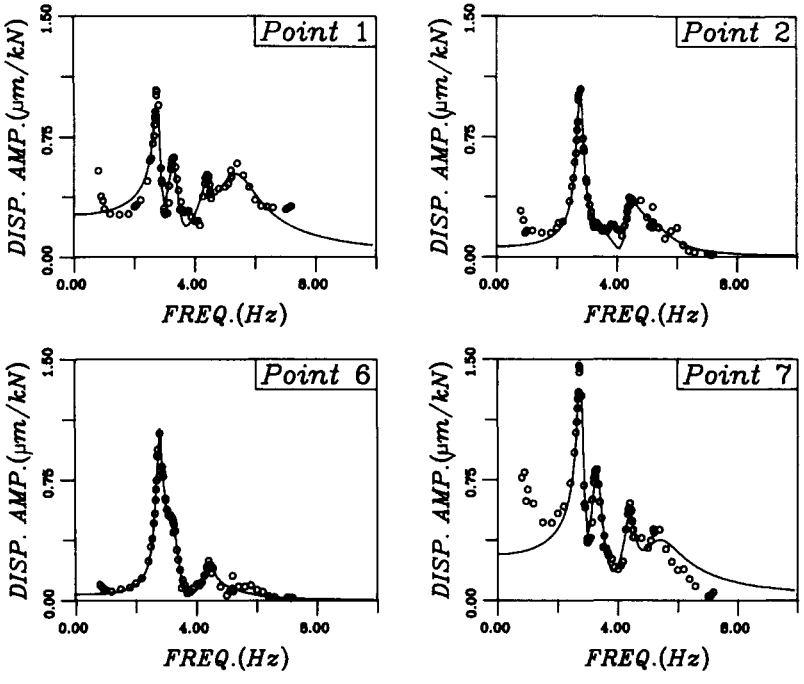

Figure 4. Generalized NDF algorithm. Fitted TF.

ratio was 2.5% for all modes of vibration considered.

This model was analysed by the finite element method, using 62 3D beam elements (fig. 5). To compute the force-displacement

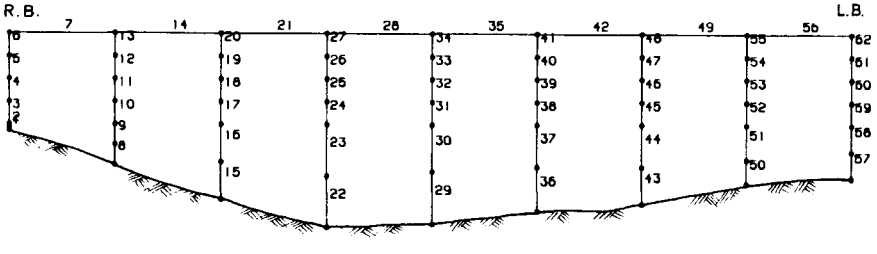

Figure 5. Finite element model.

@seismicisolation

transfer functions, the model was loaded with a frequency variable unit sinusoidal force identical to the one produced by the vibrator.

4.2. Comparison between experimental and mathematical results

Table III shows finite element results and test results. TF

Table III - Comparison of vibration frequencies

MODE	TESTS	F.E.M.
1	2.78	2.78
2	3.31	3.39
3	4.41	4.52
4	5.36	5.50

and modal vibration shapes are compared in figure 6.

This model reproduces adequately the structural behaviour computed from the forced vibration test results.

CONCLUSION

"In situ" dynamic tests, namely forced vibration tests, are important for safety assessment of large structures, such as large dams.

The fundamental part of the interpretation of forced vibration test results is modal parameter identification. It is based on either single or multiple degree of freedom algorithms. The former are used as initial guesses for the latter. NDF methods yield more significant results when used for the different points of the structure simultaneously.

The test results gave important information about the mechanical and geometrical characteristics of the structure. In fact the modal parameters obtained were used to fit the mathematical model to reproduce approximately the observed behaviour of the structure.

Future developments will concern the testing technique and the identification methods. For the testing technique the main development will be the measurement of force response phase-lag and of force amplitude. The identification methods will be adapted to the new testing technique.

@seismicisolation

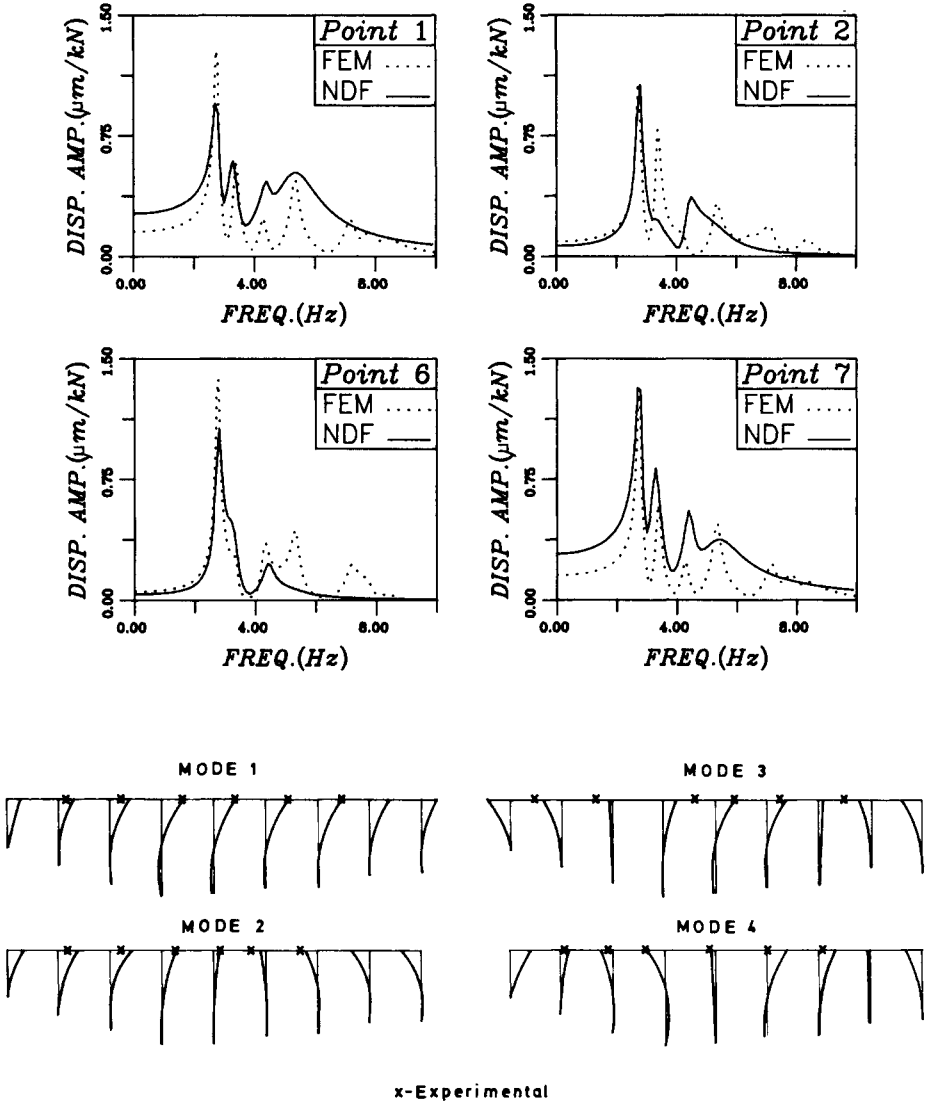

Figure 6. Comparison between experimental and analytical results.

REFERENCES

1,2,3,4 - LNEC, 1962, 1962, 1977, 1978 - "Dynamic measurements of Cabril dam", "Dynamic measurements of Bouçã dam", "Cahora-Bassa dam dynamic response", "Observation of concrete dams behaviour for dynamic loads", Internal reports, Lisbon (in portuguese).

@seismicisolation

5 - Pedro, JO; Silva, AF; Pereira, J; Florentino, CA; Pinho, JS; Câmara, R; Silva, H; 1986 - "Seismic monitoring of concrete dams and reservoirs. Portuguese experience." 8th ECEE, Lisbon.
6 - CPE - "Escalão de Crestuma. Projecto." Companhia Portuguesa de Electricidade, Oporto, May 1972 (in portuguese).
7 - Ribeiro, A; Lemos, AO; Ramos, CM - "Bed protection downstream of a big dam founded in alluvia." XIth International Congress on Large Dams, Q. 41, R. 38, Madrid, 1973.
8 - LNEC - "Mechanical vibrator. Design, construction and assemblage." Internal report, Lisbon, 1965 (in portuguese).
9 - Mau, ST; Wang, S - "Arch dam system identification using vibration test data." Earthquake Engineering and Structural Dynamics, Vol. 18, 419-505, 1989.
10 - LNEC - "Study of Crestuma dam dynamic behaviour." Internal report, Lisbon, 1990 (in portuguese).

@seismicisolation

EXPERIMENTAL STUDY OF HYSTERETIC ENERGY ABSORPTION AND LOAD CAPACITY OF REINFORCED CONCRETE COLUMNS SUBJECTED TO DIFFERENT CYCLIC LOADING RATES

G. Verzeletti, S. N. Bousias, E. Gutierrez, G. Magonette and P. Tognoli
Commission of the European Communities, Joint Research Center, Ispra 21020, ITALY

ABSTRACT

Full-scale cyclic tests on 5 reinforced concrete (R/C) slender column elements were carried out at 2 10^{-3} and 0.2 Hz at displacement amplitudes sufficient to cause considerable damage. The effect of the loading rate is studied with reference to the envelope of the load carrying capacity, and the distribution of the rotation along the column length. The equivalent viscous damping associated with the hysteretic behaviour was found to be rate independent in the range studied. The structural degradation is represented as a function of the cyclic secant stiffness normalized by the elastic stiffness.

INTRODUCTION

One of the activities to be carried out in the Reaction Wall Facility (RW) currently under construction at the JRC, Ispra, will be the behaviour of R/C structures subjected to seismic loading. This facility will provide the ability to test full-scale structures up to 16 m high, thus eliminating many of the complexities of scale effects usually encountered in tests carried out on a shaking table. One of the testing procedures to be used on the RW will be the Pseudo-Dynamic Test Method (PDTM) (1) performed at a loading rate which may be, typically, three orders of magnitude lower than under earthquake loading conditions; thus it is important to quantify possible rate effects on the structural response.

In the papers by Shah et. al [2] and Chung [4], significant rate effects were found on model R/C column-slab joints in the frequency range of 2.5 10^{-3} to 1 Hz; those results were consistent with those of Kitigawa et al. [3] on 1/2 scale 2 storey R/C structures tested using both PDTM and shaking table techniques. In view of the limited number of experimental data and the fact that they were obtained from model specimens, our research aimed at providing some analogous information on full-scale specimens. In addition, a cycle per cycle evaluation of the secant stiffness degradation and hysteretic equivalent damping parameters, as a function of the displacement amplitude, was undertaken.

@seismicisolation

DESCRIPTION OF SPECIMENS AND TEST SET-UP

The specimen elevation and the cross-sectional reinforcement are illustrated in Fig. 1. The specimen was 1.5 m high with a square section of 300 mm side. The longitudinal reinforcement consisted of six 20 mm deformed bars bolted at the top of the column on a thick steel plate used for the load transfer on the unit. The transverse reinforcement consisted of 8 mm diameter bars spaced every 70 mm up to 600 mm from the column base and every 150 mm along the rest. Prepared in-place normal density concrete with 35 MPa compressive strength was used for all specimens tested, while the yield strength of steel was 460 MPa.

As the construction of the RW has not yet been completed, a steel reaction frame was designed in the form of a truss, as depicted in Fig. 2. The loading arrangement consisted of a piston mounted on a cradle between two swivel joints. In order to avoid transverse column deformations, the column was constrained normal to the loading plane by two nylon bearings. The moment arm was effectively 1530 mm and the maximum piston stroke amplitude was 135 mm. The instrumentation layout is shown also in Fig. 2. In addition to the piston stroke displacement, the actual column end displacement at the load line was measured from a reference frame mounted on the slab. The column rotations at three levels from the base were measured by three pairs of LVDTs spaced every 300 mm (one column width). Strain gauges were mounted at different heights on the central bars.

The displacement controlled path consisted typically of four cumulative uniaxial bending cycles at a given amplitude level; this pattern was repeated with increasing levels, 130 mm being the maximum displacement applied. No axial load was applied. Limitations in the hydraulic power imposed 0.2 Hz being the maximum rate that could be applied for the displacement level sought. A typical path is shown in Fig. 3. Table 1 provides the main experimental details and specimen nomenclature.

Table 1. Summary of testing programme

Test	Frequency (Hz)	Peak Displ. (mm)	Comments
L01	0.002	100	No bar buckling
L02	0.002	120	No bar buckling
H01	0.2	120	No bar buckling
H02	0.2	130	Buckling over 100 mm
H03	0.2	120	No bar buckling

EXPERIMENTAL RESULTS

Column Behaviour

All specimens exhibited predominant flexural behaviour owing to a number of parameters (no axial load, considerable transverse reinforcement, high shear span ratio). While it can be said that both loading rates produced obvious damage around the column base, in the high strain rate tests the damage and crack formation was more concentrated around the column base whilst in the slow test some cracks extended as far as 2/3 of the column length from the top of the base. The same observation is supported by the results of Shah [2]. The different crack distribution between fast and slow tests manifests itself in the rotation measurements. This is consistent with Ref. [3] where correlation tests between dynamic and pseudo-dynamic testing procedures on half-scale R/C structures are reported; the results show cracking patterns in the dynamic event as being more concentrated than in the corresponding quasi-static PDT test.

@seismicisolation

The hysteresis loops for a low frequency test (L02) are shown in Fig. 4, and those obtained from the two fast tests (H01 and H03) in Figs. 5 and 6. At first glance no obvious difference exists, apart from a slight deterioration in the load carrying capacity in H03, with cumulative cycling. A more revealing picture of the column response, may be obtained by analysing the data on a cycle per cycle basis. In Fig. 7, the envelope of the peak loads (average peak-to-peak forces at a given displacement amplitude) versus nominal displacement level, is shown. The broken line represents the mean of the two slow tests, while the continous one that for the fast tests. The reason for averaging was the scatter in the peak load levels, probably owing to differences in concrete strengths. It is seen that the load at the faster rate is about 5% higher for displacements of 40 mm and over. Although the individual load envelopes were found to have a scatter of the same order, the highest load envelope did correspond to a fast test and conversely so for the lowest. The observations made by Shah et. al [2] that the maximum load carrying capacity of their two R/C models tested was higher at the faster frequency, seems to be verified, although in their findings a 10% increase is reported (with a loading rate five times higher than our highest)

With the set-up developed, it has been possible to observe the mean column relative rotation at levels of 300, 600 and 900 mm from the base. From 0-300 mm, the rotation is proportional to the displacement amplitude and thus the column "hinge" is below this level (Fig. 8). The position of the "plastic hinge" is as well verified by observing the rotation measured along the gage length between 300-600 mm, where the rotation is shown to be fairly independent of the displacement level. As regards the difference between fast and slow deformation rates the situation is as follows: in the lower gage length (0-300 mm) the higher damage (as verified by the cracking pattern) is exhibited by the specimen subjected to a fast deformation rate and thus higher rotations are recorded in this case. Passing to the next gage length (300-600 mm) the inverse holds; the spreading of cracking and hence of damage in the slow strain rate case makes the rotations larger than the ones recorded in the fast test.

Characterization of Hysteretic Behaviour

A column-slab joint subjected to reverse bending cycles may be modelled as a discrete parameter system consisting of a spring (column) and the associated inertial mass within the framework of a larger structure of which it is part. When the column is subjected to cyclic excursions in the plastic range, the hysteretic behaviour will provide the system with an energy absorbing mechanism and induce a change in the restoring forces which are nonlinearly related to the displacements. It is well known that this behaviour will affect the dynamic response of the system. In order to quantify these non-linearities, the hysteretic behaviour of the spring element is first studied by conducting quasi-static, cyclic, displacement controlled experiments. Typical load-deflection characteristics are shown in Fig. 9 below.

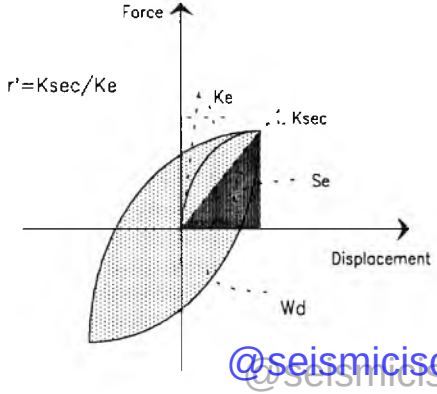

Fig. 9 Typical Hysteresis loop

@seismicisolation

The energy loss per cycle may be expressed in the same way as is done for a viscous damper described in (5), namely;

$$\eta = W_d / (4 \pi S_e) \qquad (1)$$

The term η (%) is the equivalent damping factor and W_d and S_e are the dissipated energy per cycle and the maximum strain energy, respectively.

The stiffness degradation is expressed as the ratio of the secant stiffness to the elastic stiffness thus

$$r' = K_{sec}/K_e \qquad (2)$$

For the purely hypothetical case of displacements in the elastic range, η will be equal to zero and r' will be 1. The values of η and r', as specified in equations (1) and (2), were evaluated from the experimental load-deflection loops as illustrated in Fig. 9. It should also be noted that r' is also the square of the ratio of the damaged to the initial natural frequency.

The damping factor values have been plotted versus displacement for test L02, as families of first, second pass, etc., at the given amplitude (Fig. 10). By increasing the displacement amplitude, damping increases in a manner similar to the load envelope. The first cycle at a given displacement exhibits higher damping factor than the three cycles that follow it, but the difference between the first and the second is greater than between the latter and the third and fourth. As the displacements increase beyond 80 mm the curves generally level off. What happens beyond the 100 mm range will be commented on later.

Fig. 11 shows the variation of r' with the displacement amplitude. For the loading path followed in the tests, it is seen that increasing the displacement amplitude increases the damage experienced by the column, thus reducing r'. However, repeating a cycle at the same displacement does not considerably decrease it, this is observed as the small step-like drops in Fig. 11. This figure could also be derived by using the common assumption that the response of a member in cyclic loading possesses an envelope which in good approximation can be assumed to be the monotonic force-displacement curve.

The cross-plot of r' versus η shown in Fig. 12, is an adimensional characterisation of the load-deflection hysteresis loops of test H03, once again, each curve represents the repetition cycle number at a given displacement amplitude. The physical behaviour is best understood in conjunction with the preceding r' versus displacement amplitude plot. The following is an example.

The first four cycles of test H03 had a 20 mm displacement amplitude, now for the first cycle the value of r' (from Fig. 11) was 0.33 thus η (from Fig 12.) is 16% . For the next three cycles r' varies little but η drops down to 9, 7 and then 6%. The data in Fig. 12 is represented in Fig 13, but here, the data points are joined in historical sequence and not by their position in the cycle repetition. Generally the η value for all the columns tested incresaes as a funtion of displacement up to amplitudes of 100 mm after which two cases were observed: for test H03 the pronounced pinched form of the hysteresis loops causes the equivalent damping to decrease as observed by the knee formed in the curves in Fig 12 . In test H01 no such knee was present, as in this test buckling of the corner bars influences the shape of the hysteresis loops such that the ratio of the work done to the potential energy continues to increase.

The material properties in the (r',η) plane, for a given path, are found to be quite insensitive to the rate of loading. Considering that the rate effect increases the load carrying capacity, then an increase in the S_e term in Eq. 1 is offset by an increase in W_d. In other words, the rate effect is noticable in the absolute levels of the force-displacement envelope but not in the shape of the hysteresis loops from which the terms η and r' are derived. The authors suggest that the general shape of the curves in Figs 12 and 13 is applicable to any R/C column displaying flexural response. It is proposed that from a monotonic force-displacement curve, an evaluation of r' is first made and

@seismicisolation

η is calculated using a mapping, of the form of Fig. 13, developed from the history of the response, ie. considering the number and the amplitude of the cycles. These material properties could be used within the framework of an integration scheme of the equations of motion which represent a dynamical system consisting of column-slab elements, whence, in the plastic range, the damping and stiffness matrices would be kept constant during the duration of a cycle and updated at the end of it. This approach is currently under investigation.

CONCLUSIONS

Cyclic displacement controlled uniaxial flexure tests on full-scale R/C columns were carried out at 2 10^{-3} and 0.2 Hz. The results obtained seem to confirm those reported in the literature for scaled column specimens, in the sense that at quasi-static loading rates the mean column strength is about 5% lower than in the faster tests. Although the strain rate effect is consistently observed, it is proposed to perform a test that excludes material property scatter, such as testing a single column at alternate fast and slow frequencies and observing the load decrement with repeated cycles. The observed damage in the case of slow deformation rate tests consistently produced more dispersed cracking which was also depicted in the rotation measurements along three gauge lengths at the base of the column. Referring to the application of the PDT method, to date, the results for rates of deformation one order of magnitude less than those under earthquake action show that no major problems are posed by the presence of the measured effect of the rate of loading on the R/C member response.

The equivalent damping factor characteristics of such columns was found to be in the order of 25% at the point of maximum load carrying capacity and appears to be effectively rate independent. The decrease in the normalised secant stiffness was correlated to the equivalent damping characteristics to depict the possible general dynamic behaviour of elements such as the ones tested for monotonically increasing cyclic displacements as have been presented here. With the use of the linearization technique previously described, the behaviour of R/C members under dynamic conditions can be simulated, as long as the dynamic excitation has the form of the displacement path used in the tests presented here. Hence, further experimental studies are needed for covering cases of displacement histories more representative of those in seismic conditions in order to evaluate a more general r'-η mapping relation

REFERENCES

1. Tanaka, H., "A Computer-Actuator On-Line System for Non-Linear Earthquake Response Analysis of Structures", Seisan Kenkyu Institute of Industrial Science, The University of Tokio, Japan, Vol. 27, No. 12, Dec. 1975, 15-19.

2. Shah, S.P., Wang, M.L., and Chung, L.,"Model concrete beam-column joints subjected to cyclic loading at two rates", Materials and Structrures, 1987, Vol. 20, pp. 85-95.

3. Kitagawa, Y., Kubota, T., Kaminosono, T., Kubo, T., "Correlation study on Shaking Table Tests and Pseudo-Dynamic Tests by R/C Models", 8th World Conference in Earthquake Engineering, San Fransisco, 1984, Vol. VI, pp.

4. Chung, L., Shah, S.P.,"Strain Rate Effects on Bond Stresses during Earthquake Loading", Proc. Pasific Conf. on Earthquake Eng., New Zealand, 5-8 Aug., 1987.

5. Clough., R.W., Penzien, J., "Dynamics of structures", McGraw-Hill 1975

@seismicisolation

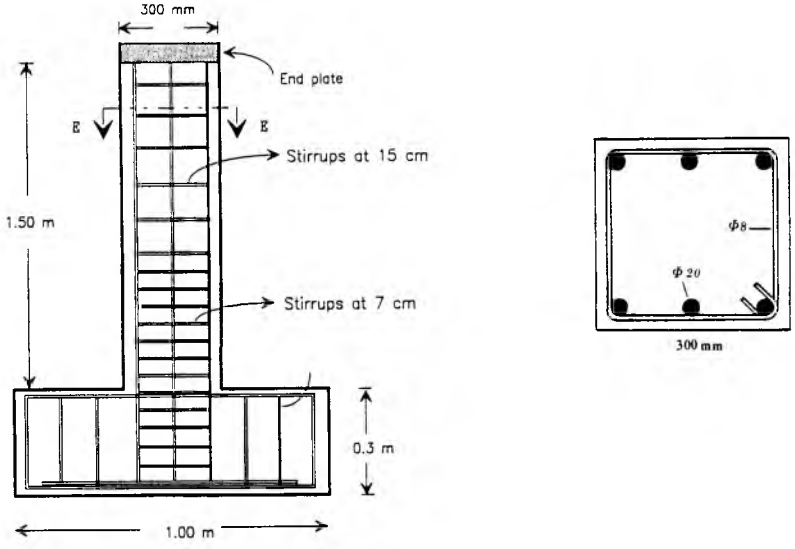

Fig. 1 Specimen elevation and cross-section

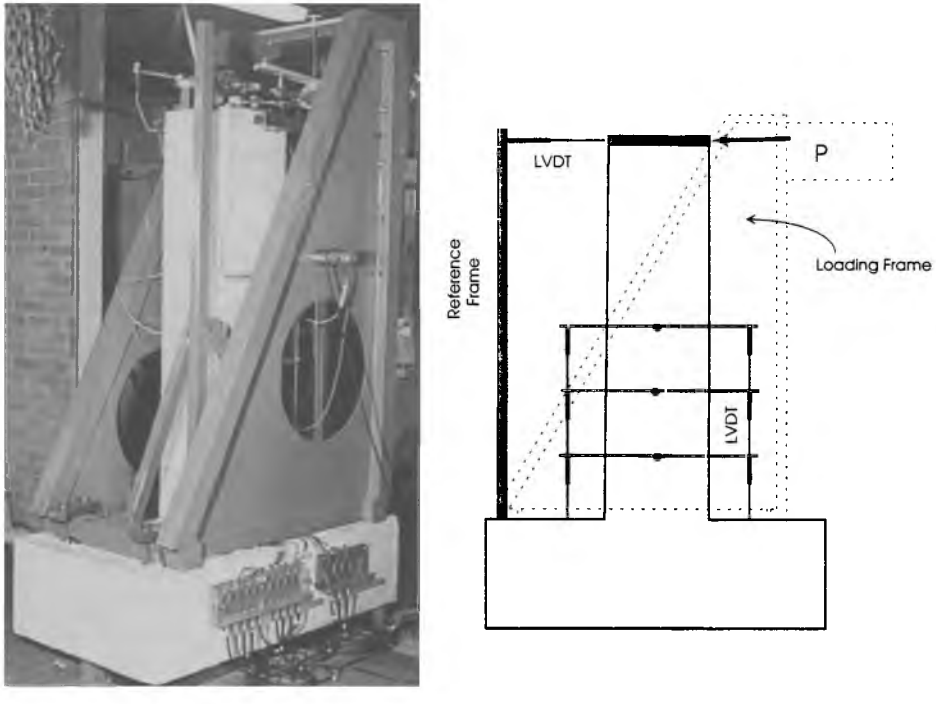

Fig. 2 Steel frame and specimen instrumentation

@seismicisolation

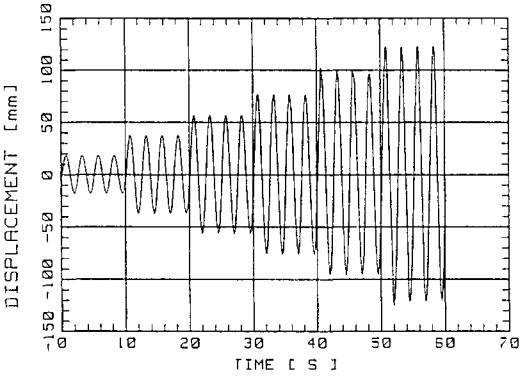

Fig. 3 Loading path

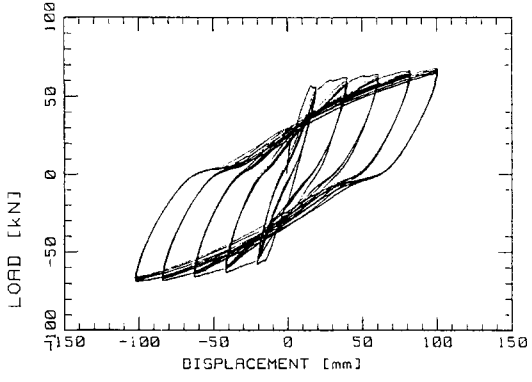

Fig. 4 Hysteresis loops for specimen L02

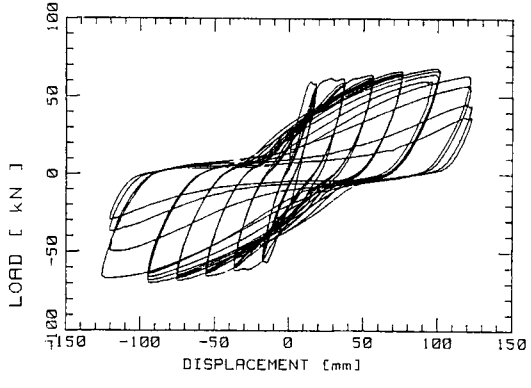

Fig. 5 Hysteresis loops for specimen H03

@seismicisolation

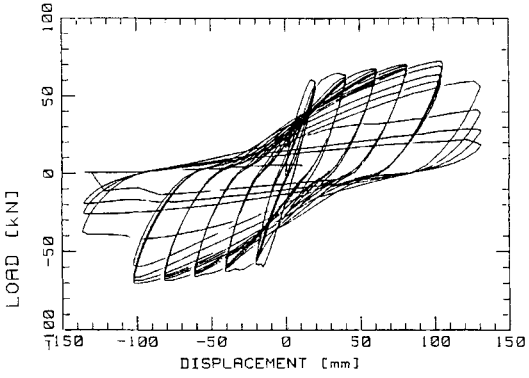

Fig. 6 Hysteresis loops for specimen H01

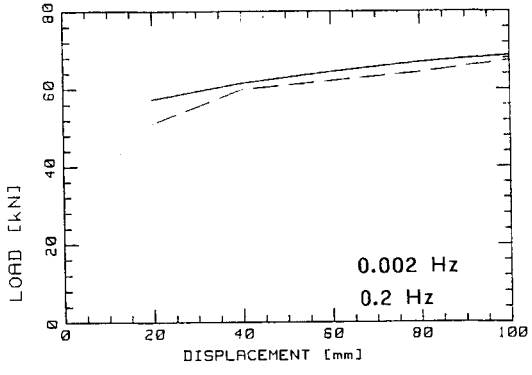

Fig. 7 Comparison of force-displacement first cycle envelopes

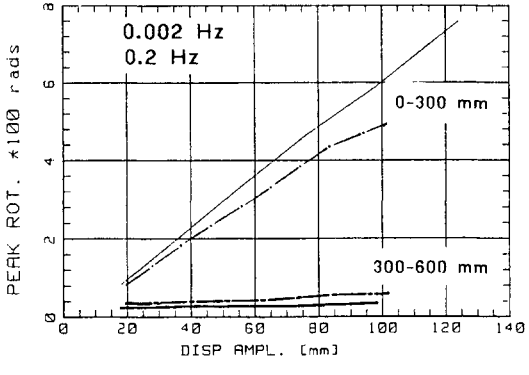

Fig. 8 Measured rotation at 300, 600 mm levels

@seismicisolation

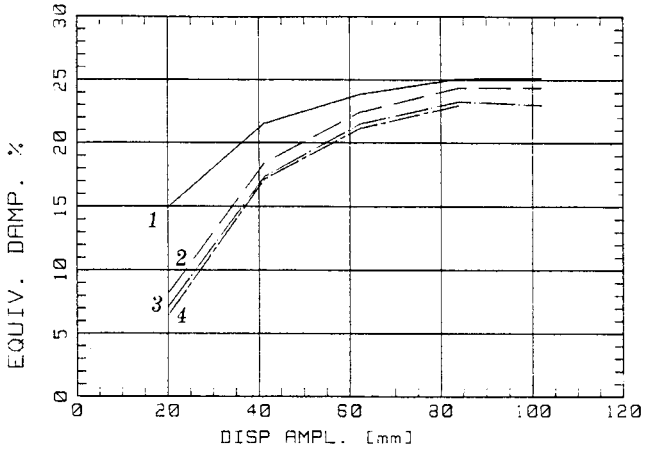

Fig. 10 Evaluated damping coefficient (L02)

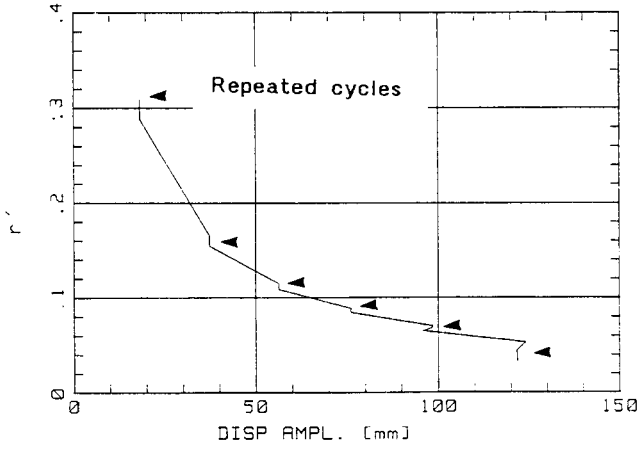

Fig. 11 Variation of normalised secant stiffness vs. displacement for H03

@seismicisolation

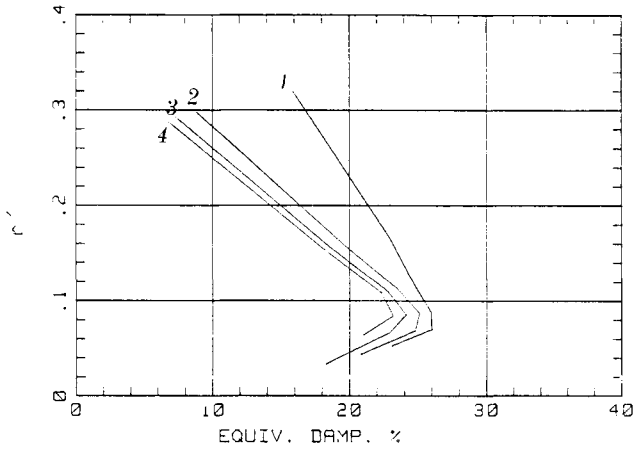

Fig. 12 Variation of normalised secant stiffness vs. damping for H03 (as families of cycle repetition number)

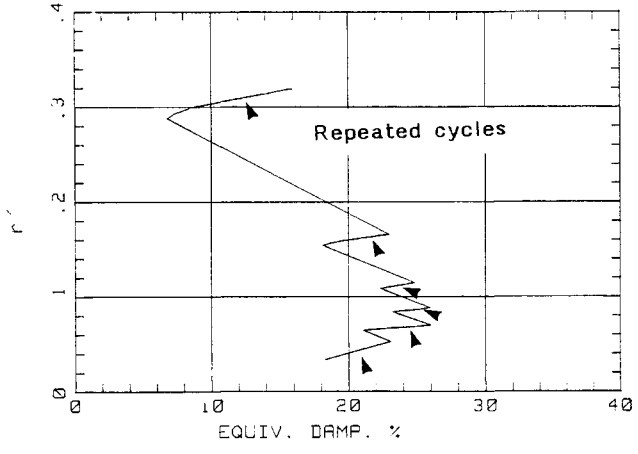

Fig. 13 Variation of normalised secant stiffness vs. damping for H03 (historical progression)

@seismicisolation

PHYSICAL MODELLING OF EARTHQUAKE EXCITATION FOR GEOTECHNICAL ENGINEERING

Dr R S Steedman
Director, BEQE Limited, 278 Cambridge Science Park, Milton Road, Cambridge.

Dr X Zeng
Research Fellow, Churchill College, Cambridge.

ABSTRACT

There have been considerable developments in recent years in dynamic modelling techniques for geotechnical engineering. These include new shaking systems, new data recording and analysis techniques and projects involving collaboration between researchers using different modelling techniques. In the literature centrifuge test data has been used to demonstrate how the physical modelling tests may help engineers to understand seismic problems in the field and hence to help prepare remedial measures and future designs. Shaking tables both working on a centrifuge (high g) and at normal gravity (1g) have been used cooperatively to study dynamic problems in geotechnical engineering.

INTRODUCTION

The technique of physical modelling has been used to study dynamic geotechnical engineering problems for many years. As early as the 1920s shaking tables were constructed in Japan to investigate soil structure interaction problems. In the late 1970s a shaking table was mounted on the Cambridge Geotechnical Beam Centrifuge, thus greatly expanding the capability of shaking table systems. The period 1980 to 1990 saw a rapid development in dynamic centrifuge modelling techniques. New shaking systems have been or are being built for centrifuges in the UK, Japan and the US. New data recording and acquisition facilities have helped to record a wide range of information during dynamic centrifuge tests. Collaboration between researchers in both physical modelling and numerical modelling is now one of the most active fields in geotechnical engineering research.

Two basic issues need to be addressed before centrifuge data can be directly applied to engineering practice. The first issue is the reliability of the data of centrifuge tests and the second is to what extent centrifuge modelling may benefit the prototype design. The experience of dynamic centrifuge modelling at Cambridge University for over a decade has shown that a great deal of valuable data can be obtained from centrifuge tests. The most outstanding achievement by far is that centrifuge modelling has made a major contribution in the understanding of the basic mechanisms of soil-structure interaction during earthquakes. As will be shown by example data of dynamic centrifuge tests have identified the fundamental mechanisms in the failure of a range of prototype soil structures during earthquakes. Based on these mechanisms simple engineering calculations can be used effectively to estimate the response of soil structures during earthquakes. With the continuing fast development in the technology of data acquisition systems it has also become possible to record data accurately enough for engineering purposes.

@seismicisolation

The most widely available technique of physical modelling is the shaking table working at normal gravity (1g). There is a great deal of published data of 1g shaking table tests carried out on a number of geotechnical engineering problems. Generally speaking the 1g shaking table has the advantage of being relatively cheap to construct and manage, and it is relatively easy to make detailed models. The 1g shaking table is therefore very useful for a parametric study, for example. The most recent development in 1g shaking table facilities in the UK is the new SERC shaking table at Bristol University which has a maximum payload of 15 tonnes. This can be compared with a giant shaking table in Japan with a maximum payload capacity of up to 1,000 tonnes which has been put into operation at the Nuclear Power Engineering Test Centre. The cost of a model test on such a large shaking table would be substantial, as each experiment takes many months.

The scaling relationships for a shaking table test at 1g create a difficulty for data interpretation especially for tests involving large strain or significant excess pore pressure. Centrifuge model tests have the advantage of having the same stress and strain at homologous points in model and prototype and thus the scaling relationships are much easier to satisfy. Furthermore the size of the prototype structure that can be modelled on a centrifuge is generally much larger. For the Cambridge Geotechnical Beam Centrifuge the maximum payload of soil for earthquake tests is currently 135kg, which when testing at a typical working speed of 80g is identical to 135×80×80×80 = 69,000 tonnes of soil at prototype scale. This payload capacity is much higher than any feasible 1g shaking table. However as the g level is increased on a shaking table both the frequency of excitation and the force required to shake the model also increase, making it more and more difficult to apply a broad band input. In the example quoted above the 135 kg of soil is contained in a stringbox giving a total shaking mass of 270 kg. At 80g this mass weights 21.6 tonnes and therefore to produce a 0.4g, 1 Hz prototype motion a force of around 9 tonnes at 80 Hz is required. Clearly the peak instantaneous power required is also rising as the g level increases and this creates substantial difficulties in the confined space available on a centrifuge for energy storage and mechanical actuators. The 1g and high g shaking table can be seen as forming part of a spectrum of modelling in which each has an important role: the 1g table at scales of 1:1 to about 1:10 and the centrifuge from about 1:10 to around 1:200. Above about 1:200 dynamic models can be tested but this requires the use of explosives. At these g levels mechanical actuation is extremely difficult with current technology. This spectrum of modelling was proposed by Steedman (1).

DEVELOPMENT IN DYNAMIC CENTRIFUGE MODELLING

The principles of centrifuge modelling tests were first discussed in detail by Pokrovsky (2) at the First International Conference on Soil Mechanics and Foundation Engineering. During a model test, the rotational motion of the centrifuge creates a radially directed acceleration field which is similar to the prototype gravitational acceleration field. The principal scaling relation is that a model constructed by the same soil with dimensions scaled down by 1/N and subject to an acceleration field increased by N times leads to identical stresses at the corresponding points in the model as in the prototype. As the mechanical properties of soil are stress-dependent, a correctly scaled centrifuge model will show identical behaviour to that of the corresponding prototype soil structure.

Although the centrifuge modelling technique has been used in geotechnical engineering research for over half a century the application of the geotechnical centrifuge to study earthquake problems began in earliest in the late 1970s with the construction of the Bumpy Road Actuator on the Cambridge beam centrifuge. The Bumpy Road Actuator is a mechanical shaking system which obtains the energy for shaking from the kinetic energy of the rotating rotor. The detail of the system was described by Schofield (3) and Kutter (4). The model earthquake it generates has a characteristic 10 cycle vibration and a fixed frequency which is determined by the testing speed. However both the number of cycles and the frequency of vibration can be varied by changing the track fixed on the wall of the chamber. Since it was commissioned in 1980, a wide variety of tests have been carried out on models of retaining walls, embankments, artificial islands, embedded structures, dykes, piles and rocking towers. The data of these tests are reported in

@seismicisolation

detail in the technical reports of the University Engineering Department and are available for both engineers and research workers. Dynamic centrifuge tests on this facilities have formed the major part of eight PhD theses alone of the Cambridge Soils Group, with two more currently in preparation. The Bumpy Road shaking system has by far the largest payload of any centrifuge shaker. New shakers are planned for Japan and the USA, however, which will dwarf even this facility.

The last decade saw a rapid development in dynamic modelling techniques on geotechnical centrifuges. For example in the US alone there are at least six universities which have the capability of carrying out dynamic centrifuge tests. In Japan there is a highly active group of researchers using shaking systems on centrifuges at a number of universities. Most of these systems were reported by Steedman (5).

At the same time as the development in new shaking systems, progress has been achieved in the techniques of data recording, data acquisition and analysis. High speed data acquisition systems, which are essential for dynamic centrifuge tests because of the high frequency of model earthquakes, are now widely available. Transducers such as accelerometers and pore pressure transducers are made smaller and more accurate. New types of transducers such as bender elements have been developed for use in dynamic centrifuge tests. Data analysing techniques such as cross-correlation, spectral analysis and windowing are frequently used. All this leads to higher quality, more reliable and accurate data which will have an important bearing on practical problems in the field.

One of the major concerns of geotechnical engineers in the field for dynamic centrifuge modelling is the boundary conditions in a model test. Most of the model packages so far used have rigid, smooth end walls and this undoubtedly causes energy reflection at these boundaries, which is different from the infinite half space in the prototype which it intends to model. A second problem with rigid boundaries is the stress and strain dissimilarity in the area near the boundaries, Figure 1. While it may be assumed that stress and strain similarity is satisfied in the centre area for a relatively large package the stress and strain conditions near rigid, smooth walls are definitely different from the corresponding points in the prototype. To what extent the rigid boundaries will affect the stress and strain field in the soil model is still a question for study. To solve these boundary problems a number of techniques have been adopted or proposed. It is quite a common practice now in dynamic modelling tests to use a industrial filler material called duxseal at the boundary, which has been found to be very effective in reducing wave reflections from the rigid walls of the model package, Steedman (5). However using duxseal introduces other

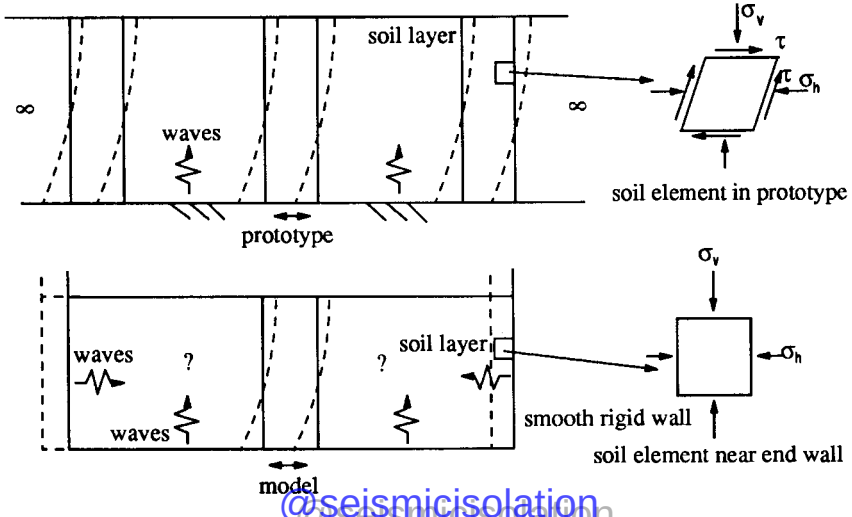

@seismicisolation

Figure 1 Stress and strain dissimilarity near the end walls

uncertainties such as the flexibility and friction at the interface between the duxseal and sand. The mechanical properties of duxseal are very difficult to determine in standard laboratory tests and therefore any consistent numerical model of this boundary is difficult to achieve.

A more favourable solution is a model package with both flexible and frictional end walls. An ideal boundary would have the same stiffness and friction as the soil column adjacent to it. The principle of a flexible boundary was first adopted in the stacked ring apparatus by MIT (Whitman et al. (6)). The apparatus was made of separate Teflon coated aluminium rings which are allowed to move relative to each other and hence create a kind of flexible boundary. Although this represented a major step forward technical problems prevented the wide spread use of the concept. Firstly there is no active control of the relative movement between the rings, resulting in the possible concentration of shear deformation at specific levels. Secondly the boundary is frictionless, and therefore cannot transfer complementary shear stresses on the vertical plane. Thirdly due to the circular shape of the packages and the low ratio of length over height, the analysis of the model response is a complex three dimensional problem.

In recent years a more advanced type of model containment has been proposed. In the US research workers have been developing laminar boxes which are intended to provide more compatible boundary conditions, Hushmand et al (7). A rectangular box with a higher length to height ratio has been used to create a two-dimensional condition. As the end walls are free its stiffness is similar to liquefied soil and has been adopted for liquefaction studies. However many centrifuge tests will not involve liquefaction of the whole soil column particularly as in some cases the behaviour of soil immediately prior to liquefaction has been seen to play a dominant role in the dynamic soil-structure interaction. This makes it necessary to use a box with rough flexible boundaries in which the stiffness of the end walls is compatible to the soil. In the UK a new approach has been adopted by Cambridge and Bristol Universities under a current SERC funded research contract. By using rubber gaskets between aluminium alloy rings with a membrane on the inner face capable of reacting the complementary shear stresses on the vertical plane, the box creates a kind of flexible and frictional boundary similar to an infinite soil layer. To mirror the increasing shear modulus in the soil the stiffness of the gaskets may be varied with depth, producing the same dynamic stiffness as a soil column. Although it is very difficult to mirror the stiffness of soil through out the test as the stiffness of soil is varying with the magnitude of the shear strain and effective stress, the use of flexible and frictional boundaries has definite advantages over a rigid boundary.

INTERPRETATION OF CENTRIFUGE TEST DATA

A typical dynamic centrifuge test generates a large amount of data which engineers might be interested in. How these data would help the design engineers in their practice depends critically on the data interpretation. Over the past 11 years, over 1,100 model earthquake tests have been carried out on the Cambridge Geotechnical Beam Centrifuge on over one hundred centrifuge models. The following examples show how the centrifuge test data has helped the understanding of fundamental mechanisms of dynamic soil structure interaction and thus has contributed to the design process.

Tests on Embankment Models

Lee and Schofield (8) reported dynamic centrifuge tests on embankment models. It was found that the degradation of stiffness within the soil structure due to excess pore pressure generation played a key role in the seismic response of the embankment. By windowing the data at different stages of the shaking and by examining the corresponding spectra from the acceleration recorded at the base and on the structure it is clear that the response of the embankment is changing during the earthquake. Initially amplification of motion was exhibited at high frequencies but due to the degradation of stiffness the natural modes dramatically reduced to much lower frequencies during the later part of shaking. This stiffness deterioration was clearly mirrored in the records of phase shift as shown in Figure 2. Initially the vibration at the top surcharge of embankment was approximately in phase with the base but a phase shift gradually built up to 150 degrees as partial liquefaction of soil took place.

@seismicisolation

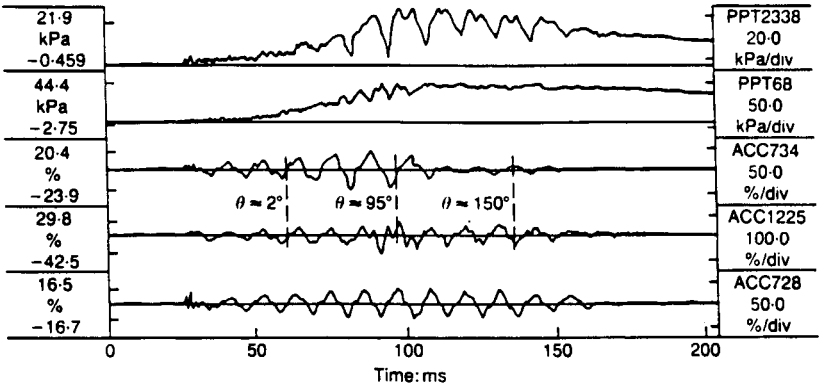

Note: accelerometers ACC728, ACC1225 were at the base and the top of the embankment model. ACC734 was on the surcharge on the top of the embankment. Pore pressure transducers PPT2338 and PPT68 were underneath the surcharge. Data are plotted at model scale.

Figure 2 Phase shift between vibration of embankment and its surcharge (after Lee and Schofield, 1988)

Tests on Dyke Models

The seismic response of coastal dykes was studied by Steedman and Habibian (9) in a research project funded by INTEVEP of Venezuela. The model was a stiff coastal dyke overlying discontinuous dense and loose sand layers. The large excess pore pressure generated by the compacting loose zones could transmit themselves to adjacent regions of dense material. Figure 3 shows the excess pore pressure contours in the foundation at an instant during a model earthquake. Differential settlement of the foundation caused large cracks in the dyke model in the directions both parallel and perpendicular to the axis of the dyke. The model tests clearly showed the phenomena of fracture, sliding of the dyke relative to the foundation and liquefaction.

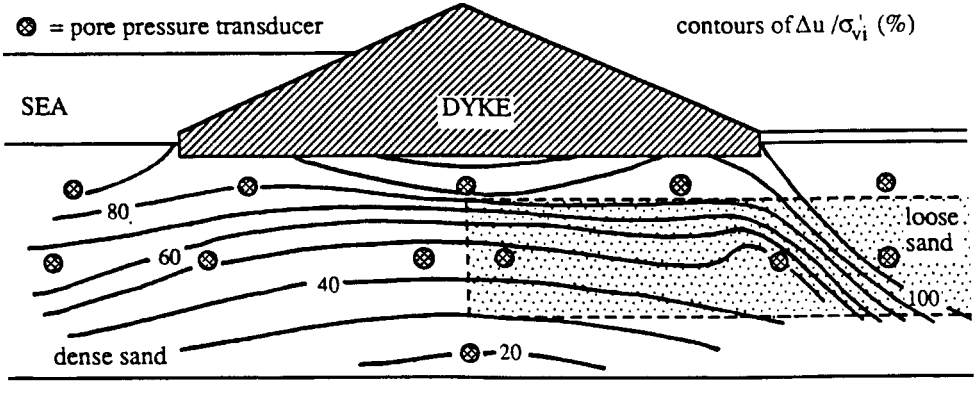

Figure 3 Contours of excess pore pressure in the foundation of a dyke model (after Steedman and Habibian, 1987)

@seismicisolation

Tests on Waterfront Retaining Walls

Probably the most widely recorded failure of soil structures in the field is waterfront retaining walls which have been reported in almost all major earthquakes in coastal areas, such the Chilean earthquake in 1960, the Niigata earthquake in 1964 and most recently the Loma Prieta earthquake in California in 1989. Centrifuge studies of the seismic response of anchored sheet pile wall models were reported by Steedman and Zeng (10) and Zeng (11). It was shown that deterioration of stiffness in the backfill soil due to excess pore pressure generation initiated the failure of the structure in advance of liquefaction. Once the excess pore pressure generated in the backfill had reached a threshold level the stiffness of the soil-structure system degraded rapidly towards resonance with large amplification of motion and phase shift. The substantial increase in dynamic earth pressure and hydrodynamic pressure due to the resonant vibration caused large bending moments in the wall and considerable displacement of the soil. Figure 4 shows the profile of one of the models before and after the earthquake tests. The model wall failed with large displacement seawards the sea coupled with significant settlements in the backfill. Large surface cracks were observed in the backfill. This failure mechanism is much like the failure of anchored sheet pile walls reported during the Niigata Earthquake in 1964 in Japan. The onset of liquefaction of the sand was of only secondary importance in the failure mechanism. An objective for design engineers arising from these tests is clearly to maintain the high stiffness of the soil-structure system during an earthquake by optimising the configuration of the structure and by reducing the possible excess pore pressure generation through increasing the density of backfill or by using gravel drains for example.

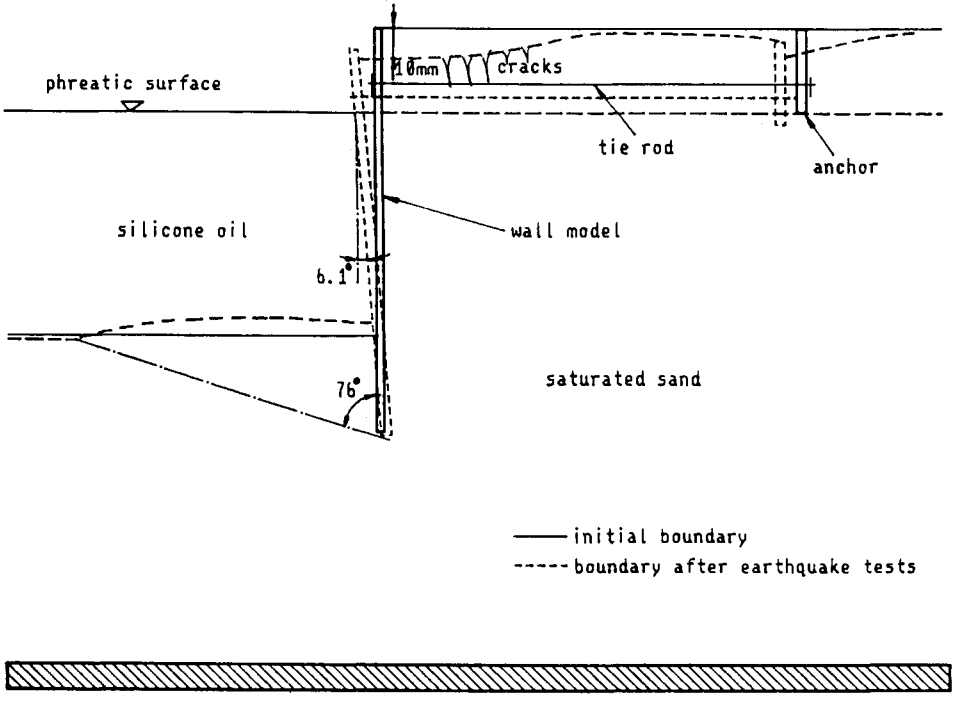

Figure 4 Failure mechanism of an anchored sheet pile wall model

@seismicisolation

Model Tests on Piles

The seismic response of pile structures has been a focus of research for both physical modelling and numerical modelling. The complex pattern of soil-structure interaction in such a 3-D problem is difficult to model in a numerical analysis and makes centrifuge modelling a very attractive alternative. Steedman et al. (12) reported some data from centrifuge tests on pile structures. It was found that stiffness degradation due to excess pore pressure led to resonant vibration of the structure and a large phase shift between the base shaking and vibration of the structure. Figure 5 shows the increase of phase shift from less than 90 degrees in a small earthquake to almost 180 degrees during a large earthquake. The resonant vibration induced very large bending moment on the model piles. Pseudo-static type calculations which assume the soil is rigid would have seriously underestimated the response of the piles in such an event.

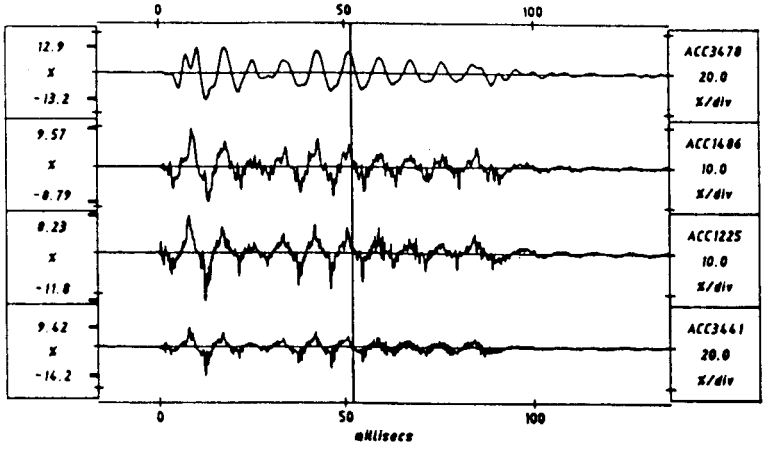

small earthquake

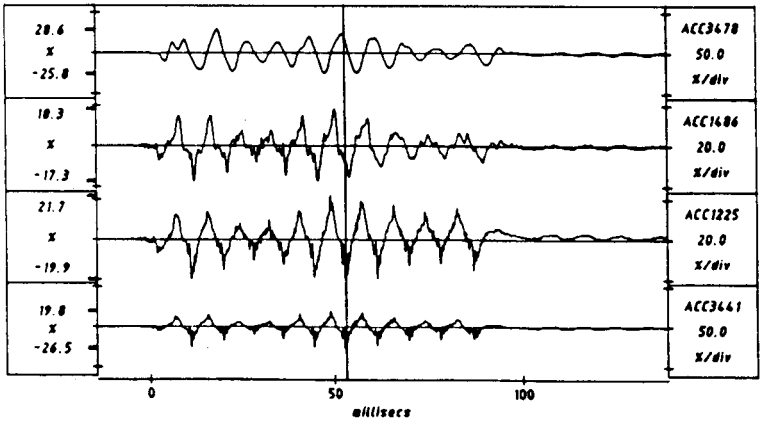

large earthquake

Note: ACC3441, ACC1225, ACC1486 and ACC3478 recorded acceleration on the model container, at the base of foundation, at the surface of soil and at the cap of the model pile.

Figure 5 Phase shift between vibration of piles and the foundation (after Steedman et al., 1990)

@seismicisolation

Model Tests on Rocking Towers
Failure of rocking tower structures was widely reported in the 1964 Niigata Earthquake and in the Mexico Earthquake in 1985. Centrifuge model tests have been carried out at Cambridge to study the response of tower structures to cyclic loading, Madabhushi (13). As expected it was found that the response of the structure reached a maximum value when the frequency of energy input coincided with one of the natural frequencies of the rocking tower. The generation of excess pore pressure in the foundation soil reduced the fundamental frequency of the structure and hence tended to increase its response.

All the abovementioned examples demonstrate how effective the centrifuge tests have been in understanding the mechanisms of failure of prototype structures. The dynamic response of these model structures clearly shows that the reduction of soil stiffness due to excess pore pressure generation is a consequence as important as the reduction of strength. These detailed observations of the evolving dynamic behaviour of a soil-structure system were possible because of the broadly harmonic input of the model earthquake. In the field, earthquakes on soft soil sites repeatedly show a predictable, strongly periodic motion; consider the time histories recorded in Oakland during the Loma Prieta event (Seed, et al.(14)), for example. Even for a more random earthquake, there is usually a certain range of frequencies where the seismic energy is concentrated. This is clearly shown in a response spectrum of an earthquake, of which there is always a range of frequency on a soft soil site within which the vibration is greatly amplified. The resonant vibration of a soil-structure system in that range is the driving force that causes failure.

1G AND HIGH G SHAKING TABLE TESTS

The wide availability of 1g shaking facilities and the relative simplicity of 1g shaking table models make 1g shaking table tests very attractive. However there are some difficulties in satisfying the scaling relationships for a 1g shaking table test. In recent years a number of researchers have investigated this problem. It is reported by Schofield and Steedman (15) that to model a stratum of uniform sand in a prototype at a unique scale it would be necessary to vary the density of the soil in the model with depth, in such a way that the density in the model be reduced. Thus the dissipation of pore fluid during partial liquefaction in such a loose model layer will probably not be similar to the dissipation in the more dense prototype. Moreover the strength of a cohesionless aggregate at a high stress level involves not only friction and interlocking of particles but also grain crushing. That can not be correctly replicated at low stress levels in a 1g model.

Iai (16) proposed an alternative group of scaling relationships for 1g shaking table tests based on a principle of normalised strain. Thus in the model both the stress and the strain are scaled down while keeping the void ratio unchanged. However the low stress level and the scaled down strain means the true behaviour of soil at high strain levels can not be correctly reproduced. In the prototype the failure of the soil-structure system quite frequently involves large deformation of soil in the presence of high excess pore pressures. Such arguments do not invalidate 1g shaking table tests but careful design of the experiments and interpretation of the data is necessary. For small strain problems the 1g shaking table test might provide very useful data and its interpretation could be straight-forward. But in the case of large deformation (and especially liquefaction) problems the 1g shaking table test may be highly unreliable and even misleading.

An effective approach is to combine the capabilities of 1g and high g shaking table tests. One option for such a study could be to model the same prototype structures using both facilities independently and to compare the data of the tests at prototype scale. The tests should cover a wide category of models, including small strain or large strain problems, dry or saturated models, and loose or dense models. The models on the two kinds of facilities would be prepared and tested in ways as comparable as possible, for example using the same type of model packages and the similar types of transducers. The data of these tests should be studied case by case in order to find out in which area these two kinds of tests have similar results and in which area the data are different. The correlation of the data will make it possible to make use of the advantages of both facilities.

@seismicisolation

The recent SERC sponsored project "The application of dynamic geotechnical modelling to design" for which Cambridge University is the principal investigator will seek to bring together the data of 1g and high g shaking table tests for comparisons, coupled to analysis by numerical modelling. The three year project will study extensively soil-structure interaction problems on the centrifuge at Cambridge and on the SERC shaking table at Bristol University. Both small and large strain problems will be studied and tests will be carried out on both dry sand and saturated sand models. Numerical predictions will involve the SWANDYNE code at Glasgow University. It is hoped that by the end of the project there will be a better understanding of and collaboration between different modelling techniques in geotechnical engineering. This will lead to recommendations on the limitations of dynamic physical modelling techniques in geotechnical earthquake engineering.

CONCLUSIONS

The following general conclusions can be drawn on the current state of the art in physical modelling for geotechnical earthquake problems:

1) There has been a rapid development of physical modelling capabilities in recent years. The wide availability of the data of dynamic centrifuge model tests will lead to more frequent use of dynamic centrifuge modelling for validation and for design.

2) Recent experience of centrifuge model tests at Cambridge clearly demonstrates the importance and effectiveness of dynamic centrifuge tests. A number of seismic problems have been successfully studied on the Cambridge Geotechnical Beam Centrifuge, which have helped to identify the fundamental mechanisms of seismic response of soil structures.

3) Shaking table tests carried out at 1g can also be effective in helping to solve certain dynamic problems in geotechnical earthquake engineering provided the limitations imposed by the 1g condition are clearly understood.

REFERENCES

1. Steedman, R.S., Discussion on: Similitude for shaking table tests on soil-structure-fluid model in 1g gravitational field, by S. Iai. Soils and Foundations, **30**, June, 1990.

2. Pokrovsky, G. and Fyodorov, L.S., Studies of soil pressure and deformation by means of a centrifuge, Proc. 1st International Conference on Soil Mechanics and Foundation Engineering, 1, No.70, 1936.

3. Schofield, A.N., Dynamic and earthquake geotechnical centrifuge modelling, Proc. Int. Conf. Rec. Adv. Geotech. Earthquake Eng. Soil Dyn., **3**, pp1081-1100, Univ. Missouri-Rolla, Rolla, 1981.

4. Kutter, B.L., Centrifuge modelling of the response of clay embankments to earthquakes, Ph.D thesis, Cambridge University, 1983.

5. Steedman, R.S., Centrifuge modelling for dynamic geotechnical studies, Second Int. Conf. Rec. Adv. Geotech. Earthquake Eng. Soil Dyn., University of Missouri-Rolla, Rolla, 1991.

6. Whitman, R.V., Lambe P.C. and Kutter B.L., Initial results from a stacked ring apparatus for simulation of a soil profile, Proc. Int. Conf. Rec. Adv. Geotech. Earthquake Eng. Soil Dyn., **1**, pp361-366, University of Missouri-Rolla, Rolla, 1981.

@seismicisolation
@seismicisolation

7. Hushmand, B., Scott, R.F. and Crouse, C.B., Centrifuge liquefaction tests in a laminar box, Geotechnique, **2**, pp253-262, 1988.

8. Lee, F.H. and Schofield, A.N., Centrifuge modelling of sand embankments and islands in earthquakes, Geotechnique, **1**, pp45-58, 1988.

9. Steedman, R.S. and Habibian, A., Modelling the failure of coastal dykes during earthquakes, Proc. 9 ECSMFE, **2**, pp633-636, Dublin, 1987.

10. Steedman, R.S. and Zeng, X., The seismic response of waterfront retaining walls, Proc. ASCE Spec. Conf. Retaining Structure, Ithaca, 1990.

11. Zeng, X., Modelling the behaviour of quay walls in earthquakes, PhD thesis, Cambridge University, 1990.

12. Steedman, R.S., Zeng, X. and Maheetharan, A., The application of dynamic geotechnical centrifuge modelling to design, IX Euro. Conf. Earthquake Eng., Moscow, Sept. 11-16, 1990.

13. Madabhushi, S.P.G., Modelling of tower structure subjected to earthquake perturbations, thesis under preparation for Ph.D degree, Cambridge University, 1991.

14. Seed, R.S., Dickenson, S.E. and Idriss, I.M., Principle geotechnical aspects of the 1989 Loma Prieta Earthquake, Soils and Foundations, Jap.SSMFE, **31**, No.1, pp1-26, March, 1991.

15. Schofield, A.N. and Steedman, R.S., Recent development of dynamic model testing in geotechnical engineering, Proc. 9th WCEE, **8**, pp813-824, Tokyo-Kyoto, 2-9 August, 1988.

16. Tai, S., Similitude for shaking table tests on soil-structure-fluid model in 1g gravitational field, Soils and Foundations, Jap.SSMFE, **29**, No.1, pp105-118, March, 1989.

@seismicisolation

UNIVERSITY OF NOTTINGHAM CYCLIC TRIAXIAL TEST FACILITY

Matthew Raybould
Lecturer
Department of Civil Engineering
University of Nottingham
Nottingham NG7 2RD

ABSTRACT

A digital control servo-hydraulic cyclic triaxial test facility with full data acquisition has been developed at Nottingham University as part of the Science and Engineering Research Council initiative in earthquake engineering. The facility has been used to investigate the behaviour of kaolin clay contaminated coarse silt subject to cyclic stress and strain. This paper describes the development of the test facility and presents some results of the cyclic triaxial tests.

INTRODUCTION

Analogue controlled servo hydraulic systems for carrying out triaxial tests have been in use at Nottingham University since the early 1960s. They were extended during the 1970s for cyclic loading problems associated with offshore structures, Hyde[1], and have been further extended to study the behaviour of subgrade in relation to road construction, Loach [2]. Most recently the system was upgraded as part of the SERC initiative in earthquake engineering including the development of a new control and data acquisition facility.

The facility provides for the testing of 76mm diameter samples with a maximum height to diameter ratio of 2. The Instrumentation described by Brown et al [3] is located in the middle third of the test sample to reduce the effect of end restraint. Instrumentation mounted on the test sample allows accurate measurement of axial and radial deformation. Pore pressures are monitored by a small pore pressure transducer consolidated into the central region of reconstituted test samples.

The loading system (Fig. 1) comprises two linear actuators, which nominally control the deviator stress ($q = \sigma_1 - \sigma_3$) and the confining stress (σ_3) and enable them to be cycled. Feedback from any monitored parameter can be used to control the applied loading. Hence, for example, sample consolidation can follow K_O conditions using feedback from radial strain transducers to control the applied stress ratio. Axial Strain and deviator stress controlled tests use feedback from the axial Linear Variable Differential Transformer (LVDT) transducers and the strain gauged diaphragm load cell respectively.

CYCLIC TRIAXIAL TEST FACILITY

Digital Control System

The proprietary digital control system (Fig. 2), supplied by Dartec Limited, Stourbridge, UK, comprises two sets of four channel microprocessor control systems programmed by a Texas Instruments PC. Proprietary software provides for setting appropriate gains for the

@seismicisolation

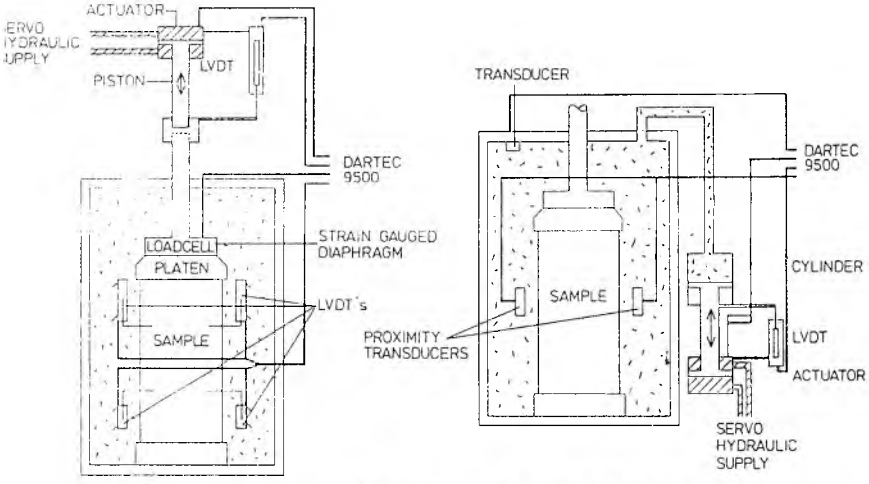

FIG. 1 LOADING SYSTEM

system, analysing frequency response, programming complex waveforms and setting various trips. The data acquisition facility comprising only four channels was too limited for the requirements of the work being undertaken and an alternative system was developed.

FIG. 2 CYCLIC TRIAXIAL FACILITY

Cyclic Triaxial Apparatus

The cyclic triaxial apparatus (Fig. 3) was first developed by Lashine [4]. Subsequent developments have brought the equipment to the state described below:

@seismicisolation

FIG. 3 TRIAXIAL INSTRUMENTATION

Axial Load:
Axial load is measured by load cells designed and built at Nottingham University. They are disc load cells and consist of a loaded web shaped to give an approximately linear strain profile with radius. The load cell is attached to a top platten by means of vacuum permitting extension or compression loading. The bush device which guides the load ram is detachable from the outer cell enabling soft samples to be assembled without the risk of failure during preparation.

Deviator stress is determined as the ratio of the axial load to the current mid height area of the sample. Changes in sample diameter and hence area are measured by radial strain transducers.

Pressure Transducers:
Cell pressure and base porewater pressure are monitored using strain-gauged silicon transducers manufactured by Druck Limited, Leicester, UK. To improve the hydraulic conductivity between the sample and transducer a domed shape porous stone protrudes the base of the sample. Internal porewater pressure is monitored by a miniature strain gauged silicon transducer introduced in to reconstituted samples at the initial consolidation stage. Back pressure on the volume change line is monitored using strain-gauged diaphragm transducers manufactured at Nottingham University. They are larger devices than the Druck transducers and are mounted adjacent to the volume change device remote from the sample.

@seismicisolation

Volume change:
A 100ml capacity volume change device produced by Soiltech Ltd is used in which a DC

LVDT is attached to the side of a piston connected to a rolling diaphragm, inside a cylinder. Back pressure is applied to one side of the diaphragm and pore fluid to the other. The device is connected to the test sample by 5mm internal diameter UPVC flexible tubing.

Deformation:
Radial deformation is measured using two Kaman proximity transducers. The transducers are mounted on a frame, hence imparting no load to the test sample. A thin metal foil target is secured to the sample inside the membrane. The signals for both transducers are electronically averaged to provide one radial displacement reading. Radial strain is defined as that displacement reading divided by the original radius of the test sample.

Axial deformations are measured 'on-sample' using four LVDT displacement transducers also mounted on a frame. The core of the LVDT is attached to the test sample by means of a brass rod screwed into a stud attached to the side of the test sample. Signals from all four transducers ar electronically averaged to provide one axial displacement reading which is necessary for feedback purposes. Individual transducer readings are also obtained for post test analysis. The accuracy of this system at low strains particularly when determining damping ratios has been critically examined.

Data Acquisition
Data obtained from cyclic triaxial tests has previously been recorded on X-Y or linear time chart recorders which tend to introduce significant electrical and mechanical damping. Transition from an analogue to a digital system was essential but was accompanied by problems. Previously smooth stress-strain loops were clouded by electrical noise.

Various software techniques were employed to analyse the nature of the noise and attempt to reduce its significance. The noise on the system was a combination of intrusive signals from A-C power supplies, both mains and transducer excitation, random noise from electronic components and radiated interference from other equipment in the vicinity. Several techniques for manipulating the noisy data were studied. Straightforward mathematical averaging and rolling weighted averages were found to round of peaks and obviously not work if the noise was greater than the signal. A sophisticated software package using Fast Fourier Transforms was examined. This highlighted the problem by revealing significant energy levels at 50hz (mains) and also at the test frequency. By passing the noisy data through an appropriate filter (eg Butterworth low pass filter) a smooth response resulted (Fig. 4).

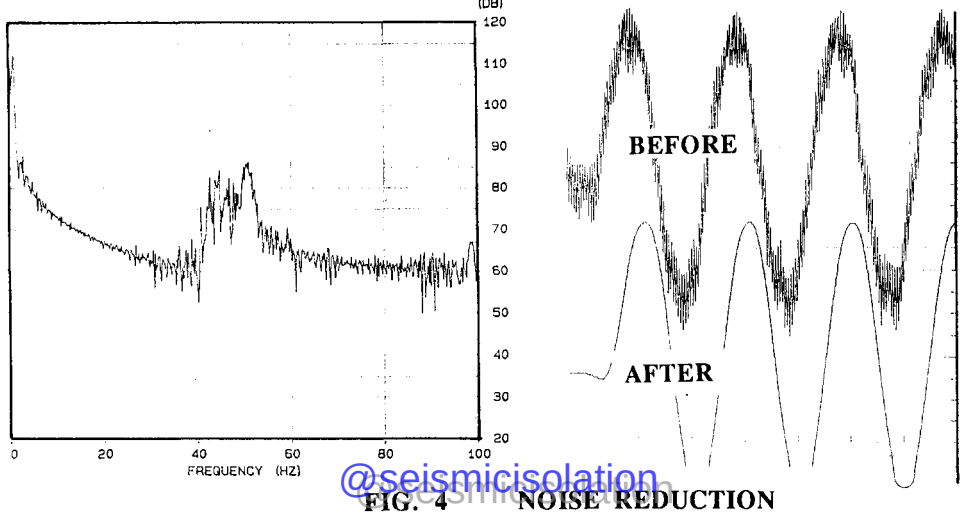

@seismicisolation

FIG. 4 NOISE REDUCTION

Manipulating data post test is time consuming and obviously does not permit real-time servo control. A system which performed real time filtering was provided by CIL Ltd, Worthing, UK. Their α-block A-D system is used in which signals from all transducers are filtered using an electronic low pass technique before being amplified to a level approaching 5 volts. All data is converted to ASCII format and transferred to a proprietary spreadsheet for manipulation.

The facility at Nottingham comprises three fully instrumented triaxial cells equipped as described above. The digital controlled servo-hydraulic system provides for the cyclic loading of one of these. A switching unit developed at Nottingham University allows manual monitoring of parameters from the two cells containing samples in various states of preparation while data from the one sample on test is recorded digitally.

EXPERIMENTAL RESULTS

Introduction

A test programme has been undertaken to investigate the response of a coarse silt (Attenborough silt) contaminated by kaolin clay subject to cyclic loading. Although some work on clean silts and silty clay has been undertaken elsewhere, the topic of clay contamination has not been addressed.

Four nominal combinations of silt and clay have been examined. Namely:

a. 100% silt
b. 75% silt - 25% clay
c. 50% silt - 50% clay
and d. 25% silt - 25% clay

Four different consolidation stress histories prior to cyclic loading have also been followed. Namely:

i. K_O - normally consolidated
ii. K_O - overconsolidated
iii Isotropically normally consolidated
and iv Isotropically overconsolidated

@seismicisolation

The undrained cyclic load tests involved applying 5 sinusoidal cycles of loading over a range of durations. The loading frequencies used were 1Hz (T = 5s), at 0.5Hz (T = 10s) and a much slower test at 0.1Hz (T = 50s) to minimise the effect of pore pressure lag behind deviator stress. Shear stiffness, damping, development of plastic and elastic strains and frequency dependency have been specifically examined.

Material

The silt was obtained from a local gravel pit, wet sieved and only material finer than 75 microns was used. Kaolin clay was purchased from the English China Clay Company.

Classification

The silt is very coarse which is consistent with high angle of internal shearing resistance. The nominal 100% silt sample contains a small amount of clay size particles whose presence enabled a value of plastic limit to be determined. This data is reproduced on a plasticity chart (Fig. 5) showing that all points plot slightly above and when joined parallel to the 'A' line.

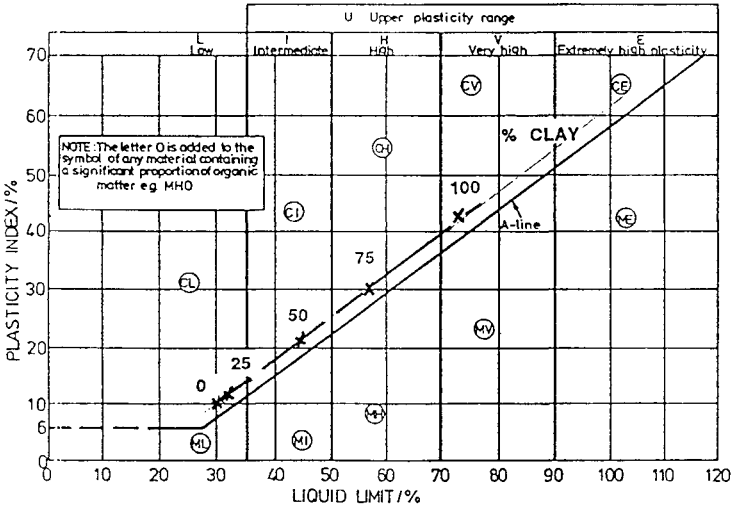

FIG. 5 PLASTICITY CHART

An indication of the Critical State parameters was obtained by carrying out a four stage triaxial test, consisting of:

1. Isotropic consolidation
2. Undrained shear test almost to failure
3. Anisotropic reconsolidation (dissipating accrued pore pressures from stage 2).
4. Drained shear test to failure.

@seismicisolation

Critical State parameters derived from these and other tests are shown in Table 1. Where:

M_c	=	Slope of Critical State line for triaxial compression tests.
M_e	=	Slope of Critical State line for triaxial extension tests.
N_o	=	Specific volume of K_o consolidated soil (p' = 1kPa).
Γ	=	Specific volume of soil at Critical State (p' = 1kPa)
λ	=	Slope of normal consolidation line.
κ	=	Slope of over-consolidation line.
η_{k_o}	=	Slope of K_o normal consolidation line in q-p' stress space.

TABLE 1

PARAMETER	PERCENTAGE SILT CONTENT			
	25	50	75	100
M_c	0.86	0.9	1.32	1.62
M_e	0.63	-	0.89	0.95
No	2.80	2.40	1.85	1.95
Γ	2.65	2.28	1.72	1.75
λ	.151	.112	.065	.036
κ	.043	.030	.017	.012
$\eta_{\kappa o}$	.42	-	.78	1.00

Sample Preparation

Air dried combinations of silt and clay are continuously mixed with de-aired water for 2 days to form a slurry with a moisture content of about twice the Liquid Limit. The slurry is then gently poured into 78mm internal diameter 300mm high perspex cylinder sitting on a vibrating table. This process assists in eliminating trapped air. A previously de-aired miniature pore pressure transducer is inserted into the slurry via one of the two porous loading platens inserted at either end of the cylinder. The cylinder is mounted vertically in a loading frame as K_o consolidation is effected. A dial gauge mounted on the loading ram and the internal pore pressure transducer monitors the state of consolidation. Having reached a predetermined consolidation state the sample is extruded from the cylinder and set up in the triaxial cell. The predefined state adopted in the work presented here is a vertical effective stress of approximately 150kPa.

Consolidation is further effected in the triaxial cell either isotropically (stress controlled) or anisotropically (stress and strain controlled) using feedback from the proximity transducers to maintain constant sample diameter. After consolidation the sample is subjected to a series of controlled stress and strain excursions.

@seismicisolation

K_o Consolidation

Fig. 6 shows the stress path followed in q - p' space during K_o consolidation in the triaxial apparatus for the 100% silt sample where:

$$p' = \frac{1}{3}[\sigma_1' + 2\sigma_3'] \quad \text{and} \quad q = \sigma_1' - \sigma_3'$$

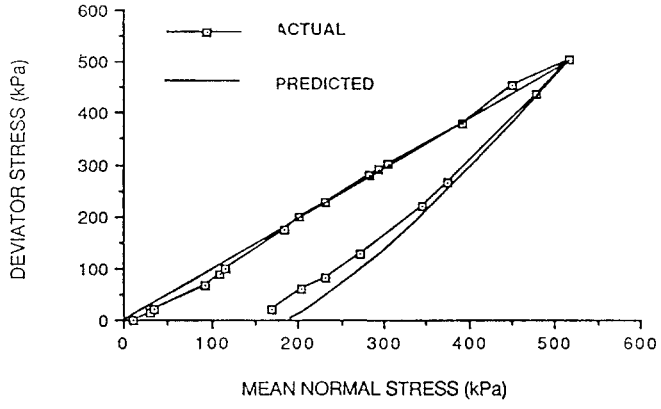

FIG. 6 K_o CONSOLIDATION

This is compared with the Mayne and Kulhawy [6] model $K_o = (1 - \sin\phi')\ OCR^{\sin\phi'}$ using a value of $\phi' = 38°$ which indicates significant similarity.

Cyclic Load Tests

In order to examine the development of secant shear modulus and plastic and resilient shear strains each cycle of loading has been inspected as shown in Fig. 7.

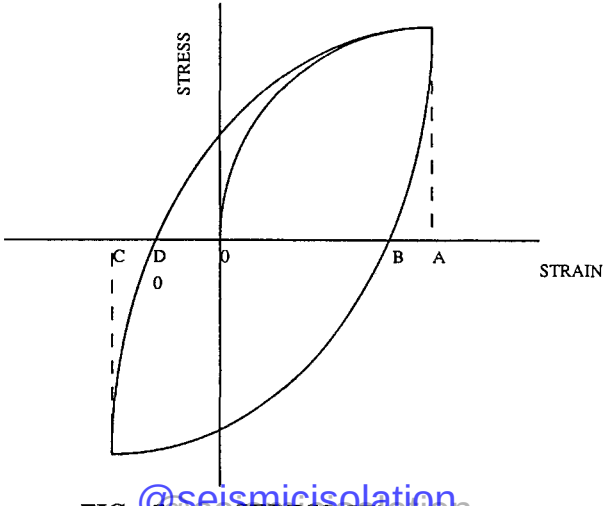

FIG. 7 STRESS-STRAIN LOOP

@seismicisolation

Five parameters as defined below are obtained:

α	=	a-b	:	resilient strain compression
β	=	b-o	:	plastic strain compression
γ	=	c-d	:	plastic strain extension
δ	=	b-d	:	resilient strain extension
ζ	=	a-c	:	peak to peak strain

α and δ are plastic strains and β and γ the resilient strains relating to the compression half cycle of loading and extension half cycle of loading respectively. ζ is the peak to peak strain used to calculate secant shear modulus.

The secant shear modulus was determined using observed axial strain values and a value of Poissons's ratio of $\nu = 0.5$, the theoretical value for full saturation assuming no volume change. Although the on sample instrumentation did monitor values of ν larger than 0.5 due probably to local barelling caused by end restraint particularly at high strains. It has been found that for those sample combinations tested that the degradation of secant shear modulus is not significantly affected by the type of consolidation history (ie one dimensional or isotropic). Fig. 8 shows the normalised shear modulus G/p'_o against shear strain for some of the cyclic load tests highlighting the apparent insignificance of type of consolidation history and showing as expected a higher stiffness for the coarser material for any given level of repeated shear strain.

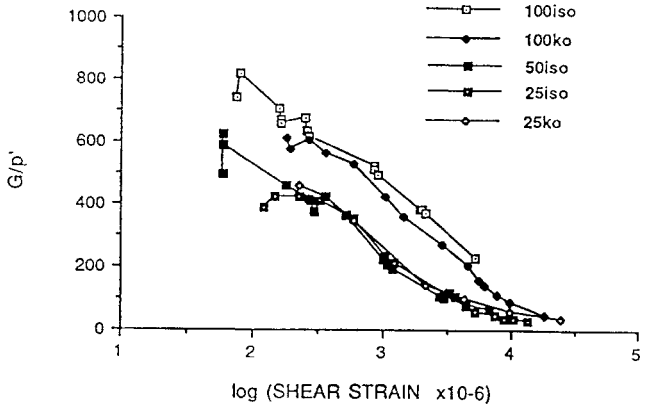

FIG. 8 G/p'_o v SHEAR STRAIN

Previous work at Nottingham, Brown and O'Reilly [7] has emphasised the importance of the η ratio when considering the strain behaviour of soil. η is the current ratio of deviator stress to mean normal effective stress (q/p'). In this work this parameter is normalised by the ratio of q/p' at critical state M.

The tests described are all isotropically consolidated. Compression parameters α and β are compared with η/M_c while extension parameters γ and δ are compared with η/M_e. Table 1 shows the difference between the values of M in compression and extension.

@seismicisolation

Fig. 9 shows α v η/M_c for tests on 25% and 100% silt isotropically overconsolidated (OCR = 4) to p'_o = 100kPa. It indicates that the development of resilient strain is similar for both series of tests. Fig. 10 shows a similar agreement between tests for β, indicating a threshold value below which very little strain occurs. The extension parameters δ and γ show similar trends but not with such agreement.

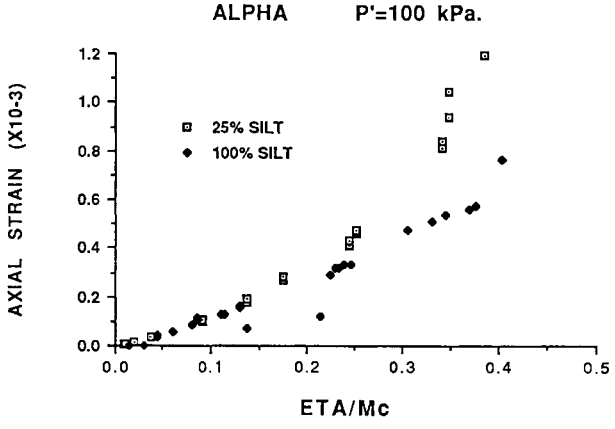

FIG. 9 ALPHA v η/Mc: p'_o = 100kPa

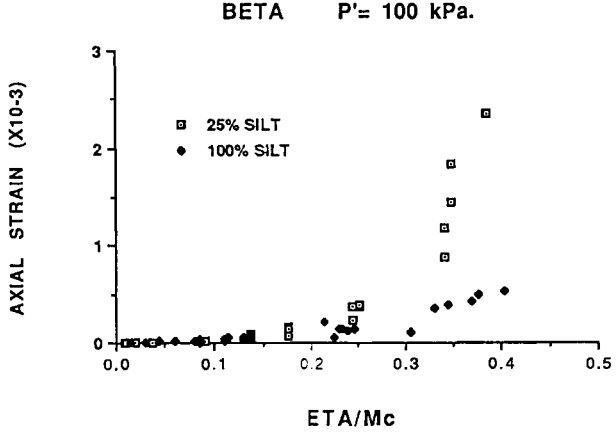

FIG. 10 BETA v η/Mc: p'_o = 100kPa

Cyclic tests on normally consolidated samples of 75 % silt and 100% silt (p'_o = 400kPa) also indicate consistent results between tests for the parameters α, β, γ and δ.

@seismicisolation

Both sets of tests have the same yield surface as in both cases p'_c = 400kPa. It would be expected therefore that the normally consolidated samples would develop plastic strains at much lower values of η/M than the overconsolidated samples. This was not observed. The treshhold value of η/M below which very little plastic strain occured: $\eta/M_c = 0.4$ and $\eta/M_e = 0.5$ was the same for both series of tests.

The development of resilient strain did show differences in behaviour (Fig. 11). The normally consolidated samples developing more resilient strain than the overconsolidated for a given value of η/M. The overconsolidated sample showing linear elasticity up to a value of $\eta/M = 1$ where as the normally consolidated samples' resilient behaviour became non-linear at $\eta/M \approx 0.4$.

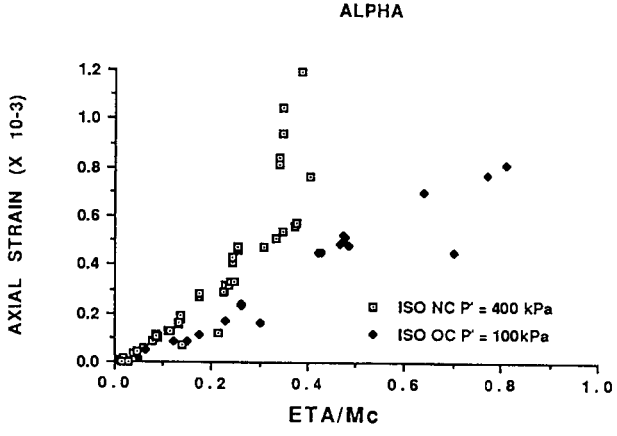

FIG. 11 ALPHA v η/Mc: OC and NC

The effect of frequency has also been considered. Fig. 12 shows the degradation of shear modulus and development of viscous damping at three frequencies for the isotropically reconsolidated 100% silt sample. Indicating higher stiffnesses and lower damping for the faster tests.

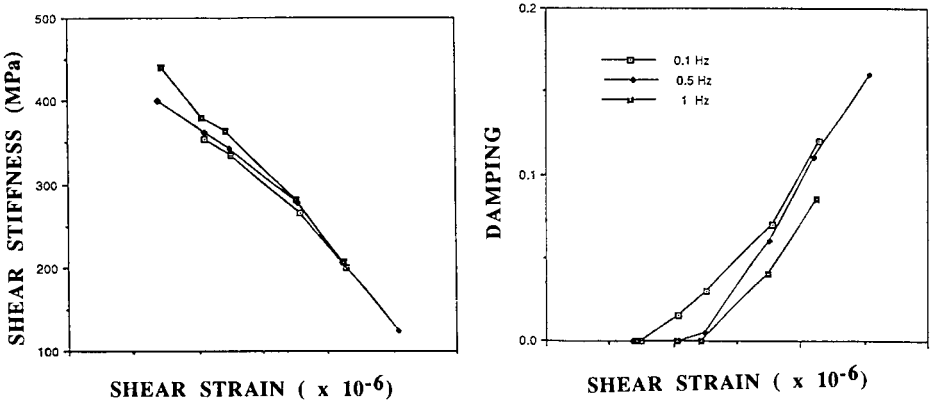

FIG. 12 SHEAR STIFFNESS AND DAMPING v SHEAR STRAIN: FREQUENCY AFFECT

@seismicisolation
@seismicisolation

CONCLUSION

The triaxial test facility developed at the University of Nottingham has enabled high quality data to be generated on the deformation characteristics of clay contaminated silt samples subject to cyclic stress and strain.

This paper has described the development of the test facility and presented some of the data generated from the current research project. This illustrates the ability of the equipment to accurately produce K_o overconsolidated samples in the triaxial configuration and the ability to determine accurate values of shear modulus at strain levels similar to those which are imposed by the resonant column apparatus. The results reported appear to indicate that the shear modulus degradation is independent of the type of consolidation history, K_o or isotropic, but controlled by the degree of overconsolidation.

A technique for examining the behaviour of soil subject to earthquake type extension and compression loading has been suggested. The results of a series of tests on isotropically consolidated soil indicate that this method of analysis will enable a model for determining the behaviour of clay contaminated silt subject to cyclic loading to be produced.

ACKNOWLEDGEMENTS

The research described in this paper was carried out in the Department of Civil Engineering, University of Nottingham under contract to the Science and Engineering Research Council. The Author is grateful to the support provided by his Head of Department, Professor S F Brown, and the assistance of many other colleagues.

REFERENCES

1. Hyde, A.F.L., Repeated Load Testing of Soils, PhD Thesis, University of Nottingham, 1974.

2. Loach, S.C., Repeated loading of fine grained soils for pavements design, PhD Thesis, University of Nottingham, 1987.

3. Brown, S.F., Austin, G. and Overy, R.F., An Instrumented triaxial cell for cyclic loading of clays Geot. Testing Journal, ASTM, 1980, Vol. 3, No. 4, pp145-152.

4. Lashine, A.K.F., Some aspects of the behaviour of Keuper Marl under repeated loading, PhD Thesis, University of Nottingham, 1971.

5. Mayne, P.W. and Kulhawy, F.H., K_o-OCR relationships in soil, Journal of the Geot. Eng. Div., ASCE, 1982. Vol. 108. No. GT6, pp851-872.

6. Seed, H.B., Pore water pressure changes during soil liquefaction, Journal of the Geot. Eng. Div., ASCE, 1976. Vol. 102, No. GT4, pp323-346.

7. Brown, S.F. and O'Reilly, M.P., The resilient shear stiffness of dry particulate material. To be published.

@seismicisolation

COMPARISON BETWEEN ANALYTICAL AND SHAKING TABLE RESULTS FOR EXTREME RESPONSE OF A MODEL STEEL BUILDING

A BLAKEBOROUGH
University of Bristol, Bristol BS8 1TR, UK

P D MURPHY and E D BOOTH
Ove Arup & Partners,
13 Fitzroy Street, London W1P 6BQ, UK

ABSTRACT

A fifteenth scale model of a 10 storey steel framed building designed to UBC:88 has been built and tested on the SERC shaking table at Bristol. The modal properties were determined from sine sweep tests. These tests were followed by earthquake time history tests of increasing severity which excited the model to ductility ratios of up to 8. The test data are currently being compared with the results of analyses using the explicit non-linear analysis code Oasys-DYNA3D; correlations are excellent.

OBJECTIVES OF THE TEST PROGRAMME

Oasys-DYNA3D [1], a program originally developed by Dr John Hallquist for impact problems, has recently been extended to enable non-linear seismic analyses to be performed on building and soil structures [2]. Whenever a new application is envisaged for a program, faith in the results is established by a series of comparisons, either of the program results with the output of known and trusted programs, or preferably with the results of experimental data obtained from field measurements or from physical model tests. Mindful of this need, Ove Arup and Partners and the University of Bristol have collaborated in a Teaching Company association [3] with the following objectives.

a) Correlation of computer analyses with test results from a model steel building shaken on the SERC Earthquake Simulator [4] at Bristol University.

b) Investigation of the usefulness of shaking tables for assisting in the development of the aseismic design of building structures.

c) Investigation of the performance of the Bristol table for a test piece larger than previously attempted.

@seismicisolation

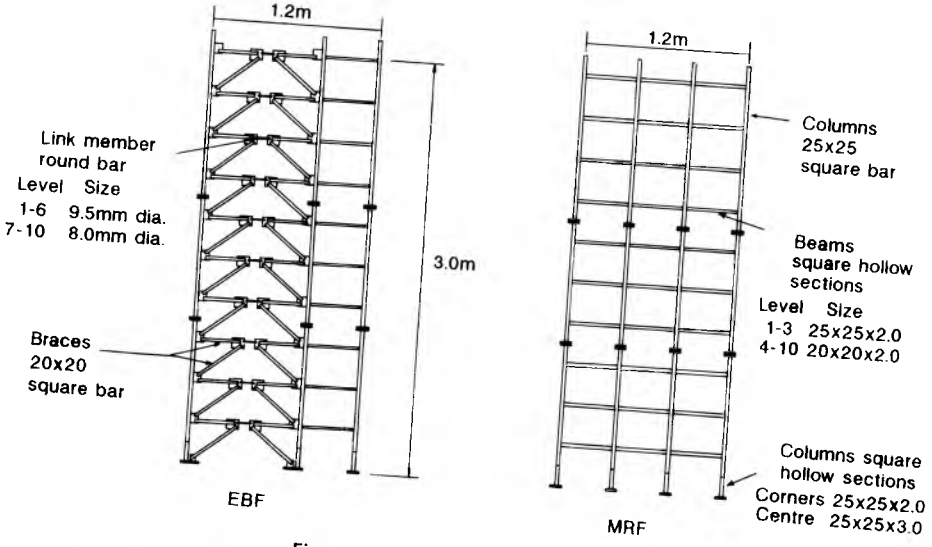

Figure 1. Elevations of model

Figure 2. Photo of model

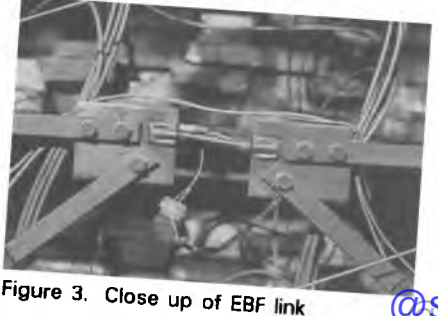

Figure 3. Close up of EBF link

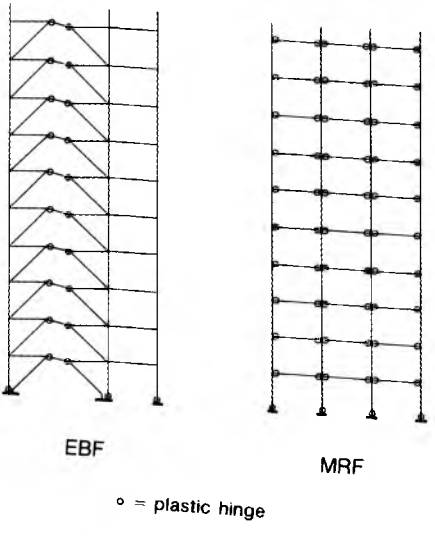

Figure 4. Sway mechanisms of frames

@seismicisolation

DESCRIPTION OF THE MODEL STEEL BUILDING

Scaling considerations

The shaking table at Bristol has a platform area of 3m x 3m and a headroom of 4.5m. Any model of a multistorey building must therefore be scaled to fit the available space. A 1:15 geometrical scaling factor was chosen which enabled a 10 storey building of a conventional 4.5m interstorey height to be fitted comfortably on the table. It is of paramount importance in designing scale models that the model reflects accurately the correct balance of the physical processes of the prototype. For a model such as this constructed of the same material as its prototype, the strains and hence stresses must be the same in model as in prototype in order to reproduce correctly the pre and post yield behaviour of the structure. Two different types of force were important in the present tests, firstly dynamic forces due to ground shaking and secondly gravity forces, which are important both for static self weight stresses and for P-delta effects. It can be shown [5] that, where the gravitational field is the same for model and structure (the case for shaking table tests but not, for example, centrifuge tests), the following scaling relationships need to apply to equalise both dynamic and gravity stresses in the model and prototype.

Time scales as	(geometrical scaling factor) ^ ½
Mass scales as	(geometrical scaling factor) ^ 2

The first relationship meant that time in the model was speeded up by a factor $\sqrt{15}$ or 3.9; all natural periods, earthquake durations etc for the model were shorter by this amount than in the prototype and this should be borne in mind when considering subsequent results. The second relationship meant that additional mass was required in the model, since with the same density in model and prototype, mass would scale as the cube of the scaling factor, and would therefore be a factor of 15 too low in the model. Accordingly, 9 tonnes of lead was added to the model.

Design of the model

The basic design of the model building was developed from a Tokyo office building designed by Ove Arup & Partners. The model (Figures 1 and 2) represents a prototype 10 storey building 45m high, weighing 2250 tonnes. It is square in plan and consists of an external perimeter tube, with conventional moment resisting frames (MRF) along two parallel sides and eccentrically braced frames (EBF) along the other two. This had several advantages for testing purposes since it combined two different framing systems in the same model and allowed each type of frame to be tested first separately and later together to study interaction effects. Stiffened steel plates formed rigid diaphragms connecting the frames at each level. The structure was designed according to the provisions of UBC:88 [6] for a hard site in the most seismically active zone. The intended plastic sway mechanisms of the frames are shown in Figure 4. The important constraints were interstorey drift in the MRF direction and yield capacity in the EBF.

@seismicisolation

The MRF construction was of RHS beams welded to solid columns. Solid columns were chosen because of the extreme difficulty of producing realistic beam-column connections

with hollow columns which would have needed stiffening. Since the columns were designed as non-yielding elements, except at their base (Figure 4), the divergence from typical building behaviour was small. The bottom halves of the ground floor columns were made of hollow sections to reproduce the yield behaviour expected to occur there.

The EBFs were made of separate components bolted together. The EBF link (Figure 3) was another area where precise scale modelling was not possible. In a standard design, the EBF link is a stiffened I beam section, but at fifteenth scale this would have been very difficult to model properly. It was decided to use instead solid round bar, yielding in flexure at its two ends, which was found to be a good analogue for the hysteretic characteristics of a conventional shear beam. The total mass of the model was 10 tonnes, including 9 tonnes of added lead mass equally distributed between floors, and its centre of mass was 1.5m above the table platform.

INSTRUMENTATION

A well designed instrumentation scheme should provide for two things. It must not only provide enough data for an acceptable comparison to be drawn between the physical and theoretical models, but it must also contain enough redundancy to allow self consistency checks on the most important data. The quantities to be measured that are of most interest to a designer of an earthquake frame, and therefore the quantities to be compared, are the peak values of the interstorey drift, the peak and cumulative ductility demand, the maximum deflection and the permanent set, and the peak values of base shear and overturning moment.

Four different instrumentation schemes were used, depending on the direction of input motion. Figure 5 shows the scheme used for monitoring MRF direction tests. LVDT gauges measured the interstorey drift on the MRF face, and the absolute displacements of the top and bottom of the corner column. Accelerometers on the corner column measured the motion of each floor in the MRF direction, and others the linear and pitching acceleration of the base. Additional accelerometers at the top of an adjacent column measured the torsion and EBF response. Strain gauges measured the axial and bending strain at the bottom of the corner column and at the ends of selected beams.

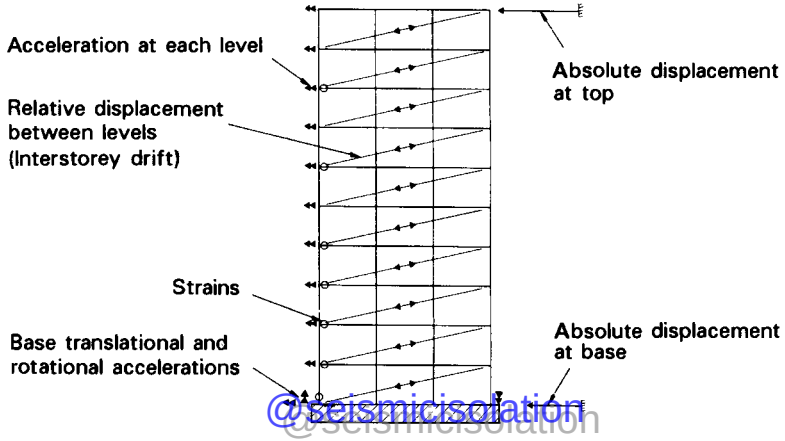

@seismicisolation

Figure 5. Instrumentation scheme for MRF direction

This instrumentation scheme allowed for three consistency checks, two comparing the acceleration and displacement of the top and bottom of the instrumented column, and and one comparing the sum of the interstorey drifts plus rigid body tilting of the model with the relative motions of the top and bottom of the instrumented column.

TESTING SEQUENCE

All testing took place at the Earthquake Engineering Research Centre of Bristol University. The model was fabricated in the workshops at Bristol and assembled on the table in three sections.

Testing was done in two phases. Firstly, static cyclical tests were performed on single storey MRF and EBF subframes, primarily to determine their hysteretic characteristics. Secondly, dynamic shaking table tests were performed on the assembled model structure, as described in more detail below.

Modal testing

An extensive series of resonant search tests was carried out to identify the modal properties of the model. Sine sweep tests excited the MRF, EBF and torsional modes of the structure by turn. Modal frequencies and damping levels were determined from the power spectra of accelerations measured on the frame. The mode shapes were obtained by comparing the relative phase and amplitude of pairs of accelerometer signals.

Earthquake tests

In all cases, the specified input earthquake time history was a modified version of an epicentral recording of the 1985 Mexican earthquake. The model was shaken with 31 separate earthquake tests of increasing severity. Different tests excited the model in the MRF and EBF directions both separately and together. The accelerations in each direction in the combined tests were designed to excite each of the frames to the same ductility ratio. The initial tests were low level tests to excite the structure linearly, but the later tests produced displacement ductility ratios (peak response divided by response at yield) of up to 8 in the structure.

Data collection and processing

The signal from the instrumentation in the earthquake tests was logged using a computer. A PC containing three analogue to digital converter boards collected data from up to 48 channels. After backing up, the data was scanned to check that all the instrumentation had worked correctly and the signals fell within expected values. More extended processing then followed to check that the ductility ratio set for the test had been achieved, and that the data was internally consistent.

EXPERIMENTAL RESULTS

The programmed tests were all completed successfully, and data of a high standard

@seismicisolation

obtained. Figure 6 shows the record of the base acceleration in the MRF direction for the test reported further in this paper, which excited the structure to a ductility of 4 and Figure 7 shows the corresponding 0.5% damped acceleration response spectrum. The 'target' response spectrum of the specified motions is superimposed on Figure 7, normalised to give a spectral acceleration equal to that recorded at 0.5Hz. The match is good over the frequency range of interest, bearing in mind the low damping ratio. However, the height and mass of the model caused the table to pitch about a horizontal axis in a way which was not intended. The table control reduced these rotations to a low level in the MRF direction, but in the more rigid EBF direction, the product of rotation times model height was of the order of 10% of the base lateral motion. This was more than had been hoped, but since the rotational motions were measured and included in the subsequent computer analyses, the objective of validating those analyses was not affected.

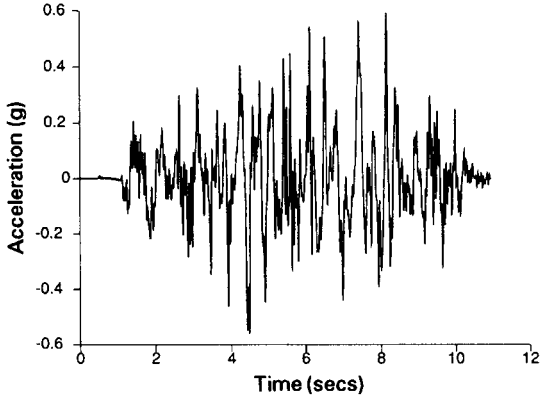

Figure 6. Base acceleration in MRF direction for test CN5

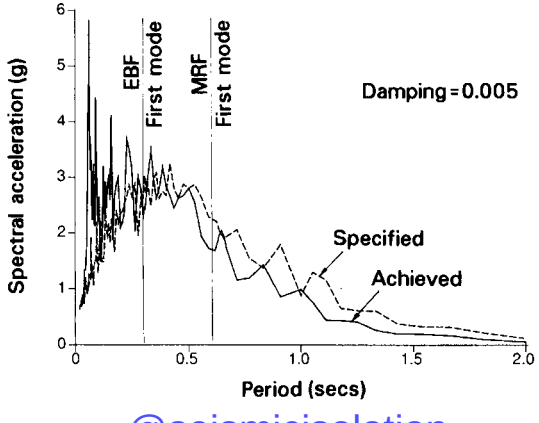

Figure 7. Acceleration response spectrum for base acceleration

@seismicisolation

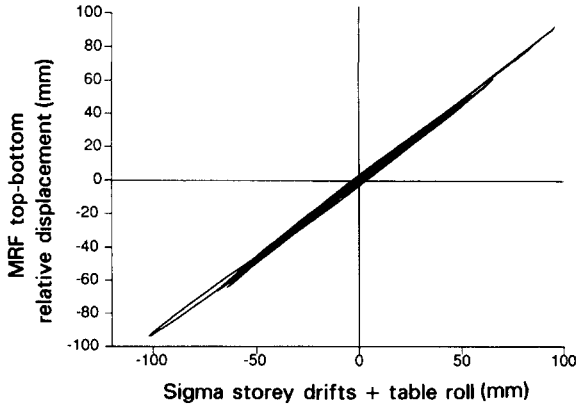

Figure 8. Consistency check between drift and displacement readings

The results of one of the consistency checks on displacements is shown in figure 8. For a zero closure error the line should be straight with a unit slope. The correlations were not always as close as shown here, but in all cases were very satisfactory for such complex instrumentation.

ANALYSIS PROCEDURES

Modal analysis

The comparisons between the non-linear experimental behaviour and analytical predictions were of primary interest in this study. However the basic modal properties, modal frequencies and modeshapes, were also investigated. The finite element computer program PAFEC [7] was used to evaluate the modal properties. A three-dimensional model was developed. Structural members were modelled with linear beam elements. The floor diaphragms were idealised with trusses of beam elements. The added lead mass was modelled with discrete lumped masses. Rotational springs restrained the column bases to simulate the stiffness of the bolted holding down connection detail with the shaking table.

The element properties were initially calculated directly from member sizes and were then adjusted in order to give good agreement with the measured modal properties of the experimental structure. In the MRF direction this adjustment was small but in the EBF direction the first frequency was overestimated by 30% and so to compensate for this the link stiffness was reduced. The original link stiffness corresponded to the pre-yield elastic stiffness measured from the static subframe tests, while the reduced stiffness corresponded to the stiffness measured after one or more yielding cycles of the frame. The adjustments to the EBF model therefore corresponded to data available before the dynamic tests. Table 1 shows the analytical frequencies by comparison with the experimental measurements. Correlation of modeshapes was also good.

@seismicisolation

TABLE 1
Modal properties from tests and analysis

Mode	Analytical frequency PAFEC (Hz)	Analytical frequency DYNA3D (Hz)	Experimental frequency (Hz)	Experimental Damping (% critical)
MRF 1	1.58	1.56	1.63	0.5
EBF 1	3.30	3.22	3.32	1.2 - 2.6
MRF 2	4.70	-	5.06	0.2
Torsion 1	6.42	-	6.56	5.0
MRF 3	8.25	-	8.80	0.1
EBF 2	9.19	-	9.75	0.6

Non-linear analysis

The non-linear time history analysis of the structural response was calculated using the program Oasys-DYNA3D [1]. This is an explicit three-dimensional finite element code for analysing the dynamic response of inelastic solids and structures. The analysis reported here is for the earthquake response in the MRF direction using a two-dimensional model. (A study of the response in the EBF direction is in progress and will be fully reported later). Structural members were modelled with beam elements. The elastic section properties used were the same as those used for the PAFEC analysis. The yielding properties of the structural members were determined from the static subframe tests. In order to reproduce the measured hysteresis behaviour of the frame, each yielding beam and column was modelled with two elements in parallel. The first element had elastic - perfectly plastic moment - rotation characteristics at each end and the other was a purely elastic element.

The added mass was modelled by increasing the element densities, in effect lumping the mass at the end of each element instead of adding discrete masses, since this improved computational efficiency [1]. Discrete nodal loads at the beam-column joints simulated gravity forces. As the measured damping ratios were low and not significant by comparison with hysteretic damping during large ductility response, equivalent viscous damping was not modelled. The elastic properties of the computer model were checked by measuring its free vibration response to a square pulse input; the frequency (Table 1) and modeshape agreed well with both PAFEC analysis and test for the first mode.

The earthquake analysis was preceded by a dynamic relaxation in order to achieve initial equilibrium of external and internal forces. The lateral and rotational earthquake accelerations measured at the base of the experimental model were then applied to the base of the analytical model in the form of a lateral and angular velocity time-history. Each run took 40 minutes to complete on a Convex C210 mini supercomputer.

COMPARISON OF ANALYTICAL AND EXPERIMENTAL RESULTS

The results presented below are for the MRF for one earthquake test achieving a ductility of 4. A time-history of the displacement at the top of the structure relative to

@seismicisolation

the base is shown in Figure 9. The analytical results were in phase with the experimental result and the peaks were of similar value. The permanent set at the top of the structure at the end of the motion was measured as -2mm and predicted as 10mm; it was small by comparison with the peak displacement.

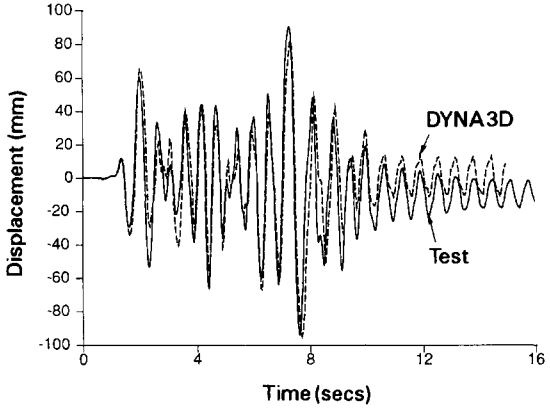

Figure 9. Displacement of top of model

The peaks of interstorey drifts (relative displacement between adjacent levels) and shears are shown in Figure 10. The experimental storey drifts were measured by the displacement transducers attached between adjacent levels. The largest drifts correspond to 6% of the storey height and a storey ductility of approximately 3.6.

The peak storey shears are also shown in Figure 10. The experimental storey shears were calculated from the accumulated storey inertial forces using the accelerometer data at each level. The peak base shear corresponded to 41% of the structure weight. Figure 11 shows the experimental and analytical storey shear - displacement hysteretic behaviour between levels 1 and 2.

The peak base overturning moment in the experimental model was calculated from the contribution of each storey inertial force as 80 kNm. The corresponding analytical result was 60 kNm. P-delta effects were assessed based on the analytical results and added 10% to the peak overturning moment.

The shear forces calculated at each level were multiplied by the relative velocity between adjacent levels (obtained from the time integrated acceleration data) and integrated over time. This represents the sum of elastic, hysteretic and viscous energy stored or absorbed at each level. Figure 12 shows the time-history of these energies summed for all levels.

The total energy absorbed at the end of the experimental test was 10.8 kJ and the analysis result was 8.9 kJ, a difference of 18%. The analysis however does not include equivalent viscous damping. With a damping ratio of 0.5% the viscous damped energy absorption is approximately 0.5 kJ.

@seismicisolation

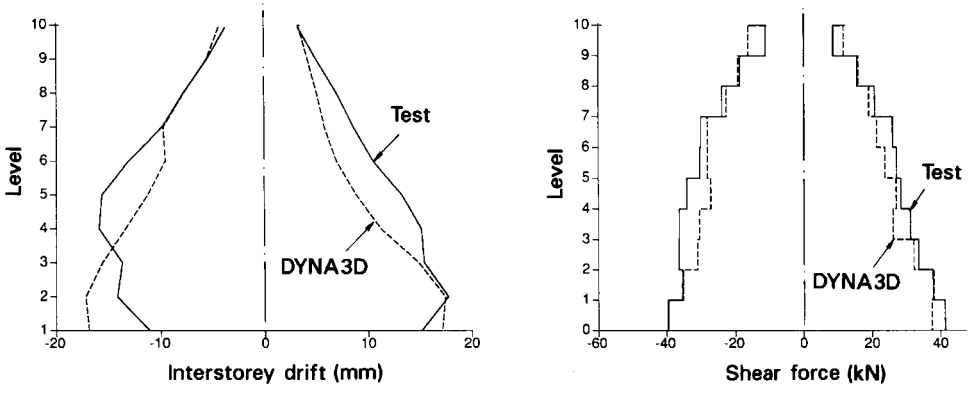

Figure 10. Comparison of peak interstorey drifts and shears

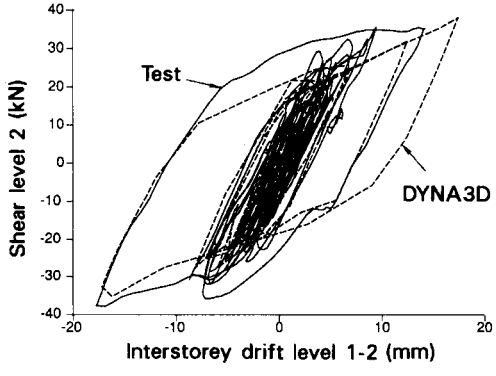

Figure 11. Hysteresis behaviour at level 2

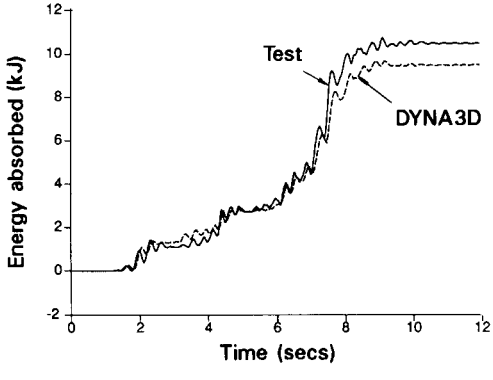

Figure 12. Total energy stored or absorbed by the model

@seismicisolation

The energy absorption at each level at 3, 6 and 10 seconds after the beginning of the earthquake is shown in Figure 13. Both analysis and experiment show the energy to be absorbed primarily by the lower half of the structure.

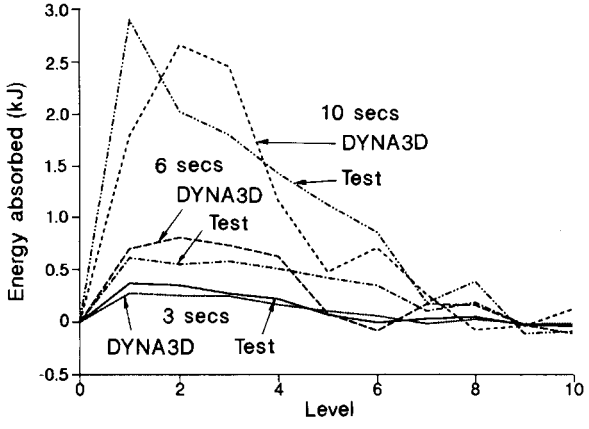

Figure 13. Distribution of absorbed energy throughout the model with time

CONCLUSIONS AND OBSERVATIONS

1) For the MRF direction excited to a ductility level of 4, the results of an Oasys-DYNA3D analysis agreed well with experiment, with excellent correlation between the responses of primary interest to designers. Preliminary results for the EBF direction show a less close, but still very satisfactory agreement. Work is in progress to see if less sophisticated analyses, using simple 'stick cantilever' models, can also produce adequate results.

2) The difficulties of modelling steel details at small scale militate against the use of shaking tables during the design development of tall steel buildings. However, computer analysis have been shown to produce reliable results involving run times of an hour or less on a Convex C210 mini supercomputer. This reduces the need for dynamic physical modelling of an entire building structure. Static cyclical tests on components or subframes of the structure at or near full scale may however be useful to establish (inter alia) the hysteretic characteristics needed as input to a non-linear computer analysis.

3) The elastic properties in the MRF direction (which had all welded connections) were well predicted by analysis, but significant adjustments had to be made to the computer model to gain agreement in the EBF direction, where the connections were mainly bolted. The reason is not fully understood but is probably associated with the post slip stiffness of bolted connections.

@seismicisolation

4) The Bristol shaking table can successfully excite a 10 tonne, 3m tall model to predetermined motions up to 0.7g. Control of pitching during the tests was less successful than hoped, but still adequate.

5) Between 40 and 50 channels of dynamic data were collected during each test and this proved feasible, though a great deal of effort was involved in setting up. The number of channels was however necessary to capture a dataset which monitored all the responses of interest and which allowed for essential checks on the internal consistency of the data. The data set captured had a satisfactory degree of internal correlation over a very wide range of response.

ACKNOWLEDGEMENTS

The authors would like to thank the UK Science and Engineeering Research Council (SERC), Teaching Company Directorate, Ove Arup & Partners and the University of Bristol for financial support of the project, and SERC for the provision of shaking table facilities. The authors would also like to express their special thanks to Britannia Refined Metals who generously loaned the lead ballast.

REFERENCES

1. Oasys-DYNA3D. User Manual Version 5.0. Oasys Ltd, 13 Fitzroy Street, London W1P 6BQ, November 1990.

2. Sturt R. and Wilson J. Seismic application of Oasys-DYNA3D. DYNA3D User Group Conference, London 1989.

3. Putting ideas to work. Teaching Company Directorate, Hillside House, London Street, Farringdon, Oxon SN7 8AA.

4. Blakeborough A., Severn R.T. and Taylor C.A., The new UK national six-axis shaking table. 8th European Conference on Earthquake Engineering, Lisbon, 1986.

5. Moncarz P.D.and Krawinkler H. Theory and application of experimental model analysis in earthquake engineering. John Blume Center, Stanford University, California, June 1981.

6. UBC:88 Uniform Building Code: International Conference of Building Officials, Whittier, California, 1988

7. PAFEC User Manual Level 6.2. PAFEC Ltd, Strelley Hall, Nottingham.

@seismicisolation

COMPARISON OF CALCULATED SEISMIC RESPONSE OF A 1/4 SCALE REACTOR BUILDING WITH MEASURED RESPONSE

JOHN M LLAMBIAS & ROBERT S JOHNSTON
Safety and Structures Department
NNC Ltd
Booths Hall, Knutsford, Cheshire, WA16 8QZ, UK

ABSTRACT

This paper describes a comparison between the calculated seismic response and the measured seismic response of a 1/4 scale model of a containment building in Lotung, Taiwan. The seismic response of the containment model is calculated using a procedure typical of that employed by NNC Ltd for the SSI analysis of buildings. The calculations are performed 'blind' (ie. without any details of the recorded response being available) and the predicted seismic response is then compared with the recorded response. The model of the soil is then refined using the results of forced vibration tests performed on the Lotung containment model and the response predicted using the refined soil model is compared also with the recorded response. The results of this comparative study show that the typical SSI methods of analysis used by NNC Ltd predict the frequency of the spectral peaks accurately and produce conservative results. The results indicate that the main source of conservatism is inherent in the method used to model the soil and take account of embedment effects.

INTRODUCTION

This paper describes a comparison between the predicted seismic response with the measured seismic response of a 1/4 scale containment building in Lotung, Taiwan.

The comparative study is divided into two phases. The first phase which is a 'blind' comparative study examines the response of the Lotung containment model to two real earthquake time histories using a procedure typical of that employed by NNC Ltd for the seismic SSI analyses of buildings. This typical procedure follows the impedance function (substructure) approach and involves the determination of high strain soil properties using either FLUSH or SHAKE, the generation of soil compliances using CLASSI and the time history response analysis using NASTRAN. The calculated seismic response of the Lotung structure is subsequently compared with its measured seismic response.

In the second phase, the results of low level forced vibration tests carried out on the Lotung structure are considered and better estimates for the soil compliances are obtained. The response of the containment model to

©seismicisolation
©seismicisolation

the same two real earthquake time histories is predicted again using these refined soil compliances and the calculated seismic response is compared with the measured seismic response.

DESCRIPTION OF LOTUNG CONTAINMENT MODEL, SITE AND INSTRUMENTATION

The containment model is located within the Taiwan Power Company, Lotung Substation in North-Eastern Taiwan. It is a 1/4 scale reinforced concrete model of a PWR containment building. The model is cylindrical in shape with an outer diameter of 10.5m and wall 300mm thick. It stands 10.67m above the ground and is embedded to a depth of 4.57m.

The response of the containment model is recorded at ten stations located within the building [1], see Figure 1. There are three accelerometers at each station to record the seismic response in three orthogonal directions, namely vertical, North-South and East-West.

The model is founded on a soft layered saturated site comprising mainly silty sand and sandy silt to a depth of between 30m and 40m and silty clay below that depth, to at least 150m, with the ground water table about 1m below the surface. A typical soil profile showing the dynamic soil properties for the Lotung site is given in Figure 2.

The ground surrounding the model is instrumented with an array of 15 strong motion triaxial accelerometers. The accelerometers are positioned along three arms which extend radially from the structure as shown in Figure 3. Each accelerometer records the ground acceleration time history in the same three orthogonal directions as the building accelerometers.

SEISMIC MOTION

A number of seismic events have been recorded by the array of ground accelerometers since it was commissioned. This study was limited to the ground time histories recorded during two of these seismic events. These were those recorded during the 20 May 1986 earthquake (event No. 7) and the 14 November 1986 earthquake (event No. 16). These two events were chosen as they were amongst the largest of the range of events recorded at the Lotung site and at the same time exhibited a different spectral content. Details on these two seismic events are given in Table 1(a).

For the analyses only one of the sets of time histories recorded by the array during each seismic event was used. The acceleration time histories recorded at station A2-3 during the 20 May event and those recorded at station A1-5 during the 14 November event were selected to calculate the high strain soil properties for the site and to predict the seismic response of the containment model. Details of these two sets of time histories are given in Table 1(b). The set of time histories recorded at station A2-3 during the 20 May event are shown in Figures 16 to 18. These time histories were selected as their frequency content was typical of the frequency content recorded during the particular seismic event by ground accelerometers located a distance away from the building, where the presence of the building did not influence the recorded seismic motion.

TABLE 1(a)
Details of Seismic Events

Event No.	Date	Duration (s)	Peak Ground Acceleration (g) E-W	N-S	Vert
7	20 May 86	35.52	0.062	0.187	0.047
16	14 Nov 86	56.00	0.125	0.150	0.122

@seismicisolation

TABLE 1(b)
Comparison of Peak Ground Accelerations for the Earthquake Time-Histories Selected for the SSI Analyses

Event No.	Station	Peak Ground Acceleration (g)		
		E-W	N-S	Vert
7	A2_3	0.169	0.215	0.047
16	A1_5	0.133	0.169	0.098

STRUCTURAL IDEALISATION

The containment model was idealised by a finite element beam-mass model using the NASTRAN beam (CBEAM) and mass (CONM2) elements.

The soil was idealised by a system of six frequency independent elastic springs and dampers representing each of the six rigid body degrees of freedom. NASTRAN scalar spring (CELAS2) and scalar damping (CDAMP2) elements were used in the discretisation and they were connected directly to the underside of the base slab of the containment model.

Frequency dependent spring stiffnesses and damping coefficients, ie. compliances were calculated using CLASSI assuming a surface mounted building. The frequency dependent compliances were then modified to take account of the embedment of the Lotung structure by modifying the stiffnesses as recommended in Ref [2]. The damping coefficients were not modified in this work. The high strain soil properties used in CLASSI to calculate the soil compliances were derived from the low strain dynamic soil properties shown in Figure 2 using both SHAKE and FLUSH. The selected time histories quoted in the previous section were used in the deconvolution studies to obtain the high strain soil properties.

The modified spring stiffnesses and damping coefficients at the containment model's lowest SSI natural frequency in each of the six rigid body degrees of freedom were used as the frequency independent soil compliances [3]. These frequency independent soil compliances which are shown in Table 2 indicate that, for the earthquake time histories considered in this comparative study, the use of soil properties generated using SHAKE and FLUSH produce similar stiffnesses and damping coefficients.

SEISMIC RESPONSE OF CONTAINMENT MODEL

The time history response analysis of the containment model was performed using a modified version of solution sequence 31 in NASTRAN. Solution sequence 31 which follows the modal superposition method was modified to incorporate composite hysteretic structural and viscous soil damping together with cross-coupling between modes [4].

The response of the containment model to the two seismic events was predicted using the soil compliances appropriate to the event under consideration, ie. the soil compliances based on the 20 May earthquake time histories were added to the building model to examine its response to the 20 May seismic event. The surface ground motion was applied directly to the soil spring/damper system. This is a conservative assumption inherent in the procedure employed by NNC Ltd for the SSI analysis of buildings.

SSI Modal Characteristics

The first mode of vibration of the combined soil structure system was a coupled rocking shear mode corresponding to a natural frequency of around 2.4Hz. The first vertical mode of vibration occurred at a natural frequency of around 4.8Hz and the first torsional mode of vibration occurred at around 5.8Hz. A comparison of the SSI natural frequencies obtained using soil

© seismicsoftware

TABLE 2
Comparison of Soil Compliances Based on High Strain Soil Properties Determined Using SHAKE and FLUSH for the Two Selected Time Histories

(a) Stiffness

	SHAKE		FLUSH	
Component	Event 7	Event 16	Event 7	Event 16
Horizontal (N/m)	3.92E+08	4.78E+08	4.00E+08	5.31E+08
Vertical (N/m)	6.17E+08	7.35E+08	5.98E+08	8.11E+08
Rocking (Nm/rad)	2.57E+10	3.05E+10	2.58E+10	3.28E+10
Torsional (Nm/rad)	1.67E+10	2.04E+10	1.74E+10	2.26E+10

(b) Damping

	SHAKE		FLUSH	
Component	Event 7	Event 16	Event 7	Event 16
Horizontal (Ns/m)	1.30E+07	1.42E+07	1.32E+07	1.46E+07
Vertical (Ns/m)	2.83E+07	2.99E+07	2.91E+07	3.19E+07
Rocking (Nms/rad)	2.19E+08	2.19E+08	2.20E+08	2.23E+08
Torsional (Nms/rad)	1.84E+08	2.00E+08	1.85E+08	2.02E+08

compliances based on SHAKE and FLUSH is given in Table 3. The differences in the SSI natural frequencies shown in this table reflect the differences in the compliances tabulated in Table 2.

Seismic Response

The predicted time histories for the containment model showed that the horizontal responses at all four stations on each level was the same. This was expected as a circular symmetric section should not show a significant response in the torsional mode. The predicted vertical response on one particular level varied from station to station but the response at a particular station at the top of the model was very similar to the response at the station directly underneath it, ie. vertical response at F4UE was very similar to vertical response at F4LE. This indicated that the structure was seismically rigid vertically and that the recorded vertical response was mainly due to soil-structure interaction. In general the predicted responses at all locations confirmed that the finite element model was behaving as expected with a predominant horizontal rocking mode.

TABLE 3
Comparison of SSI Natural Frequencies Obtained Using the Soil Compliances Based on the Two Selected Earthquake Time Histories Using SHAKE and FLUSH

	SHAKE		FLUSH		
Mode	Event 7	Event 16	Event 7	Event 16	Description
1	2.29	2.50	2.30	2.60	Rocking/Shear (N-S)
2	2.29	2.50	2.30	2.60	Rocking/Shear (E-W)
3	4.52	4.93	4.45	5.18	Vertical
4	5.40	5.94	5.50	6.25	Torsional
5	6.68	7.24	6.73	7.42	Hor. Translational
6	6.71	7.35	6.76	7.69	Hor. Translational

@seismicisolation

A comparison of the predicted and measured response at station F4UE

(see Figure 1) is given in Figures 4 to 6 for the 20 May 1986 earthquake and Figures 7 to 9 for the 14 November 1986 earthquake. The response predicted using soil compliances based on both SHAKE and FLUSH high strain soil properties is shown. Typical measured and predicted response acceleration time histories are shown in Figures 19 to 24. These figures show the response of the containment model to the 20 May event at station F4UE.

Figures 4, 5, 7 and 8 show that the predicted horizontal response spectra envelop the measured horizontal response spectra throughout the frequency range. Furthermore the comparison indicates that the peaks of the predicted spectra occur at the same frequencies as the peaks of the measured spectra and correspond with the predicted SSI natural frequencies given in Table 3. It should be noted that the measured horizontal motion at the four stations on each level were also very similar.

The comparison of the vertical response spectra shows that in general the predicted response spectra envelop the measured response spectra and that the peaks of the predicted spectra occur at the same frequencies as the peaks of the measured spectra. There are some exceptions where the measured vertical response spectra exceed the predicted vertical spectra. However it can be shown that this can be attributed directly to the choice of input time history for the analysis - a comparison of all the recorded ground time histories during a single seismic event showed considerable spatial variation in the vertical seismic motion over the site.

The differences in the response predicted using soil compliances based on SHAKE and FLUSH is consistent with the differences in the soil compliances shown in Table 2. For the 20 May earthquake, Figures 4 to 6 show that the response predicted using either the SHAKE or FLUSH soil compliances is the same. This is expected as the rocking compliances, which dominate the SSI response of the containment model, are the same when based on either SHAKE or FLUSH soil properties. On the other hand for the 14 November event, the FLUSH rocking stiffness is slightly higher than the SHAKE rocking stiffness and this results in the slight frequency shift of the main spectral peak indicated in Figures 7 and 8.

Discussion of Results

The comparison of predicted and measured seismic response shows that the seismic SSI methods used for this comparative study which are typical of those used by NNC Ltd for building analyses produce conservative results. Also the comparison shows that the SSI methods accurately predict the frequencies of the peaks of the response spectra. Further exceedance of the measured response is ensured by the broadening and amplification of these "best estimate" spectra which are normally carried out by NNC Ltd in the generation of design floor response spectra for equipment qualification.

The conservatisms in the predicted response arise due to a number of reasons. In the first place, there are conservatisms inherent in the method used to derive the high strain soil compliances. The accuracy with which the frequencies of the spectral peaks are predicted indicate that accurate values for the soil spring stiffnesses are generated. The magnitude of the spectral peaks are influenced by the damping and the level of exceedance shown by the comparison indicates that the damping may be underestimated in the analyses. This is consistent with the fact that the method employed in this study to modify the soil compliances to take account of the embedment of the structure neglects the increase in the damping due to embedment effects. This pessimistic approach with regards to the embedment damping is expected to contribute significantly to the higher spectral peaks present in the predicted response and is examined in more detail in the next section.

There is some conservatism also due to the choice of input time history for the analyses. A comparison of all the response spectra recorded during

@seismicisolation

each seismic event indicates that, in general, the selected horizontal response spectra envelop the other response spectra recorded during the particular event over the site. This spatial variation in the recorded ground motion is expected to contribute to both the higher peaks present in the predicted horizontal response spectra and the underprediction of some of the peaks in the vertical response spectra.

Finally, there are some conservatisms due to the application of the time histories recorded at the surface of the site to the underside of the basemat. This does not take account of the variation of seismic motion with depth which is expected to influence both the magnitude of the spectral peaks and the frequency content of the seismic ground motion. This is expected to contribute also to the higher spectral accelerations predicted and further work is currently being carried out to examine this conservatism in more detail.

REVIEW OF FORCED VIBRATION TESTS

In order to examine the conservatisms inherent in the generation of the soil compliances and in particular the effects of embedment damping, the results of low level forced vibration tests carried out on the containment model [5] were reviewed with the view of obtaining better estimates for the soil dynamic stiffness and hence soil compliances. During the forced vibration testing, the structure was excited in both the radial (N-S) and tangential (E-W) direction by an eccentric mass vibrator located at the southern edge of the roof. The structure was subjected to steady state excitation over a range of frequencies between 1Hz and 30Hz and the response amplitude and phase were recorded over the frequency range by 20 accelerometers installed on the roof, basemat and at the midheight of the building.

Low Strain Level Modal Characteristics

The measured response data from these tests was analysed to obtain the low-level SSI modal characteristics of the model. This was done using two different methods, namely the Half-Power Bandwidth and the Resonant Testing method [6]. This indicated that the first SSI natural frequency was around 3.8Hz and was associated with a coupled horizontal rocking/shear mode. No other modes of vibration could be identified from the test results.

Soil Compliances

The dynamic stiffness of the soil was calculated from the test results assuming that the soil model/containment system could be represented as a coupled two degrees of freedom system, ie. a rigid body on a translational and rotational spring. The low strain rocking and translational soil compliances were then calculated from the rotational and translational dynamic stiffnesses of the soil respectively and are shown in Table 4.

The high strain soil compliances were estimated by modifying the low strain soil compliances to take account of the shear modulus degradation and increase in material damping expected on the Lotung site under the two seismic events used in this study. The resulting high strain soil compliances are shown in Table 4. A comparison of Table 4 and Table 2 indicates that the high strain translational compliances estimated using the test results are considerably greater than that calculated in the previous section. However the predominant SSI response is a rocking mode and hence this increase in the soil compliances is not expected to influence the seismic response of the model significantly. On the other hand whilst the rocking stiffness derived from the tests is very similar to that calculated earlier, the rocking damping coefficient is considerably higher. This difference in the damping coefficient is expected to contribute significantly to the higher spectral peaks discussed earlier.

@seismicisolation

Seismic Response

The high strain soil compliances tabulated in Table 4 were added to the building model and the response of the containment model to the two seismic events considered above was again calculated. The resulting response spectra at station F4UE are compared with the measured response spectra in Figures 10 to 12 for the 20 May 1986 event and Figures 13 to 15 for the 14 November event. These figures show that the predicted response to the two seismic events follows a similar trend to that predicted previously except that lower spectral peaks were obtained giving a better comparison with the measured response. This was as expected due to the higher damping coefficients from the forced vibration test results and confirms that the underestimation of the damping referred to in the previous section contributes significantly to the high exceedance predicted using the SSI methods employed by NNC Ltd for building analyses.

TABLE 4
Soil Compliances Generated Using the Forced Vibration Test Results

Component	Low Strain		High Strain	
	Horizontal	Rocking	Horizontal	Rocking
Stiffness	2.79E+09 N/m	7.27E+10 Nm/rad	9.77E+08 N/m	2.55E+10 Nm/rad
Damping	2.26E+07 Ns/m	5.87E+08 Nms/rad	3.27E+07 Ns/m	8.51E+08 Nms/rad

CONCLUSIONS

The seismic SSI methods employed in this comparative study which are typical of that used by NNC Ltd for the SSI analyses of buildings have been demonstrated to produce conservative results. The SSI methods predict the frequencies of the peaks of the response spectra accurately and result in conservative design floor response spectra for equipment qualification.

A major source of conservatism lies in the method used to estimate the soil compliances in which the soil radiation damping due to embedment is neglected.

ACKNOWLEDGEMENTS

The Lotung experiment was co-sponsored by the Taiwan Power Company and the Electric Power Research Institute (EPRI). The forced vibration tests were largely sponsored by the United States Nuclear Regulatory Commission (USNRC). This work was carried out by NNC Ltd under contract to Nuclear Electric (NE). NNC Ltd and NE wish to thank the above organisations for their permission to use the Lotung test data. The authors wish to thank NNC Ltd for permission to publish this paper.

REFERENCES

1. Liu, C.C. and Yeh, Y.T., Final Instrumentation Report for the Lotung Large Scale Seismic Test Program, Report No. ASIES-ER8510, Institute of Earth Sciences, Academia Sinica, December 1985.

2. Parris, R.A., Summary of Methods used to Calculate Floor Response Spectra for the Seismic Design of Equipment and Minor Structures, NNC Report No. PWR/RX745, November 1987.

3. Gardner, D.J., Llambias, J.M. and Shepherd, D.J., Investigation of

@seismicisolation

Various Aspects of the Soil-Structure Interaction Problem, Proceedings of the 11th International Conference on Structural Mechanics in Reactor Technology, Japan, August 1991 (to be published).

4. Parris, R.A., Aspects of Seismic Analysis Using MSC/NASTRAN, Proc. of the MSC/NASTRAN European Users' Conference, Munich, June 1983.

5. ANCO Engineers Inc., Test report for Forced Vibration Testing of 1/4 Scale Containment Structure, April 1986.

6. Clough, R.W. and Penzien, J., Dynamics of Structures, McGraw-Hill, 1975.

@seismicisolation

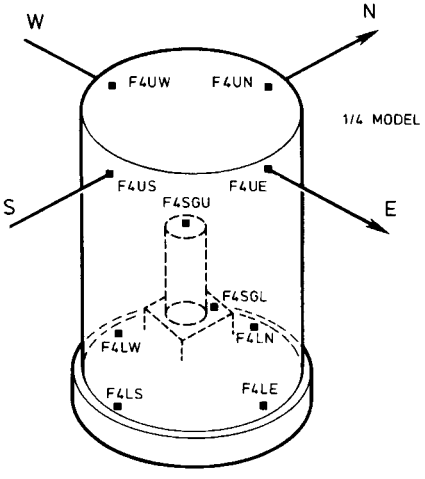

FIG. 1 ARRANGEMENT OF ACCELEROMETERS ON THE LOTUNG CONTAINMENT BUILDING

DEPTH (m)	SOIL PROFILE	Vs (m/s)	ρ (Mg/m³)	ν
0	SANDY SILT AND SILTY SAND	120	2.044	0.441
5		140	1.827	0.485
8		190	1.910	0.488
15		220	2.057	0.486
30		260	1.868	0.447
60	MAINLY SILTY CLAY	320	1.875	0.475
80		480	1.875	0.446
150				

FIG. 2 SOIL PROFILE AT LOTUNG

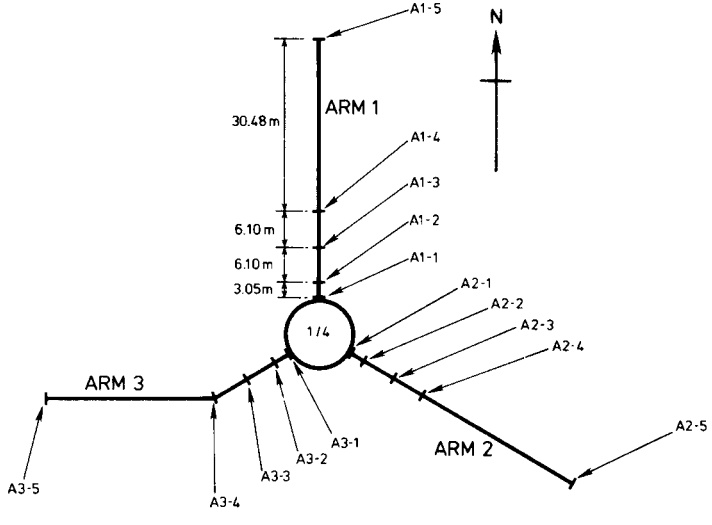

FIG. 3 LOCATION OF GROUND MEASUREMENT STATIONS

@seismicisolation

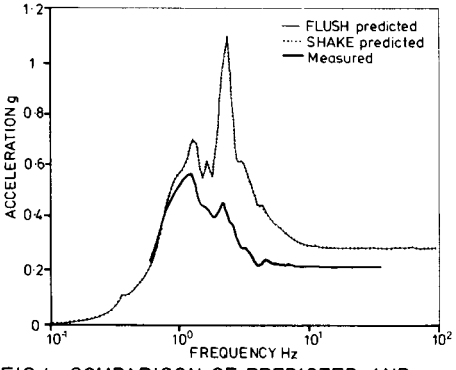

FIG 4 COMPARISON OF PREDICTED AND MEASURED RESPONSE TO EVENT No7 AT STATION F4UE (E-W DIRECTION)

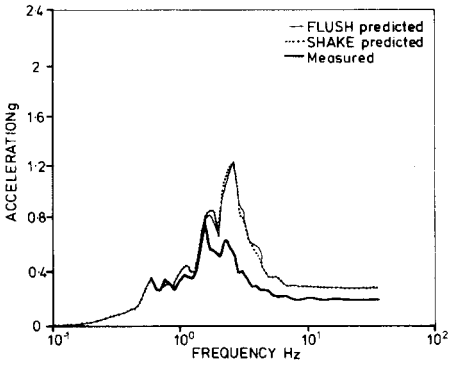

FIG 7 COMPARISON OF PREDICTED AND MEASURED RESPONSE TO EVENT No16 AT STATION F4UE (E-W DIRECTION)

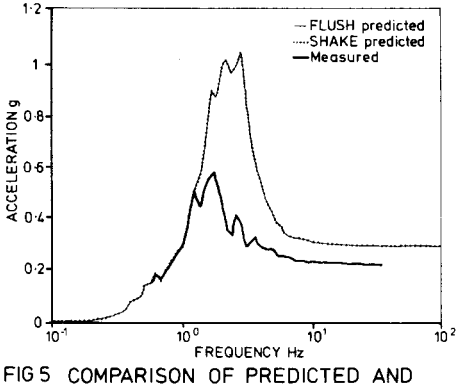

FIG 5 COMPARISON OF PREDICTED AND MEASURED RESPONSE TO EVENT No7 AT STATION F4UE (N-S DIRECTION)

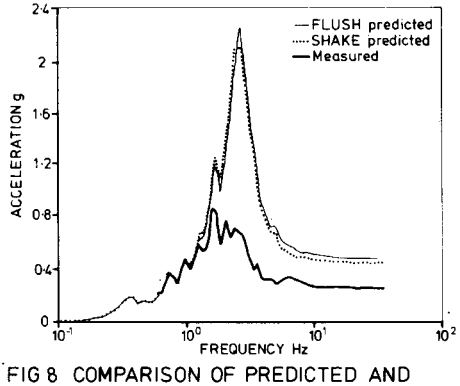

FIG 8 COMPARISON OF PREDICTED AND MEASURED RESPONSE TO EVENT No 16 AT STATION F4UE (N-S DIRECTION)

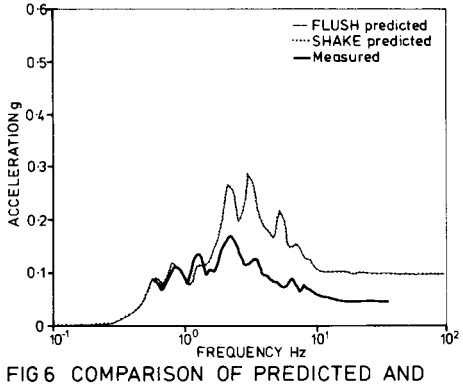

FIG 6 COMPARISON OF PREDICTED AND MEASURED RESPONSE TO EVENT No7 AT STATION F4UE (VERT DIRECTION)

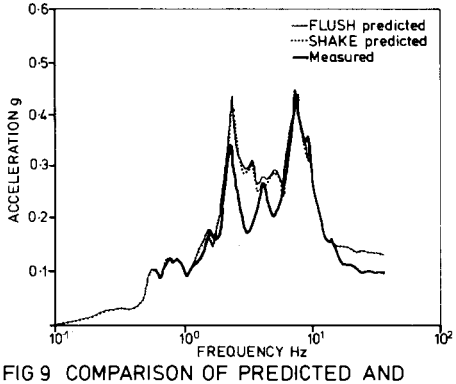

FIG 9 COMPARISON OF PREDICTED AND MEASURED RESPONSE TO EVENT No16 AT STATION F4UE (VERT DIRECTION)

@seismicisolation

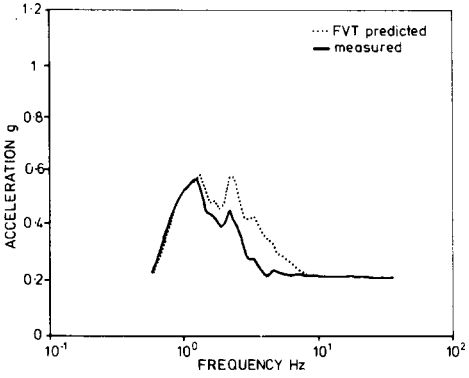

FIG 10 COMPARISON OF FVT PREDICTED AND MEASURED RESPONSE TO EVENT No 7 AT STATION F4UE (E-W DIRECTION)

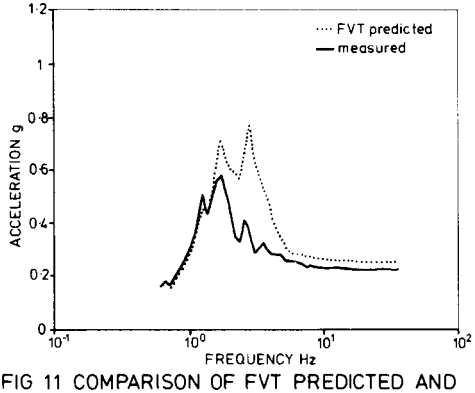

FIG 11 COMPARISON OF FVT PREDICTED AND MEASURED RESPONSE TO EVENT No 7 AT STATION F4UE (N-S DIRECTION)

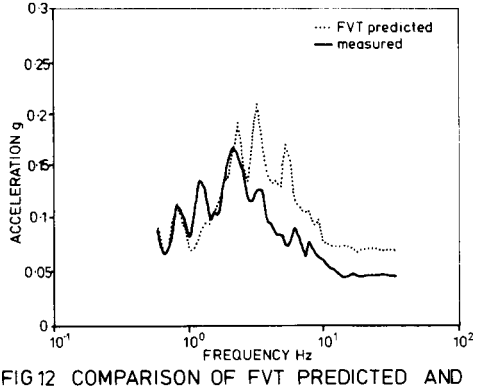

FIG 12 COMPARISON OF FVT PREDICTED AND MEASURED RESPONSE TO EVENT No 7 AT STATION F4UE (VERT DIRECTION)

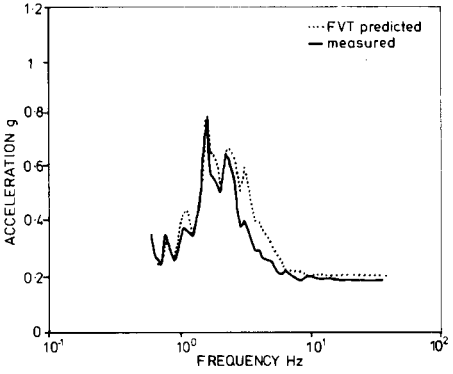

FIG 13 COMPARISON OF FVT PREDICTED AND MEASURED RESPONSE TO EVENT No 16 AT STATION F4UE (E-W DIRECTION)

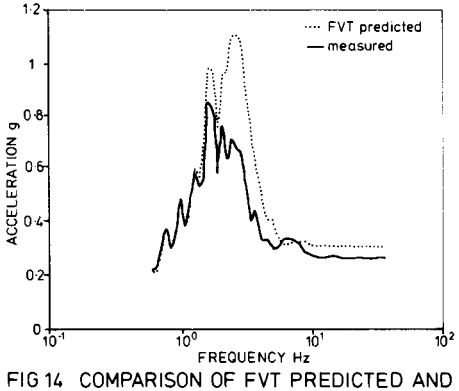

FIG 14 COMPARISON OF FVT PREDICTED AND MEASURED RESPONSE TO EVENT No 16 AT STATION F4UE (N-S DIRECTION)

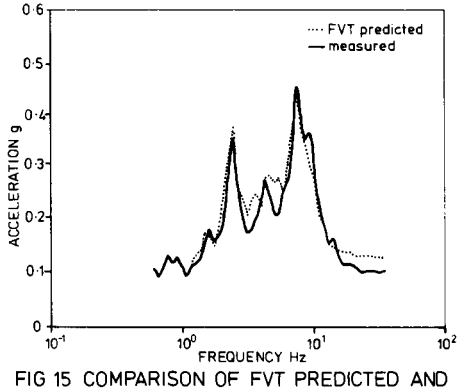

FIG 15 COMPARISON OF FVT PREDICTED AND MEASURED RESPONSE TO EVENT No 16 AT STATION F4UE (VERT DIRECTION)

@seismicisolation

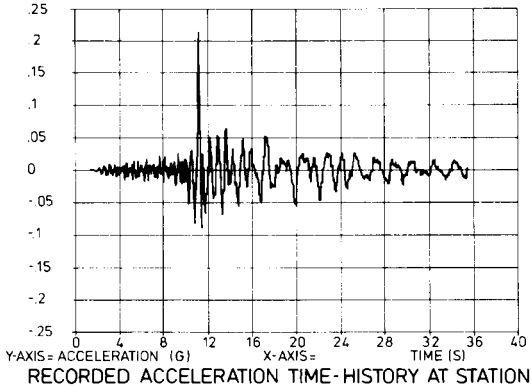

FIG. 16 RECORDED ACCELERATION TIME-HISTORY AT STATION A2-3 DURING THE 20 MAY 1986 EARTHQUAKE (N-S)

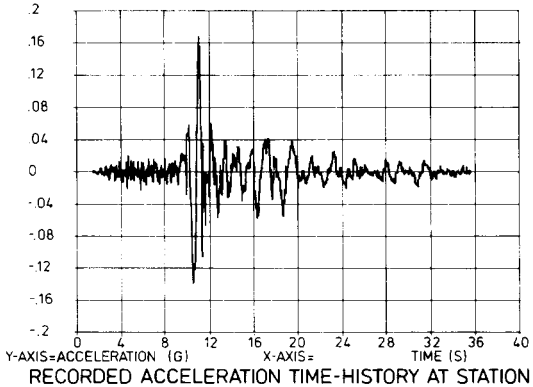

FIG.17 RECORDED ACCELERATION TIME-HISTORY AT STATION A2-3 DURING THE 20 MAY 1986 EARTHQUAKE (E-W)

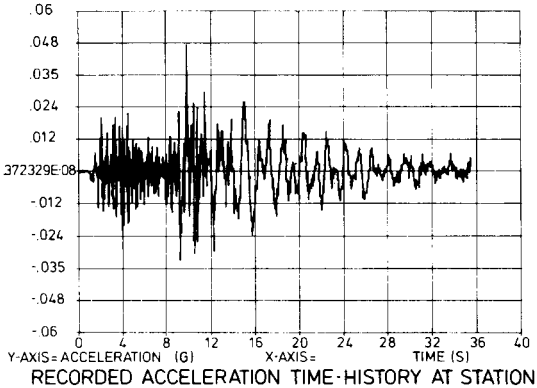

FIG.18 RECORDED ACCELERATION TIME-HISTORY AT STATION A2-3 DURING THE 20 MAY 1986 EARTHQUAKE (VERTICAL)

@seismicisolation

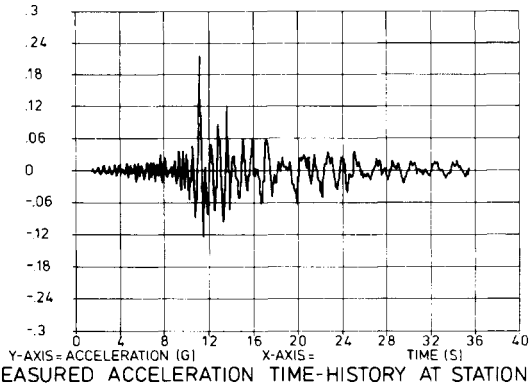

FIG.19 MEASURED ACCELERATION TIME-HISTORY AT STATION F4UE (N-S)-20 MAY 1986 EARTHQUAKE

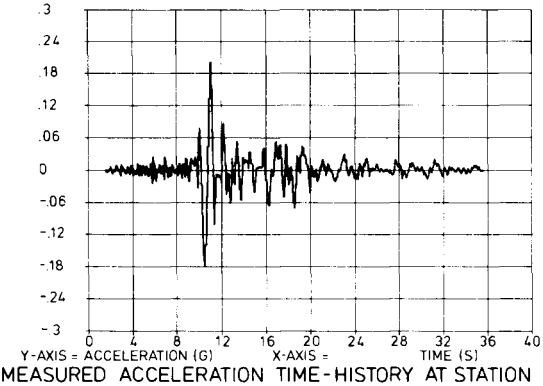

FIG.20 MEASURED ACCELERATION TIME-HISTORY AT STATION F4UE (E-W)-20 MAY 1986 EARTHQUAKE

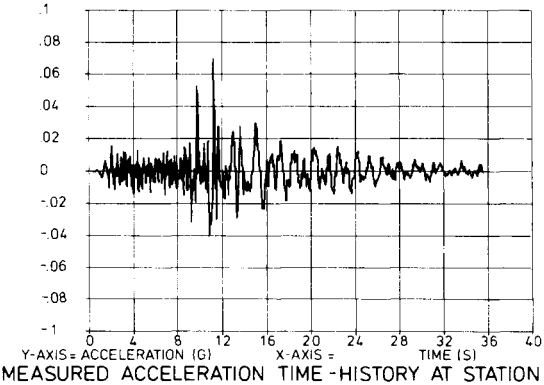

FIG. 21 MEASURED ACCELERATION TIME-HISTORY AT STATION F4UE (VERTICAL)-20 MAY 1986 EARTHQUAKE

@seismicisolation

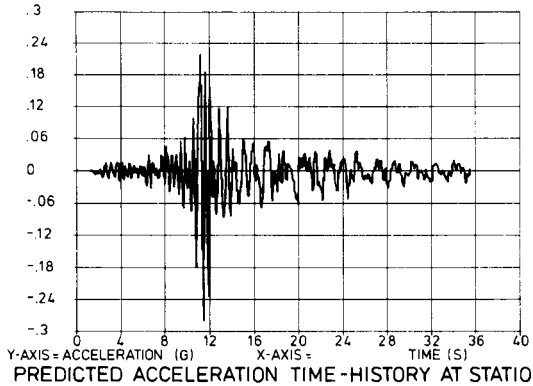

FIG. 22 PREDICTED ACCELERATION TIME-HISTORY AT STATION F4UE (N-S)-20 MAY 1986 EARTHQUAKE

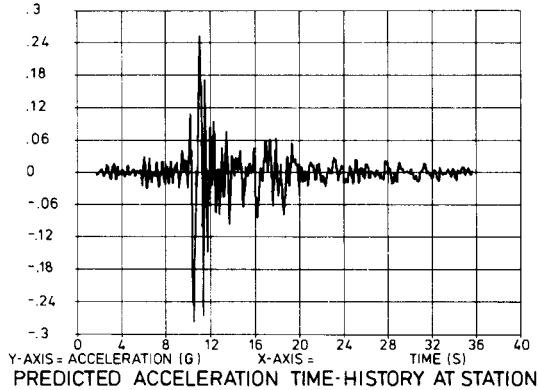

FIG. 23 PREDICTED ACCELERATION TIME-HISTORY AT STATION F4UE (E-W)-20 MAY 1986 EARTHQUAKE

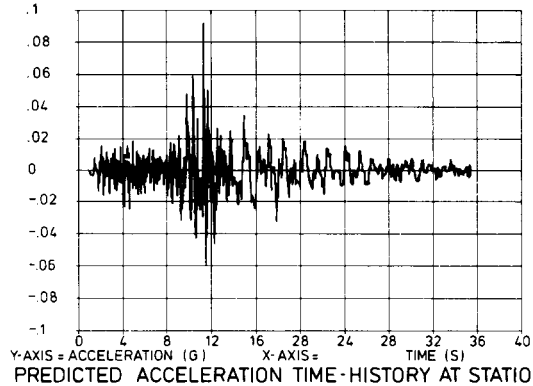

FIG. 24 PREDICTED ACCELERATION TIME-HISTORY AT STATION F4UE (VERTICAL)-20 MAY 1986 EARTHQUAKE

@seismicisolation

EFFECT OF TEST APPARATUS BOUNDARIES ON SHAKING TABLE TEST RESULTS

M. Budhu , G. Neelakantan and A. Al-Karni
Department of Civil Engineering and Engineering Mechanics
University of Arizona, Tucson, Arizona 85721, U.S.A.

ABSTRACT

Test results from seismic simulations using shake tables and centrifuges are often seriously affected by the responses of the test infrastructure, such as frames and supports, and especially the end boundaries of the test apparatus. Amplification of acceleration in shake table tests involving soil media may also significantly affect the results. Though such interferences may never be completely eliminated, proper modeling, fabrication and instrumentation of the test set up may mitigate these effects. Herein, we investigate the extent of such interferences on a model set up on a shake table which was used to study the seismic behavior of anchored retaining walls.

INTRODUCTION

A chief concern in shake table tests is the difficulty in producing a uniform acceleration field within the confines of the test region. This problem is very pronounced especially when the test medium is soil, since the horizontally applied base acceleration gets amplified along the depth of the soil. This acceleration amplification depends upon the stress-strain behavior of the soil and the applied dynamic base motion. Simplifying assumptions are often required to assess the approximate acceleration histories along the

@seismicisolation

depth of the medium. Another problem frequently encountered in shake table tests involving semi-infinite media such as soil is the proper modeling of boundaries. Often, the test boundaries do not imitate field conditions. The relative rigidity of the test boundaries with respect to the soil tends to create entirely different acceleration fields compared to those assumed.

In this paper we address the aforementioned problems by investigating (i) acceleration amplification during seismic simulation experiments and (ii) the effect of restraint conditions of the test boundaries on the interpretation of test results.

MODEL DESCRIPTION

We modeled an experimental set up to study the behavior of anchored retaining walls [1] wherein a 5.6m x 1m x 1m box with a test section 4m x 1m x 1m was used. An aluminium wall was placed in the middle of the section and dry Ottawa C-109 sand was pluviated on either sides to different depths. The longitudinal sides of the box were constructed from 12mm thick plexiglass. The test section was bounded by two plywood walls at either ends. Beyond these wall and extending up to the limits of the box were two compartments, each 0.8m long, 1m wide and 1m high, in which sand can be added to desired levels to stiffen the plywood end-walls (Fig.1). In our seismic tests on anchored retaining walls at SUNY, Buffalo [1], these end-compartments also served as over-flow regions to contain sand spillages that occurred when a mechanical sand spreader traversed the length of the test box, pluviating sand within the test region at a steady rate. The whole assembly was placed on the State University of New York (SUNY) at Buffalo seismic simulator and shaken. In this contribution we are only concerned with the stiffening effect of the sand within the end-compartments on the plywood end-wall (Fig.1). We theorize that the flexibility of this end-wall will have a significant influence on the quality of the test results.

@seismicisolation

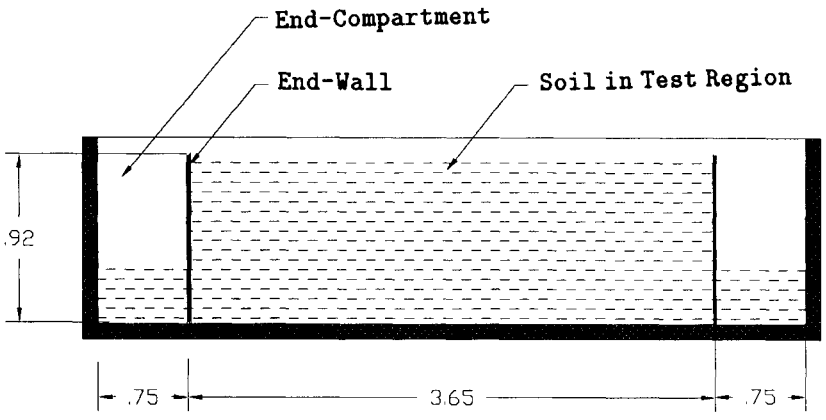

(Dimensions are in metres)

Fig. 1 - Model experimental set up

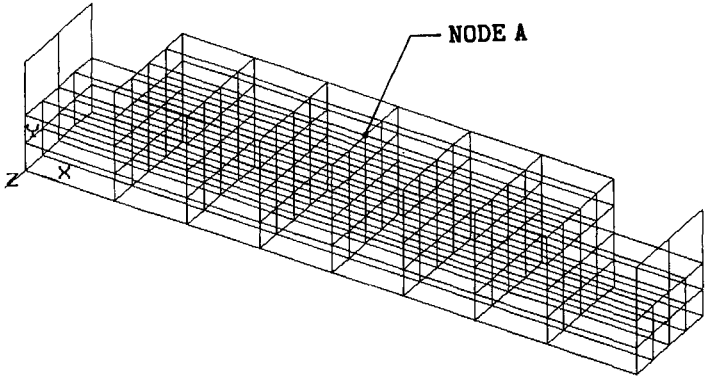

Fig. 2 - Finite element discretization of the model

@seismicisolation

NUMERICAL SIMULATION OF MODEL SET UP

We discretized the model set up into finite elements and conducted a transient dynamic analysis using ANSYS [2]. The soil elements were taken as 8-noded 3-D isoparametric solid elements and the plywood end-walls as plate elements. Interface friction between the sand and the longitudinal plexiglass sides was simulated using interface elements. The finite element discretization is as shown in Fig.2.

At the base of this model, we applied displacements consistent with a predetermined acceleration trace, with a peak acceleration of ±0.8g (Fig.3). Under such a loading condition, we studied the responses for (a) different elastic properties of the sand and (b) different restraint conditions of the end-walls.

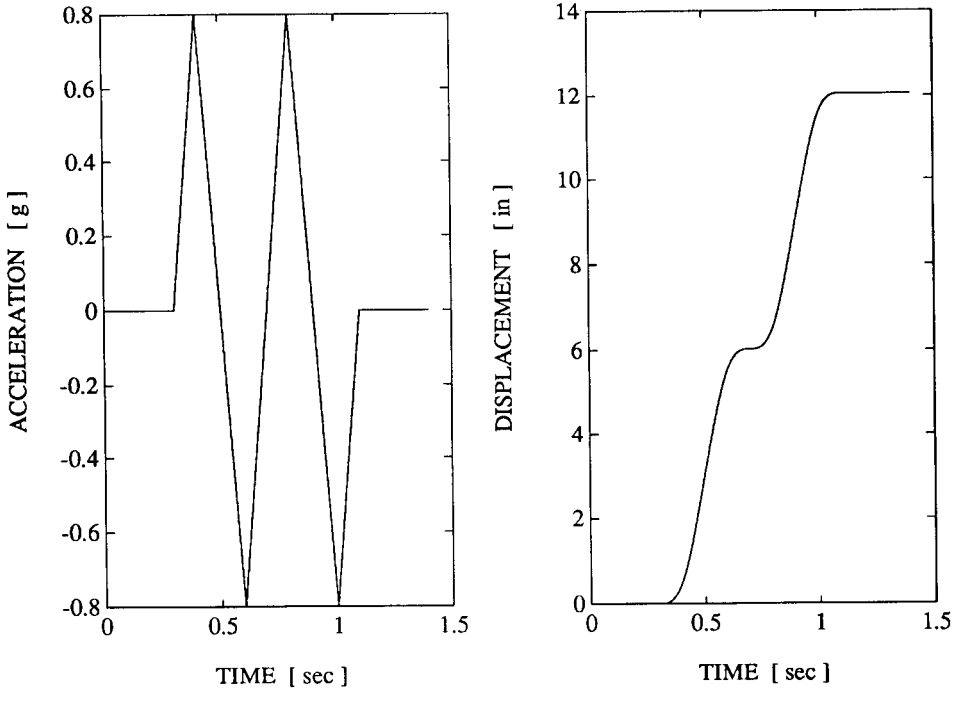

Fig. 3 - (a) Applied base acceleration and (b) displacement

@seismicisolation

ACCELERATION AMPLIFICATION

From the displacement histories of soil elements at various depths, we obtained the corresponding acceleration histories by differentiation. The variation of acceleration amplification with depth, for Ottawa C-109 sand for the maximum positive and negative acceleration peaks, is shown in Fig.4. As expected, the acceleration amplification increases upwards - away from the base.

The modulus of elasticity of the sand was varied from values representative of medium dense sand to those of dense sand. The numerical results (Fig.5) reveal that for medium dense sand the acceleration amplification could be as much as 350% while for dense sand the amplification is in the range of 200% to 300%. It may be noted that only a material of infinite elasticity would show an amplification of 1.0 - an ideal 'rigid body', for instance. These results are likely to exaggerate the amplification of real soils since only elastic deformations are assumed. However, they do show that it is important to locate accelerometers along the same horizontal plane, especially if the test material has a low elastic modulus.

RESTRAINT CONDITIONS OF END BOUNDARIES

It is desirable in shake table tests that the boundaries of the apparatus do not induce localized effects which will propagate during shaking and cause difficulties in interpreting the results with respect to a free field environment. In the case under study, if the sand elements at the end-region of the test box were to be subjected to conditions different from the mid-section as a result of restraint conditions of the end-walls, then the results of the tests will bear little resemblance to the likely field responses. As the dynamic responses are dependent upon relative stiffnesses, the restraints of the end-walls become important factors. An ideal end-wall would provide similar reaction and rotational stiffness as a semi-infinite body of soil subjected to the same base motion. Such ideal end-walls would ensure that all nodes along a specified horizontal plane would respond identically, for horizontal uniaxial shaking. On the other hand, end-walls that are rigid with respect to the soil medium may lead to considerable differences in the responses amongst the co-planar nodes.

@seismicisolation

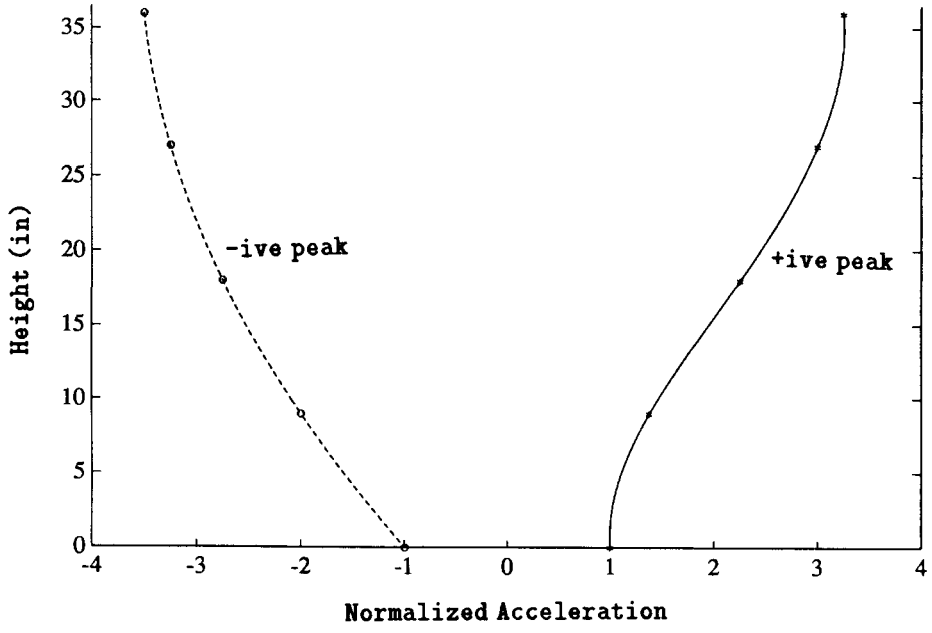

Fig. 4 - Variation of acceleration with height (Ottawa C-109 sand)

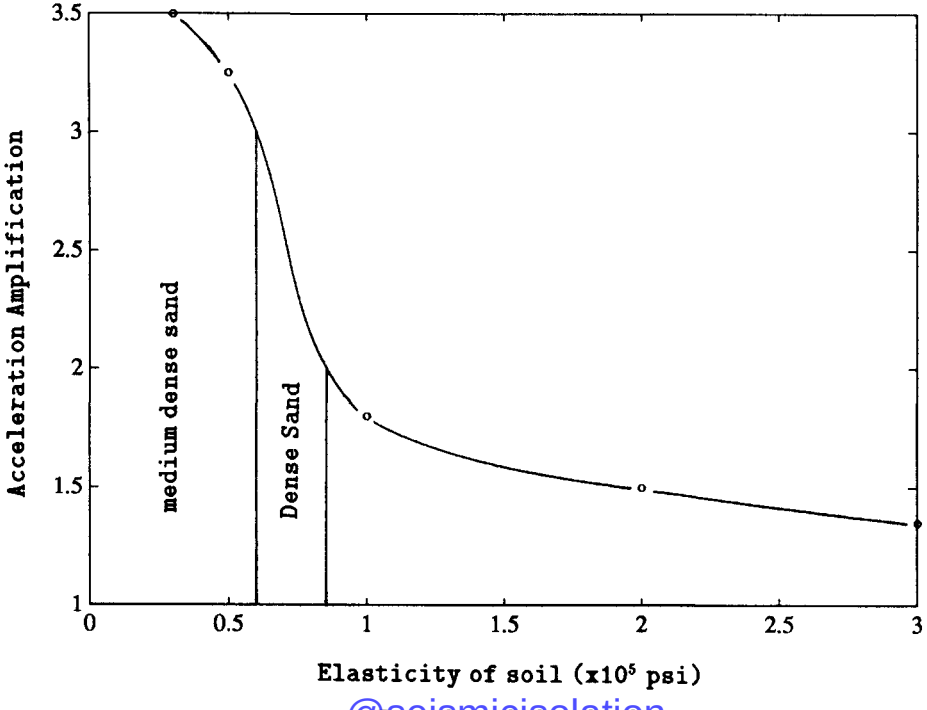

@seismicisolation

Fig.5 - Dependence of acceleration amplification on elastic modulus

In our effort to understand the extent to which the end-walls influence the response of the system, we increased the stiffness of the plywood end-wall boundaries by progressively increasing soil elements (simulating addition of layers of soil) within the end-compartments.

The difference in the predicted responses of the mid- and end-nodes, for various levels of soil in the end-compartments, is shown in Fig.6. Curve 'A' corresponds to the case for no soil in the end-compartments, curves 'B', 'C' and 'D' respectively represent the responses for end-compartments filled with sand to 25, 50 and 75 percent of the wall height. From these curves, it is observed that there is negligible difference in the responses of the mid- and end-nodes when there is no soil in the end-compartments. The difference progressively increases with increase in the amount of soil in the end-compartments.

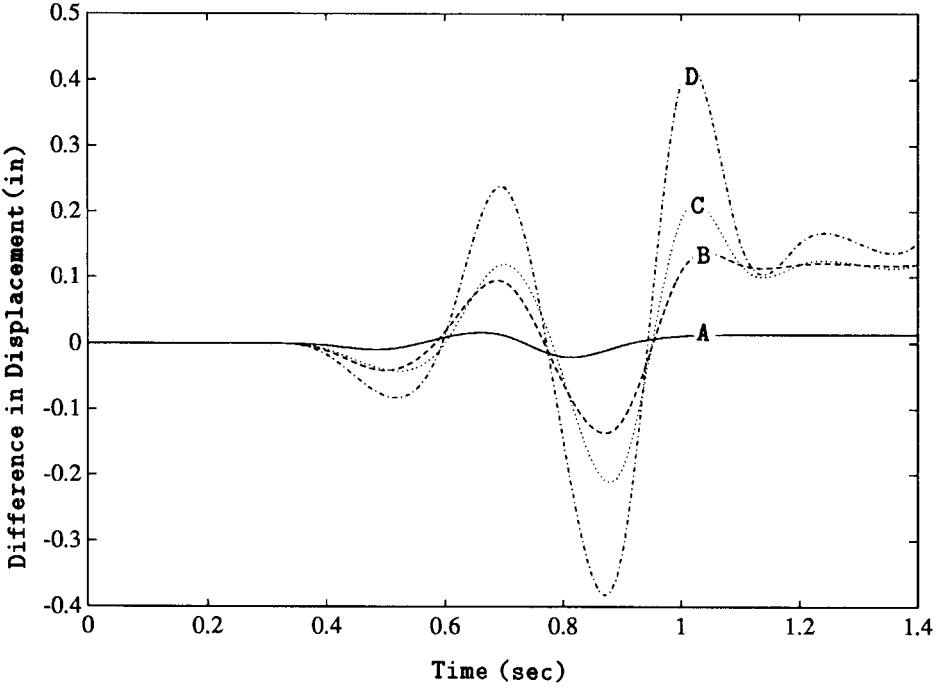

Fig.6 - Difference in responses of the mid- and end-nodes plotted for various levels of sand in the end-compartments

@seismicisolation

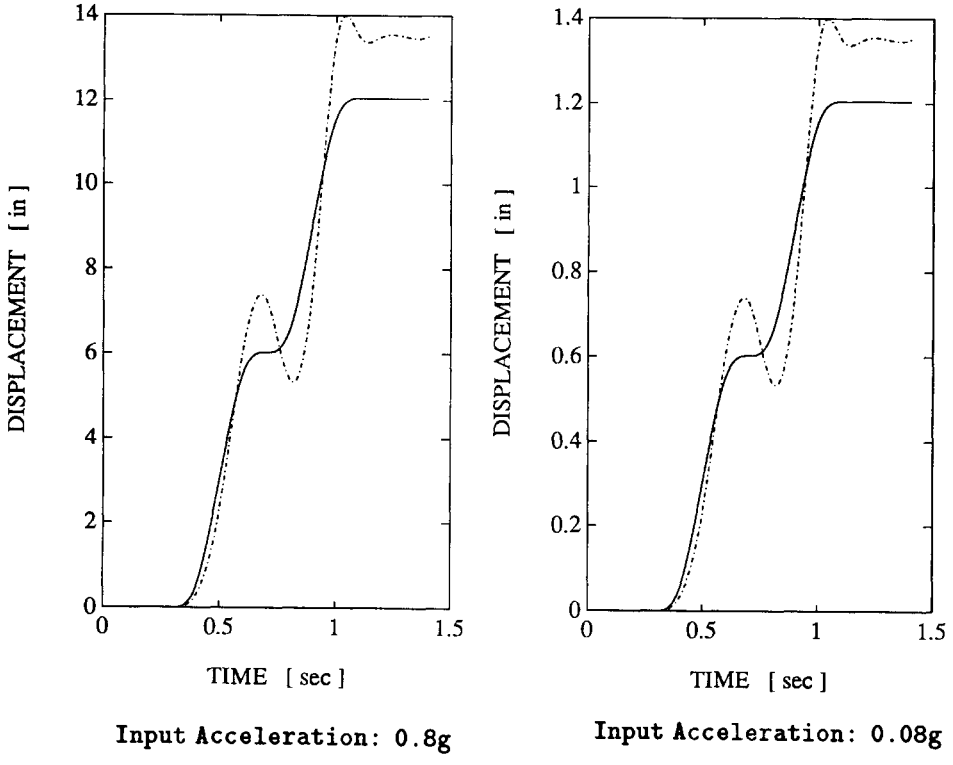

Fig. 7 - Response of node 'A' (Fig.2) for a peak acceleration input of (a) 0.8 g and (b) 0.08 g. The continuous line represents the input base motion and the dotted line represents the displacement histories of node 'A'.

@seismicisolation

It appears from the numerical simulations that when there is no soil in the end-compartments, the plywood end-wall boundaries would closely represent free field conditions. However, practical considerations such as excessive bending of the end-walls may necessitate stiffening of these walls. Such stiffening, in turn, increases the difference in the responses between the mid- and end-nodes. The minimum stiffening (minimum height of soil in the end-compartment) required would be governed by the maximum stresses and permissible deflections that can be allowed in the plywood end-walls.

The investigations carried out herein involved acceleration levels as high as 0.8g. Even if we scaled down the acceleration level by, say 1/10th, all the results of this analysis would be scaled down by the same level since we assumed linear elastic properties for all the materials. As an example, the acceleration trace in Fig.3 is scaled down by a factor of 10, so that the acceleration peaks were ±0.08g. From the curves in Figs.7a and 7b it can be seen that the responses in both the cases were identical except for a scaling factor of 10.

CONCLUSIONS

We have conducted a transient dynamic finite element analysis, to simulate a shake table test involving dry cohesionless sand. Results of our analysis show that acceleration amplification and restraint conditions of the test boundaries can have significant influence on the test results. We conclude that (i) considerable care should be taken to ensure that accelerometers are located along the same horizontal plane, especially for materials with low elastic moduli, to cater for the acceleration amplification which occur during shake table tests and (ii) the end boundaries must have sufficient flexibility if a close simulation of field conditions is desired.

REFERENCES

1. Neelakantan, G., Budhu, M. and Richards jr.,R., Mechanics and Performance of a Tied-Back Wall under Seismic Loads. Earthquake Engineering and Structural Dynamics, 1990, 19.
2. ANSYS - Engineering Systems User's Manual, Swanson Analysis Systems, Inc., Houston, Pennsylvania, 15342, U.S.A.

@seismicisolation

LABORATORY AND CENTRIFUGE MODELLING OF IMPACT LOADING ON BURIED STRUCTURES

Dr Michael C.R. Davies
School of Engineering, University of Wales College of Cardiff
P.O. Box 917, Cardiff CF2 1XH, U.K.
0222 874280

ABSTRACT

An experimental investigation of impact loading of buried structures has been conducted in two series of experiments. Models were tested in a laboratory floor apparatus in the first series and at elevated gravity in a geotechnical centrifuge in the second. In each case the model consisted of a flexible cylinder located in a medium of sand. The impulsive loading of the soil/structure system was provided by a mass impacting on a plate located at the surface of the soil immediately above the structure. Instrumentation in the soil and of the structure permitted monitoring of the propagation of the P-wave and the structural response. The results of the experiments are compared with predictions of stress wave attenuation and dynamic magnification factor.

INTRODUCTION

Buried structures may be subjected to blast and impulse loading resulting from stress waves travelling through the ground from a source of loading. Buried structures vary in size and function, from simple flexible pipelines to complex basement structures and sub-surface personnel shelters. The stresses which these structures have to withstand may be initiated by surface impact or result from an air or sub-surface explosion. Whatever the source of the impulse two aspects have to be considered in the design of buried structures. The first is the prediction of the intensity of the load reaching the structure from the source of loading. Secondly, having determined the nature of this loading the resulting soil structure interaction has to be quantified to establish the structural response.

A programme consisting of two series of experiments has been conducted to investigate the mechanisms involved when soil/buried structure systems are subjected to impulse loading resulting from surface impact. The first series consisted of small scale laboratory floor model tests [1]. In the second series the experiments were conducted at elevated gravity in a geotechnical centrifuge at the University of

@seismicisolation

Manchester [2]. In both series of model tests the structure - a flexible brass cylinder - was located in a surrounding medium of sand. Results from both these series of experiments are described herein.

Experimental Programme

In the laboratory floor experiments a comparison of the response of the soil/structure system to static and dynamic loading was investigated. To achieve this two sets of model tests were conducted. In the first set structures were located in the soil at different depths of cover and the soil immediately above the structure subjected to an increasing static pressure surface pressure until the cylinder failed. The model configurations were repeated in a second set of experiments. Dynamic loading of the soil/structure system was an impulsive force provided by a dropping weight. Cylinders buried at different depths of cover were subjected to the same surface impact allowing an assessment of the effects of stress wave attenuation on the structural response. In addition, a dynamic loading test was conducted in which there was no structure located in the sand. The purpose of this experiment was to investigate the attenuation of the pressure wave as it travelled through the "free field".

The stress/strain behaviour of soil under both monotonic and dynamic loading conditions is highly non-linear and thus stress level dependent. The centrifuge tests described herein were conducted to examine stress wave propagation and dynamic soil/structure interaction at prototype levels of stress. No specific prototype was envisaged in the design of the experiments. Rather, this was a generic study of the effects of impulsive loading on buried structures. Similarly to the laboratory floor experiments, the impulse was provided by a mass impacting at the surface of the soil immediately above the buried structure. The closest prototype situation would be a buried flexible pipeline subjected to a dynamic surface impact.

APPARATUS AND EXPERIMENTAL PROCEDURE

Laboratory Floor Models

The brass cylinder used in these tests had a diameter of 100mm and wall thickness 0.127mm; resulting in a very flexible structure. The models were placed in a 1.5m cubic tank, Fig. 1, and buried at varying depths of cover. The cylinders were fabricated from five lengths - joined together with adhesive tape - to span the tank. The intention of the segmental form of construction was to minimise end effects (as a result of confinement in the tank) on the instrumented central section; thus ensuring plane strain conditions for the instrumented section. A dry sand foundation with a repeatable density of 16.8 ± 0.1 kN/m^3 was achieved by pluviating sand from a hopper mounted on rails above the tank, Fig. 1.

In the static loading tests surface pressure was applied using an hydraulic jack acting on a 100mm wide stiffened plate (footing) which spanned the width of the tank above the buried cylinder. The longitudinal axes of both cylinder and footing being coincident. To maintain plane strain conditions during dynamic loading of the soil/structure system the impactor was a beam dropping 200mm onto a 100mm wide plate spanning the box. The impactor was located between guide rails to ensure simultaneous contact with the footing. The mass of the beam with its retaining elements was 26kg.

@seismicisolation

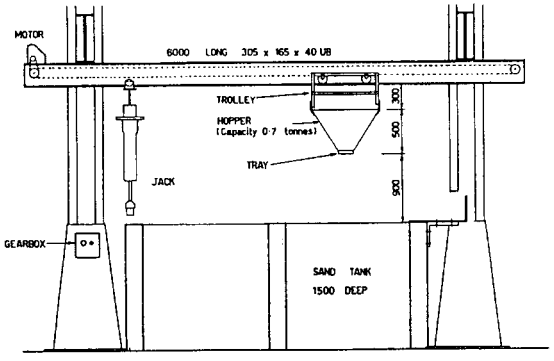

Figure 1. Laboratory floor apparatus (major features)

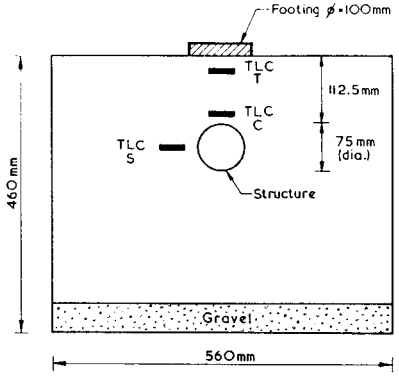

Figure 2. Section through centrifuge model showing location of buried structure and total load cells (TLC)

Centrifuge Models

The major features of the centrifuge models are shown in Fig. 2. In these experiments the structure was a cylinder 75mm in diameter, 400mm long and with a wall thickness of 0.127mm, located centrally in the strong box (560mm x 560mm x 460mm high) with a cover depth of 112.5mm (i.e 1.5 times the diameter). Tests were conducted at an acceleration of 20g. The model, therefore, represented a prototype cylinder 1.5m in diameter with 2.25m depth of cover. Similarly to the laboratory model tests, sand was placed in the centrifuge strong box by pluviation; resulting in a specimen having a density of 16.68kN/m^3.

In these experiments loading was provided by a mass impacting onto the centre of a target (footing) placed immediately above the structure at its mid-length. The target was a circular plate of diameter 100mm and thickness 25mm. These loading boundary conditions were considered to represent field conditions more closely than the idealised plane strain conditions in the laboratory floor experiments. The impactor was carefully fabricated to have a mass of exactly 1kg. This could be increased to 3kg by the addition of 1kg rings fixed to the central cylinder. When released the impactor fell through a guide tube a distance of 0.5m onto the target.

Instrumentation

In both static and dynamic laboratory floor tests stresses in the soil immediately below the footing and at locations adjacent to the crown and springing of the cylinder were measured using strain gauge diaphragm type miniature pressure cells. Circumferential strains in the cylinder wall were measured by pairs of strain gauges (one bonded to the inside of the cylinder wall and the other to the outside) positioned symmetrically around the middle segment at 45° intervals.

In the centrifuge models circumferential strains in the wall of the structure were measured by pairs of strain gauges positioned at 60°

@seismicisolation

intervals around the circumference of the cylinder at its mid-length. At three locations in the model total pressure cells measured the amplitude of the wave initiated by the surface impact. On the centreline of the model two pressure cells were situated in the soil between the target and the structure, Fig. 2, viz: 25mm below the surface (T) and 10mm above the crown of the cylinder (C). The third pressure cell (S) monitored dynamic stress in the soil 25mm from the springing of the cylinder. In both series of experiments signals were recorded on a 14 track tape recorder and later transferred to a digital signal memory recorder for analysis.

EXPERIMENTAL RESULTS

Characteristics of stress waves

The nature of the stress wave initiated by the impact of a mass on a plate located at the surface of the model was similar in both series of experiments. Figure 3 shows typical data from the series of centrifuge tests for the two pressure cells located on the centreline of the target, Fig. 2. Attenuation of the stress wave as it travelled between the two locations is apparent; this is discussed in detail below. If the stress wave pulse is approximated to a half-sin-wave, the typical frequency of the applied loading impulse measured by the pressure cell immediately above the crown of the buried cylinder was f = 0.410 kHz in the laboratory floor models and f = 3.731 kHz in the centrifuge models; yielding wave lengths, λ (= c_c/f), of 0.561 m and 0.153 m, respectively.

The velocity of the stress wave was obtained from the difference in arrival times at pressure cells located at different depths below the target, Fig. 3. The average values of P-wave velocity, c_c, were 230 ms^{-1} in the laboratory floor tests and 570 ms^{-1} in the centrifuge experiments. These values compare well with propagating wave velocities quoted for similar soils [3]. It is well established that the velocity of propagating body waves in an elastic material is a function of the stiffness of the material [4]. The in-situ stress conditions caused by the elevated value of g in the centrifuge model tests resulted in a higher soil stiffness than in the laboratory floor models, and hence a greater wave velocity.

Attenuation of stress wave

As body waves travel through the ground from a source the energy transferred to the soil is distributed over an ever increasing area. The reduction in the energy density with distance from the source of the disturbance results in a decrease in the displacement amplitude, δ, of the wave. Since the dynamic stress associated with the travelling pressure wave is proportional to the amplitude of the wave, the peak normal stress, σ_p, reduces with distance from the source of the disturbance.

For the plane strain loading conditions in the laboratory floor experiments the area of the wave front increases in proportion to the distance, r, from the source of the disturbance and it may be shown for an elastic soil

$$\sigma_p \propto \delta \propto 1/r^{1/2} \qquad (1)$$

@seismicisolation

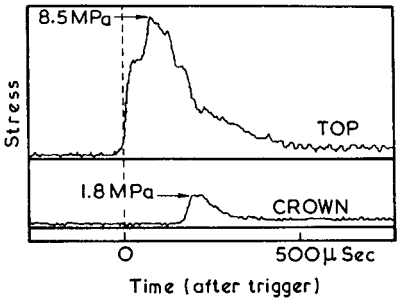

Figure 3. Typical output from total load cells located: Top - 25mm below surface and Crown - 102.5mm below surface

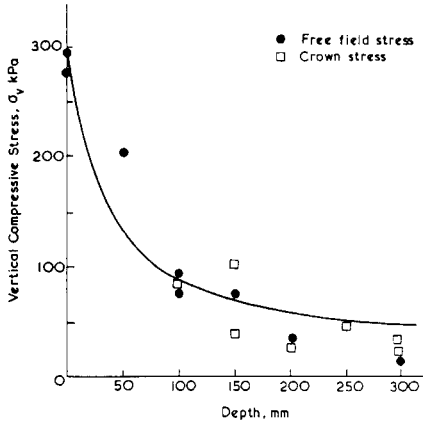

Figure 4. Measured and predicted attenuation of peak stress laboratory floor experiments

In Fig.4 the peak dynamic stresses measured 5mm above the crown of the structure in each of the laboratory floor experiments are plotted together with values of peak stress recorded in the "free-field" test. A curve of the form of Eqn. 1 is also shown in Fig. 4. The agreement between the measured and predicted attenuation is very good, although at greater depths the measured attenuation was slightly more than predicted - probably due to additional "material" or "internal" damping. The effect of this phenomenon is more pronounced in repeated dynamic loading and material damping is often ignored in impulse loading analysis because it is considered that the maximum response of a system is reached before appreciable energy is absorbed by damping.

The axi-symmetric nature of the impact in the centrifuge model tests results in spherical propagation of the wave front. Hence its area increases with the square of the radius, r. If the soil is considered to be elastic, it may also be shown that

$$\sigma_p \propto \delta \propto 1/r \qquad (2)$$

Plots of measured peak stress v. depth from the point of impact in centrifuge tests with impactors of mass 1kg and 2kg are displayed in Fig. 5. As would be expected, the peak stresses recorded in the tests in which the 2kg mass was used were greater than those measured in the experiment using the 1kg impactor, but both display very similar rates of attenuation. Curves of the form of Eqn. 2 are plotted together with the data in Fig. 5 showing close agreement between measured and predicted values of peak stress. The results of these tests and the laboratory floor experiments indicate the dominance of geometric damping in the attenuation of stress waves in soil.

@seismicisolation

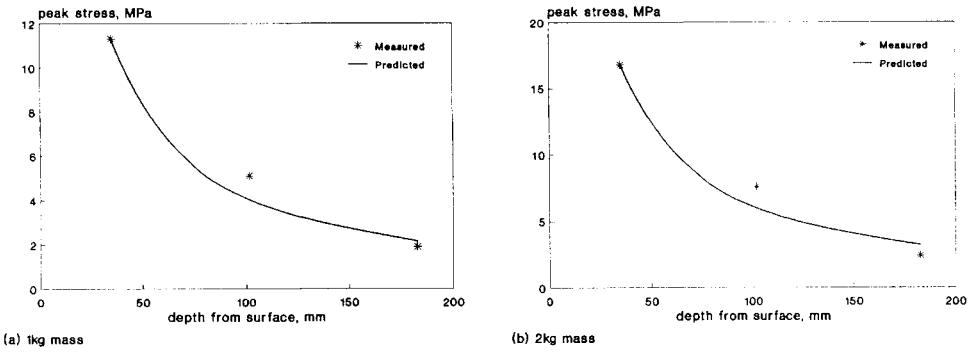

Figure 5. Measured and predicted attenuation of peak stress centrifuge experiments

Dynamic Magnification Factor, D

The response of an elastic system, with stiffness k, to dynamic loading may be expressed in terms of a dynamic magnification factor, D. This is defined as the ratio of the maximum response of a dynamically loaded system, x_{max}, to the response of the system if the peak dynamic load, P_D, had been applied monotonicly i.e.

$$D = \frac{x_{max}}{P_D/k} \tag{3}$$

Now the equivalent static load, P_S, required to produce a response equivalent to the maximum dynamic response, x_{max}, is given by,

$$P_S = k\, x_{max} \tag{4}$$

Hence, for an elastic system the dynamic magnification factor, D, may also be expressed in terms of the ratio of the static and dynamic loads, or stresses, which produce the same response in the system,

$$D = \frac{P_S}{P_D} = \frac{\sigma_S}{\sigma_D} \tag{5}$$

where σ_D and σ_S are the peak dynamic and equivalent static stresses respectively.

Values of peak dynamic stress recorded at the soil/footing interface in the laboratory experiments are plotted v. cover depth in Fig. 6, together with the static stresses at equivalent cylinder responses. The results indicate that to produce the same structural response the peak dynamic stresses were much larger than static values. The average value of the dynamic magnification factor for the soil/structure system was D = 0.15. Static loading tests were not conducted in the series of centrifuge experiments. However, it is possible to obtain an estimate of the dynamic magnification factor by calculating the equivalent static overburden

@seismicisolation

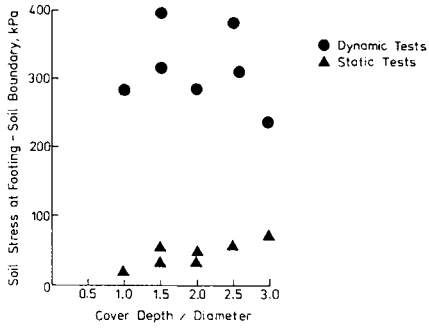

Figure 6. Dynamic and static soil/footing interface stresses at equivalent structural response

stress, σ_0, at the crown of the cylinder from the measured stresses in the cylinder wall - using ring compression theory - and comparing this value with the measured peak stress at this location. This yields an estimated value of D = 0.03 for these experiments.

For an elastic system it may be shown [5], that the dynamic magnification factor is a function of the ratio of the applied load frequency to the natural free vibration frequency. To calculate the value of D it is therefore necessary to predict the natural free vibration frequency of the soil/structure system. This may be achieved using the Rayleigh method [6]. For the laboratory experiments the forced frequency due to the impact was 2575 rad/s and the calculated value of the circular natural frequency of the soil/structure system was found to be 297 rad/s. This resulted in a dynamic magnification factor, D = 0.23. This value predicted the experimental trends, i.e. $P_D >> P_S$, and was of similar magnitude to the experimentally obtained value of D = 0.15.

Structural Response

Typical values of peak normal (i.e. hoop) strains in the cylinder are shown in Fig. 7(a) and Fig. 7(b) for the laboratory experiments and centrifuge tests respectively - the angle θ being measured from the crown of the cylinder. The rate of attenuation of peak stress decreases with depth, Fig. 4 and Fig. 5, hence there was a greater variation in stress across the structures located at shallow depths of cover. The high strains in the crown of the cylinder ($\theta = 0^o$) relative to the strains at the invert ($\theta = 180^o$) in the cylinder located at the shallowest depth, 0.5 x diameter, in Fig. 7(a) reflect the non-uniform pressure around the cylinder. As the cover depth was increased in the laboratory tests so the distribution of normal strain around the circumference became more uniform.

Greater detail of the soil/structure interaction was obtained from the centrifuge model tests. The response of three pairs of strain gauges in a test in which an impactor of 1 kg was used are shown in Fig. 8; the sets of plots represent locations (a) near the crown (b) at the springing and (c) near the invert of the model cylinder. The datum for time in Fig. 8 is the arrival of the stress wave at pressure cell T, Fig. 2. Following the arrival of the body wave at the structure two distinct types of response were observed.

@seismicisolation

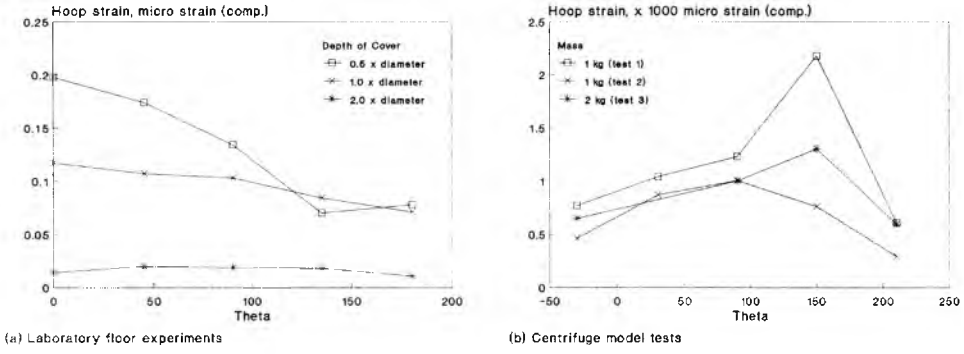

Figure 7. Cylinder hoop strains

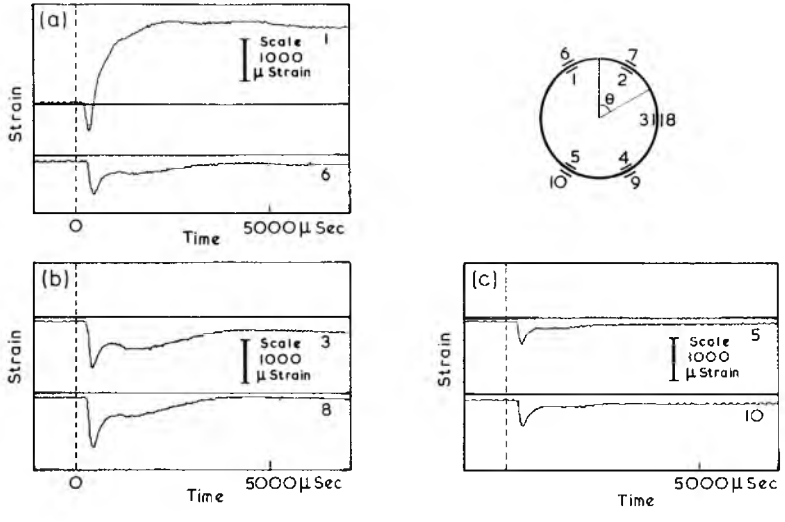

Figure 8. Typical output of internal and external strain gauge pairs following surface impact (Compression negative) (a) 1 and 6, (b) 3 and 8, (c) 5 and 10

Initially as the wave arrived at the cylinder all the gauges indicated compressive strain. There was a delay of 50 μs between the gauges at the top and the bottom of the structure responding as the impulse travelled through the structure - around its circumference. The gauges continued to show that the structure was totally in ring compression for a period of 134 μs, which corresponded to the length of the pressure pulse recorded immediately above the structure at pressure cell C. It has been shown above that the half-sin-wave length of the impulse was 76.5mm, thus as the wave passed the structure, which had a diameter of 75mm, it was completely enveloped by the compression wave. The values of peak compressive hoop strain at locations around the

@seismicisolation

circumference of the cylinder during the ring compression phase are displayed in Fig. 7(b). The magnitude of the strains around much of the circumference of the structures was very similar, i.e. approximately 1000 μ strain. A high value of 2180 μ strain was recorded at the haunch (θ = 150°) in one of the tests, probably resulting from insufficient densification of the soil around the base of the cylinder.

The strain gauge outputs, Fig. 8, indicate that the structure continued to deform under load for about 2000 μs after the commencement of loading, i.e. for a considerable time after the body waves had completely passed the structure. This deformation was caused by loading which resulted from the inertia of the soil/structure system. The internal gauge at the top of the structure, 1 in Fig. 8(a), changed from compression to tension during this period as (sagging) bending moments developed at the crown. As gauge 1 approached the yield value of 2000 μ strain, other gauges - which up to this point were showing a reduction in strain - indicated an increase in output, Fig 8(b), or a reduced rate of decrease in output, Fig 8(c), due to the redistribution of stress around the circumference of the structure. On excavation the structure displayed a permanent depression in its crown, consistent with the observations of the strain gauges.

Although ring compression was observed in both series of model tests the response to inertial forces, once the body wave had passed the structure, occurred only in the centrifuge experiments. This was a consequence of prototype stress conditions being reproduced in the centrifuge model. By contrast, in the laboratory floor experiments the soil above the cylinder was of insufficient weight to cause any measurable inertial loading of the structure. Therefore in addition to the benefits of testing a model in which the strength and stiffness of the soil were at prototype values, the technique of centrifuge modelling enabled this important loading mechanism to be observed. The necessity to conduct centrifuge tests in order to correctly model prototype scale field behaviour is clearly demonstrated by these observations.

The results of the above two series of experiments form a data set which may be used in the validation of both closed form and numerical analysis of dynamic soil/structure interaction. At present the validation of a finite difference code is being conducted. The results of the analysis of the dynamic loading laboratory floor models, in which stress wave attenuation and ring compression were closely predicted, have been published elsewhere [7]. Analysis of the centrifuge models is currently being conducted.

CONCLUSIONS

The following conclusions can be drawn from the results of the laboratory floor and centrifuge experiments:

1. In the laboratory floor models impact surface loading resulted in a body wave of frequency, f = 0.410 kHz, wave length, λ = 0.561 m and propagation velocity, c = 230 ms^{-1}. Typical characteristics of the body wave in the centrifuge models were f = 3.731 kHz, λ = 0.153 m and c = 570 ms^{-1}. The higher wave velocity in the centrifuge tests resulted from the greater stiffness of the soil in these models.

@seismicisolation

2. In both series of experiments the attenuation of stress waves was primarily caused by geometric damping. The rate of damping depended on the loading boundary conditions.

3. Comparison of the results of the static and dynamic tests in the series of laboratory floor experiments indicated that a dynamic magnification factor, D, could be used to predict the dynamic response. The predicted value of the dynamic magnification factor was of similar magnitude to the experimentally obtained value.

4. Both laboratory floor and centrifuge models exhibited ring compression as the body wave passed the structure. In the centrifuge models the structure continued to deform once the body wave had completely passed it. This was caused by the inertia of the soil/structure system.

5. The results of these experiments constitute a valuable data set for the validation of both closed form and numerical analysis of dynamic soil structure interaction.

ACKNOWLEDGEMENTS

The author wishes to thank Dr C.M. Merrifield and other members of the Centrifuge Modelling Group at Manchester University for their help in conducting the centrifuge experiments reported in this paper. The financial support of the Royal Armaments Research and Development Establishment, Christchurch, U.K. for the research in dynamic soil/structure interaction at University of Wales College of Cardiff is gratefully acknowledged.

REFERENCES

1. Spriggs, R.A., Impact loading of Buried Structures, M.Phil thesis, University of Wales College of Cardiff, 1990.

2. Davies, M.C.R., Modelling of dynamic soil structure interaction resulting from impulsive surface loading, Centrifuge 91, Proc. 2nd International Centrifuge Conference, Boulder, Colorado, U.S.A, 1991.

3. Barkan, D.D., Dynamics of bases and foundations, McGraw-Hill, New York, 1962.

4. Prakash, S., Soil Dynamics, McGraw-Hill, New York, 1981.

5. Clough, R.W. and Penzien, J., Dynamics of Structures, McGraw-Hill, New York, 1975.

6. Davies, M.C.R., Physical Modelling of Impact Loading of Buried Structures, In Structures Under Shock and Impact, ed P.S. Bulson, Elsevier, Amsterdam, 1989, pp. 431-442.

7. Claber, K.J., Davies, M.C.R. and Saunders, M.C., Validation of a finite difference code using centrifuge model tests of dynamic soil structure interaction, Proc. 5th International Symposium on the Interaction of Non-nuclear Munitions with Structures, Mannheim, Germany, 1991.

@seismicisolation

GROUND VELOCITY ATTENUATION ASSOCIATED WITH THE LOCKERBIE AIR CRASH IMPACT

D W REDMAYNE AND T TURBITT
Seismic Analysts, Global Seismology Research Group
British Geological Survey
Murchison House, West Mains Road, Edinburgh. EH9 3LA, UK

ABSTRACT

On 21 December 1988, as the result of a terrorist bomb attack, Pan Am flight 103, a Boeing 747 aircraft, crashed on the Scottish border town of Lockerbie.

The impact of the largest portion of the fragmented aircraft was detected by British Geological Survey seismometers in the Eskdalemuir network as a magnitude 1.3 ML event.

Seismometers at 17 and 24 kilometers gave direct measurement of ground velocity at their locations. Ground motions nearer to the impact site were however unknown and estimation from damage was complicated by air blast effects. To allow a full appraisal of the effect on buildings near the impact site, velocity attenuation data from a variety of sources, including measured velocities at seismometers, were extrapolated back to the impact site. The likely damage effects could then be predicted from the estimated peak velocities.

Results indicate that the impact was likely to be perceptible (peak particle velocities over 1 mm/s) within a radius of 1.1 kilometres and that structural damage was possible within 150 metres of the epicentre (peak particle velocities over 100mm/s).

A comparison is made with a number of other aircraft crashes detected by seismometer networks and efficiency and directionality effects are noted.

INTRODUCTION

Following the crash of the Pan Am Boeing 747 aircraft on the town of Lockerbie on 21 December 1988 there was considerable interest, particularly from the local authority, Dumfries and Galloway Regional Council, in the strength of ground shaking caused by the impact. At the site a number of houses had been totally destroyed, however, not far from the impact crater, buildings appeared to be structurally undamaged. For the rehabilitation of the area it was necessary to assess the level of

@seismicisolation

shaking likely to have been experienced by nearby buildings and the hidden effects on foundations and structures.

The Lockerbie aircraft impact was registered by British Geological Survey (BGS) seismometers as a 1.3 ML (Richter magnitude) event (Figure 1) and was detected up to 120 kilometres away. The location and time of the event confirmed that it was the impact of the largest portion of the Boeing 747 aircraft. Direct measurement of peak particle ground velocity, the measure of ground motion most directly related to damage, could be made from the seismograms at 17 and 22 km. Extrapolating back to the near-field of the aircraft impact, however, to the critical range where ground velocity exceeded perceptible levels, required data from other similar sources.

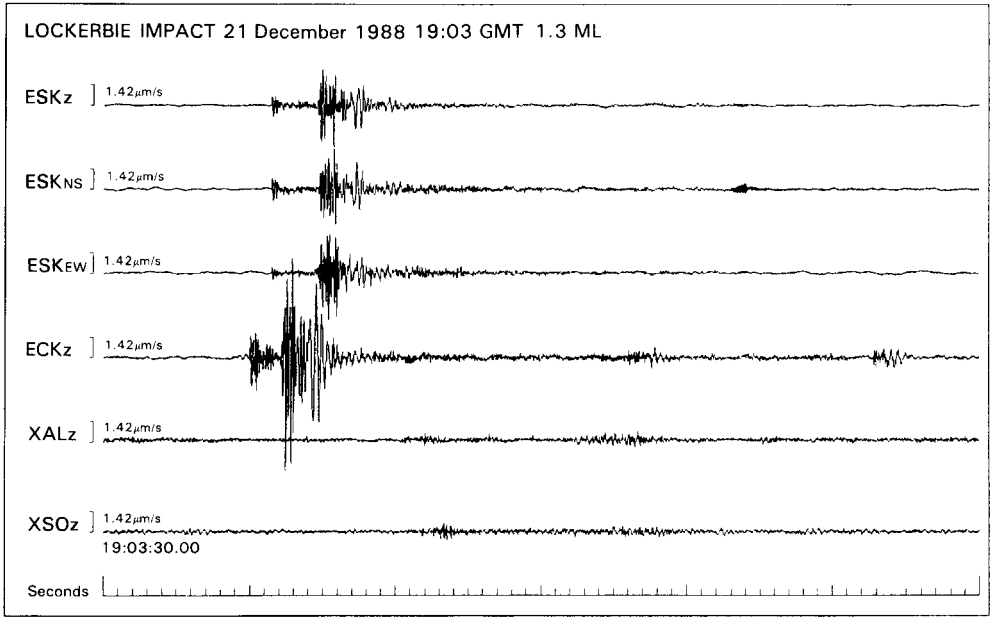

Figure 1. Seismograms of the Lockerbie impact recorded on BGS seismometers in the Eskdalemuir network.

SOURCES OF DATA

Data was collected from shallow events with magnitudes similar to the Lockerbie crash and the literature was searched for data on events of equivalent energy. BGS data from quarries, an underwater weapons test and

@seismicisolation

coalfield earthquakes was supplemented with data from environmental health quarry-blast tests and from Skipp [1] on cooling tower collapses and cratering explosions. The suite of data was chosen to cover, as completely as possible, ground velocities over the distance range of interest. Being shallow these events exhibited similar seismograms to the Lockerbie event, having pronounced surface waves and lower dominant frequencies than natural earthquakes.

Peak particle velocities from sources other than the Lockerbie impact had to be scaled to a 1.3 ML equivalent magnitude to give a consistent dataset. The relationship is straightforward: magnitude is proportional to $\log_{10}$(ground velocity).

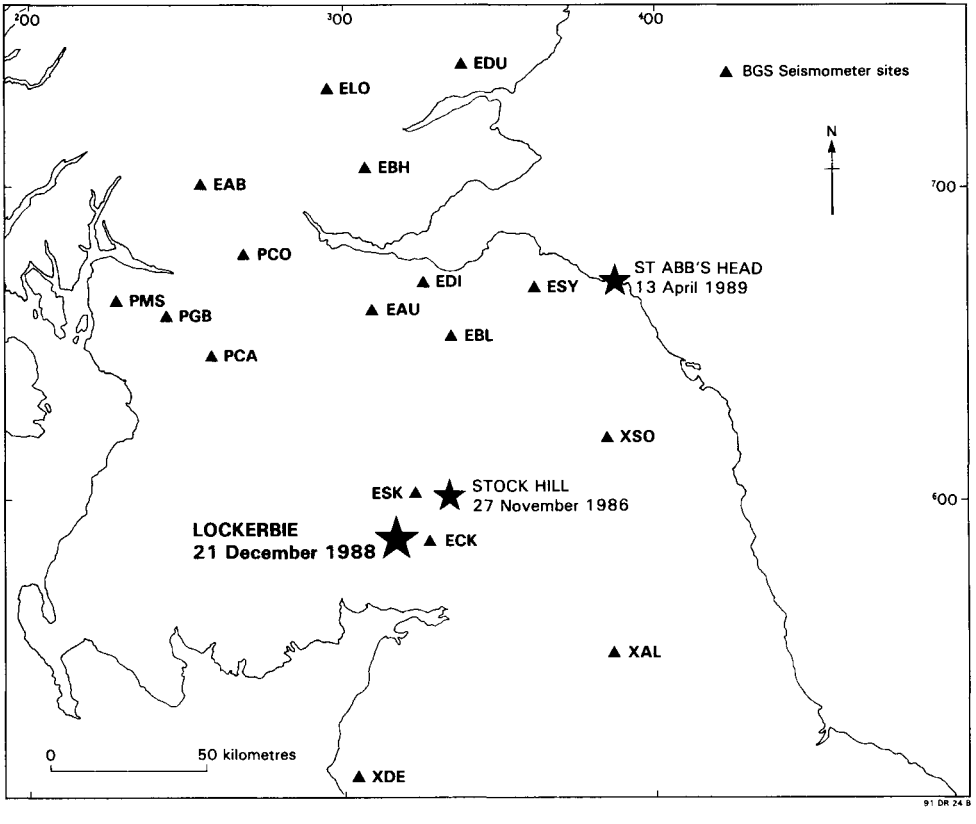

Figure 2. Locations of the Lockerbie and other crash sites with the BGS seismometer stations employed.

@seismicisolation

Measured Data

The records from seismometer stations ECK and ESK (Figure 2), 17 and 25 km distant respectively, gave direct ground velocities. Quarry blast data held by BGS for ranges from 2.9 to 29 km were scaled and added to the dataset. Ground velocities were scaled from a magnitude 1.1 ML naval underwater weapons trial monitored by BGS in 1983 at a range of 1.7 km. Collapse earthquakes induced by coalmining and recorded by BGS in the Midlothian and other coalfields gave data for the range 0.9 to 41 km from events with magnitudes from 0.5 to 1.1 ML. Near-field monitoring of Kaimes quarry, by Edinburgh District Council Environmental Health Department, gave values for 0.07 to 0.52 km which could be directly scaled having been monitored by BGS at a distance of 14 km. All the measured data collected for this study were from vertical instruments, these being more widespread than horizontal seismometers.

Published Data on Cooling Tower Collapses

Skipp [1] investigated ground vibrations induced by the demolition of power-station cooling towers at ten sites in the UK. Masses of 6,000 tonnes impacted on varying soil conditions with energies of up to 10^9 Joules. Skipp's data is presented graphically but is scaled to energy rather than magnitude.

The energy of the Lockerbie air-crash, equal to $\frac{1}{2}mv^2$, where m=130 tonnes (1.3×10^5 kg) and v=300 Knots (154.3 m/s), was 1.55×10^9 Joules. This value is very similar to that from the very much heavier, but slower, cooling tower collapses and scaling was straightforward. The regression line fitted to Skipp's data has been plotted on Figure 3(a) and gives good coverage in the near-field down to 0.05 km.

Published Data on Large Cratering Explosions

The air-crash created a very large crater in the gravels at Lockerbie. Skipp [1] also gives data for large cratering explosions. His regression lines based on this data have been scaled for equivalent charge size and give peak ground acceleration.

Peak ground acceleration was converted to peak ground velocity using the standard geophysical relationship:

$$\text{acceleration} = 2\pi f \times \text{velocity}$$

where f is the frequency of the waveform at that point (5.26 Hz for the Lockerbie air-crash, measured at ESK).

The energy of the Lockerbie impact was converted to an equivalent

@seismicisolation

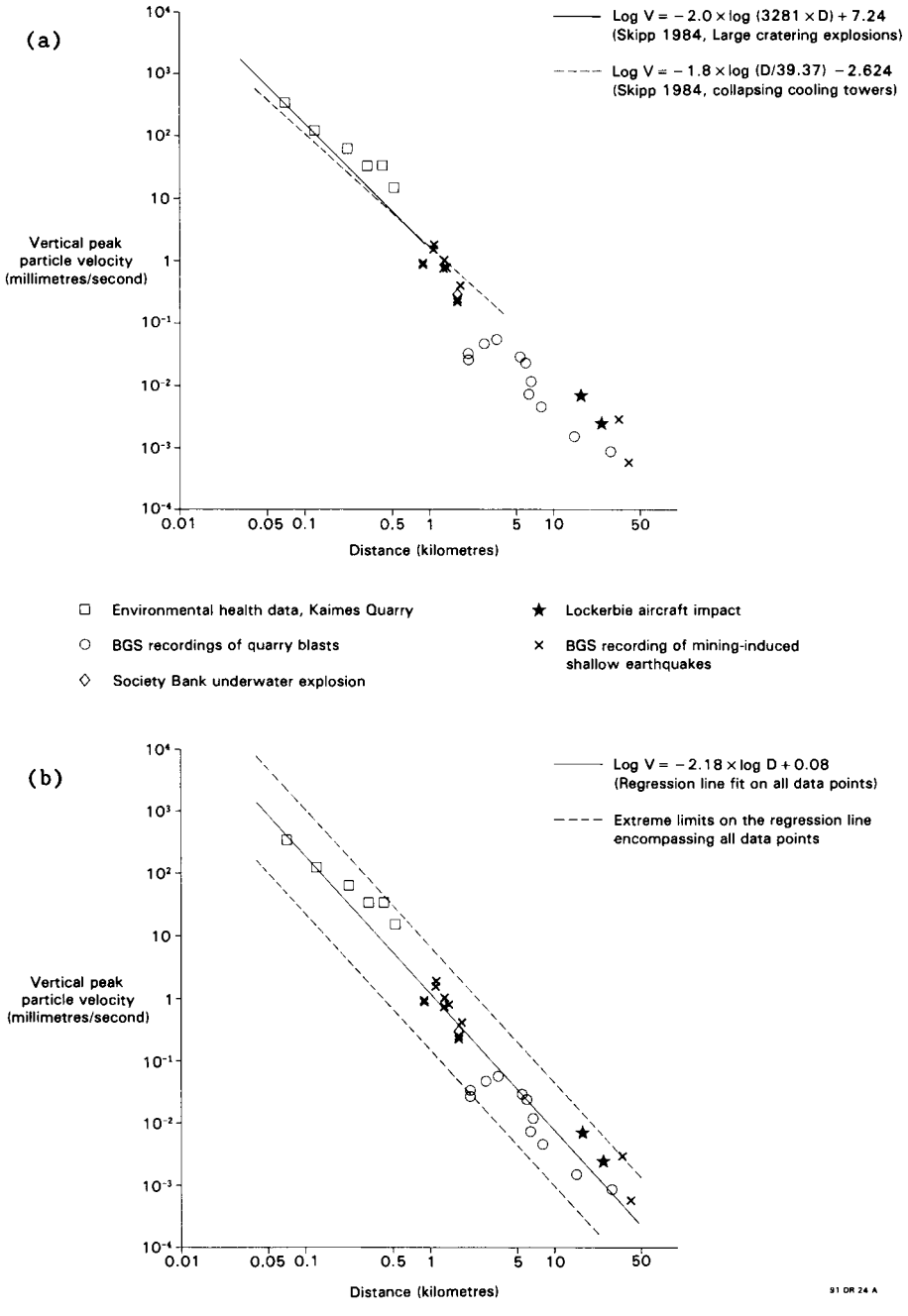

Figure 3. Peak vertical velocity attenuation data from a variety of sources, scaled to the magnitude (1.3 ML) of the Lockerbie impact. (a) All collected data. (b) Measured data with regression line and extreme limits.

@seismicisolation

charge size using a factor of 4 MJoules/Kg supplied by ICI explosives. This gives an equivalent charge size of 387.5 Kg of TNT which for convenience, and given the uncertainties involved in the efficiency of the impact and in the mass and velocity of the largest section of the aircraft, has been approximated to 0.5 tonnes. This agrees with estimates of the likely equivalent charge size estimated by ICI experts. The regression line for large cratering explosions is also plotted in Figure 3(a).

PRESENTATION OF THE DATA

All of the available data has been plotted on logarithmic axes in Figure 3(a) to show the relationship between peak particle velocity and distance from the source. It is immediately obvious that all the data fit a straight line remarkably well, even though they have come from various sources, and different scaling factors for magnitude, energy and charge size have been employed.

The near-field data, from Kaimes Quarry and Skipp's work on cooling towers and cratering explosions is, of course the most relevant. Extrapolating this data to the actual measurements for the Lockerbie crash gives a reassuring calibration.

A linear regression of the data, excluding Skipp's regression lines, is shown in Figure 3(b) along with extreme limits on the line encompassing all data points. A correlation coefficient of 0.971 confirms the good fit of the data and the slope of -2.18 indicates attenuation obeying the relationship:

$$\text{velocity} \propto 1/d^{2.18}$$

Theory predicts an inverse law for geometrical spreading plus an extra decay due to attenuation of the waves as they dissipate in the rock medium. The fit apparently holds good for these data over the range 0.05 to 50 km. The relationship obtained is:

$$\log v = -2.18 \times \log D + 0.08$$

where v is peak ground velocity in mm/s and D is epicentral distance in kilometres.

This attenuation relationship has been determined for vertical ground motion, but the attenuation observed will essentially be the same for horizontal ground motion also. For earthquakes it is generally observed that peak ground velocities are greater in the horizontal than the vertical by a factor of between two and three. For this event, however,

@seismicisolation

observation of the Eskdalemuir three component seismometer set (Figure 1) suggests that they were of the same order.

The indicated confidence limits on Figure 3(b), whilst encompassing all of the data points, may not reflect all of the inherent errors. Some of these, relating to assumptions made in scaling factors have already been discussed and are probably relatively minor compared to those due to soil effects, source radiation pattern and frequency dependent attenuation.

Differing soil conditions can introduce amplification or attenuation factors up to about four. It is also likely that the energy of the Lockerbie impact radiated asymmetrically with a maximum forward of the impact and minima at right angles to this direction.

For the data in Figure 3 no account has been taken of the frequency content of the seismogram. Attenuation is known to be frequency dependent, higher frequencies being attenuated more rapidly. This may also introduce errors into the dataset and its interpretation.

DISCUSSION

Predicted Damage at Lockerbie

Relating the ground motion at the site to the damage experienced requires reference to work carried out at quarry blasts. The seismograms of the aircraft impact recorded at the nearby BGS seismometer sites appear similar to quarry blasts in frequency content and a comparison would seem to be acceptable.

Information relating to safe blasting levels for ground motion have been produced by the United States Bureau of Mines who give peak particle velocities of 19.1 mm/s as a safe level for dry walls and 12.7 mm/s for plaster in the frequency range of the Lockerbie event. British Gas recommend that 25 mm/s should not be exceeded where their pipes are laid. These figures are for blasting and are likely to be on the low side to give a margin for uncertainty in prediction and also to allow for repeated blasting. Strictly speaking these figures relate to the overall peak particle velocity, whether in the horizontal, vertical or resultant planes.

@seismicisolation

For an assessment of damage effects Langefors and Kihlström [2] give the following for overall peak particle velocity:

less than 75mm/s - no noticeable cracks
75 - 100 mm/s - slight cracking and plaster fall
100 - 150 mm/s - cracks
150 - 225 mm/s - serious cracks

Below 1 mm/s the ground movement is unlikely to be felt. From this level up to 75mm/s the effects increase in intensity, being strongly felt over 12 mm/s where damage to unstable objects and structures may start to occur. The Manual of Seismological Observatory Practice [3], in relation to the MSK intensity scale, suggests that cracks may be caused from 12 mm/s upwards although this is for slightly lower frequencies (0.5-2.0 Hz) than the Lockerbie event (5 Hz).

Assuming, for this purpose, a symmetrical radiation pattern it can be deduced from Figure 3 that the Lockerbie air-crash impact would have been felt within 1.1 km (>1.0 mm/s), slight damage would have been possible within 0.4 km (>10.0 mm/s) and significant damage was likely within 0.15 km (>100 mm/s). Closer than 45 metres levels over 1,000 mm/s are predicted and general destruction was likely. It would be unwise to extrapolate much closer to the impact site than this as the elastic response of the ground is likely to limit and ground deformation predominate. The radius of the crater varied from 7.5 to 20 metres.

Severe damage did occur to buildings within 0.15 km of the impact site, especially forward of the point of impact. However, distinguishing the effects of air-blast, debris impact and fire from that of ground shaking was more problematical. A major aim of this study was to identify areas of likely damage from ground vibration to, for example, utilities and foundations which might otherwise remain hidden in a general survey.

Efficiency of the Lockerbie Event

Using Båth's [4] formula for the energy of an earthquake in ergs:

$$\log E = 1.27(ML) + 12.3$$

we get an efficiency for the impact of 0.6%, the magnitude having been read from seismometers close to the line of impact. This compares with quarry blast seismic efficiencies of about 0.4%. Skipp estimates efficiencies of about 1% for the cooling tower collapses.

@seismicisolation

The Nature of the Lockerbie Seismograms

The seismic signature of the Lockerbie impact was very similar to other shallow sourced seismic events. The seismogram (Figure 1) is nevertheless distinct, showing very strong shear waves (about 3 seconds after the first P arrival on station ESK) followed by a strong, longer period surface wave. The strong shear wave is characteristic of an impact source. It is not so marked for quarry blasts and coalfield events although the surface wave is, being symptomatic of a shallow source.

There are also a number of other arrivals on the seismogram. The signal on ECK about 42 seconds after the P arrival is thought to be an acoustic signature of the impact. The arrival 26 seconds after P on ECK may be the seismic signature of a smaller portion of the aircraft, possibly the cockpit, falling later. The precursor to P on ECK may have some significance, possibly an acoustic arrival from the break-up of the aircraft, but this must remain speculative.

Other Aircraft Crashes

Two smaller aircraft crashes were also examined for comparison. A Jaguar military aircraft crashed in trees at Stock Hill, 10 km east of Eskdalemuir Observatory, on 27 November 1986 and another Jaguar aircraft crashed into the cliffs near St. Abb's Head on 13 April 1989. Both aircraft weighed about 14 tonnes but were travelling at greater velocities than the Lockerbie aircraft: 232 m/s in the second case. These events generated seismograms similar to the Lockerbie event, but of lower amplitude.

The Stock Hill crash generated a magnitude 0.1 ML event, indicating a very low efficiency of 0.04%, probably because the aircraft struck at a low angle in trees dissipating much of the energy. The St. Abb's Head event showed extreme directionality, having hit vertical cliffs. Magnitudes varied from 0.06 ML from seismometers at right angles to the flight path to 0.8 ML from those directly in line with it. The latter magnitude gave an seismic efficiency similar to the Lockerbie event.

Other Attenuation Relationships

Comparison was made with two other attenuation relationships which have proved of value. Campbell [5] gives a relationship in terms of peak particle acceleration. This has been found to give good results in Britain for the 1990 Bishop's Castle earthquake. For the Lockerbie event, however, results did not agree with the attenuation relationship found

@seismicisolation

here. The likely reason for this is that Campbell's relationship was calibrated on larger deeper earthquakes in central USA and also because it is difficult to compare acceleration attenuation with velocity attenuation without taking account of frequency.

Esteva [6] gives a relationship for velocity:

$$v = 15e^{M}(R + 0.17e^{0.59M})^{-1.7}$$

where v is velocity in cm/s, R is the distance in kilometres and M is magnitude. It gives values which are higher by a factors of 10 to 1000: greatest at the farther distances. Apparently Esteva's relationship does not hold for such small events.

CONCLUSIONS

Data from various sources for vertical peak particle velocity attenuation in respect of the Lockerbie air-crash impact are found to be in good agreement for the range 50 metres to 50 kilometres. This also agrees closely with data published by Skipp [1] for cooling tower collapses and large cratering explosions.

Extrapolation of the relationship to the near-field of the impact site allows estimation of the peak ground velocity experienced by structures in this area. The range of data used in the graph (Figure 3) is believed to have significance to within 40 metres of the centre of the crash site. Closer than this ground deformation is likely and field trials would be necessary to calibrate the dataset.

Where damage to an installation can have hazardous consequences even the low probability of aircraft impact must be considered. This data provides a unique opportunity for the calibration of such events.

ACKNOWLEDGEMENTS

The authors wish to acknowledge the help of Mr R M Dixon of ICI, Nobel Explosives Ltd, Wigan and Mr A Sommerville of Edinburgh District Council's Environmental Health Department who provided data and advice used in preparing this paper. We also wish to thank Deakin Callard and Partners, surveyors, and the Air Accident Investigation Branch for Information on the Lockerbie crash and permission to publish. Thanks are also due to our colleague Mr Peter Marrow for his helpful advice and assistance. This work was supported by the Natural Environment Research

@seismicisolation

Council and is published with the approval of the Director of the British Geological Survey.

REFERENCES

1. Skipp, B.O., Dynamic ground movements - man-made vibrations. In Ground Movements and their Effects on Structures eds. P.B. Attewell and R.K. Taylor, Surrey University Press, 1984, pp 381-434.

2. Langefors, U. and Kihlström, B., The Modern Technique of Rock Blasting (3rd edn.), J. Wiley and Sons, New York, 1978.

3. Willmore, P.L. (ed.), Manual of Seismological Observatory Practice, Report No. SE-20, World Data Center A for Solid Earth Geophysics, Boulder, U.S.A, September 1979.

4. Båth, M., Structural and vibrational bedrock properties in Sweden. J. Comp. Phys., 1978, 29, pp. 344-356.

5. Campbell, K.W., A ground motion model for the central United States based on near-source acceleration data. In Earthquakes and earthquake engineering: the eastern United States, volume 1, ed. J.E. Beavers, Ann Arbor Science Publishers, Inc., Michigan, 1981, pp. 213-232.

6. Esteva, L., Seismic risk and seismic design decisions. Seminar on Seismic Design of Nuclear Power Plants, 1969, Cambridge, Mass., Massachusetts Institute of Technology Press.

@seismicisolation

DYNAMIC RESPONSE OF IMPACTED CEMENTED BACKFILL

Godwin N. Nnadi
Strata Engineering Corporation, Kingston, Canada.

ABSTRACT

Cemented backfills are commonly used as local and regional stabilizing structures during mineral extraction, although, apparently little is known about their behaviour when subjected to dynamic loadings such as blasting. Physical model studies were carried out in the centrifuge on backfill with 3 percent of cement to observe the material behaviour under simulated ring blast loadings.

The development of a method of vibration testing with impact excitation is described. The technique has many advantages for physical modelling over explosives or projectiles excitation and has been shown to be a reliable, controlled method for providing quantitative data. A brief outline of the theoretical basis is given. An impact loading mechanism mounted on the strong box of the centrifuge was used to simulate the ring blasting effects on the cemented backfill. The dynamic loadings were applied on a facial concrete slab which simulates the rock pillar being mined. Two series of tests were conducted. Series A consisted of cemented backfill with concrete slab of 20mm thickness. Series B had concrete slab of 30mm thickness. For each test series, the effect of simulated gravity was investigated. The responses of the material were monitored by accelerometers and dynamic stress gauges, and predictive relations obtained by dimensional analysis method.

INTRODUCTION

Cemented backfills have been used in several parts of the world as local and regional stabilizing structures during mineral extraction. Despite an increase in use, data on the behaviour of cemented backfill structures when subjected to dynamic loading such as blasting remain relatively scare. O'Hearn and Swan [1] reported a field instrumentation of the response of cemented backfill to blast loading, however, the blasts were not very close to the backfills.

A schematic representation of a rock-backfill system is shown in Figure 1. Askew et al. [2] reported a failure which resulted in the loss of over 15,000 tonnes of high grade ore in NBHC Mine, Broken Hill, Australia. An understanding of the dynamic behaviour

@seismicisolation

of cemented backfill will minimize the risk of such a failure. The degree of uncertainty associated with predicting the behaviour of prototype backfills subjected to explosive loadings makes the application of simple design safety factors insufficient. In developing simulation criteria, it is necessary to consider the two aspects of the problem: (1) the characteristics of
the prototype explosive environment, and (2) the dynamic behaviour of the backfill structure. The mechanics of transfer of explosive energy to backfill structures, and the resulting responses, are complex. Analysis of the behaviour of prototype backfill under such loading is not completely developed analytically, and correlation with experimental data is very expensive. Comprehensive testing or prototype instrumentation programs is required to assure reliability in the structural performance.

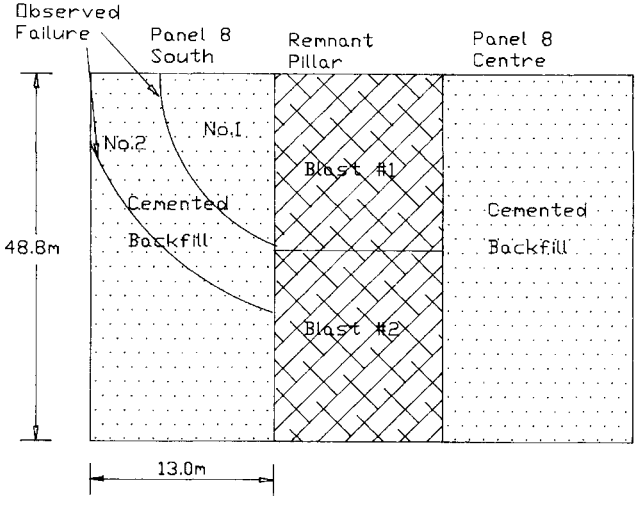

Figure 1. Vertical Section of Exposed Backfill Failure (Askew et al. 1978).

This study is directed toward improving our understanding of dynamic behaviour of cemented backfill when subjected to impact loading. Figure 2 illustrates the typical centrifuge model used in this study.

BASIC THEORY

In simulation of blasting effects in backfills, the boundary conditions, stress conditions and the type of force input are important. In this study, the backfill structure is idealized by the simplest model, the single degree of freedom system in which the response is a function of frequency. The equilibrium equation of the model leads to [3]

$$Mx + Cx + Kx = F(t) \tag{1}$$

where x is the horizontal displacement due to dynamic force F(t). The stiffness of the cemented backfill behind the rock section is K, the damping matrices is C, and M is the

@seismicisolation
@seismicisolation

mass of the rock section and the cemented backfill. The solution to equation (1) is:

$$x = x_1(t) + x_2(t) \tag{2}$$

where $x_1(t)$ is the general solution and $x_2(t)$ is the particular solution of equation (1). The function $x_1(t)$ is given for the underdamped case as:

$$x_1(t) = e^{-\xi\omega_n t}(A \sin \omega_D t + B \cos \omega_D t) \tag{3}$$

where $\omega_n = (K/M)^{0.5}$ = the undamped natural frequency; $\xi = C/2M\omega_n$ = critical damping ratio; $\omega_D = \omega_n(1 - \xi^2)^{0.5}$ = damped natural frequency; and A and B are redefined constants of integration.

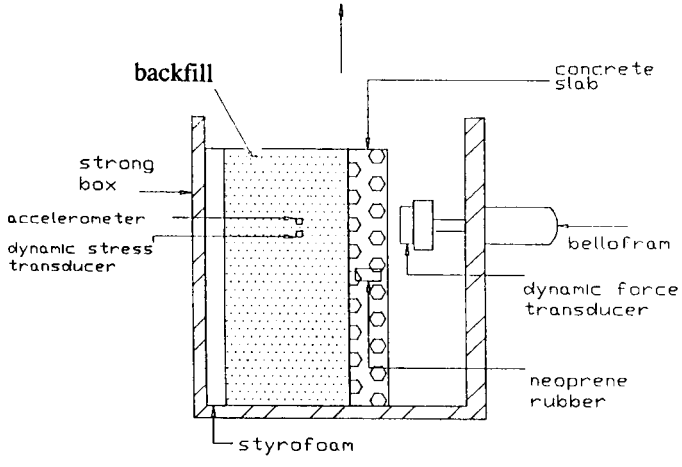

Figure 2. Typical Centrifuge Model for Backfill Structure.

If F(t) is a harmonic force, $F(t) = F_o e^{j\omega t}$, the function $x_2(t)$ is given as:

$$x_2(t) = \frac{F_o e^{j(\omega t - \theta)}}{[(K-M\omega^2)^2 + C^2\omega^2]^{0.5}} \tag{4}$$

where $\tan \theta = C\omega/(K-M\omega^2)$ The function $x_1(t)$ will die away after sufficiently long time because of the exponential term in equation (3) and the displacement x will be reduced to $x_2(t)$. Therefore, x(t) is given as

$$x(t) = \frac{F_o e^{j(\omega t - \theta)}}{[(K-M\omega^2)^2 + C^2\omega^2]^{0.5}} \tag{5}$$

@seismicisolation

and the acceleration a(t) is given as

$$a(t) = \frac{F_o \omega^2 e^{j(\omega t - \theta + 180)}}{[(K - M\omega^2)^2 + C^2\omega^2]^{0.5}} \tag{6}$$

The ratio between the acceleration response and the harmonic force is a function of ω. This function is called the transfer function of the system. The ratio of the maximum acceleration of the system and the maximum applied force is equal to the modulus of the transfer function.

A simplified confined vertical wall boundary condition is adapted for this study and the condition for identical stress is imposed on the model by the centrifuge testing method [4]. Ideally, explosive should be used, however, explosive excitation does not offer the opportunity to measure the force input. A practical approach to evaluate the behaviour of cemented backfill structure is to evaluate the response due to a known force. Basically, structural response may be defined as:

RESPONSE = PROPERTIES * INPUT (7)

For an accurate determination of the behaviour of cemented backfill structure, an input-output relationship should be developed and utilized. The concept of impact testing has been developed mainly for structural works but its potential for measuring ground vibration transmission has been demonstrated by White and Mannering [5]. It is desirable to establish the mechanical transfer function between the various parts on the system. The transfer function is derived from the relationship between the input spectral density and the response spectral density.

$$G_{yy}(\omega) = |H(\omega)|^2 \, G_{xx}(\omega) \tag{8}$$

where $G_{yy}(\omega)$ is response spectral density; $|H(\omega)|^2$ is the magnitude of the complex transfer function; and $G_{xx}(\omega)$ is the input spectral density. The complex function $H(\omega)$ has magnitude, phase, real and imaginary parts.

Signals such as acceleration, dynamic stress and force are recorded as a function of time. Yet the modulus of the transfer function $|H(\omega)|$ is a function of the frequency. Fourier transfer allows one to go from time domain to the frequency domain of the signals. It should be noted that forced vibration analysis is based on the assumption that the structure behaves in linear manner. However, for nonlinear systems such as soils, that are amplitude dependent, if the amplitude of the response is at a constant level, the system could be approximately treated as a linear system [6]. Certainly, the values obtained would be valid only for that vibration at that specific strain level. Although this method of analysis is not commonly used in backfill evaluation, it has been successfully applied to evaluate ground vibration [7-9].

An advantage of this method is that the accuracy of the testing and analysis for transfer function estimation could be evaluated by the coherence function which is defined as:

$$\gamma^2(\omega) = \frac{|G_{yx}(\omega)|^2}{G_{xx}G_{yy}} \tag{9}$$

@seismicisolation

where G_{yx} is the cross spectral density. The coherence function is basically defined for a linear, stationary system, however, for nonlinear systems the products of the nonlinearity are treated as system noise which reduces the coherence value [10]. A value of coherence function equal to unity corresponds to perfect correlation between the input and the output signals. Therefore, coherence function was checked to ensure the validity of the measurements and method of analysis. Typical coherence functions are shown in Figures 3.

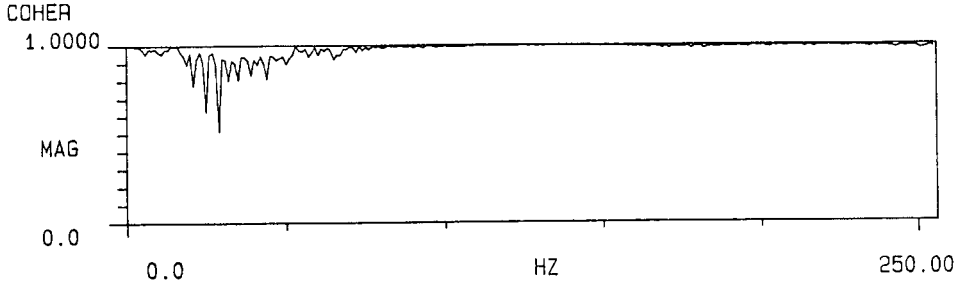

Figure 3. Typical Coherence Function at 104g for B Test Series.

Modelling Considerations

Small-scale physical models,however, may give erroneous results because the structural self weight which affects the dynamic responses are not modelled to scale. Experimental results obtained in the laboratory by using centrifuge to simulate self weight on small scale models are more reliable and reproducible. This modelling technique leads to a set of scaling relationships between the model and prototype. The relations between the quantities of interest in this study are shown in Table 1.

Centrifuge modelling offers a procedure for conducting physical scaled model tests with the gravity-induced stresses being accurately simulated. Townsend et al., [11] and other researchers have used explosives in the centrifuge, however, the impact mechanism used in this study measured accurately the force applied to the structure

TABLE 1
Scaling Relationship

Linear Dimension	L	$L_m=L_p/\lambda$
Stress	σ	$\sigma_m=\sigma_p$
Strength parameter	F	$F_m=F_p$
Energy	E	$E_m=E_p/\lambda^3$
Material density	ρ	$\rho_m=\rho_p$
Poisson's ratio	μ	$\mu_m=\mu_p$
Acceleration	g	$g_m=\lambda g_p$
Dynamic time	t	$t_m=t_p/\lambda$
Frequency	ω	$\omega_m=\lambda\omega_p$
Wave velocity	C	$C_m=C_p$

@seismicisolation

which is not possible with explosive excitation. The concept of impact mechanism is based on the consideration that the dynamic force generated by the impactor may be correlated to the dynamic force generated by blasted rock impacting on the fill.

The response of cemented backfill when subjected to dynamic loading is a function of many variables in addition to the properties of the material particle matrix. Nnadi and Mitchell, [4] observed that fifteen independent variables adequately affect the behaviour of particle motion in cemented backfill. They established functional relationships in terms of dimensionless acceleration and dynamic stress respectively. If the material properties are the same in all tests and the characteristic lengths scaled according to the induced gravity level, then for a centrifuge environment,

$$\bar{a} = f_1 [\bar{E}, \bar{S}, \bar{D}] \tag{10}$$

Equation (10) is the predictive equation for dimensionless peak particle acceleration, $\bar{a}$. Equation (10) indicates that the acceleration ratio, $\bar{a}$ is a function of energy ratio, $\bar{E}$, strength ratio, $\bar{S}$, and distance ratio, $\bar{D}$. However, if the density of the models are approximately the same, then the constitutive effects will be minimal. Nnadi [12] established that the energy ratio is linearly dependent on the inverse of the strength ratio. Therefore, the predicative equation in terms of peak particle acceleration ratio will be reduced to:

$$\bar{a} = f[g, \bar{D}] \tag{11}$$

where g is the induced acceleration level.

Similarly, the scaled dynamic stress and the response time are functions of the three independent variables.

EXPERIMENTAL TECHNIQUES

The materials used are classified sands and high early strength Portland cement, Type 30. The backfill material was premixed with 3 percent cement on a dry weight basis. Centrifuge models were prepared by pouring the design mix into form-ply moulds at 70% pulp density. A styrofoam spacer was placed at one end of the mould, prior to pouring of the design mix. 24 hours after pouring, the spacer was removed and concrete slab mix poured. Further details of model preparation procedures are described in Nnadi [12].

All model testing was carried out by increasing the centrifuge speed to produce an acceleration of 104g before conducting the individual tests at the design acceleration of either 42g, 62g or 104g which represent prototype backfill heights of 11.8m, 17.6m and 29.1m respectively. A solenoid valve controlled by an electric switch located in the control room was used to create impact loadings. A back pressure of about 10 kPa was used to return the impactor mechanism immediately after impact. Impact loadings were repeated up to twenty times to check on the repeatability of the impactor and to obtain averages for the monitored responses. One of the requirements of this work was to subject the backfill structure to a dynamic force which would produce a measurable response. Measurements of force, the response at the point of excitation and at some remote location would give the input characteristics and response behaviour as indicated in equation (7).

@seismicisolation

A PCB impact force transducer attached to the impactor was used to record the input

force on the structure. Bruel & Kjaer accelerometers and dynamic stress transducers developed by Nnadi [12] were used to record the time histories of the dynamic backfill behaviour.

RESULTS AND DISCUSSION

One of the objectives of this study was to ascertain the influence of geostatic and self weight stresses in the structural response from impact loadings. This influence was determined by comparing the structural response at various simulated gravities. Figure 4 presents the dynamic stress responses at simulated gravities of 42, 63 and 104. Figure 4 shows a steady decrease of induced dynamic stress with increase in simulated gravity as well as the effects of placement of the sensors on the dynamic response of the structure. However, Nnadi [12] found that the pulse duration, defined as the difference between the pulse arrival time and the time the pulse completes the peak half sine wave, decreases with increase in simulated gravities. These results emphasize the importance of properly accounting for the magnitude of the self weight stress and its variation with backfill height, so that a realistic measure of the dynamic responses of cemented backfill can be obtained.

The influence of simulated gravity on particle acceleration of the cemented backfill is shown in Figure 5. A linear relationship is found to exist between peak particle acceleration and simulated gravity; therefore, illustrating further the importance of correct simulation in dynamic tests. These observations indicate that at higher simulated gravity levels, the backfill structure becomes stiffer due to the confining pressures induced by the gravitational stresses and thereby, reducing the attenuation of the dynamic force.

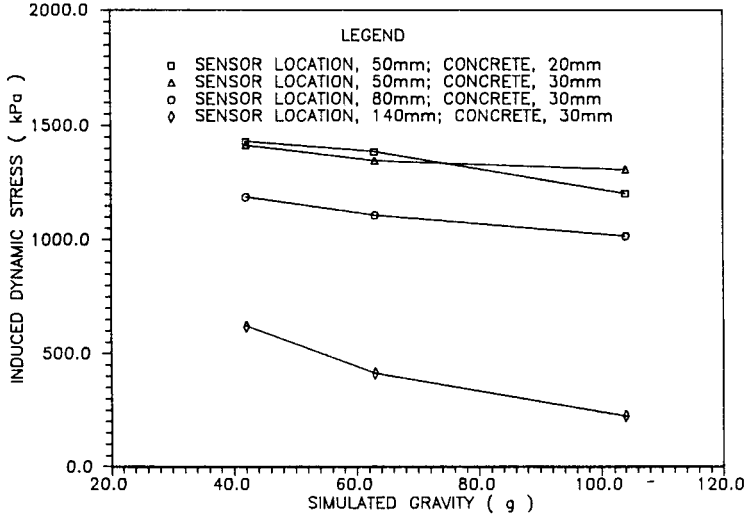

Figure 4. Effects of Simulated Gravity on Induced Dynamic Stresses.

@seismicisolation

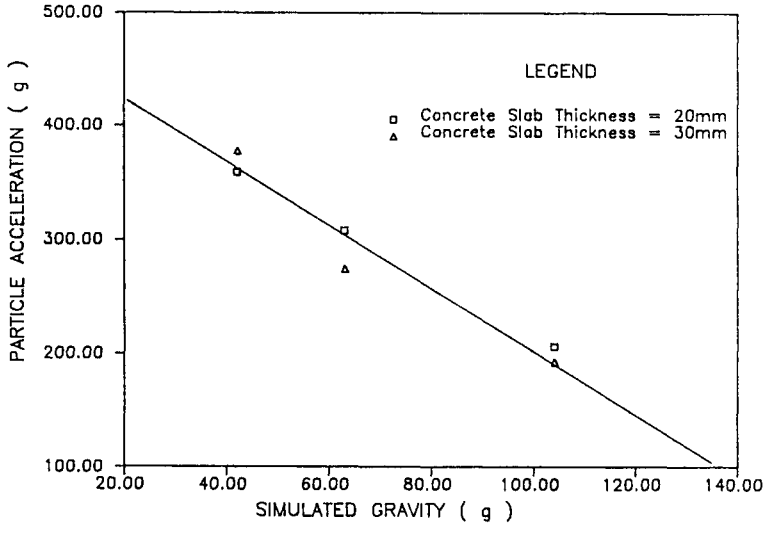

Figure 5. Effects of Simulated Gravity and Peak Particle Acceleration.

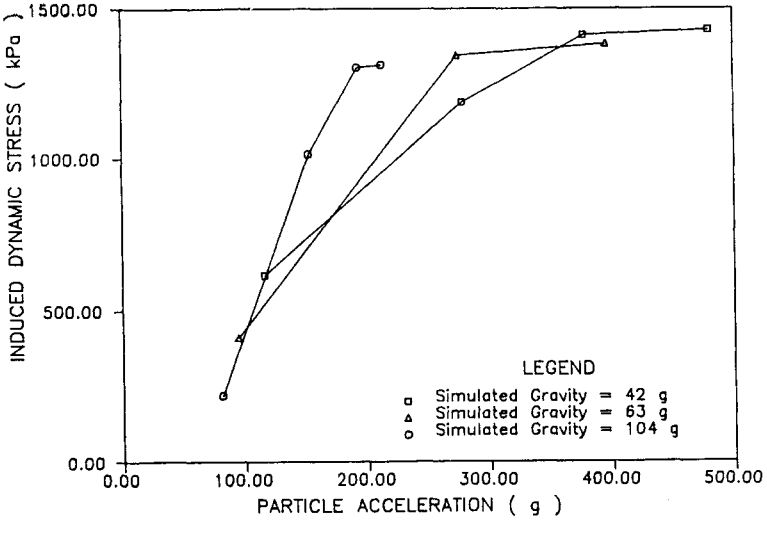

Figure 6. Relationship between the Induced Dynamic Stresses and Particle Acceleration.

@seismicisolation

Figure 6 shows the relationship between the induced dynamic stresses and the corresponding peak particle accelerations. The peak acceleration was found to generally increase with increase in the dynamic stress. However, the relationship is nonlinear but the tangential slope is found to increase with increase in gravitational field. The tangential slope of this relationship is found to increase with increase in gravitational field. Since the test conditions are the same , the nonlinearity is attributed to the changes in gravitational field.

The moduli of the transfer function of acceleration signals and the phase relations at different simulated gravities for the B test series are shown in Figures 7 and 8. The effect of simulated gravity on the resonant frequency is evident in the figures, although shapes of the transfer functions are different. The resonant frequencies of the peak moduli is seen to decrease with increase in g levels. Therefore indicating that higher frequency resonance predominated at higher stress level and confirming the validity of elastic theory assumptions made. Higher moduli are found to be associated with higher g levels.

The identification of the dynamic properties of backfills from the resonance curves was in some instances difficult because the force used to excite the backfill structure was very low and the resonant frequencies were often too closely spaced to permit identification of the modes. The peaks of some of the modes also interfered with the response at other modes. Modal damping was therefore not determined because of the closeness of some of the modes. This interference could be attributed to the nonlinearity of the material.

CONCLUSION

In this study, blast loading simulation on cemented backfills were performed in a geotechnical centrifuge. The testing program utilized dimensional analysis and transfer function methods to validate the viability of centrifugal modelling for examining the response of cemented backfills to dynamic loadings. The influence of geostatic and self-weight stresses on structural responses was clearly demonstrated.

The model studies showed that the cemented backfill acted like a low-pass filter with the magnitude of the shock wave decreasing with increase in distance from the impact source.

The results obtained via the forced vibration analysis indicated that higher resonant frequencies predominated at higher stress levels. However, further work is needed in estimating the damping of a nonlinear material like cemented backfills especially when the exciting force is low.

ACKNOWLEDGMENTS

This work was supported by National Research Council of Canada grant to R.J. Mitchell and research awards to the author from the Graduate School, Queen's University at Kingston, Canada.

@seismicisolation

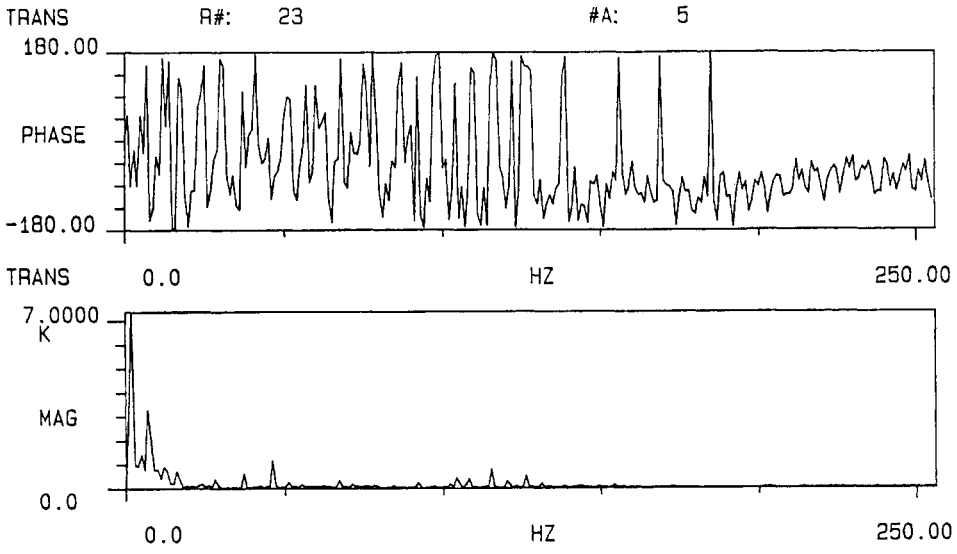

Figure 7. Transfer Functions of B Test Series at 42g.

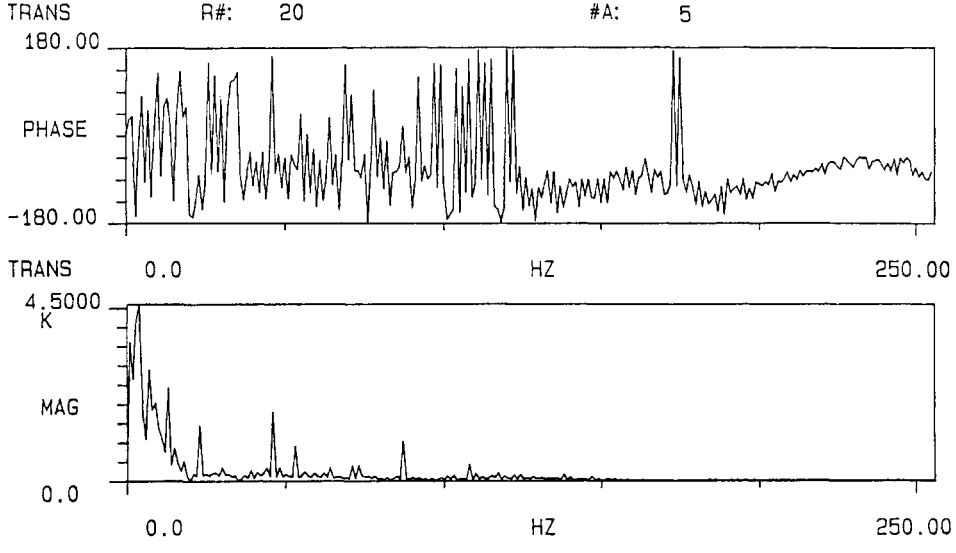

Figure 8. Transfer Functions of B Test Series at 104g.

@seismicisolation

REFERENCES

1. O'Hearn, B.O., and Swan, G. 1989. The use of models in sill mat design at Falconbridge. Proceedings Innovations in Mining Backfill Technology, pp.139-146.

2. Askew, J.E., McCarthy, P.L., and Fitzgerald, D.J. 1978. Backfill research for pillar extraction at ZC/NBHC, Mining with Backfill, Proc. 12th Canadian Rock Mech. Symp., Sudbury, pp.100-110.

3. Clough, R.W., and Penzien, J. 1975. Dynamics of structures. McGraw-Hill Book Co., New York, N.Y.

4. Nnadi, G.N., and Mitchell, R.J. 1990. Use of centrifuge models to study simulated blast loadings on backfills. Canadian Institute of Mining, Metallurgy and Petroleum, CIM. Accepted for publication.

5. White, R.G., and Mannering, M.E.J. 1975. Techniques for measuring the vibration transmission characteristics of the ground. Journal of the society of environmental engineers, March 1975.

6. Ewin, D.J. 1984. Modal testing: theory and practice. John Wiley and Sons, New York.

7. Abdel-Ghaffar, A.M. 1981. Dynamic longitudinal response of an earth dam. Proceedings, 2nd Specialty Conference on Dynamic Response of Structures: Experimentation, Observation, Prediction and Control. Atlanta, Georgia.

8. Amini, F., Tawfiq, K.S., and Aggour, M.S. 1968. Cohesionless soil behavior under random excitation conditions. Journal of Geotechnical Engineering Division, ASCE, Vol.114, No. GT8, pp.896-914.

9. Fogelson, D.E., and Dowding, C.H. 1977. Bureau of mines research on response of residence to ground vibrations from blasting. Proceedings, 18th. U.S. Symposium on Rock Mechanics, Supplemental Vol., Keystone, Colorado.

10. Bendat, J.S., and Piersol A.G. 1980. Engineering applications of correlation and spectral analysis. John Wiley and Sons, New York.

11. Townsend, F.C., McVay, M.C., Bradley, D.M., Cunningham, C.H., and Yovaish, D.J. 1985. Numerical and centrifugal modelling of buried structure response to near field blast. Proceedings, 2nd. Symposuim on the interaction of Non-Nuclear Munitions with Structures, Panama City Beach, Florida, April, 1985.

12. Nnadi, G.N. 1990. Dynamic behaviour of cemented mine backfill. Ph.D. thesis, Queen's University, Kingston, Canada.

@seismicisolation

METHODOLOGY FOR ASSESSMENT OF HIGH MASS LOW VELOCITY IMPACTS ON CONCRETE STRUCTURES

B.R. EVASON B.Sc.
Principal Dynamicist, Taywood Engineering Limited

K. FULLARD B.Sc., C.Eng., M.I.Mech.E.
Head of Circuit Rupture Consequences Group,
Berkeley Nuclear Laboratories, Nuclear Electric plc

ABSTRACT

This paper introduces a methodology for evaluating and understanding the response of concrete targets to impact from slow-moving massive missiles. Its purport is to stress the significance of different modes of behaviour and explain apparent anomalies in experimental data. It was developed on a logical basis and is independent of the data with which it is compared.

NOTATION

A	Area	P	Force
A_o	Interface area	P_c	Punching capacity
C_c	Stress wave celerity in concrete, taken as 3900 m/s	P_e	Effective applied load
E_c	Young's Modulus of confined concrete	P_p	Peak load
f_c'	Cylinder Strength	ρ	Mass density of concrete
f_t	Concrete tensile strength	r	Distance travelled by stress wave
h	Slab thickness/Target Depth	t	Time
K	Stiffness	t_p	Time to peak load
M_m	Missile mass	V	Velocity
N_k	Kinetic energy	V_o	Impact velocity
N_p	Plastic work	$\varnothing$	Missile diameter

@seismicisolation

INTRODUCTION

As is well known Nuclear Electric plc (NE, formerly part of CEGB) have, in conjunction with other interested parties (notably UKAEA), been conducting a long-term research programme to examine the response of concrete targets to a wide range of impact conditions. The experimental work spans fifteen years and has been conducted primarily at AWRE (Foulness), AEE (Winfrith) and their own Structural Test Centre (STC) at Cheddar.

With the formalisation of safety criteria for nuclear power stations, it was realised that there were a number of postulated accident conditions that had a small but unacceptable probability of occurrence. Extant methods of assessment were generally dependent on analogy to inappropriate empirical formulae, such as that of NDRC, derived for military missiles and differing widely in several parameters from the conditions of concern.

The concrete impact research programme set out to evaluate, partly by parametric study and partly on an ad hoc basis, such hazards and requirements for their obviation.

Answers to many of the questions have, for practical purposes, been found and are embodied in a Guideline Document published by the Safety and Reliability Directorate (SRD) of the UKAEA [1].

One area that has only recently received attention in the research programme is the response to massive missiles at low velocities, relevant to the problem of dropped loads. It was found that not only were the experimental results apparently less consistent, compared to the derived predictions, but that these predictions were noticeably unconservative.

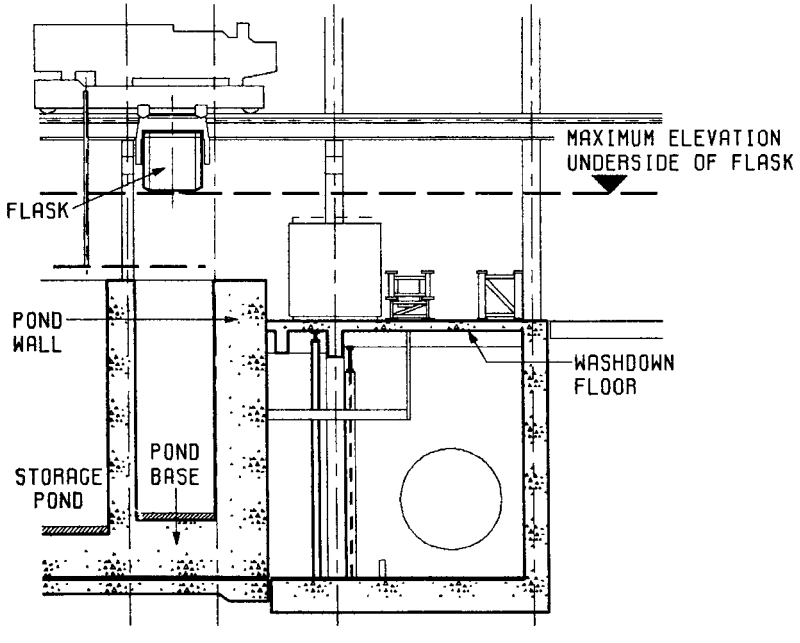

FIGURE 1 : Section Through Cooling Pond and Washdown Floor

@seismicisolation

THE DROPPED FLASK ASSESSMENT

In a contract with NE, Taywood Engineering Ltd undertook to assess the effects of accidentally dropping a loaded fuel transport flask in the Cooling Pond and Flask Handling Buildings at Heysham I or Hartlepool power stations, illustrated in Figure 1. There were three distinctly different types of structure as potential targets. These were the base and wall of the cooling pond, and the suspended washdown floor.

Even allowing for the above-mentioned doubts in the derived formulae, it is readily demonstrable that the dropped flask would not be expected to perforate any of the targets. Perforation alone, however, is clearly inadequate to describe the response for the practical purposes of assessing pond leakage or repair needs. It is also necessary to consider lesser states of damage and transmitted loads.

The objective of the methodology outlined in this paper was to describe, qualitively and with practical quantification, the type and degree of damage inflicted on the target.

THE PERFORATION PROCESS

A clear understanding of the processes leading to perforation is needed in order to try and evaluate impact response. The following sequence is depicted in Figure 2.

1. At impact a high compressive stress is generated at the area of contact, and elastic displacement is initiated.

2. This stress and concomitant deformation are transmitted into the body of the target. If the contact stress is sufficiently high, crushing will be initiated at the contact surface.

3. In the meantime the compression state propagating through the target will give rise to stress differentials. The resulting shears and tensions may initiate cracking.

4. At some stage a punching cone may be formed and undergo displacement relative to the rest of the target.

5. This cone will be restrained by the bending reinforcement in the target. If the rate of energy deposition is high the missile will fracture the cone, crush it and extrude fragments through the reinforcement mesh.

6. At lower rates of energy deposition the perforation will degrade towards a pseudo-static failure mode, typified by delamination on the reinforcement plane and a virtually complete punching cone hanging in a net of reinforcement.

Perforation is completed when failure of the reinforcement allows passage of the missile.

Clearly the relative amounts of crushing (typical of cratering in high velocity impacts) and cone-displacement (typical of 'static' failure) must have a significance in the determination of the response to low-velocity impacts. Traditionally displacement damage measured in impact experiments is recorded as a single parameter, the incursion of the missile nose into the target. The only available data giving sufficient detail to distinguish the different types of deformation is the

@seismicisolation

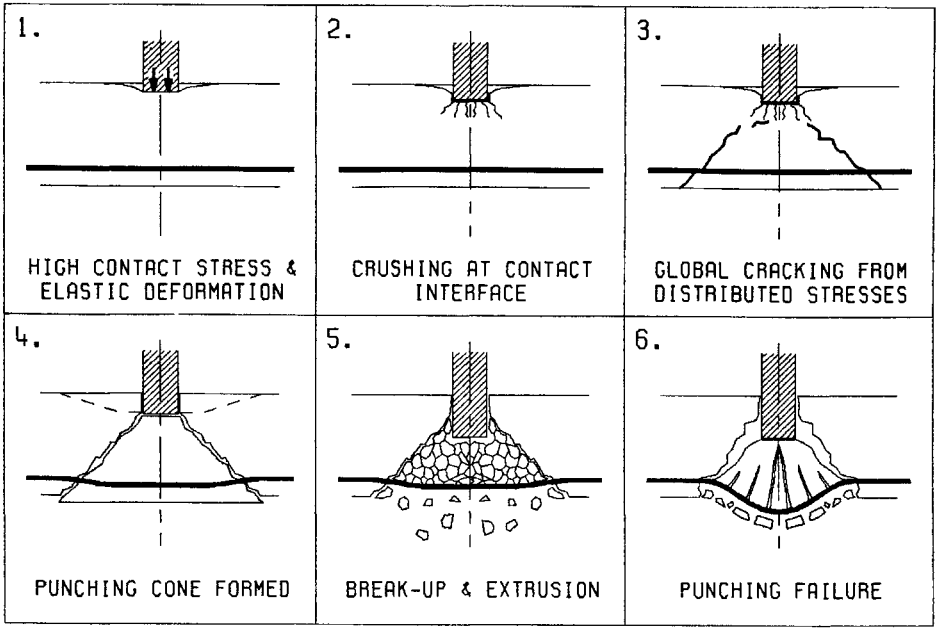

FIGURE 2 : The Perforation Process

NE data from STC. Much of this data, and the test details, were presented at the SMiRT conference in 1987. [2]

CONTACT STRESSES

If the problem were that of low velocity, co-axial impact of long thin rods, it would be a textbook case in simple one-dimensional stress wave theory. Some textbooks, such as that of Johnson [3], also explain the effects of plastic and elasto-plastic behaviour should the contact stress exceed the elastic limit of either material.

Building on the simple elastic case, the salient differences can be examined. Neither the transport flask, nor, to a lesser extent, the STC test missile, are conducive to the propagation and reflection of plane stress waves. Incoherence of reflected waves at the point of contact will smooth the steps in the theoretical thin rod transient. Due to the cooling fins and other protrusions the contact area of a standard transport flask will necessarily be small relative to its gross body dimensions. This implies that there will be no coherent axial vibration of the missile, which can for practical purposes be treated as rigid. Since the missile material is significantly stiffer than that of the target, this is not a dramatic generalisation but it peels an order of complexity from the problem.

Since the concrete rod representing the target is built into a surrounding slab not directly-loaded by the contact, its properties will be those of the confined material. Additionally, the advancing stress wave, unable to distinguish the rod core from the surround, will disperse in all directions. If the contact were a point, a spherical wave front would be anticipated. For a finite contact area, a flattened approximation could be expected such that the nearest point of the wave front to the contact face is everywhere equi-distant.

For a sufficiently hard missile, the deformation under the missile will be sensibly uniform, implying a uniform stress in the core. If the support from the surrounding target is envisaged as

@seismicisolation

an assembly of struts their common length implies a common axial stiffness per unit area while their inclination (β) implies a factor of Cos β on their deformation and also on their vertical efficiency. The resulting stress distribution varies from the peak value in the core, decaying as $\cos^2\beta$ around the wave front. This distribution accords comfortably with Timoshenko's solution for stresses under a local load in an extended solid. [4]

When the wave front has reached a depth $r(t) = C_c . t$ the effective instantaneous stiffness of the resisting target, using this distribution, is closely approximately by

$$K(t) = E_c . \pi . \varnothing \left\{ \frac{\varnothing + 1.38r(t)}{4r(t)} \right\}$$

This may be envisaged as that of a rod of length $r(t)$ and an instantaneous cross-section $A(t) = \pi . \varnothing . (\varnothing + 1.38r(t)) / 4$. For $r(t) >> \varnothing$, $K \approx 1.084\, E_c . \varnothing$. This is comparable (+14% for $\nu = 0.18$) to the mean static value for a concentrated load on an elastic half-space.

At time t the contact force will be

$$P = A(t) . p . C_c . V(t)$$

This resisting force is generated by absorption of missile momentum

$$P = -M_m \frac{dV}{dt} = A(t) . \rho . C_c . V(t)$$

whence

$$V(t) = V_o \exp \left\{ - \frac{A_o \rho C_c}{M_m} \left(t + \frac{0.69\, C_c t^2}{\varnothing} \right) \right\}$$

and $P = A_o . p . C_c . \left(1 + \frac{1.38\, C_c . t}{\varnothing} \right) . V(t)$

This enables the contact force transient for elastic impact on a target half-space to be computed (Figure 3). As deformation increases after impact, the resisting force increases up to a peak value P_p at a time t_p which may be deduced, from differentiating the momentum equation, as

$$t_p = -\frac{\varnothing}{1.38\, X_\chi} + \frac{2}{\sqrt{1.38}\, C_c} \sqrt{\frac{M_m}{\pi \rho \varnothing}}$$

If the corresponding stress (P_p/A_o) exceeds the crushing limit of the concrete, plastic indentation will occur.

SURFACE INDENTATION

The penetration resistance is typified as uniaxial crushing capacity enhanced by the confinement of the surrounding material. The magnitude of this enhancement is debatable. Based on published triaxial test data and the interpretation of other miscellaneous data, a factor between 3 and 6, weighted towards the lower value, would be expected for a flat nosed missile. A lower value could be expected for a more streamlined nose-shape.

@seismicsolutions

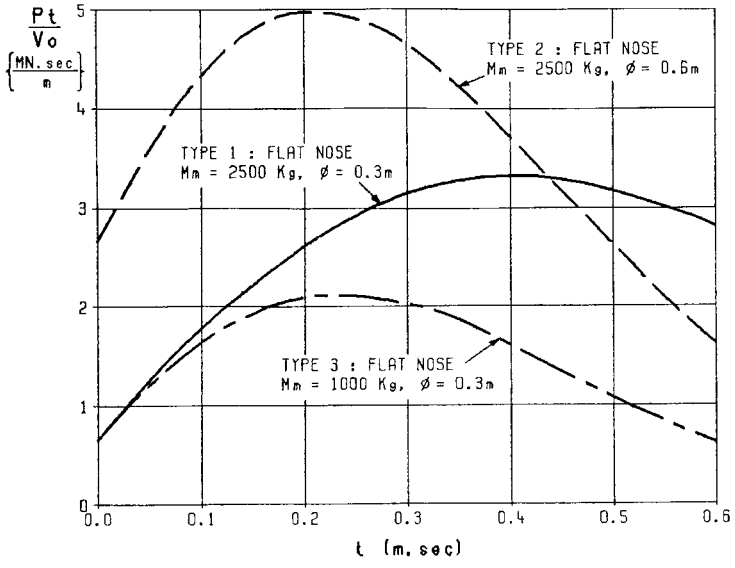

FIGURE 3 : Loading Functions for STC Missiles

At STC a value of 3.3 was deduced from accelerometer readings for a conical-nosed missile. This value was adopted and scaled in the light of the NDRC nose-shape factor, in the region of its presumed validity, yielding

Flat nose :	4.0	(Impact of flask foot)
Wedge (90°) :	3.7	(Impact of flask edge)
Conical (90°) :	3.3	(Impact of flask corner)

After impact the contact stress will increase until such time ty as crushing starts with a load P_y and interface velocity V_y. For a right cylindrical impact and an ideal elastic/perfectly plastic material, this will be the peak force generated. The concomitant elastic deformation will be maintained by the continously transmitted elastic limit stress. As the missile is slowed its capability for generating high contact stresses reduces, until, at time t_f (P_f, V_f), the instantaneous contact stress is elastically transmissible.

During this phase the energy transmitted through the contact interface is

$$N_K = M_m (V_y^2 - V_f^2) / 2$$

which is shared between crushing and elastic transmission. V_f is taken as the velocity of the missile for which the peak of the transient would not initiate crushing.

Adopting Martel's hypothesis, that work done is the product of penetration volume and flow (crushing) stress, and noting that only the kinetic energy (particle velocity) in the stress wave will be transmitted, half the input energy, during the period t_y to t_f will be absorbed plastically for a flat-nosed missile. Hence

$$N_p = \frac{1}{4} M_m (V_y^2 - V_f^2)$$

@seismicisolation

Taking a representative force as energy divided by penetration depth yields

$N_p = \frac{3}{8} M_m (V_y^2 - V_f^2)$ for a wedge shaped missile

and $N_p = \frac{5}{12} M_m (V_y^2 - V_f^2)$ for a conical missile.

Depth of penetration and the contact loading transient on a half-space can now be evaluated.

SLAB TARGET

If the target is a slab rather than a half-space, the advancing stress waves will be reflected from the remote face as tensile, or unloading waves. The reflection of the dilatational compression wave at angle β is taken to be a dilatational tension at angle $-\beta$. This is a gross simplification as Kolsky has demonstrated [5]. When the wave front reaches a point on the remote face at 45^0 from the load edge, the reflected tensile stress will be orthogonal to the incident compression implying an optimum efficiency to initiate cracking. This is compatible with cracking observed at STC.

The resistance to ejection of a 45^0 punching cone can be taken as the product of the tensile strength and the area of the curved surface

$$P_c = \pi \sqrt{2}h \, (\varnothing + h) f_t$$

Tensile strengths obtained for concrete are very dependent on the test method used. Based on Modulus of Rupture tests and on static punching tests a value of $f_t = 0.15 f_c'$ was assumed. For static punching, the effective applied load is readily identified but in the dynamic case the load at the contact interface is not directly related to the stress on the critical surface. For elastic energy transmission half the wave energy is kinetic which does not immediately represent a damage potential.

The distortion energy is input continuously to the cone through the contact surface. After a time-lag of the order of the through-thickness period of the slab ($2h/C_c$) the cone will be relieved by adjacent deformation. With due regard to periods of through-thickness and global plate deformations a realistic and not unconservative criterion for formation of the cone-crack can be expected to be:

$$Pp > (0.15 f_c')(2 . \sqrt{2} . \pi . h . (\varnothing + h))$$

$$Pp > 1.33 \, f_c' \, h \, (\varnothing + h)$$

Plastic penetration, however, represents a considerable temporal attenuation of the loading transient. The crushing zone can be envisaged as absorbing energy at the expense of applying a quasi-static load, but the continuously delivered elastic energy applies an additional component of deformation.

A simple idealisation could be to assume that all energy not absorbed in crushing represents the limiting elastic missile loading superimposed on the load required to cause plastic deformation. The loading from this pseudo-missile, with the mass of the actual missile and velocity defined by the available residual energy, can then be calculated as before. Adding the peak of this transient to the penetration load gives a peak value, P_e, which can be compared to global response criteria. This hypothesis was examined and found to give reasonable agreement with test data (q.v.). In view of the time-lag effects, and reflections from the slab boundary, the logic is somewhat specious.

@seismicisolation

For the purpose of the Dropped Flask Analysis the residual energy was assumed to be applied as strain energy in the half-space stiffness. On the basis that the half-space was the stiffest possible representation of the problem, this was assumed to be a conservative assumption since it corresponds to the maximum effective applied force. This approach gave no unconservative results when applied to the data.

Bending response and support reactions can be estimated from the response of the plate mode to the computed transient, noting that disestablishment of a punching cone will curtail the transient such that only that load transferred by the reinforcement will be applied.

The increased period for through-thickness vibration, relative to the transient duration, implies that, for a given missile diameter, cone-crack predictions would be more conservative for a thicker slab.

COMPARISON WITH TEST DATA

A hypothesis based on theoretical considerations and independent of direct data reduction has been advanced. The assumptions included are:

Martel's Hypothesis, that the energy absorbed in plastic deformation is the product of crater volume and flow stress.

A particular value of the ratio of confined flow stress to uniaxial strength, from within the expected range, was adopted from test data.

That the flow stress for different penetrator configurations can be scaled using the NDRC nose-shape factors.

A particular linear ratio of tensile to compressive cylinder strength.

Predictions on this basis were compared with STC test data as shown in Table 1.

The comparison between calculated plastic indentation, W_p, and that measured experimentally, X_p, is shown on Figure 4, and indicates close agreement.

After allowing for this indentation, if any, the effective peak applied load, P_e, from the residual energy and the load necessary to form a punching cone, P_c, were calculated. The normalised cone displacment, X_d/h, is plotted against the ratio of these loads (P_e/P_c) on Figure 5.

The ratio P_e/P_c is a form of overstress ratio for cone formation. At the critical ratio of unity a cone-crack would be expected to occur, while for lower values the target should maintain global integrity.

Higher values of the overstress ratio represent residual energy to displace the cone. Initially the resistance will be high due to friction and interlock forces. Once these have been overcome the resistance will reduce significantly when the cone is restrained solely by the reinforcement.

The form of figure 5 should therefore be a gradual increase from unity followed by a marked increase for high values of P_e/P_c. While the precise value of displacement is of little practical significance it can serve as a damage indicator. It would be helpful to know whether post-accident reinstatement was purely cosmetic, required grouting or re-concreting or involved reinforcement replacement. A calculable indicator would therefore be of value.

Figure 5 echoes these trends but is found to be unconservative for the exceptional mass/diameter ratio of the 75mm, 2500Kg missile and becomes progressively more conservative as this ratio reduces.

@seismicisolation

TABLE 1
COMPARISON BETWEEN PREDICTIONS AND TEST DATA

TEST No.	NOSE	DIA (mm)	MASS (kg)	V_o (m/s)	f_c' (MPa)	W_p (mm)	X_p (mm)	P_e/P_c	X_d (mm)
3	FLAT	300	2500	5.0	42.7	0.	0.	1.62	61.0
4	FLAT	300	2500	4.0	43.7	0.	0.	1.27	15.0
5	FLAT	300	2500	2.5	33.0	0.	0.	1.05	0.5
7	FLAT	600	2500	6.0	30.5	0.	0.	2.71	34.0
8	FLAT	600	2500	3.7	33.5	0.	0.	1.52	1.5
9	FLAT	600	2500	12.0	29.8	0.	0.	5.54	205.0
10	FLAT	600	2500	3.0	34.5	0.	0.	1.20	0.0
11	FLAT	600	2500	14.0	27.2	0.	0.	7.09	480.0
19	CONE	300	2500	5.2	37.7	57.1	55.0	1.22	1.5
23	FLAT	300	1000	2.8	37.8	0.	0.	.66	-
26	FLAT	300	1000	3.18	24.3	0.	0.	1.16	0.0
30	CONE	300	1000	6.55	28.5	54.1	55.0	1.21	0.0
33	FLAT	300	1000	4.12	34.7	0.	0.	1.05	0.8
35	FLAT	75	2500	3.35	32.5	9.9	9.0	1.05	33.0
36	FLAT	75	2500	2.07	31.3	3.6	4.5	.71	1.5
40	CONE	75	2500	5.0	35.0	73.7	78.5	.91	5.0
45	FLAT	75	1000	3.34	27.5	4.3	4.7	.81	1.0
46	CONE	75	1000	7.1	29.3	70.2	65.7	1.18	1.8
47	FLAT	50	1000	3.66	32.3	11.7	15.0	.64	-
48	FLAT	50	1000	4.25	28.5	18.7	22.0	.85	-

A value X_d = 0.0 indicates that the punching cone was fully formed but that there was no discernible displacement; a dash indicates that a coherent crack was not developed.

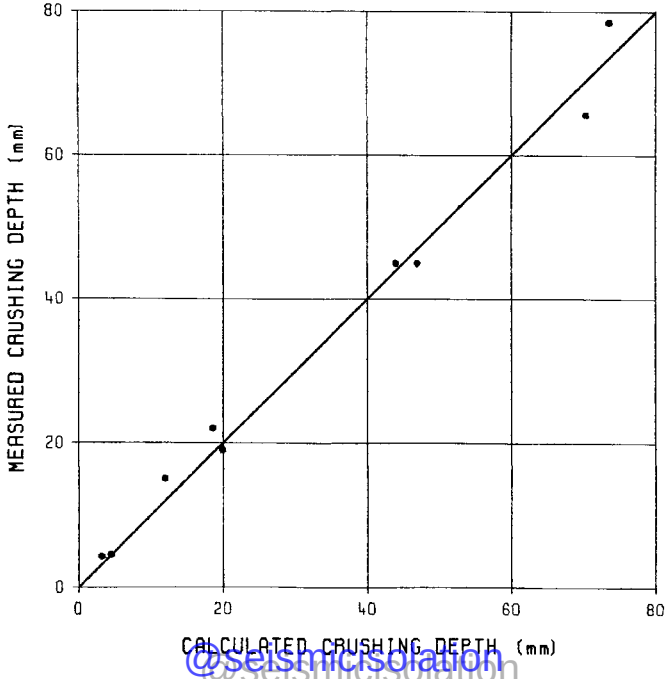

@seismicisolation

FIGURE 4 : Comparison Between Measured and Calculated Crushing

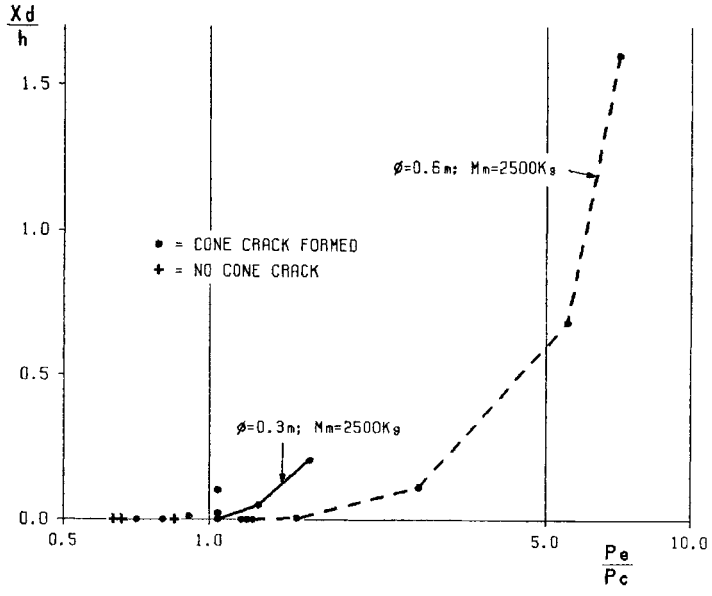

FIGURE 5 : Punching Cone Formation and Displacement

The fit between the theory and the separate lines implied on Figure 5 can be improved by any or all of the following:

- A correction factor of low orders of mass and inverse of diameter.
- A lower order of relationship of tensile to compressive concrete strength than the linear assumption used.
- Assuming a lower initial enhancement factor for calculating crushing resistance, but assuming that resistance increases with penetration depth in some fashion.

The degree of agreement between Figure 5 and the expectation is taken to imply that, to a first order approximation, the process of impact damage has been explained.

CONCLUSIONS

A method for predicting the response of concrete slabs to hard dropped loads has been advanced. It was assembled on a simplistic logical basis without recourse to data reduction.

On comparison with test data it was found that the method accurately predicted crater depths. It also indicated, realistically, the likelihood of formation of a through-thickness cone-crack. This latter prediction is not precise and indicates that there are significant second order effects. Within the range of data used the prediction can be significantly improved by factors obtained from data reduction, with implications in line with expectation.

There was no data to validate the calculated load transient for predicting support response or bending mode behaviour.

@seismicisolation

The method is considered to give a good qualification description of the damage process, particularly with regard to the relative significance of surface crushing and global punching modes of response, and a useful degree of quantification.

There are a number of areas of uncertainty implied by the need for the assumptions previously described. It is to be hoped that these can be clarified when more data, and an assessment of its reliability (repeatability) becomes available.

ACKNOWLEDGEMENT

The authors wish to thank Taywood Engineering Limited and Nuclear Electric plc for permission to publish this paper.

REFERENCES

1. P. Barr (Ed.), "Guidelines for the Design and Assessment of Concrete Structures Subjected to Impact - Issue 3" (SRD R439 - AEA Technology, HMSO 1990)

2. Sinclair, Fullard & Baker, "The Impact Resistance of Concrete Slabs under Heavy Dropped Loads" (Transactions of the 9th SMiRT Conference, Volume J; BALKEMA 1987)

3. Johnson W., "Impact Strength of Materials" (Edward Arnold, 1972)

4. Timoshenko & Goodier, "Theory of Elasticity" (McGraw-Hill, 1951)

5. Kolsky H., "Stress Waves in Solids" (Dover, 1963)

@seismicisolation

EXPERIMENTAL STUDY AND THEORETICAL ANALYSIS OF REINFORCED CONCRETE STRUCTURES UNDER ACCIDENTAL IMPACT LOADING

ALEXANDER V. ZABEGAYEV
Moscow Civil Engineering Institute,
129337 Moscow, Yaroslavskoye sh.,26,USSR

ABSTRACT

Experimental data and a method of analysis of reinforced concrete columns subjected to accidental hard impact are presented. The method allows for cracking, strain-rate effect and interaction between the structure and the striker. Two stages of the structural behaviour are considered: before cracking in the concrete member and after cracking. Bearing capacity of the column is derived from the concrete strip between inclined cracks strength condition.

Simple and reliable formulae to estimate local strenth of reinforced concrete plates and shells under low-velocity hard impacts are also given.

INTRODUCTION

The problem of the design of reinforced concrete structures to resist intensive impact loadings has been actively studied for several decades by military engineers. Simple formulae for the analysis have been obtained. However, when accidental impacts were taken into consideration, it was found out, that the results obtained from these relationships were not valid in many practical cases.

@seismicisolation

One of the main reasons is that most of accidental impact loads are low-velocity hard impacts [1] , caused by bodies of significant mass, i.e. much slower and heavier than those considered in the military field. In these cases overall behaviour of structures, as well as the local one requires modelling; in addition a contact law needs to be determined to take into account any interaction between the structure and the striker.

In this paper an approach, allowing for the interaction, is presented and illustrated by a method of analysis of reinforced concrete columns subjected to transverse hard impact. Local response experimental formulae for reinforced concrete plates and shells are also given.

EXPERIMENTAL STUDY AND THEORETICAL ANALYSIS OF COLUMNS

Axially loaded rectangular cross-section columns were placed in the horizontal position and struck vertically by a steel solid hammer with a flat indenter. The structural behaviour and crack patterns were traced by a high-speed camera and electrical strain gauges.

The experiments have shown that in most cases the inclined crack, propagating from the edge of the contact area to the column support occers in 1 - 2 ms after the beginning of the impact loading. The normal crack (Fig.1) takes place immidiately after it. Then, in 3 - 4 more milliseconds the second inclined crack propagates in parallel to the first one. Thus, the inclined compressed strip, shown in Fig.1,b, forms. Failure of the column begins when the ultimate compressive strain in the strip is reached.

According to the tests the structural behaviour can be divided into two stages: 1) before cracking and 2) after cracking up to failure of the inclined concrete strip.

Lagrange's equations are used to obtain motion equations.

Stage 1. Let the transverse deflection of the column under impact, applied at a distance $\bar{x}$ from the lower end, be

@seismicisolation

$$y\ (x,t) = X_n\ (x)\ T_n\ (t), \tag{1}$$

where X_n is the n-th mode of free vibration of the column; T_n is the corresponded time-function.

Kinetic K and potential U energies are determined, allowing for the interaction between the striker and the structure as follows [2]:

$$P = \begin{cases} K_1 \alpha & \dot{\alpha} \geqslant 0 \\ K_1' \alpha - (K_1' - K_1)\alpha_{max} & \dot{\alpha} < 0, \end{cases} \tag{2}$$

where P is the contact force, α is the penetration and K_1 is the contact zone's stiffness:

$$K_1 = \pi b\ \Delta\ /\ \bar{s}, \tag{3}$$

b is the cross-sectional width; $\Delta = 2K^2 E_c''/(3K-1)(K+1)$; $K = 1/(1-2\nu')$; $\nu' = \nu/(1+\nu)$; $\lambda = h/a$ $(\lambda \geqslant 2)$; h is the cross-sectional depth; a is the contact area half length; $\bar{s} = \ln 2\lambda - d_o - d_1/\lambda^2 - d_1^2/4\lambda^4 - 9d_2/\lambda^4$; $d_o = 0{,}527$; $d_1 = -0{,}716$; $d_2 = 0{,}245$; E_s'' is a contact modulus of concrete

$$E_c'' = (0{,}001\ f_{cu} + 0{,}11)\ E_c. \tag{4}$$

Eqs. (2) and (3) are based on the solution of corresponding problem of the theory of elastisity [3], eq. (4) has an experimental origin.

Thus, we can obtain

$$K = \frac{m}{2} \int_0^1 \dot{y}^2\ dx + \frac{M_s}{2} (\dot{y}(\bar{x}) + \dot{\alpha})^2, \tag{5}$$

$$U = \frac{B}{2} \int_0^1 (y'')^2\ dx + \frac{K_1 \alpha^2}{2}. \tag{6}$$

The work of the axial force N

$$W = \frac{N}{2} \int_0^1 (y')^2\ dx. \tag{7}$$

@seismicisolation

Substituting eq. (1) into eqs. (5)-(7) and further to

Lagrange's equations, we can obtain the system of differential equation of motion

$$\begin{cases} \sum_n \ddot{T}_n \varkappa_{1n} + \sum_n T_n \eta_{1n} + \Delta_1 \ddot{\alpha} = 0 \\ \cdots\cdots\cdots\cdots\cdots\cdots \\ \sum_n \ddot{T}_n \varkappa_{nn} + \sum_n T_n \eta_{nn} + \Delta_n \ddot{\alpha} = 0 \\ \sum_n \ddot{T}_n X_n(\bar{x}) + \ddot{\alpha} + \omega^2 \alpha = 0 \end{cases} \tag{8}$$

where $\varkappa_{in} = m \int_0^l X_i X_n dx + M_s X_i(\bar{x}) X_n(\bar{x})$; $\eta_{in} = B \int_0^l X_i'' X_n'' dx - N \int_0^l X_i' X_n' dx$; $\Delta_i = X_i(\bar{x}) M_s$; $\omega^2 = K_1/M_s$, m is mass of the column per unit length; M_s is the mass of the striker; l, B are the length of the column (Fig. 1) and its stiffness in bending.

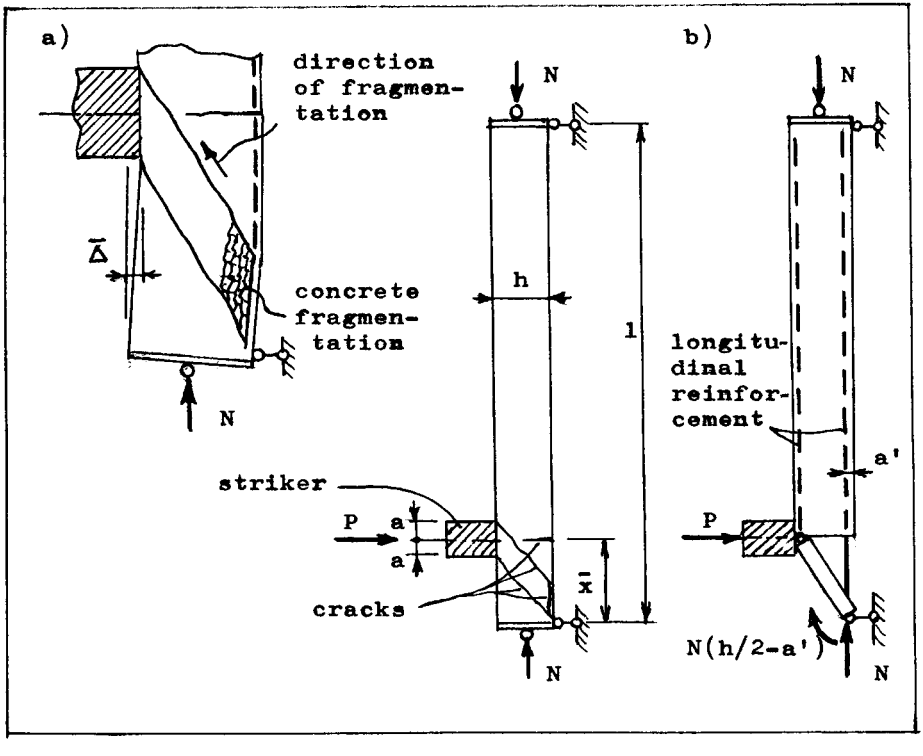

Figure 1. Mode of failure and truss model of the column

@seismicisolation

Initial conditions

$$t=0 \quad T_1=\ldots=T_n=\dot{T}_1\ldots=\dot{T}_n=\alpha=0; \quad \dot{\alpha}=V_o, \tag{9}$$

here V_o is the initial velocity of the striker.

The solution of eqs.(8) gives bending moments and shear forces as follows

$$M(x,t) = -By''-Ny \; ; \qquad Q(x,t) = -By'''-Ny', \tag{10}$$

which allow to define principal stresses $\sigma_{1,2}$ near the neutral axis of the column; time of the first crack t_1 can be derived from

$$\sigma_1(x,t) = \sigma^d_{1,u}; \tag{11}$$

here $\sigma^d_{1,u}$ is the ultimate compressive stress in the concrete just before the inclined crack initiating; $\sigma^d_{1,u}$ is recommended to define according to eq.(12), based on [5] :

$$\sigma^d_{1,u} = \frac{K_{\dot{\varepsilon},c}\, K^{if}_{IIc}}{\rho\, G(\theta_o,\bar{\lambda})}\sqrt{\frac{2}{D_M}}, \tag{12}$$

where K^{if}_{IIc} is the critical stress intensity factor referred to aggregate-cement paste interface [4]; ρ is the fraction of the interface that is initially debonded; θ_0 is the orientation of the first crack to propagate; $\theta_o = \arctan(\mu + \mu^2 + 1)$; $\mu = 0,6$; $G = (1-\bar{\lambda})\sin\theta_o\cos\theta_o - \mu(\cos^2\theta_o + \bar{\lambda}\sin^2\theta_o)$; $K_{\dot{\varepsilon},c}$ is the concrete strain-rate factor

$$K_{\dot{\varepsilon},c} = \begin{cases} 1,212 + 0,0424 \log\dot{\varepsilon}_c & 10^{-5} < \dot{\varepsilon}_c \leq 1 \\ 1,212 + 0,444 \log\dot{\varepsilon}_c & 1 < \dot{\varepsilon}_c \leq 10^2, \end{cases} \tag{13}$$

D_M is an effective diameter of the maximum size of aggregate in the concrete mix.

Equations (8) will have also be valid till a time $t_2 < t_1$, when the contact between the structure and the striker ends. The time t_2 can be taken from

@seismicisolation

$$P(t_2) = 0, \tag{14}$$

where P is determined according to the second of eqs.(2). If $t > t_2$ a free motion of the structure should be considered.

If t t_1 the second stage begins.

<u>Stage 2</u>. The truss model can reasonably be used to describe the structural behaviour (Fig.1b).

K, U, W for this stage can be given as follows

$$K = \frac{M_s \dot{\bar{\Delta}}^2}{2} + \frac{m}{2}\int_0^{\bar{x}} (\dot{y}^{I})^2 dx + \int_{\bar{x}}^{1} (\dot{y}^{II})^2 dx = (M_s + \frac{ml}{3})\frac{\dot{\bar{\Delta}}^2}{2}, \tag{15}$$

$$U = \frac{C_o \bar{\Delta}^2}{2} \tag{16}$$

$$W = N(h/2 - a')\,\bar{\Delta}/\bar{x} \tag{17}$$

here $\bar{\Delta}$ is the transverse deflection of the impacted cross-section; $y^{I} = \bar{\Delta}\, x/\bar{x}$; $y^{II} = \bar{\Delta}\,(1-x)/(1-\bar{x})$; C_o is the stiffness of the bottom $(x < \bar{x})$ block of the column:

$$C_0 = \frac{2abE_sA_sE_c''\sin^4\beta}{\gamma^2(h_oE_sA_s + (\bar{x} - a)2abE_c''\sin^2\beta\cos^2\beta)}; \tag{18}$$

E_s, A_s are modulus of elasticity and cross-sectional area of the longitudinal reinforcement of the column; γ is a coefficient, allowing for the part of the contact force, transferring into the lower support; β is the angle of the inclined cracks.

Substituting (15)-(17) into Lagrange's equations, we can obtain

$$\ddot{\bar{\Delta}} + \omega_o^2\bar{\Delta} = \Phi \tag{19}$$

where $\omega_o^2 = C_o/(M_s + \frac{ml}{3})$; $\Phi = N(\frac{h}{2} - a')/\bar{x}\,(M_s + \frac{ml}{3})$; a' is the longitudinal reinforcement covering.

The initial conditions for (19) are

$$t = 0 \quad \bar{\Delta} = \bar{\Delta}_o;\ \dot{\bar{\Delta}} = \dot{\bar{\Delta}}_o \tag{20}$$

@seismicisolation

here $\bar{\Delta}_o = y(\bar{x}, t_1)$. $\dot{\bar{\Delta}}_o$ can be determined on the base of the observed transfer of kinetic energy of the striker into cracking energy U_{crc}. Thus,

$$\frac{M_s}{2}(\dot{\alpha}(t_1) + y(\bar{x}, t_1))^2 + \frac{m}{2}\int_0^1 y^2 dx = (M_s + \frac{ml}{3})\frac{\dot{\bar{\Delta}}_o^2}{2} + U_{crc}. \quad (21)$$

The solution of eq.(19) is

$$\bar{\Delta} = \frac{\Phi}{\omega_o^2}(1 - \cos\omega_o t) + \frac{V_o}{\omega_o}\sin\omega_o t. \quad (22)$$

Bearing capacity of the mechanical system in Fig.1b will be guaranteed when

$$\sigma_1(t_{max}) = \frac{E_c''\bar{\Delta}_{max}(t_{max})}{h_o \sin^2\beta} \leq K_{v,c}R_c \quad (23)$$

here $\bar{\Delta}_{max}$ is the maximum value of $\bar{\Delta}$ from eq.(22), R_c is axial concrete strength in compression. In practice, the first half-cycle is essential only so energy dissipation can be neglected.

Fig.2 shows theoretical and experimental relationships "deflection - time" for the impacted cross-section of the pin-ended column, 800×100×120 mm in dimentions, reinforced with a mild steel (σ_y=400 MPa) and struck by a solid 120 kg mass at 300 mm from the bottom.

It can be seen that the theoretical results based on the abovementioned theory are in good coincidence with the test data. It can also be pointed out that Stage 1 is much shorter

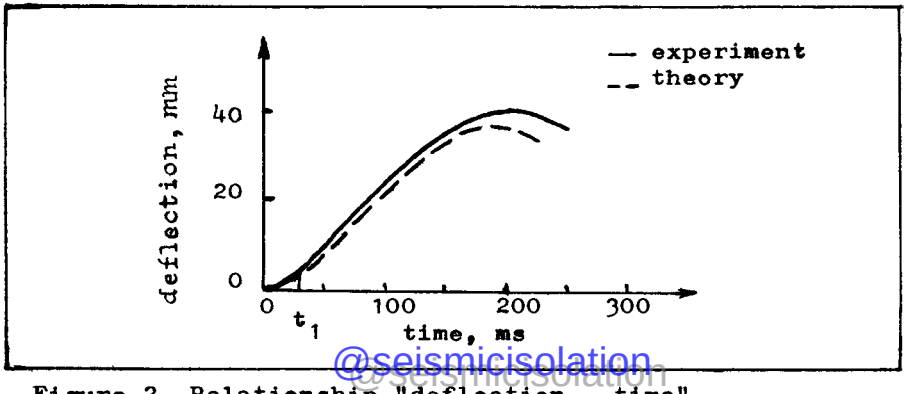

@seismicisolation

Figure 2. Relationship "deflection - time"

than Stage 2 and its influence is relatively small (as far as for energy absorbtion is concerned), so the analytic procedure can be simplified by neglecting of Stage 1.

LOCAL STRENGTH OF REINFORCED CONCRETE PLATES AND SHELLS

Plates and shells as well as columns are frequently subjected to accidental impacts. Their bearing capacity in most cases depends on their local dynamic strength.

An experimental study of reinforced concrete plates under low-velocity hard impact loadings[6] had been carried out and the results as well as the available experimental data by other authers had been generalized by means of dimensional and regression analyses to obtain the following formulae:

$$\frac{t_s}{d} = \frac{t_p}{d} = 2{,}019\ N_1\ Q^{-0{,}3439}\quad V_o \leqslant 75\ \text{m/s} \qquad (24)$$

$$\begin{cases} \dfrac{t_s}{d} = 1{,}429\ N_1\ Q^{-0{,}5673} \\ \dfrac{t_p}{d} = 0{,}943\ N_1\ Q^{-0{,}5530} \end{cases} \quad 75 < V_o \leqslant 150\ \text{m/s} \qquad (25)$$

here t_s and t_p are the minimal thickness of the plate or shell to resist scabbing and perforation, respectively; d is the diameter of the contact zone; N_1 is a coefficient, allowing for the shape of the indenter; $N_1=1$ for a flat one, $N_1=1{,}18$ for a spherical one, $N_1=1{,}26$ for sharp indenters; $Q = 10^4 f_{cu} d^3/M_s V_o^2$; f_{cu} is the concrete cube strength.

Eqs.(24),(25) are illustrated by Fig.3.

Thus, local bearing capacity will be guaranteed if $t > t_s$ or $t > t_p$. The first condition is reasonable to apply to plates and shells without link reinforcement, otherwise the second condition should be used.

@seismicisolation

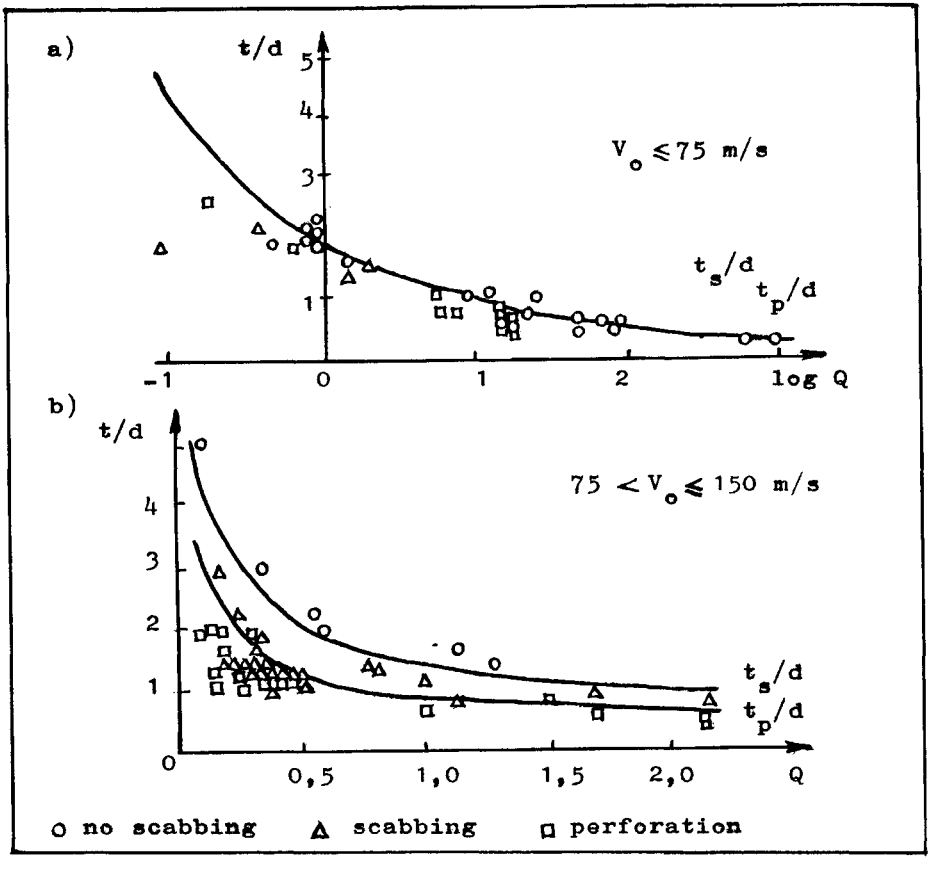

Figure 3 . Relationships "respective thickness - Q"

CONCLUSIONS

An experimentally proved mode of failure and a method of analysis of reinforced concrete columns under transverse impact (e.g. by a vehicle), including cracking, strain-rate effect and interaction between the structure and the striker is presented. Allowing for the interaction makes major theoretical parameters more reliable. The approach can also be used in analysis of overall behaviour of reinforced concrete beams and plates.

Simple formulae to ascertain local strength of plates and shells are also presented. Unlike most of similar formu-

@seismicisolation

lae they have a clear dimensionless form and cover the range of low-velocity impact loadings.

REFERENCES

1. Zabegayev, A.V., On the determination of accidental impact loadings on structures. Stroitelnaya mechanika i raschet soorugeny, 1988, 1, 5-9.
2. Zabegayev, A.V., Local behaviour of bar elements under intensive loadings. Beton i gelezobeton, 1989, 4, 38-39.
3. Vorovitch, I.I., Non-Classic Problems of Theory of Elasticity, Nauka, Moscow, 1974, pp. 230-4.
4. Mindess, S., Young, J., Concrete, Prentice-Hall, Inc., Englewood Cliffs, New York, 1981.
5. Fanella, D., A., Fracture and Failure of concrete in uniaxial and biaxial loading. J. Eng. Mech., 1990, 116, 11, 2341-62.
6. Luzhin, O.V., Zabegayev, A.V., Kuderin, M.K., Peculiarities of reinforced concrete slabs' behaviour under impact loadings Beton i gelezobeton, 1990, 2, 35-6.

NOTATION

K_1 contact zone's stiffness at the loading stage;
K_1' contact zone's stiffness at the unloading stage;
ν Poisson's ratio
E_c initial tangent modulus of concrete
$\dot{\varepsilon}_c$ strain rate in concrete in compression

@seismicisolation

ESTIMATION OF PILING-INDUCED GROUND VIBRATIONS

A. OLIVER & A.R.SELBY
School of Engineering and Applied Science
University of Durham
England

ABSTRACT

The driving of piling by impact hammer or vibrodriver causes ground vibrations which can be disturbing to neighbours and may even cause risk of damage to nearby buildings or buried service pipes. A large database has been assembled of piling-induced ground surface vibrations in the 2m to 20 m region from driven piles, with simultaneous recording of radial, transverse and vertical components at each of five stations. A selective recall facility allows perusal of appropriate records and so assists in a subjective estimate of vibrations in a proposed piling activity.

The work was then developed into a predictive device, using three databases and algorithms to build a knowledge based system. The system is capable of responding to enquiries based upon pile and soil conditions to estimate hammer energies, select appropriate hammers, estimate vibrations and compare the estimates with statutory or selected vibration levels.

INTRODUCTION

The driving of steel piles in construction projects is an increasingly common occurrence. The piles are driven by either impact or vibratory hammer through weak soils into strata of greater bearing capacity. The high levels of energy used in the driving of such piles causes vibration waves to emanate radially from the source of piling. These waves are discernible to humans and in severe cases may be damaging to structures, see for example Attewell and Farmer [1], Walton [2] and Steffens [3]. As the public becomes increasingly sensitive to "environmental" disturbances of this nature, the industry must respond through a legislative framework, in particular the draft BS 5228 Part 4 [4], by predictions of vibration levels and by modifications of working practices if necessary.

@seismicisolation

The driving of piles has one of two main functions :

1) To transfer loads from a structure to ground strata of adequate strength and stiffness to support them without intolerable displacement, or

2) To construct a continuous wall capable of carrying transverse loads from retained earth and possibly water, again without intolerable displacement.

In the former case the piles may be of steel H section; however precast concrete piles can also be employed. In addition, a wide range of piling methods is available, see Tomlinson [5], Whittaker [6] and BS8004 Foundations [7]. In the latter case, interlocking sheet piles are used, see the British Steel Piling Handbook [8]).

As inner city construction and major civil engineering projects increase, the use of piling becomes more prevalent. It may offer economic benefits over deep raft foundations and is widely used in the construction of buildings, bridges, sea defences and temporary works.

There are two main methods of driving steel piles into the ground - impact or vibration. Other methods such as jacking/vibration or jacking are much less common in site practice.

An impact hammer operates by striking the top of the pile and thereby imparting energy to that pile, which drives the pile downwards into the soil. The amount by which the pile is driven per blow depends upon the efficiency of the blow, the condition of the soil and the precise nature of the pile being driven.

A vibratory hammer uses the weight of the pile and hammer to provide the driving force. The hammer is clamped to the top of the pile and vibration is set up by contra-rotating eccentric masses, at a frequency of around 25 Hz. This vibration reduces the friction at the soil/pile interface and at the toe, partially liquefying the soil particles present. The combined weight of hammer and pile then causes the pile to be driven into the ground. This hammer is only suitable for granular soils because cohesive soils are not prone to liquefaction. Some modern vibrodrivers operate at much higher frequencies, of 40 Hz or more, in an attempt to decrease the level of the transmitted ground vibrations, and in particular to cause more rapid attenuation.

Both processes involve the input of high levels of energy into the head of the pile. This energy passes through the length of the pile as a stress wave and some enters the soil at the toe. This transfer of energy causes the vibration waves to expand radially outwards around a quasi-spherical wave front. Other sources of energy have been discussed, eg Selby [9].

@seismicisolation

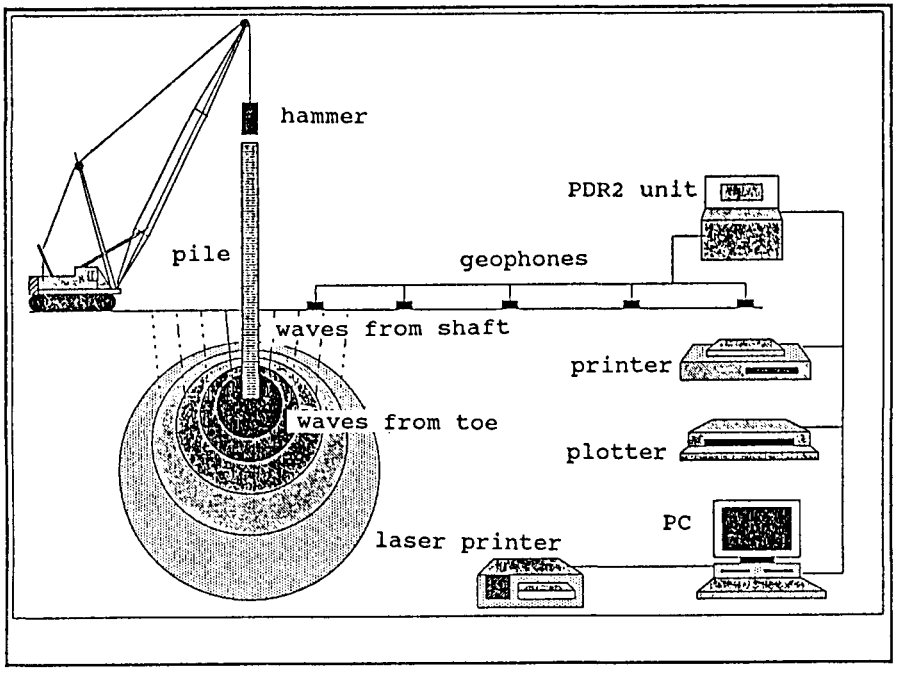

Figure 1. Schematic of vibration measurement.

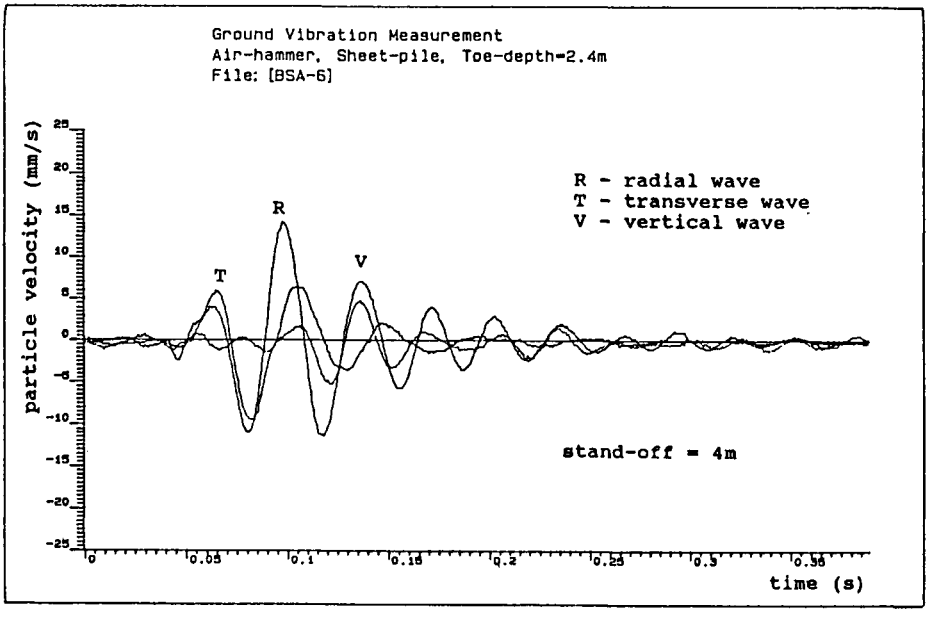

Figure 2. Typical traces of particle velocity/time records.

@seismicisolation

Measurements of ground surface vibrations should be made in three orthogonal directions (usually radial, transverse and vertical : R,T and V), at a number of stations simultaneously, see Figures 1 and 2. The transducer commonly used for this work is the geophone, which produces a voltage signal proportional to transient particle velocity. It is highly desirable that signals are recorded digitally, to allow time-based vector resolution, frequency analysis and other post processing operations. From such data patterns of vibrations can be developed.

DATABASE DESCRIPTION

A large number of vibration records have been taken during some 130 visits to piling sites throughout the United Kingdom, in the form of peak particle velocities(ppv.s) of R,T,V and resultant components, in the proximity of piling operations (usually 2m to 20m distance).

Preliminary evaluation of the data showed considerable variability in the ppv.s and also, commonly, non-uniform attenuation of signals with distance from the pile, eg. Figure 3. Consequently, as a first stage in the processing of a very large quantity of site measurements, the vibration records were stored on a database, see Attewell et al.[10].

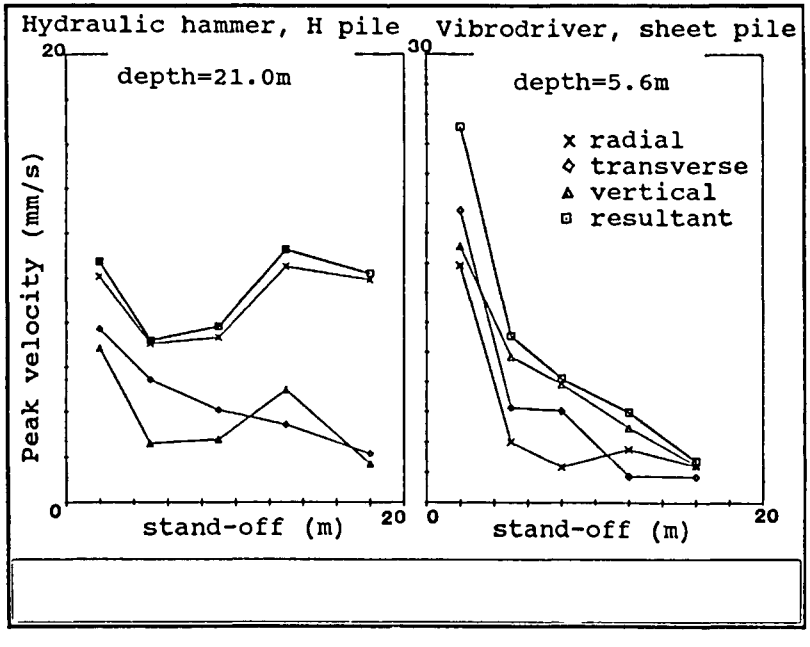

Figure 3. Non-uniform and uniform signal attenuation.

@seismicisolation

The data was then in a suitable form for analysis of trends of behaviour in terms of individual independent parameters affecting the level of ground vibrations. The database may also be used as an aid to subjective prediction of the level of probable vibrations at a new site. This is achieved by examining records from previously visited sites which closely resemble the proposed site. To this end the database was constructed in a manner which facilitated structured query routines.

The user of the system may interrogate the database by entering values in query fields and searching the database to see if these search criteria can be met. If suitable matches are found the system will choose all the relevant records and allow the user to view them in any order. The more specific the query, the fewer accurate matches will be made.

Peak particle velocities (and accelerations and displacements) from a batch of site records were described by cubic polynomial functions for interpolation between values recorded at five discrete stations, see Figure 4. The coefficients of these polynomials provided the essential stored information in the database. A suite of programs was written to allow organic growth of the database system. This suite of programs allows transfer from logger to PC, analysis and optimisation of raw data, the fitting of polynomial curves to the data and the filling of the database itself. A shell program was written to allow rapid extraction of information, using a structured query process. The database is capable of producing reports of recorded velocity, acceleration and displacement in radial, transverse, vertical and resultant components, selected by specification of a range of parameters, see Table 1.

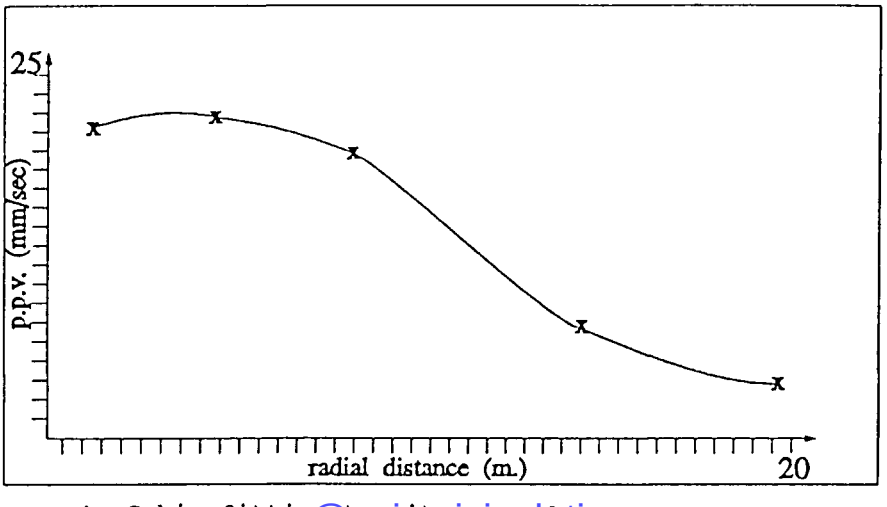

Figure 4. Cubic fitting to site records.

@seismicisolation

TABLE 1

Ground Vibration Database - Full Analysis Report

Request Date February 21, 1991

Site Location	- Blaydon (Contract 3)	**Date of Visit**	- 11 May 89
Hammer Type	- Hyd Drop	**Pile Type**	- H Pile
Hammer Model	- BSP 357 (3 tonne)	**Pile Section**	- 356*368*168 kg/m
Input Energy	- 35.3 kJ	**Pile Length**	- 21 m.
		Toe Depth	- B
Ground Type	- PFA	**Rake**	- Y
Classification	- Compressed	**Record Number**	- 2

Distance (m)	Radial Vel. (mm/s)	Transverse Vel. (mm/s)	Vertical Vel. (mm/s)	Resultant Vel. (mm/s)
6	5.02	1.77	7.75	8.35
7	3.55	1.60	6.06	6.46
8	2.54	1.44	3.57	5.00
9	1.93	1.29	4.68	3.91
11	1.66	1.04	2.05	2.67
12	1.86	0.93	1.59	2.41
13	2.20	0.84	1.28	2.33
14	2.62	0.76	1.10	2.36
15	3.04	0.70	1.01	2.46
16	3.40	0.66	1.00	2.58
17	3.63	0.63	1.02	2.67
19	3.46	0.62	1.06	2.54
20	2.93	0.64	1.01	2.22
21	2.01	0.59	0.89	1.66
22	0.63	0.55	0.67	0.81

Comments

Raking 1:4 Piling taking place in an already highly piled area

Produced by Durham University in conjunction with British Steel

@seismicisolation

KNOWLEDGE BASED SYSTEM

The production of a knowledge based system was a natural progression of the ground vibration project. The database can only supply predictive results if the user carries out an essentially subjective evaluation process on selected data. The system provides predictive estimations of expected levels of vibration by responding to user-supplied variables through rule-based procedures. These rules include calculations of the energy required to drive the pile, application of any suitable modification factors to this energy requirement, and selection of hammers. A structured set of algorithms are then applied, these algorithms being based on data from the Ground Vibration Database. The resulting predicted levels of vibration are then displayed; these levels can be referenced against values set by the user or taken from national codes.

The main aim of this stage of the project was to produce a tool that could be used for supplying a predictive estimate of vibration levels for a given piling system of hammer, ground and pile type. The database is primarily an historical filing system, in which every record represents one group of historical activities that is essentially unique. However, the database can be used in a subjective fashion as a predictive system through selective data retrieval, enhanced by the interpolation of velocity readings between values from the five actual stations.

Of course, the database can only respond positively if there are records present within the database which match the query criteria. A general query will produce numerous suitable records from the database. The user must then manually search through these records, either by tightening the selection parameters or by printing out hardcopies of the relevant reports. This process is time consuming; the knowledge based system is designed to carry out this process automatically. Also, the database can be queried only on the physical characteristics of the event recorded. Selection cannot be made with respect to levels of vibration observed or restrictions placed thereon. The knowledge based system can allow referencing to results.

The knowledge based system incorporates additional sets of data not included in the vibrations database. The system can give an indication of the energy required to drive a pile under defined conditions. Hammers capable of delivering this magnitude of energy can also be selected from a large hammer database. The suitability of a hammer which a contractor may choose to use can be assessed, by a "hammer rating index". The knowledge based system then uses sets of equations to estimate vibration levels, based upon the user-supplied information of pile and soil types, and upon deduced hammers/energies.

@seismicisolation
@seismicisolation

SmartWareII - an integrated applications package including separate database, spreadsheet and text handling modules - was the software chosen for the whole system. There were three reasons for this choice; the software existed at Durham University and British Steel, Scunthorpe, it afforded standardisation between the database and the knowledge based system, and SPL, the SmartWareII Programming Language, is a powerful 3GL clone language which was easily capable of handling all aspects of the knowledge based system.

The system utilizes an approach which can be represented graphically by Figure 5. The system gains inputs from the user via an opening user interface, a simple set of question and answer routines. After this the system will have all the data it requires to calculate the final vibration levels.

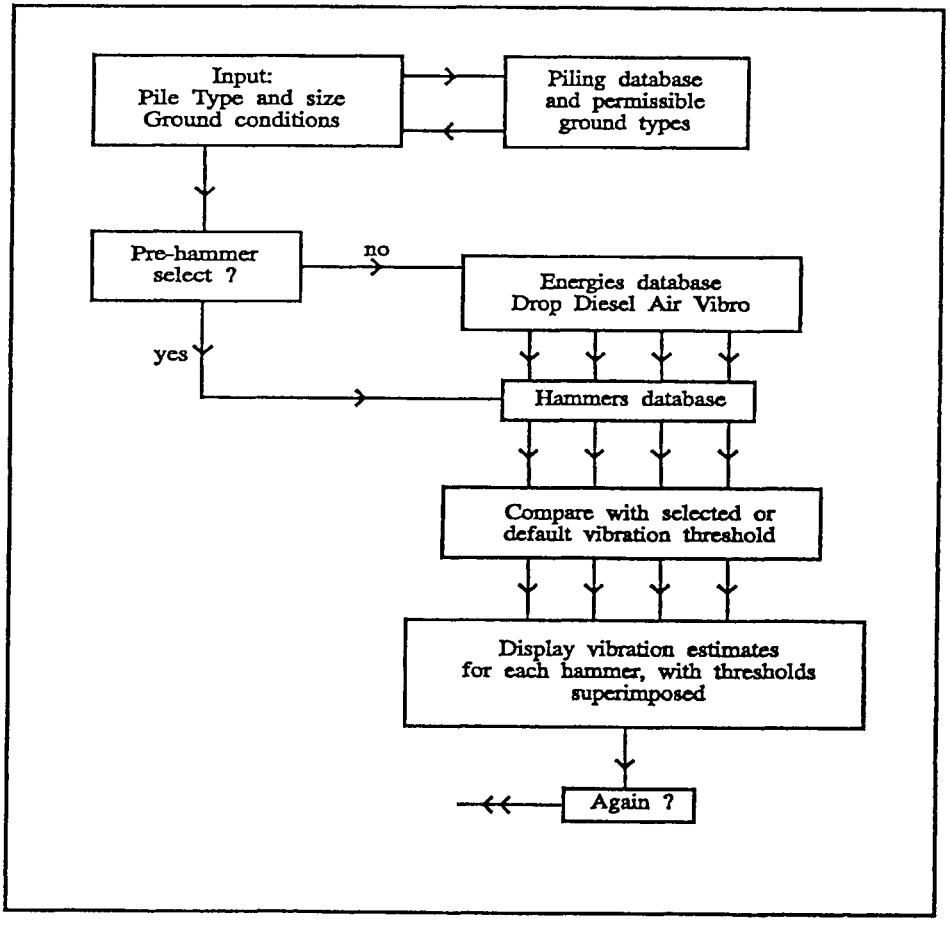

Figure 5. Logic route of knowledge based system.

@seismicisolation

This data is then applied to particular algorithms to calculate the energy required to drive the pile for the four hammer types - namely Drop, Diesel, Air and Vibrodriver. Once these energies are known, hammer models can be selected which are most appropriate for supplying this energy. The hammers are selected from a hammer database. The associated vibration levels may then be calculated, using the appropriate equations held in a sub group datafile.

The engines of the system are the algorithms which calculate the energy required to drive the pile. The four main hammer groups are calculated in three distinct stages, Drop and Diesel as one group, Air and Vibrodriver separately. However the heart of the system is the set of algorithms which lead to the predictive estimation of ground surface vibrations as a function of hammer, pile size and length and ground conditions. This sub-grouping is now discussed.

Sub Group Divisions

After consideration of data recorded and processed out of the database, it was recognised that separate equations were required to predict vibrations, dependant upon consideration of hammer, pile and soil types. For example, vibrations from a vibrodriver on sheet piles attenuate more rapidly than those caused by a drop hammer on bearing piles. The sub groups used to represent the data in the knowledge based system were chosen so as to allow representative prediction compatible with a realistic limit on subdivision. The subdivisions chosen were based on the criteria in Table 2.

TABLE 2
Hammer, pile and ground subdivisions

Hammer Type	Pile Type	Ground Type
Air Drop Diesel Vibro	Sheet Bearing	Granular Cohesive

Vibration data for the sixteen groups in the Table were analysed by logarithmic regression to produce equations giving "best estimate" resultant ppv.s in terms of hammer energy and stand-off distance, in the form proposed by Attewell and Farmer [1].

Logarithmic Sub Group Equations

The work carried out by Attewell and Farmer [1] in producing logarithmic equations to describe the levels of vibration due to pile driving has been mentioned previously. In the vibrations database project this method was not chosen, as the cubic fit was thought to provide a more precise and specific solution for any one particular case.

@seismicisolation

However, when the knowledge based system was being designed it became necessary to deduce equations giving explicit prediction of probable vibration, in preference to searching a very large database for appropriate data which may be duplicated yet conflicting.

The general form of the logarithmic equation generated by Attewell and Farmer could be stated as :

$$v=k\left(\sqrt{\frac{W}{r}}\right)^{x}$$

where
v = Resolved peak particle velocity(mm/sec)
W = Nominal input energy (J.)
R = horizontal surface distance (m)
k , x = constants

When k and x had been derived for each of the proposed sub-groups, then this system of equations could be used to predict vibration levels for a given hammer, pile and soil combination. Once the hammer was selected, its nominal energy rating could be supplied into the equation.

This would make the basic operation of the system comparatively simple as one of the most important factors, namely nominal energy input, could be regarded as an independent variable. It is important to be consistent with the use of "nominal" hammer energy; " nominal" implies the energy available from the hammer fall without reduction for energy loss during the hammer impact. Efficiency differences between hammer types are taken into consideration, as detailed later.
The equations derived from the logarithmic regression analyses were compared with the original Attewell and Farmer equations, and the results showed that the work carried out 17 years previously was validated by modern data, except in the case of vibrodrivers.

Drop and Diesel Hammer Selection

Different algorithms were built into the knowledge based system for bearing piles and for sheet piles. The reason for this is that the source of the driveability data, the British Steel Piling Handbook [8], treats the pile types separately.

Calculations of the energy requirements for driving sheet piles are based upon Table H1 of the British Steel Piling Handbook which gives an indication of the energy ranges required to drive sheet piles in pairs or as singles. These figures relate only to diesel hammers. Values used in the hammer energy database were taken as 80% of the mean of the energy range quoted in the table, which was considered to be a reasonable estimate of minimum energy which would give an

@seismicisolation

acceptably high confidence of achievement of pile penetration.

From work carried out on the relative efficiencies of diesel and drop hammers, see Testing and Analysis Internal Report, [11], representative efficiencies were chosen to be in the ratio of 80:60. The drop hammer energy requirements were thus deduced from the basis of the diesel hammer data. Application of such a simple approach is valid because the operation of both hammers is similar. Both are impact hammers, but their performance is affected differently by the ground conditions.

The table of energies was converted into a database, with individual values being related to the pile section, the pile depth and the ground type and condition. For ground conditions "soft" or "loose" energies were reduced by 10%, and for "stiff" or "dense" conditions a 10% increase was applied; these modifiers were deduced by examination of a number of records from the vibrations database. In response to user-defined pile size and soil conditions the database is searched so as to estimate the energy required to drive sheet piles by both diesel and drop hammer.

Bearing piles were treated differently, the algorithm used being:-

$$E = m*l*k$$

where

E = Energy required to drive pile (kJ)
m = mass per unit length of pile (kg/m)
l = total length of pile (m)
k = modifying constant, normally 1.0

The mass per unit length and depth of pile are user-input, and only the modifying constant needs to be system-calculated. Experience showed that for piles greater than 20 metres long a 10% enhancement is needed. The energy required is also modified on ground condition, as described previously.

Air Hammer Selection

The operation of an air hammer has been described as a sharp chiselling action with a low energy rating per impact. Their use in industry is increasingly rare since they produce high levels of noise in operation and their efficiency is lower that of the competitors. Ironically, they also typically produce lower levels of vibration.

Although air hammers are manufactured by several companies, those in most common use in this country are produced by BSP (British Standard Piling). The database has only one occurrence of an air hammer not manufactured by BSP.

@seismicisolation

To calculate the air hammer to be used to drive a specific pile, the table H2 of the British Steel Piling Handbook is used. This quotes directly the BSP model to be used for a specified pile/soil combination. This table was also built into the database of hammer energies. However instead of producing an energy level, it responds with a selected BSP hammer model.

For selection of an air hammer rating for bearing piles, tables H1 and tables H2 of the Piling Manual were effectively overlaid to produce a comparison of diesel hammers against air hammers. This comparison is then used to chose a specific air hammer based upon the selection of the other impact hammers.

Vibrodriver selection

Vibrodrivers operate on a principle which involves application of periodic forces to the head of the pile but not impact, and so the techniques employed previously must be altered. It was considered desirable that hammer definitions could be incorporated into the same hammer database despite the different mode of operation.

Several manufactures of vibrodrivers suggest methods for selecting the size of hammer to be used for a specific project. Naturally, these different methods produce different results. The method chosen was that proposed by ICE (International Construction Equipment) since it was considered to be the most reliable.

The method is based upon the centrifugal force generated by the vibrodriver, as the equivalent parameter to nominal energy input for an impact hammer. The method is described below :-

$$C = f * l$$

where

C = Centrifugal force (kN)
f = Force required per linear metre (kN/m)
l = Maximum embedded length of pile (m)

The value of force per linear metre was selected from values proposed by ICE in graphical form, which experience showed to be realistic. Throughout the hammers energy database, the centrifugal force field is carried for use in the case of vibrodrivers only. This allows the same methodology to be applied throughout the hammer selection system. This simple method also has the advantage of being suitable for both sheet and bearing pile types.

@seismicisolation

Preferred Hammer selection

This routine allows the user to force the system to choose a specific hammer. This is useful when a contractor would prefer to use a hammer in his possession, but is unsure of the effect on ground vibration levels. The user is able to pick any hammer from the database of hammer models. Only one preferred hammer may be selected in each run.

A "hammer rating" indicates the suitability of the chosen model for driving the pile in question.

Soil types and conditions

The two primary soil types included in the knowledge based system are granular and cohesive, a choice which allows the user to differentiate between the dominant soil types. This is important as the soil type and condition affect the vibration levels.

The ground condition is split into three catagories for each of the soil types; loose, medium and dense for granular soil, and soft, firm and stiff for cohesive soils. These conditions modify the calculation of energy required to drive the pile by ±10%, as mentioned previously.

In the production of the sub-groups, "fill" was classed as a loose granular soil and Pulverised Fuel Ash (PFA) as a dense granular material. Silty clays were grouped depending on the particular site in question - the proportion of silt in the clay will dictate its class. If the user is in doubt which soil classification to apply to a particular site, various types may be chosen and a consensus of vibration levels achieved.

SYSTEM OUTPUT

On completion of the user-input information the system selects the suitable hammers to drive the pile and then displays an output screen, see Table 3. The upper portion of the screen contains the user-input data as a summary, the lower portion containing the vibration levels. The screen may be hard copied by the use of the Print Screen key on most IBM standard keyboards.

Four columns are displayed, one for each of the primary hammer groups, the vibration levels being displayed as integer values. At the foot of each column is the hammer model that has been selected by the system to drive the particular pile.

@seismicisolation

TABLE 3
Predictive Ground Vibration System

Pile type: Bearing		Pile section: 305x305@110kg/m		
Maximum depth: 20m		Ground condition: Medium		
Groung type: Granular				
Comments ...				
Distance(m)	Diesel	Air	Drop	Vibro
2	45.8	12.2	32.9	26.4
4	24.0	9.3	16.4	14.3
6	16.5	7.9	11.0	10.0
8	12.6	7.1	8.2	7.8
10	10.3	6.5	6.6	6.4
12	8.7	6.0	5.5	5.5
14	7.5	5.7	4.7	4.8
16	6.6	5.4	4.1	4.2
18	5.9	5.2	3.7	3.8
20	5.4	5.0	3.3	3.5
Hammer	Delmag D16-32	BSP 700N	IHT S35	Delmag PE7001
Rating	1.23	1.15	1.07	1.30

Below the hammer model is a hammer rating, expressed as a decimal number. This hammer rating can be expressed as :

$$\text{Rating} = \frac{\text{Nominal energy rating of selected hammer}}{\text{Calculated energy required to drive pile}}$$

The closer this rating approaches unity, the more suitable is the hammer for the project required. This hammer rating is very useful when used in conjunction with the "preferred hammer" routine.

The bottom line of the output screen displays any velocity restrictions placed on the piling. The user may impose certain restrictions on the piling whilst inputting the original data. This is useful if an outside body i.e. a local authority, has imposed certain limitations. These limitations form the basis for the output screen on which a colour coding overlays the vibration levels. A deep red signifies that piling levels are expected to be greater than the restrictions placed thereupon, while a light blue signifies that levels are expected to be acceptable.

The user may then change any one of the initially entered parameters and rerun the system to monitor the effect. This adds a great deal of flexibility to the system and allows the user to investigate fully the potential of a given construction project.

@seismicisolation

Interface and error trapping

The method by which the user interfaces with the system is via question and answer routines. The responses required from the user are all one word or numerical answers - there is no natural language interface. By simplifying this interaction, error trapping becomes much more of a simple task. Each question has a finite number of correct replies and these replies are stored within the system. Automated routines can then prompt the user if either the reply given is incorrect, or indeed if the user simply requires assistance.

The facility to rerun the system whilst changing selected parameters is driven via a set of menus. These menus allow the system to be operated in an unstructured manner. However this flexibility multiplies the potential for error. The system relies upon the manipulation of user input variables to produce its results. To then go back and change one or more of the variables requires care. System-set flags are comprehensively used so that the system has a complex internal logic of its own.

By definition, the knowledge based system contains the summation of available knowledge in the Ground Vibration Team at Durham University. The experience gained while conducting field work, particularly from piling crews, proved particularly useful. The British Steel Piling handbook was used in compiling the algorithms for nominal energy required and the staff of the Piling Technical Services department were helpful throughout. Steffens [3] was a useful source of information.

CONCLUSIONS.

Ground surface vibrations caused by pile installation can disturb neighbours and may pose a risk of damage to nearby structures and buried utilities.

A major programme of multichannel vibration measurements has been completed. Analysis of the large quantity of digital data presented a problem because of the several variables in the mechanical system, including primarily the type and size of driving hammer, the accuracy of the blow, the type and weight of the pile and its degree of restraint above the ground, and the type of ground and its condition.

The first procedure was to define the data as cubic functions of stand-off distance, and to mount each record onto a large database. The database was specifically designed so as to allow structured recall of data sets.

Patterns of data were deduced from the database, and a knowledge based system was constructed to operate in a

@seismicisolation

predictive mode, such that in response to input information of pile type and length and categorisation of soil conditions, the system would select appropriate hammers, make estimates of vibration profiles, and compare these levels with statutory or selected vibration thresholds.

Despite the power of this integrated system, it should be emphasised that because of the variability of the piling process, vibration estimates are not highly accurate.

REFERENCES.

1. Attewell, P.B and Farmer, I.W, Attenuation of ground vibrations from driven piling, Ground Engineering, 1973,6(4),26-29.

2. Walton, C, A database of ground borne vibration and structural damage cases - description of the database and the initial analysis of the data, BRE/84/7/2, Buiding Research Establishment, Watford. 1990.

3. Steffens, R., Structural vibration and damage, BRE Report, Watford. 1985

4. BS 5228 Part 4 Draft. Code of practice for noise and vibration control applicable to piling operations. BSI London. 1990.

5. Tomlinson, M.J., Pile design and construction practice. Viewpoint Publ., C&CA,London. 1977

6. Whitaker, T. The design of piled foundations. Oxford Pergammon, 1970.

7. BS8004 Code of practice for Foundations. BSI London. 1986.

8. British Steel. Piling Handbook 6th ed. BS Scunthorpe. 1988

9. Selby A.R., Ground vibrations caused by pile driving. Steel Piling Seminar. Sheffield Univ. 1988

10. Attewell, P.B., Oliver, A. and Selby, A.R. Database managemen and analysis of piling-induced ground vibration records. in Int. Conf. on Signals and Systems, Rabat,April 1990.

11. Testing and Analysis Internal Report. Balken Piling Derby 1982.

@seismicisolation

DYNAMIC DEBONDING OF GROUTED PRESTRESSING TENDONS CUT DURING DEMOLITION

ALI BELHADJ, PETER WALDRON and ANTHONY BLAKEBOROUGH
University of Bristol, Department of Civil Engineering,
Queen's Building, University Walk, Bristol BS8 1TR, UK

ABSTRACT

Experimental methods are described which are being used to investigate the behaviour of bonded tendons suddenly released during demolition of post-tensioned concrete structures. Results from simplified drop tests have indicated the need for a more realistic simulation of the movement of large prestressing tendons cut during demolition. As a result, cutting tests in which bonded prestressing strands and bars cast in concrete beam models are suddenly released have subsequently been undertaken. Laboratory work in this difficult area must be limited to idealised scale models which are less than satisfactory for simulating the actual behaviour in real structures. However, important information about the complex mechanics of dynamic debonding of large tendons is being obtained before attempting more realistic field trials.

INTRODUCTION

Very little has been published about the demolition of prestressed concrete but, because of the growing number of prestressed structures that will eventually need to be demolished, the subject is attracting more and more research interest. Demolition of prestressed concrete is potentially very dangerous due to the high level of strain energy stored within the tendons. The sudden release of this energy due to the cutting of a prestressing tendon may result in excessive movement of the tendon accompanied by bursting of the end anchorages, severe cracking of the surrounding concrete with ejection of debris, and possible instability of the structure followed by uncontrolled collapse.

Three main areas of study have been identified [1] for special attention: (i) dismantling of progressively stressed structures; (ii) cutting of unbonded tendons in slabs; and (iii) cutting of large bonded tendons. Due to the very small number of progressively stressed structures that have been constructed to date, very little attention has been paid to the first of these topics. The essential difference between the two remaining topics is the degree of bond that exists between the tendons and the surrounding concrete.

@seismicisolation

Unbonded tendons
Experimental and analytical work in this general area is very limited. Williams and Waldron [2-5] have carried out a comprehensive investigation into the movement of unbonded prestressing tendons in greased plastic sheaths when cut during the demolition of slab structures. Results from an extensive programme of controlled laboratory tests were used to validate an analytical model developed for the purpose. The results from these tests and subsequent analyses indicated that large movements of unbonded tendons of the type considered in the research were unlikely to occur during demolition largely as a result of the effects of damping provided by the protective grease. This conclusion appeared to be valid irrespective of tendon length.

Bonded tendons
Some limited in-situ monitoring of a small number of prestressed concrete structures during demolition has been carried out [6-8]. The effect of cutting tendons was observed to vary from one structure to another depending on local conditions such as the degree of bond, friction between individual wires or strands within a tendon or tendon group, and the level of confinement provided by shear reinforcement. Significant debonding of the tendon, longitudinal splitting of the concrete member, and bursting of the end anchorage zones were the main forms of structural damage observed.

In pre-tensioned concrete elements many small diameter wires or strands are generally cast within the concrete section to provide the necessary prestressing force. Due to their relatively high ratio of surface area to cross-sectional area, bond stresses that arise between the steel and the concrete as a result of cutting are usually very small and the wires may generally be assumed to be perfectly bonded along their length. This feature limits the chances of unsafe dismantling of pre-tensioned precast concrete beams which are used extensively in building structures.

On the other hand, in post-tensioned concrete elements, a large number of tendons producing a very large total prestressing force may be concentrated in a single duct within a relatively small cross-sectional area of concrete. Although the remaining voids in the duct are subsequently filled with a cement grout for the dual purposes of providing corrosion protection and bond with the surrounding concrete, the effective bond area defined by the perimeter of the tendon group may be insufficient to resist the large bond stresses generated as a result of cutting. This feature makes the demolition of such structures potentially much more dangerous.

Prior to cutting a large post-tensioned tendon in practice, the duct must first be exposed by breaking away a length of the surrounding concrete. After the ducting has been stripped away, the grout is then chipped off the strands (Fig. 1). The loaded tendon may then be cut either by hand with a thermic lance or oxyacetylene cutter or remotely by the use of explosives.

After cutting, the sudden release of energy results in the formation of an impact axial stress wave which travels down the tendon from the point of release. A large amount of this energy is dissipated in the debonding process and it is possible for massive and progressive debonding to occur between the tendons and the surrounding grout resulting in severe cracking along the concrete beam. Indeed, the problem may be further compounded by the occurrence of poor or incomplete grouting which, for example, in major bridge structures has been found to occur in a very significant proportion of cases [9].

Unlike the case of unbonded tendons, for which a uniaxial solution was proposed, the problem faced is clearly a three dimensional one requiring a non-linear dynamic analytical approach which is currently under development. Uncertainty about

@seismicisolation

the condition of the grout surrounding the tendon adds to the complexity of the problem.

Figure 1. Cutting of a post-tensioned tendon by oxyacetylene torch.

DROP TESTS

A large amount of stored strain energy is released as a result of cutting the stressed tendons. This is converted to kinetic energy within the system, any movement of the tendon being resisted by the two main energy-dissipating mechanisms: (i) bond-slip between the grout and the tendon; and (ii) cracking of the surrounding concrete. A short series of simple drop tests were conducted in order to obtain preliminary information on the nature of these two mechanisms, and to identify other possible parameters. The tests also provided the opportunity of selecting the most appropriate measurement techniques to be used in the main tests planned to follow.

For each test an instrumented steel rod was cast centrally within a concrete cylinder. Each rod was formed by milling two similar smooth bars down to a half round and then machining a longitudinal groove 5mm wide by 2mm deep in each to accommodate strain gauges and their wiring. After installation of the gauges, four in each specimen, the two halves were glued together with epoxy resin to form a complete round bar. All bars were mild steel of 20 mm diameter. Two types of cylindrical concrete specimen were used: Type 1 was 150 mm dia. by 300 mm high with a characteristic concrete strength of 70 N/mm^2; Type 2 was 100 mm dia. by 150 mm high with a concrete strength of 50 N/mm^2.

Each concrete cylinder was strain gauged around its circumference at 3 positions over its height. An accelerometer was fixed to the bottom of the bar. Each specimen was loaded by dropping a 52 kg mass on to the bar from a series of heights which were increased incrementally until debonding occurred. The falling mass was instrumented with a load cell as shown in Fig. 2.

©seismicisolation

Readings of impact load, strain and acceleration were recorded either digitally on a PC or in analogue form on a 4-track FM tape recorder. These were then analysed using advanced data processing software [10,11]. An example on the response without debonding of a type 1 specimen is shown in Fig. 3. Strain outputs in the bar give an indea on the distribution of bond along the steel-concrete interface. Hoop strains on the concrete indicate that cracking did not occur. Bond between the steel and concrete was excellent in Type 1 specimens and no visible cracks appeared on the concrete. With Type 2 specimens, however, debonding occurred with a clear slip of the bar and the formation of a longitudinal crack extending across the diameter of the concrete cylinder.

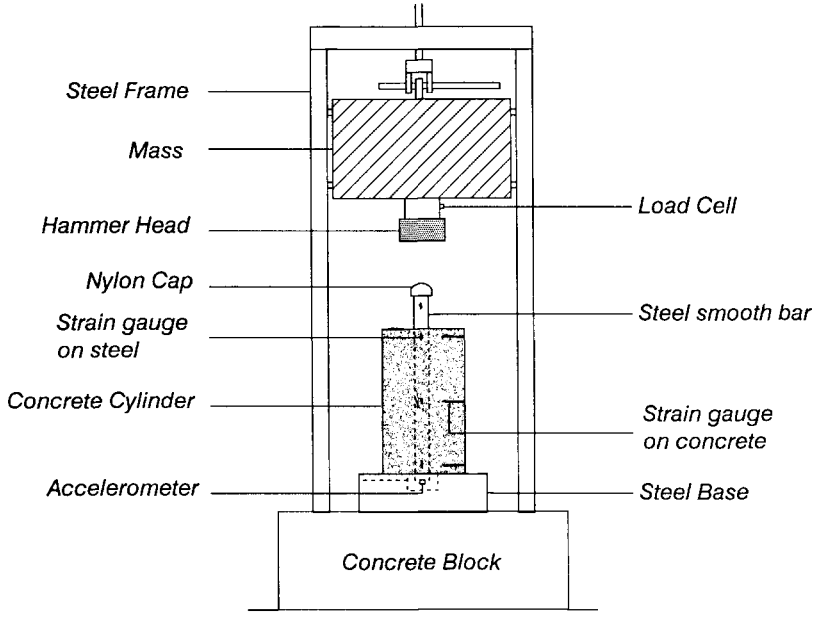

Figure 2. Details of drop rig and impact specimen

Because of the short length of the specimen and the limitations on the speed of data acquisition it was not possible to capture data regarding the axial stress wave propagation due to the compressive impact load. The models had very high axial and radial natural frequencies (4 kHz and 12 kHz respectively) and because of the low frequency content of the input load (with a maximum value of 1.2 kHz), it was not possible to excite those natural frequencies. The specimens were therefore too stiff to respond dynamically.

These simple drop tests, however, allowed the performance of the different instrumentation and software employed to be evaluated, and the usefulness of different methods of measurement and recording to be assessed. The important parameters worthy of further study were also identified and these were incorporated in the design of the main test programme.

@seismicisolation

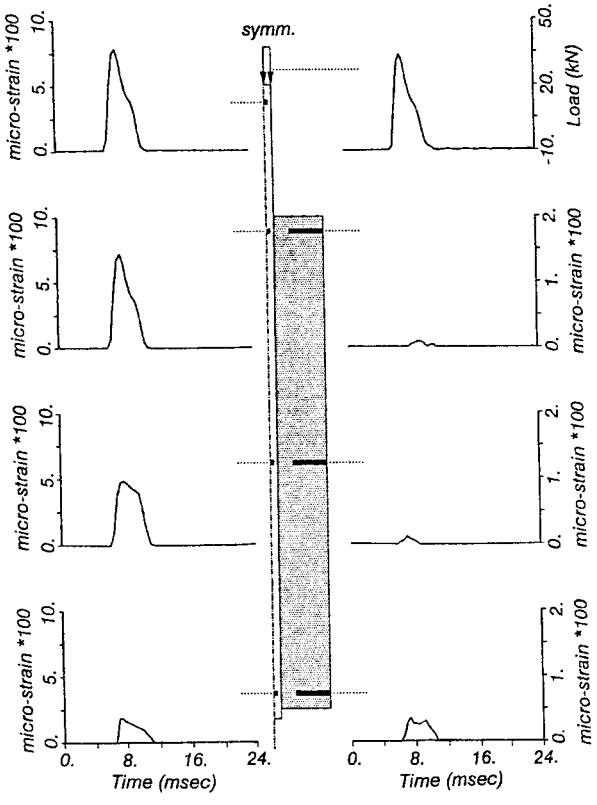

Figure 3. Typical load and strain outputs from a Type 1 drop test

CUTTING TESTS

To overcome the limitations mentioned above, more realistic cutting tests on longer beam models were designed. The longer beam length permitted a stress wave to be measured allowing for better dynamic analysis of the bond mechanism. The sudden release of load from a stressed high tensile steel tendon rather than the impact of an unstressed bar (as investigated previously in the drop tests) was also likely to result in more significant cracking of the concrete due to the Poisson's ratio effect and mechanical wedging during the bond slip process.

Test rig

Although idealised scale models of full scale beams were to be employed for these tests, cutting of the loaded tendons in a laboratory environment still posed considerable problems. A fail-safe mechanism for releasing the load had, therefore, to be designed. For safety reasons, the whole cutting mechanism and the beam specimen were enclosed between the side walls of a rigid steel testing frame. Further protection from flying debris was provided by sheets of steel-faced plywood placed top and bottom to form a completely enclosed box. The cutting mechanism consisted of a high speed 125mm diameter abrasive disk cutter its rate of advance being controlled by a suitably geared D.C. motor fixed to the frame wall, as shown in Fig.4.

@seismicisolation

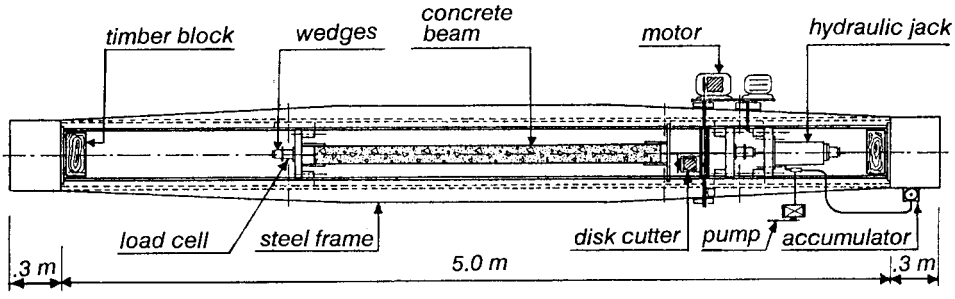

Figure 4. Plan view of the reaction frame and concrete specimen showing the prestressing and cutting mechanisms.

The tendon specimen to be cut was fixed between two 50 mm thick steel reaction plates and loaded to the required level by a hydraulic jack located at the same end as the cutting mechanism. As the concrete specimens were to be either cast in place or precast and subsequently grouted in position, it was essential that a stable load was maintained in the tendon for several days after stressing until the time of the test. Two alternative methods were adopted. In the first, the load was transferred from the jack to the adjacent reaction plate by means of conventional barrels and wedges (for 7-wire strands) or by nuts (for high tensile steel bars). In later tests a more satisfactory method was adopted whereby a constant pressure was maintained in the jack until the time of test by employing a hydro-pneumatic accumulator mounted in parallel.

Each concrete specimen was simply supported at its ends on short circular bars extending from the end reaction plates. Intermediate supports were provided in some cases using transverse bars positioned through the holes in the frame walls. Finally, to prevent excessive movement of the prestressing tendon after release, timber blocks backed with steel plates were placed vertically within the testing frame at the two ends.

Beam models

Five preliminary tests were carried out to check the performance of the cutting mechanism and the overall behaviour of different beam configurations. A redundant bridge beam monitored during demolition by Buchner et al [12] was adopted as a basic prototype for the design of the beam models using an approximate linear scaling factor of 1/2.5.

Initially concrete beams 100 mm diameter by 2.1 m long were cast vertically in a PVC pipe reinforced externally during casting by a pair of mild steel angles. Inside the pipe a 40 mm dia. corrugated steel prestressing duct was placed centrally and held in position over its length by a rigid steel bar. The steel angles and the rigid bar were fixed to a thick steel base plate to provide stability during the casting process. The concrete was placed in layers and compacted using a vibrating table.

After several days the beam was demoulded by cutting the plastic formwork longitudinally. It was then placed horizontally in the testing frame. A 7-wire strand of 15.2 mm diameter was threaded through the central duct and loaded. Finally, the duct was filled with cement grout. The grouting procedure was simple and consisted of

@seismicisolation

pouring the grout from a height of 2 m into one end of the beam through a transparent 25 mm dia. plastic tube connected to the specimen with a special end fitting. The grout was allowed to flow out from a similar assembly at the other end of the beam until all air had apparently been excluded. After a further 3 days of curing the grout filled plastic filling tubes were removed and the beam was tested.

In the later tests, concrete was cast directly around the stressed tendon without the necessity for ducting or grouting. A timber mould square in cross-section was placed in the testing frame and accurately positioned around the tendon specimen represented in all these tests by a solid high tensile steel bar rather than strand. The bar was stressed to its predetermined load, and the concrete poured into the mould and compacted in place using a vibrating hammer applied to the formwork. After several days the beam was demoulded and tested.

Data acquisition and release of load

The acquisition system consisted of signal conditioning units, a termination board, and a P.C. containing a high speed analogue to digital converter board (DT 2821-F-16SE). The data was acquired and later processed using advanced data processing software [10, 11] in the same way as for the drop tests. The appropriate frequency range governing the rate of data acquisition was determined from the preliminary tests recorded on a FM tape recorder.

Prior to cutting the loaded tendon, the disk cutter was adjusted to be very close to the surface of the tendon. The whole system was then covered by the protective steel faced sheets top and bottom. From a safe distance the cutter and the motor controlling its rate of advance were switched on remotely. The computer used for data acquisition was started simultaneously.

Test results and observations

A summary of the behaviour of the beams tested is given in Table 1.

The use of multi-wire strand in early tests further complicated the behaviour of the beam. In addition to the progressive drop of load as each component wire was cut, as can be seen in Fig. 5, the released force induced a torsional effect on the beam because of the spiral configuration of the strands. The use of solid Macalloy bars instead of 7-wire strand together with an accumulator to maintain load helped to solve these problems in later tests (Figs. 6 and 7).

Although the surface of the Macalloy bars was very smooth the desired behaviour i.e. stress wave propagation and cracking of concrete was still observed. It should be noted that friction between steel and concrete was the main factor that prevented excessive longitudinal movement of the bar.

The wall thickness of the steel sheathing used in the fabrication of the early cylindrical specimens was too thick for the scale of the beam models adopted. This additional lateral confinement entirely prevented cracking in the surrounding concrete. This was one of the principal reasons why specimens without ducts were used in later tests.

The effect of the bearing plates on the beam behaviour did not seem to be very important despite the fact that these plates have a natural frequency of 460 Hz which falls within the frequency range of principal interest (up to 2.5 kHz). This was due to the fact that most of the energy released was dissipated before the initial stress wave reached the end of the beam specimen remote from the position of cutting.

@seismicisolation

TABLE 1
Summary of preliminary cutting tests

Test	concrete specimen	tendon	grout strength	boundary conditions	response
1	circular,precast D=100 mm strength 70 N/mm^2	15.2 mm diameter 7 wire - strand	18 N/mm^2	2 ends free and simply supported	no visible cracks debonding length=.5m load in several steps (slip between wires)
2	circular,precast D=100 mm strength 65 N/mm^2	15.2 mm diameter 7 wire - strand	25 N/mm^2	one end free and simply supported one end stressed to plate	no apparent cracks debonding length=.8m individual snapping of wires during cutting
3	The Test2 beam was reused with the strand exposed and cut at a section 0.8 m from the left hand support (The strand was still under about 70 percent of the initial load when it reanchored during Test2)				total debonding with no cracking
4	square,in-situ 100x100 mm^2 strength 45 N/mm^2	20 mm dia. stainless Macalloy bar	N/A	one end stressed to plate and two intermediate simple supports	total debonding with no visible cracks big drop of load before release
5	rectangle,in-situ 80x100 mm^2 strength 15 N/mm^2	same as in Test4	N/A	same as in Test4	1 m long longitudinal crack total debonding faster impact load

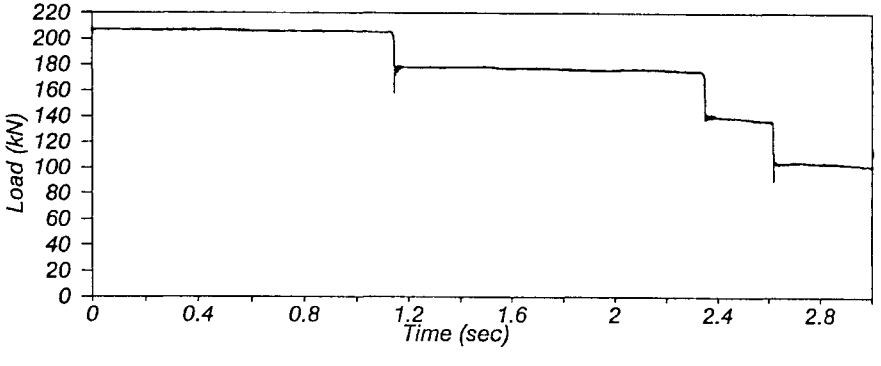

Figure 5. Test2 released end load during cutting of the first 3 wires of the strand

@seismicisolation

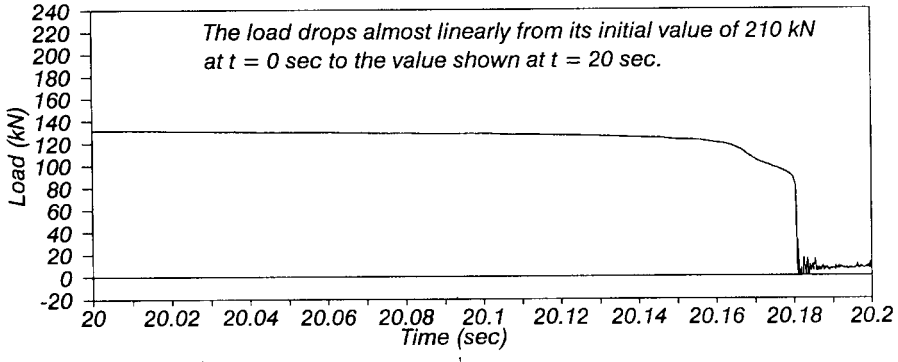

Figure 6. Released end load history of test4 where no accumulator was used

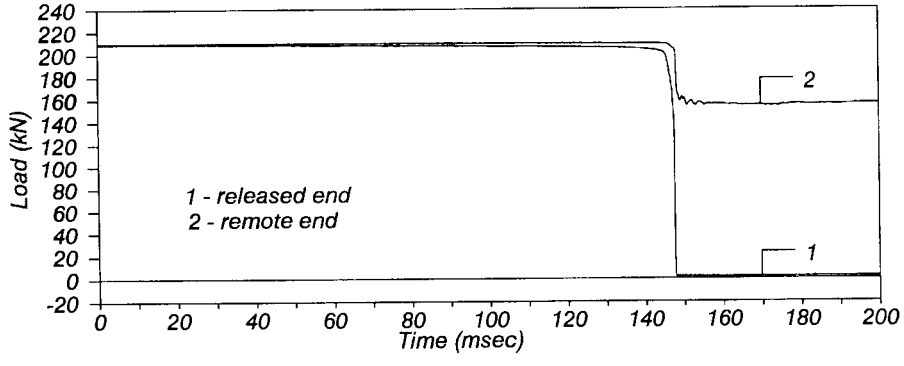

Figure 7. Time histories of Test5 loads where an accumulator was used

CONCLUSIONS

(a) The drop tests and the preliminary cutting tests were useful in designing a main series of tests which are currently being undertaken. In particular they permitted a successful cutting mechanism to be developed and a method to be established for the desired prestressing load to be maintained until release. The tests also helped to define the important dimensions and parameters of the tests specimens.

(b) Although the tests specimens and methods used in the laboratory were idealised and only modelled the real situation to be found in full-scale structures, they have proved to be sufficiently realistic to provide important information on local behaviour of the dynamic debonding mechanism.

(c) The initial model testing in the laboratory described here is seen as a preliminary study to subsequent investigations in this new complex area of research. The principal objective of this programme of laboratory research was to provide useful and reliable data for the development and validation of a computer model that will be able to simulate the general mechanism of dynamic debonding. In particular this could be used in planning the strategy for the demolition of large post-tensioned concrete structures.

@seismicisolation

REFERENCES

1. Williams, M. S. and Waldron, P., Demolition of structures containing unbonded tendons. Report No. UBCE/C/86/2, Department of Civil Engineering, Bristol University, Dec. 1986.

2. Williams, M. S., The cutting of unbonded prestressing tendons during demolition. University of Bristol, PhD thesis, 1988.

3. Williams, M. S. and Waldron, P., Demolition of structural concrete containing unbonded tendons. Proc. of Intl. Conf on Decommissioning, UMIST, Inst. of Civil Engrs. NW Assoc., March 1988, pp. 121-130.

4. Williams, M. S. and Waldron, P., Dynamic response of unbonded prestressing tendons cut during demolition. ACI Structural Journal, Nov-Dec 1989, 686-696.

6. Lindsell, P., Demolition of post-tensioned concrete. Concrete, Jan. 1975, Vol 9, No. 1., pp. 22-25.

7. Felstead, A. E. and Lindsell, P., Controlled demolition of a post-tensioned beam. Concrete, Sept. 1981, Vol 15, No. 9., pp. 20-23.

8. Lindsell, P. and Buchner, S. H., Dismantling of continuous post-tensioned structures. Proc. of Intl. Conf on Decommissioning, UMIST, Inst. of Civil Engrs. NW Assoc., March 1988, pp. 131-135.

9. Woodward, R. J., Conditions within ducts in post-tensioned prestressed concrete bridges, TRRL report 980, 1981.

10. Taylor, C. A., DSP - A fully interactive digital signal processing program, Version 1.17, Bristol Earthquake Engineering Data Acquisition and Processing System, EERC, Department of Civil Engineering, Bristol University, 1991.

11. Brownjohn, J. M. W., Acquiring data using the data translation (DT) hardware and ASYST software. EERC Technical Instruction TI23002, Department of Civil Engineering, Bristol University, March 1990.

12. Buchner, S. H., Lindsell, P. and Robinson, S., Prestress losses in full-scale structures. Internal report, R/M/CVL 842, Department of Civil Engineering, University of Surrey, 1984.

ACKNOWLEDGEMENTS

The Authors wish to acknowledge the financial assistance of the Algerian Ministry of Higher Education.

@seismicisolation

GROUND AND STRUCTURAL VIBRATIONS INDUCED BY EXPLOSIVE DEMOLITION OF ADJACENT STRUCTURES

J.M.W.Brownjohn[1], Z.A.Lubkowski[2], J.W.Pappin[2] and C.A.Taylor[1]
(1) University of Bristol, EERC, Dept of Civil Engineering, Bristol BS8 1TR, UK
(2) Ove Arup & Partners, 13 Fitzroy Street, London W1P 6BQ, UK

SYNOPSIS

In what is believed to be one of the largest controlled explosion in Europe since the Second World War, three large reinforced concrete tobacco warehouses in the centre of Bristol were demolished in 1988. Acceleration response measurements were taken in another warehouse only 30m away and at various points on the ground. The monitored warehouse, adjacent to the docks, was founded on alluvium and fill, with piled foundations.

This paper is a factual report presenting the effects of a major demolition on adjacent structures. It compares observed and theoretical structural responses and examines ground response, including the attenuation of motions with distance from the centre of demolition. Structural responses were small and no structural damage was observed.

INTRODUCTION

On the 29 April 1988 three tobacco warehouses adjacent to Cannons Road and The Butts Road, Cannons Marsh, Bristol were demolished by a controlled explosive sequence. The site, adjacent to the Floating Harbour, is a relatively flat area with an average ground level of 9mOD. The ground profile consists of 14m of Estuarine Alluvium (clays, sands and gravels) overlying sandstone [1]. The tobacco warehouses were seven storey reinforced concrete frame structures with brick infill panels and founded on spread footings. Each warehouse had an approximate mass of 10,000

@seismicisolation

tonnes. The dynamic response of a transit shed (referred to as 'Z' shed) was monitored. This was a two storey reinforced concrete frame structure founded on piles, which was within 30m of the demolition. A plan of the site and cross section of 'Z' shed are shown in Figure 1.

DEMOLITION

The method of demolition involved the systematic removal of supporting members by a series of explosive charges, detonated in sequence to achieve a progressive inward folding collapse leaving a compact debris pile. The demolition was a series of two explosions, with a three second interval to provide sufficient time for the structure to respond to the forces mobilised by the first blast before the second blast was initiated. Figure 2 shows a series of photographs which illustrate this progressive collapse. The instrumented 'Z' shed is shown on the left of the photographs.

MEASUREMENT SYSTEM

Acceleration response signals were recorded digitally on a personal computer. Horizontal and vertical accelerations were measured within 'Z' shed and vertical accelerations at several ground locations (Figure 1). Piezoelectric accelerometers were used in 'Z' shed, while high gain, servo accelerometers were used at the ground locations. The frequency band width of this data acquisition system was set to 30Hz. The digitised time histories were then processed using interactive signal processing software [2].

PROCESSING SCHEME

The digitised time histories were processed to remove unwanted noise, drift and d.c. shift components. An Ormsby low pass filter with 40Hz cut-off frequency and 5Hz filter ramp was used to remove the high frequency noise. A high pass filter with 1Hz cut-off frequency and 0.5Hz filter ramp removed the drift component. The signals were then base line corrected using the principle of a minimum sum of the squares of the deviations for the whole length of the record. This procedure produced the time histories in Figures 3 and 4.

These acceleration time histories were integrated twice to produce velocity and displacement time histories. Maximum and minimum values for all three sets of records

@seismicisolation

were calculated. These are shown in Table 1. The frequency content of the acceleration time histories were found from calculating the complex Fourier spectra and the velocity response spectra; the latter are shown in Figures 3 and 4.

The frequency response functions (transfer functions) of the horizontal acceleration time histories within 'Z' shed were calculated. These used auto power and cross power spectra calculated from the complex Fourier spectra and enabled the modal response characteristics of 'Z' shed to be derived. Table 2 shows the modal response frequencies.

DISCUSSION OF PROCESSED DATA

Ground Response

At the nearest ground location to the demolition the peak vertical ground acceleration was measured to be 0.032g. The recorded acceleration time histories (Figure 3) show the peak response reduces with distance from the demolition. Furthermore the 5% damped response spectra show the frequency of this peak reduces from 10Hz to 4Hz. This shows that, as expected, the high frequency component of the waves drop off faster than the low frequency components, as the waves travel through the ground.

From the measured values at the three monitored ground points, the attenuation of the peak velocity was plotted (Figure 3). The energy attenuation relationships given in [3] have been used to estimate the maximum instantaneous energy released by the demolition. This was calculated as 5.4MJ, which is about 1.2% of the potential energy that was stored in the tobacco warehouses.

Structural Response

The maximum accelerations recorded in 'Z' shed were 0.040g vertically and 0.023g horizontally. The amplitudes of vibration were larger in the vertical direction since the collapse of the tobacco warehouses caused a vertical impact on the ground beneath it. The 5% damped velocity response spectra show the peak response is 6Hz in the vertical direction and between 1.3 and 3Hz in the horizontal direction (Figure 4). The peak particle velocity measured was 6.8mm/s, at the horizontal first floor motion. It has been found [4] that peak particle velocities in excess of 50mm/s cause plaster to crack in buildings. No structural damage within 'Z' shed was observed after the demolition.

The vertical time histories (Figure 4) show that the ground motion lasted approximately 5 seconds. The remaining 3 seconds was a pure structural response. This

@seismicisolation

time period was used to determine the first two free vibration structural sway modes. Since the time histories were measured on one column, only the sway modes could be analysed although 3-D finite element analyses showed several torsional modes at frequencies around 1.9Hz and 5.6Hz. The first two dominant mode shapes derived from the accelerometer data were at frequencies of 1.46Hz and 5.37Hz. The finite element programs SAPIV and ANSYS were used to calculate the structural modes. To obtain the structural properties for these analyses the beam, column and slab dimensions were measured on site [5]. A gross concrete stiffness of 30 x 10^6 kPa and a concrete density of 2430kg/m^3 were assumed. A rigid foundation was used in these analyses. FREDA, a simple frequency domain analysis was also used to model 'Z' shed. This program uses a 1-dimensional lumped mass model and both soft soil and rigid foundations were used to model the sway modes. Table 2 shows general agreement between measured data and all the programs used. It was noted that the addition of a horizontal foundation, flexibility, calculated using conventional methods [6] in FREDA made no difference to the modal frequencies.

CONCLUSIONS

From the measured data it can be seen that in this case the induced ground motions were small, compatible with a peak energy source of about 1% of the available potential energy. Whilst there was no damage to an adjoining structure the response was sufficiently large to enable the frequency characteristics to be determined. Comparisons of the structural response with finite element and 1-dimensional frequency domain computer programs show reasonable correlation.

REFERENCES

1. Arup Associates, Cannons Marsh Development, Bristol. Geotechnical Report. November 1988.

2. Taylor, C.A., DSP A Fully Interactive Digital Signal Processing Program, Version 1.8. University of Bristol, August 1983.

3. Woods, R.D., Jedele, L.P., Energy - Attenuation Relationships from Construction Vibrations. Vibration Problems in Geotechnical Engineering, ASCE, 1985.

4. List, B.R., Lord, E.R.F. and Fair, A.E., Investigations of Potential Detrimental Vibrational Effects Resulting from Blasting in Oilsand. Vibration Problems in Geotechnical Engineering, ASCE, 1985.

@seismicisolation

5. Gatrell, M.D. and Goldman, J.R., Demolition Induced Vibrations. Final year research project, University of Bristol, April 1989.

6. Werkle, H. and Waas, G., Dynamic Stiffness of Foundations on Inhomogeneous Soils. Proceedings of the 8th European Conference on Earthquake Engineering. Lisbon 1986.

TABLE 1

Peak Measured Values

Location	Acceleration (m/s^2)	Velocity (mm/s)	Displacement (mm)
'Z' Shed			
Horizontal Ground	0.227	6.64	0.39
Horizontal First	0.187	6.77	1.10
Horizontal Second	0.142	5.42	0.45
Vertical Ground	0.247	5.74	0.31
Vertical Second	0.391	6.37	0.54
Ground			
A	0.310	5.04	0.12
B	0.152	2.35	0.06
C	0.043	1.88	0.04

TABLE 2

Measured and calculated modal frequencies (Hertz)

Mode	Measured	SAPIV	ANSYS	FREDA	FREDA
Foundation	Rigid	Rigid	Rigid	Rigid	Flexible
1	1.46	1.64	1.62	1.67	1.67
2	5.37	5.30	5.36	4.64	4.64

Mode 1 (1.46Hz) Mode 2 (5.37Hz)

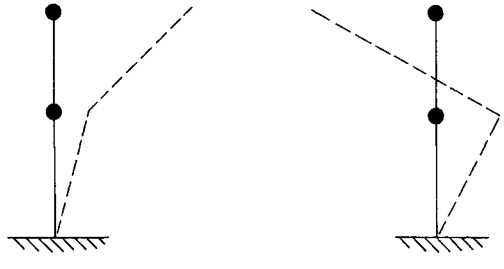

@seismicisolation

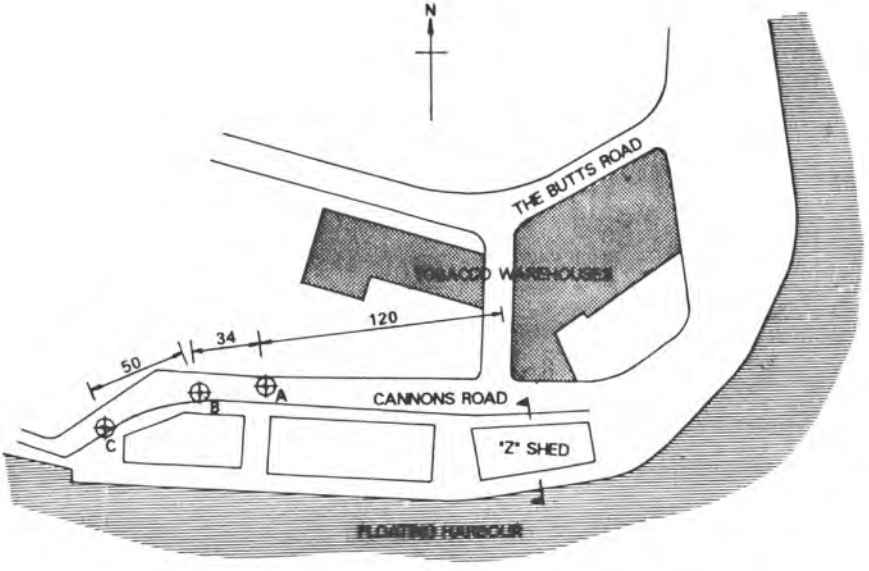

PLAN OF SITE

0 50 100
metres

⊕ Accelerometers

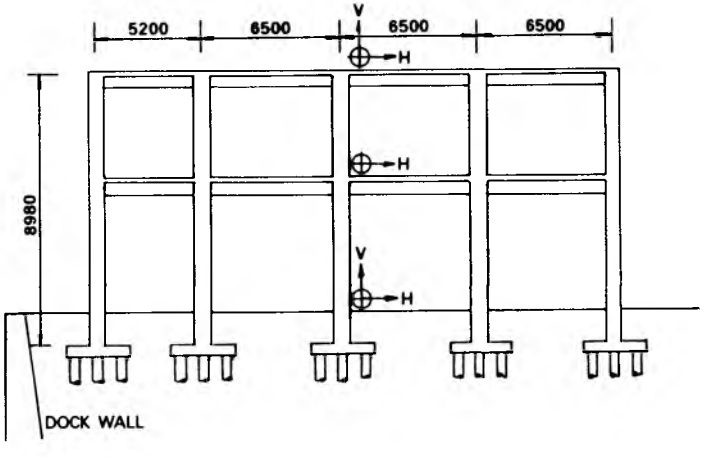

"Z" SHED CROSS SECTION

FIGURE 1

@seismicisolation

"Z" SHED

DEMOLITION OF TOBACCO WAREHOUSES

FIGURE 2

@seismicisolation

Wave Attenuation Graph

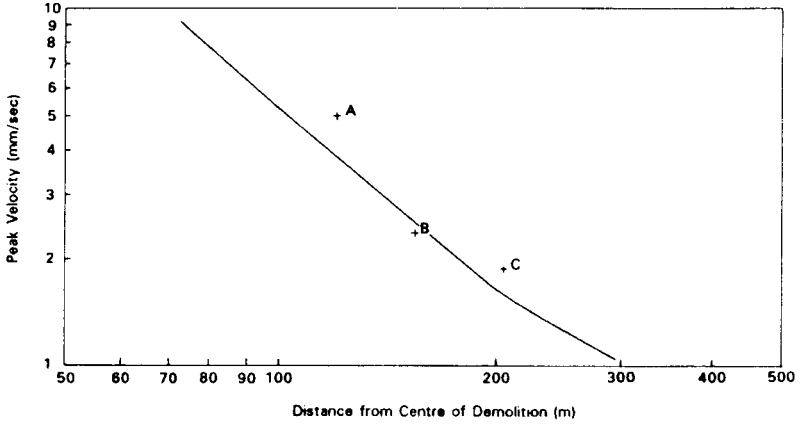

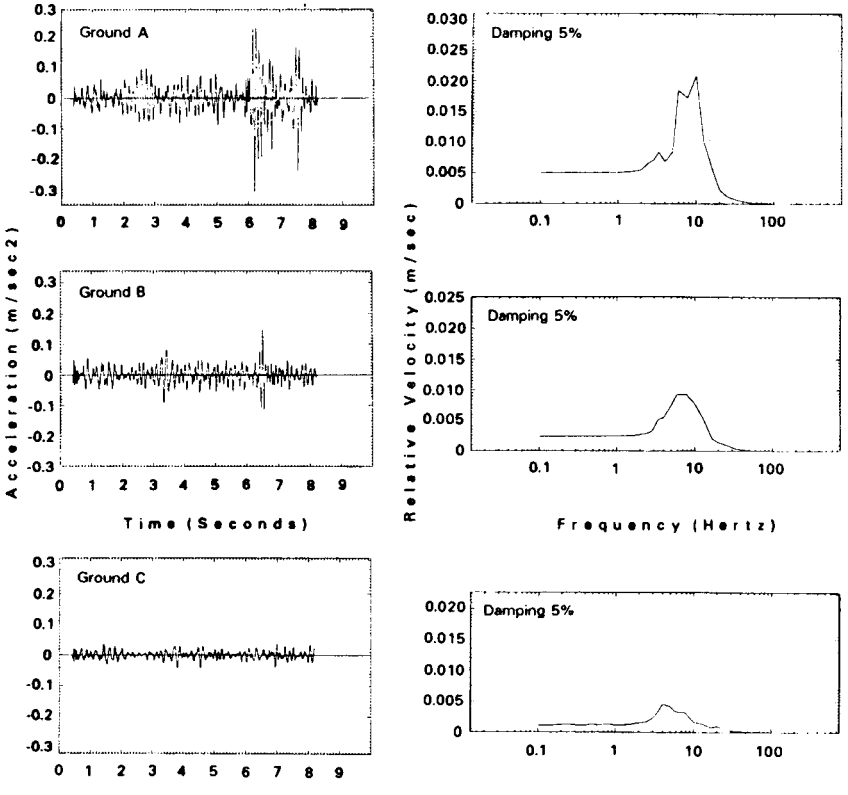

GROUND RESPONSE : Acceleration Time Histories and Velocity Response Spectra

FIGURE 3

@seismicisolation

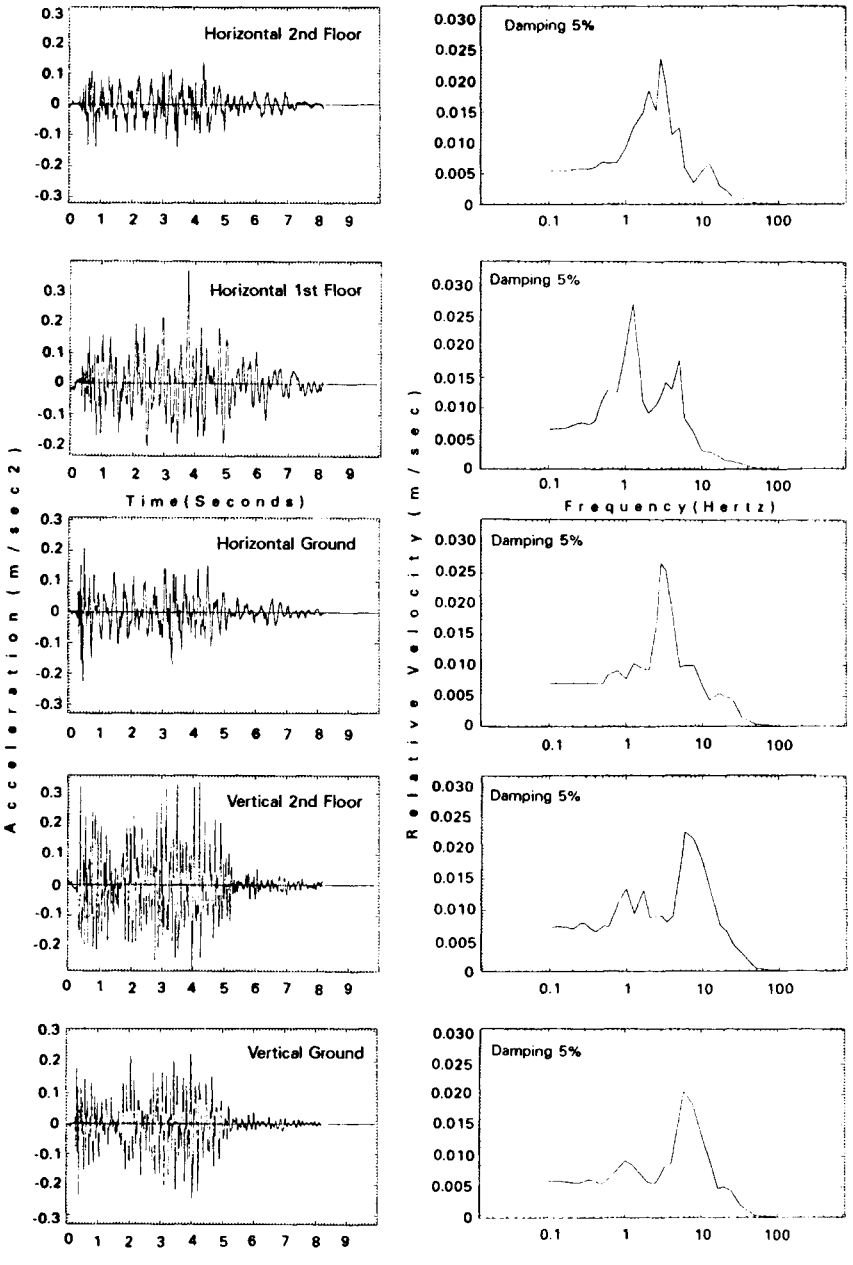

BUILDING RESPONSE : Acceleration Time Histories and Velocity Response Spectra

FIGURE 4

@seismicisolation

DYNAMIC MONITORING OF LARGE DIAMETER DRIVEN PILES NEW GALATA BRIDGE, ISTANBUL, TURKEY

JEFFREY S YOUNG
Associate of Bridge Division
Mott MacDonald Group
St Anne House
20/26 Wellesley Road, Croydon
Surrey, CR9 2UL, UK.

ABSTRACT

The new Galata Bridge is currently under construction in the historic centre of Istanbul and will replace the existing floating bridge which was constructed in 1917.

The new bridge with an overall length of 470m will incorporate a four leaf bascule bridge with a clear span of 80m and double decked insitu post-tensioned concrete approach spans. It is largely founded on 2m diameter driven steel tube displacement piles up to 80m in length.

The new bridge's foundation piles are required to sustain working loadings in excess of 1200 tonnes each and in addition to satisfy an exacting differential settlement criteria of 5mm.

During construction it was therefore essential to develop procedures to confirm that the piles had been driven satisfactorily into the intended founding strata. Dynamic monitoring was used in conjunction with detailed manually recorded pile driving data and physical load tests up to 2000 tonnes to ensure satisfactory pile installation.

@seismicisolation

INTRODUCTION

This paper describes the procedures developed during construction to confirm that the bridges piles has been satisfactorily installed. To achieve the load carrying and differential settlement criteria set by the structural design of the superstructure the piles were required to be driven into the gravel/cobble founding strata. Figure 1 shows the arrangement of the soil strata though which the piles were driven. The piles were 2m diameter steel tubes, the majority of which were driven closed ended and functioned as end bearing piles.

Prior to the commencement of construction, a driveability analysis was performed by advisors to the Contractor to determine the appropriate choice of piling hammer. As a result the Contractor elected to use a Delmog D-100 diesel hammer with a maximum rated energy of approximately 35 tonne metres.

The short length of the double decked approach spans and the need to ensure a reliably rigid foundation to the bascule section resulted in the requirement that the piles achieve a differential settlement criteria of 5mm.

The bridge is designed to carry 6 traffic lanes, two footways and has the additional capacity to accommodate a twin track light railway in the future. This necessitated an overall deck width of 42 metres. Furthermore the lower deck of the approach spans to the bascule sections are to be utilised as a shopping and public amenity area. The loads transmitted to the foundations were therefore high and this coupled with the desire, for reasons of economy, to reduce the number of piles to a minimum, resulted in the choice of a limited number of high capacity piles with working loads in excess of 1200 tonnes.

The primary requirement for pile installation was therefore that the piles be driven to virtual refusal in the gravel/cobble foundation layer. The load carrying capacity of the piles and their settlement characteristics were demonstrated by a limited number of confirmatory physical load tests of up to 2000 tonnes, preformed at key stages during piling operations.

Detailed manually collected pile driving data and dynamic monitoring records were obtained for piles that were to be subsequently load tested. This data had two uses, firstly to enable assessments to be made as to the adequacy of the pile installation to satisfy subsequent load test requirements, and secondly to provide characteristic pile driving data by which to judge subsequent piles that were to be driven but which would not be subjected to physical load testing. Thus standardised pile installation requirements were evolved. All piles driven were carefully observed throughout their installation and a full manually collected set of data was recorded. In addition every fourth pile driven was dynamically monitored over the final stages of driving to enable comparison with the records obtained for earlier and representative load tested piles. The dynamic monitoring also yielded valuable data on pile hammer efficiency and stresses generated in the pile during driving.

@seismicisolation

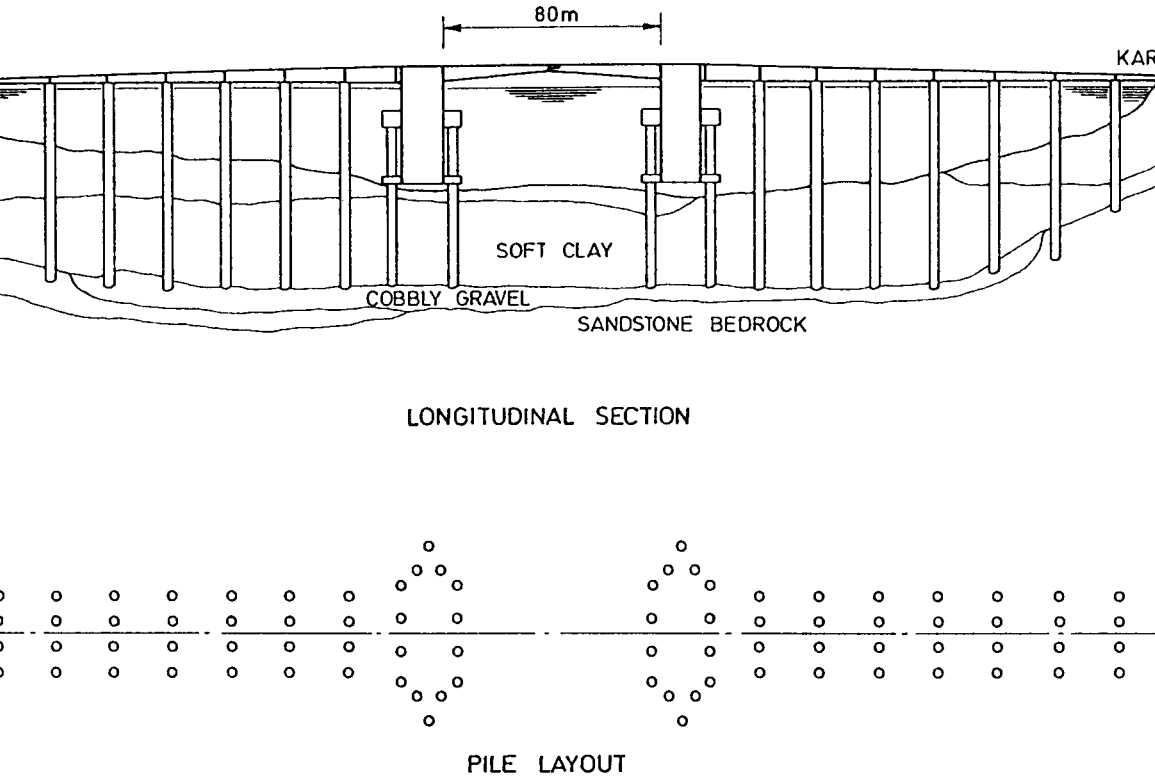

Figure 1. NEW GALATA BRIDGE

@seismicisolation

INSTRUMENTATION FOR DYNAMIC MONITORING

Instrumentation for the dynamic monitoring was provided and operated for the Main Contractors and their advisors, TNO of the Netherlands. The basic equipment consisted of strain and acceleration transducers attached to the pile head which in turn were connected to a micro-computer with appropriate software.

This paper is not concerned with the technical details of the instrumentation or its subsequent processing but deals with the practical interpretation of the resulting record and its use as a confirmatory tool to verify satisfactory pile installation.

OBSERVATIONS DURING THE DRAWING

During piling a full account was manually recorded for each pile driven. Times. durations and comment were recorded for all events that took place during the installation of the piles. Piles were accurately marked at intervals along their length prior to pitching to enable all recorded events to be accurately related to pile toe level. The most important data collected was driving resistance, recorded in terms of the number of hammer blows per 25cm of pile penetration.

This manual record was of vital importance because of the unexpected behaviour of the piles during their installation. Pre-construction drivability analyses performed on behalf of the Contractor indicated that a modest resistance to driving would be encountered when passing through the soft normally consolidated clay which would increase rapidly as the pile entered the gravel/cobble founding layer. It was initially estimated that a blow count of 250 blows per 25cm of penetration would be adequate to achieve the necessary load carrying performance of the piles. To avoid possible damage to the piling hammer and pile an upper limit of driving resistance of 650 blows per 25cm was set.

Boreholes sunk at the site had enabled the level of the founding strata to be defined accurately at specific locations. However variations in the level of the founding strata between boreholes could not be determined to an accuracy commensurate with the limited penetration achievable in the founding strata.

In practice the upper levels of the soft clay were penetrated fairly easily as had been predicted. However the piles reached a driving resistance of 250 blows per 25cm well above the expected level of the founding strata. Continued driving resulted in the driving resistance rising to the 650 blows per 25cm limit with the pile toes still well above the founding strata's predicted level and supposedly still within soft clay. Such a situation was unacceptable because of the possibility of excessive settlement of piles in service.

@seismicisolation

Reasons were initially suggested for the apparent premature refusal of the piles as follows:

(1) Malfunction of the piling hammer resulting in reduced driving energy being imparted to the pile: Observation of the piling hammer in operation however did not indicate abnormal functioning of the hammer. Indeed dynamic monitoring records clearly showed that the energy being delivered to the pile was well up to the hammers rated energy.

(2) Founding strata level higher than predicted: This could not readily be confirmed for all piles without further borehole investigation for which there was insufficient time within the construction program.

In line with conventional practice confirmatory redrives were performed and showed a reduced resistance to driving. This clearly showed that the founding strata had not previously ben reached. Experience further showed that increasing the length of time allowed to elapse between redrives increased the reduction in driving resistance. This phenomenon was attributed to disturbance of the pore water pressure surrounding the pile during the driving of these large diameter displacement piles. With time pore water pressures were believed to return to near normal thereby allowing further penetration to be achieved.

The concern was therefore to ensure that pile driving was not halted and piles accepted before they has reached refusal in the founding strata. Manually collected data enabled redrives to be assessed and further redriving ordered until such time as reduction in driving resistance did not occur between redrives. Typical driving resistance data recorded manually is shown in Figure 2, which for clarity of presentation has been simplified. For comparison purposes drivability predictions are also shown.

DYNAMIC MONITORING OF PILES

Whilst the manually collected data discussed above was felt to provide adequate assessment of the acceptability of the pile installation, confirmation was essential bearing in mind the high working loads and exacting differential settlement requirements for the piles. As has been stated before it was of primary importance that the piles were driven into the founding strata so as to develop end bearing. Uncertainty surrounding the precise level of the founding strata meant that refusal of the pile within the final 5m of the predicted pile length required confirmation. In this respect redriving and assessment of manually collected data used in conjunction with dynamic monitoring provided the necessary assurance,

Every fourth pile was dynamically monitored over the final 5 to 10 metres of driving, Data obtained during the monitoring provided the following information, the use of which

@seismicisolation

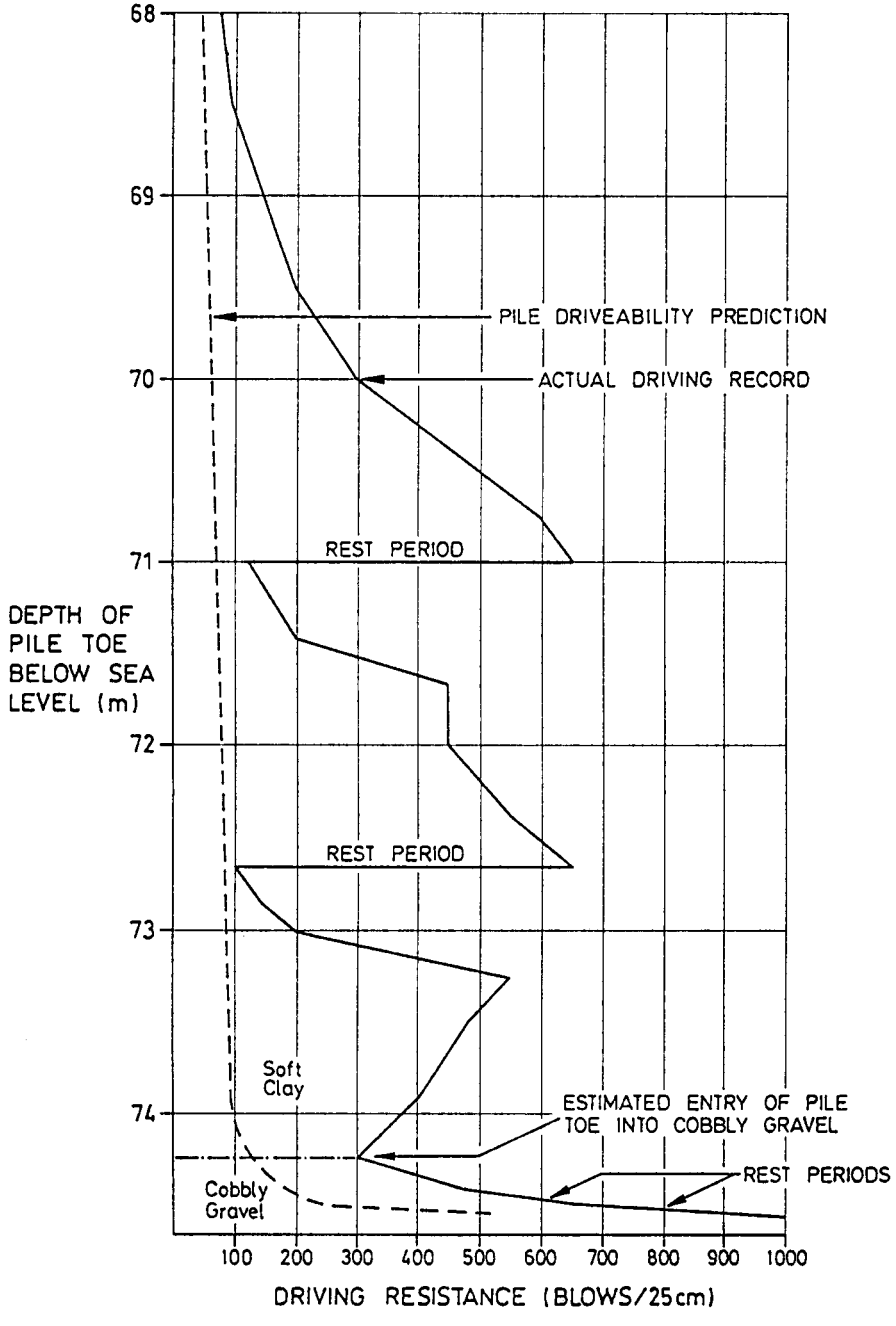

PILE DRIVEABILITY PREDICTION & ACTUAL DRIVING RECORD

@seismicisolation

Figure 2.

is briefly explained:

(1) Pile hammer energy imparted to the piles (enthru energy):
Consistent and correct operation of the piling hammer could be checked objectively.

(2) Pile stresses during driving:
Multiple redrives with a very high total number of hammer blows were necessary to complete the installation of each pile, and it became essential to assess possible fatigue damage to the piles resulting from the pile driving. Manual records were unable to provide any data on pile stresses and hence dynamic monitoring provided the only data available to assess fatigue damage.

(3) Driving resistance and estimate of the static resistance;
This data was of little practical use on site in that the resistance recorded did not show the transient increased resistance which was found to decrease with time as discusses earlier. However careful review of the record did show a small but significant increase as the pile toe entered the founding strata. No doubt with further study the soil/pile model represented in the computer program could have been refined for the sites specific conditions to provide more exact and useful interpretation of the monitoring record. This was not necessary however since alternative representation of the monitoring record did provide the clear indication necessary to show penetration into the founding strata.

(4) Analysis of individual hammer blows:
Represented graphically in terms of force against time, the characteristics of the shock waves passing through the pile driving could readily be reviewed during pile driving or subsequently by replaying the stored data. Three characteristics were found to provide data that could be assessed and checked against established wave forms to confirm satisfactory pile installation.

(a) Time against Force.

(b) Time against Velocity x Impedance

(c) Time against Upward Travelling Wave Force

@seismicisolation

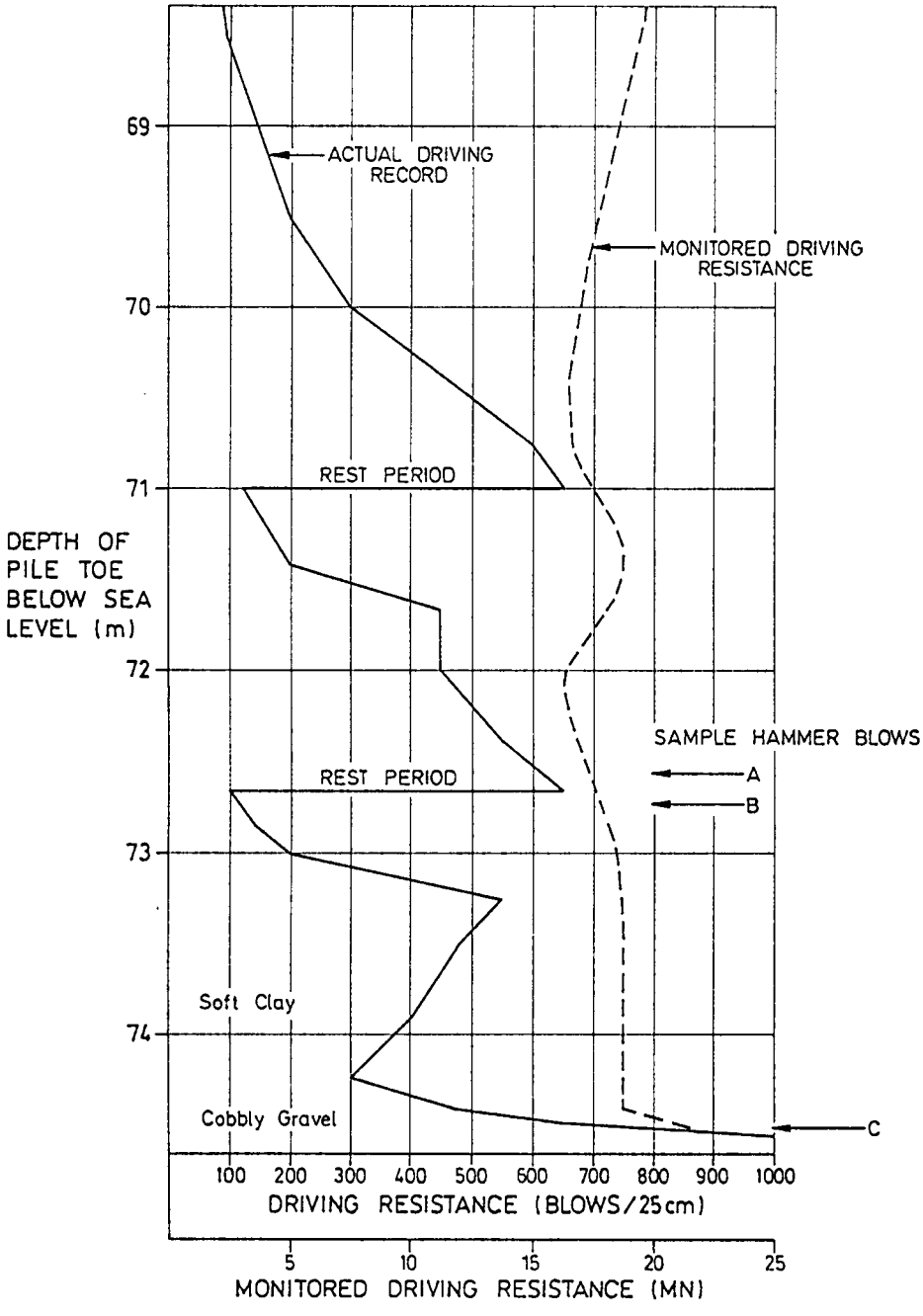

MONITORED DRIVING RESISTANCE AND ACTUAL DRIVING RECORD

@seismicisolation

Figure 3.

INTERPRETATION AND COMPARISON OF PILE DRIVING RECORD

Typical manually recorded pile driving record is shown in Figure 3 which clearly shows the characteristic reduction of driving resistance found in practice following a period of rest when the pile toe was in the soft clay. Furthermore the increasing driving resistance even after rest periods, can be seen in the final phases of pile driving.

Characteristic dynamic monitoring records related to the above manual record are shown in Figures 4 and 5. Figure 4 shows Force and Velocity x Impedance plotted on the same time axis whilst Figure 5 shows the Upward Travelling Wave plot.

It should be noted that the key characteristic is to be found at an elapsed time representative of signal response from the pile toe.

$$t = 2L/C \tag{1}$$

t = elapsed time
L = length of pile
C = velocity of the stress wave = $(E/p)^{\frac{1}{2}}$
E = Young's modulus of pile
p = density of pile

The typical change in response shown at t = 2L/C as the pile toe passed from the soft clay to the gravel/cobble founding strata is very marked and was found to correspond with observations of the manually recorded data.

Absolute values obtained by dynamic monitoring were not important since the objective was to confirm that the pile toe had penetrated into the founding strata. It was necessary to provide confirmation of the interpretation made of the recorded data and this was achieved by observing the characteristic changes in dynamically monitored data as the pile entered the founding strata.

CONCLUSIONS ON PILE DRIVING MONITORING

Premature refusal of the piles when the toe of the piles clearly remained in the soft clay led to considerable concern. The situation was further compounded when viewed against the limited penetration that could be achieved in the founding strata. It was therefore of critical importance that the final phases of pile driving were observed very carefully and that

@seismicisolation

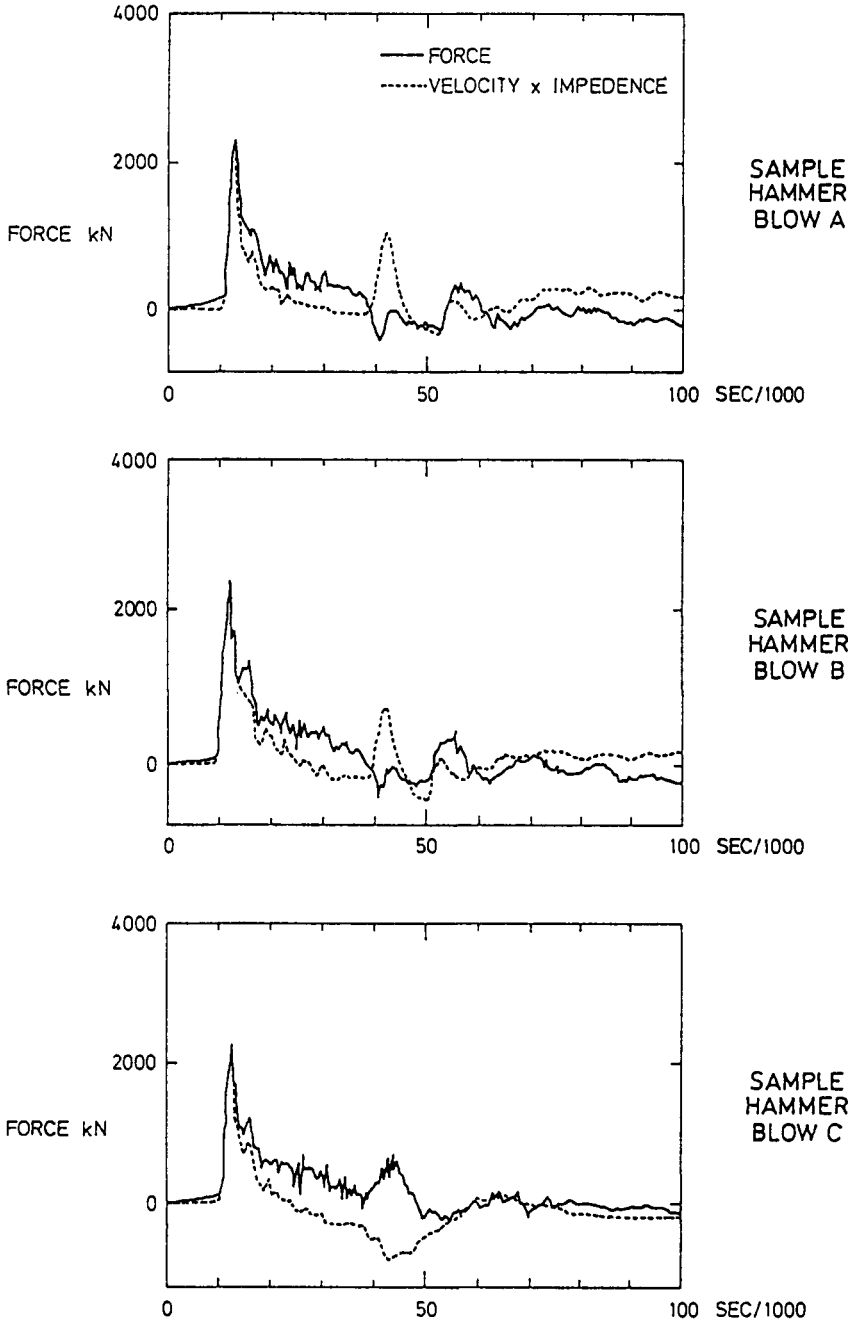

SAMPLE HAMMER BLOWS : TIME VERSUS FORCE AND VELOCITY x IMPEDENCE

@seismicisolation

Figure 4.

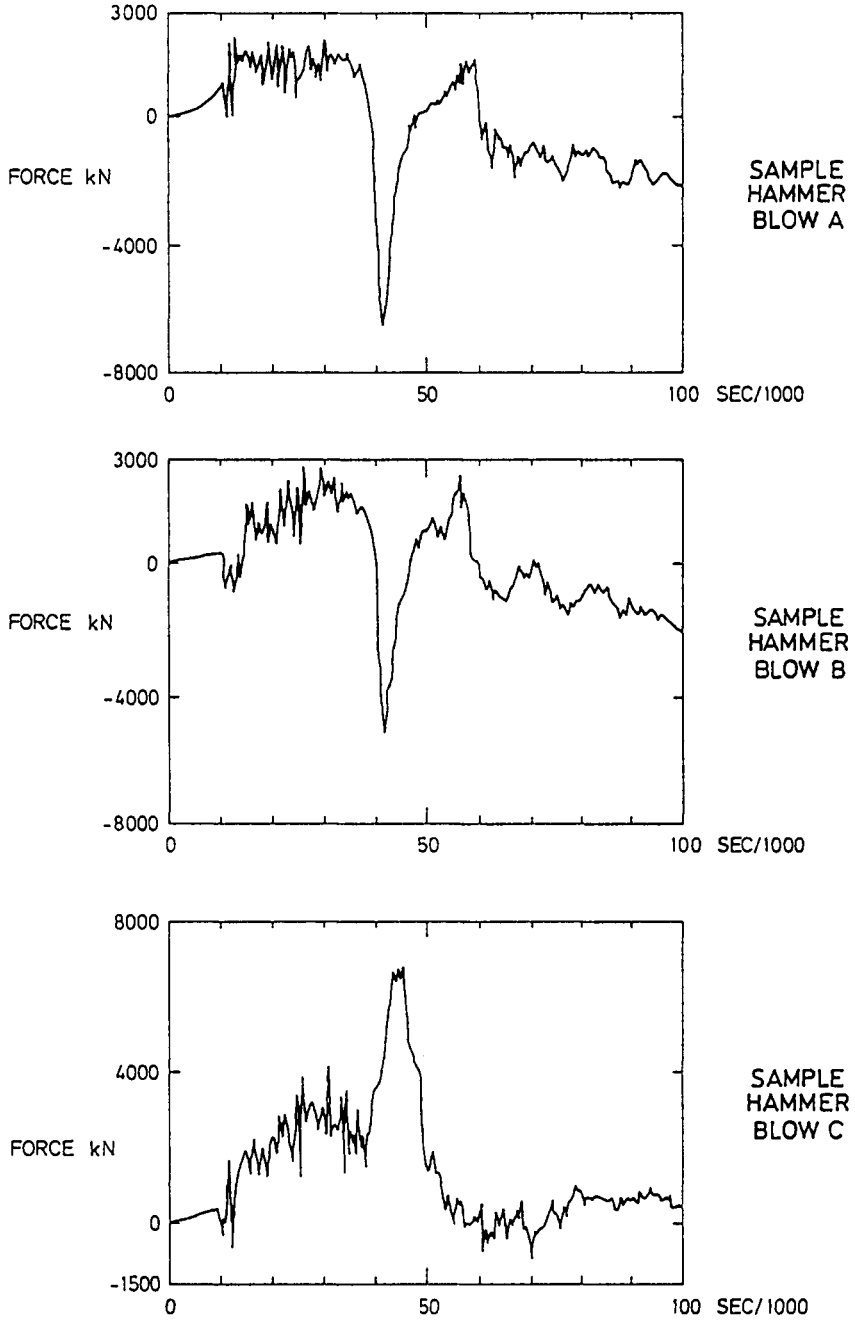

SAMPLE HAMMER BLOWS : TIME VERSUS FORCE
(UPWARD TRAVELLING WAVE)

@seismicisolation

Figure 5.

characteristic response was observed as the piles entered the founding layer. The careful evaluation of both manual and dynamically monitored results enabled the acceptability of pile installation to be judged objectively and with certainty.

Physical load tests performed on four of the piles provided the final confirmation of acceptability. The piles that were load tested performed extremely well giving results that fully complied with pre-set criteria for compliance.

MONITORING OF ANCIENT BUILDINGS DURING PILE DRIVING

The construction site is in the centre of Istanbul with one end of the bridge adjacent to a famous 16th century mosque, the Yeni Camii. Concern had been expressed that the large energies that would be required to drive the piles may have resulted in unacceptably high levels of vibration being set up in the mosque.

Piling was to commence at the closest point to the mosque and during the driving of the first pile accelerations were recorded at locations on the mosque. These were compared with nominally acceptable levels of acceleration and background vibrations generated by the heavy local traffic.

Although the mosque was only 150m from the closest pile the resulting effects on the mosque were deemed of no influence. Frequency of vibrations recorded were around 5Hz with peak accelerations of 1.0cm/sec^2 vertically and 0.5cm/sec^2 horizontally. As a result of these observations indicating that piling induced vibrations were comparable to traffic generated vibrations and recognising that the actual values recorded were in themselves low, piling was allowed to continue with the confidence that damage would not be caused to the mosque by pile driving.

New Galata Bridge, Istanbul, Turkey

Client:	Republic of Turkey General Directorate of Highways 17th Division Directorate
Project Consultant:	Mott MacDonald (Formerly Mott Hay & Anderson) in Association with GAMB
Contractor:	STFA Construction Co/Thyssen Engineering GMBH
Piling Sub-Contractor:	Temel Pile Construction Co
Dynamic Monitoring Advisors:	TNO Institute of Building Materials and Structures The Netherlands

@seismicisolation

EFFECTS OF CONSTRUCTIONAL VIBRATIONS UPON AN URBAN ENVIRONMENT

I.D. ISAAC BSc; CEng; FICE: FGS
Principal Engineer, Mott MacDonald UK Ltd.

ABSTRACT

In an urban environment, the public is conscious of induced vibrations and noise from a number of man made sources such as passing traffic, including overlying aircraft. Occasionally, natural phenomena, such as earthquakes are felt or are the cause of considerable damage.

This paper addresses the man-made effects of vibrations and noise which arise from constructional activities. These principally comprise blasting and piling operations. It identifies some of the prime causes and principal elements and underlines the need for a reliable procedure for determining potential damage criteria relating to rocks and soils, adjoining structures, instrumentation, plant and equipment - particularly where operations are carried out close to the sources of induced vibrations.

These features are highlighted through the presentation of some case histories including where tunnels have been driven immediately below city dwellings and in close proximity to very sensitive structures.

INTRODUCTION

The effects of vibratory motions can be caused by many different sources and such effects need effective and reliable control from their inception to completion in order to avoid and/or limit damage or nuisance. **Figure 1 refers.**

@seismicisolation

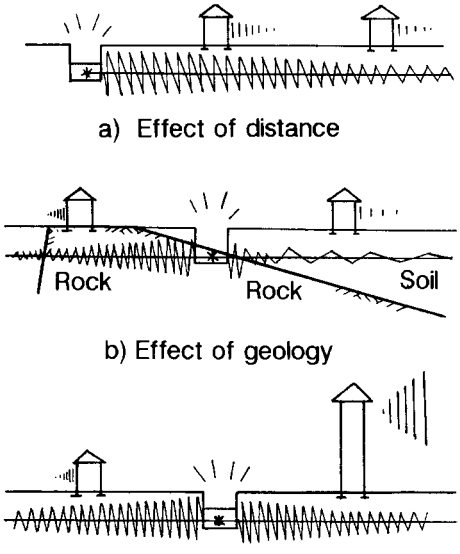

Figure 1. Illustration of the effects of vibratory motions

It is considered essential that industry and communities at large base their awareness of the effects of vibrations on an informed appreciation of potential dangers while recognising the variable problems which may occur within the spectrum of vibratory motions.

This paper addresses the effects from blasting and piling vibrations upon the urban environment and reviews the state of the art with respect to:

GENERAL CHARACTERISTICS

Elements Effecting Vibrations
Vibration Wave Motion
Principal Frequency
Peak Particle Component
Vibration and Damage Criteria

PRINCIPAL CAUSES
Blasting
Piling Operations

Case histories are provided in the penultimate section of the paper to illustrate these principles and a final section discusses some aspects of the law relating to blasting.

GENERAL CHARACTERISTICS

Elements Effecting Vibrations

Blasting and piling operations are, in the main, the cause of greater concern with regard to structural damage and environmental nuisance where such operations effect a wide spectrum of energy release and propogated frequencies.

©seismicisolation

With respect to the effects on personnel, it has been found that complaints from the public in particular, increases as duration of vibration induced activities increase. However it has been recognised also, that in particular situations, early and effective planning and communication with the public has the affect of allaying particular fears and developing improved cooperation with less complaints occurring during operations.

Vibration Control

The potential problems of damage to such areas as buildings, permanent concrete or rock structures, rock support surrounding rock mass etc are constantly recognised. As blasting and piling technology develops, methods become more sophisticated with increasing concern from clients and other interested parties with regard to potential damage due to blasting and piling operations. Therefore nowadays, very tight controls may be effected to either minimise or ensure no damage occurs to any form of structure.

Blasting and piling is best controlled with a performance criterion such as an allowable peak particle velocity at different frequencies rather than a specification of procedures. Unfortunately, such practice usually allows criteria to be specified without an understanding of the difficulties faced by the blaster and piling operators. Therefore, it is also important to be constantly aware and fully acquainted with the blast designs, piling regimes and adopted methods for blasting and piling.

Monitoring

During the initial stages of examining the likely effects of vibrations, the response of structures to blasting or piling cannot be known with any certainty. Figure 1 refers. To determine such response, monitoring and regression trials are necessary to establish the appropriate 'Site Laws' for the different types of induced vibrations which would enable a satisfactory basis to be derived for control and reassurance that vibration limits will not be exceeded.

For control and monitoring of blasting and piling activities, vibrations are normally defined in terms of peak particle velocity (ppv) relative to other parameters such as propogation frequencies, particle displacement (amplitude) and particle acceleration.

By utilising well developed techniques, an economic as well as a safe procedure can be effected to reduce the potential risks of damage.

It is also important to consider the following aspects when determining the basis for monitoring:

- the environment,
- the criteria to be assumed for establishing ground vibration and overpressure parameters,
- the likely effects of blasting and piling at very close distances to all types of structures.
- how these effects are to be monitored and how the results could be used to further design development.

@seismicisolation

- The primary information for deriving a relationship between vibration levels, distance from the blasts and explosive charge weight per delay, propogation frequencies and zones of influence. For piling, the charge weight per delay is usually replaced by pile hammer energy.

Vibration Wave Motion

With vibratory wave motion the three main wave types (compressive, shear and surface) can be divided into two categories, namely:

- body waves which propogate through the body of the rock and soil and/or other form of ground medium.

- surface waves, which are transmitted along a surface (usually the upper ground surface), the most important being the Rayleigh Wave.

Body waves can be further subdivided into compressive(compression/tension) or sound-like waves,and distortional or shear waves. Explosive and piling energies predominately produce body waves at small distances which propagate outward in a spherical manner until they intersect a boundary such as another rock layer, soil, or the ground surface. Figure 1 refers. At this intersection, shear and surface waves are produced and Rayleigh surface waves then become important at larger transmission distances. At shorter distances, all three wave types will arrive together and greatly complicate wave-type identification, whereas at large distances, the more slowly moving shear and surface waves begin to separate from the compressive wave hence allowing them to be clearly identified.

The longitudinal (compressive) wave produces particle motions in the same direction as it is propagating. On the other hand, the shear wave produces motions perpendicular to its direction of propagation, either horizontally, or vertically. The Rayleigh wave (the most complicated) produces motions both in the vertical direction and parallel to its direction of propagation.

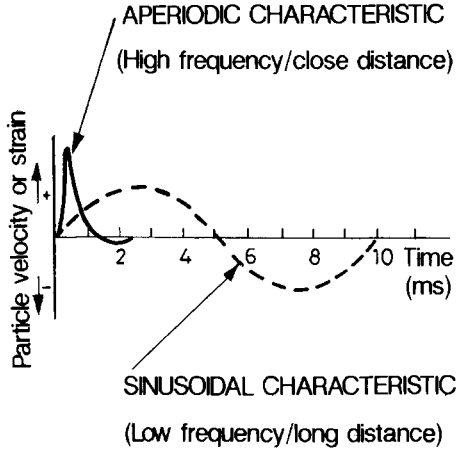

Figure 2. Comparison of wave formations

@seismicisolation

Close explosions usually produce the single spiked pulse, by direct transmission. Figure 2 refers. At longer distances from the source, say > 15 metres, explosions can simulate the relatively sinusoidal pulse through a combination of direct transmission, reflection and and refraction. The close distance blasting produces transient pulses which usually last 1 to 2 milliseconds On the other hand, at relatively large distances, the single sinusoidal type pulses have durations of 10 to 100 milliseconds. Combination of these single pulses mainly produce commonly observed waves which may approximate to sinusoidal characteristics depending upon the rate of attenuation.

Principal Frequency

Principal frequencies are defined as those associated with the greatest particle displacement and usually vary between 0.5 to 250 Hertz. Their magnitude depend upon the transmission medium and certain types of blasting or piling techniques which tend to produce frequencies in a more limited range.

Explosions propogating through low density rock or soil conditions tend to produce vibrations with lower principal frequencies than in ground conditions of higher density such as with hard rock etc. Small distances between a structure and a blast as well as tight joints in rock transmission paths tend to influence higher frequencies which are usually aperiodic (non-sinusoidal).

When relatively high propogation frequencies are exhibited rapid motions usually occur at frequencies higher than the natural frequency of structures and hence tend to minimise the extent of strain imposed on structures. Such high frequency motions are advantageous but certain frequencies could attenuate over shorter distances in soil than in rock.

It is important to ensure there is no superpositioning of wave forms and recognise that shear waves can resonate within a soil or rock at particular frequencies. It is known that at particular distances, principal frequencies range from almost approx 1 to 40Hz when propogating through soil thicknesses greater than 2 to 3m and between 10 to 250Hz in rock.

Peak Particle Component

The passage of blast and piling vibration forces the ground to move in an elliptical manner in three dimensions. To define this elliptical or spherical motion it is necessary to measure the mutually perpendicular components, namely the transverse, longitudinal (radial) and vertical directions. None of these perpendicular components consistently dominate and each component varies with each situation with peaks occurring at different times and at different frequencies.

Vibration and Damage Criteria

The safe quantity of explosives or piling energy which could be used without causing damage to buildings, reinforced concrete structures surrounding rock mass and its support is usually determined by:
(a) predicting the intensity of ground vibration as a function of charge weight per delay or piling energy, distance of the structure etc from the source of detonated charge or piling hammer, transmission characteristics of the rock mass or ground conditions;

@seismicisolation

(b) assessing the level of ground vibrations which could be accommodated by structures, rock mass and support etc without causing damage.

Many controlled studies of damage effects due to blast and piling vibrations indicate that peak particle velocity is the best criterion for assessing levels of vibration damage in media such as rock, reinforced concrete structures, varying ground conditions. Before determining the permissible charge and design of the drilling and blasting patterns or piling techniques the levels of acceptable vibrations should be assessed and discussed between the respective parties involved.

The industry should recognise areas of natural frequency and strain levels which could be accommodated by the rock mass, structural concrete or any other medium and relate also, threshold vibration limits to propogated frequencies and zones of influence.

PRINCIPAL CAUSES

Blasting

It is realised that some degree of damage, however small, will occur at any excavated rock profile. To assess these effects it is also necessary to consider the geotechnical parameters of the rock mass.

The extent of damage to rock depends mainly upon:

- The strain induced in the rock
- The extent of fissures and/or joints existing in the rock mass
- The design of the blast patterns

The effects of vibrations on reinforced concrete structures at close distances depend mainly upon:

(a) Natural frequency of RC structure

(b) Frequencies induced by blasting

(c) Peak particle velocity from blast vibration

(d) Propogation velocity of wave motion through RC structure

(e) Peak particle displacement and acceleration

(f) Density of the RC structure

(g) Modulus of elasticity of the RC structure

(h) Poisson's ratio of the structure

(j) Distance of blast source from structure

(k) Maximum charge weight per delay

(l) Depth of RC structure

@seismicisolation

Figure 3 illustrates some typical relationships between peak particle velocity (ppv) and concrete strengths relating to varying concrete designs.

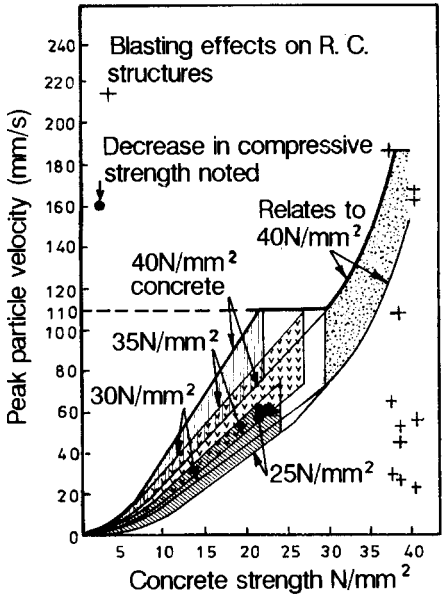

Figure 3. Dinorwig. Typical relationship between ppv and concrete strength for varying concrete design strengths

Air Blast (Noise/Overpressure)

The air blast from an explosion or other vibration energies is a compressional wave in air producing an overpressure which could result in some structural damage. The overpressure is usually monitored on the same basis as ppv using the scaled distance as a co-ordinate with pressure.

An air blast usually contains high energy at frequencies below $20H_z$ which on occasions would damage structures directly, but more commonly, could excite higher frequencies vibrations which are perceived as noise. For direct noise appreciation the pressure is related to decibels, which is normally used as a basis for monitoring and controlling the effects of air blast.

The magnitude of noise/overpressure is sensitive to changes in atmospheric condition and therefore considered that this may affect the perception of blasting by the public. However, the limited explosive charge weights permitted to control the ground vibrations are usually considered sufficient to avoid structural damage as well as annoyance.

Each blast should be monitored at strategic locations and levels of noise checked and controlled to ensure compliance with acceptable practices. For reference, the USBM reports recommend the following limits for air blast to minimise the possibility of both annoyance and structural damage:-

@seismicisolation

Safe level - 128 decibels (dB)
Maximum level - 136 decibels (dB)

Piling

Ground-borne vibrations from piling can be disturbing to neighbouring people and may cause damage to nearby property. There are subjective criteria based on human perception of vibration, and 'rule of thumb' and empirical guidelines on vibration levels which might cause property damage. These criteria are not specific to piling vibrations, are limited in their applicability and difficult for regulating authorities to set practical limits for control of the effects of piling operations.

Potential Damage

An important indirect cause of building damage through piling results from dynamic/vibration-induced ground settlements in granular soils. Structural damage, to a varying extent can result but is most pronounced where shallow foundations overlie loose or medium dense deposits. Dynamic settlement predominantly affects uniform fine sands and silty sands below the groundwater level, and produces movements that are differential in nature. The degree of induced movement will depend on the initial density of the soil, level of vibration and distance from source. Various authors (NAVFAC 1982, Heckman and Hagerty 1978 and D'Appolonia 1971) suggest settlements can be expected for a distance of up to 10 pile diameters and occasionally as much as 10 to 15m distance from driven piles.

Whilst piling operations occur, it is essential that settlement readings are taken and reconciled with the ground vibration readings monitored at particular locations. Should it be considered that ground settlements are directly related to piling vibrations the regression curves should be used to effect suitable control of the piling energies to ensure no damage occurs and identify advantages of using impact or continues high frequency vibration hammers.

Propogation frequencies resulting from vibrations have a significant influence when determining threshold levels for structure foundations and other more sensitive elements such as brickwork, wall panels etc. **Table 1** illustrates the types of threshold limits which have been used successfully for piling through granular ground conditions.

TABLE 1
Typical Threshold Piling Vibrations Limits

Structure Elements	peak particle velocities related to predominant frequencies			
	<3Hz	3<10Hz	10<50Hz	50 <100Hz
Concrete Foundations	6mm/s	6-10mm/s	10-25mm/s	25-40mm/s
Building Fabric (Brickwork/wall panels)	3mm/s	3-5mm/s	5-12mm/s	12-20mm/s

It is important to record the peak particle velocities whilst at the same time determining the minimum frequencies and maximum amplitude/displacement. To establish the appropriate "site-laws" a minimum of four vibrographs should be located at varying distances from the piling locations to establish a suitable range of readings which would enable

@seismicisolation

meaningful regression curves to be established for ppv (mm/s) against scaled distance ie $\frac{(\text{Distance})}{(\text{Energy})^{\frac{1}{2}}} = \frac{(\text{metres})}{(\text{joules}))^{\frac{1}{2}}}$

CASE HISTORIES

To illustrate the various approaches and techniques in applying vibration control within an urban environment some case histories are described briefly as follows;

Edinburgh Castle Tunnel
1989/1990 - Historic Buildings and Monuments

Preliminary studies indicated that a tunnel could be excavated under Edinburgh Castle by utilising drill and blast techniques; the potential problems of nuisance and damage occurring to historical and other structures, including rock slopes and surrounding rock mass, were recognised.

In particular, the presence of the 12th Century St. Margaret's Chapel which has its foundations located at around 17 metres above the crown of the tunnel and the sensitivity of the alarm system surrounding the Honours of Scotland (crown jewels) were of particular concern. It was apparent that very close control would be required during construction over the elements of ground vibrations, noise, airblast and overpessure to ensure there were no structural damage or annoyance to the public.

Blasting Trials

Having appreciated the nature of damage criteria that could be tolerated by the structures it was then necessary to experience and confirm the performance and effect of using particular explosive charges in the sedimentary and basalt rock at the Castle by carrying out blasting trials.

@seismicisolation

Examination of the vibration data showed significant variance between blast characteristics in the different strata of basalt and sedimentaries. In all cases the vibration data used for the regression analysis were the maximum ppv's in any one plane. (Figures 4 and 5 refer)

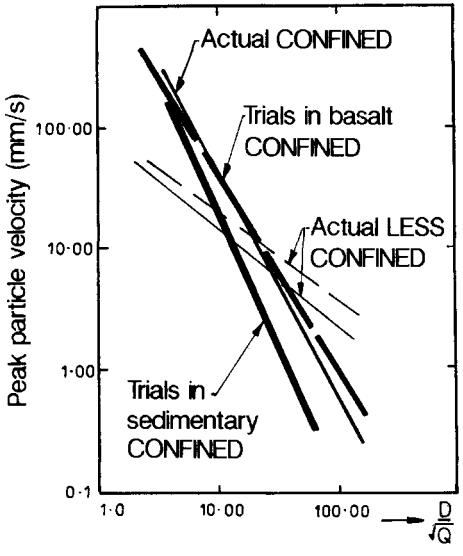

Figure 4. Edinburgh Castle Comparison of Regression Curves for varying rock conditions

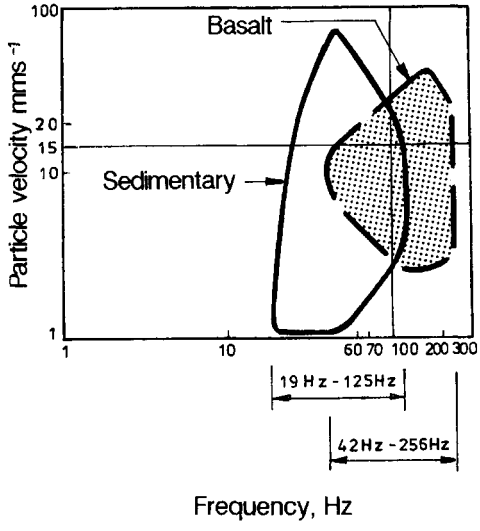

Figure 5. Edinburgh Castle Comparison of envelopes of ppv and frequencies for varying rock conditions

Blast Vibration Criteria

Having acquired the regression curves from the trials, further examination of the related frequencies confirmed the original assumption that much higher frequencies were exhibited through the basalt than through the sedimentary rocks. Studies of the potential damage effects on the historical buildings and other structures revealed the wide spectrum of natural frequencies of buildings in the vicinity.

It was recognised that where propogation frequencies were much higher than the natural frequencies of particular structures then the strain to their foundations would be minimised if those foundations were directly located onto the basalt bed rock. However, when propogating through fill material and/or the sedimentary rock the decay in frequency could result in somewhat larger strains than those experienced in structures founded directly onto rock.

Following examination of these phenomena and recognising the need to ensure that the Contractor had sufficient flexibility to design and control his blasting, it was determined that vibration constraints should be categorised accordingly in terms of ppv and frequencies generated. The categories which were adopted for the specification, are shown in the following table:

@seismicisolation

TABLE 2
Categories of threshold limits relating to Edinburgh Castle

Category	range of frequency	ppv not greater(in any one plane) than	Structure considered
1	all frequencies	15mm/sec	St Margaret's Chapel
2	<50Hz	15mm/sec	within 15m of the source of the blast other than St. Margaret's Chapel
	>50Hz	20mm/sec	
3	<20Hz	15mm/sec	All structures more than 15m from the source of the blast other than St. Margaret's Chapel
	20< f<50Hz	20mm/sec	
	50< f<100Hz	25mm/sec	
	100Hz	30mm/sec	

Monitoring and Control

In recognition of the rock conditions and the severe constraints imposed by the specification in terms of vibration criteria and access, the Contractor adopted three forms of blasting:

Unconfined/surface wave blasting which applied to open cut benching (Charge weights varied between 0.690 and 1.0 kg per delay.)

Confined/body wave blasting which applied to the top heading and full face tunnel drives (limited to 0.690kg per delay).

Less confined blasting which involved the tunnel bench and "shaft" open cut at the portal. (Charge weights were limited to 1.0kg per delay).

The close liaison and relationship between Client, Engineer and Contractor contributed significantly towards the success of the tunnelling while ensuring there were no detrimental affects upon the urban environment.

Dundee Inner Ring Road
1990/1991 - Tayside Regional Council

The project involves the excavation for and construction of the main inner ring road which runs through the centre of the City of Dundee. Ancillary work involves also the construction of shafts and tunnels to accommodate sewerage and water diversions within the city. The periphery of the main excavations are located at very close distances (within 2 metres) to surrounding buildings, structures and their basements.

Blast damage to these surrounding structures was recognised to be a potential problem and therefore it was considered necessary to effect very tight control to minimise the risk of such damage occurring.

@seismicisolation

Blasting Trials

During the initial stages of examining the likely effects of blasting, response of structures to blast vibrations was not known with any certainty. To determine such response blasting trials were effected which comprised 8No 10 metre deep holes within the dolerite, basalt and siltstone with maximum charge weights per delay varying from 0.2kg to 0.6kg of special gelatine 80 explosive with high velocity of detonation.

Blast Vibration Criteria

Examination of the regression curves and vibration data did not show significant differences between those exhibited through the dolerite, basalt and siltstone media. **(Figures 6 and 7 refer)**

The vibration data was obtained, in all cases, from confined shots which provided some degree of conservatism when determining the control parameters during production blasts which were assumed would exhibit lower ppv results due to less restrictive energy release. The confined shots at close distances are considered to resemble the effects from tunnelling within 2 metres from foundations of town and city buildings.

@seismicisolation

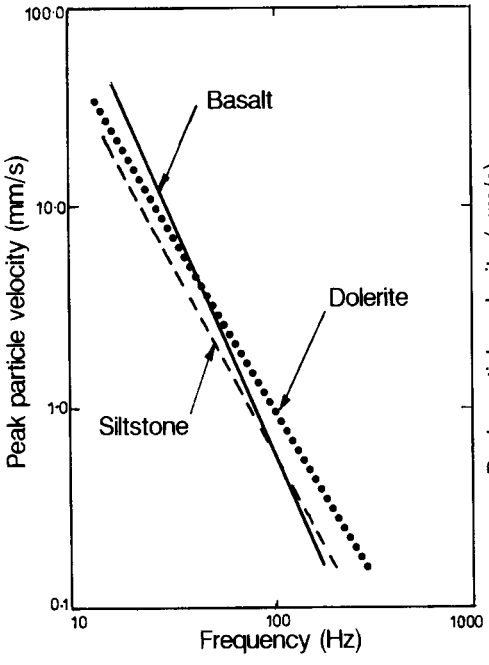

Figure 6. Dundee Inner Ring Road Comparison of Regression Curves for varying rock conditions

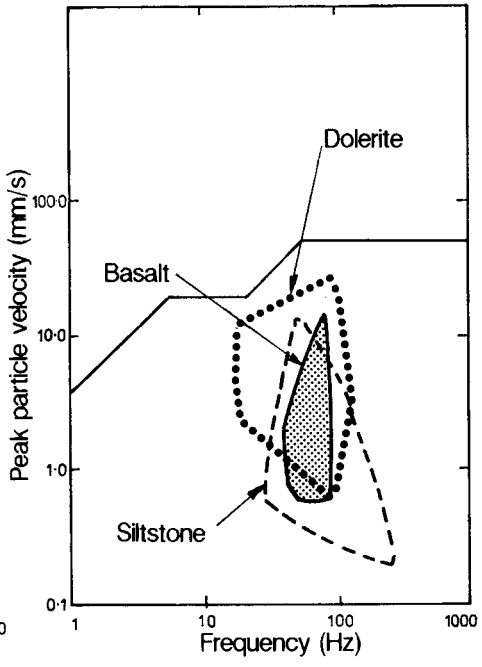

Figure 7. Dundee Inner Ring Road Comparison of envelopes of ppv and frequencies for varying rock conditions

Some concern was also expressed relating to the possible effects of blast induced vibration on computer installation within a major shopping complex adjacent to the main excavations. No main frame computers were identified and it was considered that PC or desk top type computers would be relative insensitive to vibration and therefore not adversely affected by routine blasting operations.

Following examination of these phenomena and recognising the need to ensure sufficient flexibility for design and control, it was determined that vibration constraints should be categorised in accordance with ppv, propogated frequencies and zones of influence as shown in the following table:

@seismicisolation

TABLE 3

Categories of threshold limits relating to Dundee Inner Ring Road

Structures	Category 1 ppv limits on structures within 15m of source of blast (mm/sec)		Category 2 ppv limits on structures more than 15m from source of blast (mm/sec)	
	<50Hz	>50Hz	50<f<100Hz	>100Hz
Supermarket	15	20	20	20
Shop basement	15	20	20	25
Building in very poor condition	15	15	15	20
Building in reasonable condition	15	20	25	30
Base of brick retaining wall	15	20	20	20
Gas, Water, Sewerage, Drainage Services and the like	15	20	20	25
All other structures	15	20	25	30

Dundee Sewer Renewal
1990/1991 - Tayside Regional Council

This project comprised a series of shafts (5m excavated diameter and up to 14 metres deep) and tunnels (1.7m excavated diameter) with major inlet and outlet structures which were excavated by drill and blast methods within the city centre of Dundee. The shafts and tunnels were located as near as 2 metres to major brick and stone masonry retaining walls, foundations of major high rise buildings and to within a zone of 10 metres from 30 metre high multistorey buildings.

@seismicisolation

Blasting Trials

Due to early difficulties with access the basic vibration criteria and threshold limits were established within the Contract by recognising previous experience on projects under similar rock conditions.

During the commencement of the Contract, and in particular during the initial stages of excavating the shafts, cautious blasting trials were undertaken under confined conditions to establish appropriate "Site Laws" for the different rock conditions.

Early blasting comprised a total of 10 initiations which were recorded at six discrete locations providing a total of 60 readings with 6No. RE4 Digital Seismographs. The maximum explosive charge per delay varied from 0.2kg/delay to 0.8kg/delay.

The results enabled a series of regression curves to be established and relationships between ppv and frequencies to be determined to allow the blast criteria to be monitored and controlled. **Figure 8 refers**.

The sewer runs at some depth partly through basalt and partly through sedimentary rocks with steeply dipping bedding planes. Its tunnels and shafts are located very close to old masonry brick and reinforced concrete retaining walls which were also very closely monitored with sophisticated precise surveying techniques.

@seismicisolation

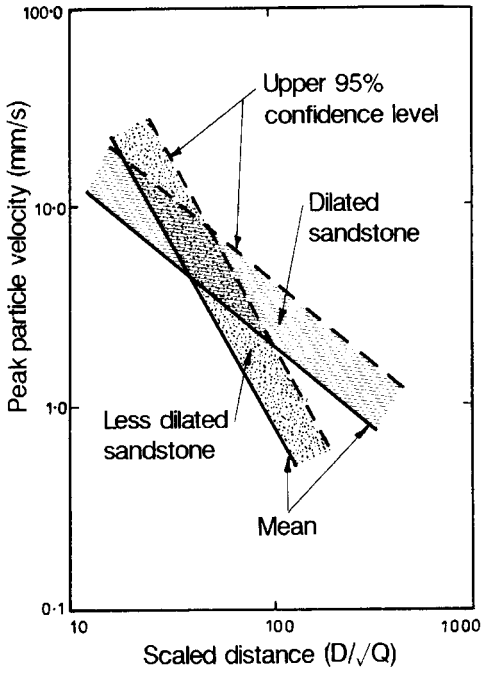

Figure 8. Dundee Sewer Renewal
Comparison of Regression Curves within short distances from blasting sources for varying rock conditions

Blast Vibration Criteria

Due to the sensitivity and closeness of the structures it was decided to limit ppvs to 20mm/sec at all frequencies at locations of all foundations of buildings and retaining walls. This limitation assumed propogation frequencies not less than 50 Hz and was originally based upon the Swiss Association Standards, which are generally perceived as being rather cautious for buildings with masonry walls.
Prior to work commencing, a dilapidation survey of particular adjacent properties were carried out, some of which comprised deep basements at around the same levels as the tunnels. These structures are accessible to the public and in addition to monitoring blast vibrations a programme for further monitoring of movement, crack width propogation and noise levels was implemented to ensure effective control.

Monitoring and Control

During the execution of the works it was necessary to restrict the maximum charge per delay to around 100 grms and in certain cases to 75 grms. This necessitated the need to double deck charges, ensure the explosives had as high a velocity of detonation as possible and provide 44 magnadets at the face of the tunnel drive at any one time to effect and limit such maximum charge weights per delay.

@seismicisolation

Due to the nature of the tunnel drive, small explosive charge weights per delay were adopted and contrary to expectations, there were occasions when

it proved necessary to increase the charge weight per delay from 75 grammes to 100 grammes in order to reduce the ppv. During tunnel driving it was determined that the 75 grammes/delay did not allow sufficient breakage of the rock and therefore, its containment exhibited higher ppv than with a slightly higher charge per delay. An interesting phenomenon.

Vibrations induced by land based piling in UK

During piling adjacent to buildings and structures etc concern is usually expressed relating to the effects of such operations on foundations, freshly placed concrete, construction of brickwork, manholes, structures, steelwork services, electrical and communication elements etc.

Trials

Prior to allowing full production of pile driving it is considered prudent to identify and determine suitable vibration criteria, establish whether potential damage exists and develop a basis for appropriate control.

Trials should be undertaken to establish ground geotechnical parameters the site laws for ground vibrations and their peak values in the three orthogonal axes, time period of operations, peak particle velocities, ground displacements, acceleration and propogation frequencies.

@seismicisolation

Recordings should be carried out using a minimum of three self triggering digital seismographs.

Vibration Criteria

From examination of regression curves from various projects it can be shown that levels of vibration for similar energy levels are greater when using impact piling hammers than with the continuous vibrating high frequency hammers. **Figures 9 and 10 refer.**

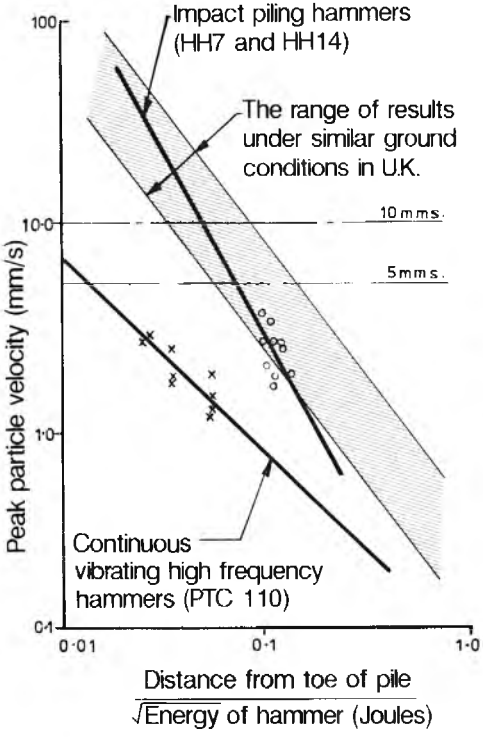

Figure 9. Land based piling Comparison of Regression Curves for different piling hammers in granular material

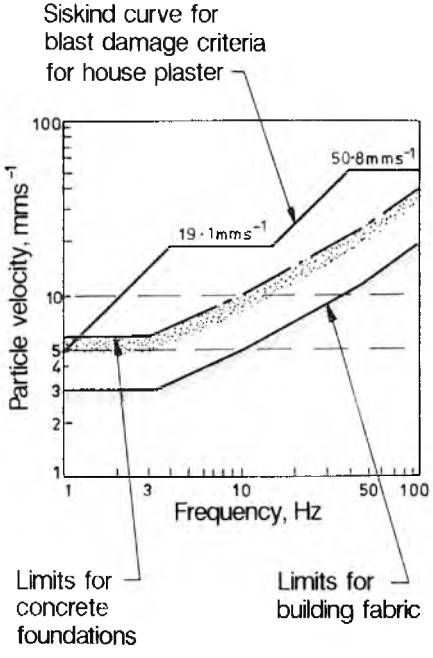

Figure 10. Land based piling Relationships between ppv and piling frequencies for effects on concrete structures and building fabric

The regression curves show that all the readings for piling through granular soil fall within a satisfactory zone and adjustment of energy levels to the piling hammers may be carried out effectively and without too much difficulty.

It was recognised that at very low predominant frequencies there was a risk of damage should ppv be correspondingly high, developing high displacement and hence relatively high strain.

Under these circumstances however, particular trials indicated that relatively low predominant frequencies related also to low ppvs which signified little risk of damage occurring to the buildings and structures provided that vibration energies were contained within the determined threshold ppv limits and propogated frequencies. It was also found

©seismicisolation

necessary to determine the level of energy required to comply with ppv for a particular distance to the toe of the piles based upon the regression curves and in particular, their scaled distances.

Monitoring and Control

Close monitoring should be undertaken to ensure that piling energies are compatible with safe scaled distances.

The critical period for placed concrete at the foundation of buildings and structures is after the concrete has taken its initial set and before it has acquired appreciable strength. It is therefore considered that, in general, piles should not be driven close to newly cast concrete between its age of 4 hours and 24 hours unless very stringent investigation and controls are effected.

On particular projects the permissible criteria for piling near concrete were adopted satisfactorily as follows:-

a ppv of not more than 5mm/s for concrete < 4 hrs old
a ppv of not more than 10mm/s for concrete >24 hrs old <35 hrs old
a ppv of not more than 25mm/s for concrete >35 hrs old

Brickwork should be tied effectively and adequate bond strengths achieved before piling operations and it is suggested that planning of projects should assume that no brickwork, within zones of influence, should be in the course of construction whilst piling operations are being carried out.

It was also accepted that piling induced vibrations affecting brickwork/wall/panels should be avoided unless the mortar bonding of the brickwork was at least:

12 hours old for ppv < 5mm/sec
24 hours old for ppv < 10mm/sec
36 hours old for ppv < 25mm/sec
and the brickwork had been bonded structurally.

All settlement points and vibration readings from a minimum of three vibrographs were also collated and plotted frequently to ensure that the energies generated by the piling operations were within the required threshold levels.

BLASTING AND THE LAW

The laws governing explosives in the urban environment are no different to those in the open countryside situation, except where local byelaws have been enacted, giving the Local Authority additional powers to control or ban the use of explosives.

The principal areas of legislation likely to come under scrutiny are:

- the carriage of explosives
- the storage of explosives
- the control of explosives

@seismicisolation

The actual use of explosives is likely to come under British Standards 5607. 'The Safe Use of explosives in the Construction Industry'.

In most large towns and cities, there are local byelaws which govern the use of explosives and in the main, are usually negative in that they ban the use of explosives without a permit. Such bans may come from one or more of a number of departments or even the local police. It is not unusual for a permit to be granted on the limited condition that explosives are used in safe manner and according to the manufacturer's instructions. In towns, where explosives are to be regularly used, it is likely that a City Council's Engineering Department, and often a Consultant, will be involved and a set of rules and thershold limits governing noise and ground vibration will be specified. Often, the Environmental Health Department are also likely to be involved, particularly on noise, dust and vibration.

Litigation to prevent or stop blasting taking place is reasonably common and lawyers make a tidy sum each year writing threatening letters with dire consequencies.

The main complaint obviously is from ground vibration and its potential effect on property. Happily, references show that the difference in magnitude between complaint level and damage level is at least 10 times and whilst much concern is usually expressed, the matter rarely lands up in court. Generally, if noise levels are reduced vibration concerns tend to disappear.

In cases where 'fly' occurs, then the offending party is liable to prosecution and occasionally, there will be litigation to settle damage for injury or loss.

Due to the proximity of blasting to the public and considering the potential dangers it is likely that the Health and Safety Executive will take a very close interest. Often, it is a requirement of a contract that they approve or comment on a method statement and local police may become involved because of road closures and restrictions on the public during the period of blasting.

ACKNOWLEDGEMENTS

The Author wishes to acknowledge the assistance and support received from all his colleagues during preparation of this paper and, in particular, wishes to acknowledge the following for their kind permission to publish particular aspects relating to projects used in the case histories section.

1) The Historic Buildings and Monuments, Scotland who were the client for the Edinburgh Castle Tunnel Project.

2) The Tayside Regional Council, Roads and New Works Department, who are the client for the Dundee Inner Ring Road Project.

3) The Tayside Regional Council, Water Services Department, who are the Client for the Dundee Sewer Renewal Project.

4) C.I.R.I.A. working party which relates to ground-borne vibrations arising from piling.

5) Rock Environmental Ltd who have provided assistance and instruments, particularly during monitoring of trials of vibration.

@seismicisolation

6) Rocklift Co. Ltd (Glasgow) for their support and assistance during various blasting trials within urban environs and advice relating to particular issues within this paper.

7) Lilley Construction Co. Ltd for information relating to particular piling events within an urban environment.

REFERENCES

1. DOUGLAS T.H., KEEBLE S. "Design and Construction of a New Service Tunnel at Edinburgh Castle"

2. ISAAC I.D. "Soft Blasting the Way to Fortress Rock at Edinburgh Castle" - Tunnels and Tunnelling January 1990.

3. ISAAC I.D. BUBB C., - Study of Blast Vibration, Tunnels and Tunnelling 1981 (July and September issues)

4. "CIRIA" Report Draft D on "Ground borne vibrations arising from piling"

5. Rock Environmental Ltd "Field records and range of results of piling vibrations"

6. TRRL Report No.53 - "Ground Vibration caused by Civil Engineering Works"

7. ISAAC I.D., WU E., - "Design and Construction of Dens Brae Sewer Renewal Project"- Tunnelling in Tayside Conference, March 1991.

8. Construction Safety Newsletter (January 1977) "Effects of Impact - Driven piles on nearby Structures"

9. CIRIA Report Pg 9 October 1990 "Noise and Vibration from Piling Operations"

10. DOWDING C., "Blast Vibrations, Monitoring and Control"

11. NEW BM.1990 "Ground Vibration caused by Construction Works".

@seismicisolation

NON-MONOTONICAL DECAY OF GROUND SURFACE VIBRATIONS CAUSED BY PILE DRIVING

P.B. ATTEWELL, A.R. SELBY and A. UROMEIHY

School of Engineering and Applied Science
University of Durham
England

ABSTRACT

Driving of piles by impact hammer or vibrodriver causes ground surface vibrations which generally attenuate with distance from the pile because of geometrical divergence and to a lesser extent soil material damping. A large body of records has been taken on many sites in the UK using a multichannel digital recorder which allows simultaneous recording at different standoff distances, usually in the 2m to 20m range. On a significant number of occasions the vibrations have shown a maximum amplitude at some 10m from the pile, usually when a long bearing pile was being driven at large toe depth. One effect of this 'anomalous' amplitude/distance phenomenon is to render inapplicable any scaled distance law of a form sometimes used for initial vibration estimation purposes by construction site staff in order to ensure conformance with any consent to work agreement entered into with a local authority under Section 61 of the Control of Pollution Act 1974.

The probable cause of this peak is identified as the overlap of surface waves caused by pile movement at surface level with waves emanating from the pile toe. This explanation has been validated by detailed time increment analysis of a number of vibration records in terms of estimated arrival times of direct surface waves and of waves from the toe. These estimates of arrival times require knowledge of wave velocities in the ground; a 'P' wave velocity can be derived by perusal of the

@seismicisolation

simultaneously recorded vertical and horizontal radial components of ground vibrations, given a multiaxis recording facility.

Other causes of non-uniform attenuation are identified: sheet pile panels and ground surface profiles. Severe anomalies have been observed in cases of steep banks of loose or uncompacted soil material.

Finally, and notwithstanding these anomalies, it is demonstrated that reasonable best estimate vibrations caused by impact hammers can be made using an equation published several years ago. Estimates of vibrations caused by vibrodrivers should be based on a newly proposed equation.

INTRODUCTION

When attempting to specify ground vibration transmission from driven piling it is usually found convenient to refer to the mechanics outlined in 1973 by Attewell and Farmer [1]. Two sources of energy transfer were proposed (see Figure 1): the pile toe, from which a quasi-spherical wavefront emanates, and the pile shaft from which the wavefront projected into the soil as a result of shaft friction is of quasi-cylindrical form. There is further discussion in Attewell [2] on the operational energy distribution during the driving process, but reference is substantially to source mechanisms within the body of the soil through which the vibration is transmitted. No explicit consideration is given to the different vibration propagation environments associated with the several types of piles (for example, sheet piles and H-section end-bearing piles) nor to the possibility of eccentric impacts on the head of a pile, which leads to the direct initiation of surface waves.

An underlying assumption is that the imposed vibration is most intense in the soil at the steel-soil interface and thereafter decays monotonically with transmission distance from source. Two controls on diminishing amplitude, albeit conceptually over-simple, have been well recognised:

(a) Spherical and cylindrical divergence of wavefronts, whereby in the former case the vibration amplitude of the wave decreases directly in proportion to the distance from the source and in the latter case the amplitude decreases in proportion to the square root of the distance from the source.

@seismicisolation

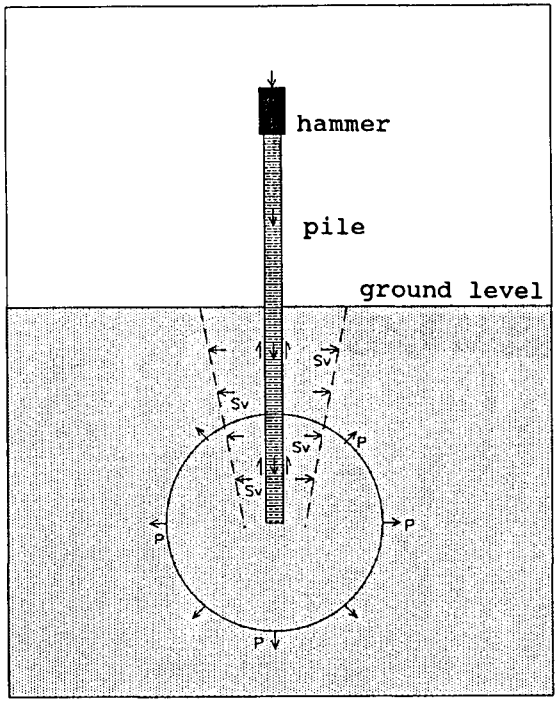

Figure 1. **Wave fronts emanating from pile shaft and toe.**

(b) Friction in the soil during wave passage, which causes the amplitude of the disturbance to reduce in some negative exponential manner as a function of distance travelled.

Transducers monitor vibration at or near to ground surface, and most of the foundations of buildings prone to the effects of vibration are often shallow. Quasi-cylindrical waves associated with shaft friction originate at the pile shaft/soil interface and diverge along and beneath the surface of the half-space. They would be expected to produce, in theory at least, transient disturbances of vertical shear (SV) form which reduce in amplitude as noted in (a) above. Definition of spherical waves from the toe of the pile implies refraction of the waves at ground surface during divergence and thereby a decrease in amplitude of these waves approximately proportional to the distance from the pile toe.

@seismicisolation

It is not difficult to show that the dominant control on wave attenuation (decrease in vibration amplitude) is divergence, of the forms noted above, rather than the negative exponential style of reduction imposed by soil friction mechanisms. The distances of practical concern in these civil engineering sources of wave transmission ensure the dominance of geometry over friction.

Identification of discrete sources of vibration from a driven pile is simply an analytical convenience. Wave 'forms' interact and merge at and in the vicinity of the pile-source interface and continue to interact during transmissions, reflections and refractions through stratifications (having different acoustic impedances), voids, water tables, and the free ground surface. For this reason, estimates of ground vibration likely to be created by different piles and piling plant are best achieved on the basis of precedent and empiricism. Field measurements and laws based on those measurements, from which future estimates can be made, are therefore one of the pre-requisites in the design of piling systems in urban areas, in the formulation of consent to work agreements under Section 61 of the Control of Pollution Act 1974 [3], and in the apportionment of responsibility for any disruption that might be attributed to those operations.

VIBRATION MEASUREMENT

Measurements are usually, but not invariably, made at ground surface using velocity transducers or accelerometers which replicate (or are assumed to replicate) the ground motions. In order to resolve the styles of those motions*, three transducers are usually arranged in a right angle configuration at each of several locations set out in a line along ground surface from the vibration source. Placements, digital recording techniques, signal processing systems and new methods of data presentation used by the writers have been reported in several publications [4,5,6].

GROUND MOTION AS A FUNCTION OF TRANSMISSION DISTANCE

An initial and simple assumption, based on the concepts of wavefront divergence, is that the vibration amplitude decreases with distance (r) in a manner that is proportional to r^n, where n lies between 0.5 and 1. Vibration estimation equations of the type suggested by Attewell and Farmer [1], and reviewed at Durham University in the light

* The full character of the motion, normal displacements and rotations, requires analysis of the motions from two orthogonal transducer sets in close proximity and at the same radial horizontal distance from source.

@seismicisolation

of more recent work, also assume that the fall-off in vibration amplitude from source to receiver will be smooth. Yet evidence from numerous episodes of piling on different sites shows this not to be the case. Frequently there is an initial rise in vibration amplitude fairly close to the driven pile, to be followed by a smooth reduction in amplitude further away. Figure 2 is such an example. One simple explanation for this form of amplitude-distance curve depends on considerations of the components of vibration transmitted from the pile shaft and toe as they arrive at different points along the ground surface transmission path.

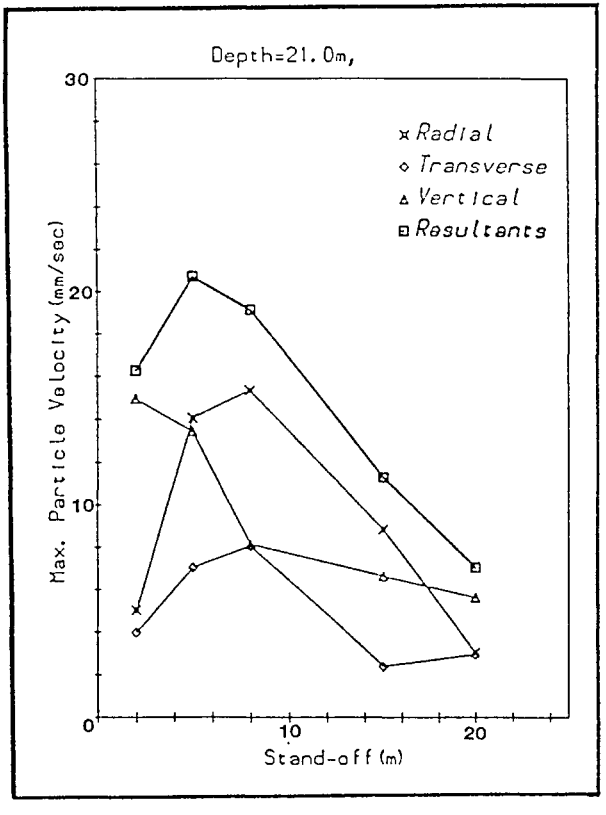

Figure 2. Non-uniform vibration attenuation.

A pre-requisite for an understanding of a vibration attenuation curve is knowledge of the relevant wave velocities in the pile (c_p) and in the ground (c_g). The one-dimensional transmission velocity in the former may be set at 5000m/s. Adopting a multi-station linear array of ground surface vibration transducers, and on the same time

@seismicisolation

base stacking the outputs from transducers sensing surface motions of the same (vertical, radial or transverse) mode, wave velocities in the ground can readily be deduced from the staggered arrival times at each transducer point. Examples of traces which provide this facility, being output on site by the digital data acquisition, processing and recording facility, are shown in Figure 3. Taking, for convenience, two adjacent recording points, distance r_n and r_{n-1}, where n can (theoretically) vary from zero to infinity, from the pile, the wave velocity in the ground can be expressed as

$$c_g = (r_n - r_{n-1})/(t_n - t_{n-1})$$

where r is the radial distance from the pile toe to the respective transducers and t is the equivalent arrival time of the vibration.

The radial distance r is a function of the position of a vibration source along the pile shaft. Writing h for the buried depth along the pile shaft and x for ground surface (assumed horizontal) distance to the particular transducer point, then

$$r = (x^2 + d^2)^{0.5}.$$

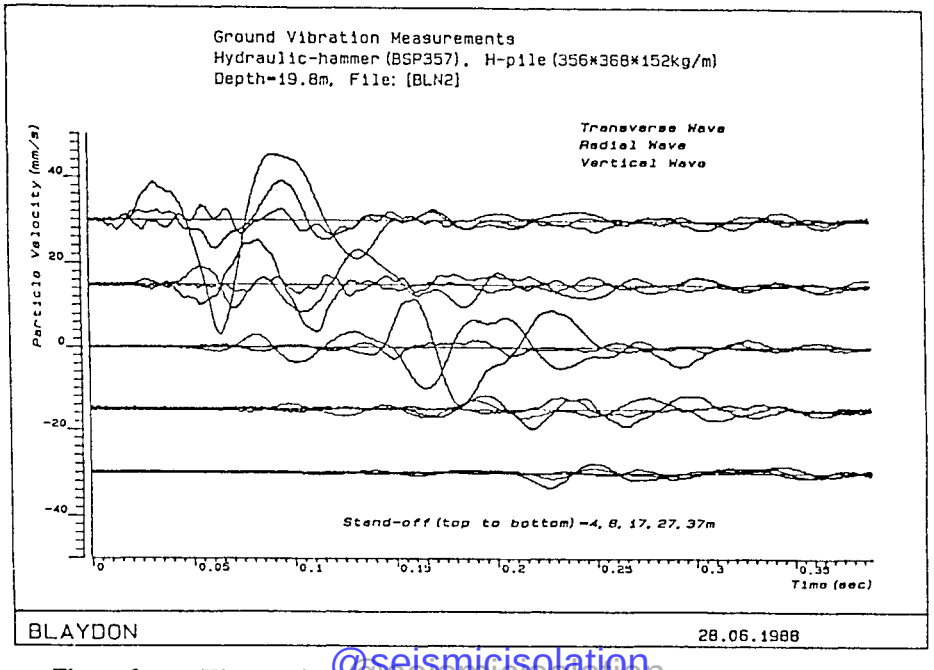

Figure 3. **Wave arrivals at measurement stations.**

@seismicisolation

For a P-type wave transmitted with an assumed spherically expanding wavefront for the pile toe,

$$r_{(t)} = (x_n^2 + d_{(t)}^2)^{0.5}.$$

For an SV-type wave generated at and advancing from the head,

$$r_{(h)} = x_n.$$

The SV wave, initiated by friction at the pile-soil interface, advances as a surface wave from the head of the pile at a speed, c_s, which is approximately half that of the body wave, c_p, from the toe of the pile.

Now consider the arrival times of the disturbances associated with the pile toe body wave front and the surface wave front. Time $t = 0$ is when the hammer strikes the head of the pile and initiates c_s. The body wave arrival time from the pile toe is

$$t_{(n)p} = (r/c_p) + (h/5000),$$

where t, r, h and c_p are in units of seconds, metres, metres and metres per second, respectively, since 5000m/s is entered directly for the wave velocity in the steel pile. The surface wave arrival time from the head of the pile is simply

$$t_{(n)h} = x_{(n)}/c_s.$$

The point on the ground surface where the amplitudes of these two significant wave types coincide masks the attenuation of the constitutive wave amplitudes by introducing an apparent increase in vibration amplitude at small stand-off distances from the pile.

EXAMPLES

A few plots of vibration attenuation recordings are used to illustrate the wave interaction effects discussed above.

(a) A 25m long steel H-pile was driven by a 5000kg hydraulic hammer at a site in Blaydon, Tyne and Wear. Vibration amplitude traces as a function of time (5 line locations, 3 orthogonal recording modes per location, providing 15 time-base traces)

@seismicisolation

are shown in Figure 3. There was evidence of incremental increases in radial mode vibration amplitude as the distance x from the pile increased, to be followed by amplitude decrease at greater distances. The form of this vibration curve is shown in Figure 2.

A P-wave velocity, c_p, was calculated from vibration records at standoff distances x of 4m and 37m, equivalent to radial transmission distances of 20m and 42m for the particular depth of penetration. It was found that

$$c_p = (42 - 20)/(0.225 - 0.06) = 134\text{m/s}$$

and

$$c_s = 67\text{m/s}.$$

The times of the vibration arrivals at the transducer location, 17m from the pile, were

$$t_{(17)p} = (26.2/134) + (20/5000) = 0.199\text{s}$$

and

$$t_{(17)s} = 17/67 = 0.25\text{s}.$$

A similar procedure was followed for calculation of arrival times of the vibration fronts at the several transducer stations. The results are shown in Table 1 which also includes other relevant information about the site, pile and hammer.

From the wave arrival time information plotted in Figure 4 it can be seen that there is quite reasonable agreement between coincidence of the two travel time lines at a standoff distance x of 12m and the recorded peaking of the radial vibration peak particle velocity at a distance x of about 10m.

@seismicisolation

Table 1. Calculation of wave arrival times, Blaydon, Tyne and Wear, Record 28/06/88.

Pile

Type	Size	Depth
H-Section	356 x 368 x 152kg/m	20.0m

Hammer

Weight	Type and Model	Drop-Height
5000kg	Hydraulic BSP 357	800mm

Vibration Recording

Geophone Set	Distance Horizontal (x) m	Distance Radial (r) m	Arrival Time* $t_s=x/c_s$ s	Arrival Time* $t_p=r/c_p$ s	Radial Vibration mm/s
A	4.0	20.39	0.060	0.156	9.36
B	8.0	21.54	0.119	0.165	11.15
C	17.0	26.25	0.254	0.199	14.48
D	27.0	33.60	0.403	0.255	4.69
E	37.0	42.06	0.552	0.318	3.49

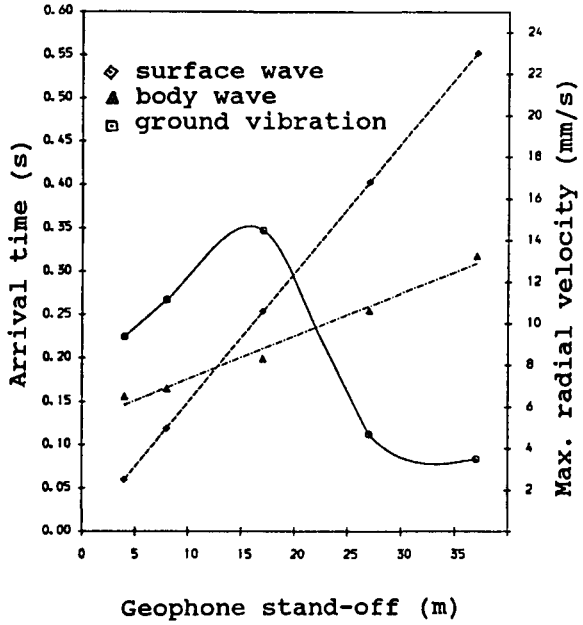

Figure 4. Overlap of surface and body waves, Blaydon.

@seismicisolation

* A time of 0.004s been added to the t_p figures to accommodate the wave travel time down the pile from head to toe.

(b) Measurements of ground vibration were taken at a site in Keighley, Yorkshire during the driving of a 32m long H-pile by 3 tonne hydraulic hammer. Particle velocities in three orthogonal modes were, as above, measured at five positions on the ground surface along a line from the pile. Figure 5 shows the form of the radial mode velocity amplitude versus transmission distance curve, this time with a peak amplitude at a standoff distance of about 10m. From information in Table 2 and the additional plots in Uromeihy [7] but not reproduced here, approximate wave velocities of 422m/s and 211m/s can be assigned to the body wave c_p and the surface wave c_s, respectively. The prediction, through convergence of the two wave types, of an amplitude boost at a standoff distance x of 12m is a reasonable approximation to the distance at which the ground surface actually received maximum vibration.

Table 2. Calculation of wave arrival times, Keighley, Yorkshire., Record 02/03/87

Pile

Type	Size	Depth
H-Section	305 x 305 x 126kg/m	20.0m

Hammer

Weight	Type and Model	Drop-Weight
3000kg	Hydraulic BSP 357	800mm

Vibration Recording

Geophone Set	Distance Horizontal (x) m	Distance Radial (r) m	Arrival Time* $t_s=x/c_s$ s	Arrival Time* $t_p=r/c_p$ s	Radial Vibration mm/s
A	4.0	20.39	0.019	0.055	10.35
B	7.0	21.19	0.033	0.057	10.51
C	10.0	22.36	0.047	0.059	10.95
D	15.0	25.00	0.071	0.066	9.92
E	20.0	28.28	0.095	0.073	8.99

* A time of 0.004s been added to the t_p figures to accommodate the wave travel time down the pile from head to toe.

@seismicisolation

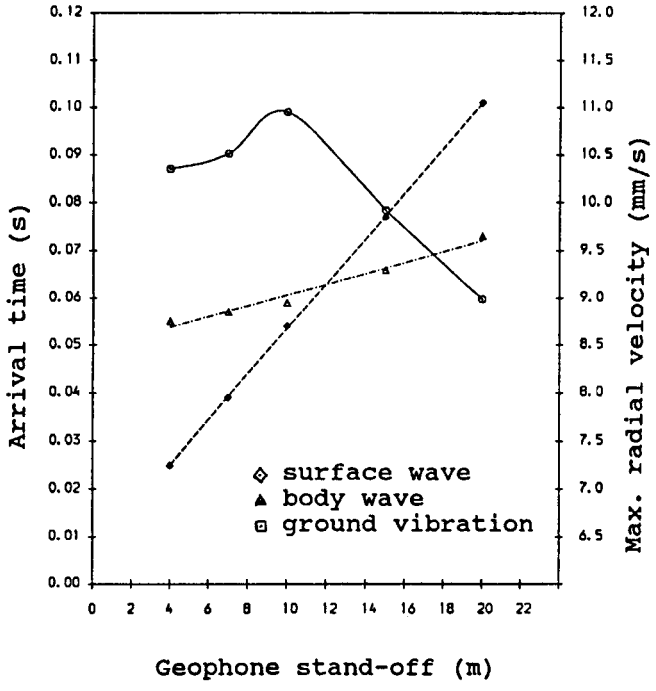

Figure 5. **Overlap of surface and body waves, Keighley.**

(c) The final example of pile driving records to be presented here, this time from a site at St. Annes on the Lancashire coast, concerns the driving of 15m long sheet piles using a BSP 357 seven tonne hydraulic hammer. Figure 6 shows the velocity amplitude-transmission distance curve to have a peak at a distance of about 8m. From information in Table 3 and the plots in Figure 6, approximate wave velocities are 120m/s for c_p and 60m/s for c_s. The point of intersection of the two wave velocity plots suggests a ground vibration velocity enhancement at a distance of 7m, which is a reasonable approximation to the 8m standoff distance at which the peak was recorded.

@seismicisolation

Table 3. Calculation of wave velocity arrival times, St. Annes, Lancashire, Record 01/12/87.

Pile

Type	Size	Depth
Sheet-Pile	Larssen (32W)	10.65m

Hammer

Weight	Type and Model	Drop-Height
7000kg	Hydraulic BSP 357	800mm

Vibration Recording

Geophone Set	Distance Horizontal (x) m	Distance Radial (r) m	Arrival Time* $t_s=x/c_s$ s	Arrival Time* $t_p=r/c_p$ s	Radial Vibration mm/s
A	2.0	10.84	0.034	0.092	21.78
B	5.0	11.76	0.083	0.100	16.44
C	8.0	13.32	0.134	0.113	22.21
D	12.0	16.04	0.200	0.136	10.01
E	18.0	20.91	0.300	0.176	5.12

Each piling operation from which measurements of consequential ground vibration are taken needs to be assessed for its possible contribution to anomalous vibration transmission behaviour. Eccentric impact on the head of the pile causes accentuation of radial mode vibration at ground surface along the line of the pile's horizontal motion. If the transducer array line is set out normal to this latter horizontal motion there is then an accentuation of measured transverse vibration in the ground in response to the horizontal shear (SH) at source. Such recorded behaviour is particularly associated with more flexurally compliant sheet piles. In the case of a (relatively) flexurally stiff H-section bearing pile undergoing eccentric impact, modal vibration is dominantly a function of ground stiffness in compression and shear. Flexurally more responsive sheet piles tend more readily to control the rate at which the ground vibrates.

* A time of 0.002s has been added to the figures to accommodate the wave travel time down the pile from head to toe.

@seismicisolation

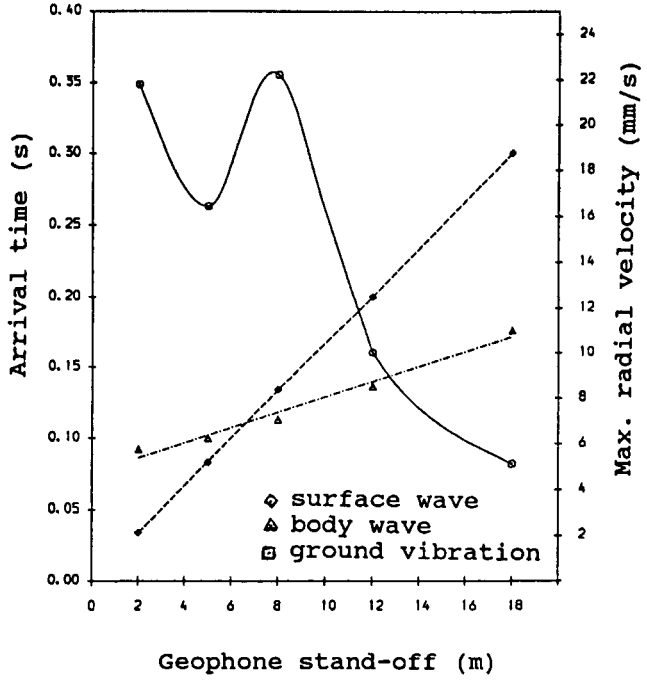

Figure 6. **Overlap of surface and body waves, St Annes.**

ANOMALIES DUE TO GROUND TOPOGRAPHY

Two cases of anomalous vibration attenuation have been observed on several occasions. These are attributed either to the geometry of the ground with respect to the piling operation or to instability of loose soil on a steep bank.

(i) A case of piling in front of an existing quay wall

A common example of sheet piling, associated with urban renewal and redevelopment of river side areas, is the driving of a line of piles in front of a deteriorating old quay wall. The space between the new and old walls is then backfilled. Vibration measurements taken on top of the existing quay wall in response to the sheet piling show the strong influence of the construction geometry. Vibration amplitudes closest to the quay wall are quite small, with a maximum value occurring about 7m back from the wall before recorded attenuation develops with increasing distance therefrom (see Table 4). This 'anomaly' arises because the divergent vibration waves do not

@seismicisolation

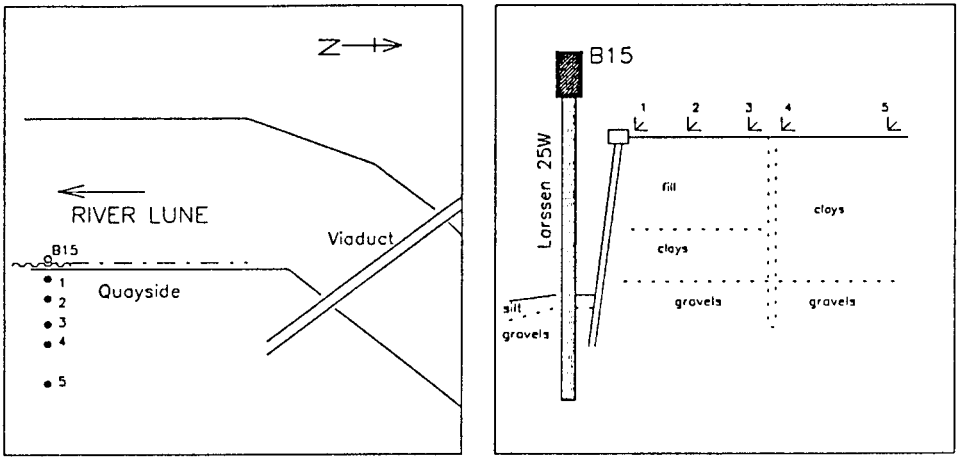

Figure 7. Quayside piling, Lancaster.

experience a clear, straight path to the quay head, a situation which is modelled in Figure 7. The position of the pile toe is an obviously important control on the transmission mechanics.

Table 4. Vibration levels, quayside, River Lune, Lancaster

Station	1	2	3	4	5
Horizontal Distance x (m)	2	3	5.5	7	11
Resultant peak ppv (mm/s)	5.5	6.3	9.4	13.9	3.5

(ii) Slope surface instability

Anomalous vibrations have also been recorded from transducers fixed into relatively loose soil on slopes that could be shown to be close to critical equilibrium. Such vibrations were particularly noticeable at a site in Sheffield where a diesel hammer was driving steel H-piles on either side of the River Don. On the south bank of the river the geophones were fixed into well-compacted, near-horizontal ground, the vibrations maximising at values of some 20mm/s close to the pile and with the radial and vertical components contributing dominantly to the resultant values. On the other (north) bank, however, the first set of transducers was fixed into relatively loose soil on a

@seismicisolation

crossfall of the steep river bank and they recorded uncharacteristically high transverse component peak particle velocities of up to 45mm/s (see Table 5). A similar effect was observed for the radial component of the second set of transducers.

Table 5. Extracts from ground vibration measurements, River Don site, Sheffield, Records 25/10/88 and 23/02/89.

Pile

Type	Dimensions	Length
H-Section	305 x 305 x 79kg/m	15m (N) 12m (S)

Hammer

Blow Rate	Model	Energy/Blow
80-100bl/min	Diesel Hammer (B15/7)	37.2kJ

Peak Particle Velocity Measurements (mm/s) North Bank

Depth (m)	Standoff Mode	2.0m	4.0m	6.0m	8.0m	10.0m
4.0	Radial	24.43	46.45	5.94	13.23	3.80
	Transverse	45.36	11.26	4.57	8.55	0.98
	Vertical	15.98	14.10	3.23	13.30	1.59
	Resultant	59.72	46.66	8.06	17.92	3.83

Peak Particle Velocity Measurements (mm/s) South Bank

Depth (m)	Standoff Mode	2.0m	5.0m	7.0m	13.0m	15.0m
5.0	Radial	16.69	6.85	4.61	0.81	1.53
	Transverse	11.97	3.24	2.66	0.65	0.84
	Vertical	17.69	3.41	2.13	1.18	1.86
	Resultant	22.76	6.94	5.21	1.41	2.15

@seismicisolation

Although vertical accelerations do not affect a statically-determined factor of safety against surface shear failure of a scree slide, transverse acceleration can cause transient instability which promotes downslope movements. Appendix 1 contains an analysis of this situation.

DISCUSSION

In a current UK legislative setting, vibration is a form of noise, which in turn is a type of pollution [3]. There are currently no official guidelines expressing tolerable ground vibration levels with respect to structural damage and other disruptive effects, although a revision of BS 5228 Part 4 [8] is addressing this deficiency with respect to driven piling. Notwithstanding the problems inherent in offering 'blanket guidance' for structurally diverse building with respect to ground motions in the soil, the requirement is for case history data which will generate a simple rule or rules that relate the likelihood of damage arising from pile driving to the distance from a pile driving source and the energy put into the ground at source.

It seems clear from the earlier examples that simple attenuation relations, as proposed by Attewell and Farmer [1], may not suitably describe input energy/distance/vibration velocity relations at standoff distances less than about 10 metres. For distances greater than about 10m, major measurement programmes throughout Britain, together with substantial data processing, have produced an equation for vibration estimation from impact hammers:

$$v = 1.33(W^{0.5}/x)^{0.73}$$

where v is the ground vibration velocity in units of millimetres per second, W is the nominal pile driver energy in units of joules (Newton.metres), and x is the radial standoff distance from the pile in units of metres. This equation is substantially the same as would be generated by the original Attewell and Farmer impact data alone, the non-impact data (eg vibroflotation vibration measurements) being removed from the consideration.

In the case of vibration from vibrodrivers, the relevant equation is

$$v = 1.18(W^{0.5}/x)^{0.98}$$

@seismicisolation

with the same units as above. In this case W is taken as the energy per cycle and is calculated as power divided by frequency.

These equations do not discriminate between the type of soil nor the type of pile being driven. Empirical equations which permit a more refined estimate of vibration levels by accommodating this additional information have been formulated by the authors and are currently under consideration by the BS 5228 Part 4 drafting committee.

CONCLUSIONS

Vibration amplitude at ground surface resulting from pile driving does not decay progressively as distance from the pile increases. Up to distances of about 10m there can be an increase in amplitude caused by superposition of pile toe body wave and pile head surface wave dynamic energy. An empirical equation for driven piling, published by Attewell and Farmer in 1973 [1] and recently re-validated via extensive case history studies throughout Britain, is therefore best applied to standoff distances greater than about 10m from the driven pile. This same recommendation is applied to the use of a new empirical equation for estimating ground vibration from vibrodrivers. When engaged on a measurement programme and appraisal of the results from that programme it is important to take due account of the site conditions. Both piling geometry and ground topography can influence recorded amplitudes of transient vibration.

REFERENCES

1. Attewell, P.B. and Farmer, I.W., Attenuation of ground vibrations from driven piling, Ground Engineering, 1973, **6**(4), 26-29.

2. Attewell, P.B., Estimation of ground vibration caused by driven piling in soil. In Contributions on the Influence of Earthwork Construction on Structures (Proc. XII Conf. on Soil Mech. and Found. Engrg, Aug. 11-16, 1985, San Francisco, Calif.), eds D. Resendiz and M.P. Romo, 1-11.

3. Control of Pollution Act 1974 Chapter 40, HMSO, London, 136p.

4. Selby, A.R. and Swift, J.S., Recording and processing ground vibrations caused by pile driving, Proc. Int. Conf. "Signals and Systems", Brighton, UK, July 12-14,

@seismicisolation

1989, AMSE Press (Association for the Advancement of Modelling and Simulation Techniques in Enterprises), **6**, 101-113.

5. Selby, A.R., Acquisition by microcomputer of some ground vibration data during pile driving, In Computer and Physical Modelling in Geotechnical Engineering (Proc. Conf. December 3-6, 1989, Bangkok), eds A.S. Balasubramaniam, G. Rantucci, S. Chandra, D.T. Bergado, Noppadol Phienweja, S. Saran and Prinya Nutalaya, A.A. Balkema, Rotterdam, 1989, 133-147.

6. Attewell, P.B., Selby, A.R. and Uromeihy, A., Appraisal of ground vibration from civil engineering construction, Int. J. Min. and Geol. Engrg, **7**, 183-208.

7. Uromeihy, A., Ground vibration measurements with special reference to pile driving, unpublished PhD Thesis, 1990, University of Durham, England.

8. British Standards Institution, Noise Control on Construction and Open Sites, BS 5228 1986, Part 4 Code of Practice for Noise and Vibration Control Applicable to Piling Operations (Draft 19 July 1990), London.

APPENDIX 1

As in Figure A1 consider an element of loose soil near to the slope surface. In terms of total stress

$$\tau = c + \sigma \tan\phi.$$

Resistance R to transient downslope motion is

$$R = c \cos^{-1}\beta + W \cos\beta \tan\phi .$$

The downslope disturbing force is $W \sin\beta$.

Thus, factor of safety is given as

$$F = (c \sec\beta + \gamma z \cos\beta \tan\phi)/(\gamma z \sin\beta) .$$

@seismicisolation

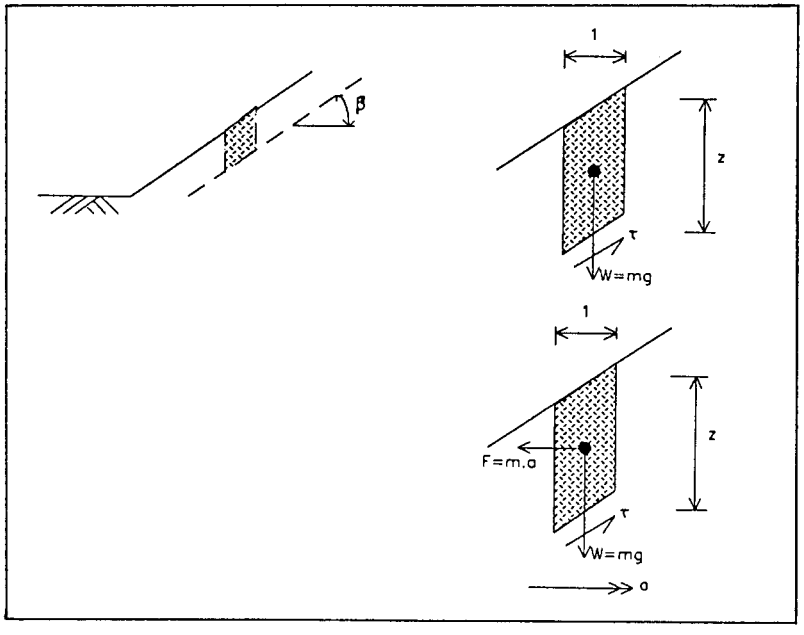

Figure A1. Slope instability

If $c = 0$, then $F = \tan \phi / \tan \beta$. Hence, vertical acceleration, which temporarily reduces the normal pressure on the shear surface, does not modify the static stability, but a small amount of outward transverse acceleration has a strong effect. For example, if horizontal acceleration is equal to 0.1g, then

$$\text{downslope force} = W \sin \beta + 0.1 \rho g z \cos \beta$$

$$= \rho g z \sin \beta + 0.1 \rho g z \cos \beta$$

$$= \rho g z (\sin \beta + 0.1 \cos \beta).$$

If $\beta = 30^{o}$, then static force = $\rho g z$ x 0.5,

and dynamic force = $\rho g z$ x 0.59, which is an 18% increase.

@seismicisolation

CHOICE OF DESIGN SEISMIC HAZARD PARAMETERS FOR EUROCODE 8 IN AREAS OF LOW SEISMICITY

E.D. Booth (Ove Arup & Partners)
B.O. Skipp (Soil Mechanics Associates)

ABSTRACT

The current UK and European progress in developing methodologies for defining seismic hazard parameters for Eurocode 8 is discussed, particularly in the context of low seismicity, intraplate areas such as the UK. A tentative methodology for the UK is proposed.

INTRODUCTION

In May 1990, a draft of the seismic Eurocode, EC8 (1) was circulated for comment to the member nations of CEN (Comite Europeen de Normalisation). The basis for lateral force selection procedure in the code contained a zoning parameter α defined in terms of peak ground acceleration. However, unlike other recent codes such as UBC:88 (2), an associated return period was not given and the guidance on the choice of α given in the previous draft of EC8, which related to maximum intensities, was removed. Without a common approach to this basic parameter and also the parameters defining the shape of the site dependent response spectra, some of the benefits of a unified European seismic code may be lost. The Drafting Committee of EC8 are well aware of these issues and in July 1990, they convened a workshop in Lisbon to try and make progress towards such a common approach, as discussed later.

Low seismicity areas such as Northern Europe have particular difficulties in defining appropriate seismic hazard parameters. This is principally because the maximum credible hazard can be so much larger than the maximum probable hazard associated with a return period of say 500 years. The seismic hazard in low seismicity areas is therefore dominated by the low probability tail of the distribution (3) and the instrumental records of the last 40 years are insufficient to define this. Historical records are therefore essential to increase the length of the record, but these are only complete in populated areas with good written records. Moreover, apparently sensible checks on hazard given by the maximum intensity experienced in a given region may be highly unreliable, unless exceptionally long periods of good historical records are available; even if they are, damage from past periods may be difficult to interpret in present day terms.

There are other difficulties associated with the low seismicity rates inherent to a region

@seismicisolation

like the UK. Firstly, dense seismic monitoring networks are needed to locate accurately the events that do occur and in the UK these have been available only in the last 40 years or so. Secondly, there are no accompanying surface expressions of the activity to give clues on the underlying geological processes. Finally, few strong motion records exist for intraplate regions (there are none for the UK) and so information on the attenuation of earthquake motion, which is essential for seismic hazard analysis, must be deduced indirectly, either from the few strong motion recordings made in tectonically similar environments or from macroseismic data.

The potential risk to ordinary structures from shallow earthquakes in areas of low seismicity has been demonstrated by recent events such as that in Newcastle, Australia (4) and cannot be dismissed in the UK where it has been subject to a recent major study (5). As a member nation of CEN, the UK will have to make a decision on the seismic zoning under EC8 to apply to its territory, even if that decision is effectively to remove the UK from the application of EC8. The BSI committee CSB/65 charged with reviewing EC8 has therefore addressed the issue of definition of the seismic zone factor α in its comments to CEN on EC8 (6).

THE LISBON WORKSHOP OF JULY 1990

This workshop was convened to discuss a document by Hosser et al (7) which described a model seismic zoning exercise for Germany. A number of other papers were tabled at the workshop, including one by the UK delegate (8) and this documentation was discussed over a period of two days.

The German Study

The German pilot study was generally well received by delegates. Its principal features were as follows:

1. Use of historical, instrumental and seismo-tectonic data to carry out a probabilistic seismic hazard assessment.

2. Use of effective peak acceleration (EPA, see NEHRP, 9), rather than peak ground acceleration (PGA), as an anchor for the design spectrum.

3. Generation of spectral shapes both by statistical analysis of real accelerograms and by source and site propagation models.

4. Use of hard ground response to characterise seismic hazard, with subsequent local allowance for soil effects.

5. Use of actual maximum recorded intensities (on hard ground) as a deterministic limiting curb on the results of the probabilistic analysis. There was strong support for this, particularly from the Italians, but as discussed below there was also some dissent.

Other Contributions

Recent national seismic hazard studies were presented for Greece, Italy, Portugal, Spain and the UK (in addition to the German study). Spain has been developing uniform hazard spectra, following lines similar to those adopted recently in the US. France and Italy have been investigating reliability and cost/benefit methods of

@seismicisolation

determining appropriate annual probabilities for design, partly echoing recent UK work (3).

The UK Contribution

The UK contribution (8) made the following conclusions and observations relevant to EC8.

1. Many points of the methodology adopted in the German study were endorsed, including the adopted probabilistic hazard assessment procedures, the use of EPA and the relation of basic regional seismic hazard to hard ground conditions.

2. The methods of allowing for site effects were also endorsed, though work was cited (10) which showed that the amplification of rock motions by soil layers was significantly amplitude dependent, implying that site response factors might vary between low and high seismicity areas.

3. The proposal to relate seismic zoning to maximum recorded seismic intensity was not favoured for areas of low seismicity because, as noted previously, a very long historical record was needed, which was unlikely to be uniformly available.

4. A probabilistic method was proposed (3) for establishing an appropriate annual probability for design seismic motions, which suggested a figure of around 10^{-3} for the UK. This produced the same risk as for a high seismicity area adopting an annual probability of 2×10^{-3}, a figure commonly used in high seismicity regions such as California.

5. For the level of seismicity found in the UK, simple robustness clauses were recommended as the most appropriate means of providing adequate seismic resistance to structures of normal importance. The use of EC8 was therefore considered unnecessary. This was also the view of the Belgian and Dutch delegations for their countries.

   A simple statement in EC8 was recommended which would define the level of zone factor α at which the robustness provisions of the non-seismic Eurocodes were deemed sufficient to provide adequate seismic resistance. On the basis that the robustness clauses conformed to the recommendations of Ref 3, an α value of around 0.05 was suggested as an appropriate threshold. This assumes α is the design EPA (in 'g' units) for the annual probability recommended in Point 4 above.

6. Choice of appropriate design motions cannot be done independently from the definition of structural behaviour factor Q, for the following reasons. (Q is the reduction factor in EC8 applied to elastic response, accounting primarily for ductility).

   - The short duration of motions in areas of low seismicity lessens the need for lateral strength in such areas, for a given level of ductile detailing. Therefore, either Q values should be a function of seismic hazard, to take this into account, or the seismic hazard parameter should include an allowance for duration effects.

   - The magnitude of structural behaviour factor implies a certain level of structural damage, the acceptability of which will be related to the probability of the design motions. Thus the relatively higher R_w factors of UBC:88 may

@seismicisolation

imply a lower annual probability for design motions than that appropriate to the Q values of EC8.

Events since the Lisbon Workshop

At the end of the Workshop, an international task group was set up, with the task of establishing common methodologies for defining seismic hazard in EC8. The situation at the end of March 1991 was that the task group hoped to receive approval from the European Commission to start its work in the summer of 1991.

A meeting of the CEN committee with responsibility for EC8 chaired by Prof P.Pinto was held in December 1990. Among other resolutions, it was agreed that a project team should be established to draft the requirements, criteria and rules for the definition of seismic input data for the Eurocode on Actions, EC1. The project team has yet to report.

CURRENT UK WORK ON SEISMIC HAZARD ASSESSMENT

In order to understand the current work on seismic hazard and use being made of existing published, and sometimes unpublished, results, it will be helpful to set out the background for what is a rapidly evolving scene. The current awareness of seismic hazard in the UK is largely due to the nuclear industry. As public enquiry procedures became more rigorous and onerous, the nominal inclusion of some seismic action into the design of nuclear power plants was supplanted from the early 80's by explicit data supported assessments of seismic hazard using probabilistic methods. Re-examination of geological and tectonic settings for a wide range of existing and proposed nuclear facilities was accompanied by re-examination of the earthquake database. The progress of the work up to 1985 is well summarised in Ref. 11. Subsequent developments up to March 1991 are discussed by Mallard et al (12).

As the hazard assessments became more sophisticated, it was recognised that the likely characteristics of the design basis earthquake for the intraplate/passive margin setting of the British Isles would render the standard US tripartite design response spectra stipulated in USNRC 1.60 (13) overly conservative. These spectra although developed in the US for the nuclear industry were by the late 70's being imported into Europe and used also for non-nuclear but potentially high risk industrial projects such as certain petrochemical installations, not always appropriately. The questionable appropriateness of the USNRC spectra led to the formulation in 1981 of the 'PML (Principia Mechanica Ltd) piecewise linear spectra'. These spectra were developed from a suite of strong motion records of moderate sized earthquakes.

In tandem with this work on design response spectra, the Central Electricity Generating Board (CEGB), following the initial studies for the Sizewell 'B' nuclear power station (Irving, paper 19 in Ref 11) set up the Seismic Hazard Working Party to appraise the seismic hazard at a number of nuclear power plant and waste disposal sites. These evaluations where completed have used 'logic tree' methodology. (Logic trees (14) are helpful where uncertainty in the value of input parameters such as the maximum magnitude of earthquake needs to be incorporated into the hazard assessment, particularly where expert judgement is used (15). There is of course considerable uncertainty attached to most of the input parameters of a seismic hazard assessment. Different weights are assigned to the possible range of input assumption and this procedure is repeated for all the input parameters to produce the branching 'logic tree' shown in Figure 2. The final weighted outcomes at the right hand end of the logic tree

@seismicisolation

can be summed to produce a 'best estimate' result, but the method is also valuable for investigating the sensitivity of the result to input assumptions).

During the past decade, site specific studies for seismic hazard have also been carried out for petrochemical installations and more recently for defence related projects. These studies have often drawn upon those parts of the nuclear industry funded work which have found their way into the public domain, such as the earthquake database and PML 1981 spectra referred to previously. Of more general interest has been a recent comprehensive study (5) which is reviewing UK seismic hazard and the vulnerability of the normal built environment (other than high risk installations) and estimating the consequent overall seismic risk. The review of seismic hazard has collated available data on both historical and more recent earthquakes and has incorporated several attenuation laws for similar continental intraplate regions (16-18). The study makes use of both logic tree methodology and 'uniform hazard spectra', defined below. It complements a number of other recent studies into seismic hazard and risk in the context of EC8 funded by the UK Department of Environment.

Within the last two years, work has been carried out to test the effect of reasonable variations in the UK seismological parameters on low frequency seismic motions (12). There has also been increasing interest in the use of site specific uniform hazard spectra. A uniform hazard spectrum is defined as one which provides a constant probability of exceedence for the maximum response of a single degree of freedom system of any frequency. Its use implies a strong link between the hazard assessment process and its final application in terms of 'seismic actions' or forces. By contrast, the more traditional form of hazard assessment, where a single hazard variable such as PGA is used to anchor a response spectrum whose shape is determined independently, implies a much looser coupling between hazard assessment and 'seismic action'.

One objection to using a uniform hazard spectrum is that it does not necessarily reflect the shape of any particular earthquake, but is an amalgam of contributions from distant large magnitude events and nearer, smaller ones. This is a definite drawback if the spectrum is to be used directly for a multi-mode analysis or to generate a strong motion record. However, for normal buildings in low seismicity areas, the main need is to provide a single, frequency dependent indicator of lateral strength requirement, for which the refinement of considering multi-mode effects is not necessary. Moreover, the uniform hazard spectrum can be used as an envelope criterion for the spectra from a set of real time histories which can then be used in more sophisticated designs. Thus, use of uniform hazard spectra can be justified when employed properly.

A POSSIBLE METHODOLOGY FOR UK CONDITIONS

Figure 1 shows a proposed flowchart for establishing seismic hazard parameters for EC8 in the UK. Comments on the various steps involved are as follows.

Step 1: Probabilistic hazard assessment

Use of a probabilistic hazard assessment following lines originally proposed by Cornell (19) and more recently developed by the US National Research Council (20) and Whitman (21) is now generally accepted as the most appropriate means of establishing seismic hazard. The range of possible input assumption can be accomodated into the analysis using logic tree methodology (Figure 2) as previously described.

@seismicisolation

Step 2: Uniform hazard spectrum

The wealth of strong motion data now available means that uniform hazard spectra can be established, using frequency dependent attenuation laws. References 16-18 are suggested as providing laws suitable for UK conditions.

Step 3A: Comparative risk studies

Annual return periods appropriate for design tend to lengthen with reducing seismicity and must be established by approriate means. As noted previously, the exercise must be done with proper reference to the structural behaviour factors, Q. Ref 22 contains further useful information on assessing comparative risks to society.

Step 3B and 4: Site response studies & site dependent design spectra

The effects of uniform soil layers on bedrock motions can be predicted analytically using one dimensional soil column models (10), although these procedures are currently under review. Less work and confidence attaches to the case of ground motion amplification by sedimentary deposits in steeply sloping valleys where two dimensional effects may become important.

The site response analysis requires appropriate strong motion records. The theoretical difficulty in deriving such records from uniform hazard spectra, noted previously, can be overcome if the analysis is performed on real time histories of suitable amplitude and tectonic origin taken at rock or hard ground sites. The effect of the soil layers can then be calculated as 'spectral ratios' or amplification factors at a range of frequencies. These ratios can then be applied direct to the uniform hazard hard site spectrum to produce site dependent spectra corresponding to the annual probability for design established in step 3A.

Step 5: EC8 design values

The site dependent parameters describing spectral shape can be derived by obtaining the best fit for the site dependent spectra obtained in step 4.

Step 6 & 7: Robustness studies and threshold value for α

The seismic hazard may be sufficiently low that the robustness provided by following non-seismic codes that gives adequate seismic resistance. This is partly a matter of the minimum lateral strength required, which is tractable to analysis, and partly a matter of more qualitative provisions, like continuity, redundancy and regularity. The discussion by Booth (3) on these matters concludes that the robustness inherent in tall buildings in the UK conforming to current codes is quite sufficient for seismic purposes. However, in low to medium rise buildings, they may not always be adequate. Rather than recommending the use of EC8 for such buildings, it is suggested either that there should be an increased minimum lateral strength requirement or that additional detailing requirements should be applied.

CONCLUSIONS

The goal of a common EC8 methodology for establishing design ground motion parameters may still be some way off, but is well worth pursuing. There are particular difficulties attached to the low seismicity areas of northern Europe, which may require

@seismicisolation

a different approach from the Alpide seismic belt affecting southern Europe. The considerable expertise acquired in the UK from the extensive and still continuing seismic hazard work of the last 20 years should be a valuable resource in helping both to resolve the problems and to achieve a common European approach.

REFERENCES

1. EC8. Structures in seismic regions. Council of the European Communities, Luxembourg, 1989.

2. UBC:88. Uniform Building Code. International Conference of Building Officials, Whittier, California, 1988.

3. Booth E., Baker J. Code provisions for engineered building structures in areas of low seismicity. 9 Eur. Conf. Earthq. Engg, Moscow 1990.
4. The Newcastle, Australia earthquake of December 1989. A field report by EEFIT. Institution of Structural Engineers, April 1991.

5. Ove Arup and Partners. Preliminary study of UK seismic hazard and risk. Department of the Environment, 1991.

6. UK Comments on May 1988 Draft of EC8. BSI Committee CSB/65, British Standards Institute, London September 1990.

7. Hosser D, Keintzel E, and Schneider G. Proposal for harmonised rules for the determination of seismic input data. Universitaet Karlsruhe, 1989.

8. Booth E. Current studies of UK seismicity and their relevance to EC8. Paper tabled at EC8 Workshop, Lisbon, July 1990.

9. NEHRP. Recommended provisions for the development of seismic regulations for new buildings. Building Seismic Safety Council, Washington DC 1988.

10. Pappin J.W., Heidebrecht A.C., Henderson P. and Naumoski N. Influence of site response on seismic ground motion in regions of low seismicity. Proc. 9 Eur. Conf. Earthq. Engg, Moscow, Vol 4A pp44-52, 1990.

11. Earthquakes and Earthquake Engineering in Britain. Thomas Telford 1985.

12. Mallard D.J., Higginbottom, I., Muir Wood R. and Skipp B.O. Recent developments in the methodology of seismic hazard assessment, Institution of Civil Engineers Conference "Civil Engineering in the Nuclear Industry", Windermere, UK, March 1991.

13. USNRC 1.60. US Nuclear Regulatory Commission, Washington D.C.

14. Coppersmith K. and Youngs R.R. Capturing uncertainty in probabilistic seismic hazard assessments within intraplate tectonic environments. Third US national conference on earthquake engineering, 1986.

15. Budnitz R.J. Seismic PRA: Recent Developments in Methodology and Applications. Proc Conf. Prob. Safety Assessment, pp1225-1231, Pittsburg, 1989.

@seismicisolation

16. Atkinson G.M. and Boore D.M. Recent trends in ground motion and spectral response relations for North America. Earthquake Spectra Vol 6/1, 1990.

17. Toro G.R. and Maguire R.K. An investigation in earthquake ground motion characteristics in Eastern North America. BSSA, Vol 17 No 2, 1987.

18. Dahle A., Bungum H. and Kvamme L. Attenuation models inferred from intraplate earthquake recordings. Earthquake Engineering and Structural Dynamics, Vol 19 pp 1125-1141, 1990.

19. Cornell C.A. Engineering seismic risk analysis. Bull. Seism. Soc. America, Vol 58 No 5, 1968.

20. US National Research Council. Probalistic seismic hazard assessment. National Academy Press, Washingon DC 1988.

21. Whitman R. (ed). Workshop on ground motion parameters for seismic hazard mapping. NCEER, Buffalo, New Nork, December 1989.

22. Health and Safety Executive. Quantified risk assessment: its input to decision making. Her Majesty's Stationery Office, London 1989.

@seismicisolation
@seismicisolation

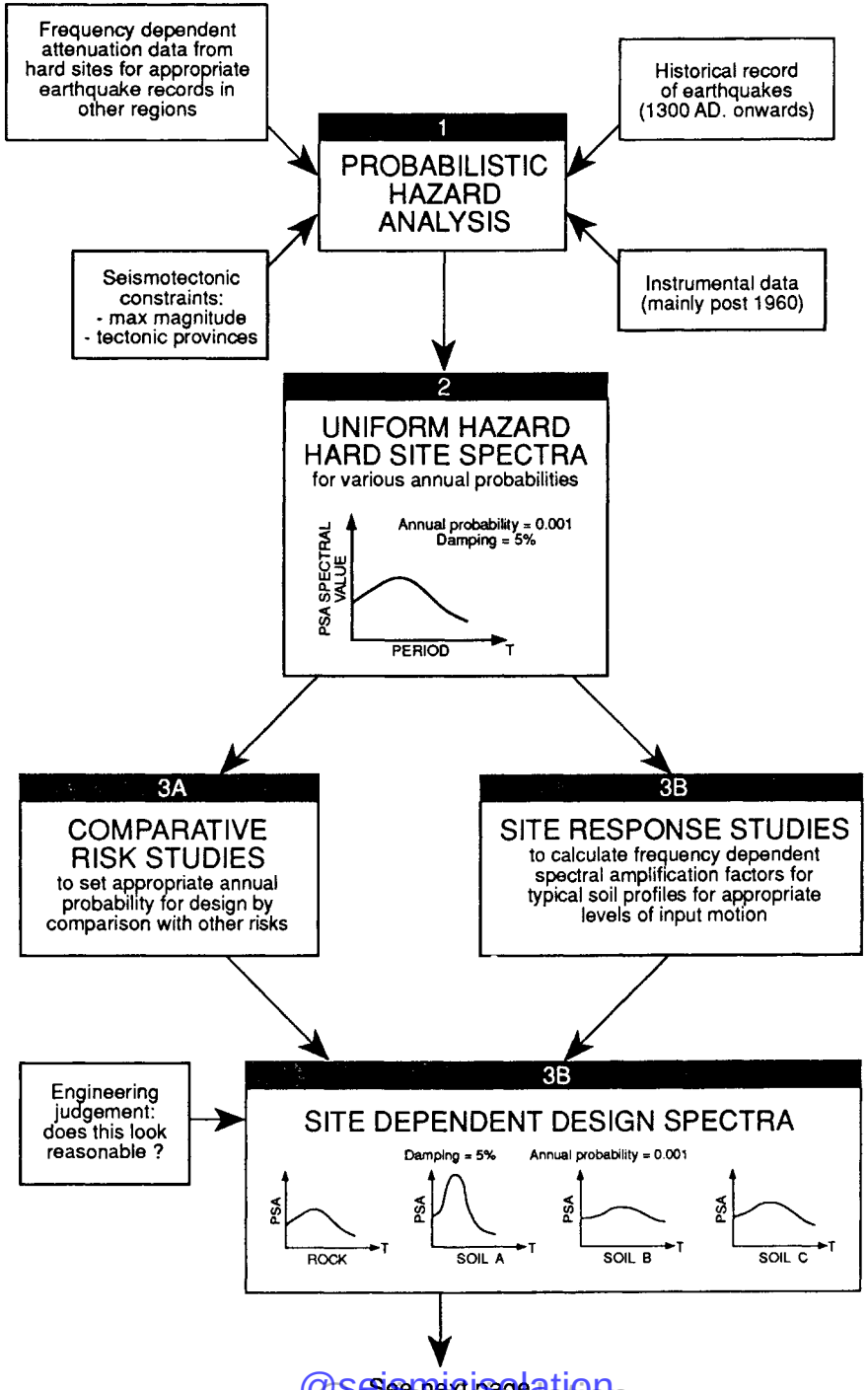

@seismicisolation
@seismicisolation

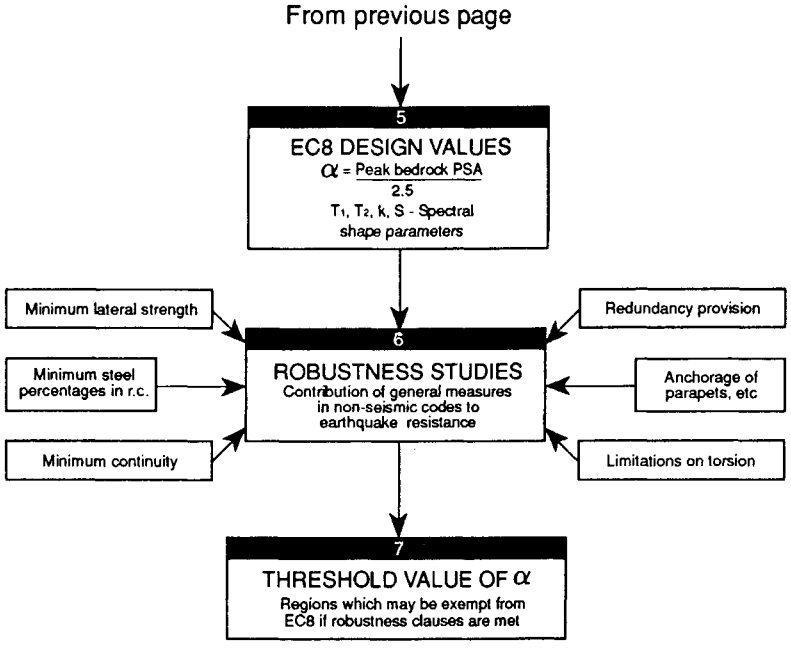

FIGURE 1: ESTABLISHING EC8 SEISMIC HAZARD PARAMETERS FOR THE UK

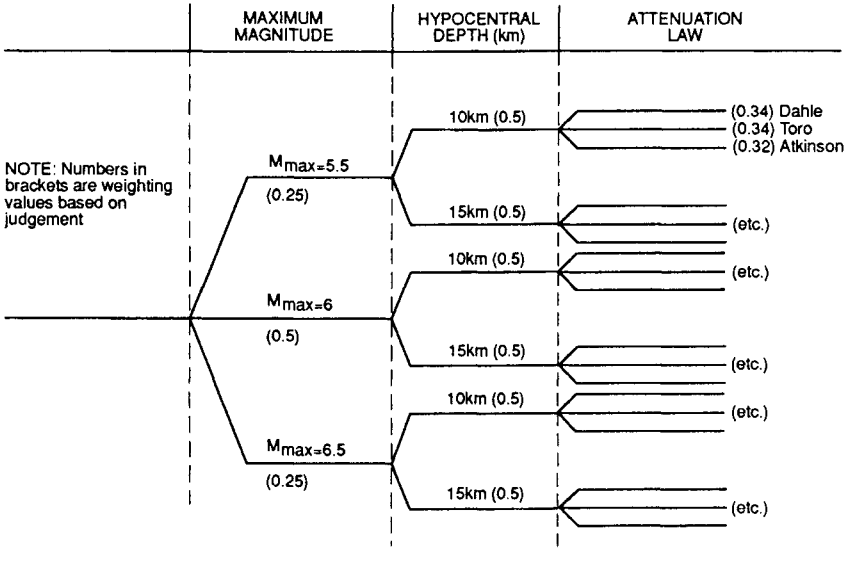

FIGURE 2: ILLUSTRATION OF LOGIC TREE FORMULATION FOR SEISMIC HAZARD ASSESSMENT

@seismicisolation

EVALUATION OF EFFECTS OF SIMPLIFICATION USED IN CURRENT SEISMIC RELIABILITY ANALYSIS

Sharif Rahman

Battelle, Columbus, Ohio 43201

ABSTRACT

An investigation is undertaken to examine the validity of current methods for reliability analysis of building structures subjected to seismic ground motion. Both static and dynamic methods are applied to estimate component reliability indices of a 5-story reinforced concrete frame designed according to a building code. Several seismic zones with various levels of site seismicity which are representative of contiguous United States are considered. Results suggest that the analysis based on static method underestimates seismic reliability.

INTRODUCTION

A major objective of seismic design is the generation of structures that can survive earthquakes. Traditional structures are usually designed in accordance with provisions in building codes and standards, such as *Uniform Building Code* (UBC) [7], *Standard Building Code* (SBC) [14], and *American National Standard ANSI A58.1* [2]. Current code provisions for seismic design are usually based on simplified methods for estimating seismic hazard (*e.g.*, the zone factor Z of *Uniform Building Code*), seismic load effects (*e.g.*, the static method for stress analysis) and elementary simplified failure criteria (*e.g.*, failure occurs when load effects exceed resistance at any one structural component). Effects of frequency content and duration of ground motions, structural dynamic characteristics, nonlinear dynamic analysis, and structural redundancy are not generally accounted for in seismic design. There is no doubt that building codes should utilize simplified rules and formulas to facilitate operational convenience of design process. However, the validity of these rules and formulas and their impact on building safety and reliability must be investigated.

Current estimates of seismic reliability measures for building structures are also obtained by static method. It is based on simplified methods for modeling (*i*) seismic hazard *e.g.* by the 50-year maximum peak ground acceleration, (*ii*) stress analysis by static method, and (*iii*) limit states by strength-related elementary failure criteria at a particular structural component. These simplified methods have also been used in recent studies [6,9,12,13] to perform reliability analysis for code-designed buildings subject to seismic ground shakings. Resultant

©seismicisolation
©seismicisolation

reliability indices have much lower values than those for gravity loads. It is suspected that the seismic reliability indices obtained from static analysis may not provide satisfactory means of structural performance, because their determination involves several gross approximations.

This paper examines the validity of static reliability analysis which is evaluated by the proposed dynamic reliability analysis. The dynamic analysis is based on random process representation of seismic ground acceleration, nonlinear dynamics for structural analysis, and damage-related failure criteria. The objective is to assess seismic performance of structural systems designed according to existing building codes. Both static and dynamic methods and various failure criteria are used to (*i*) calculate reliability indices for these structures, (*ii*) evaluate sensitivity of above indices to particular method of analysis, and (*iii*) investigate the adequacy of current provisions for codified seismic design.

SEISMIC LOAD PROCESS

Consider a site where the lifetime largest load effect during exposure time τ of seismic environment can be represented by a nonstationary colored process $W_\tau(t)$ with strong motion duration T_s. Suppose, the ground acceleration process $W_\tau(t)$ can be modeled as a uniformly modulated random process

$$W_\tau(t) = \psi(t)\widetilde{W}_\tau(t) \tag{1}$$

where $\widetilde{W}_\tau(t)$ is a *zero* mean stationary Gaussian colored noise with one-sided mean power spectral density

$$\widetilde{G}(\omega) = G_0 \frac{1 + \left[2\zeta_g(\frac{\omega}{\omega_g})\right]^2}{\left[1 - (\frac{\omega}{\omega_g})^2\right]^2 + \left[2\zeta_g(\frac{\omega}{\omega_g})\right]^2} \tag{2}$$

in which G_0 is one-sided spectral intensity and ω_g, ζ_g are spectral parameters, and

$$\psi(t) = \begin{cases} 0 & t \le 0 \\ \left(\frac{t}{t_1}\right)^2, & 0 \le t \le t_1 \\ 1, & t_1 \le t \le t_2 \\ \exp[-c_\psi(t - t_2)], & t_2 \le t \end{cases} \tag{3}$$

is the modulation function with parameters c_ψ, t_1, and t_2. Note that the characterization of lifetime largest seimic load defined here does not take into account serial description of pre-shocks, main events, and after-shocks. The issues related to more realistic hazard model and damage accumulation between consecutive seismic events are discussed in Ref. 12.

During the stationary strong motion phase of $W_\tau(t)$, the distribution of lifetime peak ground acceleration Y_{50} with $\tau = 50\ yr$ can be obtained from spectral characteristics of $\widetilde{W}_\tau(t)$ as

$$\bar{F}_{50}(y) \stackrel{\text{def}}{=} \Pr\left(\max_{0<t<T_s} |W_\tau(t)| < y\right) =\simeq \exp\left[-2\tilde{\nu}(y)T_s\right] \tag{4}$$

in which $\bar{F}_{50}(y)$ is the cumulative distribution function of Y_{50},

$$\tilde{\nu}(y) \simeq \frac{1}{2\pi}\sqrt{\frac{\tilde{\lambda}_2}{\tilde{\lambda}_0}} \exp\left(-\frac{y^2}{2\tilde{\lambda}_0}\right) = \tilde{\nu}(0)\exp\left(-\frac{y^2}{2\tilde{\lambda}_0}\right) \tag{5}$$

is the stationary mean y-upcrossing rate of $\widetilde{W}_\tau(t)$ with

@seismicisolation

$$\tilde{\nu}(0) = \frac{1}{2\pi}\sqrt{\frac{\tilde{\lambda}_2}{\tilde{\lambda}_0}} \tag{6}$$

as the stationary mean *zero*-upcrossing rate of $\widetilde{W}_\tau(t)$, and $\tilde{\lambda}_i$ is ith spectral moment of $\widetilde{W}_\tau(t)$ defined by

$$\tilde{\lambda}_i \stackrel{\text{def}}{=} \int_0^\infty \omega^i \tilde{G}(\omega) d\omega. \tag{7}$$

When the expression for $\tilde{G}(\omega)$ in Eq. 2 is substituted in Eq. 7, the spectral moments $\tilde{\lambda}_0$ and $\tilde{\lambda}_2$ can be obtained as

$$\tilde{\lambda}_0 = \rho_0 G_0, \qquad \tilde{\lambda}_2 = \rho_2 G_0 \tag{8}$$

in which

$$\rho_0 = \frac{\pi\omega_g}{4\zeta_g}\left[J_0(\Omega^*)\left(1+4\zeta_g{}^2\right)\right], \qquad \rho_2 = \frac{\pi\omega_g{}^3}{4\zeta_g}\left[J_2(\Omega^*) + 4\zeta_g{}^2 J_4(\Omega^*)\right] \tag{9}$$

$$J_i(\Omega^*) = \frac{4\zeta_g}{\pi}\int_0^{\Omega^*} \frac{\Omega^i d\Omega}{(1-\Omega^2)^2 + 4\zeta_g{}^2\Omega^2}, \tag{10}$$

$\Omega^* = \omega^*/\omega_g$, ω^* is the cutoff frequency which replaces the upper integration limit of infinity in Eq. 7.

Site Consistent Spectral Intensity

Consider the lifetime peak ground acceleration Y_{50} at a site which has the cumulative distribution function shown in Eq. 4. From this distribution function, it can be shown that the approximate expected value of Y_{50} is

$$\mathrm{E}\left[Y_{50}\right] \simeq \left(\sqrt{2\log[2\tilde{\nu}(0)T_s]} + \frac{\gamma}{\sqrt{2\log[2\tilde{\nu}(0)T_s]}}\right)\tilde{\lambda}_0^{\frac{1}{2}} \tag{11}$$

where $\gamma \simeq 0.5772$ is the Euler's constant. Consider now the alternative description of the distribution function of Y_{50} given by [4,6]

$$\tilde{F}_{50}(y) = \exp\left[-\left(\frac{y}{u}\right)^{-k}\right] \tag{12}$$

with the parameters $k \simeq 2.3$, and $u = 0.38a_{10}$ where a_{10} is the 10% upper fractile of Y_{50}. The expected value of Y_{50} from this Extreme Type-II distribution function in Eq. 12 is

$$\mathrm{E}\left[Y_{50}\right] = u\Gamma\left(1-\frac{1}{k}\right) = 1.58u = 0.60a_{10}. \tag{13}$$

When the two expected values in Eqs. 11 and 13 are equated, they give rise to an expression for the site specific spectral intensity

$$G_0 = \frac{1}{\rho_0}\left[\frac{0.6a_{10}}{\sqrt{2\log[2\tilde{\nu}(0)T_s]} + \frac{\gamma}{\sqrt{2\log[2\tilde{\nu}(0)T_s]}}}\right]^2 \tag{14}$$

which is consistent with the site specific value of a_{10}. For a given T_s and spectral parameters ω_g and ζ_g, ρ_0 and ρ_2 can be calculated by using Eq. 9. Using these values, $\tilde{\nu}(0)$ can be obtained from Eq. 6. Finally, for any site specified value of a_{10}, the corresponding spectral

@seismicisolation
@SeismicIsolation

intensity G_0 can be computed from Eq. 14. Note that when the quantities T_s, ω_g, ζ_g are treated as random variables, G_0 also becomes random. However, the same algorithm can be applied by using their relevant realizations.

Generation of Synthetic Seismograms

Consider a discrete approximation of $\tilde{G}(\omega)$ consisting of N_ω spikes each of which has magnitude $\tilde{G}(\omega_k)$ at the frequency ω_k. The associated stationary process $\widetilde{W}_\tau(t)$ can thus be represented by a superposition of harmonic components giving the discrete spectral decomposition of $W_\tau(t)$ as

$$W_\tau(t) = \psi(t) \sum_{k=1}^{N_\omega} \sigma_k \left[A_k \cos(\omega_k t) + B_k \sin(\omega_k t)\right] \tag{15}$$

where $\sigma_k = \sqrt{\tilde{G}(\omega_k)\Delta\omega_k}$, A_k and B_k are independent and identically distributed standard Gaussian random variables. When random numbers are generated according to the distributions of A_k and B_k, the realization of $W_\tau(t)$ can be obtained from given $\tilde{G}(\omega_k)$ and $\psi(t)$. The generated time series is consistent with site specific spectral parameters and the 10% upper fractile a_{10} of lifetime peak ground acceleration.

STATIC RELIABILITY ANALYSIS

Building codes and standards used in structural design contain provisions for ensuring structural safety under extreme loads. The general form of equation from these provisions obtained from the Load and Resistance Factor Design (LRFD) format [5] provides the nominal code-specified (deterministic) resistance at a particular structural component. The load combinations usually involve several load components, such as, D_n, L_n, and E_n representing code-specified nominal dead load, live load, and earthquake load respectively. Representative values of these nominal loads used in a wide variety of buildings can be obtained from the specification in *American National Standards Institute (ANSI) A58.1-82* [2], *Uniform Building Code* (UBC) [7] and many others. For example, the nominal seismic base shear E_n obtained from the *Uniform Building Code* [7] is given by

$$E_n = ZIKCSW \qquad \text{where } C = \frac{1}{15\sqrt{T_0}} \tag{16}$$

in which Z is seismic zone factor, I is importance factor, K is building system factor, S is soil factor, T_0 is initial fundamental period of structure, and W is weight of structure. Due to distinct statistical scatter exhibited by the data, resistance at a structural component is assumed to be random variable. Means, coefficients of variation and probability distribution for structural strengths are available in Refs. 6 and 12.

The load effects due to seismic ground shaking are currently determined by the inverted triangular loads applied laterally to building structures. These loads are proportional to base shear E which can be obtained from [3,6]

$$E = \frac{1.2 Y_{50} SW}{R {T_0}^{2/3}} \tag{17}$$

where Y_{50} is the 50-yr extreme peak ground acceleration (PGA), and R is the response modification factor. According to Refs. 4 and 6, the cumulative distribution function of Y_{50} at a site can be modeled as *Extreme Type-II* distribution and is already specified in Eq. 12. Means, coefficients of variation and probability distributions of 50-yr maximum and arbitrary-point-in-time loads are also available in Refs. 6 and 12.

@seismicisolation

Seismic Performance

The reliability of a structural component can be computed from the condition that the margin of safety $M_i = R_i - S_i > 0$ where R_i and S_i denote random resistance and random load effect, respectively. This condition can be expressed in the conventional form $M_i = g(\mathbf{X}) > 0$ where $\mathbf{X} \in \Re^n$ is a vector of basic random parameters characterizing uncertainty in both loads and resistances, and $g(\mathbf{x})$ is the performance function of the structural component. In the $\mathbf{x}$ space, this function $g(\mathbf{x})$ also known as limit state function separates the domain $\mathcal{D} = \mathcal{S} \cup \mathcal{F}$ of $\mathbf{X}$ into safe set $\mathcal{S} = \{\mathbf{x} : g(\mathbf{x}) > 0\}$ and failure set $\mathcal{F} = \{\mathbf{x} : g(\mathbf{x}) < 0\}$. The component probability of failure P_F which is the complement of component reliability P_S ($P_F = 1 - P_S$) can be defined as

$$P_F \stackrel{\text{def}}{=} \Pr\left[g(\mathbf{X}) < 0\right] = \int_{g(\mathbf{x})<0} f_{\mathbf{X}}(\mathbf{x}) d\mathbf{x} \tag{18}$$

in which $f_{\mathbf{X}}(\mathbf{x})$ is the joint probability density function of random vector $\mathbf{X} \in \Re^n$. The *generalized reliability index* β_G of the structural component can be obtained from

$$\beta_G = \Phi^{-1}(-P_F) \tag{19}$$

in which $\Phi(\cdot)$ is the cumulative distribution function of a standard Gaussian random variable. In general, the n-fold integral in Eq. 18 cannot be calculated analytically. Alternatively, numerical integration can be performed, however, the computational effort becomes prohibitive when $n > 2$.

First- and Second-Order Reliability Methods (FORM/SORM) are used to approximate the member probability of failure and the corresponding reliability index in Eqs. 18 and 19, respectively. These methods are based on linear and quadratic approximations of the limit state surface $g(\mathbf{x}) = 0$ that are tangent to the closest point of this surface (the β point, design point, etc.) to the origin of the space. The determination of the β point can be formulated as a nonlinear optimization problem which is performed here in standard Gaussian image $\mathbf{u}$ of original space $\mathbf{x}$. The distance β_{HL} of this point to the origin of the $\mathbf{u}$ space is referred to as *Hasofer-Lind reliability index.*

The approximate values of P_F and β_G by FORM and SORM are [8,12]

$$P_{F,1} = \Phi(-\beta_{HL}) \tag{20}$$

$$\beta_{G,1} = \beta_{HL} \tag{21}$$

and

$$P_{F,2} \simeq \Phi(-\beta_{HL}) \prod_{i=1}^{n-1} \left[1 - \kappa_i \Psi(-\beta_{HL})\right]^{-\frac{1}{2}} \tag{22}$$

$$\beta_{G,2} = \Phi^{-1}\left(-P_{F,2}\right), \tag{23}$$

respectively, where $\Psi(-\beta_{HL}) = \phi(-\beta_{HL})/\Phi(-\beta_{HL})$, $\phi(u) = 1/\sqrt{2\pi}\exp(-1/2\ u^2)$ is the probability density function of a standard Gaussian variable, and κ_i is the principal curvatures of the limit state surface at the design point.

DYNAMIC RELIABILITY ANALYSIS

Consider a discrete, nonlinear structural system subjected to seismic ground acceleration. The equation of motion satisfy the following governing system of ordinary differential equation

@seismicisolation

$$\mathbf{m}\ddot{\mathbf{Z}}_t + \mathbf{c}\dot{\mathbf{Z}}_t + \mathbf{g}\left(\{\mathbf{Z}_s, 0 < s < t\}; \alpha\right) = -\mathbf{m}\mathbf{d}W_\tau(t) \tag{24}$$

with the initial conditions $\mathbf{Z}_0 = \mathbf{0}$ and $\dot{\mathbf{Z}}_0 = \mathbf{0}$ in which $\mathbf{Z}_t$ is the real vector of generalized displacement, $\mathbf{m}$ is the constant mass matrix, $\mathbf{c}$ is the linear time-invariant viscous damping matrix, $\mathbf{g}$ is a vector functional representing general nonlinear hysteretic degrading restoring forces, $\boldsymbol{\alpha}$ is a constant vector of hysteretic parameters determining rules for structural degradation, and $\mathbf{d}$ is a influence coefficient vector.

The restoring force used to describe the hysteretic behavior of reinforced concrete structures due to seismic ground shaking depends on the type of structural component to be modeled. A three parameter hysteretic model developed by Park *et al.* [10] is used for the nonlinear dynamic analysis conducted in this study. This model consists of piecewise linear segments in the hysteretic loops and is capable of representing various types of reinforced concrete members with appropriate choice of parameters. The values of the three components of $\boldsymbol{\alpha} = \{\alpha_1, \alpha_2, \alpha_3\}^T$ determine the properties of (i) stiffness degradation, (ii) strength deterioration, and (iii) pinching behavior of the material model. An elaborate study of the effects of all the components of $\boldsymbol{\alpha}$ can be obtained from the original reference [10].

Seismic Performance

Seismic performance of structural systems can be evaluated in terms of the condition that a specific response or damage level is not exceeded during ground motion $W_\tau(t)$. Both ground acceleration and structural and material characteristics are assumed to be random. Hence, a realistic assessment requires computation of the exceedance probability of a response quantity of interest.

Structural damage during earthquake depends primarily on maximum deformation and the hysteretic energy dissipated during repeated load cycles The damage of any structural members can be measured by the index [11]

$$DI = \frac{\delta_m}{\delta_u} + \frac{\beta_e}{Q_y \delta_u} \int dE \tag{25}$$

where δ_m is the maximum deformation, δ_u is the ultimate deformation under monotonic loading, Q_y is the calculated yield strength, dE is the incremental absorbed hysteretic energy, and β_e is a non-negative parameter which can be estimated from the experimental data. The probabilistic evaluation of seismic performance based on this damage index requires the computation of component probability of failure P_F given by

$$P_F \stackrel{\text{def}}{=} \Pr(DI > d_0) \tag{26}$$

where d_0 is some allowable value of structural damage. Accordingly, the dynamic reliability index β_L becomes

$$\beta_L = \Phi^{-1}(-P_F). \tag{27}$$

APPLICATIONS

A 5-story, 3-bay R/C planar frame is analyzed and designed in accordance with the appropriate provisions of *1985 Uniform Building Code* [7] and *ACI Code 318-83* [1] for seismic zones-2 and -3. Thus, the static method and elementary failure criteria have been used in the analysis. Fig. 1(a) shows the typical plan of the building system. An interior frame is chosen to perform seismic analysis in the transverse direction and is shown in the Fig. 1(b).

The nominal dead load D_n consists of mainly self-weight of structure and superimposed load of 30 psf for the floors and 10 psf for the roof. The nominal live load L_n is also assumed to be 30 psf for the floors and 10 psf for the roof. The nominal seismic base shear E_n can be obtained from Eq. 16 and are found to be 34 *kips* and 64 *kips* for seismic zones-2 and

©seismicsolution

-3, respectively. The calculated base shears are based on $Z = 3/8$ for zone-2 and 3/4 for zone-3, $I = 1$, $K = 0.67$ for ductile moment resisting frame, C=0.10, S=1.2 for stiff clay, and $W = 1043$ *kips*. For load combination involving earthquake, this nominal base shear is distributed along the height of building frame and is applied laterally to the structural systems. Design details of the frames can be obtained from Ref. 12.

The structural dynamic modeling of the frames are done by using beams and columns with critical cross-sections at their ends. The trilinear backbone curve of a structural component is defined by various component properties, such as cracking moments, cracking curvature, yield moment, yield curvature, etc. which are calculated from empirical equations reported in the current literatures [10,11]. The post-yielding stiffness is taken as 1.5% of the initial elastic stiffness of the member.

The uniaxial constitutive law for each individual critical cross-section of the frame is described by the trilinear backbone curve and the model parameters α_1, α_2, and α_3 that determine the properties of hysteretic loops. The stiffness degradation parameter α_1 is taken as 2.0 for both beams and columns which is found to be fairly representative for reinforced concrete structures. The strength deterioration parameter α_2 of an individual member is calculated from the empirically developed expression in Ref. 10. No slippage of the reinforcement is allowed either in beam or in column and the pinching parameter α_3 is set to an extreme value which does not account for pinching effect in the restoring force. A typical hysteretic rule for beam or column element is shown in Fig. 2.

The concrete strength f_c' and yield strength F_y of steel reinforcement are treated as independent random variables with mean 3.39 *ksi* and 67.5 *ksi*, and coefficients of variation 18% and 9.8%, respectively. The probability distribution of f_c' and F_y are modeled as Gaussian and lognormal variables, respectively.

Mass is assumed to be lognormal random variable with mean value equal to the nominal value and coefficient of variation 11%. The damping property is specified by damping ratio in the first mode with mean 0.02, coefficient of variation 65%. and lognormal distribution function. The uncertainty in the stiffness property will be determined by the variabilities in the basic parameters such as concrete strength, yield strength of steel, etc.

The spectral parameters ω_g and ζ_g are assumed to be independent random variables with their mean values 16.5 rad/s and 0.8 and coefficients of variation 42.5% and 42.6%, respectively. These values are consistent with the intermediate soil condition for which the frames are designed. The probability distribution functions of ω_g and ζ_g are modeled as gamma and lognormal, respectively. The strong motion duration T_s is also treated as a random variable with mean 6.9 s, coefficient of variation 42%, and lognormal cumulative distribution function. The modulation function $\psi(t)$ in Eq. 3 is chosen with $t_1 = 0.15T_s$, $t_2 = 1.15T_s$, and $c_\psi = 2.0/T_s$. The total duration T_d of ground motion is assumed to be 1.5 times the strong motion duration T_s. The artificial earthquakes are generated in accordance with the algorithm described earlier.

Static Reliability Analysis

FORM/SORM algorithms are employed to determine the performance of above frames designed for seismic zones-2 and -3 of *Uniform Building Code* [7]. The reliability analysis is carried out for the load combination $D + L_{apt} + E$, where D, L_{apt} and E denote dead load, arbitrary-point-in-time live load, and earthquake load, respectively.

The seismic performance of this frame is evaluated by calculating component reliability indices at the critical cross-sections. The corresponding limit states are obtained from flexural action for beams and combined action of axial force and bending moment for columns. Several representative values of $a_{10} = 0.1g$, $0.15g$, $0.2g$ and $a_{10} = 0.2g$, $0.3g$, $0.4g$ within the seismic zones-2 and -3 are considered. The smallest reliability indices by FORM at zone-2 with $a_{10} = 0.1g$ are found to be 2.19 for the beam and 2.26 for the column. Comparisons of these results with more accurate estimates by SORM confirm previous results with slight variation

©seismicisolation

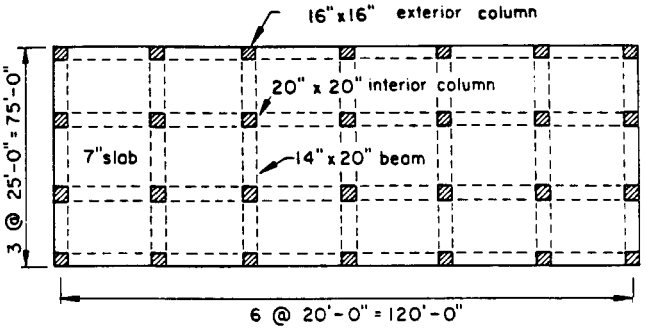

(a) Plan of Building System

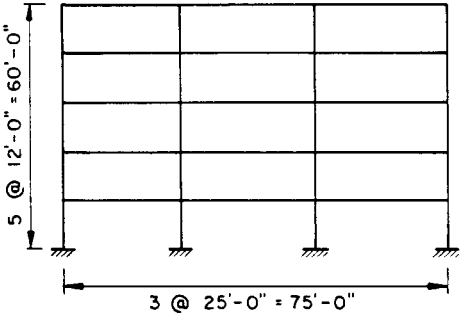

(b) Interior Frame of Building System

Figure 1. Plan and Interior Frame of Building System

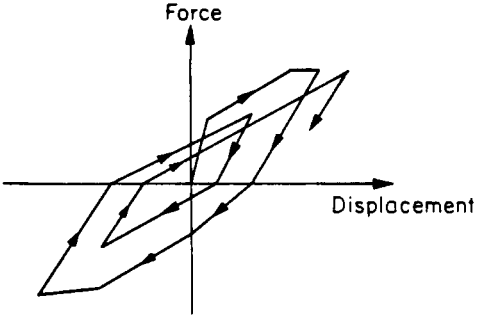

Figure 2. Three Parameter Model with Degrading Hysteresis

@seismicisolation

Table 1: Static and Dynamic Reliability Indices

Zone	a_{10}	Minimum β_L (Eq. 27)	Minimum $\beta_{G,1}$ (Eq. 21)
Zone-2	0.1g	7.69	2.19
	0.15g	6.57	1.81
	0.2g	5.13	1.50
Zone-3	0.2g	5.12	2.04
	0.3g	3.60	1.59
	0.4g	2.91	1.30

in the values of above indices. Results also suggest that the indices based on FORM for zone-2 can be as low as 1.81 if $a_{10} = 0.15g$ and 1.5 if $a_{10} = 0.2g$.

The static reliability indices are also obtained by various estimates for the the 5-story R/C frame structure designed for seismic zone-3 of *Uniform Building Code* with several cases of $a_{10} = 0.2g$, $a_{10} = 0.3g$, and $a_{10} = 0.4g$. Based on FORM estimate, the smallest values of the above indices are 2.04 for $a_{10} = 0.2g$, 1.59 for $a_{10} = 0.3g$, and 1.30 for $a_{10} = 0.4g$. Comparisons of these results with those for zone-2 structure suggest that that current designs by *Uniform Building Code* [7] is less safe in areas of high seismicity.

Dynamic Reliability Analysis

One major objective of this numerical example is the evaluation of static reliability estimates. This can be accomplished by comparing the static reliability indices with the reliability indices β_L (Eq. 27) obtained from nonlinear dynamic analyses. In this paper, the indices are estimated by direct Monte Carlo simulation with 1500 number of samples. The associated deterministic nonlinear dynamic analysis for a particular sample of simulation is performed by a computer code IDARC [10]. This program computes the deterministic structural response by direct step-by-step numerical integration using the Newmark algorithm.

Table 1 shows the smallest reliability index β_L in Eq. 27 based on the damage index DI (Eq. 25) which is obtained for the 5-story frame designed for seismic zones-2 and -3. The critical threshold of $d_0 = 0.4$ proposed in Ref. 10 is used here to calculate the above quantities in the table. Although the failure criteria (in static and dynamic reliability analyses) are different, these member level reliability indices can be compared with corresponding static reliability measures obtained previously and is also shown in the same table. Comparisons of minimum reliability indices for the 5-story frame obtained for various combinations of seismic zone and a_{10} exhibit significant differences due to the static and the dynamic methods. However, note that the comparisons are valid only when the component reliabilities are considered. Concepts of system reliability are not explored in this study.

In a recent work of O'Connor and Ellingwood [9], a similar study regarding adequacy of static reliability indices for simple structural systems was performed. Their findings suggest that the static method provides satisfactory seismic structural performance when compared to dynamic method. However, in Ref. 9, the analysis is based on elementary stochastic modeling of ground motion in which the peak ground acceleration is assumed to be random with the cumulative distribution function defined be Eq. 12 and the frequency contents are obtained from an ensemble of actual seismograms. Also their study involves simple 1-story portal frame and ideal elasto-plastic material model without any degrading characteristics. It is interesting to note that in this study, static reliability indices are found to significantly underestimate structural reliability particularly at sites with low seismicity.

@seismicisolation

CONCLUSIONS

An investigation is carried out to evaluate current methods for seismic reliability analysis of building structures. Both static and dynamics methods are applied to obtain component reliability indices of a 5-story reinforced concrete frame designed according to a building code. Results of analysis suggest that the static method underestimates seismic reliability, particularly at sites with low seismicity.

REFERENCES

1. American Concrete Institute, "Building Code Requirements for Reinforced Concrete," *ACI Standard 318-83*, Detroit, Michigan.

2. American National Standard Institute, "Minimum Design Loads for Buildings and Other Structures," ANSI A58.1-1982, New York, New York.

3. Applied Technolgy Council, "Tentative Provisions for the Development of Seismic Regulations for Buildings," *National Bureau of Standards Special Publication No. SP* 510, *ATC*3 – 06, Washington, D.C., June 1978.

4. Cornell, C. A., "Engineering Seismic Risk Analysis," *Bulletin of the Seismological Society of America*, Vol. 58, No. 5, pp. 1583-1606, 1968.

5. Ellingwood, B., MacGregor, J. C., Galambos, T. V., and Cornell C. A., "Probability Based Load Criteria - Load Factors and Load Combinations," *Journal of Structural Division*, ASCE, Vol. 108, No. ST5, Proc. Paper 17068, pp. 978-997, May 1982.

6. Ellingwood, B., Galambos, T. V., MacGregor, J. C., and Cornell C. A., "Development of a Probability Based Load Criterion for American National Standard *A*58," *National Bureau of Standards Special Publication No. SP* 577, Washington, D.C., June 1980.

7. International Conference of Building Officials, *Uniform Building Code*, Whittier, California, 1985.

8. Madsen, H. O., Krenk, S., and Lind, N. C., Methods of Structural Safety, Prentice-Hall, Inc., Englewood Cliffs, New Jersey, 1986.

9. O'Connor, M. J., and Ellingwood, B., "Reliability of Nonlinear Structures with Seismic Loading," *Journal of Structural Division*, ASCE, May 1987.

10. Park, Y. J., Reinhorn, A. M., and Kunnath, S. K., "IDARC:Inelastic Damage Analysis of Reinforced Concrete Frame-Shear Wall Structures," Technical report, *NCEER-87-0008*, State University of New York at Buffalo, Buffalo, New York, July 1987.

11. Park, Y. J. and Ang, A. H-S., "Mechanical Seismic Damage Model for Reinforced Concrete," *Journal of Structural Division*, ASCE, 111(4), 722-739, 1985.

12. Rahman, S., "A Markov Model for Local and Global Damage Indices in Seismic Analysis," Dissertation presented to the Graduate School of Cornell University, in partial fulfillment of the requirements for the degree of Doctor of Philosophy, 1991.

13. Rahman, S., and Grigoriu, M., "Reliability Based Design Codes," *Proceedings of the International Conference of Structural Safety and Reliability*, San Francisco, California, August 1989.

14. Southern Building Code Congress International, *Standard Building Code*, Birmingham, Alabama, 1985.

@seismicisolation

SEISMIC BEHAVIOUR OF STRUCTURES DURING THE MANJIL EARTHQUAKE, 1990 IN IRAN

HASSAN A. MOGHADDAM
Lecturer, Sharif University of Technology
Tehran, Iran

ABSTRACT

The Manjil earthquake of June 1990 destroyed many building and structures in Northern parts of Iran. In the meizoseismal region, the effect on low rise buildings with rather short fundamental periods was more predominant. On the other hand, in distant regions, structures with longer periods were affected more severely. A spatial distribution of the acceleration has been calculated, based on the results obtained from the strong motion network. These accelerations were used to evaluate the seismic response of a variety of structures and the results are compared with the response of structures observed during the earthquake.

INTRODUCTION

On Thursday June 21 1990 at 30 minutes past midnight local time (9.0am Wednesday June 20, Greenwich Mean Time) a destructive earthquake occurred in the Gilan province in Northern Iran. The magnitude of this earthquake was estimated at 7.3 by the Institution of Geophysics of Tehran University, and at 7.6 by the US Geological Survey. The epicentre has been reported to be approximately 200 km northwest of Tehran between the towns of Manjil and Rudbar. The earthquake caused strong shaking in a large part of Iran including Tehran and Tabriz some 200 and 300 km away, respectively. It caused widespread damage in areas within 100 km radius of the epicentre including the city of Rasht, some 60 km away and hundreds of towns and villages in Gilan and Zanjan provinces. Manjil was almost totally destroyed. Most of the brick dwellings located in the meizoseismal region collapsed and those located as far as 50 km from the epicentre were severely damaged.

@seismicisolation

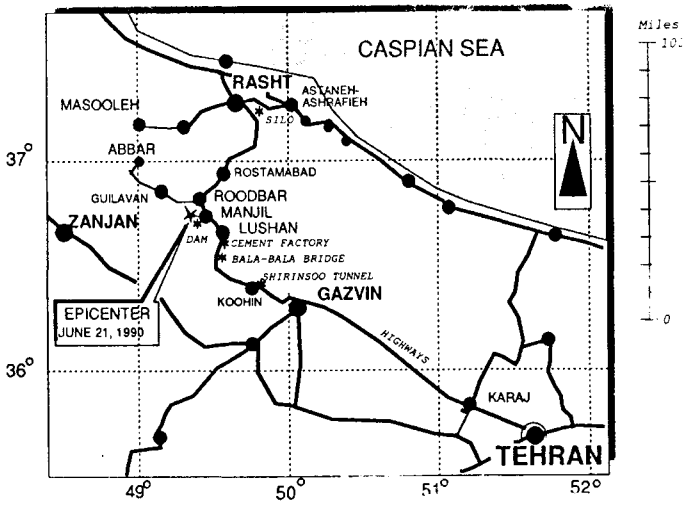

Figure 1. Area affected by the Manjil earthquake

ATTENUATION OF ACCELERATION

Peak accelerations were recorded in various positions by the Iranian network of accelerographs. Ab-bar is the nearest town to the epicentre (apart from Manjil and Rudbar from which no record is available) with a peak acceleration of 0.65 g. The following relation was used to evaluate the attenuation of acceleration.

$$a_D = a_0 \left(\frac{1.25}{1 + D/76.8}\right)^n \qquad (1)$$

where

$$n = 1/(2.5\ Tp) + 1$$

a_0 and a_D are the peak accelerations at the meizoseismal area and a place D km from the epicentre respectively. T_D is the predominant period ranging from 0.25 sec in the meizoseismal region to 0.6 sec for a distance of 200 km from the epicentre. On the basis of this approach, the peak acceleration in Manjil is estimated as 0.71g. Replacing a_0 in Equation (1) with 0.71, the peak acceleration at any point can be readily evaluated and used for back analysis of certain structures.

UNREINFORCED MASONRY

Masonry structures are usually categorized as low strength and brittle. Investigations and observations indicate that while the strength of masonry structures is not lower than the average for various types of structures, the brittle behaviour undermines their seismic performance significantly. As indicated in Figure 2, ductility plays a much more significant role than strength when a structure is subjected to severe earthquakes. During such earthquakes, the demand strength is much higher than the strength of ordinary structures.

@seismicisolation

Consequently, brittle structures collapse as a result of large inelastic displacements, whereas ductile structures can undergo large plastic displacements without failure.

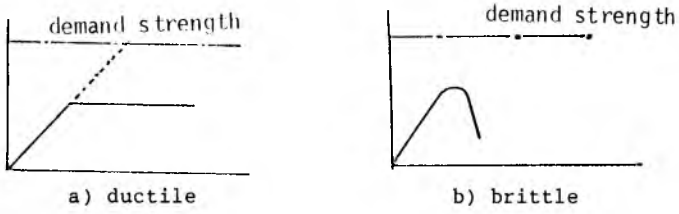

Figure 2. A comparison of ductile and brittle behaviour

Figure 3. Collapse of masonry warehouse near Manjil

RURAL DWELLINGS

Typical rural dwellings consist of thick walls made of round stones. Mud is normally the only type of mortar used in rural houses. It is commonplace to use bamboo to cover the roof and a layer of clay with a thickness of approximately 15 cm proofs it against rain and snow. Although roofs were not very heavy, the lack of sufficient strength and ductility in walls resulted in the collapse of rural dwellings in places like Ghazvin, some 75 km from the epicentre, where the peak acceleration was recorded as 0.19g. The behaviour of the rural houses indicates that the weight of the walls themselves had been enough for collapse, especially if we consider the out of plane component of seismic force. In the meizoseismal region, modern warehouses with masonry shear walls collapsed.

@seismicisolation

These shear walls were made of high quality stones and cement mortar. Therefore, it can be concluded that, unless special seismic provisions are considered, stone shear walls are not sufficiently strong to undergo seismic forces. Sometimes, the stone walls are strengthened by putting timbers horizontally into the wall. This has been proved to enhance the seismic resistance significantly. The reason for this phenomenon has been discussed elsewhere (1.2). The state of stress in masonry shear walls is as shown in Figure 4. It is equally possible to have horizontal and vertical sliding. Vertical stress becomes predominant as precompression increases. Therefore, it is easier to slide vertically than horizontally. Timbers can prevent this mode of sliding and consequently strength increases.

Figure 4. (a) timbers in shear walls
(b) the state of stress in shear walls

Figure 5. Typical rural dwellings in Northern Iran

@seismicisolation

BRICK BUILDINGS

In general, brick buildings had a better performance than rural dwellings. The closest place to the epicentre in which a few single storey brick buildings collapsed was Koohin, some 48 km south of Manjil. The peak acceleration at Koohin from Equation (1) was estimated as 0.36g. Since most of the brick buildings in Koohin remained intact, it can be concluded that ordinary unreinforced brick buildings can resist base accelerations as high as 0.36g. Assuming a dynamic magnification factor of 1 for short brick buildings (one or two storeys), a seismic coefficient of 0.36 is obtained as the threshold of collapse for brick buildings. Howver, due to the brittle nature of unreinforced brick buildings, the number of collapsed buildings increases drastically as we approach the epicentre. In Manjil and Rudbar almost all unreinforced brick buildings were fully destroyed, no matter what type of brick and mortar had been used. From the lessons learned from the Manjil earthquake, it can be concluded that the ordinary brick buildings cannot resist the typically high seismic forces in the meizoseismal region during severe earthquakes. This has been accounted for in the new seismic code of the Islamic Republic of Iran in which special reinforcing arrangements are required.

EFFECTS OF REINFORCED CONCRETE BOUNDARY FRAME

It is a long time now since RC boundary frames were first introduced as efficient means for enhancing the seismic resistance of brick buildings. The behaviour of framed walls during all previous earthquakes including the Manjil earthquake is in agreement with this assumption. This system has been enforced in the new Iranian seismic code. The theory of seismic behaviour of framed walls has been discussed elsewhere [3 - 6]. The interaction between frame and wall significantly enhaces seismic behaviour of both wall and frame. A method has been suggested for seismic analysis and design of this type of structure [6].

Figure 6. A brick building in Manjil which survived due to the enhancing effect of horizontal RC bond beams

@seismicisolation

Rasht is a modern city located 63 km north of Manjil. Most residential blocks are 4 to 8 storey buildings in which steel or concrete frames are infilled with brick panels. Usually, the connections of these steel frames are not deigned for seismic forces and, therefore, the moment capacity and regidity are very low and do not provide enough lateral resistance to comply with the requirements of the seismic code (typically about one tenth of the weight of the building). From Equation (1), the peak acceleration in Rasht was evaluated as 0.3g. The magnification factor for a mid-rise building is greater than one. Thus, the seismic forces that these buildings underwent during the Manjil earthquake were greater than 0.3 times their weight. Now, the question is how they could withstand these strong forces? The author believes that the interaction between wall and frame has had a significant role in improving the seismic performance of mid-rise buildings. The occurrence of diagonal cracks and corner crushings indicate that a large portion of loads have been taken by infills and that they can be repaired and strengthened to resist probable earthquakes in the future.

INVERTED PENDULUMS

The old water tank of Rasht which was an inverted pendulum with a capacity of 1500 m^3 was totally destroyed during the earthquake. The size and weight of this tank are given in Figure 7.

a) before earthquake

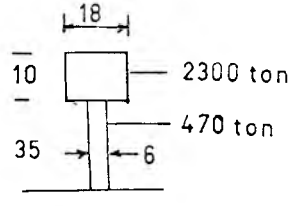

b) size and weight

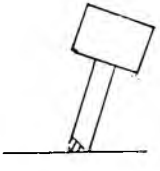

c) failure mechanism

Figure 7. The concrete water tank in Rasht which collapsed during the Manjil earthquake

@seismicisolation

The seismic design forces given by the previous seismic code and the recent one are 115 ton and 483 ton, respectively. The peak acceleration at the base was evaluated by Equation (1) to be equal to 0.3g. The dynamic magnification factor was estimated as 0.77. Hence the seismic force V is:

$$V = 0.77 \times 0.3 \times 2300 = 531 \text{ ton} \qquad (2)$$
$$M = 531 \times 40 = 21252 \text{ ton.m} \quad \text{seismic moment at the base}$$

The pendulum which had been designed in accordance with the previous seismic regulation, which does not alter the minimum amount of reinforcement. The ultimate moment capacity of the pendulum has been:

$$M = A_s f_y R \qquad (3)$$

A_s and f_y are the area of reinforcement and yield stress, respectively, and R is the radius of the cylindrical pendulum. The thickness of the cylinder was 0.3m and the amount of reinforcement was 0.002 of the gross area. Hence:

$$A_s = 0.002 \times 6.28 \times 300 \times 30 = 133 \quad cm^2$$
$$M = 113 \times 3000 \times 3/1000 = 1017 \quad t.m \qquad (4)$$
$$M_w = W.R = 2300 \times 3 = 6900 \quad t.m$$
$$M_s - M_w = 21252 - 6900 = 14352 >> 1017$$

This difference should be taken by the moment capacity of the pendulum, which is obviously far less than the required one. The result was the full collapse of the water tank.

CONCLUSION

On the basis of the observations and back analysis of the behaviour of structures during the Manjil earthquake, the following conclusions may be drawn:

a) low strength and lack of ductility of rural dwellings made them very vulnerable to strong earthquakes. The use of timber in walls can enhance strength and ductility and reduce vulnerability.

b) unreinforced brick buildings in the meizoseismal region usually collapse regardless of the type of mortar and brick. The introduction of boundary frames significantly improves mechanical characteristics and reduces vulnerability.

c) the composite behaviour of wall and frame enable mid-rise buildings to resist seismic forces much greater than the capacity of frames alone. Infills took a large portion of lateral forces and dissipated seismic energy through diagonal cracks and corner crushing.

d) failure of inverted concrete pendulums indicates the need for change in the requirements for seismic design of this type of structure. This need has already been met in the new seismic code of the Islamic Republic of Iran.

@seismicisolation
@seismicisolation

ACKNOWLEDGMENT

The field trip was sponsored by the International Institute of Engineering Seismology and Earthquake Engineering in Iran. This support is gratefully acknowledged.

REFERENCES

1. Moghaddam, H.A. and Dowling, P.J., The state of the art in infilled frames. ESEE Report No. 87-2, Imperial College, London, 1987.

2. Moghaddam, H.A. and Dowling, P.J., Earthquake resistant design of brick infilled frames. Proc. 8th International brick/masonry conference, Dublin, 1988.

3. Moghaddam, H.A., et al., A shaking table study of brick masonry infilled frames subjected to seismic excitations, 9th WCEE, Vol VIII, p.913, 1988.

4. Moghaddam, H.A., Dynamic out of plane behaviour of infilled frames, 9th EAEE, Moscow, 1990.

5. Moghaddam, H.A., Dynamic inplane behaviour of infilled frames, 9th EAEE, Moscow, 1990.

6. Moghaddam, H.A., Seismic design of infilled frames, 9th EAEE, Moscow, 1990.

@seismicisolation

SEISMIC DESIGN OF DUCTILE R/C MEMBERS

K.PILAKOUTAS [1] AND A.S.ELNASHAI
Department of Civil Engineering, Imperial College, London SW7 2BU

ABSTRACT

In this paper, the procedure used in EC8 for design of ductile reinforced concrete (RC) members is reviewed. Whereas the EC8 sequence of calculations is maintained, the formulations used in the calculation of the critical section curvature ductility demand and provision of confinement to satisfy the required curvature ductility are appraised and alternatives are proposed. In deriving the suggested formulations, use is made of a newly developed computer program (CRELIC) for the analysis of reinforced concrete sections, incorporating realistic cyclic models for steel and concrete. The program is used to conduct extensive parametric studies, the results of which shed light on the behaviour of critical zones in R/C members and possible improvements in existing EC8 design techniques.

INTRODUCTION

In seismic design of RC members, the aim is to achieve ductile behaviour through the development of plastic hinge areas. Codes such as the ACI 318-83 [1], UBC (1988) [2] and the New Zealand Standard 3101 (1982) [3] impose dimensional limitations and include provisions for hoop reinforcement. However, the above codes do not quantify the ductility achieved by the prescribed detailing. In this respect Eurocode 8 (EC8) [4] outlines a procedure for designing the critical structural components so as to achieve the required structural behaviour. In this paper the four stages involved in the EC8 design procedure are presented. An appraisal of the assumptions made in determining the curvature ductility and the corresponding confinement requirement follows and alternative recommendations are proposed.

[1] Department of Civil and Structural Engineering, University of Sheffield, Mappin Street, Sheffield, S1 3JD

@seismicisolation

Conventional design for ductility

From experiments conducted on RC columns, Zahn, Park, Priestley and Chapman [5] reported that the New Zealand code-recommended confinement would yield a value of maximum curvature ductility '$\mu_{1/r}$' of about 20. The relationship between curvature and displacement ductilities is accepted by researchers in New Zealand [6] to be a function of the aspect ratio of the wall and the length of the plastic hinge. Paulay and Uzumeri [7] considered two different equations for the length of the plastic hinge, which form the limits of the shaded bands depicted in figure 1.Some of these concepts are implicitly included in the Eurocode 8 and are hereafter further discussed.

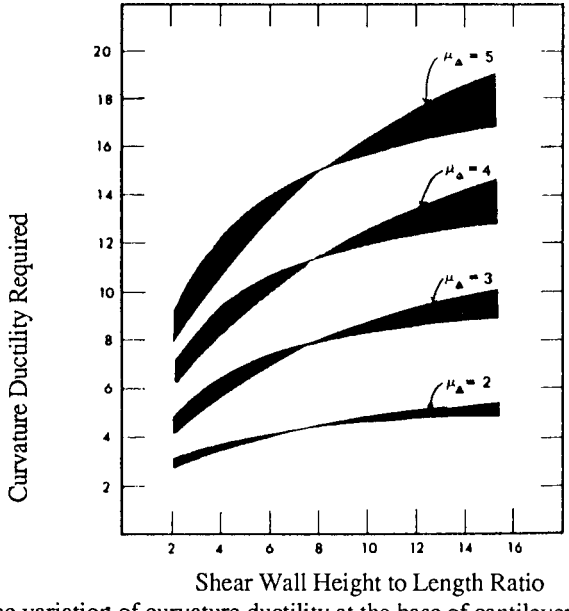

Figure 1 The variation of curvature ductility at the base of cantilever shear walls with aspect ratio of the walls and the imposed ductility demand (Paulay and Uzumeri, 1975)

Ductility design in Eurocode 8 (EC8)

Eurocode 8 [4] utilises behaviour ('q') factors to implicitly account for non-linear behaviour and other force-reduction effects. The 'q' factor can be derived as the average ratio between the seismic loads inducing an ultimate limit state in the structure taking into account its actual nonlinear behaviour, and the design seismic loads obtained by conventional linear analysis [8]. For RC structures the value of this parameter is given in the code as a function of the building regularity and the structural system for three different ductility classes.

The 'q' factor depends on, amongst other effects, the structural configuration and the ability of critical members to undergo inelastic deformations. In order to design the critical members of a RC structure so that they exhibit the required ductility, EC8 implicitly defines the design procedure shown in the flow chart of figure 2. Dimensional limitations ensure that the confinement is evenly distributed where is needed in a similar manner with other codes of practice.

@seismicisolation

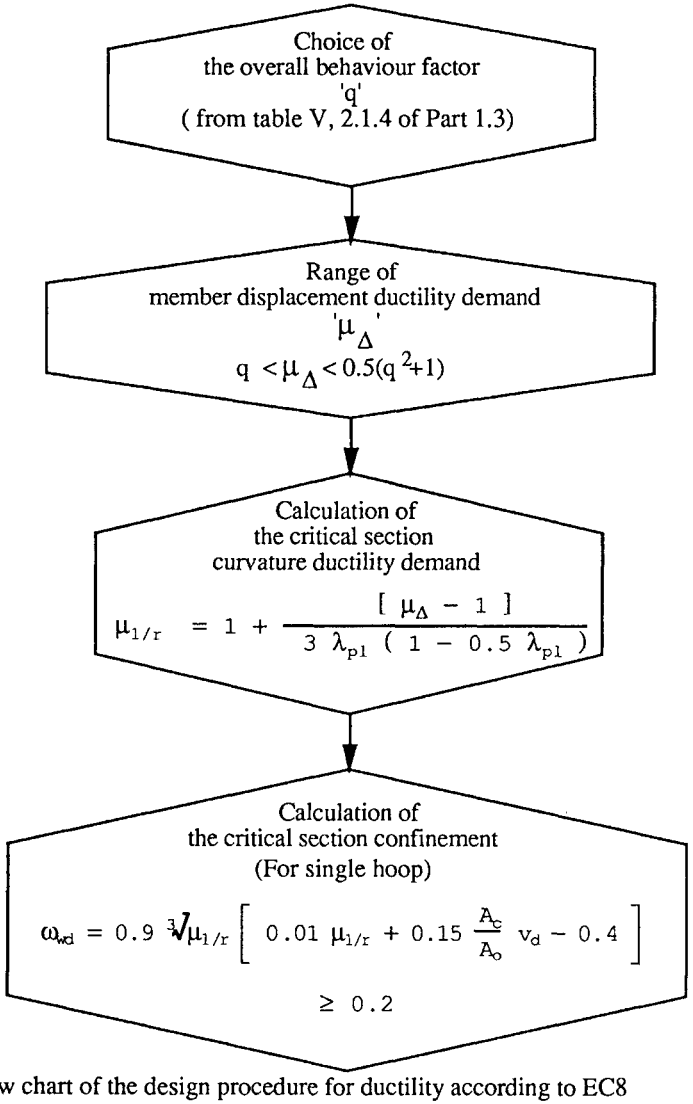

Figure 2. Flow chart of the design procedure for ductility according to EC8

Table 1 gives the first three parts of the flow chart for the different ductility classes [9] for both coupled and isolated walls. Two methods are used giving the two bounding values for displacement ductility, $\mu_{\Delta 1}$ and $\mu_{\Delta 2}$. The second value is based on the equal energy principle, but the average of the two is used to calculate the curvature ductilities.

@seismicisolation

TABLE 1
Relation between q-values and curvature ductility [9]

DC	q	$\mu_{\Delta 1}$ $0.5(q^2+1)$	$\mu_{\Delta 2}$ q	μ_{Δ} $0.5(\mu_{\Delta 1}+\mu_{\Delta 2})$	$\mu_{1/r}$ $1+2.5(\mu_{\Delta}-1)$ (coupled walls)	$\mu_{1/r}$ $1+3.5(\mu_{\Delta}-1)$ (isolated walls)
"L"	1.5	1.63	1.5	1.56	2.40	2.97
	2.0	2.5	2.0	2.35	4.13	---
"M"	2.5	3.63	2.5	3.06	6.16	8.22
	3.0	5.0	3.0	4.00	8.50	---
"H"	3.5	6.63	3.5	5.06	11.16	15.21
	4.0	8.5	4.0	6.25	14.13	---
	4.5	10.63	4.5	7.56	17.41	---
				Approximation	$\mu_{1/r} \cong q^2$	$\mu_{1/r} \cong 1.2\, q^2$

EC8 regulations recognise an increase in the concrete strain at failure due to hoop reinforcement as shown in figure 3. The value of 'α' depends on the hoop configuration. Confinement is also considered to enhance the ultimate concrete strength as well as the strain corresponding to ultimate stress.

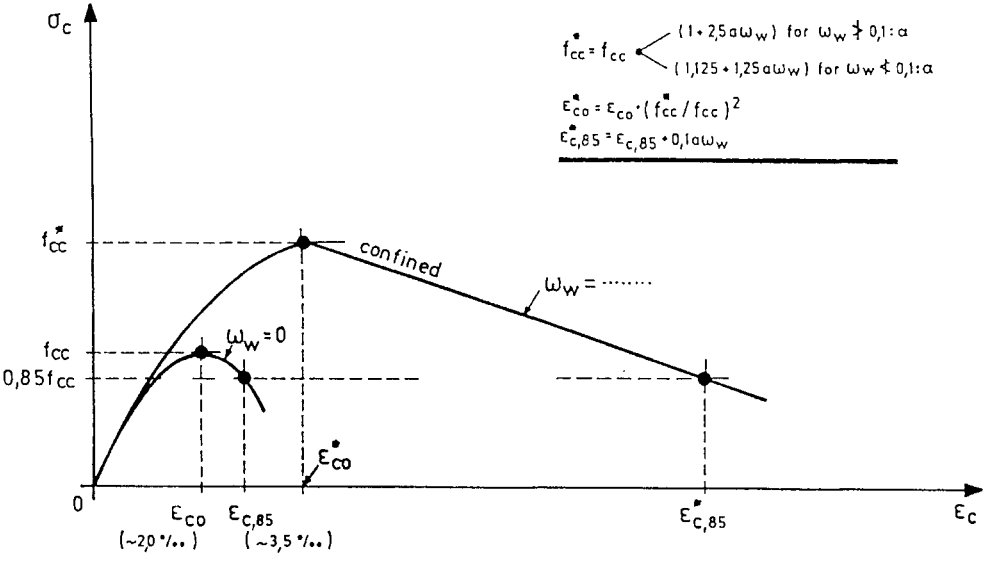

Figure 3 Modified constitutive relationship for confined concrete [7]

@seismicisolation

CALCULATION OF CURVATURE DUCTILITY

The relationship between displacement and curvature ductilities in Appendix "D" of EC8 is given by:

$$\mu_{1/r} = 1 + \frac{[\ \mu_\Delta - 1\ ]}{3\ \lambda_{pl}\ (\ 1 - 0.5\ \lambda_{pl}\ )} \qquad (3)$$

The above expression is based on the curvature distribution shown in figure 4.

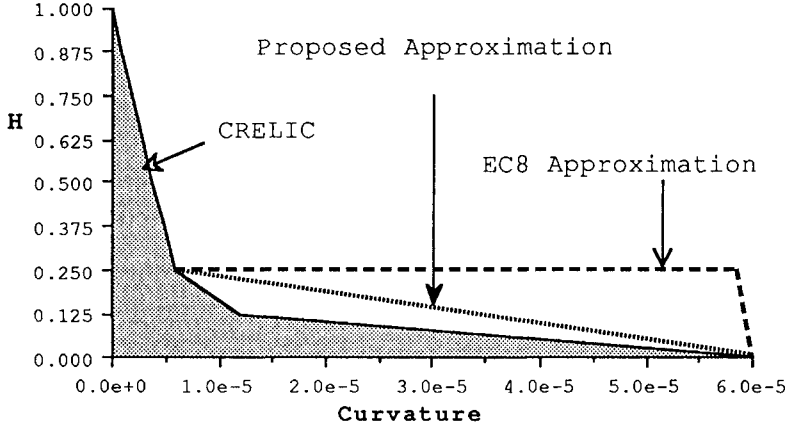

Figure 4 Curvature distribution for a cantilever wall at ultimate load

As demonstrated in figure 4, the EC8 assumption overestimates the curvature at the lower part of the wall, hence, it will underestimate the curvature ductility demand. This was demonstrated analytically as shown in figure 5 for a number of walls analysed by a computer program CRELIC developed by the writers [10].

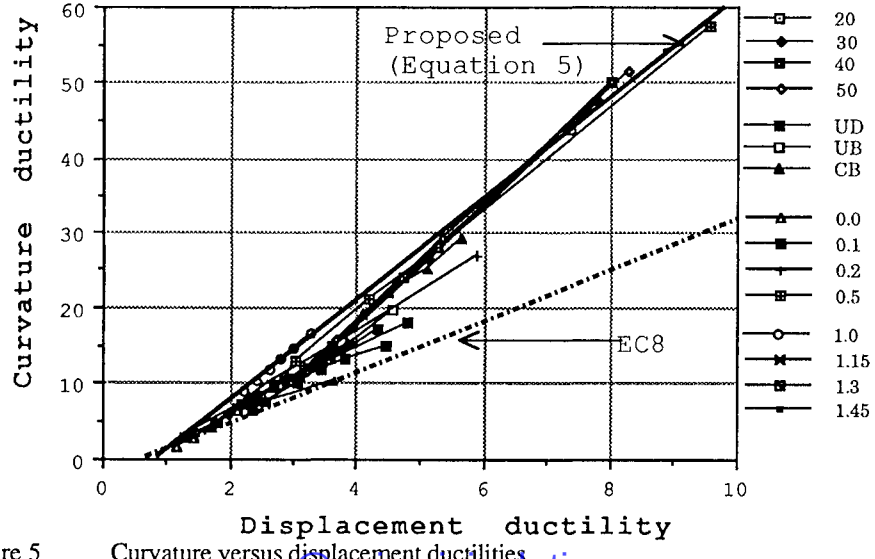

Figure 5 Curvature versus displacement ductilities

@seismicisolation

Based on the proposed curvature distribution of figure 4 (the derivation is given in the Appendix) the following equation for curvature ductility evaluation is proposed.

$$\mu_{1/r} = 1 + \frac{[\mu_\Delta - (1 + \lambda_{pl})]}{\lambda_{pl}(1.5 - 0.5\lambda_{pl})} \tag{4}$$

By assuming a minimum plastic hinge length of 0.1 h_w, then substituting in equation 4, the relationship between curvature and displacement ductilities is given by:

$$\mu_{1/r} = 1 + 6.9(\mu_\Delta - 1.1) \approx 1 + 7(\mu_\Delta - 1) \tag{5}$$

The equation proposed above is shown in figure 5 to be conservative for most of the examined walls except for the cases with high confinement levels for which estimates are very close to the analytical predictions. Nonetheless, since the extent of the plastic hinge is of paramount significance to the derivation of equation 5, a closer examination of the assumed value of 0.1 h_w is required.

Estimation of plastic hinge length

The plastic hinge height is given by several researchers to be a function of the aspect ratio based on equations proposed by Mattock [11]. However, since the effect of shear is not taken into account in curvature calculations, there is no reason why the plastic hinge height should be a function of the section width. If it is assumed that the normalised length of the plastic hinge zone is given by:

$$\lambda_{pl} = 1 - \frac{M_y}{M_{pl}} \tag{6}$$

then the extent of the plastic hinge can easily be obtained analytically. It was demonstrated through a parametric study by using CRELIC that the plastic hinge length is affected by the amount and distribution of the flexural reinforcement, the characteristics of the reinforcement and the presence of axial load. Plots of λ_{pl} versus a number of different parameters are shown in figure 6.

In figure 6 it is demonstrated that the value of λ_{pl} does not fall below the value of 0.2 except in the presence of very high axial load. If this value of λ_{pl} is used in equation (4) then the equation for curvature ductility becomes:

$$\mu_{1/r} = 1 + 3.6(\mu_\Delta - 1.2) \approx 1 + 3.5(\mu_\Delta - 1) \tag{7}$$

The above equation approximates to that used in EC8 for a plastic hinge length of 0.1. However, as seen from figure 5, this is still on the unsafe side which implies that even the new derivation for curvature ductility of equation 4 is unconservative. A better representation than the linear approximation between the yield and ultimate curvatures in figure 3 would be a parabolic curve. Nonetheless, the proposed approximation of equation (4) based on an assumed plastic hinge height of 0.1h_w seems, in general, to yield conservative results.

@seismicisolation

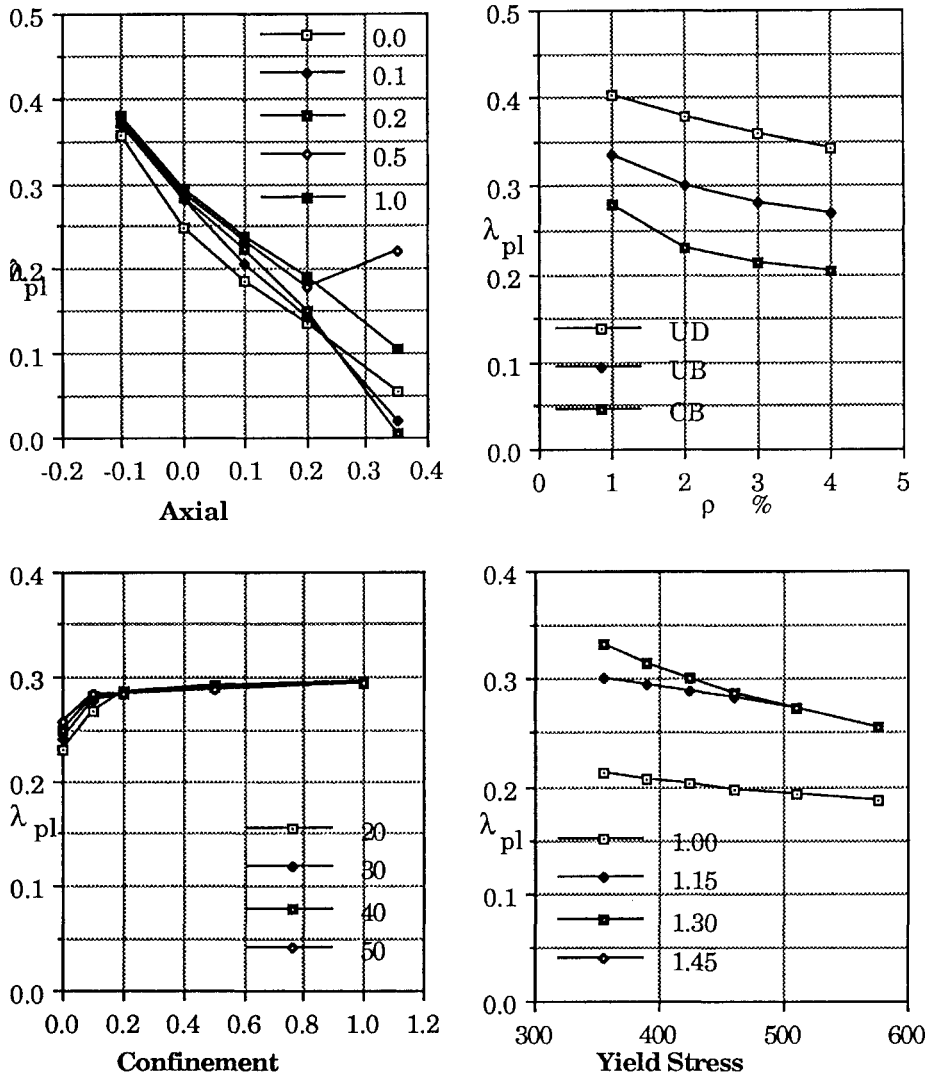

Figure 6 Variation of plastic hinge length

ESTIMATION OF REQUIRED CONFINEMENT

The final stage of converting curvature ductility to confinement is a more onerous task, since many parameters influence the ductility of an unconfined section. It is proposed that a reference curvature ductility μ_{1/r_0} is calculated first for the unconfined section by establishing the curvatures at yield and ultimate conditions based on accurate estimates of the neutral axis depth. Thereafter, the controlling curvature parameters at yield and at ultimate are the steel

@seismicisolation

strain ε_{sy} and the concrete ultimate strain ε_{cu}. In which case, the unconfined curvature ductility is given by:

$$\mu_{1/ro} = \frac{\varepsilon_{cu}\,(1-\xi_y)}{\varepsilon_y\ \xi} \geq \frac{\varepsilon_{cu}\,(1-2\,\xi)}{\varepsilon_y\ \xi} \tag{8}$$

The value of ξ_y is always larger than ξ (almost twice) and hence a conservative assumption would be to use the value of 2ξ at ultimate conditions in order to by-pass the extra calculation required for the evaluation of ξ_y.

The final equation for calculating the confinement should include the ratio of ductility demand to $\mu_{1/ro}$, as well as the confinement pattern as shown in equation (9) below. This is obtained through a parametric study by using CRELIC. This is given by:

$$\omega_{wd} = \frac{1}{32\,\alpha}\left(\frac{\mu_{1/r}}{\mu_{1/ro}} - 1\right) \tag{9}$$

The above equation could be improved by further studies and comparisons with experimental data. The novelty of this approach is in accounting for section properties in the determination of the required level of confinement.

CONCLUSIONS

(a) The EC8 procedure of design for ductility provides a complete framework for detailing the critical members in accordance with the chosen behaviour factor.

(b) The EC8 implicit assumption that curvature ductility is constant within the plastic hinge zone will lead to unconservative design. A better approximation of the curvature distribution is presented in this paper.

(c) The available ductility of unconfined RC members $\mu_{1/ro}$ is not accounted for in the EC8 detailing requirements. A new approach which includes estimating $\mu_{1/ro}$ is proposed based on analytical studies.

ACKNOWLEDGEMENT

The work described herein was funded by the UK Science and Engineering Research Council, as part of a research programme on the seismic performance of reinforced concrete structural walls.

REFERENCES

1. ACI 318-83, " Building Code Requirement for Reinforced Concrete", American Concrete Institute, Detroit,1983, 111 pp.

2. Uniform Building Code, International Conference of Building Officials, Whittier, California, 1988

3. NZS 3101:1982, Parts 1 &2, "Code of Practice for the Design of Concrete Structures", Standards Association of New Zealand, Wellington, 1982, 283 pp.

@seismicisolation

4. EC8, "Eurocode No.8 : Structures in seismic regions - Design ", Part 1, General and building, Report EUR 12266 EN, Industrial Processes, Building and Civil Engineering, Commission of the European Communities, May 1988

5. Zahn, F.A., Park, R., Priestley, J.N. and Chapman, H.E., "Development of design procedures for the flexural strength and ductility of reinforced concrete bridge columns", Bulletin of the New Zealand Society for Earthquake Engineering, Vol. 19, No.3, September 1986, pp. 200-212

6. Paulay, T. and Williams, R.L., "The analysis and design of and the evaluation of design actions for reinforced concrete ductile shear wall structures", Bulletin of the New Zealand National Society for Earthquake Engineering, Vol. 13 No. 2, June 1980, pp 103-143

7. Paulay, T. and Uzumeri, S.M., "A Critical Review of the Seismic Design Provisions for Ductile Shear Walls of the Canadian Code and Comments", Canadian Journal of Civil Engineering, Vol.2, December 1975, pp. 592-601

8. Seminar on Eurocode 8, "Structures in seismic regions - Design ", Report EUR 12266 EN, Industrial Processes, Building and Civil Engineering, Commission of the European Communities, May 1988

9. Tassios, T.P., "Specific rules for concrete structures", In Background Document for Eurocode 8 - Part 1, Volume 2 - Design Rules, Commission of European Communities, 1989, pp. 1-123

10. Pilakoutas K., "Earthquake resistant design of reinforced concrete walls", PhD Thesis, University of London, 1990

11. Mattock A. H., Discussion of "Rotational capacity of reinforced concrete beams", by Corley W. G., in J. Struct. Div. Am. Soc. Civ. Eng., 93 (ST2), April 1967, pp. 519-522

APPENDIX

Derivation of ductility based on linear distribution of curvature within the plastic hinge zone

The definition of curvature ductility $\mu_{1/r}$ and μ_Δ is given by:

$$\mu_{1/r} = \frac{k_p}{k_e}, \qquad \mu_\Delta = \frac{\delta_p}{\delta_e} \tag{A1}$$

The elastic and plastic deformations are obtained by integrating the product of curvature and h over the wall height.

$$\delta_e = \int_0^{h_w} \left(\frac{k_e\, h}{h_w} \right) h\, dh = \frac{k_e\, h_w^2}{3} \tag{A2}$$

By considering $\lambda_{pl} = l_{pl} / h_w$ and a linear distribution of curvature within the plastic hinge zone the plastic displacement is given by:

@seismicisolation

$$\delta_p = \frac{k_e h_w^2}{3}\left(1 + \lambda_{pl} - \frac{\lambda_{pl}^2}{2}\right) + \frac{k_e(\mu_{1/r} - 1)h_w^2}{3}\lambda_{pl}[1.5 - 0.5\lambda_{pl}] \tag{A3}$$

Hence, by dropping second order values and dividing A3 by A2, an expression for deflection ductility is achieved, as shown below.

$$\mu_\Delta = \frac{\delta_p}{\delta_e} = (1 + \lambda_{pl}) + (\mu_{1/r} - 1)\lambda_{pl}[1.5 - 0.5\lambda_{pl}] \tag{A4}$$

By rearranging the above equation, the curvature ductility is obtained:

$$\mu_{1/r} = 1 + \frac{[\mu_\Delta - (1 + \lambda_{pl})]}{\lambda_{pl}(1.5 - 0.5\lambda_{pl})} \tag{A5}$$

@seismicisolation

Taylor & Francis
Taylor & Francis Group
http://taylorandfrancis.com

@seismicisolation
@seismicisolation

INDEX OF CONTRIBUTORS

Ahmadi, H.R., 141
Al-Karni, A., 333
Aspinall, W.P., 1, 41
Attewell, P.B., 463

Bassett, R.H., 231
Belhadj, A., 411
Beshara, F.B.A., 249
Billings, L.J., 121
Blakeborough, A., 307, 411
Bongiovanni, G., 201
Booth, E.D., 53, 307, 482
Bousias, S.N., 275
Breitwieser, K., 63
Brownjohn, J.M.W., 421
Budhu, M., 333

Câmara, R., 264
Chandler, A.M., 53, 231
Clark, P., 110
Coburn, A.W., 19, 53
Colloff, J., 31
Constantinou, M.C., 151
Coveney, V.A., 141

Daniell, W.E., 91
Davies, M.C.R., 342
Donald, J., 9
Dowling, P.J., 211
Durrani, A.J., 241

Elghazouli, A.Y., 211
Ellis, B.R., 193
Elnashai, A.S., 211, 510
Evason, B.R., 374

Fashole-Luke, P.S., 79
Fenwick, R., 221
Fullard, K., 374
Fuller, K.N.G., 141

Gorelli, V., 201
Gutierrez, E., 275

Hinks, J.L. 91

Isaac, I.D., 442

Johnston, R.S., 319

Key, D., 131
Khabbazan, M.M., 79
Kunar, R., 9

Llambias, J.M., 319
Lubkowski, Z.A., 421

Mackay, D.C., 79
Magonette, G., 275
Maguire, J.R., 100
Makris, N., 151
Mallard, D.J., 1, 41
Menu, J., 31
Moghaddam, H.A., 502
Murphy, P.D., 307

Neelakantan, G., 333
New, B.M., 163
Newell, J.P., 176
Nichol, E.A., 231
Nnadi, G.N., 363

Oliver, A., 395

Pappin, J.W., 421
Pilakoutas, K., 510
Pomonis, A., 19
Portugal, A., 264
Prakash, S., 186
Puri, V.K., 186

Rahman, S., 492

@seismicisolation

Raybould, M., 295
Redmayne, D.W., 352
Riding, J.B., 110
Rienzo, G., 201
Rinaldis, D., 201
Rogers, C., 110

Sakai, S., 19
Sarma, S.K., 63
Selby, A.R., 395, 463
Shepherd, R., 121
Skipp, B.O., 41, 482
Spence, R.J.S., 19
Steedman, R.S., 285

Taylor, C.A., 91, 421
Thompson, D.B., 79
Tognoli, P., 275
Turbitt, T., 352

Uromeihy, A., 463

Verzeletti, G., 275
Virdi, K.S., 249

Waldron, P., 411
Williams, M.S., 176
Wong, P.K.C., 53
Woo, G., 1

Young, J.S., 430

Zabegayev, A.V., 385
Zeng, X., 285

@seismicisolation